

Oliver M. O'Reilly

Modeling Nonlinear Problems in the Mechanics of Strings and Rods

The Role of the Balance Laws

Interaction of Mechanics and Mathematics

Series editor

Lev Truskinovsky, Laboratoire de Mechanique des Solid, Palaiseau, France
e-mail: trusk@lms.polytechnique.fr

About this Series

The Interaction of Mechanics and Mathematics (IMM) series publishes advanced textbooks and introductory scientific monographs devoted to modern research in the wide area of mechanics. The authors are distinguished specialists with international reputation in their field of expertise. The books are intended to serve as modern guides in their fields and anticipated to be accessible to advanced graduate students. IMM books are planned to be comprehensive reviews developed to the cutting edge of their respective field and to list the major references.

Advisory Board

D. Colton, USA

R. Knops, UK

G. DelPiero, Italy

Z. Mroz, Poland

M. Slemrod, USA

S. Seelcke, USA

L. Truskinovsky, France

IMM is promoted under the auspices of ISIMM (International Society for the Interaction of Mechanics and Mathematics).

More information about this series at <http://www.springer.com/series/5395>

Oliver M. O'Reilly

Modeling Nonlinear Problems in the Mechanics of Strings and Rods

The Role of the Balance Laws



Springer

Oliver M. O'Reilly
Department of Mechanical Engineering
University of California, Berkeley
Berkeley, CA, USA

ISSN 1860-6245 ISSN 1860-6253 (electronic)
Interaction of Mechanics and Mathematics
ISBN 978-3-319-50596-1 ISBN 978-3-319-50598-5 (eBook)
DOI 10.1007/978-3-319-50598-5

Library of Congress Control Number: 2016961219

Mathematics Subject Classification (2010): 73-01, 73G05, 73K05, 73K03, 34B60, 74K10, 74-01

© Springer International Publishing AG 2017

This work is subject to copyright. All rights are reserved by the Publisher, whether the whole or part of the material is concerned, specifically the rights of translation, reprinting, reuse of illustrations, recitation, broadcasting, reproduction on microfilms or in any other physical way, and transmission or information storage and retrieval, electronic adaptation, computer software, or by similar or dissimilar methodology now known or hereafter developed.

The use of general descriptive names, registered names, trademarks, service marks, etc. in this publication does not imply, even in the absence of a specific statement, that such names are exempt from the relevant protective laws and regulations and therefore free for general use.

The publisher, the authors and the editors are safe to assume that the advice and information in this book are believed to be true and accurate at the date of publication. Neither the publisher nor the authors or the editors give a warranty, express or implied, with respect to the material contained herein or for any errors or omissions that may have been made. The publisher remains neutral with regard to jurisdictional claims in published maps and institutional affiliations.

Printed on acid-free paper

This Springer imprint is published by Springer Nature
The registered company is Springer International Publishing AG
The registered company address is: Gewerbestrasse 11, 6330 Cham, Switzerland

*Dedicated with love and gratitude to my
mum, Anne, for her inspiration and strength.*

Preface

The aim of this graduate-level textbook is to show how the balance laws for theories of rods and strings can be applied in a systematic manner to develop models for a wide range of problems. My goal for the reader is to enable them to formulate models for problems involving one-dimensional continua such as rods and strings that apply to many interesting applications ranging from the human spine, to columns, and plant stems. The formulation of the models presented in the book presumes an introductory graduate-level familiarity with continuum mechanics and intermediate engineering dynamics. The analyses of the models that are discussed in the book require an elementary knowledge of the solutions to ordinary differential equations. The balance laws discussed in the text include the material momentum balance law and, depending on the problem, this law can serve to provide conservation laws and differential equations of motion. The applications include steadily moving strings, ribbon-like models for DNA, an elastica arm scale, and a series of problems with chains that are subject to shocks and impact. These examples have been chosen to be tractable and interesting, and hopefully they will serve as an inspiration for readers to explore the wealth of recent applications of rod theory to problems ranging from tendril perversion in morning glories to DNA supercoiling.

I have always greatly admired the beauty and elegance of continuum mechanics as it is presented in graduate-level courses. Among the highlights that still resonate nearly 30 years after I first saw them are the manner in which restrictions on constitutive relations are established using invariance requirements under superposed rigid body motions, the method of describing deformation gradients using curvilinear coordinate systems, and Rivlin's exact solutions for deformations of isotropic incompressible elastic materials. However, translating this wealth of material to problems was challenging for me. During my graduate studies, I worked on nonlinear dynamics of elastic strings and found it frustrating that I struggled to apply the material I had learned in courses on continuum mechanics to establish the equations of motion for an application with an elastic string. Because I knew that I would spend months analyzing the resulting equations of motion, I found the lack of confidence in my ability to derive equations of motion to be quite disconcerting.

Subsequently, while I was a junior faculty member at the University of California, Berkeley, I had the opportunity to delve into the works of Green and Naghdi on theories of deformable media. Although I experienced a steep learning curve, their seminal works enabled me to bridge the gap between my understanding of continuum mechanics and the development of feasible models in the form of partial and ordinary differential equations for a range of systems that can be modeled using theories of elastic rods and strings. Substantial portions of this book are summaries of the work that has resulted from these early explorations on the application of rod theories. While Green and Naghdi's works influenced the writing of every single page of this book, I have also benefitted greatly from the works of Antman, Gurtin, Maugin, and many others that are referenced in these pages. I am fortunate to work in a field where the standards for excellence in writing include Antman's *Nonlinear Problems of Elasticity* [12] and Love's *A Treatise on the Mathematical Theory of Elasticity* [213].

The opening chapters of this book are designed to enable a reader to explore how the theory of a deformable elastic string or elastic rod can be formulated for classes of problems. I place great emphasis on examining how the balance laws interplay with constitutive relations to form a set of governing equations. In contrast to other texts, I show how a balance of material momentum can play a key role in forming the equations of motion for a variety of well-known systems. I have found that most of the expertise needed to manipulate the balance laws so as to constitute a closed system of equations of motion can be understood by considering examples using the theory of the string. Consequently, discussions and applications of the theory of inextensible strings and elastic strings form the first part of the book. The second part of the book is devoted to rod theories. I start with a planar theory due to Euler and present several classic and new applications of this wonderful theory. To discuss nonplanar problems, Kirchhoff's theory of an elastic rod is needed. This theory is a nonplanar extension of Euler's work and involves an inextensible, unshearable elastic rod. After discussing both recent and classic applications of Kirchhoff's theory, a more elaborate theory of an extensible, shearable elastic rod is discussed. This theory has been championed by the works of Antman dating to the early 1970s and is ideally suited to many biophysical applications. The book concludes with a discussion of Green and Naghdi's rod theory. This theory subsumes the aforementioned rod theories and can accommodate shear, extension, flexural, and torsional modes of deformation. For the reader's convenience, two supplemental chapters are incorporated into the text. The first of these chapters is a review of continuum mechanics and the second is an equally rapid review of variational methods.

Several colleagues and students have generously given of their time and reviewed drafts of this book during its lengthy gestation period. Despite my best efforts, I doubt if all possible typographical errors or inconsistencies have been removed from the published version. If you find such errors or inconsistencies in this text, I would be most grateful if you could bring them to my attention by sending me an email at oreilly@berkeley.edu. A list of errata for the book will become available on my homepage in due course. Finally, part of the pleasure of writing a book is describing the works of others. On the other hand, it is challenging to decide which works

to exclude in an effort to produce a book of manageable scope and size. I hope the works I have chosen to discuss form an interesting and engaging blend for the reader and apologize in advance to the many researchers whose works I was not able to include in these pages.

Berkeley, CA, USA
September 2016

Oliver M. O'Reilly

Acknowledgements

When I started as a junior faculty member in the Department of Mechanical Engineering at the University of California, Berkeley, in 1992, I was fortunate to have had James Casey and Paul M. Naghdi (1924–1994) as mentors and colleagues. I attended their courses on continuum mechanics and over the course of the next five years was able to have the time to read and appreciate Paul’s extensive series of works on rod theories with his longtime collaborator Albert E. Green (1912–1999). These works left an indelible impression on me. I greatly admired the precision and ingenuity with which Green and Naghdi developed models for mechanical systems and the clarity of their thoughts and writings.

In terms of the enormous volume of works discussing applications of rod theory that have appeared over the past thirty years, the theories of Antman, Kirchhoff, and Bernoulli-Euler are arguably the most popular nonlinear rod theories. A unifying perspective on these theories can be gained by examining the more general theory that Green and Naghdi along with several coworkers, including N. Laws, M. Wenner, and M. B. Rubin, developed in a series of works spanning 30 years. Their rod theory is currently the most general rod theory available. It is capable of including electromagnetic effects and can be constrained and restricted to the classical rod theory of Kirchhoff, Euler’s theory of the elastica, and a rod theory developed by Antman. Green and Naghdi also spent considerable time developing their rod theory from three-dimensional considerations and consequently a unique perspective (that is very useful when applying the theory to concrete applications) can be readily gained.

In the late 1990s, I developed a course on the dynamics of rods and strings. This course provided an introduction to the rod theories of Green and Naghdi and sought to apply them to a range of problems. I had believed up until then that Green and Naghdi’s rod theory was complete, but a student in this course, Carmel Majidi, showed me an adhesion problem that was not accommodated in a satisfactory manner by their rod theory. A similar issue had arisen a few years earlier with a classic problem of a folded chain that Hans Troger (1943–2010) had brought to my attention. After working with Carmel on the adhesion problem and Peter Varadi on

folded chain problems, I came to the realization that Green and Naghdi’s rod theory was lacking a balance law. Fortunately, at this time, R. Abeyaratne, M. E. Gurtin, J. K. Knowles (1931–2009), and G. A. Maugin (1944–2016) were leading the charge in pointing out that a similar issue arises with continuum theories. Leveraging the works of others, I was eventually able to postulate the missing balance law, which is now known as a balance of material momentum, in 2007. The local form of this balance law is always identically satisfied and the jump condition associated with the balance law resolved the earlier issues that I had with the adhered rod and folded chain problems. Subsequently, along with several collaborators, I used this balance law with various rod theories to explore problems including the growth of plants, chains modeled as inextensible strings, and the buckling instabilities of rods which are partially adhered to a surface.

Much of the material in this book has been the subject of my research and teaching for the past two decades. I have been privileged to teach several courses at the University of California, Berkeley, including ME175 (Intermediate Dynamics), ME271 (Calculus of Variations and Optimal Control), and ME290A (Nonlinear Dynamics of Continuous Systems), where the material has been presented and constantly revised in response to feedback from students. It is a pleasure to be able to thank these former students. In particular, Rubens Goncalves Salsa Junior, Evan Hemingway, Hyung-Taek Kim, Matthew Kury, and Alyssa Novelia generously provided feedback on a draft of this book that I used in my most recent offering of ME290A in the Spring Semester of 2016.

Prior to becoming a faculty member, I was extremely fortunate to have been a graduate student in the Department of Theoretical and Applied Mechanics at Cornell University during the latter half of the 1980s. There, I was exposed to a wide range of research on the nonlinear dynamics of mechanical systems, and the papers and teachings of John Guckenheimer, Tim Healey, Phil Holmes, and Frank Moon have had a profound influence on my career. During my time as an undergraduate student at University College Galway (now the National University of Ireland, Galway), I was first introduced to continuum mechanics and variational calculus by Jim Flavin (1936–2012). Little did I know then that Jim, who was a former student of Albert Green, would become such an influential mentor and friend.

I have benefited greatly from working with my former graduate students and research collaborators, Christopher Daily-Diamond, Wyatt O. Davis, Nur Adila Faruk Senan, Wayne Huang, Daniel T. Kawano, Patrick “Patch” Kessler, Nathan Kinkaid, Todd Lauderdale, Jeffrey C. Lotz, Cheng Luo, Carmel Majidi, Tom R. Nordenholz, Kristin M. de Payrebrune, Daniel M. Peters, Arun Srinivasa, Timothy N. Tresierras, Jeffrey S. Turcotte, Peter C. Varadi, John A. Williams, and Xuance Zhou. Without them, writing this book would not have been possible. In particular, much of the material on stability and variational methods that appears in Chapter 4 is adapted from papers [219, 220] and [268, 269] that I have coauthored with Carmel, John, and Daniel. Their influence and the influences of my other collaborators are evidenced by the citations to our joint works that appear throughout this book.

Several researchers generously provided images from their research. My thanks to James Hanna (Virginia Polytechnic Institute and State University) for kindly

supplying the image used in Figure 2.1 and to Jean-Christophe Géminard (École Normale Supérieure de Lyon) for graciously providing the image of the falling chain used in Figure 2.11. Davide Bigoni (University of Trento) provided the image of his research group’s elastica arm scale that is presented in Figure 4.14. Tyler McMillen (California State University, Fullerton) and Alain Goriely (Oxford University) generously supplied the code used to construct the solutions shown in Figures 5.23 and 5.24.

I also wish to take this opportunity to thank Alain Goriely and Apala Majumdar (University of Bath) for helpful comments on their papers [221, 222], Gert van der Heijden (University College London) for his helpful comments on a paper by Mielke and Holmes [238], Tim Healey (Cornell University) and Gabor Domokos (Budapest University of Technology and Economics) for insightful commentary on their paper [90] and related works on bifurcations of the equilibrium configurations of rods, Miles Rubin (Technion) for constructive comments on an earlier draft of this book, James Hanna for pointing out the distinctions between link chains and bead chains and his comments on the chain problem discussed in Section 2.5 of Chapter 2, Daniel Kawano (Rose-Hulman Institute of Technology) for his invaluable editorial advice and thorough proofreading, Harmeet Singh (Virginia Polytechnic Institute and State University) for several discussions on jump conditions in inextensible strings, and Lev Truskinovsky (École Polytechnique) for his helpful comments on the penultimate draft of this book.

As always, it has been a great pleasure working with Achi Dosanjh at Springer-Verlag. The constructive anonymous reviews of earlier drafts that she commissioned have helped improve the book and her support and guidance have been invaluable. I am delighted that the electronic version of this book will be available free of charge to large numbers of students worldwide.

The writing of this book has taken several years. In this endeavor, I have had the great fortune to be a member of the faculty at the University of California, Berkeley, for nearly a quarter of a century. Throughout this time, I have benefited from the support provided by alumni, benefactors, students, and taxpayers of the State of California to this remarkable institution. This sustenance has given me the freedom to explore, discover, assimilate, and ultimately write the material discussed in this book and for this I am immensely grateful.

Berkeley, CA, USA
September 2016

Oliver M. O’Reilly

Contents

Part I Mechanics of Strings

1	Mechanics of a String	3
1.1	Introduction	3
1.2	Notation and Nomenclature	4
1.3	Space Curves	5
1.3.1	The Frenet Triad, Torsion, and Curvature	6
1.3.2	The Frenet-Serret Relations	8
1.3.3	A Plane Curve	9
1.3.4	A Circular Helix	10
1.4	A Material Curve	13
1.4.1	Stretches, Derivatives, and Velocities	14
1.4.2	Functions and Their Derivatives	16
1.4.3	Discontinuities	17
1.4.4	Eulerian Formulation	19
1.4.5	Superposed Rigid Body Motions	21
1.5	Balance Laws	22
1.5.1	Assigned Forces, Contact Forces, and Material Forces	23
1.5.2	The Postulated Balance Laws	25
1.5.3	Localization Procedure	26
1.5.4	Local Balance Laws	27
1.5.5	Jump Conditions	28
1.6	Elastic Strings and Inextensible Strings	30
1.6.1	Gibbs Free Energy	33
1.6.2	Inextensibility	34
1.6.3	Identities	34
1.7	Summary of the Governing Equations	35
1.8	An Elementary Example Involving Material Forces	37
1.8.1	Interpretations of B_{ℓ_1} and C	39
1.8.2	A Uniform Bar	42

1.9	Closing Remarks	42
1.10	Exercises	43
2	Applications of the Mechanics of a String	49
2.1	Introduction	49
2.2	Steady Axial Motions of Elastic Strings and Inextensible Strings	51
2.2.1	Closed Loops of String	53
2.3	Inextensible Strings with Shocks	56
2.3.1	General Considerations	57
2.3.2	Boundary Conditions, Sources, Sinks, and Reservoirs	58
2.4	Cayley's Problem	60
2.5	A Chain of Finite Length Falling off the Edge of a Table	64
2.6	"Chains that Suck"	68
2.7	The Falling Folded Chain	72
2.8	The Chain Fountain	78
2.8.1	An Inverted Catenary	78
2.8.2	The String Leaving the Heap	81
2.8.3	The String at the End of the Catenary	82
2.8.4	Characteristics of the Chain Fountain	83
2.9	Closing Comments	86
2.10	Exercises	87
3	Link, Writhe, and Twist	93
3.1	Introduction	93
3.2	Space Curves, Ribbons, and Framings	94
3.2.1	Ribbons	98
3.2.2	Gauss-Bonnet Theorem	99
3.3	Gauss' Linking Number of Two Space Curves	101
3.4	Total Geometric Torsion of a Space Curve and Total Twist of a Ribbon	106
3.5	Călugăreanu's Theorem	108
3.6	Examples of Computing Writhing Numbers	111
3.7	Self-Linking of a Space Curve with Application to Strands of DNA	113
3.8	Exercises	115
Part II Mechanics of Rods		
4	Theory of the Elastica and a Selection of Its Applications	121
4.1	Introduction	121
4.2	Kinematical Considerations	123
4.3	Balance Laws	127
4.3.1	Local Balance Laws and Constitutive Relations	128
4.3.2	Jump Conditions	130
4.3.3	Summary of the Governing Equations	132
4.4	A Terminally Loaded Elastica and the Kinetic Analogue	132

4.5	The Adhesion of a Rod	137
4.5.1	General Considerations	138
4.5.2	Summary of the Solution Procedure	140
4.5.3	Examples	143
4.6	The Elastica Arm Scale	147
4.6.1	Background	148
4.6.2	The Deformable Arm Scale	149
4.6.3	The Operation of the Arm Scale	153
4.6.4	Insights from a Pair of Pendula	154
4.7	Potential Energies and a Variational Formulation	161
4.7.1	A Terminally Loaded Rod Deforming Under a Conservative Assigned Force	161
4.7.2	Application to an Adhesion Problem	164
4.8	Conditions for Stability from the Second Variation	167
4.8.1	A Representation for the Second Variation	168
4.8.2	Conjugate Points and the Riccati and Jacobi Equations	171
4.8.3	The Criterion N1	172
4.8.4	The Criterion B1	173
4.8.5	The Criterion S1	173
4.9	Simple Examples of Buckling	174
4.9.1	Compressing an Adhered Rod	174
4.9.2	Buckling of a Clamped Rod	176
4.9.3	Stability of Peeling	178
4.10	Additional Areas of Application of the Elastica	182
4.11	Exercises	183
5	Kirchhoff's Rod Theory	187
5.1	Introduction	187
5.2	The Directed Curve	189
5.2.1	An Approximation	189
5.3	Kinematics of Kirchhoff's Rod Theory	191
5.3.1	Parameterizations of the Rotation Tensor	193
5.3.2	Strains	197
5.3.3	Inertias	200
5.4	Further Kinematics and Discontinuities	202
5.5	Momenta and Kinetic Energy	204
5.6	A Strain Energy Function	205
5.7	Balance Laws for the Rod Theory	207
5.7.1	Assigned Forces, Assigned Director Forces, and Assigned Moments	208
5.7.2	Conservation Laws	210
5.8	Local Balance Laws and Jump Conditions	211
5.8.1	Local Balance Laws	211
5.8.2	Jump Conditions	212
5.9	Constitutive Relations	213

5.10	Twist, Torsion, and Tortuosity	215
5.11	Summary of the Governing Equations for Kirchhoff's Rod Theory	217
5.12	Relation to the Theory of the Elastica	218
5.13	A Terminally Loaded Rod and a Kinetic Analogue	219
5.13.1	Kirchhoff's Kinetic Analogue	220
5.14	The Simplest Problem: Bending and Torquing into a Helical Shape	222
5.15	Hocking of Cables, Loop Formation, and Localized Buckling	225
5.15.1	Development of the Reduced Dynamical System	227
5.15.2	The Straight Rod and a Pair of Rods Bent into a Helical Form	229
5.15.3	Nontrivial and Localized Equilibrium States of the Rod	233
5.15.4	Comments	239
5.16	Rods with Intrinsic Curvature: Tendril Perversion, Helical Solutions, and Buckling	240
5.16.1	Balance Laws for an Intrinsically Curved Rod	241
5.16.2	Helical Solutions: Solving for the Geometric Torsion, Curvature, and Angle of Twist	241
5.17	Buckling of a Clamped Rod	247
5.18	Spiral Springs and a Stiffness Matrix	252
5.18.1	The Reference Configuration	253
5.18.2	The Balance Laws	254
5.18.3	A Stiffness Matrix	255
5.19	Closing Remarks	258
5.20	Exercises	258
6	Theory of an Elastic Rod with Extension and Shear	269
6.1	Introduction	269
6.2	Kinematical Considerations	270
6.3	Summary of the Governing Equations for the Rod Theory	273
6.3.1	Constitutive Relations for \mathbf{n} and \mathbf{m}	274
6.4	Treatments of Material Symmetry	277
6.4.1	The Case of a Constant Transformation \mathbf{Q}	278
6.4.2	Transverse Isotropy and Transverse Hemitropy	281
6.4.3	Application to Kirchhoff's Rod Theory	284
6.5	Application to Torsion and Extension	284
6.6	Erickson's Uniform States	287
6.6.1	Kinematical Considerations	288
6.6.2	Forces and Moments	290
6.7	Closing Comments	290
6.8	Exercises	291

7 Green and Naghdi's Rod Theory	295
7.1 A Hierarchy of Rod Theories	295
7.2 Kinematics of Green and Naghdi's Rod Theory	296
7.2.1 Three-Dimensional Considerations	298
7.3 Strains	298
7.3.1 Infinitesimal Strains	299
7.4 Momenta and Kinetic Energy	302
7.5 The Strain Energy Function	303
7.5.1 Infinitesimal Theory	305
7.6 Conservation Laws for the Rod Theory	307
7.6.1 Assigned Forces and Director Forces	307
7.6.2 Singular Supplies	309
7.6.3 Conservation Laws	311
7.7 Local Balance Laws and Jump Conditions	312
7.7.1 Local Balance Laws	312
7.7.2 Jump Conditions	314
7.8 Constitutive Relations	315
7.8.1 Constrained Elastic Rods	316
7.9 Summary of the Governing Equations for an Elastic Rod	318
7.10 Boundary Conditions	319
7.11 Kirchhoff's Rod Theory as a Constrained Rod Theory	320
7.12 Prescriptions and Three-Dimensional Considerations	323
7.12.1 Kinematical Considerations	323
7.12.2 Inertias	325
7.12.3 Preliminary Identities Pertaining to Volume Integrals	325
7.12.4 Integrating the Balance of Linear Momentum	328
7.12.5 Balance of Linear Momentum for the Directed Curve	329
7.12.6 Balances of Director Momenta for the Directed Curve	330
7.12.7 The Moment of Momentum and the Energy Balances for the Directed Curve	331
7.12.8 Balance of Material Momentum for the Directed Curve	332
7.12.9 Comments on the Integration Process	334
7.13 Applications	335
7.14 Exercises	335

Part III Background Material

8 A Rapid Review of Some Elements of Continuum Mechanics	345
8.1 Introduction	345
8.2 Some Kinematical Results	346
8.2.1 Curvilinear Coordinates	347
8.2.2 A Material Curve	350
8.2.3 Metric Tensors and Identities	351
8.2.4 Convected Coordinates	351

8.3	Stress Tensors and Divergences	355
8.3.1	Divergences	356
8.3.2	The Traction Vector and a Divergence	357
8.4	Balance Laws	359
8.5	Invariance Requirements under Superposed Rigid Body Motions ..	359
8.6	Constitutive Relations for Hyperelastic Bodies	361
8.6.1	A Mooney-Rivlin Material	364
8.6.2	Additional Remarks	365
8.7	Configurational, Material, or Eshelbian Forces	365
8.8	A Material Momentum Balance Law	366
8.8.1	The Local Form	367
8.8.2	The Jump Condition	369
8.9	Closing Comments	370
8.10	Exercises	371
9	Variational Methods	377
9.1	Introduction	377
9.2	Variations and Necessary Conditions	378
9.3	The Euler-Lagrange Necessary Condition	379
9.3.1	Varying Boundary Conditions	381
9.3.2	Weierstrass-Erdmann Corner Conditions	382
9.3.3	Examples	384
9.4	Hamilton's Principle of Least Action	387
9.5	The Wave Equation	387
9.6	Application to Green and Naghdi's Rod Theory	389
9.7	Closing Remarks	390
References	393
Index	423

Part I

Mechanics of Strings

Chapter 1

Mechanics of a String

“In a theory ideally worked out, the progress which we should be able to trace would be, in other particulars, one from less to more, but we may say that, in regard to the assumed physical principles, progress consists in passing from more to less.”
A. E. H. Love [213, Page 1] commenting on the historical development of theories for continuous media.

1.1 Introduction

A purely mechanical theory of a string provides a simple model for several systems. In particular, it has been used to model axially moving media and biological filaments. The former is present in cable laying, band saws, textile processes, and drilling strings, among others. Our interest in this chapter lies in establishing the equations of motion for such systems when modeled using a mechanical theory of a string. The developments we present are hopefully of sufficient generality that they provide a unified perspective on the applications which follow in the subsequent chapters.

Among the topics of interest are the possibilities that the string will undergo large motions and large deformations (see Figures 1.1 and 1.2), that it may be subject to singular supplies of power and momentum, and that its motion may have points of discontinuity in strain, unit tangent vector, or velocity vector, among others. In the theory that is presented here, all of these issues are addressed. We base our developments on a series of works by the late Albert E. Green and Paul M. Naghdi and their coworkers. These works are supplemented with a recently developed balance law for material momentum from [264, 278]. The latter allows us to present a systematic development of models for strings that have discontinuities in their motion.

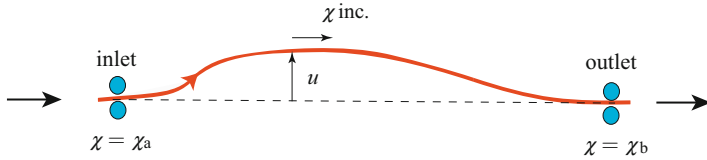


Fig. 1.1 The moving threadline problem. Here, an inextensible string is drawn between the outlet and inlet, and external body forces, such as gravity, are ignored. During the steady motion, the material points of the string move in rectilinear motion at a constant speed which is denoted by V , the string has a constant density ρ , and is in a state of uniform tension which is denoted by P . The transverse perturbations $u(\chi, t)$ to this steady motion are governed by a partial differential equation $\rho u_{,\text{tt}} + 2\rho Vu_{,\chi t} + \rho V^2 u_{,\chi\chi} = Pu_{,\chi\chi}$ (see, e.g., [57, 363]). For the threadline shown in this figure, $\chi_b - \chi_a = \ell$ where ℓ is a constant and χ is a coordinate.

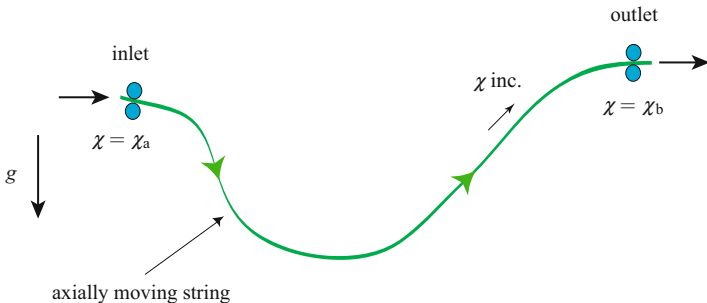


Fig. 1.2 Schematic of a string which is being drawn between an inlet and an outlet. The coordinate χ is used to label the material points passing through the inlet and the outlet and also to parameterize the steady motion that the string performs. The problem shown in this figure was analyzed by O'Reilly [259] and Perkins and Mote [287, 288] for the case when $\chi_a = 0$, $\chi_b = \ell$, and ℓ is a constant.

1.2 Notation and Nomenclature

A wide range of notation and nomenclature will be introduced in this chapter and it is convenient here to summarize the major quantities that we will introduce. In the first table, Table 1.1, most of the kinematical quantities we use are defined. The second table, Table 1.2, presents kinetic quantities.

We denote Euclidean three-space by \mathbb{E}^3 and denote a right-handed, fixed Cartesian basis for this space by $\{\mathbf{E}_1, \mathbf{E}_2, \mathbf{E}_3\}$. We also make frequent use of the set of right-handed orthogonal polar coordinate basis vectors:

$$\{\mathbf{e}_r = \cos(\theta)\mathbf{E}_1 + \sin(\theta)\mathbf{E}_2, \mathbf{e}_\theta = \cos(\theta)\mathbf{E}_2 - \sin(\theta)\mathbf{E}_1, \mathbf{E}_3\}. \quad (1.1)$$

Here, θ is measured counterclockwise about \mathbf{E}_3 .

Table 1.1 Notation and units for a selection of kinematical quantities.

Kinematical quantity	Description	SI units
ξ	material coordinate	m
s	arc-length parameter	m
\mathbf{r}	position vector	m
$\mathbf{v} = \dot{\mathbf{r}}$	velocity vector	m/s
$\mathbf{a} = \ddot{\mathbf{r}}$	acceleration vector	m/s ²
$\mu = \left\ \mathbf{r}' \right\ $	stretch	dimensionless
ρ_0	mass density per unit length of ξ	kg/m
ρ	mass density per unit length of s	kg/m
$P = -\mu \rho \mathbf{v} \cdot \mathbf{r}'$	material momentum	kgm/s
\mathbf{v}_γ	velocity vector of the material point $\xi = \gamma(t)$	m/s
\mathbf{e}_t	unit tangent vector	dimensionless
\mathbf{e}_n	unit normal vector	dimensionless
\mathbf{e}_b	unit binormal vector	dimensionless
κ	curvature	1/m
τ	geometric torsion	1/m
$\omega_{SF} = \tau \mathbf{e}_t + \kappa \mathbf{e}_b$	Darboux vector	1/m

Table 1.2 Notation and units for a selection of kinetic quantities.

Kinetic quantity	Description	SI units
ψ	strain energy function per unit mass	m ² /s ²
\mathbf{n}	contact force	Newton (N) = kgm/s ²
\mathbf{f}	assigned force per unit mass	N/kg
\mathbf{b}	assigned material force	N
\mathbf{C}	contact material force	N
\mathbf{B}	singular (point) contact material force	N
\mathbf{F}	singular supply of linear momentum	N
\mathbf{M}_O	singular supply of angular momentum relative to O	Nm
Φ_E	singular supply of power	Nm/s

1.3 Space Curves

We first discuss the case of a curve in Euclidean three-dimensional space (see Figure 1.3). To start, we define the Frenet triad $\{\mathbf{e}_t, \mathbf{e}_n, \mathbf{e}_b\}$, and the space curve's curvature κ and torsion τ . We also discuss the Serret-Frenet relations,

$$\frac{\partial \mathbf{e}_t}{\partial s} = \kappa \mathbf{e}_n, \quad \frac{\partial \mathbf{e}_n}{\partial s} = -\kappa \mathbf{e}_t + \tau \mathbf{e}_b, \quad \frac{\partial \mathbf{e}_b}{\partial s} = -\tau \mathbf{e}_n, \quad (1.2)$$

and the handedness of space curves.

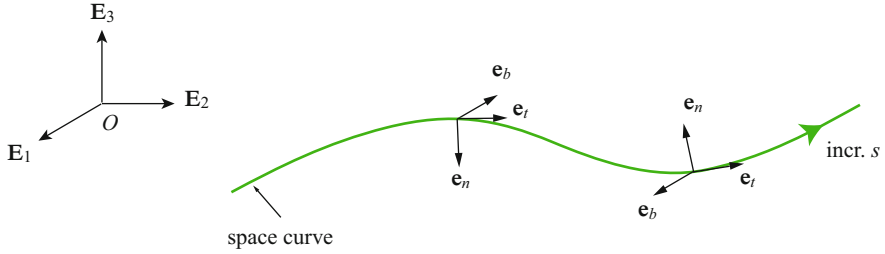


Fig. 1.3 A space curve showing the evolution of the Frenet triad.

1.3.1 The Frenet Triad, Torsion, and Curvature

We assume that the curve is parametrized by an arc-length parameter s . Hence the position of a point on the curve can be defined by specifying its value of s :

$$\mathbf{r} = \mathbf{r}(s) = x_1(s)\mathbf{E}_1 + x_2(s)\mathbf{E}_2 + x_3(s)\mathbf{E}_3. \quad (1.3)$$

A unit tangent vector \mathbf{e}_t to the curve can be defined:

$$\mathbf{e}_t = \frac{\partial \mathbf{r}}{\partial s}. \quad (1.4)$$

The derivative of this vector defines the curvature κ and the unit normal vector \mathbf{e}_n :

$$\frac{\partial \mathbf{e}_t}{\partial s} = \kappa \mathbf{e}_n. \quad (1.5)$$

That is,

$$\kappa = \left\| \frac{\partial \mathbf{e}_t}{\partial s} \right\|, \quad \mathbf{e}_n = \frac{1}{\kappa} \frac{\partial \mathbf{e}_t}{\partial s}. \quad (1.6)$$

We now use the tangent and normal vectors to define an orthonormal, right-handed triad, known as the Frenet triad:

$$\{\mathbf{e}_t, \mathbf{e}_n, \mathbf{e}_b = \mathbf{e}_t \times \mathbf{e}_n\}. \quad (1.7)$$

Here, \mathbf{e}_b is the unit binormal vector. The Frenet frame is the pairing of the Frenet triad $\{\mathbf{e}_t(s_1), \mathbf{e}_n(s_1), \mathbf{e}_b(s_1)\}$ and a point P_1 on the space curve. The value of the arc-length parameter $s = s_1$ at the associated point P_1 .

Using the fact that the Frenet triad is orthonormal, one defines the (geometric) torsion of the space curve by the relation

$$\frac{\partial \mathbf{e}_b}{\partial s} = -\tau \mathbf{e}_n. \quad (1.8)$$

Here, the minus sign is conventional.

The curvature and torsion define two important measures for a space curve and we can define them without referring explicitly to the Frenet triad:

$$\kappa = \left\| \frac{\partial^2 \mathbf{r}}{\partial s^2} \right\|, \quad \tau = \frac{1}{\kappa^2} \left[\frac{\partial \mathbf{r}}{\partial s}, \frac{\partial^2 \mathbf{r}}{\partial s^2}, \frac{\partial^3 \mathbf{r}}{\partial s^3} \right], \quad (1.9)$$

where $[\mathbf{a}, \mathbf{b}, \mathbf{c}]$ denotes the scalar triple product. A curve is said to be right-handed if $\tau > 0$ and left-handed if $\tau < 0$ (see Kreyszig [188]). For a curve where $\mathbf{r} = \mathbf{r}(s, t)$ we can still calculate the Frenet triad, however we would do so at each instant of time t .

While the relations (1.9) are useful, often a curve is parametrically described by a parameter that is not the arc-length parameter s . In this case, we can establish equivalent relations by repeated application of the chain rule. To elaborate, suppose that $\mathbf{r} = \mathbf{r}(x)$ where x is a parameter which can be expressed as a function of s : $x = x(s)$. Then, we have

$$\begin{aligned} \frac{\partial \mathbf{r}}{\partial s} &= \frac{dx}{ds} \frac{\partial \mathbf{r}}{\partial x}, \\ \frac{\partial^2 \mathbf{r}}{\partial s^2} &= \frac{d^2 x}{ds^2} \frac{\partial \mathbf{r}}{\partial x} + \left(\frac{dx}{ds} \right)^2 \frac{\partial^2 \mathbf{r}}{\partial x^2}, \\ \frac{\partial^3 \mathbf{r}}{\partial s^3} &= \frac{d^3 x}{ds^3} \frac{\partial \mathbf{r}}{\partial x} + 3 \left(\frac{dx}{ds} \right) \left(\frac{d^2 x}{ds^2} \right) \frac{\partial^2 \mathbf{r}}{\partial x^2} + \left(\frac{dx}{ds} \right)^3 \frac{\partial^3 \mathbf{r}}{\partial x^3}. \end{aligned} \quad (1.10)$$

We can conclude from these three representations that

$$\begin{aligned} \frac{dx}{ds} &= \pm \left\| \frac{\partial \mathbf{r}}{\partial x} \right\|^{-1}, \\ \kappa &= \left\| \frac{d^2 x}{ds^2} \frac{\partial \mathbf{r}}{\partial x} + \left(\frac{dx}{ds} \right)^2 \frac{\partial^2 \mathbf{r}}{\partial x^2} \right\|, \\ \tau &= \frac{1}{\kappa^2} \left(\frac{dx}{ds} \right)^6 \left[\frac{\partial \mathbf{r}}{\partial x}, \frac{\partial^2 \mathbf{r}}{\partial x^2}, \frac{\partial^3 \mathbf{r}}{\partial x^3} \right]. \end{aligned} \quad (1.11)$$

These relations, and particularly the expression for τ , will be used in Chapter 3.

The radius of curvature is the inverse of the curvature κ . As can be seen by considering the case of a circle of radius R (cf. Figure 1.4), the radius of curvature is the radius of the largest circle that would be tangent to the curve at the point of interest. Thus, the radius of curvature of a straight line is infinite while the radius of curvature of a circle of radius R is R .

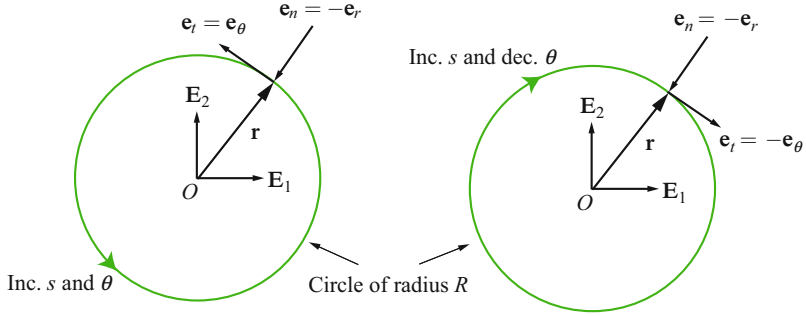


Fig. 1.4 The Frenet triad for a circle of radius R . For this curve, the torsion $\tau = 0$ (because the curve is planar) and the curvature $\kappa = \frac{1}{R}$. On the left, the direction of increasing s and θ are identical, whereas they are opposite to each other in the right-hand side image.

1.3.2 The Frenet-Serret Relations

The Frenet-Serret relations are compact expressions of the rate of change of the Frenet-triad basis vectors expressed in the basis $\{\mathbf{e}_t, \mathbf{e}_n, \mathbf{e}_b\}$. They are obtained using the definitions (1.5) and (1.8) and by differentiating the relation $\mathbf{e}_n = \mathbf{e}_b \times \mathbf{e}_t$:

$$\frac{\partial \mathbf{e}_t}{\partial s} = \kappa \mathbf{e}_n, \quad \frac{\partial \mathbf{e}_n}{\partial s} = -\kappa \mathbf{e}_t + \tau \mathbf{e}_b, \quad \frac{\partial \mathbf{e}_b}{\partial s} = -\tau \mathbf{e}_n. \quad (1.12)$$

We can express the Frenet-Serret relations using the compact notation

$$\frac{\partial \mathbf{f}_i}{\partial s} = \boldsymbol{\omega}_{SF} \times \mathbf{f}_i, \quad (1.13)$$

where

$$\mathbf{f}_1 = \mathbf{e}_t, \quad \mathbf{f}_2 = \mathbf{e}_n, \quad \mathbf{f}_3 = \mathbf{e}_b, \quad \boldsymbol{\omega}_{SF} = \tau \mathbf{e}_t + \kappa \mathbf{e}_b. \quad (1.14)$$

Noting that the Frenet triad is a right-handed frame, then the compact form (1.13) is a statement of the fact that

$$\mathbf{f}_i(s) = \mathbf{Q}_{SF}(s) \mathbf{f}_i(0) \quad (1.15)$$

where \mathbf{Q}_{SF} is a rotation (or proper-orthogonal) tensor. That is, $\det(\mathbf{Q}_{SF}) = 1$ and $\mathbf{Q}_{SF}^T \mathbf{Q}_{SF} = \mathbf{I}$. There are numerous parameterizations for rotation tensors, including Euler angles parameterizations and a unit quaternion parameterization. The former will be discussed at length in Section 5.3.1 of Chapter 5.¹

Differentiating the identity $\mathbf{Q}_{SF}^T \mathbf{Q}_{SF} = \mathbf{I}$ with respect to s , it can be shown that $\frac{\partial \mathbf{Q}_{SF}}{\partial s} \mathbf{Q}_{SF}^T$ is skew-symmetric and has an associated axial vector:

$$\boldsymbol{\omega}_{SF} = \text{ax} \left(\frac{\partial \mathbf{Q}_{SF}}{\partial s} \mathbf{Q}_{SF}^T \right). \quad (1.16)$$

¹ For additional background on Euler angles and other parameterizations of a rotation, the interested reader is referred to the authoritative review [321] by Malcolm Shuster (1943–2012).

The vector ω_{SF} is often called the Darboux vector after the French mathematician Gaston Darboux (1842–1917). The Darboux vector is unusual because it has no \mathbf{e}_n component: $\omega_{SF} \cdot \mathbf{e}_n = 0$. Curiously, if we consider a particle moving along a fixed space curve with a speed v , then the acceleration vector \mathbf{a} of the particle is $\mathbf{a} = \dot{v}\mathbf{e}_t + \kappa v^2\mathbf{e}_n$ and $\mathbf{a} \cdot \mathbf{e}_b = 0$.

Given ω_{SF} and the initial conditions $\mathbf{e}_t(s_0)$, $\mathbf{e}_n(s_0)$, and $\mathbf{e}_b(s_0)$, we can integrate (1.13)₁ to find the Frenet triad as a function of s . A further integration, of the differential equation $\frac{\partial \mathbf{r}}{\partial s} = \mathbf{e}_t(s)$, using the resulting values of $\mathbf{e}_t(s)$ and the initial value $\mathbf{r}(s_0)$ will yield the space curve $\mathbf{r}(s)$.²

To help verify the computation of ω_{SF} in later examples, we note that given a skew-symmetric tensor \mathbf{A} ,

$$\begin{aligned} \mathbf{A} = & a_3(\mathbf{p}_2 \otimes \mathbf{p}_1 - \mathbf{p}_1 \otimes \mathbf{p}_2) + a_2(\mathbf{p}_1 \otimes \mathbf{p}_3 - \mathbf{p}_3 \otimes \mathbf{p}_1) \\ & + a_1(\mathbf{p}_3 \otimes \mathbf{p}_2 - \mathbf{p}_2 \otimes \mathbf{p}_3), \end{aligned} \quad (1.17)$$

where $\{\mathbf{p}_1, \mathbf{p}_2, \mathbf{p}_3\}$ is a right-handed orthonormal basis for \mathbb{E}^3 , then the associated axial vector is

$$\begin{aligned} \mathbf{a} &= \text{ax}(\mathbf{A}) \\ &= a_1\mathbf{p}_1 + a_2\mathbf{p}_2 + a_3\mathbf{p}_3. \end{aligned} \quad (1.18)$$

We leave it as an exercise to verify that $\mathbf{Ab} = \text{ax}(\mathbf{A}) \times \mathbf{b}$ for any vector \mathbf{b} and skew-symmetric tensor \mathbf{A} . For future use, we also define an operator which transforms a vector into a skew-symmetric tensor:

$$\begin{aligned} \text{skew}(\mathbf{a}) = & a_3(\mathbf{p}_2 \otimes \mathbf{p}_1 - \mathbf{p}_1 \otimes \mathbf{p}_2) + a_2(\mathbf{p}_1 \otimes \mathbf{p}_3 - \mathbf{p}_3 \otimes \mathbf{p}_1) \\ & + a_1(\mathbf{p}_3 \otimes \mathbf{p}_2 - \mathbf{p}_2 \otimes \mathbf{p}_3), \end{aligned} \quad (1.19)$$

where $\mathbf{a} = a_1\mathbf{p}_1 + a_2\mathbf{p}_2 + a_3\mathbf{p}_3$. It is straightforward to verify that $\text{skew}(\mathbf{a})\mathbf{b} = \mathbf{a} \times \mathbf{b}$ for any pair of vectors \mathbf{a} and \mathbf{b} .

1.3.3 A Plane Curve

For a plane curve,

$$\mathbf{r} = \mathbf{r}(s) = x_1(s)\mathbf{E}_1 + x_2(s)\mathbf{E}_2. \quad (1.20)$$

Hence,

$$\mathbf{e}_t = \frac{\partial x_1}{\partial s}\mathbf{E}_1 + \frac{\partial x_2}{\partial s}\mathbf{E}_2. \quad (1.21)$$

² It is an interesting exercise to perform this integration for a space curve where ω_{SF} is constant. As can be seen from the developments in Section 1.3.4, the resulting curve will either be a circle or a circular helix.

We define an angle β such that

$$\cos(\beta) = \frac{\partial x_1}{\partial s}, \quad \sin(\beta) = \frac{\partial x_2}{\partial s}. \quad (1.22)$$

Consequently, we can use β and two unit vectors,

$$\mathbf{e}_1 = \cos(\beta)\mathbf{E}_1 + \sin(\beta)\mathbf{E}_2, \quad \mathbf{e}_2 = \cos(\beta)\mathbf{E}_2 - \sin(\beta)\mathbf{E}_1, \quad (1.23)$$

to conveniently represent the vectors

$$\mathbf{e}_t = \mathbf{e}_1, \quad \frac{\partial \mathbf{e}_t}{\partial s} = \frac{\partial \beta}{\partial s} \mathbf{e}_2. \quad (1.24)$$

Hence,

$$\kappa = \left| \frac{\partial \beta}{\partial s} \right|, \quad \mathbf{e}_n = \operatorname{sgn} \left(\frac{\partial \beta}{\partial s} \right) \mathbf{e}_2. \quad (1.25)$$

After taking the cross product of \mathbf{e}_t with \mathbf{e}_n , we observe that

$$\mathbf{e}_b = \operatorname{sgn} \left(\frac{\partial \beta}{\partial s} \right) \mathbf{E}_3. \quad (1.26)$$

Hence, for a plane curve, the torsion τ is zero. With some further calculations, we find that the Darboux vector for the plane curve is

$$\mathbf{w}_{SF} = \frac{\partial \beta}{\partial s} \mathbf{E}_3. \quad (1.27)$$

We leave it as an exercise to write down a representation for \mathbf{Q}_{SF} for a plane curve. In mechanics, the curve with constant curvature and zero torsion is the arc of a circle (see Figure 1.4). Because this is indicative of a constant bending moment, such curves are prominent in the design of many mechanical systems.

1.3.4 A Circular Helix

The equation for a circular helix (see Figure 1.5) can be expressed as

$$\mathbf{r} = R\mathbf{e}_r + R\alpha\theta\mathbf{E}_3. \quad (1.28)$$

Here, θ is a cylindrical polar coordinate, and we also recall that

$$\mathbf{e}_r = \cos(\theta)\mathbf{E}_1 + \sin(\theta)\mathbf{E}_2, \quad \mathbf{e}_\theta = \cos(\theta)\mathbf{E}_2 - \sin(\theta)\mathbf{E}_1. \quad (1.29)$$

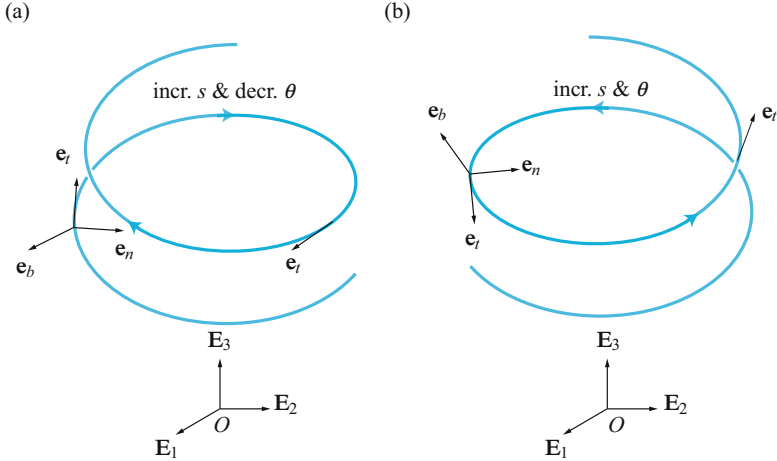


Fig. 1.5 Examples of circular helices showing the evolution of the Frenet triad. The helix in (a) is left-handed ($\tau < 0$) and the helix in (b) is right-handed ($\tau > 0$).

It is common to define a helix using the pitch parameter α . As can be seen from Figure 1.6, the pitch parameter relates θ to z . That is, we can use θ and z as coordinates on a cylinder of radius R . If we cut the cylinder along a vertical line and unfold it, sections of the helix will appear as straight lines with a slope αR .

For the helix, we can determine the Frenet triad by first differentiating \mathbf{r} with respect to s and using the chain rule:

$$\frac{\partial \mathbf{r}}{\partial s} = \frac{\partial \theta}{\partial s} (R\mathbf{e}_\theta + R\alpha\mathbf{E}_3). \quad (1.30)$$

Because \mathbf{e}_t is a unit vector, we can infer that $\frac{\partial \theta}{\partial s} = \pm \frac{1}{R\sqrt{1+\alpha^2}}$ and then calculate \mathbf{e}_t and the other two basis vectors easily. When $\frac{\partial \theta}{\partial s} > 0$, we find that

$$\mathbf{e}_t = \frac{1}{\sqrt{1+\alpha^2}} (\mathbf{e}_\theta + \alpha\mathbf{E}_3), \quad \mathbf{e}_n = -\mathbf{e}_r, \quad \mathbf{e}_b = \frac{1}{\sqrt{1+\alpha^2}} (\mathbf{E}_3 - \alpha\mathbf{e}_\theta). \quad (1.31)$$

Alternatively, when $\frac{\partial \theta}{\partial s} < 0$, then

$$\mathbf{e}_t = \frac{-1}{\sqrt{1+\alpha^2}} (\mathbf{e}_\theta + \alpha\mathbf{E}_3), \quad \mathbf{e}_n = -\mathbf{e}_r, \quad \mathbf{e}_b = \frac{-1}{\sqrt{1+\alpha^2}} (\mathbf{E}_3 - \alpha\mathbf{e}_\theta). \quad (1.32)$$

Some straightforward calculations of the derivatives of the Frenet triad basis vectors and the use of the chain rule will show that

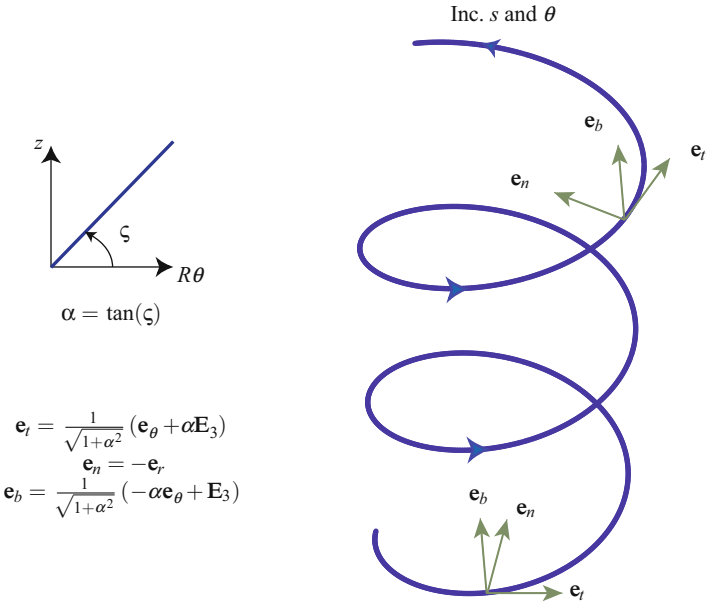


Fig. 1.6 Examples of Serret-Frenet triads for a portion of a (right-handed) circular helix. The inset image shows the relationship between the pitch angle ζ and the parameter α .

$$\kappa = R \left(\frac{\partial \theta}{\partial s} \right)^2 = \frac{1}{R(1+\alpha^2)} = \frac{\cos^2(\zeta)}{R},$$

$$\tau = \frac{\alpha}{R(1+\alpha^2)} = \frac{\cos(\zeta)\sin(\zeta)}{R}. \quad (1.33)$$

Hence, if $\alpha = \tan(\zeta) > 0 (< 0)$, then the helix is right-handed (left-handed).

Surprisingly, a helix is the only curve with constant curvature and constant nonzero torsion. The Darboux vector for the helix has the interesting representations

$$\begin{aligned} \boldsymbol{\omega}_{SF} &= \tau \mathbf{e}_t + \kappa \mathbf{e}_b \\ &= \kappa (\alpha \mathbf{e}_t + \mathbf{e}_b) \\ &= \frac{\partial \theta}{\partial s} \mathbf{E}_3. \end{aligned} \quad (1.34)$$

The Darboux vector is the axial vector of the skew-symmetric tensor $\frac{\partial \mathbf{Q}_{SF}}{\partial s} \mathbf{Q}_{SF}^T$ and an explicit representation for the rotation \mathbf{Q}_{SF} for the helix can be found in Eqn. (5.99). We also note that $\boldsymbol{\omega}_{SF}$ is constant and is parallel to the axis of the helix. Observing the complex motion of the Frenet triad as one moves along the helix, this result is surprising and has connections to constant angular velocity motions of rigid

bodies, geodesics of the rotation group $SO(3)$, and optometry.³ We also note that the results for a circle can be obtained by setting $\alpha = 0$ in the previous developments. Whence, $\kappa = \frac{1}{R}$ and $\tau = 0$ for a circle (cf. Figure 1.4).

In applications of rod theories, one often finds that the centerline of the rod is a helical space curve with a known curvature κ and geometric torsion τ . Given τ and κ , one can easily invert (1.33) to determine α and R :

$$\alpha = \frac{\tau}{\kappa}, \quad R = \frac{\kappa}{\kappa^2 + \tau^2}. \quad (1.35)$$

Observe that if the curve is planar, then $\alpha = 0$ and $R = \frac{1}{\kappa}$ as expected. An application of the identities (1.35) to a rod bent by terminal moments can be found in Section 5.14 of Chapter 5.

1.4 A Material Curve

We recall, from Green and Naghdi [133, 134], the concept of a material curve \mathcal{L} which is embedded in three-dimensional Euclidean space \mathbb{E}^3 . The current configuration \mathcal{C} of this curve is defined by the vector-valued function $\mathbf{r} = \mathbf{r}(\xi, t)$. Here, ξ is a coordinate along \mathcal{C} which uniquely identifies material points of \mathcal{L} and \mathbf{r} is the position vector of a material point of \mathcal{L} with respect to a fixed origin (cf. Figure 1.7). As the material curve moves in space, the coordinate ξ associated with a material point remains the same. Consequently, the material coordinate ξ is also known as a convected coordinate. Associated with the inertia of \mathcal{L} in the present configuration is its mass density per unit length of the coordinate ξ : $\rho = \rho(\xi, t)$. A fixed reference configuration \mathcal{C}_0 of the material curve is defined by the vector field $\mathbf{R} = \mathbf{R}(\xi)$. For convenience, we shall assume that ξ is the arc-length parameter of the space curve occupied by \mathcal{L} in its reference configuration \mathcal{C}_0 . The arc-length parameter of the space curve occupied by \mathcal{L} in its present configuration \mathcal{C} is denoted by s . As we shall presently discuss, the coordinates ξ and s can be related.

The position vector \mathbf{r} is assumed to be defined relative to a fixed origin O . Taking the partial derivative of $\mathbf{r}(\xi, t)$ with respect to t and keeping ξ fixed, we can compute the velocity vector \mathbf{v} of the material point:

$$\mathbf{v} = \dot{\mathbf{r}}. \quad (1.36)$$

The superposed dot denotes the material time derivative:

$$\dot{f} = \frac{\partial f}{\partial t}(\xi, t). \quad (1.37)$$

That is, this derivative keeps the material point (identified by ξ) fixed but varies t .

³ The interested reader is referred to [252, 253, 267] for further details and references.

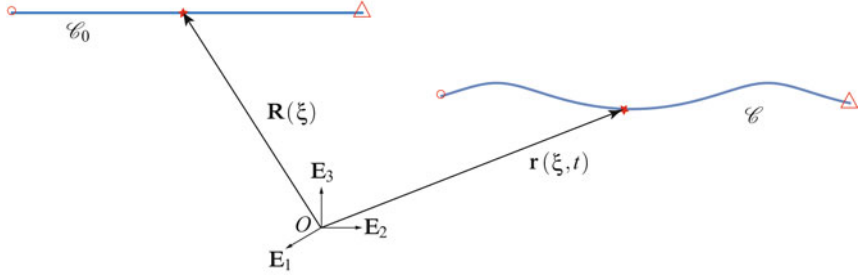


Fig. 1.7 The present \mathcal{C} and reference \mathcal{C}_0 configurations of a material curve \mathcal{L} which has a length ℓ in the reference configuration. The material points $\xi = 0$ and $\xi = \ell$ are labeled \circ and \triangle , respectively.

1.4.1 Stretches, Derivatives, and Velocities

The stretch μ at a material point of \mathcal{L} in its present configuration is defined to be the magnitude of $\partial \mathbf{r} / \partial \xi$:

$$\mu = \left\| \frac{\partial \mathbf{r}}{\partial \xi} \right\|. \quad (1.38)$$

As a result, the unit tangent vector at a point of \mathcal{L} in \mathcal{C} is

$$\mathbf{e}_t = \left(\frac{1}{\mu} \right) \mathbf{r}', \quad (1.39)$$

where the prime denotes the partial derivative with respect to ξ of a function of ξ and t . Because \mathbf{e}_t is a unit vector, $\mathbf{e}_t \cdot \dot{\mathbf{e}}_t = 0$. It follows from the definition of \mathbf{e}_t above that

$$\dot{\mu} = \mathbf{v}' \cdot \mathbf{e}_t. \quad (1.40)$$

The arc-length parameter s of the space curve occupied by the material curve in its present configuration depends on ξ and t : $s = s(\xi, t)$. We tacitly assume that $\frac{\partial s}{\partial \xi} > 0$ and consequently $\frac{\partial s}{\partial \xi} = \mu$. Integrating this equation, we see that

$$s = s(\xi, t) = s_0 + \int_{\xi_0}^{\xi} \mu(u, t) du. \quad (1.41)$$

It is a good exercise to use (1.40) to show that $\dot{s} = 0$ for inextensible curves. For inextensible material curves, $\mu = 1$, and s and ξ are often synonymous. The identity (1.40) for such curves implies that either $\mathbf{v}' \perp \mathbf{e}_t$ or $\mathbf{v}' = \mathbf{0}$. In the latter case, which is commonly found, the velocity vector is a piecewise constant function of ξ and can only change its dependency on ξ at discontinuities.

Apart from the coordinates ξ and s , it is also common with axially moving media to use another coordinate system to parameterize the motion of the string:

$$\chi = \xi + ct, \quad (1.42)$$

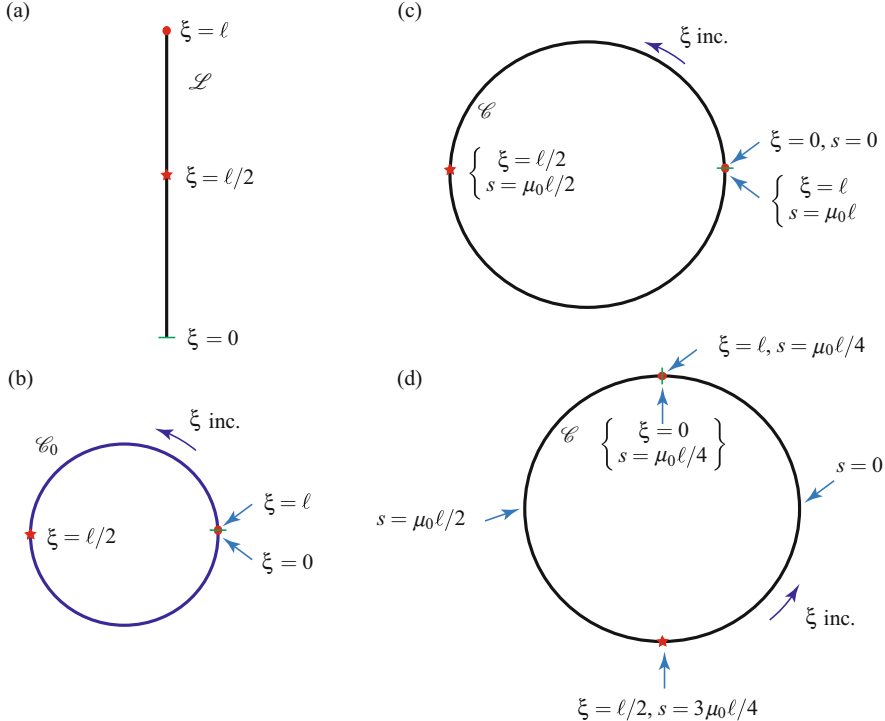


Fig. 1.8 (a), Example of a material curve \mathcal{L} ; (b), a reference configuration \mathcal{C}_0 ; (c), a deformed configuration where the reference configuration has been given a uniform stretch $\mu = \mu_0$; and (d), a deformed configuration where the string has been given a uniform stretch $\mu = \mu_0$ and rigidly rotated by 90° .

where c is a constant which can be judiciously chosen to simplify the governing equations. As μ is assumed to be strictly positive, $s' = \mu > 0$. In addition, $\chi' = 1$. Examples of strings, chains, and cables undergoing motions of this type are considered in Chapter 2.

Distinguishing the space curve occupied by the present configuration \mathcal{C} of \mathcal{L} and the material curve itself is important. For instance, there are numerous examples in the sequel where the space curve occupied by \mathcal{L} is fixed in space yet the material curve performs an axial motion. For such motions, the material points of the string move along its length. That is,

$$\mathbf{v} = \frac{\partial \mathbf{r}}{\partial t} = v(\xi, t) \mathbf{e}_t, \quad (1.43)$$

where \mathbf{e}_t is the unit tangent vector to the space curve. As an example, consider the material curve shown in Figure 1.8(a). We join the ends of this curve to form a circular reference configuration \mathcal{C}_0 that is illustrated in Figure 1.8(b). The configuration

\mathcal{C}_0 is then given a uniform stretch μ and rigidly rotated. Two distinct examples of present configurations of \mathcal{L} are shown in Figures 1.8(c) and (d). In Figures 1.8(c) and (d), the space curve that corresponds to the present configuration is parameterized by an arc-length parameter s and, because of the motion of the material curve along its length, at each instant in time the coordinate s of a material point will vary. The pair of configurations and the labeling of the material points shown in Figures 1.8(c) and (d) are intended as examples to illustrate these aspects of the coordinates ξ and s . The forces required to achieve the deformations shown in Figure 1.8 are discussed in Section 1.7.

While the linear momentum of a material point of the material curve is $\rho\mathbf{v}$, we also introduce the material momentum P per unit length of the curve:

$$P = -\rho\mu\mathbf{v} \cdot \frac{\partial\mathbf{r}}{\partial\xi}. \quad (1.44)$$

The minus sign in the definition of the material momentum is conventional and follows from Eshelby's definition of this quantity for a three-dimensional continuum in [103, Eqn. (55)] (cf. Eqn. (8.94) on Page 365). We also note that P is sometimes known as the pseudomomentum. With the help of the definition of the unit tangent vector, it is not difficult to see that P is related to the momentum of the material point along the curve, $P = -\rho\mathbf{v} \cdot \mathbf{e}_t$. Later, in Section 2.2.1 of Chapter 2, we shall discuss how P is related to a kinematical quantity championed by William Thomson, Baron Kelvin (1824–1907) that is known as the circulation.

1.4.2 Functions and Their Derivatives

Any function $\mathbf{b}(\xi, t)$ can also be unambiguously written as a function of s and t or of χ and t :

$$\mathbf{b} = \mathbf{b}(\xi, t) = \tilde{\mathbf{b}}(\chi = \xi + ct, t) = \hat{\mathbf{b}}(s = s(\xi, t), t). \quad (1.45)$$

We shall also need to take various partial derivatives of the representations for a function \mathbf{b} and it is convenient to define notations for them here:

$$\mathbf{b}_{,\chi} = \frac{\partial\tilde{\mathbf{b}}}{\partial\chi}, \quad \mathbf{b}_{,s} = \frac{\partial\hat{\mathbf{b}}}{\partial s}, \quad \mathbf{b}_{,t} = \frac{\partial\tilde{\mathbf{b}}}{\partial t}. \quad (1.46)$$

It should be clear that

$$\frac{d\mathbf{b}}{dt} = \dot{\mathbf{b}} = s\mathbf{b}_{,s} + \frac{\partial\hat{\mathbf{b}}}{\partial t} = c\mathbf{b}_{,\chi} + \mathbf{b}_{,t}. \quad (1.47)$$

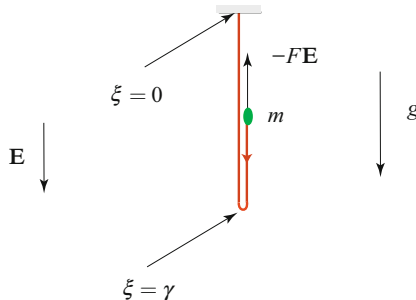
We also emphasize that $\mathbf{b}_{,t} \neq \frac{\partial\hat{\mathbf{b}}}{\partial t}$.

In the sequel we need to evaluate the derivatives of integrals with respect to time. To do this, we use the Leibnitz rule:

$$\frac{d}{dt} \int_{\xi_0=g(t)}^{\xi_1=f(t)} \mathbf{a}(u, t) du = \int_{\xi_0=g(t)}^{\xi_1=f(t)} \dot{\mathbf{a}}(u, t) du + \mathbf{a}(f(t), t) \dot{f} - \mathbf{a}(g(t), t) \dot{g}. \quad (1.48)$$

Notice how this result simplifies if ξ_1 and ξ_0 are constants.

(a)



(b)

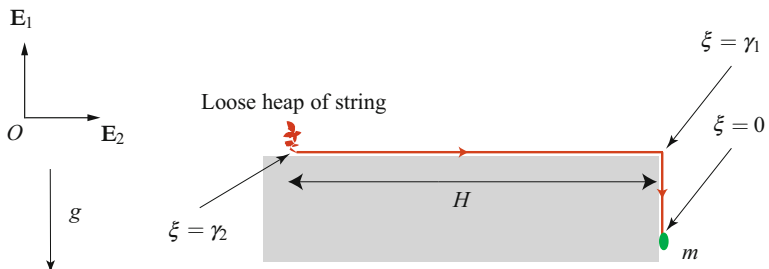


Fig. 1.9 Two classic examples of systems with points of discontinuity. In (a), an inextensible string of length ℓ hangs from one point and exhibits a fold (discontinuity). A particle of mass m is attached to the point $\xi = \ell$ and an external force $\mathbf{F} = -F\mathbf{E}$ acts on the particle. In (b), a string leaves a loose heap of stationary string and moves along the table before falling off the edge of the table.

1.4.3 Discontinuities

We next consider a point of discontinuity or singular supply at a material point $\xi = \gamma(t)$ along a string. Such instances are common in applications and a pair of illustrative examples of systems with discontinuities are shown in Figure 1.9. While our developments are quite general and the conditions we present below enable several interesting kinematical results for these systems to be easily inferred, we restrict attention to situations where $\mathbf{r}(\xi, t)$ is a continuous function of ξ (i.e., the string does not break apart).

To accommodate discontinuities in a function $\chi(\xi, t)$ at $\xi = \gamma$, we need to recall standard notation for left- and right-sided limits, and jumps and averages of functions across discontinuities. Thus, the bracket $[\![\chi]\!]_\gamma$ denotes the jump of a function $\chi(\xi, t)$ at $\xi = \gamma$, while $\{\chi\}_\gamma$ denotes the average value of the left-sided and right-sided limits of the function:

$$\chi^\pm = \lim_{\sigma \rightarrow 0} \chi(\gamma \pm \sigma, t), \quad [\![\chi]\!]_\gamma = \chi^+ - \chi^-, \quad \{\chi\}_\gamma = \frac{1}{2} (\chi^+ + \chi^-), \quad (1.49)$$

where $\sigma > 0$. Because we will be dealing with examples having multiple points of discontinuity, we often use the designations

$$\chi^+ = \chi(\gamma^+, t), \quad \chi^- = \chi(\gamma^-, t), \quad (1.50)$$

so the appropriate point of discontinuity can be identified.

Now suppose we are tracking a point P which occupies a different material coordinate ξ at each instant of time: $\xi = p(t)$. Such a situation can be visualized by imagining a bead moving along a string. At a time t , the velocity vector \mathbf{v}_P of the point P can be considered to have two components: one component can be attributed to the change in the material coordinate of P , and the other arises because of the velocity vector of the material point ξ at $\xi = p(t)$:

$$\begin{aligned} \mathbf{v}_P &= \frac{d}{dt} (\mathbf{r}(p(t), t)) \\ &= \mathbf{v}(p(t), t) + \frac{\partial \mathbf{r}}{\partial \xi}(p(t), t) \dot{p}. \end{aligned} \quad (1.51)$$

You should notice that the velocity vector which can be attributed to the change in $p(t)$ is (as expected) tangent to the material curve. As a simple example, suppose

$$\mathbf{r}(\xi, t) = \xi \mathbf{E}_1 + 20t \mathbf{E}_2, \quad p(t) = t^2. \quad (1.52)$$

In this instance, we find that

$$\mathbf{r}(p(t), t) = t^2 \mathbf{E}_1 + 20t \mathbf{E}_2, \quad \mathbf{v} = 20 \mathbf{E}_2, \quad \mathbf{v}_P = \mathbf{v} + 2t \mathbf{E}_1. \quad (1.53)$$

Thus, if the string was stationary, P 's velocity vector would be exclusively tangent to the string.

We use the previous construction of the velocity vector of a point P to compute representations for the velocity vector \mathbf{v}_γ of the point of discontinuity. Here, however, we need to take left-sided and right-sided derivatives because the differentiability of \mathbf{v} and $\frac{\partial \mathbf{r}}{\partial \xi}$ are not certain. Consequently, we arrive at two equivalent representations for \mathbf{v}_γ :

$$\begin{aligned}\mathbf{v}_\gamma &= \lim_{\sigma \rightarrow 0} \left(\frac{d}{dt} \mathbf{r}(\gamma(t) \pm \sigma, t) \right) = \mathbf{v}^+ + \dot{\gamma} \mathbf{r}'^+ \\ &= \mathbf{v}^- + \dot{\gamma} \mathbf{r}'^-. \end{aligned}\quad (1.54)$$

Because the pair of representations are equal we can also write

$$\mathbf{v}_\gamma = \left\{ \mathbf{v} + \dot{\gamma} \mathbf{r}' \right\}_\gamma. \quad (1.55)$$

The corresponding acceleration vector can be defined in a similar manner:

$$\begin{aligned}\mathbf{a}_\gamma &= \mathbf{a}^+ + 2\dot{\gamma} \mathbf{v}'^+ + \dot{\gamma}^2 \mathbf{r}''^+ + \ddot{\gamma} \mathbf{r}'^+ \\ &= \mathbf{a}^- + 2\dot{\gamma} \mathbf{v}'^- + \dot{\gamma}^2 \mathbf{r}''^- + \ddot{\gamma} \mathbf{r}'^-, \end{aligned}\quad (1.56)$$

where $\mathbf{a} = \dot{\mathbf{v}}$. From the representations for \mathbf{v}_γ and \mathbf{a}_γ follow well-known compatibility conditions:

$$\begin{aligned}[[\mathbf{v}]] + [[[\mathbf{r}']]] \dot{\gamma} &= \mathbf{0}, \\ [[\mathbf{a}]] + 2[[[\mathbf{v}']]] \dot{\gamma} + [[[\mathbf{r}'']] \dot{\gamma}^2 + [[[\mathbf{r}']]] \ddot{\gamma}] &= \mathbf{0}. \end{aligned}\quad (1.57)$$

For convenience, we temporarily dropped the subscripts γ that would ornament $[[\cdot]]$ and $\{\cdot\}$ in (1.57)–(1.59). The conditions (1.54) and (1.56) express the facts that the velocity \mathbf{v}_γ and acceleration \mathbf{a}_γ vectors can be calculated using either left-sided or right-sided limits.

The following identity, which is straightforward to establish, is very useful for manipulating jump conditions:

$$[[\mathbf{c} \cdot \mathbf{d}]] = [[\mathbf{c}]] \cdot \{\mathbf{d}\} + \{\mathbf{c}\} \cdot [[\mathbf{d}]], \quad (1.58)$$

where \mathbf{c} and \mathbf{d} are arbitrary vector-valued functions of t and ξ . Another result that is very useful is the ability to move functions which only depend on time into and out of $[[\cdot]]$ and $\{\cdot\}$:

$$[[\mathbf{c}f(t)]] = [[\mathbf{c}]] f(t), \quad \{\mathbf{c}f(t)\} = \{\mathbf{c}\} f(t), \quad (1.59)$$

for any function f that is independent of ξ .

1.4.4 Eulerian Formulation

In many areas of application, particularly gas dynamics, the jump conditions are represented in terms of an Eulerian (or spatial) formulation rather than the Lagrangian (or material) formulation which is emphasized in this book. To establish the spatial

form of a jump condition one uses the identity $\mu \frac{\partial}{\partial s} = \frac{\partial}{\partial \xi}$ and the fact that Eqn. (1.41) assigns to each s a unique value of ξ for each instant in time. Thus, we can express any function $\chi = \chi(\xi, t)$ as a function of s and t :

$$\chi = \chi(\xi, t) = \tilde{\chi}(s, t). \quad (1.60)$$

With the help of Eqn. (1.54), we find that

$$\dot{\gamma} = (\mathbf{v}_\gamma - \tilde{\mathbf{v}}(s_\gamma^+, t)) \cdot \frac{\tilde{\mathbf{e}}_t(s_\gamma^+, t)}{\tilde{\mu}(s_\gamma^+, t)} = (\mathbf{v}_\gamma - \tilde{\mathbf{v}}(s_\gamma^-, t)) \cdot \frac{\tilde{\mathbf{e}}_t(s_\gamma^-, t)}{\tilde{\mu}(s_\gamma^-, t)}. \quad (1.61)$$

Here, s_γ corresponds to the value of the arc-length parameter s at the material point $\xi = \gamma$:

$$s_\gamma = s(\gamma, t) = s_0 + \int_{\xi_0}^{\gamma} \mu(u, t) du. \quad (1.62)$$

It is now easy to show that

$$[\![\rho_0 \chi]\!]_\gamma \dot{\gamma} = \left[\left[\frac{\tilde{\rho}_0 \tilde{\chi}}{\tilde{\mu}} (\mathbf{v}_\gamma - \tilde{\mathbf{v}}) \cdot \tilde{\mathbf{e}}_t \right] \right]_{s_\gamma}. \quad (1.63)$$

We refer the reader to texts, such as Liepmann and Roshko [206], on gas dynamics where the Eulerian forms of the forthcoming jump conditions are used and the identity (1.63) can be used to show the relationship between the spatial and Lagrangian formulations of the forthcoming jump conditions.

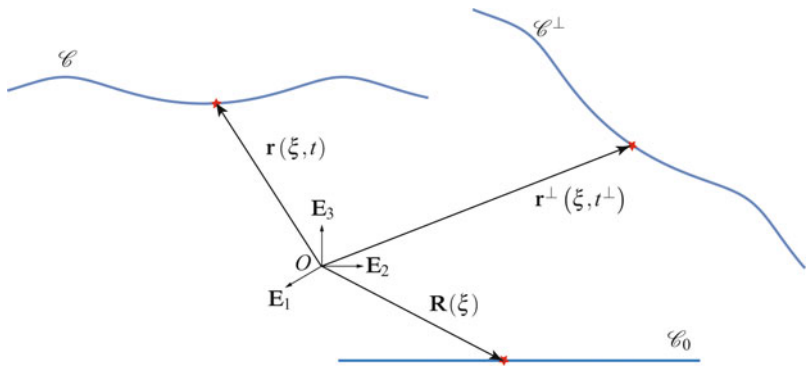


Fig. 1.10 An example of two motions of a material curve which differ by a rigid body motion. Observe that both motions are relative to the same reference configuration \mathcal{C}_0 .

1.4.5 Superposed Rigid Body Motions

Consider a string that is deformed in its current configuration \mathcal{C} at time t . Now, at a time t^\perp , imagine rigidly rotating and translating this configuration into another configuration which we denote by \mathcal{C}^\perp (see Figure 1.10). We say that the motions \mathbf{r} and \mathbf{r}^\perp of the string differ by a superposed rigid body motion:

$$\mathbf{r}^\perp(\xi, t^\perp) = \mathbf{Q}(t)\mathbf{r}(\xi, t) + \mathbf{q}(t). \quad (1.64)$$

Here, \mathbf{Q} is a proper-orthogonal tensor-valued function of time, $\mathbf{q}(t)$ is a vector-valued function of time, and $t^\perp = t + a$ with a being constant. Proper-orthogonal tensors are synonymous with rotations and, as mentioned previously, have the properties $\mathbf{Q}^T\mathbf{Q} = \mathbf{I}$ and $\det(\mathbf{Q}) = 1$. While there are a wealth of interesting parameterizations for \mathbf{Q} , for the present purposes it suffices to recall that a rotation tensor \mathbf{Q} can be uniquely described by an axis of rotation \mathbf{i} and an angle of rotation θ . The axis of rotation is unaltered by the action of \mathbf{Q} : $\mathbf{Qi} = \mathbf{i}$.⁴

Motions which differ by a rigid body motion arise when considering choices of appropriate strain measures and strain energy functions.⁵ If two motions differ by a rigid body motion, we expect the strain and strain energy functions for an elastic string to be the same for both motions. This expectation places restrictions on the strain measures and strain energy functions that we can use.

In the sequel, we will use the stretch μ as a strain measure. It is of interest to compare μ and its counterpart μ^\perp for the pair of motions which differ by a rigid body motion. To this end, we compute that

$$(\mathbf{r}^\perp)' = \mathbf{Q}\mathbf{r}', \quad \mu^\perp = \left\| (\mathbf{r}^\perp)' \right\| = \left\| \mathbf{r}' \right\| = \mu. \quad (1.65)$$

To establish the second of these results, we used the identities $\mathbf{a} \cdot (\mathbf{Q}\mathbf{b}) = (\mathbf{Q}^T\mathbf{a}) \cdot \mathbf{b}$ and $\mathbf{Q}\mathbf{Q}^T = \mathbf{I}$. Having shown that $\mu = \mu^\perp$, we conclude that μ is invariant under superposed rigid body motions. This invariance explains its prominent role as a strain measure for elastic strings.

By way of contrast, suppose we were to propose using $\mathbf{r}' \cdot \mathbf{E}_1$ as a strain measure. Now if we consider a motion which differs from \mathbf{r} by a rigid body motion, then

$$(\mathbf{r}^\perp)' \cdot \mathbf{E}_1 = (\mathbf{Q}\mathbf{r}') \cdot \mathbf{E}_1 = \mathbf{r}' \cdot (\mathbf{Q}^T \mathbf{E}_1). \quad (1.66)$$

⁴ The representation for a rotation tensor \mathbf{Q} in terms of the angle of rotation and axis of rotation is known as Euler's representation and can be found in Eqn. (5.14) on Page 194.

⁵ As first shown by Green and Rivlin [139] some fifty years ago, superposed rigid body motions can be exploited to furnish elegant formulations of the balance laws. The paper [139] has influenced numerous researchers seeking to develop balance laws (governing equations) for deformable media.

Whence,

$$(\mathbf{r}^\perp)' \cdot \mathbf{E}_1 \neq \mathbf{r}' \cdot \mathbf{E}_1 \quad (1.67)$$

unless we only consider rotations which leave \mathbf{E}_1 unchanged: $\mathbf{Q}^T \mathbf{E}_1 = \mathbf{E}_1$. That is, rotations whose axis of rotation are parallel to \mathbf{E}_1 . However, confining attention to such rotations is overly restrictive and so we conclude that the component $\mathbf{r}' \cdot \mathbf{E}_1$ is not an appropriate strain measure.

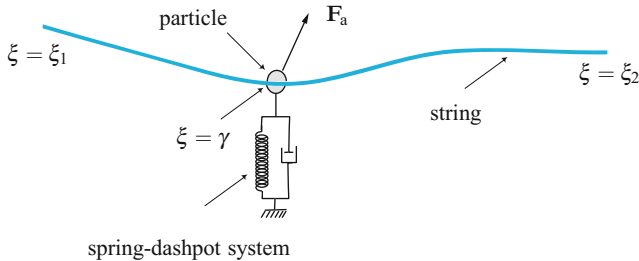


Fig. 1.11 Schematic of a string in contact with a spring-mass-dashpot system. The mass m of the spring-mass-dashpot is assumed to be concentrated at the eyelet through which the string can pass, and the position vector of this particle is denoted by \mathbf{x} . An applied force \mathbf{F}_a is assumed to act on the particle. The sole material point of the string in contact with the eyelet is $\xi = \gamma$ and a force \mathbf{F}_γ can be used to model the contact force between the eyelet and the string at this material point (cf. [279]).

1.5 Balance Laws

We are interested in being able to formulate the equations of motion of systems such as that shown in Figure 1.11. This well-studied system has a spring-mass-dashpot system in point contact with a string.⁶ As a result of the point contact at the material point $\xi = \gamma$, discontinuities in the contact force \mathbf{n} and velocity vector $\dot{\mathbf{r}}$ are to be expected, and it is nontrivial to formulate the governing equations for this system. Our treatment below is designed to make this task far easier for the system shown in Figure 1.11 and related systems.

Motivated by the developments in [12, 132, 230, 251], all of the balance laws we present are of the form

$$\frac{d}{dt} \int_{\xi_1}^{\xi_2} \mathbf{a} d\xi = \int_{\xi_1}^{\xi_2} \mathbf{e} d\xi + [\mathbf{c}]_{\xi_1}^{\xi_2} + \int_{\xi_1}^{\xi_2} \mathbf{d} \delta(\xi - \gamma) d\xi, \quad (1.68)$$

where $\delta(\cdot)$ is the Dirac delta distribution and ξ_1 and ξ_2 are fixed. The fields \mathbf{a} , \mathbf{c} , \mathbf{d} , and \mathbf{e} denote functions that are either scalar valued or vector valued. Following

⁶ See, for example, [56, 58, 201, 279, 316, 342, 343].

[277], we shall assume that the field a is integrable and has a finite number of points of discontinuity where \dot{a} is undefined. Apart from this finite number of points, a is assumed to possess a continuous and bounded material time derivative. The function e is assumed to be a bounded function of ξ with a finite number of points of discontinuity. Finally, the function c is assumed to be a bounded function of ξ with a finite number of points where c' is undefined but elsewhere this derivative is assumed to be continuous.

1.5.1 Assigned Forces, Contact Forces, and Material Forces

Preparatory to writing the conservation laws for the material curve, we introduce some additional fields. Pertaining to forces, we introduce the contact force $\mathbf{n} = \mathbf{n}(\xi, t)$ and the assigned force per unit mass $\mathbf{f} = \mathbf{f}(\xi, t)$.⁷ The forces \mathbf{n} and \mathbf{f} are familiar forces for string theories and an interpretation of the former is presented in Figure 1.12. The contact force is often known as the tension force and we say that the string is in tension at a point $\xi = x$ if $\mathbf{n}(x^-, t) \cdot \mathbf{r}'(x^-, t) > 0$. As will become evident in the examples considered in Chapter 2, body forces, such as a gravitational loading, and applied forces on the lateral surface of the string are accommodated by the assigned force $\rho \mu \mathbf{f}$. Examples of applied forces on the lateral surface include reaction forces when the string is in contact with a surface and forces modeling an elastic foundation in moving load problems.

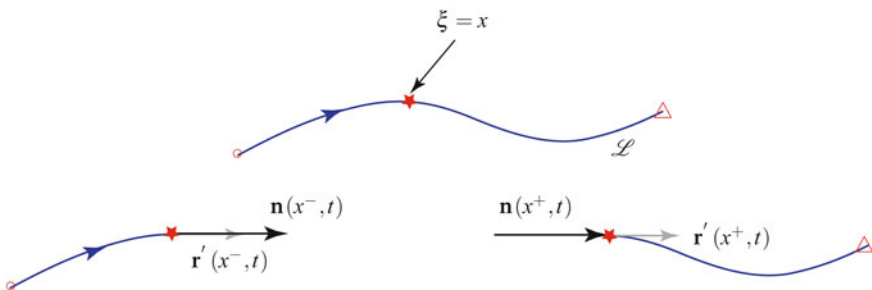


Fig. 1.12 A material curve \mathcal{L} in its present configuration and the contact forces $\mathbf{n}(x^\pm, t)$ at a point $\xi = x$ along its length. The force $\mathbf{n}(x^-, t)$ is the force exerted by the segment to the right of $\xi = x$ on the segment $\xi \in [0, x]$ and the force $-\mathbf{n}(x^+, t)$ is the force exerted by the segment to the left of $\xi = x$ on the segment $\xi \in (x, \ell]$. The jump condition from the balance law of linear momentum (cf. Eqn. (1.86)₂) at $\xi = x$ dictates that $\mathbf{n}(x^-, t) = \mathbf{n}(x^+, t)$. Additionally, the local form of the balance of angular momentum for a string (cf. Eqn. (1.84)) requires that \mathbf{n} and \mathbf{r}' are parallel. The material points $\xi = 0$ and $\xi = \ell$ are labeled \circ and \triangle , respectively.

⁷ Details on the continuity and boundedness assumptions on these fields can be inferred from our discussion following (1.68).

To introduce the two other forces of interest, we first define the strain energy function ψ per unit mass of the string. This enables us to introduce the contact material force C :

$$C = \rho\mu\psi - \mathbf{n} \cdot \frac{\partial \mathbf{r}}{\partial \xi} - \frac{\rho\mu}{2} \mathbf{v} \cdot \mathbf{v}. \quad (1.69)$$

Associated with this force, we also have the assigned material body force b per unit length of ξ . Observe that while C has unit of Newtons it can also be interpreted as an energy-density. Throughout the remainder of this book, we will see that changes to C reflect impacts in chains (in Chapter 2), and both the presence (in Section 4.5.3) and absence (in Section 4.6) of adhesion. An elementary example which highlights a role that C can play in examining problems with inhomogeneities is presented in Section 1.8 at the conclusion of the present chapter.

In contrast to \mathbf{n} and \mathbf{f} , the material (also known as configurational or Eshelbian) forces C and b have only recently garnered attention in the literature. As discussed in the texts [149, 182, 232], this attention has been inspired by the seminal works of Eshelby [101–103].⁸ To help relate the developments in this book to those arising in continuum theories for three-dimensional media, a rapid review of material momentum and its related balance law for a three-dimensional continuum is presented in Sections 8.7 and 8.8 in Chapter 8.

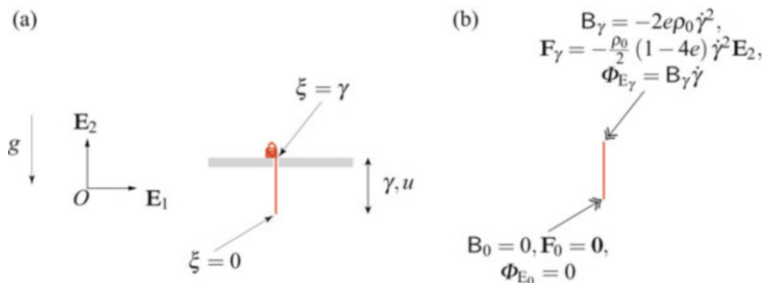


Fig. 1.13 Cayley's problem of an inextensible chain. (a) Schematic of the chain as it falls through a hole on a horizontal table and (b) a graphical summary of the singular supplies acting on the chain. A reaction force \mathbf{F}_γ acts, and a dissipation $-\Phi_{E_\gamma}$ of power occurs, at the point where the chain leaves the table. This problem is discussed at length in Section 2.4 of Chapter 2.

In order to cover a wide range of applications, we admit singular supplies of momentum, \mathbf{F}_γ , material momentum, \mathbf{B}_γ , angular momentum relative to a fixed point O , \mathbf{M}_{O_γ} , and power, Φ_{E_γ} , at a specific material point $\xi = \gamma(t)$. For ease of exposition, and without loss of generality, we assume that there is at most one such point. By way of motivation, the force \mathbf{F}_γ can model a reaction force on a rod or string

⁸ Eshelby's collected works were recently assembled and published in [104]. The recent collection [332] of articles by researchers in this area provides an interesting panorama and a variety of perspectives on the legacy of Eshelby's work.

passing over a sharp obstacle or knife edge (cf. Figure 1.13), an applied force that features in moving load problems (cf., e.g., [112, 255, 280]), or the contact force on a string as it passes through an eyelet such as the one shown in Figure 1.11. The supply B_γ will appear in adhesion problems with elastic rods, dissipative shocks in the dynamics of chains (such as the problem shown in Figure 1.13), the deformation of an inhomogeneous bar discussed in Section 1.8, and branching points in rod-based models for tree-like structures [109, 269, 274]. In certain circumstances, $-B_\gamma$ can be identified with an energy release rate and the driving force f in the influential works of Abeyaratne and Knowles [2, 5] on phase transformations.⁹

The supplies \mathbf{F}_γ and B_γ can both perform work and the former can introduce a moment. These respective contributions are related to the sources Φ_{E_γ} and \mathbf{M}_{O_γ} using the forthcoming identities Eqns. (1.87) and (1.88) on Page 29.¹⁰ Motivated by the treatments proposed in Green and Naghdi [132] and Marshall and Naghdi [230], for many problems we will find it convenient to prescribe B_γ and \mathbf{F}_γ and then use the identities to determine \mathbf{M}_{O_γ} and Φ_{E_γ} .

1.5.2 The Postulated Balance Laws

We adopt the following balance laws for any segment (ξ_1, ξ_2) of the material curve. First, we record the conservation of mass:

$$\frac{d}{dt} \int_{\xi_1}^{\xi_2} \rho \mu d\xi = 0. \quad (1.70)$$

The balance of linear momentum is

$$\frac{d}{dt} \int_{\xi_1}^{\xi_2} \rho \mathbf{v} \mu d\xi = \int_{\xi_1}^{\xi_2} \rho \mu \mathbf{f} d\xi + [\mathbf{n}]_{\xi_1}^{\xi_2} + \int_{\xi_1}^{\xi_2} \mathbf{F}_\gamma \delta(\xi - \gamma) d\xi. \quad (1.71)$$

The balance of material momentum is

$$\frac{d}{dt} \int_{\xi_1}^{\xi_2} \mathbf{P} d\xi = \int_{\xi_1}^{\xi_2} \mathbf{b} d\xi + [\mathbf{C}]_{\xi_1}^{\xi_2} + \int_{\xi_1}^{\xi_2} \mathbf{B}_\gamma \delta(\xi - \gamma) d\xi. \quad (1.72)$$

The balance of angular momentum relative to the fixed point O is

$$\frac{d}{dt} \int_{\xi_1}^{\xi_2} \mathbf{r} \times \rho \mathbf{v} \mu d\xi = \int_{\xi_1}^{\xi_2} \mathbf{r} \times \rho \mathbf{f} \mu d\xi + [\mathbf{r} \times \mathbf{n}]_{\xi_1}^{\xi_2} + \int_{\xi_1}^{\xi_2} \mathbf{M}_{O_\gamma} \delta(\xi - \gamma) d\xi. \quad (1.73)$$

⁹ We refer the reader to the example considered in Section 1.8, Exercises 1.7 and 2.7, and Section 8.8.2 of Chapter 8 for further details on these correspondences.

¹⁰ These identities have counterparts in the continuum mechanics of a three-dimensional body that can be found in the papers [230, 263]. The counterpart to Eqn. (1.88) is also discussed in Section 8.8.2 of Chapter 8.

One also has the balance of energy:

$$\begin{aligned} \frac{d}{dt} \int_{\xi_1}^{\xi_2} \left(\frac{1}{2} \mathbf{v} \cdot \mathbf{v} + \psi \right) \rho \mu d\xi &= \int_{\xi_1}^{\xi_2} \rho \mathbf{f} \cdot \mathbf{v} \mu d\xi \\ &\quad + [\mathbf{n} \cdot \mathbf{v}]_{\xi_1}^{\xi_2} + \int_{\xi_1}^{\xi_2} \Phi_{E_\gamma} \delta(\xi - \gamma) d\xi. \end{aligned} \quad (1.74)$$

Notice that we are not admitting singular supplies of mass.

As regards dissipation, we note from Eqn. (1.74) that if $\Phi_{E_\gamma} > 0 (< 0)$, then it serves to increase (decrease) the kinetic energy of the string. As a result, we term the case where $\Phi_{E_\gamma} < 0$ as dissipative. Situations with dissipative Φ_{E_γ} arise in the dynamics of chains such as the chain fountain in Section 2.8 and falling folded chains in Section 2.7. As discussed in [231, Appendix A5.2], some researchers view a balance of material momentum as a secondary law, while others grant it a primary status on par with a balance of linear momentum. Based in part on our experiences solving problems in the dynamics of strings and rods with discontinuities, we agree with the latter viewpoint. We also take this opportunity to note that alternative treatments of, and motivations for, a material momentum balance law can be found in the literature. These works include Gurtin [148, 149] who invokes invariance requirements, Kienzler and Herrmann [182, 183] who use Noether's theorem, and Tomassetti [347] who employs the Principle of Virtual Power.

1.5.3 Localization Procedure

In the balance laws, we assume that there is one point of discontinuity. Consequently, for the balance of linear momentum (1.71), with the help of Leibnitz rule (1.48),

$$\begin{aligned} \frac{d}{dt} \int_{\xi_1}^{\xi_2} \rho \mathbf{v} \mu d\xi &= \frac{d}{dt} \int_{\xi_1}^{\gamma} \rho \mathbf{v} \mu d\xi + \frac{d}{dt} \int_{\gamma}^{\xi_2} \rho \mathbf{v} \mu d\xi \\ &= \int_{\xi_1}^{\gamma} \frac{d}{dt} (\rho \mathbf{v} \mu) d\xi + \int_{\gamma}^{\xi_2} \frac{d}{dt} (\rho \mathbf{v} \mu) d\xi - [\rho \mathbf{v} \mu \dot{\gamma}]_{\gamma^-}^{\gamma^+} \\ &= \int_{\xi_1}^{\gamma} \frac{d}{dt} (\rho \mathbf{v} \mu) d\xi + \int_{\gamma}^{\xi_2} \frac{d}{dt} (\rho \mathbf{v} \mu) d\xi - [[\rho \mathbf{v} \mu \dot{\gamma}]]. \end{aligned} \quad (1.75)$$

With this result, Eqn. (1.71) becomes

$$\begin{aligned} \int_{\xi_1}^{\gamma} \frac{d}{dt} (\rho \mathbf{v} \mu) d\xi + \int_{\gamma}^{\xi_2} \frac{d}{dt} (\rho \mathbf{v} \mu) d\xi - [[\rho \mathbf{v} \mu \dot{\gamma}]] &= \int_{\xi_1}^{\xi_2} \rho \mu \mathbf{f} d\xi + [\mathbf{n}]_{\xi_1}^{\xi_2} \\ &\quad + \int_{\xi_1}^{\xi_2} \mathbf{F}_\gamma \delta(\xi - \gamma) d\xi. \end{aligned} \quad (1.76)$$

We now establish the local form of this equation and the associated jump condition. The procedure we discuss is known as the localization procedure (see, e.g., [55] or [105]).

The law (1.76) is supposed to hold for all material segments. So we first choose a segment where there are no sources or discontinuities:

$$\int_{\xi_1}^{\xi_2} \frac{d}{dt} (\rho \mathbf{v} \mu) d\xi = \int_{\xi_1}^{\xi_2} \rho \mu \mathbf{f} d\xi + [\mathbf{n}]_{\xi_1}^{\xi_2}. \quad (1.77)$$

With the aid of the fundamental theorem of calculus, this equation reduces to

$$\int_{\xi_1}^{\xi_2} \left(\frac{d}{dt} (\rho \mathbf{v} \mu) - \rho \mu \mathbf{f} - \frac{\partial \mathbf{n}}{\partial \xi} \right) d\xi = \mathbf{0}. \quad (1.78)$$

Assuming that the integrand is continuous and bounded, then as ξ_1 and ξ_2 are arbitrary, we conclude that

$$\frac{d}{dt} (\rho \mathbf{v} \mu) - \rho \mu \mathbf{f} - \frac{\partial \mathbf{n}}{\partial \xi} = \mathbf{0}. \quad (1.79)$$

This equation is known as the local form of the balance law.

To establish the jump condition associated with Eqn. (1.76), we shrink the interval: $\xi_1 \rightarrow \gamma^-$ and $\xi_2 \rightarrow \gamma^+$. Noting the fact that the integral of a continuous and bounded function goes to zero as the region of integration goes to zero, we find that the balance law (1.76) reduces to

$$-[\![\rho \mathbf{v} \mu \dot{\gamma}]\!]_\gamma = [\![\mathbf{n}]\!]_\gamma + \mathbf{F}_\gamma. \quad (1.80)$$

This is the jump condition associated with the balance of linear momentum (1.76). It can be shown that Eqn. (1.79) combined with Eqn. (1.80) is equivalent to Eqn. (1.71).

1.5.4 Local Balance Laws

The balance laws (1.70)–(1.74) are used to establish the local balance laws and jump conditions using the procedure discussed in Section 1.5.3. The following local balance laws pertain to all $\xi \neq \gamma$: mass conservation,

$$\rho_0 = \rho_0(\xi) = \rho \mu, \quad (1.81)$$

and a balance of linear momentum and a conservation of energy, respectively,

$$\begin{aligned} \rho_0 \dot{\mathbf{v}} &= \rho_0 \mathbf{f} + \frac{\partial \mathbf{n}}{\partial \xi}, \\ \rho_0 \dot{\psi} &= \mathbf{n} \cdot \frac{\partial \mathbf{v}}{\partial \xi}. \end{aligned} \quad (1.82)$$

As ξ is the arc-length parameter of the reference configuration \mathcal{C}_0 , ρ_0 is the mass-density per unit reference length of ξ . We also obtain the local form of the balance of material momentum and the balance of angular momentum:

$$\dot{\mathbf{P}} = \mathbf{b} + \frac{\partial \mathbf{C}}{\partial \xi}, \quad (1.83)$$

and

$$\frac{\partial \mathbf{r}}{\partial \xi} \times \mathbf{n} = \mathbf{0}. \quad (1.84)$$

The previous equation shows that \mathbf{n} must be tangent to the string.

Paralleling a methodology used in continuum mechanics, in the sequel the local form of the five balance laws will be used to generate a partial differential equation to determine $\mathbf{r}(\xi, t)$, to provide constitutive equations for $\mathbf{n}(\xi, t)$, and to prescribe \mathbf{b} :

$$\begin{aligned} \rho_0 \dot{\mathbf{v}} &= \rho_0 \mathbf{f} + \frac{\partial \mathbf{n}}{\partial \xi}, && \leftarrow \text{partial differential equation for } \mathbf{r}(\xi, t), \\ \rho_0 \dot{\psi} &= \mathbf{n} \cdot \frac{\partial \mathbf{v}}{\partial \xi}, \\ \frac{\partial \mathbf{r}}{\partial \xi} \times \mathbf{n} &= \mathbf{0}, \end{aligned} \quad \left. \right\} \leftarrow \text{constitutive relations for } \mathbf{n}(\xi, t),$$

$$\dot{\mathbf{P}} = \mathbf{b} + \frac{\partial \mathbf{C}}{\partial \xi}, \quad \leftarrow \text{prescription for } \mathbf{b}(\xi, t). \quad (1.85)$$

As will become evident from the examples in the subsequent chapters, this procedure produces a closed set of equations for $\mathbf{r}(\xi, t)$. We also take this opportunity to note that our developments are in accordance with Green and Naghdi's methodology whereby Eqns. (1.82)₂ and (1.84) are assumed to be identically satisfied by the constitutive relations for \mathbf{n} (cf., e.g., [133]), and Gurtin [149] and Maugin's [231, Sect. 3] methodology of prescribing a \mathbf{b} -like term so that an associated balance law (in our case Eqn. (1.83)) is identically satisfied. An example of such a prescription for an elastic string is discussed in Section 1.6.3 below.

1.5.5 Jump Conditions

From the balance laws, we find that the following jump conditions must hold at $\xi = \gamma(t)$:

$$[\![\rho_0]\!]_{\gamma} \dot{\gamma} = 0,$$

$$[\![\mathbf{n}]\!]_{\gamma} + [\![\rho_0 \mathbf{v}]\!]_{\gamma} \dot{\gamma} + \mathbf{F}_{\gamma} = \mathbf{0},$$

$$\begin{aligned} \llbracket C \rrbracket_\gamma + \llbracket P \rrbracket_\gamma \dot{\gamma} + B_\gamma &= 0, \\ \llbracket \mathbf{r} \times \mathbf{n} \rrbracket_\gamma + \llbracket \mathbf{r} \times \rho_0 \mathbf{v} \rrbracket_\gamma \dot{\gamma} + \mathbf{M}_{O\gamma} &= \mathbf{0}, \\ \llbracket \mathbf{n} \cdot \mathbf{v} \rrbracket_\gamma + \left[\left[\rho_0 \psi + \frac{1}{2} \rho_0 \mathbf{v} \cdot \mathbf{v} \right] \right]_\gamma \dot{\gamma} + \Phi_{E\gamma} &= 0. \end{aligned} \quad (1.86)$$

In writing these conditions, some rearrangements have been performed using Eqn. (1.59).

The jump condition from the mass balance, $\llbracket \rho_0 \rrbracket_\gamma \dot{\gamma} = 0$, shows that if the mass density ρ_0 is continuous, then this jump condition is identically satisfied. This situation arises if there are no discontinuous changes in the cross-sectional area of the string or in the mass density per unit volume of the three-dimensional body that it is modeling. Most frequently, it occurs when the string is assumed to be homogeneous. On the other hand, if ρ_0 has a discontinuity at $\xi = \gamma$, then this jump condition implies that $\dot{\gamma} = 0$. That is, the discontinuity is stationary at the material point $\xi = \gamma$.

Since it is assumed that $\llbracket \mathbf{r} \rrbracket_\gamma = \mathbf{0}$, the jump condition (1.86)₂ reduces the jump condition (1.86)₄ to the identity

$$\mathbf{M}_{O\gamma} = \mathbf{r}(\gamma, t) \times \mathbf{F}_\gamma. \quad (1.87)$$

That is, the resultant moment relative to the point $\xi = \gamma$ is $\mathbf{0}$. We can also interpret this result as implying that the string cannot support a moment. It is interesting to contrast this to the case of a rod which can support a bending moment (cf. Eqn. (5.83)). The jump condition (1.86)₅ from the energy equation can be expressed in the form¹¹

$$\Phi_{E\gamma} = \mathbf{F}_\gamma \cdot \mathbf{v}_\gamma + B_\gamma \dot{\gamma}. \quad (1.88)$$

Note that the force \mathbf{F}_γ is associated with the velocity of the point on which it acts and B_γ is associated with the velocity of the discontinuity along the material curve. The identity (1.88) states that the combined power of these forces is equal to the net power transmitted to the string. In applications of the theory, we will use the identity (1.87) to prescribe $\mathbf{M}_{O\gamma}$ and we will employ the identity (1.88) to prescribe $\Phi_{E\gamma}$. Hence, $\mathbf{M}_{O\gamma}$ and $\Phi_{E\gamma}$ are not considered to be independent supplies: they are determined by \mathbf{F}_γ and B_γ .

Paralleling the summary presented in Eqn. (1.85) for the local form of the balance laws, for the jump conditions we have

¹¹ This identity was first established in [264]. An outline of the derivation of the identity (1.88) is presented in Exercises 1.3 and 1.4.

$$\left. \begin{array}{l} [[\mathbf{v}]] + [[\mathbf{r}']]_\gamma \dot{\gamma} = \mathbf{0}, \\ [[\rho_0]]_\gamma \dot{\gamma} = 0, \\ [[\mathbf{n}]]_\gamma + [[\rho_0 \mathbf{v}]]_\gamma \dot{\gamma} + \mathbf{F}_\gamma = \mathbf{0}, \\ [[\mathbf{C}]]_\gamma + [[\mathbf{P}]]_\gamma \dot{\gamma} + \mathbf{B}_\gamma = 0, \\ \mathbf{M}_{O_\gamma} = \mathbf{r}(\gamma, t) \times \mathbf{F}_\gamma, \\ \Phi_{E_\gamma} = \mathbf{F}_\gamma \cdot \mathbf{v}_\gamma + \mathbf{B}_\gamma \dot{\gamma}, \end{array} \right\} \begin{array}{l} \text{conditions for } [[\mathbf{r}']]_\gamma \text{ and } [[\mathbf{n}]]_\gamma, \\ \text{differential equation for } \gamma(t), \\ \text{prescription for } \mathbf{M}_{O_\gamma}, \\ \text{prescription for } \Phi_{E_\gamma}. \end{array} \quad (1.89)$$

The role of the jump conditions for energy (1.86)₅ and material momentum (1.86)₃ has been the subject of many recent papers (see [264] for references and further discussion). We note in particular that the role of the jump condition for energy (1.86)₅ in producing a differential equation for the evolution of γ as in, e.g., [3, 39, 277, 297] is provided by the material momentum condition (1.86)₃. Furthermore, if a variational formulation of the equations of motion for a string is performed, then, with the help of the forthcoming constitutive relations and in the absence of singular supplies, the Weierstrass-Erdmann corner conditions (see Section 9.3.2 in Chapter 9) can be used to establish the jump conditions for linear momentum and material momentum.

1.6 Elastic Strings and Inextensible Strings

For an elastic string, we assume that the strain energy function ψ depends on the stretch μ and ξ :

$$\psi = \psi(\mu, \xi). \quad (1.90)$$

If the string is homogenous, then the strain energy function will be independent of ξ : $\psi = \psi(\mu)$. We can use our earlier results on motions which differ by a rigid body motion from Section 1.4.5 where we showed that $\mu^\perp = \mu$ to also show that ψ for two such motions will have identical values for each material point ξ :

$$\psi^\perp = \psi(\mu^\perp, \xi) = \psi(\mu, \xi) = \psi. \quad (1.91)$$

In other words, ψ as given by Eqn. (1.90) is invariant under superposed rigid body motions. This invariance is appealing on physical grounds: it implies that the only method of changing the strain energy at a material point is to change the stretch. In addition, if we subject the entire string to a rigid motion, then its strain energy will not change.

A useful representation for the material time derivative of the function $\psi(\mu, \xi)$ can be found with the help of the identity (1.40) for $\dot{\mu}$:

$$\dot{\psi} = \frac{\partial \psi}{\partial \mu} \dot{\mu} = \frac{1}{\mu} \frac{\partial \psi}{\partial \mu} \mathbf{r}' \cdot \mathbf{v}'. \quad (1.92)$$

To establish the constitutive equation for an elastic string, we assume that the local form of the balance of energy (1.82)₂ is satisfied for all motions¹²:

$$\rho_0 \dot{\psi} = \mathbf{n} \cdot \frac{\partial \mathbf{v}}{\partial \xi}. \quad (1.93)$$

Substituting for $\dot{\psi}$, this equation reduces to

$$\left(\frac{\rho_0}{\mu} \frac{\partial \psi}{\partial \mu} \mathbf{r}' - \mathbf{n} \right) \cdot \frac{\partial \mathbf{v}}{\partial \xi} = 0. \quad (1.94)$$

From the balance of angular momentum (1.84), we know that $\mathbf{n} = n \mathbf{e}_t$. Consequently, the identity (1.94) simplifies to

$$\left(\left(\frac{n}{\mu} - \frac{\rho_0}{\mu} \frac{\partial \psi}{\partial \mu} \right) \mathbf{r}' \right) \cdot \frac{\partial \mathbf{v}}{\partial \xi} = 0. \quad (1.95)$$

This equation is assumed to hold for all \mathbf{v}' . Hence, with the additional assumption that n does not depend on \mathbf{v}' , we conclude that

$$\mathbf{n} = \frac{\rho_0}{\mu} \frac{\partial \psi}{\partial \mu} \mathbf{r}' = \rho \frac{\partial \psi}{\partial \mu} \mathbf{r}' = \rho_0 \frac{\partial \psi}{\partial \mu} \mathbf{e}_t. \quad (1.96)$$

This is the constitutive equation for a nonlinearly elastic string.

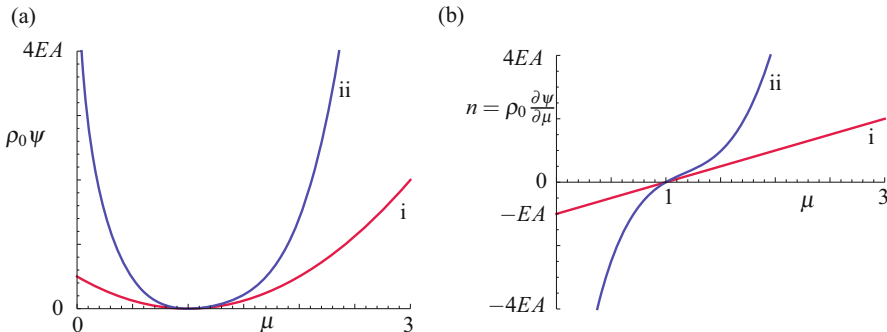


Fig. 1.14 (a) A pair of representative strain energy functions $\rho_0 \psi$ and (b) their associated forces $n = \rho_0 \frac{\partial \psi}{\partial \mu}$. For the examples shown, (i) $\rho_0 \psi = \frac{EA}{2} (\mu - 1)^2$ and (ii) $\rho_0 \psi = EA \left(\log \left(\mu + \frac{1}{\mu} - 1 \right) + (\mu - 1)^4 \right)$.

¹² This parallels the methodology used in establishing constitutive relations for a three-dimensional continuum. For the reader's convenience, a rapid summary of this procedure is presented in Section 8.6 of Chapter 8. Additional developments are presented in Exercise 8.4.

In addition to invariance requirements, it is necessary to consider physically meaningful restrictions on the strain energy function.¹³ For example, if the string is neither in compression nor tension when unstretched ($\mu = 1$), then we should expect that

$$\lim_{\mu \rightarrow 1} \left(n = \rho_0 \frac{\partial \psi}{\partial \mu} \right) = 0. \quad (1.97)$$

Further, compressing an element of the string to zero length should require infinite amounts of energy and compressive force:

$$\lim_{\mu \searrow 0} \rho_0 \psi = \infty, \quad \lim_{\mu \searrow 0} \left(n = \rho_0 \frac{\partial \psi}{\partial \mu} \right) = -\infty. \quad (1.98)$$

We also expect that infinite amounts of energy and tensile force are needed to stretch the string indefinitely:

$$\lim_{\mu \rightarrow \infty} \rho_0 \psi = \infty, \quad \lim_{\mu \rightarrow \infty} \left(n = \rho_0 \frac{\partial \psi}{\partial \mu} \right) = \infty. \quad (1.99)$$

As an example, the strain energy function labeled (ii) and its associated n that are shown in Figure 1.14 satisfy the limit (1.97) and also exhibit the desired extreme behaviors (1.98) and (1.99).

Not all popular strain energy functions exhibit the extreme features (1.98) and (1.99). For example, consider an elastic string where

$$\rho_0 \psi = \frac{EA}{2} (\mu - 1)^2. \quad (1.100)$$

Referring to the graph labeled i in Figure 1.14(b), such a string has a tension $n = EA(\mu - 1)$ that is a linear function of the extension of the string and has the desired behavior (1.97). However, this function does not satisfy Eqn. (1.98). Indeed a finite compressive force $-EA$ is all that is needed to reduce a section of the string to zero length. Consequently, a string modeled with a strain energy function (1.100) would provide questionable results when $\mu \ll 1$.

An additional example of a strain energy function for elastic strings is highlighted in Exercises 1.9 and 2.7 and is a three-parameter nonlinear function of the stretch μ . A simplified version of this energy appears in Eqn. (2.10) and is used in the analysis of a steady motion of a closed loop of string. The examples of strain energy functions discussed in this book are far from exhaustive and other examples are easy to construct. However, the parameters in the resulting functions must be evaluated by comparison with experiment and this can be a very challenging task.

¹³ Restrictions of this type are common in continuum mechanics and the interested reader is referred to [351, Section 87] for a review of these restrictions. In the context of one-dimensional continua, Antman's masterful discussion in [12, Chapter III, Section 3] has greatly influenced our exposition.

1.6.1 Gibbs Free Energy

Consider an elastic string with a strain energy function $\rho_0 \psi(\mu, \xi)$ and suppose that the constitutive relations

$$n = \mathbf{n} \cdot \mathbf{e}_t = \rho_0 \frac{\partial \psi}{\partial \mu} \quad (1.101)$$

can be inverted, at least locally, to solve for the stretch μ as a function of n :

$$\mu = \hat{\mu}(n, \xi). \quad (1.102)$$

Then, with the help of a Legendre transformation, we can define a Gibbs free energy function¹⁴:

$$\rho_0 \phi_G = \rho_0 \phi_G(n, \xi) = \rho_0 \psi(\hat{\mu}(n, \xi), \xi) - n \hat{\mu}(n, \xi). \quad (1.103)$$

This function can be considered as a dual to the strain energy function.

To see the usefulness of the Gibbs free energy function, observe that

$$\begin{aligned} \rho_0 \frac{\partial \phi_G}{\partial n} &= \frac{\partial}{\partial n} (\rho_0 \psi(\hat{\mu}(n, \xi), \xi) - n \hat{\mu}(n, \xi)) \\ &= \underbrace{\rho_0 \frac{\partial \psi}{\partial \mu} \frac{\partial \hat{\mu}}{\partial n}}_{=n} - \hat{\mu}(n, \xi) - n \frac{\partial \hat{\mu}}{\partial n} \\ &= -\hat{\mu}(n, \xi). \end{aligned} \quad (1.104)$$

Whence, we find the pair of relations

$$n = \rho_0 \frac{\partial \psi}{\partial \mu}, \quad \mu = -\rho_0 \frac{\partial \phi_G}{\partial n}. \quad (1.105)$$

The Gibbs free energy function can be used to interpret the material contact force C in static problems for elastic strings (cf. [5, Chapter 2]). This energy function is also used by Green et al. [137, 138] to determine constitutive relations for elastic rods.

As an example, consider the strain energy function given by Eqn. (1.100). The associated Gibbs free energy function is readily computed with the help of the intermediate results

$$n = EA(\mu - 1), \quad \hat{\mu} = \frac{n}{EA} + 1. \quad (1.106)$$

Substituting into the definition (1.103), we find that

¹⁴ For further details on the Legendre transformation, we refer the reader to the lucid discussion of this transformation in Lanczos [195].

$$\rho_0 \phi_G = -n \left(\frac{n}{2EA} + 1 \right). \quad (1.107)$$

The resulting Gibbs free energy function is a quadratic function of n . An additional example of a Gibbs free energy function is highlighted in Exercise 1.10.

1.6.2 Inextensibility

In a purely mechanical string theory, inextensibility is the only internal constraint on a material curve which is invariant under superposed rigid body motions of the curve. Assuming that ξ is the arc-length parameter of \mathcal{C}_0 , then this constraint is

$$\mu = \|\mathbf{r}'\| = 1. \quad (1.108)$$

In this case, \mathbf{r}' is the unit tangent vector \mathbf{e}_t to the material curve \mathcal{L} in \mathcal{C} . The local form of the balance of angular momentum (1.84) implies that $\mathbf{n} = n\mathbf{e}_t$, and the strain energy function is constant. As a result, the local form of the balance of energy (1.82)₂ implies that

$$\mathbf{n} \cdot \frac{\partial \mathbf{v}}{\partial \xi} = 0. \quad (1.109)$$

This equation is assumed to hold for all \mathbf{v}' where $\mathbf{r}' \cdot \mathbf{v}' = 0$.¹⁵ After assuming that \mathbf{n} does not depend on \mathbf{v}' , we conclude that \mathbf{n} is parallel to the tangent vector to the material curve in its present configuration:

$$\mathbf{n} = p\mathbf{r}' = p\mathbf{e}_t, \quad (1.110)$$

where the scalar-valued function $p = p(\xi, t)$ is known as the tension. As we shall see in the sequel, p must be determined from the balance laws and boundary conditions.¹⁶

1.6.3 Identities

Either set of the constitutive relations given by Eqns. (1.96) and (1.110) identically satisfy the local balance of energy (1.82)₂ and the local form of the balance of angular momentum (1.84). This parallels the situation presented in Section 1.5.5 for the power Φ_{E_γ} and moment \mathbf{M}_{O_γ} , respectively.

¹⁵ For an inextensible string $\mu = 1$ and, after computing $\dot{\mu}$, one finds that $\mathbf{r}' \cdot \mathbf{v}' = 0$.

¹⁶ We follow Casey and Carroll [49] and do not presume that $p^\perp = p$. Related invariance requirements for \mathbf{F}_γ and Φ_{E_γ} are discussed in [277].

In addition to the identical satisfaction of the balances of angular momentum and energy, we prescribe the assigned material force \mathbf{b} so that the local form of the balance of material momentum is identically satisfied. Thus,

$$\mathbf{b} = \mathbf{b}_p. \quad (1.111)$$

With the help of Eqns. (1.82), (1.83), (1.96), and (1.110), we find that the material force needed to identically satisfy the balance of material momentum is given by the expression

$$\begin{aligned} b_p &= \dot{\mathbf{P}} - \frac{\partial C}{\partial \xi} \\ &= -\rho_0 \mathbf{f} \cdot \mathbf{r}' - \left(\frac{\partial}{\partial \xi} \left(\rho_0 \psi - \frac{\rho_0}{2} \mathbf{v} \cdot \mathbf{v} \right) \right)_{\text{exp}}. \end{aligned} \quad (1.112)$$

Here, we have used the derivative $\left(\frac{\partial f}{\partial \xi} \right)_{\text{exp}}$ of a function $f = f(\mathbf{r}, \mathbf{r}', \mathbf{v}, \xi)$:

$$\left(\frac{\partial f}{\partial \xi} \right)_{\text{exp}} = \lim_{\Delta \xi \rightarrow 0} \frac{f(\mathbf{r}, \mathbf{r}', \mathbf{v}, \xi + \Delta \xi) - f(\mathbf{r}, \mathbf{r}', \mathbf{v}, \xi)}{\Delta \xi}. \quad (1.113)$$

For example,

$$\left(\frac{\partial}{\partial \xi} \left(\frac{\rho_0}{2} \mathbf{v} \cdot \mathbf{v} \right) \right)_{\text{exp}} = \frac{\rho'_0}{2} \mathbf{v} \cdot \mathbf{v}. \quad (1.114)$$

Clearly, this derivative is zero if ρ_0 is uniform throughout the string. Furthermore, the derivative of the function $\rho_0 \psi$ in Eqn. (1.112) will be zero if $\rho_0 \psi$ is not an explicit function of ξ . That is, if the string is homogeneous in its reference configuration, then $b_p = -\rho_0 \mathbf{f} \cdot \mathbf{r}'$.

1.7 Summary of the Governing Equations

For future reference, it is convenient at this stage to summarize the governing equations of motion for the string. For regions of the string where discontinuities are absent, the motion $\mathbf{r}(\xi, t)$ of the string is determined by solving the following partial differential equation:

$$(n \mathbf{e}_t)' + \rho_0 \mathbf{f} = \rho_0 \dot{\mathbf{v}}, \quad (1.115)$$

where ρ_0 and \mathbf{f} are specified and $n = \rho_0 \frac{\partial \psi}{\partial \mu}$ for elastic strings (cf. Eqn. (1.96)) or $n = p$ for inextensible strings (cf. Eqn. (1.110)). For the latter, Eqn. (1.115) is supplemented by the constraint equation (1.108) and the condition that ψ is constant. At a point of discontinuity, the following jump conditions need to be satisfied:

$$\begin{aligned} \llbracket \rho_0 \rrbracket_\gamma \dot{\gamma} &= 0, \\ \llbracket (n - \rho_0 \mu \dot{\gamma}^2) \mathbf{e}_t \rrbracket_\gamma &= -\mathbf{F}_\gamma, \\ \left[\left[\rho_0 \psi - \mathbf{n} \cdot \frac{\partial \mathbf{r}}{\partial \xi} - \frac{\rho_0}{2} \mathbf{v} \cdot \mathbf{v} \right] \right]_\gamma - \left[\left[\rho_0 \mathbf{v} \cdot \frac{\partial \mathbf{r}}{\partial \xi} \right] \right]_\gamma \dot{\gamma} + \mathbf{B}_\gamma &= 0. \end{aligned} \quad (1.116)$$

In writing these conditions some rearrangements of Eqns. (1.57) and (1.86)_{2,4} were performed with the assistance of the identities (1.58) and (1.59). The jump conditions (1.116) are supplemented by the compatibility conditions:

$$\begin{aligned} \llbracket \mathbf{v} \rrbracket_\gamma + \llbracket [\mathbf{r}'] \rrbracket_\gamma \dot{\gamma} &= \mathbf{0}, \\ \llbracket \mathbf{a} \rrbracket_\gamma + 2 \llbracket [\mathbf{v}'] \rrbracket_\gamma \dot{\gamma} + \llbracket [\mathbf{r}''] \rrbracket_\gamma \dot{\gamma}^2 + \llbracket [\mathbf{r}'] \rrbracket_\gamma \ddot{\gamma} &= \mathbf{0}. \end{aligned} \quad (1.117)$$

You may have noticed that the set of jump conditions (1.116) does not contain the jump condition for energy or angular momentum. Their absence is due to the fact that they are considered to be identities for \mathbf{M}_{O_γ} and Φ_{E_γ} (see Section 1.5.5).

To illuminate the summary presented above we consider the example of the present configuration of the string shown in Figure 1.8(c). Here, an undeformed circular section of string of length ℓ is given a uniform stretch $\mu = \mu_0$, so that its present configuration is described by

$$\mathbf{r}(\xi, t) = \frac{\mu_0 \ell}{2\pi} \left(\cos\left(\frac{\pi \xi}{\ell}\right) \mathbf{E}_1 + \sin\left(\frac{\pi \xi}{\ell}\right) \mathbf{E}_2 \right). \quad (1.118)$$

The associated unit tangent vector to \mathcal{L} in \mathcal{C} is

$$\mathbf{e}_t = \cos\left(\frac{\pi \xi}{\ell}\right) \mathbf{E}_2 - \sin\left(\frac{\pi \xi}{\ell}\right) \mathbf{E}_1. \quad (1.119)$$

Substituting into the balance law (1.115) we find that the applied forces needed to sustain this configuration are

$$\rho_0 \mathbf{f} = - \left(\rho_0 \frac{\partial \psi}{\partial \mu} (\mu = \mu_0) \mathbf{e}_t \right)' . \quad (1.120)$$

Assuming that the string is homogeneous and that $\mathbf{F}_\gamma = \mathbf{0}$ and $\mathbf{B}_\gamma = \mathbf{0}$, we find that the jump conditions (1.116) are all identically satisfied for this configuration. For a homogeneous string, ρ_0 , ψ , and, consequently, $\rho_0 \frac{\partial \psi}{\partial \mu} (\mu = \mu_0)$ are independent of ξ and we conclude that $\rho_0 \mathbf{f}$ points in the radial direction: $\mathbf{f} \parallel \mathbf{r}$ as expected.

1.8 An Elementary Example Involving Material Forces

One of the distinct aspects of the summary presented in the previous section is the presence of material forces and material momentum. While many examples involving B_γ , C , P , and b will be developed in the coming chapters, it is interesting to consider an elementary example which has distinct ties to earlier works on material forces in continua with defects and inhomogeneities. The example we consider is inspired by the bending of a beam considered in Eshelby [102, Page 142] and Kienzler and Herrmann [183] and studies on phase transformations by Abeyaratne and Knowles [5], Ericksen [98], Heidug and Lehner [161], and Truskinovsky [352, 354], among others. In particular, we explore how the material force C can be related to a potential energy density function and the material supply B_γ can be interpreted as an energy release rate and related to Eshelby's force on a singularity F_E and Abeyaratne and Knowles' driving force f .

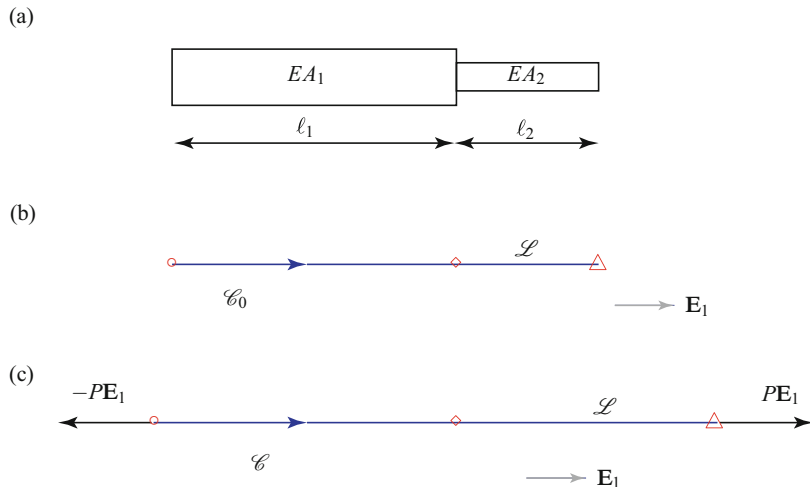


Fig. 1.15 Modeling the static deformation of a bar which has a piecewise constant stiffness. A schematic of the geometry of the undeformed bar of total length $\ell_1 + \ell_2$ is shown in (a). In (b), the reference configuration \mathcal{C}_0 of a string (material curve \mathcal{L}) that is used to model the bar is shown. The material points $\xi = 0$, $\xi = \ell_1$, and $\xi = \ell$ are labeled \circ , \diamond , and \triangle , respectively. The configuration \mathcal{C} of the deformed material curve \mathcal{L} after it has been subjected to terminal forces is shown in (c). For the situation shown in (c), it is assumed that $EA_2 < EA_1$.

Referring to Figure 1.15, we consider a bar which has a discontinuity in its stiffness EA . The undeformed bar has a length $\ell = \ell_1 + \ell_2$. The segment of the bar of length ℓ_1 has a stiffness EA_1 and the remaining segment has a stiffness EA_2 . Terminal forces $\pm PE_1$ are applied to the ends of the bar and we seek to determine the total energy of the bar and its associated loadings. To proceed, we model the bar as a string which, in a reference configuration \mathcal{C}_0 , has a length $\ell = \ell_1 + \ell_2$, a

strain energy function given by Eqn. (1.100), and a piecewise constant stiffness EA . The deformed string is assumed to be held in a state of static equilibrium by terminal forces $\mathbf{F}_0 = -P\mathbf{E}_1$ and $\mathbf{F}_\ell = P\mathbf{E}_1$ applied to its ends. No assigned forces are assumed to act on the string: $\rho_0\mathbf{f} = \mathbf{0}$. In the notation of the previous sections, the discontinuity occurs at $\gamma = \ell_1$ with $\dot{\gamma} = 0$. Furthermore, $\mathbf{r} = x\mathbf{E}_1$ and $\mu = \frac{\partial x}{\partial \xi}$.

We can use the jump condition (1.116)₂ to show that $\mathbf{n}(0^+, t) = P\mathbf{E}_1$ and $\mathbf{n}(\ell^-, t) = P\mathbf{E}_1$.¹⁷ It is easy to check that the balance of linear momentum, $\mathbf{n}' = \mathbf{0}$, is satisfied by the constant contact force $\mathbf{n} = P\mathbf{E}_1$ acting in the string. With the help of the constitutive relations $\mathbf{n} = \rho_0 \frac{\partial \psi}{\partial \mu} \mathbf{e}_t$ we conclude that the string is in a state of piecewise constant stretch:

$$\mu = \begin{cases} \mu_1 = \frac{P}{EA_1} & \forall \xi \in (0, \ell_1), \\ \mu_2 = \frac{P}{EA_2} & \forall \xi \in (\ell_1, \ell). \end{cases} \quad (1.121)$$

As a consequence, we find that the contact material force C is piecewise constant:

$$C = \frac{EA}{2} (\mu - 1)^2 - \mathbf{n} \cdot \mathbf{r}' = \begin{cases} -\frac{EA_1}{2} (\mu_1^2 - 1) & \forall \xi \in (0, \ell_1), \\ -\frac{EA_2}{2} (\mu_2^2 - 1) & \forall \xi \in (\ell_1, \ell). \end{cases} \quad (1.122)$$

In agreement with the prescription (1.112), we also observe that the local form of the balance of material momentum, $C' + b = 0$, is satisfied by the prescription $b = b_p = 0$.

The jump condition (1.116)₃ associated with the balance of material momentum yields some interesting results. With the help of the expressions presented in Eqn. (1.122) for C , Eqn. (1.116)₃ implies that a source of material momentum B_{ℓ_1} acts at the point where the discontinuity in stiffness occurs:

$$\begin{aligned} B_{\ell_1} &= C(\ell_1^-) - C(\ell_1^+) \\ &= \frac{EA_2}{2} (\mu_2^2 - 1) - \frac{EA_1}{2} (\mu_1^2 - 1). \end{aligned} \quad (1.123)$$

If the bar was homogeneous, i.e., $EA_1 = EA_2$, then B_{ℓ_1} would vanish. Furthermore, for the unloaded bar, $P = 0$ and $\mu_1 = \mu_2 = 1$. In this case,

$$B_{\ell_1}|_{P=0} = 0. \quad (1.124)$$

The behavior of B_{ℓ_1} for various values of the load P and the parameter $\frac{EA_2}{EA_1}$ are shown in Figure 1.16. For the purposes of our forthcoming discussion on an interpretation for B_{ℓ_1} , it is worthy of note that this quantity can have positive and negative values depending on the ratio of EA_2 to EA_1 .

¹⁷ A detailed description of this procedure can be found in Section 2.3.2 of Chapter 2.

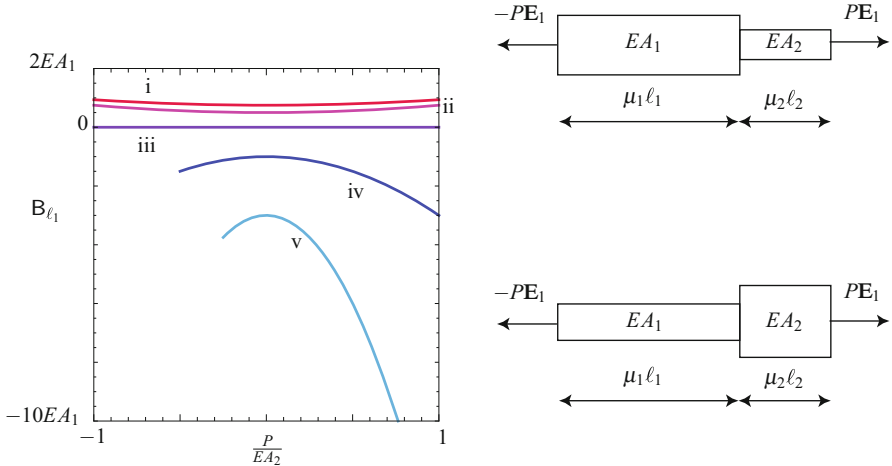


Fig. 1.16 Graphs of the material momentum supply B_{ℓ_1} defined by Eqn. (1.123) as a function of the loading parameter $\frac{P}{EA_2}$ for various values of the parameter $\frac{EA_2}{EA_1}$. For the graphs shown in this figure: i, $\frac{EA_2}{EA_1} = 0.25$; ii, $\frac{EA_2}{EA_1} = 0.5$; iii, $\frac{EA_2}{EA_1} = 1$; iv, $\frac{EA_2}{EA_1} = 2$; and v, $\frac{EA_2}{EA_1} = 4$. Observe that the value of the force P is limited by the fact that μ_1 and μ_2 must remain positive.

1.8.1 Interpretations of B_{ℓ_1} and C

While B_{ℓ_1} and C both have units of Newtons, they do not correspond to physical forces that are required for equilibrium. For the problem of the terminally loaded bar, we now start the process of exploring interpretations for B_{ℓ_1} and C . To this end, it is illuminating to establish an expression for the total potential energy of the string. This energy is the sum of the strain energy of the string and the potential energy of the terminal forces. As the potential energy of a constant force is the negative of the inner product of the force vector and the displacement of the material point on which it acts, we find that the potential energy of the string is

$$\begin{aligned}\Pi &= \int_0^{\ell_1} \frac{EA_1}{2} (\mu_1 - 1)^2 d\xi - (-P\mathbf{E}_1) \cdot \mathbf{r}(0, t) \\ &\quad + \int_{\ell_1}^{\ell} \frac{EA_2}{2} (\mu_2 - 1)^2 d\xi - (P\mathbf{E}_1) \cdot \mathbf{r}(\ell, t) \\ &= \int_0^{\ell_1} \frac{EA_1}{2} (\mu_1 - 1)^2 - \mathbf{n} \cdot \mathbf{r}' d\xi + \int_{\ell_1}^{\ell} \frac{EA_2}{2} (\mu_2 - 1)^2 - \mathbf{n} \cdot \mathbf{r}' d\xi, \quad (1.125)\end{aligned}$$

where we used the result that $\mathbf{n} = P\mathbf{E}_1$ throughout the entire string. From the final representation for Π , it should be apparent that we can express the potential energy simply in terms of C :

$$\Pi = \int_0^{\ell_1} Cd\xi + \int_{\ell_1}^{\ell} Cd\xi. \quad (1.126)$$

Thus, we can interpret the contact material force C as an energy density. This interpretation is useful when attempting to relate the presentation in this book to other works where variational formulations are emphasized.

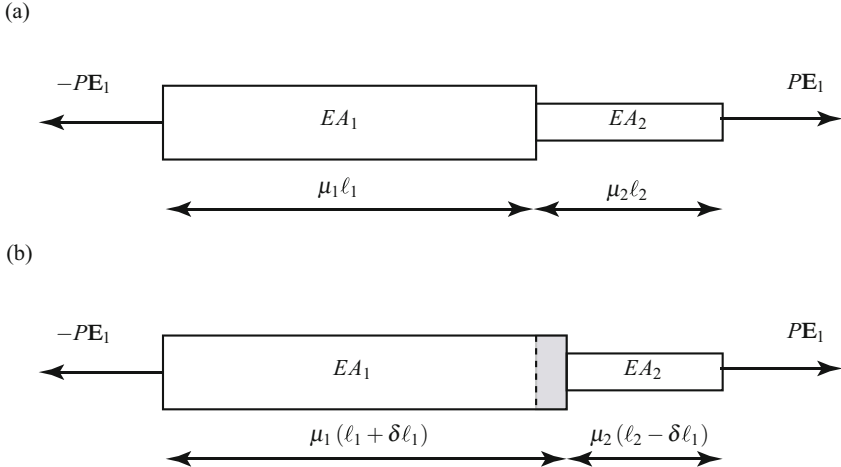


Fig. 1.17 The static deformations of a pair of bars loaded at their ends by equal and opposite forces. The bars, labeled I and II, are identical in every respect except that the lengths of their undeformed constituent components differ by an amount $\delta\ell_1$: (a) bar I and (b) bar II.

An interpretation of the material momentum supply B_{ℓ_1} can be found using insights on a related problem of a Bernoulli-Euler beam that appears in works by Eshelby [102, Page 142] and Kienzler and Herrmann [183]. Returning to the terminally loaded bar, we now compare two different bars. The first bar, known as bar I, is identical to the one shown in Figure 1.15 and reproduced in Figure 1.17(a). We also consider a similar bar, known as bar II and shown in Figure 1.17(b). In contrast to bar I, the length of the segment whose stiffness is EA_1 has an unloaded length $\ell_1 + \delta\ell_1$ and the segment of stiffness EA_2 has an unloaded length of $\ell_2 - \delta\ell_1$. Both bars are loaded with the same terminal forces $\pm PE_1$. In the loaded state, the segment of length $\delta\ell_1$ of bar II has a length $\mu_1 \delta\ell_1$. Computing the stretch μ and material contact force C for bar II in its loaded state is straightforward. Indeed, the resulting expressions for μ and C can be inferred from Eqns. (1.121) and (1.122) with a minimal amount of work. In the sequel, we distinguish quantities associated with the two bars by the respective subscripts *I* and *II*.

We now seek to determine which of the two bars have the greater potential energy. It is important to note that both bars have the same overall length ℓ and are subject to the same terminal forces $\pm PE_1$. Comparing the potential energies of both bars, we find the following expression:

$$\Pi_{II} - \Pi_I = \int_0^{\ell_1 + \delta\ell_1} Cd\xi + \int_{\ell_1 + \delta\ell_1}^{\ell} Cd\xi - \int_0^{\ell_1} Cd\xi - \int_{\ell_1}^{\ell} Cd\xi. \quad (1.127)$$

We evaluate the integrals on the right-hand side of this expression to find that¹⁸

$$\Pi_{II} - \Pi_I = (C(\ell_1^-) - C(\ell_1^+)) \delta\ell_1. \quad (1.128)$$

However, the jump in the contact material force is none other than the supply of material momentum. Whence,¹⁹

$$\Pi_{II} - \Pi_I = B_{\ell_1} \delta\ell_1. \quad (1.129)$$

Referring to Figure 1.16, we observe that $B_{\ell_1} > 0$ if $EA_1 > EA_2$ and B_{ℓ_1} is negative if $EA_1 < EA_2$. Consequently, if $EA_1 > EA_2$ and $\delta\ell_1 > 0$, then bar II has a greater potential energy than bar I. Expressed in another fashion, given a bar of length ℓ and a given terminal loading, by increasing the portion of material of stiffness EA_1 , where $EA_1 > EA_2$, we increase the potential energy of the bar.

We can also conduct a thought experiment where we imagine that an amount $\delta\ell_1$ of material of stiffness EA_1 is added (accreted) on bar I at $\xi = \ell_1$. The addition of this material is at the expense of a portion of length $\delta\ell_1$ of material which has a stiffness EA_2 . During the accretion process, the terminal loads $\pm PE_1$ remain unchanged. The potential energy of the bar is altered in this process and, following Eshelby (cf. [101, Eqn.(28)], [102, Eqn.(10.1)], or [103, Eqn.(17)]) and his definition of a force on a singularity, we define a material force F_E :

$$F_E = -\frac{d\Pi}{d\ell_1}, \quad (1.130)$$

where the minus sign in this definition parallels the definition of a conservative force as the negative of the gradient of a potential energy. After observing that

$$\frac{d\Pi}{d\ell_1} = \lim_{\delta\ell_1 \rightarrow 0} \frac{\Pi_{II} - \Pi_I}{\delta\ell_1} = -[C]_{\ell_1} = B_{\ell_1}, \quad (1.131)$$

we conclude that Eshelby's force on a singularity F_E is none other than the negative of the supply of material momentum:

$$F_E = -B_{\ell_1}. \quad (1.132)$$

Indeed, one can imagine $F_E = -B_{\ell_1}$ as a force moving the material at $\xi = \ell_1$ to $\xi = \ell_1 + \delta\ell_1$. The displacement associated with this force is $\delta\ell_1$ and the product $F_E \delta\ell_1 = -B_{\ell_1} \delta\ell_1$ is the work performed by this force.

The change in stiffness achieved by the accretion process we have just considered can also be attained by a phase transformation. Here, a segment of length $\delta\ell_1$ of

¹⁸ Alternatively, we could use the Leibnitz rule and the constancy of C to establish the sought-after expression.

¹⁹ Observe that Eqn. (1.129) is simply a restatement of the identity $\Phi_{E_\gamma} = B_\gamma \dot{\gamma} + \mathbf{F}_\gamma \cdot \mathbf{v}_\gamma$ (where $\mathbf{F}_\gamma = \mathbf{0}$) applied to the present problem.

material with stiffness EA_2 is transformed to a material with a stiffness EA_1 .²⁰ As emphasized in the works of Abeyaratne and Knowles, a driving force f plays a key role in continuum models for these problems. For the case of interest here, it can be shown that $f = -B_{\ell_1}$.²¹ Thus, for the static problem at hand where $\mathbf{F}_{\ell_1} = \mathbf{0}$, we conclude that

$$[\![C]\!]_{\ell_1} = F_E = f = -B_{\ell_1}. \quad (1.133)$$

In summary, the singular supply of material momentum B_{ℓ_1} is closely related to Eshelby's force on a singularity F_E and Abeyaratne and Knowles' driving force f . Because f , F_E , and B_{ℓ_1} can be expressed as a change in potential energy, these quantities can also be identified with an energy release rate.

1.8.2 A Uniform Bar

To gain additional perspective on the results we have just presented, the problem of a terminally loaded bar composed of a material of uniform stiffness EA is discussed in Exercise 1.8. The results of this exercise demonstrate that, for a bar of a given length ℓ and given terminal forces $\pm PE_1$, the total potential energy of the bar is an increasing function of EA . This conclusion is in agreement with the observations about B_{ℓ_1} that we have previously stated.

1.9 Closing Remarks

This concludes our presentation of a purely mechanical theory of a one-dimensional elastic string. The applications of the theory we will discuss in the next chapter include a wide range of classic problems featuring inextensible strings, the problem of an axially moving elastic string, and a static analysis of a bar with a non-convex strain energy function. These examples are chosen primarily to illuminate the roles played by \mathbf{F}_γ and B_γ in the dynamics of strings. The applications will also provide additional perspectives on the material forces C , b , and B_γ , and the material momentum P .

If one assumes uniaxial motions of the string, i.e., $\mathbf{r}(\xi, t) - \mathbf{R}(\xi) = u(\xi, t)\mathbf{E}_1$ and $\mathbf{e}_t = \mathbf{E}_1$, then the theory can also be used to formulate the equations governing the longitudinal displacement u of an elastic bar. The partial differential equation governing $u = u(\xi, t)$ is

²⁰ The strain energy function $\rho_0 \psi = \frac{EA}{2} (\mu - 1)^2$ is insufficient to examine the phase transformation. Instead, what is required is a strain energy function such as the one shown in Figure 2.5 (cf. Eqn. (2.10)). The computation of C and B_{ℓ_1} for this strain energy function follows our previous developments, but the algebraic details are more complicated and are presented in Exercise 2.7.

²¹ We refer the reader to Eqn. (1.144) in Exercise 1.7 and Abeyaratne and Knowles [5, Chapter 2].

$$\rho_0 \frac{\partial^2 u}{\partial t^2} = \frac{\partial}{\partial \xi} \left(\rho_0 \frac{\partial \psi}{\partial \mu} \right), \quad (1.134)$$

where the strain energy function $\rho_0 \psi$ depends on $\frac{\partial u}{\partial \xi}$ and (if the bar is inhomogeneous) ξ . This equation is supplemented by boundary conditions, initial conditions, and a set of jump conditions. The dynamic solutions $u(\xi, t)$ have a storied history. In particular, the solutions can exhibit shocks and nonuniqueness. This has lead researchers, including Abeyaratne and Knowles [5], Dafermos [80], LeFloch [202, 203], and Truskinovsky [354], to establish admissibility criteria for solutions, nucleation criteria for shocks to develop, and kinetic relations for driving forces so that unique solutions to problems can be established. Given the excellent texts, such as [5, 80, 202], available on this class of problems they are not discussed in great detail in this book.

1.10 Exercises

Exercise 1.1: Consider an elastic string of length ℓ . The reference configuration for the string is defined by $\mathbf{R}(\xi) = \xi \mathbf{E}_1$ where $\xi \in [0, \ell]$. During a motion of the string, it is stretched around the circumference of a circle of radius $R = R(t)$:

$$\mathbf{r}(\xi, t) = R(t) \left(\cos \left(\frac{\pi \xi}{\ell} \right) \mathbf{E}_1 + \sin \left(\frac{\pi \xi}{\ell} \right) \mathbf{E}_2 \right). \quad (1.135)$$

Compute the stretch μ and the arc-length parameter $s = s(\xi, t)$ of the string in its present configuration.

Exercise 1.2: Suppose a bead P of mass m moves along the present configuration of the string in Exercise 1.1. The material point of the string in contact with the bead at time $t \in [0, 0.5]$ is $\xi = \ell \sin(\pi t)$. Show that the velocity vector \mathbf{v}_P of the bead is

$$\begin{aligned} \mathbf{v}_P &= \dot{R} \left(\cos \left(\frac{\pi \xi}{\ell} \right) \mathbf{E}_1 + \sin \left(\frac{\pi \xi}{\ell} \right) \mathbf{E}_2 \right) \\ &\quad + \pi^2 R \cos(\pi t) \left(-\sin \left(\frac{\pi \xi}{\ell} \right) \mathbf{E}_1 + \cos \left(\frac{\pi \xi}{\ell} \right) \mathbf{E}_2 \right). \end{aligned} \quad (1.136)$$

Exercise 1.3: To establish the identity (1.88) several intermediate results are first established. This exercise explores two of these results. First, with the help of the definition of \mathbf{v}_γ and the identity (1.58), show that

$$[\![\mathbf{G}]\!]_\gamma \cdot \mathbf{v}_\gamma = \left[\left[\mathbf{G} \cdot (\dot{\mathbf{r}} + \gamma \mathbf{r}') \right] \right]_\gamma, \quad (1.137)$$

where the linear momentum density $\mathbf{G} = \rho_0 \mathbf{v}$. With the help of this identity, show that

$$[\![2T]\!]_\gamma \dot{\gamma} = [\![\mathbf{P}\dot{\gamma}]\!]_\gamma \dot{\gamma} + [\![\mathbf{G}\dot{\gamma}]\!]_\gamma \cdot \mathbf{v}_\gamma, \quad (1.138)$$

where the kinetic energy density $T = \frac{1}{2}\rho_0 \mathbf{v} \cdot \mathbf{v}$.

Exercise 1.4: With the help of Exercise 1.3, show that the jump conditions (1.86)_{1,...,4} and the definition of \mathbf{v}_γ can be used to reduce the energy jump condition (1.86)₅ to the identity (1.88).

Exercise 1.5: Consider an elastic string, and suppose that the function

$$f = \alpha \|\mathbf{r}\|^2 + \beta \left(\|\mathbf{r}'\|^2 - 1 \right) \quad (1.139)$$

is being proposed as a candidate strain energy function $\rho\psi$. Show that f is not invariant under superposed rigid body motions of the string and argue why it should not be used as a strain energy function.

Exercise 1.6: Consider a string of length ℓ which has the following mass density function:

$$\rho_0(\xi) = 10 \text{ for } \xi \in \left[0, \frac{\ell}{2}\right), \quad \rho_0(\xi) = 2 \text{ for } \xi \in \left(\frac{\ell}{2}, \ell\right]. \quad (1.140)$$

Show that \mathbf{v} , \mathbf{a} , and (in the absence of \mathbf{F}_γ) \mathbf{n} are continuous at $\gamma = \frac{\ell}{2}$.

Exercise 1.7: Recall from Section 1.7 that the jump conditions for material momentum and energy can be expressed in the following manner:

$$\begin{aligned} [\![\mathbf{C}]\!]_\gamma + [\![\mathbf{P}]\!]_\gamma \dot{\gamma} + \mathbf{B}_\gamma &= 0, \\ \mathbf{F}_\gamma \cdot \mathbf{v}_\gamma + \mathbf{B}_\gamma \dot{\gamma} &= \Phi_{E_\gamma}. \end{aligned} \quad (1.141)$$

- (a) Assuming that the string is elastic with a strain energy function ψ , show that the pair of jump conditions (1.141) can be expressed as

$$\begin{aligned} [\![\rho_0 \psi]\!]_\gamma - \{\mathbf{n}\}_\gamma \cdot [\![\mathbf{r}']]\!]_\gamma &= -\mathbf{F}_\gamma \cdot \{\mathbf{r}'\}_\gamma - \mathbf{B}_\gamma, \\ \left([\![\rho_0 \psi]\!]_\gamma - \{\mathbf{n}\}_\gamma \cdot [\![\mathbf{r}']]\!]_\gamma \right) \dot{\gamma} &= -\Phi_{E_\gamma} + \mathbf{F}_\gamma \cdot \{\dot{\mathbf{r}}\}_\gamma. \end{aligned} \quad (1.142)$$

- (b) From the representations (1.142), argue that the jump condition for energy will be trivially satisfied in a statics problem, whereas the jump condition for material momentum is not necessarily identically satisfied.
(c) Show that the driving force f defined in Abeyaratne and Knowles (see [2, Eqn. (2.11)] or [5, Eqn. (2.25)]) corresponds to

$$f = [\![\rho_0 \psi]\!]_\gamma - \{\mathbf{n}\}_\gamma \cdot [\![\mathbf{r}']]\!]_\gamma. \quad (1.143)$$

In addition, show that f can be identified with supplies of linear and material momenta:

$$f = -\mathbf{F}_\gamma \cdot \left\{ \mathbf{r}' \right\}_\gamma - \mathbf{B}_\gamma. \quad (1.144)$$

The corresponding result for a three-dimensional continuum is discussed on Page 370.

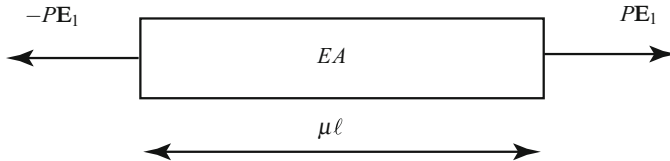


Fig. 1.18 Schematic of a bar of stiffness EA that is loaded at its ends by equal and opposite forces $\pm PE_1$. The bar is uniformly stretched by the applied forces and its length changes from ℓ to $\mu\ell$.

Exercise 1.8: This exercise is intended to complement the discussion in Section 1.8 of the terminally loaded bar. As shown in Figure 1.18, consider a bar of length ℓ composed of a material with a stiffness EA . The bar is modeled as a uniform string with a strain energy function $\rho_0 \psi = \frac{EA}{2} (\mu - 1)^2$.

- (a) Show that the stretch in the string is $\mu = \frac{P}{EA}$.
- (b) Show that the contact material force in the string is

$$C = -\frac{EA}{2} \left(\left(\frac{P}{EA} \right)^2 - 1 \right). \quad (1.145)$$

- (c) Show that the potential energy of the terminally loaded string is

$$\Pi = -\frac{EA\ell}{2} \left(\left(\frac{P}{EA} \right)^2 - 1 \right). \quad (1.146)$$

- (d) For a given load P , show that Π is an increasing function of the stiffness EA . That is, for a given load, a stiffer bar will have a greater potential energy.
- (e) For a given stiffness EA , show that Π is a decreasing (increasing) function of the load $P > 0$ ($P < 0$).

Exercise 1.9: Consider the following strain energy function:

$$\rho_0 \psi = \alpha_1 \left(\frac{1}{4} (\mu - \alpha_2)^4 + \mu \left(1 + \alpha_2 - \frac{\mu}{2} \right) \right) + \alpha_1 \alpha_3 \log \left(\mu - 1 + \frac{1}{\mu} \right), \quad (1.147)$$

where α_1 , α_2 , and α_3 are constants.

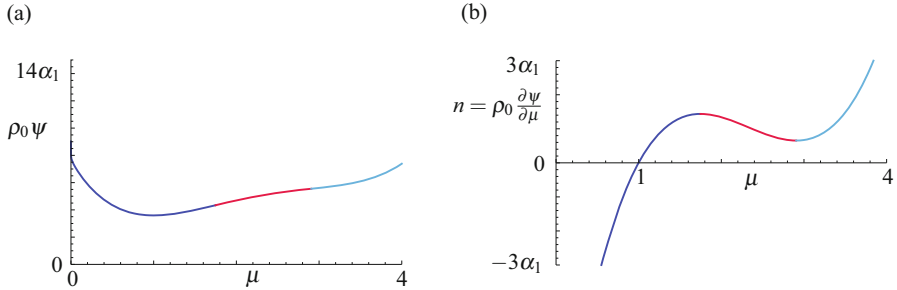


Fig. 1.19 (a) The strain energy function $\rho_0 \psi$ given by Eqn. (1.147) and (b) the associated contact force $n = \rho_0 \frac{\partial \psi}{\partial \mu}$. For the graphs shown, $\alpha_2 \approx 2.32472$ and $\alpha_3 = 0.1$.

(a) Show that the \mathbf{e}_t component of the contact force $\mathbf{n} = n \mathbf{e}_t$ is

$$n = \alpha_1 \left((\mu - \alpha_2)^3 + 1 + \alpha_2 - \mu \right) + \alpha_1 \alpha_3 \left(\frac{\mu^2 - 1}{\mu^3 + \mu - \mu^2} \right). \quad (1.148)$$

(b) If n is assumed to be zero when the string is unstretched, show that

$$\alpha_2 \approx 2.32472. \quad (1.149)$$

(c) Verify the results shown in Figure 1.19.

(d) Establish the conditions on α_1 and α_3 whereby $\rho_0 \psi$ and n become unbounded as $\mu \searrow 0$ (cf. Eqn. (1.98)).

(e) Suppose that $\alpha_1 > 0$, α_2 is given by Eqn. (1.149), and $\alpha_3 = 0.1$. Show that the equation

$$\rho_0 \frac{\partial \psi}{\partial \mu} = P_0 \quad (1.150)$$

can have multiple solutions depending on the value of the constant P_0 .

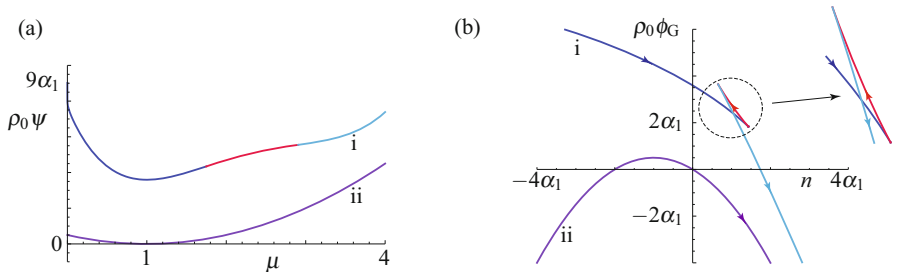


Fig. 1.20 (a) The strain energy function $\rho_0 \psi$ defined by Eqn. (1.147) (labeled i) and the strain energy function $\rho_0 \psi$ defined by Eqn. (1.151) (labeled ii), and (b) the associated Gibbs free energy functions. For the graphs shown, $\alpha_2 \approx 2.32472$ and $\alpha_3 = 0.1$. The arrows in (b) indicate the direction of increasing μ as a function of n .

Exercise 1.10: Consider the strain energy function (1.147) and the quadratic strain energy function

$$\rho_0 \psi = \frac{\alpha_1}{2} (\mu - 1)^2, \quad (1.151)$$

where α_1 is a constant which can be identified with the stiffness EA .

- (a) Using the definition (1.103) of the Gibbs free energy function $\rho_0 \phi_G$, compute the corresponding free energy functions.
- (b) Verify the results shown in Figure 1.20. The dramatic difference in the behaviors of $\rho_0 \phi_G$ can be attributed to the lack of convexity of the strain energy function (1.147) as a function of μ .
- (c) For the pair of strain energy functions (1.147) and (1.151), compute the corresponding static material contact force C both as a function of μ and as a function of n .
- (d) Relate the results of Exercise 1.9(e) to the behavior of $\rho_0 \phi_G$ shown in Figure 1.20 when $n \in (0.654306\alpha_1, 1.43586\alpha_1)$.

Chapter 2

Applications of the Mechanics of a String

“Books on dynamics usually include a number of problems on the motion of chains. Though hardly important in themselves, such problems furnish excellent illustrations of dynamical principles.”

H. Lamb [193, Page 142].

2.1 Introduction

In this chapter we present tractable applications of the theory developed in Chapter 1. Our primary aim is to demonstrate a systematic procedure to establish and analyze the motion of a string using the balance laws. We start with the simplest dynamic problem of a steady axial motion of a string. After exploring recent results for this problem, we then turn to examining a classic set of chain problems. An example of the latter class of problems is shown in Figure 2.1. All but one of the examples we explore are adopted from classic texts in dynamics and mechanics. The chain is modeled as a heavy inextensible string and we shall find that the string is often in states of rectilinear motion which are separated



Fig. 2.1 A link chain which is subject to a steady pull from the right (out of frame) emerges from a stationary pile and forms an arch-like shape. Image courtesy of James Hanna and Wes Royston.

by shocks where the velocity vector \mathbf{v} is discontinuous (cf. Figure 2.2). The methodology we use to arrive at the equations of motion contrasts to the semi-inverse method used in textbooks. With the help of the balance laws for material momentum and linear momentum along with some kinematical considerations, we demonstrate a systematic framework with which to arrive at the governing equations of motion for these problems. The resulting equations of motion are then analyzed and several interesting features of the individual problems are explored. The set of problems we consider is far from exhaustive and some additional examples are explored in the exercises at the end of this chapter.

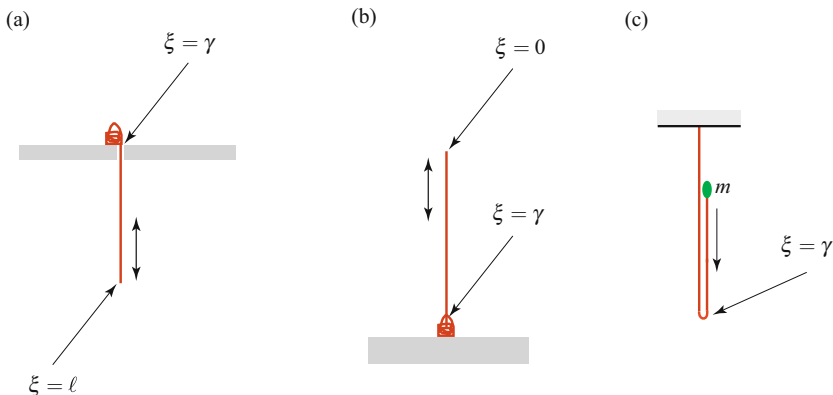


Fig. 2.2 Three singularities commonly encountered in classic problems in the dynamics of inextensible strings. (a) A string issuing from a heap, (b) a string descending into or being drawn from a pile, and (c) a string with a fold.

Typically, the class of problems we consider involve impacting segments of the chain - especially when a stationary heap of chain is present in the problem. In our model for the chain, which is an inextensible, perfectly flexible string, the dissipation associated with the impact is modeled using the material momentum B_γ and the associated source of power Φ_{E_γ} at a point of discontinuity $\xi = \gamma$. We find that we will need to prescribe B_γ and, based on experimental results in the literature, some of the constitutive quantities associated with the prescription for B_γ will need to be found from experiments. In this chapter, the prescription we use is

$$B_\gamma = -2e\rho_0\dot{\gamma}^2 \frac{\dot{\gamma}}{|\dot{\gamma}|},$$

where e is a constant which must be determined by experiments. We also take this opportunity to acknowledge that our exposition in this chapter was greatly facilitated by the recent experimental works of Biggins [23], Grewal et al. [142], and Hamm and Géminard [151]. These works provided invaluable insights and helpful

experimental results. We also note that many of the paradoxes and much of the controversy associated with this class of problems stems from the inappropriate use of energy conservation.¹

2.2 Steady Axial Motions of Elastic Strings and Inextensible Strings

In a class of motions of strings, which occupies a central role in many applications, the string only moves along its length (cf. Figures 1.2 and 2.3). Such motions are known as axial motions. For motions of this type which are classified as steady axial motions, the following three conditions hold²:

- (i) The material curve \mathcal{L} of the string moves along a fixed space curve.
- (ii) Suppose the position vector \mathbf{c} of any point on the space curve is uniquely identified by the arc-length parameter χ (i.e., $\mathbf{c} = \mathbf{c}(\chi)$), then the velocity vector \mathbf{v} of a material point of \mathcal{L} is a function of χ only.
- (iii) The vector \mathbf{r}' is a function of χ only.

It has been proven for both inextensible and elastic strings that these three conditions are equivalent to the statement that the position vector \mathbf{r} of a material point of the string has the representation³

$$\mathbf{r} = \tilde{\mathbf{r}}(\chi) = \mathbf{r}(\xi, t) \quad (2.1)$$

where $\chi = \xi + ct$ and c is a constant (which has units of speed).

For steady axial motions, straightforward application of the chain rule can be used to show that

$$\frac{\partial \tilde{\mathbf{r}}}{\partial \chi} = \frac{\partial \mathbf{r}}{\partial \xi}, \quad \mathbf{v} = \dot{\mathbf{r}} = c \frac{\partial \tilde{\mathbf{r}}}{\partial \chi}, \quad \mathbf{a} = \ddot{\mathbf{r}} = c^2 \frac{\partial^2 \tilde{\mathbf{r}}}{\partial \chi^2}. \quad (2.2)$$

Thus, the speed of a material point $v = \|\mathbf{v}\| = \mu |c|$. From the compatibility condition $[\mathbf{v} + \dot{\gamma} \mathbf{r}']_{\gamma} = \mathbf{0}$ for a steady motion, we can conclude that

$$\dot{\gamma} = -c. \quad (2.3)$$

We also find, from the definition of \mathbf{v}_{γ} (see Eqn. (1.54)), that during a steady motion $\mathbf{v}_{\gamma} = \mathbf{0}$. In other words, the point of discontinuity (if one exists) is stationary - as expected. Because c is a constant for a steady axial motion, only one of the examples

¹ Our perspective on this matter is influenced by the works of Troger and his coworkers [315, 331] and statements on the lack of energy conservation in some chain problems in the textbooks authored by Lamb [193] and Love [212].

² These conditions were first enunciated in a work by Green and Laws [129] on ideal jets of fluid.

³ The proof is presented in [250].

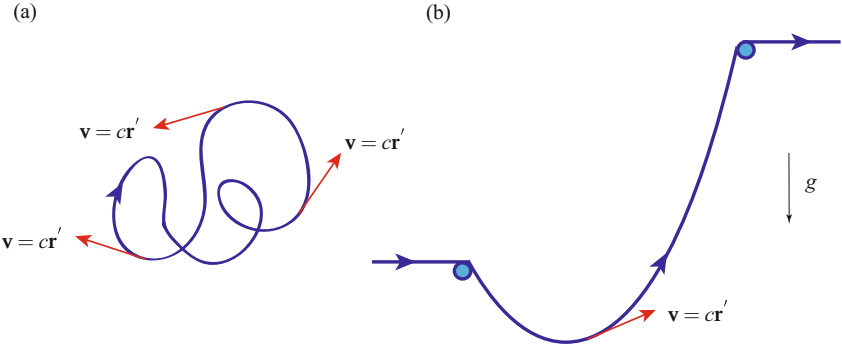


Fig. 2.3 Two representative examples of steady axial motions of strings. (a) A closed loop of string propagating along its length studied by Healey and Papadopoulos [160] and (b) the axially moving catenary studied by Perkins and Mote [287, 288].

that we consider in the sequel qualifies as an example of a steady axial motion. This example, which is discussed in Section 2.8, is known as the chain fountain and involves an inverted catenary.

The representation (2.1) has been used for inextensible strings dating to the mid-19th century (cf. [305, Sections 594 & 595]) and for extensible strings it was first used by Healey and Papadopoulos [160]. It has since presented itself in a large number of studies on the dynamics of strings and rods (cf., e.g., [63, 65, 157, 279] and references therein). One of the reasons for the popularity of these motions lies in a result noted by Routh [305, Sections 594 & 595] for inextensible strings which has since been applied to extensible rods and strings.

To see Routh's result and its extensions, we consider the balance of linear momentum (1.115) for a homogeneous string undergoing a steady axial motion:

$$\mathbf{n}' + \rho_0 \mathbf{f} = \rho_0 \dot{\mathbf{v}}. \quad (2.4)$$

Appealing to Eqn. (2.1) and noting that

$$\frac{\partial f(\xi, t)}{\partial \xi} = \frac{\partial \tilde{f}(\chi, t)}{\partial \chi}, \quad \rho_0 = \mu \rho, \quad \mathbf{n} = n \mathbf{e}_t = \frac{n}{\mu} \frac{\partial \mathbf{r}}{\partial \xi} = \frac{n}{\mu} \frac{\partial \tilde{\mathbf{r}}}{\partial \chi}, \quad (2.5)$$

we can write the balance law as follows:

$$\frac{\partial}{\partial \chi} \left((n - \rho_0 \mu c^2) \frac{1}{\mu} \frac{\partial \tilde{\mathbf{r}}}{\partial \chi} \right) + \rho_0 \mathbf{f} = \mathbf{0}. \quad (2.6)$$

Thus, it is possible for the shape taken by the string performing a steady axial motion to be identical to that taken by a stationary string provided the tension n is replaced by $n - \rho_0 \mu c^2$. For an inextensible string, this result was proven by Routh, while for an elastic string it is the extension to Routh's theorem published by Healey and Papadopoulos [160] nearly a century later.

Referring to the summary of the governing equations in Section 1.7, we note that several of the jump conditions (1.116) remain to be discussed for the aforementioned steady axial motion. For the motions of interest, no sources of linear or material momentum are assumed to be present: $\mathbf{F}_\gamma = \mathbf{0}$ and $\mathbf{B}_\gamma = 0$. Thus, the jump conditions (1.116) imply that

$$[(n - \rho_0 \mu c^2) \mathbf{e}_t]_\gamma = \mathbf{0}, \quad [\rho_0 \psi - \mu (n - \rho_0 \mu c^2)]_\gamma = 0. \quad (2.7)$$

We conclude from this pair of conditions that if $n \neq \rho_0 \mu c^2$, then the tangent vector \mathbf{e}_t varies continuously along the material curve and that, depending on ψ , the stretch μ might be continuous. For an inextensible string, one can deduce that n is continuous and that, provided $n \neq \rho_0 c^2$, \mathbf{e}_t must be continuous.

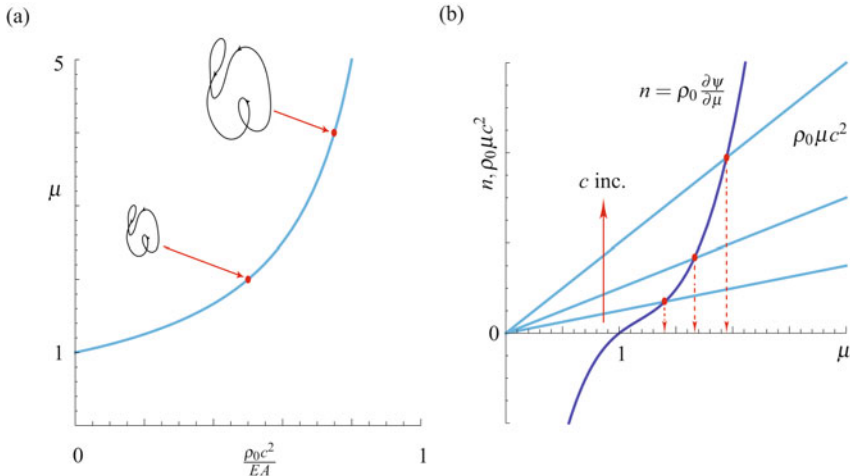


Fig. 2.4 (a) The stretch μ as a function of $\frac{\rho_0 c^2}{EA}$ for a steady axial motion of a string whose strain energy function is $\rho_0 \psi = \frac{EA}{2} (\mu - 1)^2$ (cf. Eqn. (2.9)). The inset images are representative steady axial motions of loops of string. These solutions are stable according to the stability criterion discussed on Page 56. (b) Schematic of a graphical solution procedure for the equation $n = \rho_0 \mu c^2$ (cf. Eqn. (2.8)) to determine the stretch μ in a steady axial motion of a closed loop of elastic string as the parameter c varies. The strain energy function shown in the figure is identical to one shown in Figure 1.14.

2.2.1 Closed Loops of String

As a specific example, consider the case where $\mathbf{f} = \mathbf{0}$. If the string is inextensible, then the string can take the form of *any* closed loop provided $n = \rho_0 c^2$, a result which dates to Routh [305]. Similarly, as shown more recently by Healey and

Papadopoulos [160], an elastic string can take the form of *any* closed loop provided the stretch μ satisfies

$$\rho_0 \frac{\partial \psi}{\partial \mu} = \rho_0 \mu c^2. \quad (2.8)$$

That is, $n - \rho_0 \mu c^2 = 0$. For the elastic string with the simple strain energy function $\rho_0 \psi = \frac{EA}{2} (\mu - 1)^2$ mentioned earlier (cf. Eqn. (1.100)), Eqn. (2.8) can be solved analytically:

$$\mu = \frac{EA}{EA - \rho_0 c^2}. \quad (2.9)$$

This solution is shown in Figure 2.4(a). We observe that as $c^2 \rightarrow \frac{EA}{\rho_0}$ the stretch will become infinite. However, the speed in this case approaches the speed of longitudinal waves in the string and the constitutive relation for $\rho_0 \psi$ is questionable for such high stretches.⁴ For more complex strain energy functions, it is easy to conceive a graphical representation of Eqn. (2.8) for a given ψ (cf. Figure 2.4(b)). In the example shown, there is a unique μ for every c . Furthermore as c increases, the stretch in the axial motion increases from its value of 1 when $c = 0$.

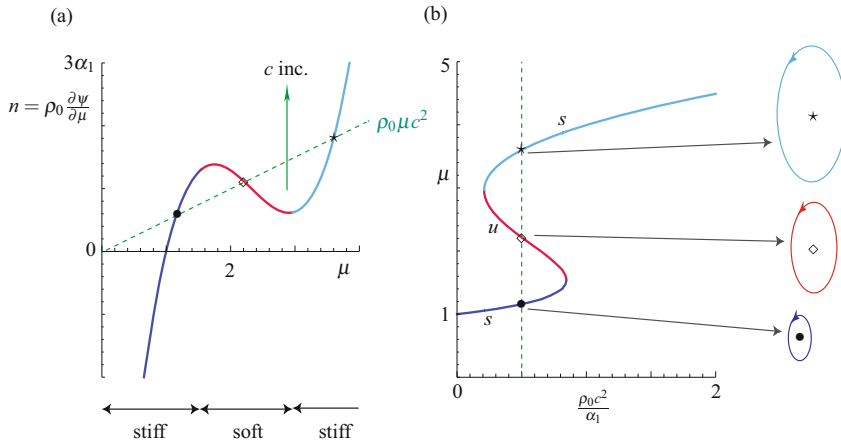


Fig. 2.5 (a) The tension n as a function of the stretch μ for a specific strain energy function given by Eqn. (2.10). (b) Solutions $\mu(\rho_0 c^2)$ of Eqn. (2.14) which determine the stretch μ in a steady axial motion of an elastic string as the parameter c varies. Observe the pair of saddle-node bifurcations as $\rho_0 c^2$ is varied. At these bifurcations, the number of possible solutions changes from 1 to 3 and 3 to 1, respectively. The labels s and u on this figure denote stable and unstable steady motions and the inset images are representative images of the simplest possible axial motions.

⁴ For a string modeling a three-dimensional linearly elastic body with a cross-sectional area A and mass density per unit volume ρ_0^* , we find that $\rho_0 = \rho_0^* A$ and so $\frac{EA}{\rho_0} = \frac{E}{\rho_0^*}$. We also recall that $\sqrt{\frac{E}{\rho_0^*}}$ is the propagation speed for longitudinal waves in an infinitely long bar [346, Section 168].

As a further example, consider the strain energy function that produces the function $n(\mu)$ shown in Figure 2.5(a).⁵ Here,

$$\rho_0 \psi = \alpha_1 \left(\frac{1}{4} (\mu - \alpha_2)^4 + \mu \left(1 + \alpha_2 - \frac{\mu}{2} \right) \right), \quad (2.10)$$

where α_1 and α_2 are constants. The strain energy function is a simplified version of the function which arises in Exercise 1.9. A differentiation of (2.10) with respect to μ shows that

$$\begin{aligned} n &= \rho_0 \frac{\partial \psi}{\partial \mu} \\ &= \alpha_1 \left((\mu - \alpha_2)^3 + 1 + \alpha_2 - \mu \right). \end{aligned} \quad (2.11)$$

Because we assume that the force n is zero when the string is unstretched, α_2 is the real root of the equation $(1 - \alpha_2)^3 + \alpha_2 = 0$:

$$\alpha_2 \approx 2.32472 \quad (2.12)$$

We also note that the stiffness of the string when $\mu = 1$ can be found from the second partial derivative of μ ⁶:

$$\begin{aligned} \rho_0 \frac{\partial^2 \psi}{\partial \mu \partial \mu} &= \alpha_1 \left(3(\alpha_2 - 1)^2 - 1 \right) \\ &= 4.26463 \alpha_1. \end{aligned} \quad (2.13)$$

For a given c , the stretch for a steady motion is obtained by solving Eqn. (2.8):

$$\alpha_1 \left((\mu - \alpha_2)^3 + 1 + \alpha_2 - \mu \right) = \rho_0 \mu c^2. \quad (2.14)$$

Depending on the value of $\rho_0 c^2$, it is possible for 1, 2, or 3 distinct values of μ to exist. Consequently, as shown in Figure 2.5(b), for a given closed loop of string, multiple axial motions are possible and the three motions are scaled versions of each other. The values of $\rho_0 c^2$ where the number of solutions changes are known as critical values. For the example shown, these critical values are $\rho_0 c^2 \approx 0.2099 \alpha_1$ and $\rho_0 c^2 \approx 0.845 \alpha_1$ and the bifurcation that occurs at these points is often referred to as a saddle-node bifurcation.

⁵ The functional form of $n(\mu)$ with its local minimum and local maximum is motivated by constitutive relations for one-dimensional continua that are used in studies on phase transformations by Abeyaratne and Knowles [2, 5], Ericksen [98], and Purohit and Bhattacharya [296] (among many others).

⁶ The corresponding stiffness for the strain energy function $\rho_0 \psi = \frac{EA}{2} (\mu - 1)^2$ is EA .

It is interesting to examine the balance of material momentum (1.72) and balance of energy (1.74) applied to the closed loop of string⁷:

$$\frac{d}{dt} \oint \rho_0 \mathbf{v} \cdot \frac{\partial \mathbf{r}}{\partial \xi} d\xi = 0, \quad (2.15)$$

and

$$\frac{d}{dt} \oint \left(\frac{1}{2} \mathbf{v} \cdot \mathbf{v} + \psi \right) \rho_0 d\xi = 0. \quad (2.16)$$

Thus, we observe that two kinematic quantities are conserved: the flow or integral of the circulation $\rho_0 \mathbf{v} \cdot \frac{\partial \mathbf{r}}{\partial \xi}$ and the integral of the energy density. These conserved quantities were used by Healey [157] to establish stability criteria for steady axial closed loops of string where the perturbations conserved both the total energy and the integral of the material momentum. Specifically, he showed that a nonlinear stability criterion could be established when the string was stiff. A string is termed stiff at $\mu = \mu_0$ if the constitutive relations satisfy the following inequality and is otherwise termed soft:

$$\rho_0 \frac{\partial^2 \psi}{\partial \mu^2}(\mu_0) - \frac{\rho_0}{\mu_0} \frac{\partial \psi}{\partial \mu}(\mu_0) > 0. \quad (2.17)$$

Thus, for the constitutive relation shown in Figure 2.5(a), the string is soft when $\mu \in [1.54, 2.96]$ and is otherwise stiff. With the help of these observations, the stability results presented in Figure 2.5(b) can be easily established. We have taken the liberty of defining the solutions where the criterion (2.17) is violated as unstable even though a formal proof of instability is not known to us. By way of contrast, the string discussed in Figure 2.4(b) is stiff and the steady motions shown in Figure 2.4(a) are stable.

2.3 Inextensible Strings with Shocks

Consider the motions of strings shown in Figure 2.2. All three examples involve inextensible strings performing piecewise rectilinear motions. In the remainder of this chapter, our goal is to establish the governing equations of motion and to solve for the motion of the string. Here, we summarize the equations needed to establish the equations of motion for the series of examples that follow.

⁷ For the homogeneous strings of interest here, $\oint \rho_0 \mathbf{v} \cdot \frac{\partial \mathbf{r}}{\partial \xi} d\xi = \rho_0 \oint \mathbf{v} \cdot \mathbf{e}_t ds$, and thus, the material momentum P and its integral can be related to the circulation $\mathbf{v} \cdot \mathbf{e}_t$ and “flow” that were first defined by Kelvin in 1869 and play a prominent role in fluid mechanics. For further details on this topic, the reader is referred to [52, 194, 349].

2.3.1 General Considerations

For an inextensible string, the stretch $\mu = 1$ and consequently, $\frac{\partial \mathbf{r}}{\partial \xi} = \mathbf{e}_t$. For many of the problems of interest in this chapter, $\mathbf{v} = v\mathbf{E}$ where \mathbf{E} is a (piecewise) constant unit vector that is equal to \mathbf{e}_t . As $\mathbf{v}' \cdot \mathbf{e}_t = 0$ for inextensible strings (see Eqn. (1.40)), it follows that $v = v(t)$. Further, from the definition (1.54) of \mathbf{v}_γ , we can conclude that

$$\begin{aligned}\mathbf{v}_\gamma &= ((v + \dot{v})\mathbf{E})^+ = ((v + \dot{v})\mathbf{E})^-, \\ [[v\mathbf{E} + \dot{v}\mathbf{E}]]_\gamma &= \mathbf{0}.\end{aligned}\quad (2.18)$$

These results are very useful for solving boundary-value problems.

We will find it convenient to use the balance of material momentum (1.83) to establish conservation laws. For an inextensible string, $\mathbf{n} = n\mathbf{e}_t$ and the strain energy function $\psi = 0$. Consequently, the material contact force C is

$$\begin{aligned}C &= -\frac{\rho_0}{2}\mathbf{v} \cdot \mathbf{v} - n \\ &= -\frac{\rho_0}{2}v^2 - n.\end{aligned}\quad (2.19)$$

In this chapter, we shall assume that ρ_0 is a continuous function of ξ and this implies that the prescription (1.112) for b_p simplifies considerably. As a result, Eqn. (1.83) now reads:

$$-\rho_0 \mathbf{f} \cdot \mathbf{r}' = \dot{P} - \frac{\partial C}{\partial \xi}. \quad (2.20)$$

The local balance law which is neither trivially nor identically satisfied comes from the balance of linear momentum:

$$\mathbf{n}' + \rho_0 \mathbf{f} = \rho_0 \ddot{\mathbf{r}}. \quad (2.21)$$

We emphasize that the material momentum balance (2.20) is identically satisfied by the solutions to Eqn. (2.21) and it finds application in establishing conservation laws (such as (2.99) for the chain fountain problem).

The jump conditions which need to be satisfied are obtained from Eqn. (1.86):

$$\begin{aligned}[[\mathbf{n} + \rho_0 \mathbf{v} \dot{v}]]_\gamma + \mathbf{F}_\gamma &= \mathbf{0}, \\ [[C - \dot{v} \rho_0 \mathbf{v} \cdot \mathbf{r}']]_\gamma + B_\gamma &= 0.\end{aligned}\quad (2.22)$$

As emphasized earlier in Section 1.5.5, the jump conditions for angular momentum and energy provide identities for \mathbf{M}_{O_γ} and Φ_{E_γ} :

$$\begin{aligned}\mathbf{M}_{O_\gamma} - \mathbf{r}(\gamma, t) \times \mathbf{F}_\gamma &= \mathbf{0}, \\ \mathbf{F}_\gamma \cdot \mathbf{v}_\gamma + \mathbf{B}_\gamma \dot{\gamma} &= \Phi_{E_\gamma}.\end{aligned}\quad (2.23)$$

In the sequel, we will often use the identity (2.23)₂ to establish Φ_{E_γ} given \mathbf{F}_γ and \mathbf{B}_γ . The force \mathbf{F}_γ will represent an impulse on the string at a point where there is an abrupt change in its motion and \mathbf{B}_γ will represent an energy loss associated with impacts of the links of the chain that the string is modeling. We shall find that the following prescription for \mathbf{B}_γ is useful for problems where the string's motion has an abrupt change in speed:

$$\mathbf{B}_\gamma = -2e\rho_0\dot{\gamma}^2 \frac{\dot{\gamma}}{|\dot{\gamma}|}. \quad (2.24)$$

While the constant e in this expression has a value of $e = 0.25$ for many classic formulations, recent experimental results by Biggins [23] and Hamm and Géminard [151] have lead us to believe that e can have values lower than this ideal number depending on the type of chain that the string is modeling and the nature of the shock that the string is experiencing. The chains in question are primarily of two types: a link chain or a bead chain (cf. Figure 2.6). The latter type of chain is sometimes known as a ball chain. Among others, we anticipate that the value of e will depend on the nature of the connections between the segments of the chain. In all of the examples considered in the sequel, there will be several points where singular supplies are present and so the subscript β in \mathbf{F}_β , \mathbf{B}_β , and Φ_{E_β} will be used to distinguish the point $\xi = \beta$ where the supply acts.

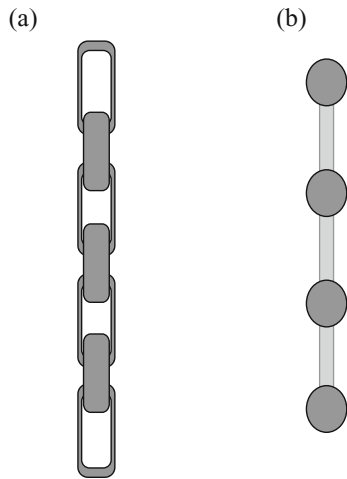


Fig. 2.6 Two types of chain: (a) a link chain and (b) a bead chain.

2.3.2 Boundary Conditions, Sources, Sinks, and Reservoirs

A primary use of the jump conditions (which is hard to find a published discussion of) is to establish boundary conditions for terminally loaded strings. For instance, suppose a force $-P_0\mathbf{E}_1$ is applied at the end $\xi = 0$ of a string and a force $P_1\mathbf{E}_1$ is applied at the end $\xi = \ell$. Questions arise as to what precisely $\mathbf{n}(0^+, t)$ and $\mathbf{n}(\ell^-, t)$ are for these loadings. To answer such questions, we can appeal to the jump condition (2.22)₁, $[\![\mathbf{n} + \rho_0\mathbf{v}\dot{\gamma}]\!]_\gamma + \mathbf{F}_\gamma = \mathbf{0}$, and apply this condition twice, once at each end.

To elaborate, let us consider the end $\xi = 0$. As the string terminates at this point, $\mathbf{n}(0^-, t)$ and $\mathbf{v}(0^-, t)$ are nonexistent. Further, because $\gamma = 0$ which is fixed, $\dot{\gamma} = 0$. The last ingredient is to model the applied force by \mathbf{F}_0 : $\mathbf{F}_0 = -P_0 \mathbf{E}_1$. Now invoking the jump condition (2.22)₁, we find

$$\mathbf{n}(0^+, t) = -\mathbf{F}_0 = P_0 \mathbf{E}_1. \quad (2.25)$$

We typically drop the + ornamenting the 0 and simply write: $\mathbf{n}(0, t) = P_0 \mathbf{E}_1$. For the end $\xi = \ell$, we follow the same procedure but now $\mathbf{n}(\ell^+, t)$ and $\mathbf{v}(\ell^+, t)$ are nonexistent. Using Eqn. (2.22)₁ with $\gamma = \ell$ and $\mathbf{F}_\ell = P_1 \mathbf{E}_1$, we find

$$\mathbf{n}(\ell^-, t) = \mathbf{F}_\ell = P_1 \mathbf{E}_1. \quad (2.26)$$

If we now consider a string of length ℓ which is loaded by equal and opposite forces, $P_0 = P_1$, then this procedure leads to the satisfying conclusion that the tension in the string is constant: $\mathbf{n} = P_0 \mathbf{E}_1$.

Several problems in the dynamics of heavy inextensible strings (also sometimes known as chains) involve a string being drawn from a heap of quiescent string (cf. the examples shown in Figure 2.2(a) & (b)). We often refer to the heap as a source, sink, or reservoir; others refer to the heap shown in Figure 2.2(a) as a top pile and the heap shown in Figure 2.2(b) as a bottom pile. To examine the boundary conditions at the exit point of the string from the heap, two cases need to be considered. The first, an example of which is shown in Figure 2.2(a), arises when the parameterization of ξ is such that γ decreases as an increasing amount of string is pulled from the heap. In this case, we denote the end point of the string by $\xi = \gamma^+$, and assume that the heap exerts a force \mathbf{F}_γ and a material force \mathbf{B}_γ on the string. The jump conditions at the point where the string exits the heap then read

$$\begin{aligned} \mathbf{n}(\gamma^+, t) + \rho_0 \mathbf{v}(\gamma^+, t) \dot{\gamma} &= -\mathbf{F}_\gamma, \\ C(\gamma^+, t) - \dot{\gamma} \rho_0 \mathbf{v}(\gamma^+, t) \cdot \mathbf{r}'(\gamma^+, t) &= -\mathbf{B}_\gamma, \end{aligned} \quad (2.27)$$

where

$$C(\gamma^+, t) = -\frac{\rho_0}{2} \mathbf{v}(\gamma^+, t) \cdot \mathbf{v}(\gamma^+, t) - n(\gamma^+, t). \quad (2.28)$$

The identity $\Phi_{E_\gamma} = \mathbf{B}_\gamma \dot{\gamma} + \mathbf{F}_\gamma \cdot \mathbf{v}_\gamma$ is used to identify if the source is dissipative, energetic, or energy conserving. Note that our implementation of the jump conditions (2.27) is tantamount to assuming that the string is stationary and slack in the heap: $\mathbf{n}(\gamma^-, t) = \mathbf{0}$ and $\mathbf{v}(\gamma^-, t) = \mathbf{0}$. We will shortly explore an example showing how the conditions (2.27) are used in Section 2.4.

The complementary case to the heap discussed above occurs when the parameterization of ξ is such that γ increases as an increasing amount of string is pulled from the heap (i.e., the bottom pile). An example of this situation is shown in Figure 2.2(b). We proceed as before to examine the boundary conditions on the string at the point $\xi = \gamma^-$ and assume that the heap exerts a force \mathbf{F}_γ and a material force \mathbf{B}_γ on the string. Applying the jump conditions in a similar manner to our earlier work, we find the following pair of conditions:

$$\begin{aligned} \mathbf{n}(\gamma^-, t) + \rho_0 \mathbf{v}(\gamma^-, t) \dot{\gamma} &= \mathbf{F}_\gamma, \\ C(\gamma^-, t) - \dot{\gamma} \rho_0 \mathbf{v}(\gamma^-, t) \cdot \mathbf{r}'(\gamma^-, t) &= \mathbf{B}_\gamma, \end{aligned} \quad (2.29)$$

where

$$C(\gamma^-, t) = -\frac{\rho_0}{2} \mathbf{v}(\gamma^-, t) \cdot \mathbf{v}(\gamma^-, t) - n(\gamma^-, t). \quad (2.30)$$

As with the case discussed earlier, the identity $\Phi_{E_\gamma} = \mathbf{B}_\gamma \dot{\gamma} + \mathbf{F}_\gamma \cdot \mathbf{v}_\gamma$ is also very helpful in determining the energetic properties of this heap. We close by remarking that the most celebrated problem associated with a heap of this type involves lowering a string into a pile atop a horizontal table. As noted by Ruina et al. [142] this problem involves chains which are “sucked” into the pile which we shall explore in Section 2.6.

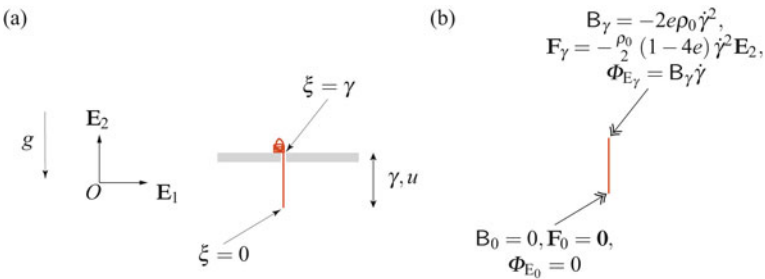


Fig. 2.7 (a) Schematic of a chain falling from a hole on a horizontal surface or table and (b) summary of the singular supplies acting on the chain. The chain is supplied from a heap which lies at rest on the surface. In classic formulations of this problem, the parameter $e = 0.25$.

2.4 Cayley's Problem

In an influential work [53] by the celebrated English mathematician Arthur Cayley (1821–1895), he presented the equations of motion for a chain that issues from a quiescent heap and falls freely under gravity over the edge of a table. If u denotes the length of chain that is below the table surface, then Cayley established the following differential equation governing $u(t)$:

$$u(\ddot{u} - g) = -\dot{u}^2. \quad (2.31)$$

A representation of Cayley's problem is shown in Figure 2.7. This problem has attracted much attention in the past 150 years and we refer the interested reader to [142, 171, 366, 367] for additional references and perspectives, some of which we will discuss below.

Referring to Figure 2.7(a), a segment of string of length γ is falling under gravity. A discontinuity is present where the string moves over the edge of the table. At this point, which we label as $\xi = \gamma$, in addition to possible supplies of power Φ_{E_γ} and material momentum B_γ , a reaction force \mathbf{F}_γ acts on the string.

As the shock is stationary, $\mathbf{v}_\gamma = \mathbf{0}$, and we also note that $\mathbf{r}'(\gamma^-, t) = \mathbf{E}_2$. Using the definition of \mathbf{v}_γ , we find that

$$\mathbf{v}(\gamma^-, t) = -\dot{\gamma}\mathbf{E}_2. \quad (2.32)$$

In the sequel, it is convenient to define a variable u :

$$u = \gamma, \quad \dot{u} = \dot{\gamma}. \quad (2.33)$$

Thus, for the section of chain that is freely falling,

$$\mathbf{v} = -\dot{u}\mathbf{E}_2. \quad (2.34)$$

A body force $-\rho_0 g \mathbf{E}_2$ acts on the string and so the balance of linear momentum (2.22) with $\mathbf{n} = n\mathbf{E}_2$ reads

$$(n\mathbf{E}_2)' - \rho_0 g \mathbf{E}_2 = -\rho_0 \ddot{u} \mathbf{E}_2. \quad (2.35)$$

We solve this equation for n using the boundary condition that $\mathbf{n}(0) = \mathbf{0}$:

$$n(\gamma^-, t) = -\rho_0 (\ddot{u} - g) u. \quad (2.36)$$

The tension $n(\gamma^-, t)$ is unknown and we now invoke the jump conditions (2.29) at the heap:

$$\begin{aligned} n(\gamma^-, t) - \rho_0 \dot{u}^2 &= \mathbf{F}_\gamma \cdot \mathbf{E}_2, \\ \frac{\rho_0}{2} \dot{u}^2 - n(\gamma^-, t) &= B_\gamma, \end{aligned} \quad (2.37)$$

where we used the substitution $C(\gamma^-, t) = -\frac{\rho_0}{2} \dot{u}^2 - n(\gamma^-, t)$.

To proceed with the classic formulation, we assume that the heap does not exert a force on the string:

$$\mathbf{F}_\gamma = \mathbf{0}. \quad (2.38)$$

Whence, the tension $n(\gamma^-, t)$ along with the supplies B_γ and Φ_{E_γ} are

$$\begin{aligned} n(\gamma^-, t) &= \rho_0 \dot{u}^2, \\ B_\gamma &= \frac{\rho_0}{2} \dot{u}^2 - n(\gamma^-, t) = -\frac{\rho_0}{2} \dot{u}^2, \\ \Phi_{E_\gamma} &= \mathbf{F}_\gamma \cdot \mathbf{v}_\gamma + B_\gamma \dot{\gamma} = -\frac{\rho_0}{2} \dot{u}^3. \end{aligned} \quad (2.39)$$

We used the identity (2.23)₂ to establish the result for Φ_{E_γ} . A graphical summary of the singular supplies acting on the chain is presented in Figure 2.7(b).

As an alternative to the classic formulation, we assume that the material momentum supply acting at $\xi = \gamma$ is

$$\mathbf{B}_\gamma = -2e\rho_0\gamma^2 \frac{\dot{\gamma}}{|\dot{\gamma}|}, \quad (2.40)$$

where e is a constant which is determined by experiment. With this prescription for \mathbf{B}_γ , along with the assumption that $\dot{\gamma} = \dot{u} > 0$, we find from Eqns. (2.37) and (2.23)₂ that

$$\begin{aligned} n(\gamma^-, t) &= \frac{\rho_0}{2} (1 + 4e) \dot{u}^2, \\ \mathbf{F}_\gamma &= -\frac{\rho_0}{2} (1 - 4e) \dot{u}^2 \mathbf{E}_2, \\ \Phi_{\mathbf{E}_\gamma} &= -2e\rho_0 \dot{u}^3. \end{aligned} \quad (2.41)$$

If we set $e = 0.25$, then we will recover the classic formulation.

Now that $n(\gamma^-, t)$ has been determined in terms of \dot{u} , we are in a position to combine Eqns. (2.36) and (2.41)₁ to arrive at a differential equation for $\gamma(t) = u(t)$:

$$\frac{\rho_0}{2} (1 + 4e) \dot{u}^2 + \rho_0 u (\ddot{u} - g) = 0. \quad (2.42)$$

When $e = 0.25$, this equation is identical to the differential equation (2.31) established by Cayley. We can non-dimensionalize the differential equation (2.42) by defining a dimensionless time τ and a dimensionless variable $x = x(\tau)$:

$$x = \frac{u}{\ell_0}, \quad \tau = \sqrt{\frac{g}{\ell_0}} t. \quad (2.43)$$

The dimensionless equation is

$$x \frac{d^2x}{d\tau^2} + \frac{1}{2} (1 + 4e) \frac{dx}{d\tau} \frac{dx}{d\tau} = x. \quad (2.44)$$

Observe that this equation has an equilibrium point when $(x, \frac{dx}{d\tau}) = (0, 0)$. However, this equilibrium point is unstable: an instability which manifests in the chain falling and the heap unraveling.

Restricting attention to the classic case $e = 0.25$, we use Eqn. (2.44) to construct the phase portrait for the ordinary differential equation (2.42) which is shown in Figure 2.8. What is interesting to observe from this portrait is the asymptotic behavior of $(u(t), \dot{u}(t))$ to the following exact solution of Eqn. (2.42)⁸:

$$u(t) = \frac{g}{6} t^2, \quad \dot{u}(t) = \frac{g}{3} t. \quad (2.45)$$

⁸ This solution was first determined by Cayley [53, Page 511] and is labeled c in Figure 2.8.

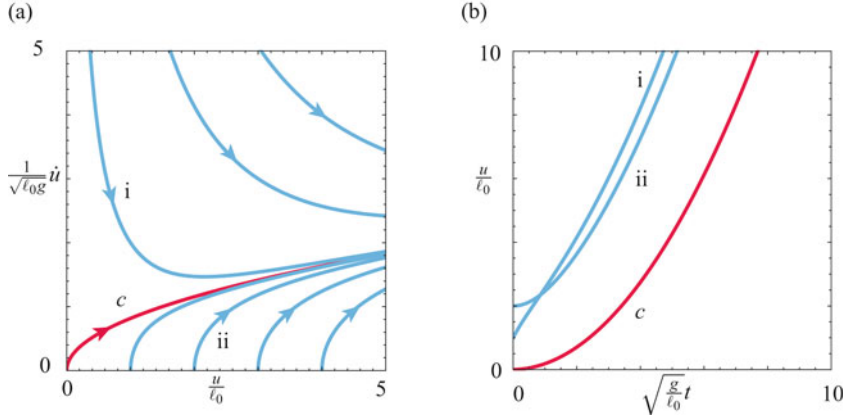


Fig. 2.8 (a) Phase portrait for the differential equation (2.42) governing $u(t) = \gamma(t)$ and (b) three representative solutions of (2.42). The solution labeled c corresponds to Cayley's exact solution (2.45). The arrows in (a) indicate the direction of increasing time t . For the solutions shown here, the parameter $e = 0.25$ in order to agree with Cayley's formulation.

This solution corresponds to a body falling freely under a gravitational force $g/3$ and asymptotes backwards in time to the equilibrium at the origin. Thus the chain falls slower than it would were it not attached to the heap. It is also interesting to return to Eqn. (2.39) and examine the asymptotic behavior of \mathbf{n} using Eqn. (2.45):

$$\begin{aligned} \mathbf{n}(\gamma^-, t) &= n(\gamma^-, t) \mathbf{E}_2 = \rho_0 \dot{u}^2 \mathbf{E}_2 \\ &= \frac{\rho_0}{9} g^2 t^2 \mathbf{E}_2 \\ &= \frac{2\rho_0 g}{3} u(t) \mathbf{E}_2. \end{aligned} \quad (2.46)$$

This tension is 33.3% less than its static counterpart for a string of the same length (i.e., $\rho_0 g u$).

We now revisit Eqn. (2.41) and examine the energy dissipated at the heap: $\Phi_{E_\gamma} = -2e\rho_0 \dot{u}^3$. Thus, the shock at the heap dissipates energy. To elaborate, let us examine an expression for the total energy of the string:

$$E = \frac{1}{2} \int_0^\gamma \rho_0 \mathbf{v} \cdot \mathbf{v} dy + \int_0^\gamma \rho_0 g \mathbf{E}_2 \cdot \mathbf{r} dy. \quad (2.47)$$

Substituting for $\mathbf{r} = y\mathbf{E}_2$ where $y \in (-\gamma, 0)$, $u = \gamma$, and $\mathbf{v} = -\dot{\gamma}\mathbf{E}_2$, we find that

$$E = \frac{\rho_0}{2} u \dot{u}^2 - \frac{\rho_0 g}{2} u^2. \quad (2.48)$$

Whence, with the help of the equation of motion (2.42) and our earlier result Eqn. (2.41)₃ for Φ_{E_γ} ,

$$\begin{aligned}
\dot{E} &= \rho_0 \dot{u} \left(\frac{\dot{u}^2}{2} + u \ddot{u} - g u \right) \\
&= -2e \rho_0 \dot{u}^3 \\
&= \Phi_{E_\gamma}.
\end{aligned} \tag{2.49}$$

Thus $\dot{E} = \Phi_{E_\gamma}$, and, so, assuming $e > 0$, $\Phi_{E_\gamma} < 0$ and E decreases in time. It is initially puzzling that the shock at the heap should be dissipative. However, it should be emphasized that this dissipation is responsible for the chain's retarded rate of fall that we mentioned earlier.

The dissipation present in Cayley's model has not been universally adopted. Some of the controversy can be attributed to the (far from transparent) manner in which Cayley's equation of motion (2.31) was established by him in [53]. The remainder of the controversy stems from the belief by some authors⁹ that this problem should conserve energy. As shall be shown in Exercise 2.1, for the string's motion to conserve energy, the tension in the string reduces by 50% compared to the dissipative case we have just considered and a nonzero force $\mathbf{F}_\gamma = -\frac{\rho_0}{2} \dot{u}^2 \mathbf{E}_2$ is needed to push down on the chain at the point where it leaves the heap. In contrast, for the dissipative case we have just considered when $e = 0.25$, we found that $\mathbf{F}_\gamma = \mathbf{0}$ (cf. Eqn. (2.38)).

2.5 A Chain of Finite Length Falling off the Edge of a Table

The previous example's dynamics are complicated by the heap of chain that serves as a reservoir. As a result, it is interesting to consider a closely related classic problem discussed in a marvelous dynamics text from 1929 by Horace Lamb (1849–1934) (see [193, Section 49]). As shown in Figure 2.9, we consider a homogeneous inextensible string of length ℓ . At the end labeled $\xi = 0$, a particle of mass m is attached. Initially, the particle is placed over the edge of the table, and proceeds to fall under gravity, pulling the string along with it. Eventually, the end $\xi = \ell$ falls off the edge of the table. Assuming that the surface of the table is smooth, we now discuss how to establish and analyze a differential equation governing the motion of the string.

To proceed we note that a discontinuity is present where the string moves over the edge of the table. At this point, which we label by $\xi = \gamma$, a reaction force \mathbf{F}_γ is exerted on the string. Further, $\mathbf{v}_\gamma = \mathbf{0}$, $\mathbf{r}'(\gamma^-, t) = \mathbf{E}_2$, and $\mathbf{r}'(\gamma^+, t) = -\mathbf{E}_1$. Using the definition of \mathbf{v}_γ , we find that

$$\mathbf{v}(\gamma^-, t) = -\dot{\gamma} \mathbf{E}_2, \quad \mathbf{v}(\gamma^+, t) = \dot{\gamma} \mathbf{E}_1. \tag{2.50}$$

As a consequence, the velocity vector of the particle of mass m is $\mathbf{v}_0 = -\dot{\gamma} \mathbf{E}_2$.

⁹ See [142, 366, 367] for the relevant citations.

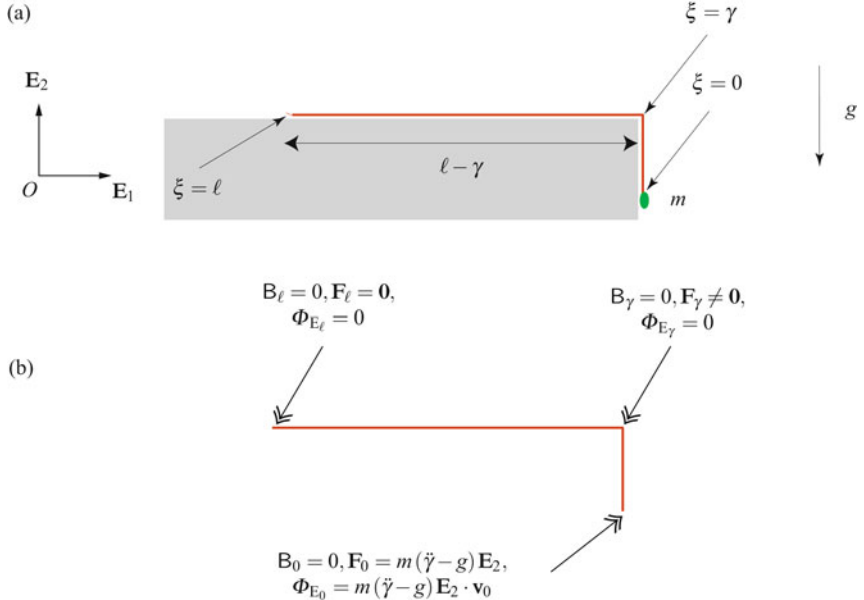


Fig. 2.9 Schematic of an inextensible string of length ℓ which is falling off the edge of a smooth horizontal table. (a) Geometric parameters of the system and (b) schematic of the singular supplies at the points $\xi = 0$, $\xi = \gamma$, and $\xi = \ell$.

To establish the boundary condition at the particle of mass m , we denote the force acting on the particle by $-\mathbf{F}_0$ and the corresponding force acting on the string at $\xi = 0$ by \mathbf{F}_0 . Thus, for the particle of mass m ,

$$-m\ddot{\gamma}\mathbf{E}_2 = -mg\mathbf{E}_2 - \mathbf{F}_0. \quad (2.51)$$

We can use this balance to determine \mathbf{F}_0 and then invoke Eqn. (2.27)₁ to find that

$$\mathbf{n}(0^+, t) = -m(\ddot{\gamma} - g)\mathbf{E}_2. \quad (2.52)$$

Now, integrating the local form of the balance of linear momentum with $\rho_0\mathbf{f} = -\rho_0 g\mathbf{E}_2$ for the hanging section of the chain, we find that

$$\begin{aligned} \mathbf{n}(\gamma^-, t) &= \mathbf{n}(0^+, t) - \rho_0\gamma(\ddot{\gamma} - g)\mathbf{E}_2 \\ &= -(m + \rho_0\gamma)(\ddot{\gamma} - g)\mathbf{E}_2. \end{aligned} \quad (2.53)$$

Notice that we used Eqn. (2.52) to establish the final expression above.

For the portion of the string in contact with the table $\rho_0\mathbf{f} = (N - \rho_0 g)\mathbf{E}_2$, where N is the normal force (per unit length of ξ) exerted by the table on the lateral surface of the string. Here, the assigned force $\rho_0\mathbf{f}$ is perpendicular to the tension \mathbf{n} in the

string. Integrating the local form of the balance of linear momentum, and noting that $\mathbf{n}(\ell, t) = \mathbf{0}$, we find that

$$\mathbf{n}(\gamma^+, t) = -\rho_0(\ell - \gamma)\dot{\gamma}\mathbf{E}_1. \quad (2.54)$$

We have now completed assembling the pieces needed to solve the problem.

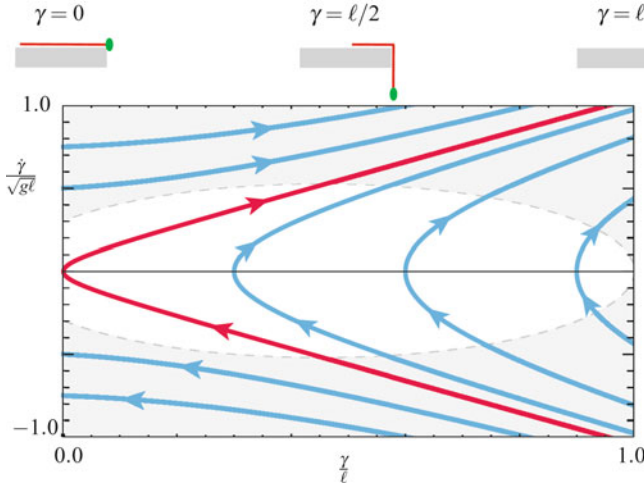


Fig. 2.10 Phase portrait of the solutions to the differential equation (2.58). When $\dot{\gamma} < 0$, the particle of mass m moves upwards, and, for some of the solutions shown in this portrait, can eventually reach the same level as the horizontal surface. The trajectories where $\dot{\gamma} > 0$ show that the string will eventually fall off the table. The shaded region in the figure corresponds to the physically unrealistic situation where $F_\gamma < 0$ (cf. Eqn. (2.61)). For the solutions shown in this figure, $\frac{m}{\rho_0\ell} = 0.1$.

The unknowns in this problem are the reaction force \mathbf{F}_γ at $\xi = \gamma$, the material momentum supply B_γ at $\xi = \gamma$ and $\gamma(t)$. Using the identity

$$\Phi_{E_\gamma} = B_\gamma \dot{\gamma} + \mathbf{F}_\gamma \cdot \mathbf{v}_\gamma, \quad (2.55)$$

and assuming that the discontinuity at $\xi = \gamma$ does not dissipate energy (i.e., $\Phi_{E_\gamma} = 0$), we find that $B_\gamma = 0$. We then use the jump condition from the balance of linear momentum to compute \mathbf{F}_γ :

$$\begin{aligned} \mathbf{F}_\gamma &= \mathbf{n}(\gamma^-, t) + \rho_0 \dot{\gamma} \mathbf{v}(\gamma^-, t) - \mathbf{n}(\gamma^+, t) - \rho_0 \dot{\gamma} \mathbf{v}(\gamma^+, t) \\ &= (\rho_0(\ell - \gamma)\dot{\gamma} - \rho_0\dot{\gamma}^2) \mathbf{E}_1 - ((m + \rho_0\gamma)(\dot{\gamma} - g) + \rho_0\dot{\gamma}^2) \mathbf{E}_2. \end{aligned} \quad (2.56)$$

The final equation of interest is obtained from the jump condition for the balance of material momentum at $\xi = \gamma$: $[\![P\dot{\gamma} + C]\!]_\gamma + B_\gamma = 0$. For this problem, this equation reduces to

$$[[\mathbf{n} \cdot \mathbf{r}']]_\gamma = 0. \quad (2.57)$$

That is, the tension $n = \mathbf{n} \cdot \mathbf{e}_t$ in the string is unaltered by the discontinuity. Substituting into Eqn. (2.57) from Eqns. (2.53) and (2.54), we find a differential equation for $\gamma(t)$:

$$\ddot{\gamma} = \left(\frac{m + \rho_0 \gamma}{m + \rho_0 \ell} \right) g. \quad (2.58)$$

Observe that $m + \rho_0 \gamma$ is the mass of the string over the edge of the table, while $m + \rho_0 \ell$ is the total mass of the string. Thus as $\gamma \rightarrow \ell$, the acceleration of m approaches g .

A phase portrait of the differential equation (2.58) is shown in Figure 2.10. Some of the solutions shown in this portrait correspond to m initially moving upwards and then moving down, and others correspond to m eventually reaching the surface of the table (when $\gamma = 0$). The solutions of particular interest arise when $\gamma > 0$ and the particle is released from rest. It is easy to see from Figure 2.10 that these solutions result in $\gamma \rightarrow \ell$ in a finite time. This behavior is also evident from the analytical expression for the solution to the differential equation (2.58). This solution can be found using standard methods and provides $\gamma(t)$:

$$\gamma(t) = (\cosh(\alpha t) - 1)\varepsilon + \gamma(0) \cosh(\alpha t) + \left(\frac{\sinh(\alpha t)}{\alpha} \right) \dot{\gamma}(0), \quad (2.59)$$

where

$$\alpha = \sqrt{\frac{g}{1 + \varepsilon}}, \quad \varepsilon = \frac{m}{\rho_0 \ell}. \quad (2.60)$$

The analytical expression for $\gamma(t)$ can be used to determine $\mathbf{n}(\xi, t)$ and \mathbf{F}_γ . In particular,

$$\mathbf{F}_\gamma = F_\gamma (\mathbf{E}_1 + \mathbf{E}_2), \quad (2.61)$$

where

$$F_\gamma = \left(\frac{m + \rho_0 \gamma}{m + \rho_0 \ell} \right) \rho_0 (\ell - \gamma) g - \rho_0 \dot{\gamma}^2. \quad (2.62)$$

Observe from this expression that as the string falls off the table, the inertial term $\rho_0 \dot{\gamma}^2$ will dominate and the possibility of a physically meaningless \mathbf{F}_γ will arise.¹⁰ That is, $F_\gamma < 0$. This is the shaded region in the phase portrait shown in Figure 2.10. When $F_\gamma < 0$, we suspect that the contact condition at the end of the table is invalid. Indeed, an experimental demonstration of the loss of contact can be seen in the recent work by Cambou et al. [45]. As discussed in the recent work by Brun et al. [38], a similar lift off phenomenon occurs in a chain moving over a pulley.

Setting $m = 0$ in Eqn. (2.58), we find the differential equation established by Lamb for this problem (see [193, Section 49]). He did not use a balance of material momentum, rather he argued that the tension in the string was unaltered by the discontinuity. As we have seen, this is equivalent to using the jump condition $[\![P\dot{\gamma} + C]\!]_\gamma + B_\gamma = 0$. In consonance with our assumption that $\Phi_{E_\gamma} = 0$, the total energy of the string is conserved for this problem.

¹⁰ I am most grateful to James Hanna for pointing this out.

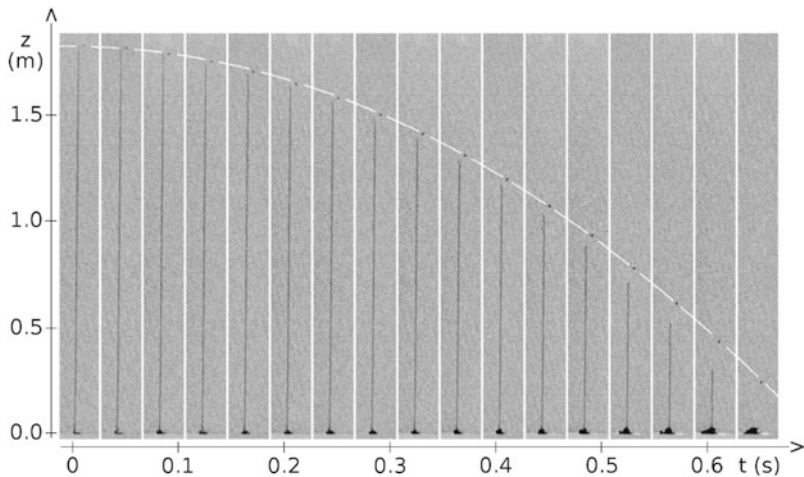


Fig. 2.11 Time lapse images of a chain falling into a heap demonstrating that the top segment of the chain is falling faster than a freely falling particle. Image courtesy of Luis Hamm and Jean-Christophe Géminard.

2.6 “Chains that Suck”

For our third example, we consider the problem of a section of string that is falling into a heap on a horizontal surface (cf. Figures 2.2(b), 2.11 and 2.12). This classic problem is discussed in some textbooks, such as [174, Problem 17, Page 252], [193, Exercise 4, Page 149], and [236, Ex. 536], and is interesting for several reasons. First, if one assumes that the chain is in free fall (i.e., accelerating at a rate of g), then the weight of the chain recorded by a weighing scale located under the heap will asymptote to three times the weight of the chain.¹¹ However, recent experiments by Hamm and Géminard [151] show that the chain actually falls faster than a free falling particle and the (dynamic) weight measured can be much higher than a factor of three times the weight of the chain. Their results on free fall are shown in Figure 2.11.

We call the problems of interest here “chains that suck” following Andy Ruina who noted that these chains appear to be sucked into the heap (cf. [142]). Referring to Figure 2.13(a), the explanation for this phenomenon in [142] is as follows: The links of the chains can be considered as pin-jointed rigid bodies. When one end of the rigid body collides with the ground, the reaction force at the contact point

¹¹ Problem 17 on Page 252 of Jeans’ textbook [174] is reproduced in Exercise 2.5 at the end of this chapter.

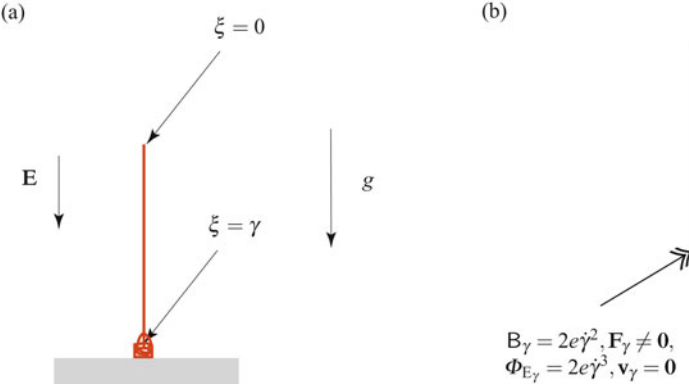


Fig. 2.12 A string falling under gravity into a stationary heap. (a) Schematic of the string and (b) schematic of the supplies at the shock $\xi = \gamma$. Referring to Eqn. (2.67), it will be shown that $F_\gamma = -\frac{\rho_0}{2} \left(1 - 4e\frac{\dot{\gamma}}{|\dot{\gamma}|}\right) \dot{\gamma}^2 E$.

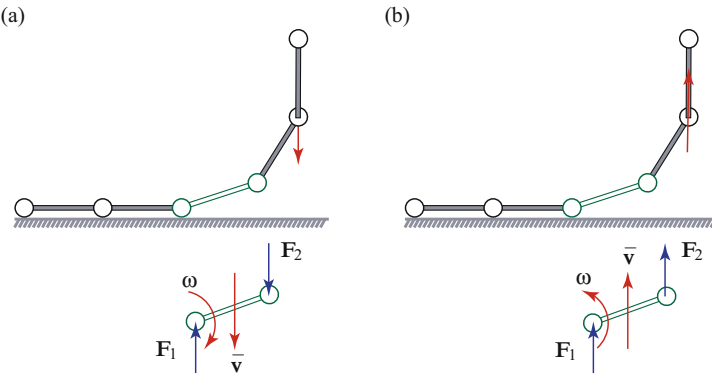


Fig. 2.13 Multi-rigid body dynamics models of chains that are used by Biggins [23] and Grewal et al. [142] to explain the anomalous behavior of chains. (a) A chain falling onto a horizontal surface. The presence of the reaction force F_1 manifests in the chain segment developing a clockwise angular acceleration ω which increases the acceleration \bar{v} of its center of mass. (b) A chain being pulled from a horizontal surface. The reaction force F_1 is synonymous with a heap of stationary chain segments apparently pushing the chain segment upward.

produces a moment on the body which gives the body an angular acceleration $\dot{\omega}$ and results in the body pulling its pin-jointed neighbor downwards.¹² As noted by

¹² We use the symbol ω to denote the angular velocity of a rigid body in this discussion. It should not be confused with the same symbol for the velocity ω that appears in later chapters and is associated with a set of directors.

Biggins [23], the opposite effect happens when the chain is being raised out of a heap and the heap appears to push the chain upwards (cf. Figure 2.13(b)).¹³

We follow the methods used in the two previous systems to establish the equations governing the motion of the falling string and start by presenting some kinematical preliminaries. The string, which has a length ℓ , is suspended above a horizontal surface and released from rest. The string falls vertically onto the surface and collects in a heap. We assume that the heap is quiescent and label the point of the string where the transition from free falling motion to rest occurs by $\xi = \gamma$.

It is straightforward to show that

$$\mathbf{v}^- = -\dot{\gamma}\mathbf{E}, \quad (2.63)$$

where $\mathbf{r}' = \mathbf{E}$ is a unit vector which also is parallel to the gravitational force on the string. The balance of linear momentum for the string (2.21)₁ where $\rho_0\mathbf{f} = \rho_0 g\mathbf{E}$ and $\rho_0\mathbf{v} = -\rho_0\dot{\gamma}\mathbf{E}$ can be integrated to find the tension in the string:

$$\mathbf{n}(\gamma^-, t) = n(\gamma^-, t)\mathbf{E} = \mathbf{n}(0, t) - \rho_0\gamma(\dot{\gamma} + g)\mathbf{E}. \quad (2.64)$$

In the sequel, we shall assume that there is no external applied force at $\xi = 0$, so $\mathbf{n}(0, t) = \mathbf{0}$.

We appeal to the jump conditions (2.29) established earlier to find that

$$\begin{aligned} (n(\gamma^-, t) - \rho_0\dot{\gamma}^2)\mathbf{E} &= \mathbf{F}_\gamma, \\ \frac{\rho_0}{2}\dot{\gamma}^2 - n(\gamma^-, t) &= \mathbf{B}_\gamma. \end{aligned} \quad (2.65)$$

To determine $\gamma(t)$, we now need to prescribe either \mathbf{F}_γ or \mathbf{B}_γ . We shall assume that the process by which the string's motion ceases when $\xi = \gamma$ is one where energy is dissipated and prescribe¹⁴

$$\mathbf{B}_\gamma = -2e\rho_0\dot{\gamma}^2 \frac{\dot{\gamma}}{|\dot{\gamma}|}. \quad (2.66)$$

Here, e is a constant and the presence of the term $\frac{\dot{\gamma}}{|\dot{\gamma}|}$ is needed to ensure that this prescription for \mathbf{B}_γ is independent of our parameterization of the string. That is, this prescription is valid whether we label the end point of the string $\xi = 0$ (as we have done here) or $\xi = \ell$. As a result of the prescription for \mathbf{B}_γ , Eqn. (2.65) now yields an equation for $n(\gamma^-, t)$ and \mathbf{F}_γ :

$$\begin{aligned} n(\gamma^-, t) &= \frac{\rho_0}{2} \left(1 + 4e \frac{\dot{\gamma}}{|\dot{\gamma}|} \right) \dot{\gamma}^2, \\ \mathbf{F}_\gamma &= -\frac{\rho_0}{2} \left(1 - 4e \frac{\dot{\gamma}}{|\dot{\gamma}|} \right) \dot{\gamma}^2 \mathbf{E}. \end{aligned} \quad (2.67)$$

¹³ For additional commentary, including slow-motion videos of chain fountains and falling chains, on these works see [114] and Ruina's website <http://ruina.mae.cornell.edu/>.

¹⁴ This prescription is identical to the one we used earlier with Cayley's problem (cf. Eqn. (2.40)).

As summarized in Figure 2.12(b), the dissipation produced at $\xi = \gamma$ can be computed from the identity $\Phi_{E_\gamma} = B_\gamma \dot{\gamma} + \mathbf{F}_\gamma \cdot \mathbf{v}_\gamma$ where $\mathbf{v}_\gamma = \mathbf{0}$:

$$\Phi_{E_\gamma} = -2e\rho_0 |\dot{\gamma}^3|. \quad (2.68)$$

In this problem, $\dot{\gamma} < 0$, so setting $e > 0$ means that the shock at $\xi = \gamma$ will dissipate energy while setting $e = 0$ implies that energy will be conserved there. The parameter e must be determined from experiments.

Having determined that $n(\gamma^-, t) = \frac{\rho_0}{2} \left(1 + 4e \frac{\dot{\gamma}}{|\dot{\gamma}|}\right) \dot{\gamma}^2$, the governing equation for $\gamma(t)$ with $\dot{\gamma} < 0$ now follows from Eqn. (2.64):

$$\rho_0 \gamma (\ddot{\gamma} + g) + \frac{\rho_0}{2} (1 - 4e) \dot{\gamma}^2 = 0. \quad (2.69)$$

This equation has been established previously in a variety of manners (cf. [142, 151, 356]).¹⁵ It is interesting to note that if $e = \frac{1}{4}$, then $\ddot{\gamma} = -g$ and so the string would be in free fall. On the other hand, if $e = 0$, then energy is conserved during the impact process of the string with the heap.

Returning to the weighting scale, we note that the weight W recorded by a scale placed under the heap corresponds to the sum of the force $-\mathbf{F}_\gamma \cdot \mathbf{E}$ and the weight of the quiescent chain. An expression can be found for this dynamic weight:

$$W(t) = \frac{\rho_0}{2} (1 + 4e) \dot{\gamma}^2 + (\ell - \gamma) \rho_0 g. \quad (2.70)$$

In principle, and if the model is adequate, then by measuring $W(t)$ and $\gamma(t)$, the parameter e can be determined. Indeed, Hamm and Géminard [151] performed experiments on a falling chain and established a value of $4e = 0.83$ for a particular chain falling onto a variety of horizontal surfaces.

The free-falling case, which as noted by Grewal et al. [142], is discussed in several textbooks, corresponds to the assumption that $e = 0.25$. In this case, Eqns. (2.64) and (2.67) can be used to show that the string is slack and find an interesting expression for \mathbf{F}_γ :

$$\mathbf{n}(\xi, t) = \mathbf{0}, \quad \mathbf{F}_\gamma = -\rho_0 \dot{\gamma}^2 \mathbf{E}. \quad (2.71)$$

That is, the heap pushes up on the string at the point $\xi = \gamma$ where the string impacts the heap. Assuming that the string is released from rest, we can determine $\gamma(t)$, the time T when $\gamma(T^-) = 0$, and $W(t)$:

$$\gamma(t) = \ell - \frac{g}{2} t^2, \quad T = \sqrt{\frac{2\ell}{g}}, \quad \frac{W(t)}{\rho_0 g \ell} = \frac{3g}{2\ell} t^2. \quad (2.72)$$

¹⁵ For instance, Eqn. (2.65) is equivalent to the governing equation for the same problem established by Virga in [356, Eqn. (5.10)] with $(\frac{1}{2} - 2e, \gamma)$ identified with his $(1 - f, y)$. The same differential equation is also equivalent to Grewal et al.’s work with $(\dot{\gamma}, \gamma)$ identified with their $(-v = -\dot{x}, L - x)$ and $e = \frac{1}{6}$ for [142, Eqn. (18)] and $e = 0$ for [142, Eqn. (19)]. Finally, Eqn. (2.65) is equivalent to [151, Eqn. (5)] with $(\frac{1}{2} - 2e, \gamma)$ identified with their $(1 - \gamma, y)$.

Thus, $W(T^-)$ is three times the weight $\rho_0 g \ell$ of the string.

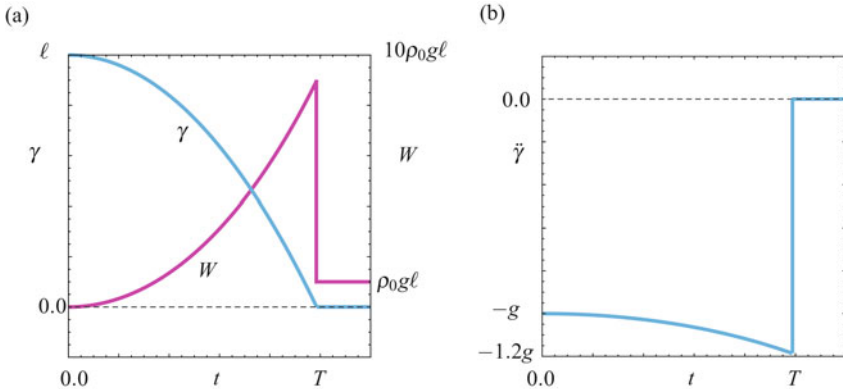


Fig. 2.14 Simulation results for the chain falling into a heap governed by the differential equation (2.69). (a) Results for $\gamma(t)$ and $W(t)$ and (b) the normalized acceleration $\dot{\gamma}(t)$. For the results shown, $\gamma(0) = \ell$, $\dot{\gamma}(0) = 0$, $4e = 0.83$, $T = \sqrt{\frac{2\ell}{g}}$, and it takes $0.98589T$ seconds for the top of the chain (labeled $\xi = 0$) to reach the heap.

However, as shown in the experiments by Hamm and Géminard [151], e is not necessarily 0.25 and the string can fall faster than a free-falling particle. To see these results, let us now use their experimental value of $4e = 0.83$. We dimension the time t using the free-fall time for a particle $T = \sqrt{\frac{2\ell}{g}}$, $t = T\tau$. Additionally, the variable γ is non-dimensionalized using the length ℓ : $\ell u = \gamma$. After integrating the differential equation (2.69) and evaluating $W(t)$ and $\dot{\gamma}$ using the resulting expressions for $\gamma(t)$, we find that the string falls slightly faster than a free-falling particle. Referring the reader to Figure 2.14, the time taken between the release of the tip $\xi = 0$ of the chain and the time it lies at rest on the heap is $0.98589T$. We also observe from this figure that the tip of the chain is accelerating (slightly) faster than gravity. While the difference in time of flight is arguable imperceptible to the naked eye, the same cannot be said of the weight $W(t)$. With the help of Eqn. (2.70), we find that the largest weight recorded by the scale is $W(T^-) = 8.9789$ times the weight of the chain!

2.7 The Falling Folded Chain

For our next example, we consider the string of length ℓ shown here in Figure 2.15 (and earlier in Figure 1.9(a)). One end of the string is fixed at a point which we conveniently take to be the origin, $\mathbf{r}(\xi = 0, t) = \mathbf{0}$. The other end of the string is attached to a particle of mass m which is acted upon by a force $-P_0 \mathbf{E}$. An applied

force $\rho_0 \mathbf{f} = \rho_0 g \mathbf{E}$ acts on the string. The interesting feature of this problem is the fold at $\xi = \gamma$. The question we ask is as follows: If the particle is released from rest, then what is the velocity and position of the particle as it falls?

Our presentation of this classic problem follows [277]. We modify their treatment to incorporate the notion of material momentum in this problem that was noted in [264]. Other relevant works on this problem include the treatment by Augustus E. H. Love (1863–1940) in [212] and the (more recent) papers by Reeken [297] and Hans Troger (1943–2010) and his coworkers [315, 331].

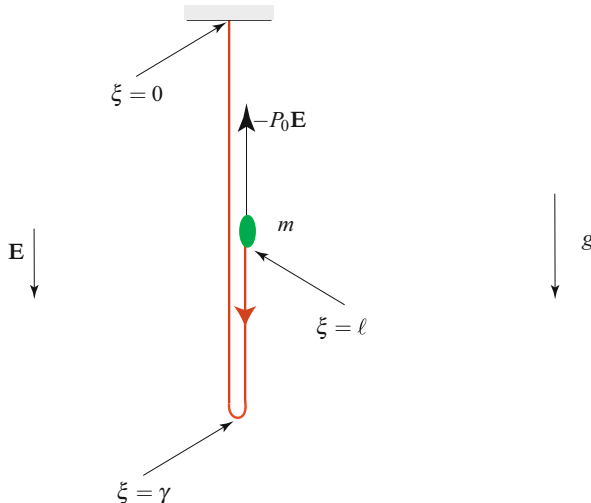


Fig. 2.15 Graphical representation of a heavy inextensible string (also known as a cable) of length ℓ with a fold located at a point $\xi = \gamma$ below the point of support. At the other end of the cable, a mass particle of mass m is attached and an applied force $-P_0 \mathbf{E}$ acts on this particle where \mathbf{E} is a unit vector in the direction of gravity.

As the chain is at rest for $\xi \in [0, \gamma^-)$ and $\mathbf{e}_t = \pm \mathbf{E}$, the following results hold:

$$\mathbf{v}(\gamma^-, t) = \mathbf{0}, \quad \mathbf{v}(\gamma^+, t) = 2\dot{\gamma}\mathbf{E}, \quad \mathbf{v}_\gamma = \dot{\gamma}\mathbf{E}. \quad (2.73)$$

It is important to note the dramatic change in velocity that occurs at $\xi = \gamma$.

Referring to Figure 2.16, at the end of the chain, we can use the jump condition $[\mathbf{n} + \rho_0 \dot{\ell} \mathbf{v}]_\ell + \mathbf{F}_\ell = \mathbf{0}$ where $\dot{\ell} = 0$ to compute the boundary condition. First, we consider a balance of linear momentum for the particle of mass m attached to the end $\xi = \ell$ of the chain:

$$-P_0 \mathbf{E} + mg \mathbf{E} - \mathbf{F}_\ell = m \ddot{\mathbf{r}}(\ell, t). \quad (2.74)$$

As $\mathbf{v}(\ell^-, t) = 2\dot{\gamma}\mathbf{E}$, we find that

$$\mathbf{F}_\ell = -(2m\ddot{\gamma} + (P_0 - mg)) \mathbf{E}. \quad (2.75)$$

Now at the end $\xi = \ell$ of the string, we have the jump condition

$$-\mathbf{n}(\ell^-, t) + \mathbf{F}_\ell = \mathbf{0}. \quad (2.76)$$

Consequently, dropping the $-$ ornamenting the ℓ and rearranging,

$$\mathbf{n}(\ell, t) = -(2m\ddot{\gamma} - mg + P_0)\mathbf{E}. \quad (2.77)$$

In interpreting this result, it is important to note that for the moving section of chain $\mathbf{r}'(\xi, t) = -\mathbf{E}$.

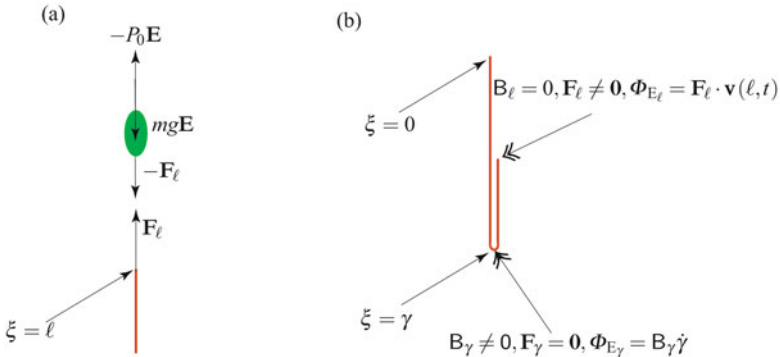


Fig. 2.16 Graphical representation of the forces acting at certain locations for the free-falling folded string problem. In (a), the particle of mass m is shown and in (b) the singular supplies acting at the points $\xi = \gamma$ and $\xi = \ell$ are shown.

Noting that an applied body force $\rho_0 g \mathbf{E}$ acts on the chain, integrating the balance of linear momentum (2.21) on the intervals $\xi \in (0, \gamma^-)$ and $\xi \in (\gamma^+, \ell)$, and then using (2.77), we find that

$$\begin{aligned} \mathbf{n}(0, t) &= \mathbf{n}(\gamma^-, t) + \rho_0 g \gamma \mathbf{E}, \\ \mathbf{n}(\gamma^+, t) &= -(P_0 + (m + \rho_0(\ell - \gamma))(2\dot{\gamma} - g))\mathbf{E}. \end{aligned} \quad (2.78)$$

The jump in \mathbf{n} across the fold can be computed using the jump condition $[\mathbf{n} + \rho_0 \dot{\gamma} \mathbf{v}]_\gamma + \mathbf{F}_\gamma = \mathbf{0}$. In this case $\mathbf{F}_\gamma = \mathbf{0}$, and so

$$\mathbf{n}(\gamma^-, t) = \mathbf{n}(\gamma^+, t) + 2\rho_0 \dot{\gamma}^2 \mathbf{E}. \quad (2.79)$$

The equations (2.78) and (2.79) enable us to compute $\mathbf{n}(\xi, t)$ once $\gamma(t)$ is known.

The most interesting part of this problem is to provide prescriptions for Φ_{E_γ} and B_γ at the fold. As pointed out by Love [212] in 1897, “energy is dissipated in the impulsive action at the place where the discontinuous change of motion occurs.”

He then proceeded with a semi-inverse solution where he assumed that $\mathbf{n}(\gamma^-, t) = \mathbf{0}$ to show that, in our notation,

$$\Phi_{E_\gamma} = -2\rho_0\dot{\gamma}^3. \quad (2.80)$$

To see how he arrived at this result, we start with the jump condition (1.86)₅, the results (2.73), and assume that $\mathbf{n}(\gamma^-, t) = \mathbf{0}$ in (2.79). In this case, the following set of identities hold:

$$\mathbf{n}(\gamma^+, t) = -2\rho_0\dot{\gamma}^2\mathbf{E}, \quad (2.81)$$

and

$$\begin{aligned} \Phi_{E_\gamma} &= -[\mathbf{n} \cdot \mathbf{v}]_\gamma - \left[\left[\rho_0\psi + \frac{1}{2}\rho_0\mathbf{v} \cdot \mathbf{v} \right] \right]_\gamma \dot{\gamma} \\ &= -\frac{1}{2}\rho_0(\mathbf{v}^+ \cdot \mathbf{v}^+) \dot{\gamma} \\ &= -2\rho_0\dot{\gamma}^3. \end{aligned} \quad (2.82)$$

As was recently pointed out in [331], some formulations of this problem erroneously set $\Phi_{E_\gamma} = 0$ thereby ignoring the dissipation of energy that occurs at the fold.¹⁶ With the help of the identity $\Phi_{E_\gamma} = B_\gamma\dot{\gamma} + \mathbf{F}_\gamma \cdot \mathbf{v}_\gamma$, we see that the corresponding prescription for B_γ is

$$B_\gamma = -2\rho_0\dot{\gamma}^2. \quad (2.83)$$

We shall shortly choose more general prescriptions for Φ_{E_γ} and B_γ than those implied by Love's analysis. Our motivation for doing so is two-fold. First, it enables us to incorporate experimental results which suggest in related problems that (2.80) is too restrictive. Second, the generalization allows us to readily compare Love's formulation to the energy-conserving formulations.

It remains to compute $\gamma(t)$ and the jump condition from the balance of material momentum (i.e., Eqn. (2.22)) provides the differential equation for this quantity once B_γ has been prescribed. For the present purposes, we generalize the prescription provided by Love's analysis to¹⁷

$$B_\gamma = -2e\rho_0\dot{\gamma}^2 \left(\frac{\dot{\gamma}}{|\dot{\gamma}|} \right), \quad (2.84)$$

where e is a constant. The constant $e = 1.0$ for Love's analysis in [212] of this problem that we previously discussed. Because \mathbf{F}_γ is zero at the fold, the prescription (2.84) for B_γ implies that

¹⁶ See, for example, [150, 189, 304].

¹⁷ This prescription is identical to the prescriptions (2.40) and (2.66) for B_γ that were used in Sections 2.4 and 2.6, respectively. As with these prescriptions, observe that the prescription (2.84) accommodates cases where $\dot{\gamma} < 0$.

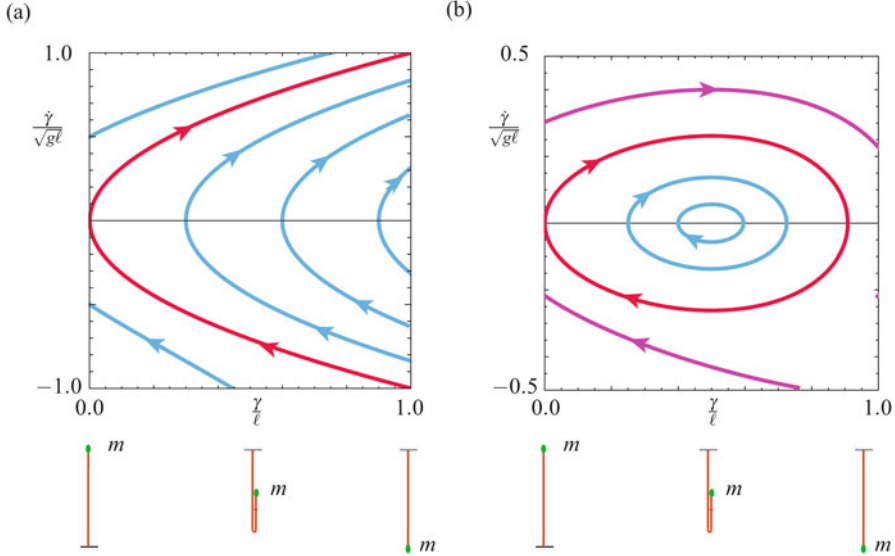


Fig. 2.17 Phase portraits of the solutions to (2.89). When $\dot{\gamma} < 0$, the particle of mass m moves upwards. For some of the trajectories shown in these portraits $\gamma \rightarrow 0$, which implies that the string will become completely vertical. For the solutions shown in this figure, $\frac{m}{\rho_0 \ell} = 1.0$ and $e = 1.0$. For (a) $\frac{P_0}{\rho_0 g \ell} = 0$ and for (b) $\frac{P_0}{\rho_0 g \ell} = 1.5$. The equilibrium in (b) corresponds to the static configuration where the applied force P_0 balances the combined weight of the particle and a length of the string.

$$\begin{aligned}\Phi_{E_\gamma} &= B_\gamma \dot{\gamma} \\ &= -2e\rho_0 |\dot{\gamma}|^3.\end{aligned}\quad (2.85)$$

Thus, if $e > 0$, the fold will dissipate energy. We now start with Eqn. (2.22):

$$C(\gamma^+, t) + \dot{\gamma}P(\gamma^+, t) - C(\gamma^-, t) - \dot{\gamma}P(\gamma^-, t) + B_\gamma = 0. \quad (2.86)$$

Substituting for C and P yields an intermediate result:

$$-n(\gamma^+, t) + n(\gamma^-, t) + B_\gamma = 0. \quad (2.87)$$

We next use (2.79) to eliminate $n(\gamma^-, t)$:

$$2\rho_0 \dot{\gamma}^2 - 2n(\gamma^+, t) + B_\gamma = 0. \quad (2.88)$$

Finally, we use Eqn. (2.78)₂ and the prescription (2.84) for B_γ to find the desired differential equation for $\gamma(t)$:

$$(m + \rho_0(\ell - \gamma))(2\ddot{\gamma} - g) = -P_0 + \rho_0 \dot{\gamma}^2 \left(1 - e \frac{\dot{\gamma}}{|\dot{\gamma}|}\right). \quad (2.89)$$

Given a pair of initial conditions $\dot{\gamma}(0)$ and $\gamma(0)$, this equation can be integrated to determine $\gamma(t)$.

It is interesting to note from Eqn. (2.89) that if P_0 is sufficiently large then the string has a static equilibrium $(\gamma, \dot{\gamma}) = (\gamma_0, 0)$ where $\gamma_0 = \ell - \left(\frac{P_0 - mg}{\rho_0 g}\right)$. A representative sample of the solutions of (2.89) when $P_0 \neq 0$ is shown in Figure 2.17(b). Observe that in addition to the solutions where $\gamma(t) \rightarrow 1$, we also find solutions $\gamma(t)$ which are periodic and oscillate back and forth about the equilibrium point $(\gamma_0, 0)$. This is in stark contrast to the case where $P_0 = 0$ and no equilibrium is present (cf. Figure 2.17(a)).

Further discussion of the solutions to the ordinary differential equation (2.89) for various values of P_0 , m , and e can be found in the literature. Of particular interest in some of these works, such as [277, 315, 356] is the fact that in the energy conserving case when $m = 0$ and $P_0 = 0$ (presented in the influential textbooks by Hamel [150] and Rosenberg [304]), the tip of the chain (at $\xi = \ell$) develops an infinite speed as $\gamma \rightarrow \ell$. This singular behavior can be easily explained: in the absence of dissipation all the potential energy of the chain is converted into the kinetic energy of an increasingly smaller portion of the chain and eventually the speed of the tip becomes unbounded.

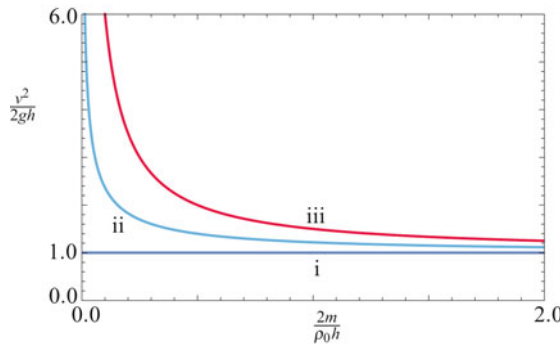


Fig. 2.18 Solutions $\frac{v^2}{2gh}$ to Eqn. (2.90) for the terminal velocity of the mass particle m at the tip of the folded chain as a function of the mass ratio and three values of the energy dissipation parameter e : i corresponds to $e = 1.0$, ii corresponds to $e = 0.5$, and iii corresponds to the energy conserving case $e = 0.0$. The choice $e = 1$ corresponds to the formulation of this problem in Love [212] and Steiner and Troger [331].

To elaborate further on this matter, we recall a result from [277]. These authors examined the solution to the differential equation (2.89) when the particle of mass m was released from a height h (i.e., $\gamma(t = 0) = \ell - h/2$) and the terminal load $-P_0 E$ was absent. They showed that the velocity $v = 2\dot{\gamma}(t = T)$ that the particle has when $\gamma(t = T) = \ell$ and the mass m had fallen a height h is provided by the equation

$$\frac{v^2}{2gh} = \frac{1}{2-e} \left(\frac{2m}{\rho_0 h} \right) \left(\left(1 + \frac{\rho_0 h}{m} \right)^{2-e} - 1 \right). \quad (2.90)$$

For a free-falling mass, the corresponding velocity is $\sqrt{2gh}$. We can examine the expression for $\frac{v^2}{2gh}$ as a function of e and m provided by Eqn. (2.90). It is easy to observe from Figure 2.18 that for all cases, except $e = 1$, the mass m will fall faster than its free-falling counterpart.

2.8 The Chain Fountain

Despite the number of investigations of chains during the past two centuries, it was surprising to see Hanna and Santangelo's 2012 demonstration of an arch-like shape formed by a link chain [153, 154] (cf. Figure 2.1) and Steve Mould's 2013 video demonstration of a chain fountain formed by a chain of beads (also known as self-siphoning beads).¹⁸ In addition to a relatively large number of popular press articles, Mould's demonstration inspired a series of papers [23, 24, 356, 357] devoted to explaining the chain fountain. For our analysis, we shall assume that the motion of the chain is a steady axial motion.¹⁹

We now examine the steady motion of the chain fountain using the framework that includes the material momentum balance. Referring to Figure 2.19, we divide the string that models the chain into three parts. First, the material point $\xi = \gamma_0(t)$ where the string exits a quiescent heap; second, the material point $\xi = \gamma_1(t)$ where the string ceases its motion and forms a quiescent heap; and third, the segment of string $\xi \in (\gamma_0, \gamma_1)$ between the heaps. For the latter portion of the string, we assume that the motion is steady and the space curve formed by the string is planar:

$$\mathbf{r} = x\mathbf{E}_1 + y\mathbf{E}_2, \quad (2.91)$$

where \mathbf{E}_2 is in the direction of gravity.

2.8.1 An Inverted Catenary

To describe the dynamics of the segment between the heaps, we assume that the motion of the string is a steady axial motion (cf. Section 2.2):

$$\mathbf{r}(\xi, t) = \tilde{\mathbf{r}}(\chi), \quad \chi = \xi + ct, \quad (2.92)$$

where c is a constant. From our earlier results (cf. Eqn. (2.3)) we know that $c = -\dot{\gamma}$ and so we conclude that

$$c = -\dot{\gamma}_0 = -\dot{\gamma}_1. \quad (2.93)$$

¹⁸ The video can be accessed at <http://stevemould.com/siphoning-beads/>.

¹⁹ It might be helpful for some readers to review the three conditions for a steady axial motion discussed in Section 2.2 and to see how they pertain to the chain fountain shown in Figure 2.19.

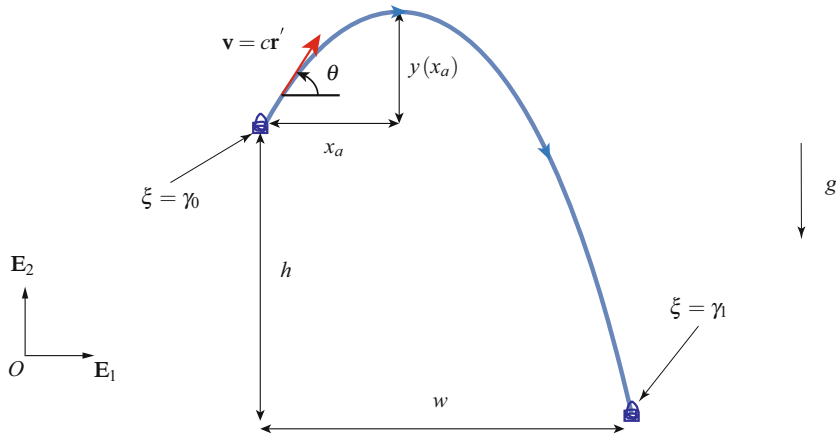


Fig. 2.19 Schematic of the chain fountain.

If ξ is taken as the arc-length parameter in a reference configuration, then χ can be identified as the arc-length parameter for the space curve formed by the string:

$$s = \chi = \xi + ct. \quad (2.94)$$

We also have the following equivalencies among partial derivatives for any function $f(\xi, t) = \tilde{f}(s = \xi + ct)$:

$$\frac{\partial f}{\partial \xi} = \frac{\partial \tilde{f}}{\partial s}, \quad \frac{\partial f}{\partial t} = c \frac{\partial \tilde{f}}{\partial s}, \quad \frac{\partial^2 f}{\partial t^2} = c^2 \frac{\partial^2 \tilde{f}}{\partial s^2}. \quad (2.95)$$

These identities are invoked without comment in the sequel.

We can parameterize the string using ξ in such a manner that $\dot{\gamma}_0 < 0$. As $\mathbf{v} = c\mathbf{r}_s$, we have that

$$v = c = \|\mathbf{v}\|, \quad \mathbf{v} = v\mathbf{r}', \quad \mathbf{a} = \kappa v^2 \mathbf{r}'', \quad (2.96)$$

where κ is the curvature of the space curve formed by the string. It is convenient to parameterize the unit tangent vector to the space curve by an angle θ :

$$\mathbf{r}' = \frac{\partial \mathbf{r}}{\partial \chi} = \cos(\theta)\mathbf{E}_1 + \sin(\theta)\mathbf{E}_2, \quad (2.97)$$

where the gravitational force on the string acts in the \mathbf{E}_2 direction: $\rho_0 \mathbf{f} = -\rho_0 g \mathbf{E}_2$.

The local form of the balance of material momentum $\dot{\mathbf{P}} = \mathbf{b} + \mathbf{C}'$ (cf. Eqns. (1.83) and (2.20)) can be used to establish a useful conservation. For the problem at hand,²⁰

²⁰ It may be helpful to examine Eqn. (1.112) to find the prescription for \mathbf{b} that we are using here. Note that because the string is assumed to be homogeneous, the expression for this force simplifies dramatically to the derivative of a potential energy density.

$$\begin{aligned} P &= -\rho_0 \mathbf{v} \cdot \mathbf{r}' = -\rho_0 c, \\ C &= -\mathbf{n} \cdot \frac{\partial \mathbf{r}}{\partial \xi} - \frac{\rho_0}{2} \mathbf{v} \cdot \mathbf{v} = -n - \frac{\rho_0 c^2}{2}, \\ b = b_p &= -\rho_0 \mathbf{f} \cdot \mathbf{r}' = (\rho_0 g y)' . \end{aligned} \quad (2.98)$$

Thus the balance of material momentum (Eqn. (2.20)) yields the conservation

$$n - \rho_0 c^2 - \rho_0 g y = U, \quad (2.99)$$

where U is a constant.

We are now in a position to involve the balance of linear momentum $\mathbf{n}' + \rho_0 \mathbf{f} = \rho_0 \dot{\mathbf{v}}$. With some rearranging, this law can be expressed in a more convenient form:

$$\left((n - \rho_0 c^2) \mathbf{r}' \right)' - \rho_0 g \mathbf{E}_2 = \mathbf{0}. \quad (2.100)$$

From this equation, we infer a conservation in the horizontal direction and a differential equation in the vertical direction:

$$(n - \rho_0 c^2) \cos(\theta) = H, \quad ((n - \rho_0 c^2) \sin(\theta))' = \rho_0 g, \quad (2.101)$$

where H is a constant and we used the earlier result that $v = c$. Because we anticipate that the solution will be an inverted catenary, $H < 0$ and $n < \rho_0 c^2$.²¹

From geometric considerations, along the space curve formed by the string, we have

$$\frac{ds}{dx} = \sqrt{1 + \frac{dy}{dx} \frac{dy}{dx}}, \quad \tan(\theta) = \frac{dy}{dx}. \quad (2.102)$$

By combining Eqns. (2.101)_{1,2} to eliminate $n - \rho_0 v^2$ and invoking Eqn. (2.95)₁ we find that

$$\begin{aligned} \frac{d}{ds} (\tan(\theta)) &= \frac{\rho_0 g}{H}, \\ \frac{d}{dx} \left(\tan(\theta) = \frac{dy}{dx} \right) &= \frac{\rho_0 g}{H} \frac{ds}{dx} = \frac{\rho_0 g}{H} \sqrt{1 + \frac{dy}{dx} \frac{dy}{dx}}. \end{aligned} \quad (2.103)$$

Thus, we arrive at the familiar equation for a catenary²²:

$$\frac{d^2 y}{dx^2} = \frac{\rho_0 g}{H} \sqrt{1 + \frac{dy}{dx} \frac{dy}{dx}}. \quad (2.104)$$

The solution $y(x)$ of this differential equation and the companion solution $s(x)$ are

²¹ We are closely following the discussion of the inverted axially moving catenary in Perkins and Mote [288] and its extension to the nonlinearly elastic case that is discussed in [259].

²² For extensions of the classic catenary problem to the case where the string is extensible, the reader is referred to Antman [11, 12] and Dickey [87, 88].

$$\begin{aligned}y(x) &= \frac{H}{\rho_0 g} \left(\cosh \left(\frac{\rho_0 g}{H} (x - x_a) \right) - 1 \right) + y(x_a), \\s(x) &= \frac{H}{\rho_0 g} \sinh \left(\frac{\rho_0 g}{H} (x - x_a) \right) + s(x_a).\end{aligned}\quad (2.105)$$

Here, $y(x_a)$, x_a , and $s(x_a)$ are constants where $(x_a, y(x_a))$ are the Cartesian coordinates of the apex of the catenary and $s(x_a)$ is the arc-length coordinate at this point (cf. Figure 2.19).

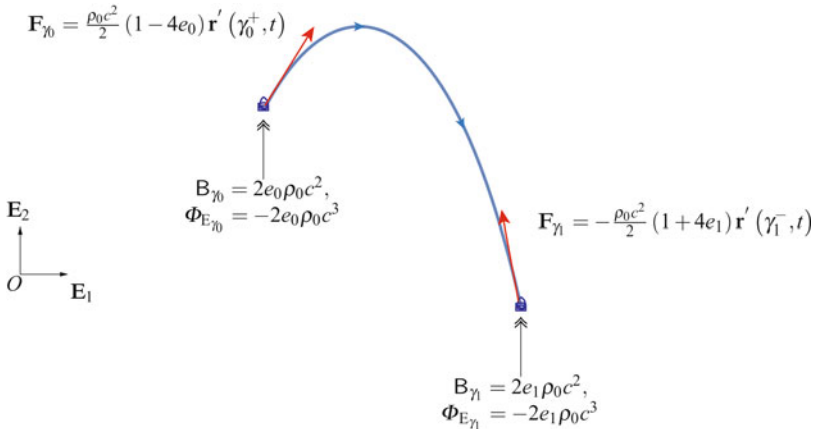


Fig. 2.20 Summary of the singular supplies at $\xi = \gamma_0$ and $\xi = \gamma_1$.

2.8.2 The String Leaving the Heap

We now turn our attention to the point $\xi = \gamma_0(t)$ where the string leaves the quiescent heap. The tangent vector to the string is

$$\mathbf{r}'(\gamma_0^+, t) = \cos(\theta_0) \mathbf{E}_1 + \sin(\theta_0) \mathbf{E}_2. \quad (2.106)$$

As the shock at $\xi = \gamma_0(t)$ is stationary (i.e., $\mathbf{v}_{\gamma_0} = \mathbf{0}$) and $\dot{\gamma}_0 = -c$ (cf. Eqn. (2.93)), we conclude that

$$\mathbf{v}(\gamma_0^+, t) = c \mathbf{r}'(\gamma_0^+, t). \quad (2.107)$$

The appropriate jump conditions were established earlier (cf. Eqn. (2.27)). Substituting for C , \mathbf{v} , and \mathbf{r}' , we find that

$$\begin{aligned}n(\gamma_0^+, t) - \rho_0 c^2 &= -\mathbf{F}_{\gamma_0} \cdot \mathbf{r}'(\gamma_0^+, t), \\\frac{\rho_0}{2} c^2 - n(\gamma_0^+, t) &= -B_{\gamma_0}.\end{aligned}\quad (2.108)$$

Next, we proceed to prescribe B at γ_0 as²³

$$B_{\gamma_0} = -2e_0\rho_0\dot{\gamma}_0^2 \left(\frac{\dot{\gamma}_0}{|\dot{\gamma}_0|} \right), \quad (2.109)$$

where e_0 is a constant which needs to be determined experimentally. Because we expect the process that occurs at γ_0 to be dissipative, e_0 is expected to be positive: $e_0 > 0$.

Substituting into the prescription (2.109) and noting that $\dot{\gamma}_0 < 0$, we can solve for $n(\gamma_0^+, t)$ and \mathbf{F}_{γ_0} :

$$\begin{aligned} n(\gamma_0^+, t) &= \frac{\rho_0}{2} (1 + 4e_0) c^2, \\ \mathbf{F}_{\gamma_0} \cdot \mathbf{r}'(\gamma_0^+, t) &= -n(\gamma_0^+, t) + \rho_0 c^2 \\ &= \frac{\rho_0}{2} (1 - 4e_0) c^2. \end{aligned} \quad (2.110)$$

Referring to Figure 2.20, observe that the heap exerts a singular force \mathbf{F}_{γ_0} on the string which has a positive component in the direction of \mathbf{v}^- and $\rho_0 c^2 - n(\gamma_0^+, t) > 0$ provided $e_0 < 0.25$. In addition, \mathbf{F}_{γ_0} only has a component in the tangential direction $\mathbf{r}'(\gamma_0^+, t)$.

2.8.3 The String at the End of the Catenary

We now turn our attention to the point $\xi = \gamma_1(t)$ where the string comes to a halt in a quiescent heap. The tangent vector to the string at this point is

$$\mathbf{r}'(\gamma_1^-, t) = \cos(\theta_1) \mathbf{E}_1 + \sin(\theta_1) \mathbf{E}_2. \quad (2.111)$$

As the shock at $\xi = \gamma_1(t)$ is stationary (i.e., $\mathbf{v}_{\gamma_1} = \mathbf{0}$), and $\dot{\gamma}_1 = -c$ (cf. Eqn. (2.93)), we conclude that

$$\mathbf{v}(\gamma_1^-, t) = c \mathbf{r}'(\gamma_1^-, t). \quad (2.112)$$

The appropriate jump conditions were established earlier (cf. Eqn. (2.29)). Substituting for C , \mathbf{v} , and \mathbf{r}' , we find that

$$\begin{aligned} n(\gamma_1^-, t) - \rho_0 c^2 &= \mathbf{F}_{\gamma_1} \cdot \mathbf{r}'(\gamma_1^-, t), \\ \frac{\rho_0}{2} c^2 - n(\gamma_1^-, t) &= B_{\gamma_1}. \end{aligned} \quad (2.113)$$

We now proceed to prescribe B at γ_1 in a manner identical to B_{γ_0} :

²³ This prescription is identical to the prescriptions (2.40), (2.66), and (2.84) for B_{γ} that were used in Sections 2.4, 2.6, and 2.7, respectively.

$$B_{\gamma_1} = -2e_1\rho_0\dot{\gamma}_1^2 \left(\frac{\dot{\gamma}_1}{|\dot{\gamma}_1|} \right) = 2e_1\rho_0c^2, \quad (2.114)$$

where e_1 is a constant which needs to be determined experimentally and we substituted for $\dot{\gamma}_1 = -c$. Again, we anticipate that e_1 is positive, but there is no reason for us to expect that $e_1 = e_0$. It is straightforward at this point to solve for $n(\gamma_1^-, t)$ and $\mathbf{F}_{\gamma_1} \cdot \mathbf{r}'(\gamma_1^-, t)$:

$$\begin{aligned} n(\gamma_1^-, t) &= \frac{\rho_0}{2}(1-4e_1)c^2, \\ \mathbf{F}_{\gamma_1} \cdot \mathbf{r}'(\gamma_1^-, t) &= n(\gamma_1^-, t) - \rho_0c^2 \\ &= -\frac{\rho_0}{2}(1+4e_1)c^2. \end{aligned} \quad (2.115)$$

As with the other shock condition, it is easy to conclude that $\rho_0c^2 - n(\gamma_1^-, t) > 0$ provided $e_1 < 0.25$. In addition, if $e_1 > -0.25$, then \mathbf{F}_{γ_1} has a negative (retarding) component in the direction of $\mathbf{r}'(\gamma_1^-, t)$.

2.8.4 Characteristics of the Chain Fountain

To gain a complete picture of the chain fountain we need to combine the analyses of the inverted catenary and the shocks at $\xi = \gamma_0$ and $\xi = \gamma_1$.²⁴ The catenary is typically determined by prescribing $y(x)$ at two known values of x . Here, we assume that the location for $\xi = \gamma_0$ is the origin and that $\xi = \gamma_1$ is located at a known distance h below the origin (cf. Figure 2.19). Rather than assuming that we know the x coordinate of the point $\xi = \gamma_1$, we assume that $\theta_0 = \theta(\gamma_0^+, t)$ is known. In summary, the following quantities are prescribed:

$$\mathbf{r}(\xi = \gamma_0, t) = \mathbf{0}, \quad \mathbf{r}(\xi = \gamma_1, t) \cdot \mathbf{E}_2 = -h, \quad \theta(\gamma_0^+, t) = \theta_0. \quad (2.116)$$

In addition, we assume e_0 , e_1 , g , and ρ_0 are prescribed.

Applying the conservation (2.99) to points on the catenary, we find the value of the constant U and some additional physical interpretations of its value:

$$\begin{aligned} U &= -\mathbf{F}_{\gamma_0} \cdot \mathbf{r}'(\gamma_0^+, t) = -\frac{\rho_0}{2}(1-4e_0)c^2 \\ &= -\frac{\rho_0}{2}(1+4e_1)c^2 + \rho_0gh. \end{aligned} \quad (2.117)$$

Thus, a relationship between the distance h and the speed c can be determined and U can be expressed in a convenient manner:

²⁴ Our presentation and scope here is strongly influenced by the earlier analytical and experimental work of Biggins [23].

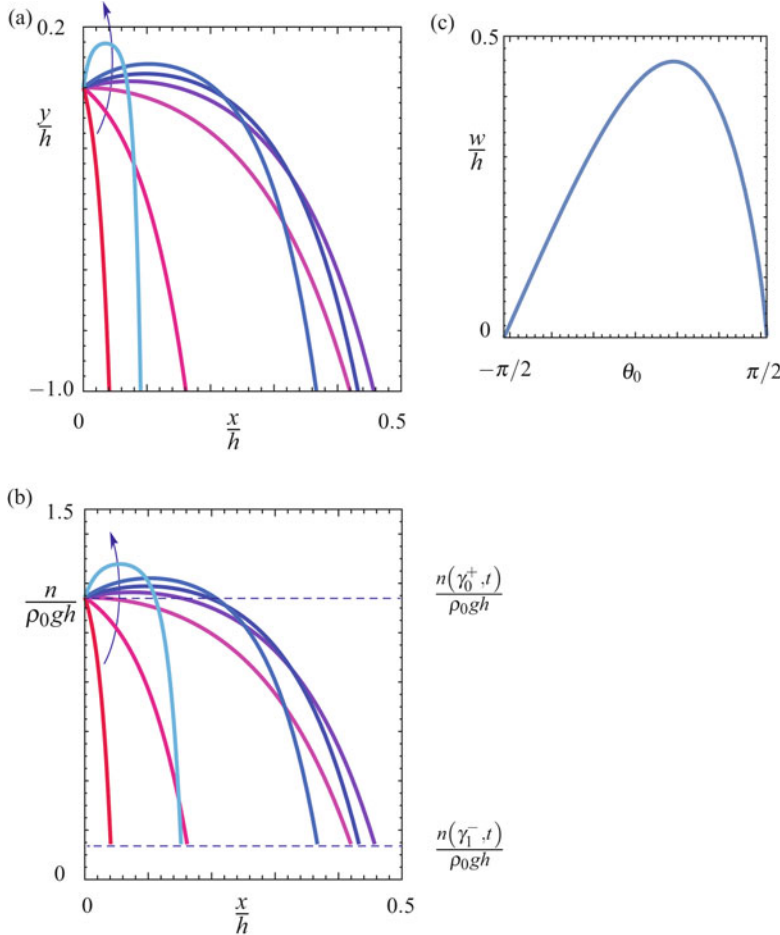


Fig. 2.21 Plots of (a) $y(x)/h$ using (2.105)₁, (b) $n(x)/\rho_0 gh$ using (2.123), and (c) w/h for various values of θ_0 . The arrow in (a) and (b) indicates the direction of increasing θ_0 . For the results shown in this figure, $e_0 = 0.190$, $e_1 = 0.195$, and θ_0 takes the discrete values $-11\pi/24$, $-\pi/3$, 0 , $\pi/6$, $\pi/4$, $\pi/3$, and $11\pi/24$. The constants y_a , x_a , and H in (2.105)₁ and (2.123) are determined using (2.120) and (2.121).

$$\begin{aligned} c^2 &= \frac{gh}{2(e_0 + e_1)}, \\ U &= -\left(\frac{\rho_0 gh}{4}\right)\left(\frac{1 - 4e_0}{e_0 + e_1}\right). \end{aligned} \quad (2.118)$$

The identity (2.118)₁ places further restrictions on e_0 and e_1 . A material point of the string gains a kinetic energy $\frac{1}{2}\rho_0 c^2$ in exiting the heap at $\xi = \gamma_0$. This energy must be less than the net loss in potential energy that the material point experiences as

it moves from $\mathbf{r} = \mathbf{0}$ to $-h\mathbf{E}_2 + w\mathbf{E}_1$. Thus, in addition to the energetic restrictions $e_0 > 0$ and $e_1 > 0$ that we discussed earlier,

$$e_0 + e_1 > \frac{1}{4}. \quad (2.119)$$

This energetic restriction was first shown by Biggins [23, Page 4].²⁵ It is interesting to note that Biggins' energetic restriction (2.119) complements the condition $e_1 < 0.25$ needed to ensure that the string does not become slack at $\xi = \gamma_1$.

Conservation of $H = (n - \rho_0 c^2) \cos(\theta)$ (cf. Eqn. (2.101)) enables us to determine H and the slope at γ_1 given the slope at γ_0 :

$$\begin{aligned} \cos(\theta_1) &= \left(\frac{1 - 4e_0}{1 + 4e_1} \right) \cos(\theta_0), \\ H &= U \cos(\theta_0), \end{aligned} \quad (2.120)$$

where $\theta_1 = \theta(\gamma_1^-, t)$. Turning to the equation (2.105) for $y(x)$, we now solve for $(x_a, y(x_a))$ by examining the slope $\frac{dy}{dx}$ at $x = 0$ and using the boundary condition $y(x = 0) = 0$ and the conservations (2.99) and (2.101)₁:

$$\begin{aligned} x_a &= -\frac{H}{\rho_0 g} \sinh^{-1}(\tan(\theta_0)) \\ &= \left(\frac{h}{4} \right) \left(\frac{1 - 4e_0}{e_0 + e_1} \right) \cos(\theta_0) \sinh^{-1}(\tan(\theta_0)), \\ y(x_a) &= -\frac{U}{\rho_0 g} (1 - \cos(\theta_0)) \\ &= \frac{h}{4} \left(\frac{1 - 4e_0}{e_0 + e_1} \right) (1 - \cos(\theta_0)). \end{aligned} \quad (2.121)$$

Note that $y(x_a)$ is the maximum height that the string attains. In addition, w as a function of the boundary conditions (2.116) and parameters e_0 , e_1 , and ρ_0 can be determined:

$$w = w(\rho_0, e_1, e_2, h, \theta_0) = -\frac{H}{\rho_0 g} \cosh^{-1} \left(-\frac{\rho_0 g}{H} (h + y(x_a)) + 1 \right) + x_a. \quad (2.122)$$

With this last result, $y(x)$ can be determined. The reader is referred to Figure 2.21(a) for examples. We found it convenient to non-dimensionalize distance using h and energies by $\rho_0 g h$ as this reduces the number of independent parameters.

²⁵ In [23], the parameters α and β are used to prescribe $n(\gamma_0^+, t) = T(0) = (1 - \alpha) \rho_0 c^2$ and $n(\gamma_1^-, t) = T(w) = \beta \rho_0 c^2$. Thus, examining Eqns. (2.110) and (2.115), we can conclude that $\alpha = \frac{1}{2} - 2e_0$ and $\beta = \frac{1}{2} - 2e_1$. The values of $\alpha = 0.12$ and $\beta = 0.11$ that are used in [23] are equivalent to $e_0 = 0.190$ and $e_1 = 0.195$ that are used to construct the results shown in Figure 2.21.

Having determined w , $y(x)$, and c , it remains to use Eqn. (2.99) to determine the variation in $(n - \rho_0 c^2)$ as we move from $\xi = \gamma_0$ to $\xi = \gamma_1$ (i.e., as x varies from 0 to w)²⁶:

$$n - \rho_0 c^2 = U + \rho_0 g y = H \cosh \left(\frac{\rho_0 g}{H} (x - x_a) \right). \quad (2.123)$$

As anticipated, and shown in Figure 2.21(b), the maximum tension in the string as it ranges from $n(\gamma_0^+, t) = \frac{\rho_0}{2} (1 + 4e_0) c^2$ to $n(\gamma_1^-, t) = \frac{\rho_0}{2} (1 - 4e_1) c^2$ that is predicted by this expression occurs at the apex $x = x_a$.

Solving the chain fountain problem involves an interesting synthesis of background on steady axial motions, the classic solution for a catenary, and models for heaps of strings that was present in some of the earlier problems, such as the one studied by Cayley, that were discussed in the present chapter. Hopefully, it also demonstrates the usefulness of the prescription for B_γ that has been used for a variety of problems throughout this chapter. In contrast to the earlier problems, the solution is assumed to be steady, $\dot{y}(t) = -c$, and the differential equation that is normally provided by the material momentum jump condition is not present in the analysis.

Our discussion and analysis of the chain fountain is far from complete. In the actual chain fountain, it is easy to observe instances where the shape formed by the chain is far more complex than an inverted catenary. In addition, we have not discussed the transient phases of the fountain when it is first set into motion and when the end of the chain finally exits the reservoir at $\xi = \gamma_0$. There is also the issue of drag forces on the chain and impact phenomena that occur when the segments of chain rattle against each other during the motion. While many of these effects can be incorporated into the string model we have used, other models, such as a multibody dynamics model involving a large number of rigid bodies modeling the individual segments of the chain, are required to provide additional insight and to capture effects that are beyond the capabilities of a string model.

2.9 Closing Comments

We cannot do justice to the enormous volume of literature on the application of the string model in the limited number of pages available to us. However, we hope this chapter has given the reader a flavor of some of the problems and a thorough introduction on how to use local balance laws, constitutive relations, and jump conditions to formulate a determinate system of equations from which the motion of the string can be computed. When we use the theory of a string to model any flexible one-dimensional continuum, such as a telephone cord, it quickly becomes apparent that the resistance to an applied bending moment that is absent in the string is present in

²⁶ It is left as an exercise for the interested reader to substitute for H , x_a , and U in terms e_0 , e_1 , θ_0 , ρ_0 , and h in the expressions for w and $n - \rho_0 c^2$ to convince themselves that knowledge of these parameters suffices to determine w and $n - \rho_0 c^2$.

the phone cord. While more elaborate theories, known as rod theories, are needed to accommodate bending, and we shall devote considerable attention to such theories, the structure of the rod theories will be similar to those we have just encountered for a string.

2.10 Exercises

Exercise 2.1: In direct contrast to Cayley's formulation of the problem of a chain falling from a heap that was discussed in Section 2.4, let us turn to formulating this problem *assuming* that energy is conserved.²⁷ For this problem, one can parallel the developments leading to Eqn. (2.37). However, we now make the assumption that

$$\Phi_{E_\gamma} = 0. \quad (2.124)$$

That is, the shock at the heap is not dissipative.

- (a) Show that the assumption that the shock is not dissipative implies that

$$\mathbf{F}_\gamma = -\frac{\rho_0}{2}\gamma^2 \mathbf{E}_2, \quad \mathbf{B}_\gamma = 0. \quad (2.125)$$

- (b) With the help of the previous results, show that the equation governing $\gamma = w$ is

$$w(\ddot{w} - g) = -\frac{1}{2}\dot{w}^2. \quad (2.126)$$

Construct a phase portrait for the ordinary differential equation (2.126) and compare the solutions to those for Eqn. (2.42) that are shown in Figure 2.8.

- (c) By paralleling the developments leading to Eqn. (2.48), show that the total energy E of the chain is

$$E = \frac{\rho_0}{2}w\dot{w}^2 - \frac{\rho_0 g}{2}w^2. \quad (2.127)$$

Verify that $\dot{E} = 0$.

- (d) Show that the differential equation (2.126) admits the exact solution

$$w(t) = \frac{g}{4}t^2. \quad (2.128)$$

Identify this solution on your phase portrait and then show the well-known result that this solution implies that the terminal acceleration of the chain is $\frac{g}{2}$. How does this compare to the case considered in Section 2.4 with $e = 0.25$?

²⁷ For further references on, and discussion of, the energy-conserving formulation, we refer interested readers to [142, 366, 367].

Exercise 2.2: An inextensible string of mass density ρ_0 per unit length hangs over the edge of a smooth horizontal table (see Figure 2.22). A particle of mass m is attached at the end $\xi = 0$ of the string. At time $t = 0$, the string and the particle are

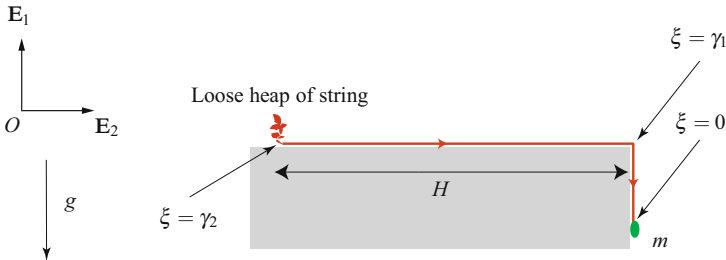


Fig. 2.22 A string leaves a loose heap of stationary string and moves a distance H along the smooth table before falling off the edge.

released from rest. The particle subsequently falls, and as it does it draws additional string from the loose heap of string. This is in contrast to the problem considered in Section 2.5, and the energy loss at the exit point from the heap changes the nature of solutions from those considered previously.

- For an inextensible string, show that if $\mathbf{r} = r(\xi, t)\mathbf{c}$ where \mathbf{c} is a constant, then $\mathbf{v} = v(t)\mathbf{c}$. HINT: Use the inextensibility constraint.
- The velocity vector of the material points of the string experiences two points of discontinuity, one at $\xi = \gamma_1$ and the other where the string exits the heap at $\xi = \gamma_2$. Give representations for $\mathbf{v}_{\gamma_{1,2}}$, $\mathbf{v}(\gamma_1^\pm, t)$, and $\mathbf{v}(\gamma_2^\pm, t)$, and show that $\dot{\gamma}_1 = \dot{\gamma}_2$.
- Give prescriptions for the applied force $\rho_0\mathbf{f}$ acting on the string. Using the local form of the balance of linear momentum, establish expressions for

$$\mathbf{n}(\gamma_2^-, t) - \mathbf{n}(\gamma_1^+, t), \quad \mathbf{n}(\gamma_1^-, t) - \mathbf{n}(0, t). \quad (2.129)$$

- At $\xi = \gamma_1$, assume that no energy is lost (i.e., $\Phi_{E\gamma_1} = 0$). Determine the supply of material momentum B_{γ_2} at this point.
- At $\xi = \gamma_2$, prescribe $\Phi_{E\gamma_2} = -2e\rho_0\dot{\gamma}_2^3$. Determine an expression for the material force B_{γ_2} at this point.
- Using the results of (a)–(d), the appropriate jump conditions, and assuming that $e = 0.25$, show that

$$\dot{\gamma} = \frac{1}{m + \rho_0 H + \rho_0 \gamma} ((m + \rho_0 \gamma)g - \rho_0 \dot{\gamma}^2), \quad (2.130)$$

where $\gamma = \gamma_1$. HINT: The jump condition from the material momentum balance law plays a key role in establishing the desired differential equation.

- (g) After nondimensionalizing the differential equation in (f), numerically integrate the resulting equation and determine the motion of the mass particle m .
- (h) How do the results for $e = 0.25$ compare to those for $e = 0$ and $e = 0.20$. Verify that the case $e = 0$ corresponds to a formulation where it is assumed that energy is conserved.

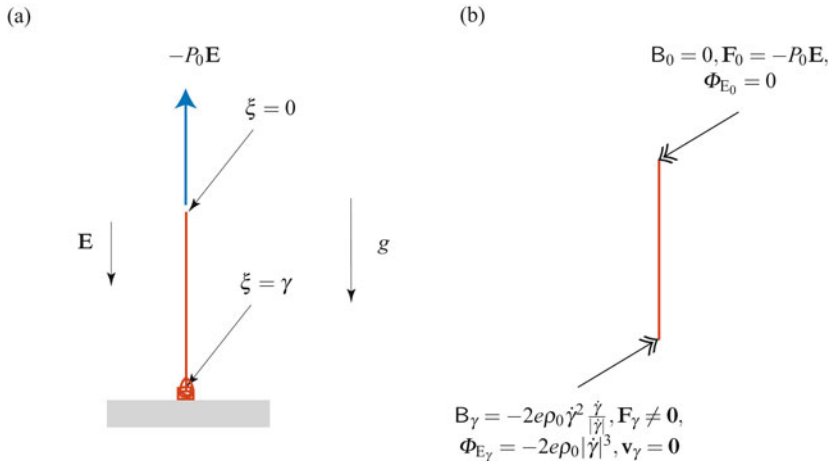


Fig. 2.23 Raising a chain from a stationary heap. (a) Schematic of the string and (b) schematic of the supplies at the shock $\xi = \gamma$ and the terminal point $\xi = 0$.

Exercise 2.3: As shown in Figure 2.23, an inextensible string of mass density ρ_0 per unit length is being pulled from a quiescent heap by a force $-P_0 \mathbf{E}$ applied at $\xi = 0$.²⁸ At time $t = 0$, the length of the string above the heap is ℓ_0 and is at rest when the force is applied.

- (a) Show that the tangent vector \mathbf{r}' and velocity vector \mathbf{v} of any point $\xi \in (0, \gamma)$ on the string have the representations

$$\mathbf{r}' = \mathbf{E}, \quad \mathbf{v} = v \mathbf{E} = -\dot{\gamma} \mathbf{E}. \quad (2.131)$$

- (b) Using an appropriate jump condition, show that the contact force at $\xi = 0$ is $\mathbf{n}(0, t) = P_0 \mathbf{E}$.
- (c) Show that the contact force immediately above the heap has the representation

$$\mathbf{n}(\gamma^-, t) = P_0 \mathbf{E} - \rho_0 \gamma (\dot{\gamma} + g) \mathbf{E}. \quad (2.132)$$

²⁸ Versions of this classic problem are discussed in several textbooks (cf. [174], Problem 8, Page 238], [236], Problem 526], and [237], Sample Problem 4/10]). We highly recommend reading [142] and [237], Sample Problem 4/10] for additional perspectives on the present problem.

- (d) With the help of the appropriate jump conditions and assuming that $B_\gamma = -2e\rho_0\dot{\gamma}^2 \frac{\dot{\gamma}}{|\dot{\gamma}|}$, show that

$$\mathbf{n}(\gamma^-, t) - \rho_0\dot{\gamma}^2 \mathbf{E} = \mathbf{F}_\gamma, \\ \frac{\rho_0}{2}\dot{\gamma}^2 - n(\gamma^-, t) = -2e\rho_0\dot{\gamma}^2 \frac{\dot{\gamma}}{|\dot{\gamma}|}. \quad (2.133)$$

- (e) Show that the differential equation governing the string is

$$\rho_0\gamma(\ddot{\gamma} + g) + \frac{\rho_0}{2} \left(1 + 4e \frac{\dot{\gamma}}{|\dot{\gamma}|}\right) \dot{\gamma}^2 = P_0. \quad (2.134)$$

- (f) After non-dimensionalizing (2.134), construct a phase portrait of the resulting equation of motion for a given value of $P_0/\rho_0 g \ell_0$ and a value of $e \neq 0$ of your choice.²⁹ Your phase portrait should have an equilibrium point where P_0 balances the weight of a section of the string.

- (g) Show that the total energy E of the string has the following representation:

$$E = \frac{\rho_0\gamma}{2} (\dot{\gamma}^2 + g\gamma) - P_0\gamma. \quad (2.135)$$

Using this identity, show that $\dot{E} = \Phi_{E_\gamma}$.

- (h) Show that the assumption that the tension in the string immediately above the heap vanishes corresponds to the choice $e = -0.25$ and implies that a force from the heap pushes upwards on the string at $\xi = \gamma$ and the shock at the heap supplies energy to the string.

Exercise 2.4: With the help of results from Exercise 2.3, solve the following problem from Jeans' classic textbook [174, Problem 8, Page 238]: "A uniform chain is coiled in a heap on a horizontal plane, and a man takes hold of one end and raises it uniformly with a velocity v . Show that when his hand is at a height x from the plane, the pressure on his hand is equal to the weight of a length $x + \frac{v^2}{g}$ of the chain."

Exercise 2.5: With the help of results from Section 2.6, solve the following problem from Jeans' classic textbook [174, Problem 17, Page 252]: "A heavy, perfectly flexible uniform string hanging vertically with its lowest point at a height h above an inelastic horizontal plane is suddenly allowed to fall on to the plane. Show that the pressure on the table when a length x of the string has fallen on to the table is $(3x + 2h)mg$."

Exercise 2.6: The following problem is adapted from the textbooks of Lamb [193, Exercise 4, Page 149] and Tait and Steele [339, Section 316]. Suppose a flexible and uniform chain of length 2ℓ hangs over a smooth pulley and let x be the length of

²⁹ It should not be surprising given the earlier comments on the classic formulations of these problems that the choice $e = 0.25$ corresponds to the case considered in [236, Problem 526] and [237, Sample Problem 4/10].

cable hanging on one side at time t . Show that the differential equation governing the motion of the string is

$$2\rho_0\ell(\ddot{x} - g) = 2\rho_0gx. \quad (2.136)$$

If the chain starts at rest with $x = \ell_0 + \varepsilon$, where ε is a small positive number, then how long does it take for the chain to leave the pulley? Show that the velocity of the chain when it leaves the pulley is $\sqrt{g\ell}$.

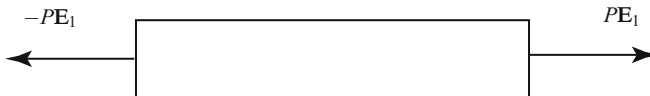


Fig. 2.24 Schematic of a bar which has an undeformed length ℓ and is loaded at its ends by equal and opposite forces $\pm PE_1$. The bar is composed of a material whose strain energy function is prescribed by Eqn. (2.137).

Exercise 2.7: This problem is inspired by the works of studies on phase transformations in bars by Abeyaratne and Knowles [5] and Ericksen [98]. The exercise can be considered as an extension to Exercises 1.8, 1.9, and 1.10 and the aim of the exercise is to show how multiple solutions to this simple problem can be present. We refer the reader to [5] for further analyses, including stability and propagation of $\gamma(t)$, and discussions of related works including [80, 202, 203, 354], on this intriguing well-studied example.

As shown in Figure 2.24, consider a bar of length ℓ in its undeformed state which is then loaded by terminal forces $\pm PE_1$. The bar is modeled by an elastic string with a strain energy function:

$$\rho_0\psi = \alpha_1 \left(\frac{1}{4}(\mu - \alpha_2)^4 + \mu \left(1 + \alpha_2 - \frac{\mu}{2} \right) \right) + \alpha_1 \alpha_3 \log \left(\mu - 1 + \frac{1}{\mu} \right), \quad (2.137)$$

where α_1 , α_2 , and α_3 are constants. As discussed in Exercise 1.9, we choose $\alpha_1 > 0$, $\alpha_2 \approx 2.32472$, and $\alpha_3 \geq 0$. The contact force n associated with the strain energy function is (cf. Eqn. (1.148))

$$n = \alpha_1 \left((\mu - \alpha_2)^3 + 1 + \alpha_2 - \mu \right) + \alpha_1 \alpha_3 \left(\frac{\mu^2 - 1}{\mu^3 + \mu - \mu^2} \right). \quad (2.138)$$

Referring to Figure 2.25, each of three regions of the function $n = n(\mu)$ are known as phases. There are three such phases, I, II, and III, for the strain energy function (2.137).

- (a) Assuming a static uniaxial solution to the boundary-value problem where $\mathbf{r} = x\mathbf{E}_1$, establish an expression for the material contact force C in the bar as a function of the stretch μ .

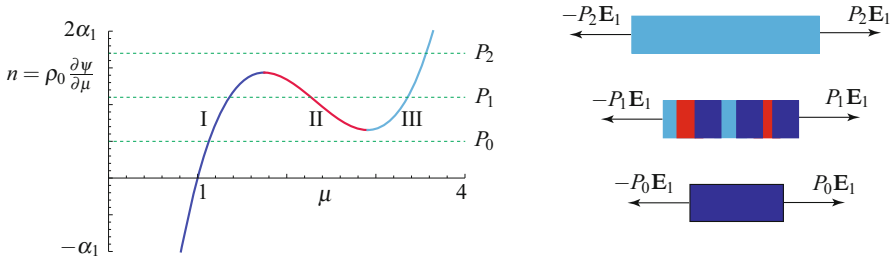


Fig. 2.25 The force n as a function of μ for the strain energy (2.137) and associated solutions to a boundary-value problem for a terminally loaded bar. For the examples shown, $\alpha_2 \approx 2.32472$, $\alpha_3 = 0.1$, $P_0 < 0.654306\alpha_1$, $P_1 \in (0.654306\alpha_1, 1.43586\alpha_1)$, and $P_2 > 1.43586\alpha_1$.

- (b) Numerically compute the graph of C as a function of n for $\alpha_2 \approx 2.32472$ and various values of α_3 . It is helpful to note the direction of increasing μ along the branches of this graph.³⁰
- (c) Suppose that $\alpha_2 \approx 2.32472$, $\alpha_3 = 0.1$, and $P = \alpha_1$. Show that solutions to the boundary-value problem for phase I with $\mu = 1.30595$, phase II with $\mu = 2.37068$, and phase III with $\mu = 3.30683$ are possible. At the interface $\xi = \gamma$ between these phases show that a singular supply of material momentum is typically present (i.e., $B_\gamma \neq 0$).³¹
- (d) Argue that, depending on the magnitude of P , the stretch in the bar is either uniquely determined or an infinite number of solutions are possible.

³⁰ The results shown in Figure 1.20 might be of assistance with these computations.

³¹ The relationship between B_γ and the driving force f is discussed in Exercise 1.7 on Page 45.

Chapter 3

Link, Writhe, and Twist

“In drawing the various closed curves which have a given number of double points, I found it desirable to have some simple mode of ascertaining whether a particular form was a new one, or only a deformation of one of those I had already obtained.”

P. G. Tait [337, Page 289].

3.1 Introduction

In many experiments, a pair of coupled rods or strings are subject to various forces and moments. It is natural to ask if any features of the original structure are preserved in the deformed state? The answer is sometimes yes and in this case the preserved feature is often a quantity known as the linking number L_k . While the linking number dates to the early 19th century and finds application in astronomy, electromagnetism, and knot theory, there has been an explosion of interest in L_k starting in the 1950s which can be attributed to two factors. The first factor is Watson and Crick’s discovery in the early 1950s of the double helix structure of DNA. The second factor is a series of works [42–44] by Gheorghe Călugăreanu (1902–1976) where he showed that the linking number could be decomposed additively into a twist and a writhe. This result is now known as Călugăreanu’s theorem [85, 239] and has enabled deep insights into the differential geometry of pairs of curves which are known as ribbons. This theorem provides a heuristic explanation for coil or loop formation (also known as writhing) of a rod when it is twisted. As a result, it has been applied to experiments on rope, tangled polymers, telephone cords, and DNA in order to gain an understanding of the supercoiling that often accompanies twist (cf. [67–70, 124, 169, 248] and references therein).

Our purpose in this chapter is to give a broad overview on the topics of linking number, twist, writhe, and relative rotations. If we consider the two tangled space curves shown in Figure 3.1, then, by the end of this chapter, the reader should be able to calculate the self-linking of each of the curves and their linking number. Much of

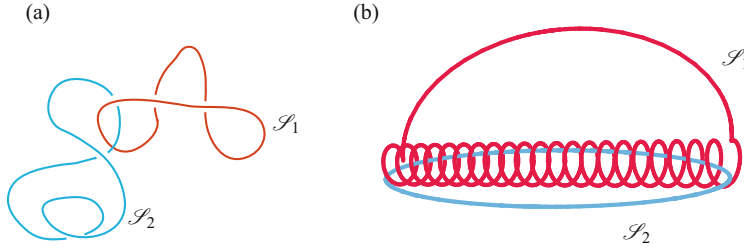


Fig. 3.1 Examples of linked space curves \mathcal{S}_1 and \mathcal{S}_2 . For the curves shown in (a), $L_k(\mathcal{S}_1, \mathcal{S}_2) = \pm 1$ and, for the curves shown in (b), $L_k(\mathcal{S}_1, \mathcal{S}_2) = \pm 21$. These values for the linking numbers were obtained by applying Eqn. (3.34).

what we discuss in this chapter pertains to closed non-self-intersecting space curves. Such curves are also known as knots and there are a wealth of additional analytical tools and perspectives that can be applied to these curves. As we have neither the space nor expertise to cover these topics here, we refer the reader to the accessible text on knot theory by Livingston [210]. In a similar spirit, for further details on the application of the twist, link, and writhe to DNA, we recommend the expository articles by Crick [77] and Pohl [294].

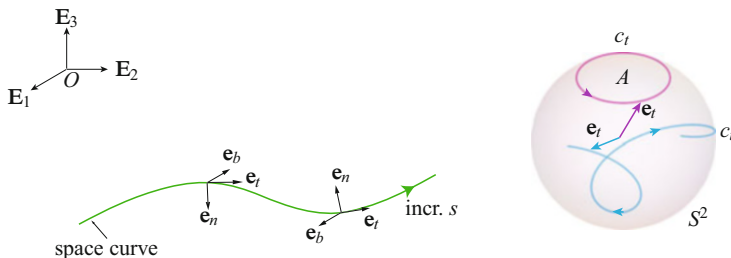


Fig. 3.2 A space curve showing the evolution of the Frenet triad. A pair of representative tantrices or tangent indicatrices c_t on a unit sphere are also shown.

3.2 Space Curves, Ribbons, and Framings

Consider a space curve \mathcal{S} in Euclidean three-dimensional space \mathbb{E}^3 (see Figure 3.2). As usual, we define the position vector of a point on the curve:

$$\mathbf{r} = \mathbf{r}(s) = x_1(s)\mathbf{E}_1 + x_2(s)\mathbf{E}_2 + x_3(s)\mathbf{E}_3. \quad (3.1)$$

Recall that the Frenet triad to this curve can be defined by the set of three vectors $\{\mathbf{e}_t, \mathbf{e}_n, \mathbf{e}_b\}$, and that these vectors satisfy the Serret-Frenet relations:

$$\frac{\partial \mathbf{e}_t}{\partial s} = \kappa \mathbf{e}_n, \quad \frac{\partial \mathbf{e}_n}{\partial s} = -\kappa \mathbf{e}_t + \tau \mathbf{e}_b, \quad \frac{\partial \mathbf{e}_b}{\partial s} = -\tau \mathbf{e}_n, \quad (3.2)$$

where τ is the geometric torsion of the space curve and κ is the curvature. You may also recall that the Serret-Frenet relations can be expressed in a compact form by using the Darboux vector $\boldsymbol{\omega}_{SF} = \tau \mathbf{e}_t + \kappa \mathbf{e}_b$. One undesirable feature of the Frenet frame arises when the curvature vanishes and \mathbf{e}_n is not uniquely defined. As the parameter s passes through such a point, \mathbf{e}_n suffers a discontinuous change.

We can also construct another triad of vectors by defining a unit vector \mathbf{u} which is normal to \mathbf{e}_t . The (right-handed orthonormal) triad or frame is completed by defining $\hat{\mathbf{u}} = \mathbf{e}_t \times \mathbf{u}$. If we denote the vector $\boldsymbol{\omega}_t$ as the angular velocity vector associated with this triad, then we have

$$\frac{\partial \mathbf{e}_t}{\partial s} = \omega_3 \mathbf{u} - \omega_2 \hat{\mathbf{u}}, \quad \frac{\partial \mathbf{u}}{\partial s} = -\omega_3 \mathbf{e}_t + \omega_1 \hat{\mathbf{u}}, \quad \frac{\partial \hat{\mathbf{u}}}{\partial s} = \omega_2 \mathbf{e}_t - \omega_1 \mathbf{u}, \quad (3.3)$$

where

$$\boldsymbol{\omega}_t = \omega_1 \mathbf{e}_t + \omega_2 \mathbf{u} + \omega_3 \hat{\mathbf{u}}. \quad (3.4)$$

Examples of the $\{\mathbf{e}_t, \mathbf{u}, \hat{\mathbf{u}}\}$ triad that we shall see later include the triad $\{\mathbf{r}', \mathbf{d}_1, \mathbf{d}_2\}$ in the theory of the elastica and Kirchhoff's rod theory and the Bishop frame.

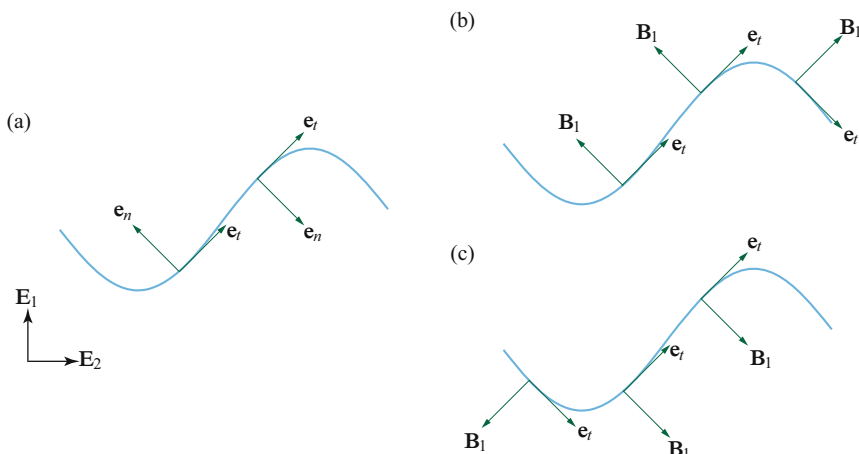


Fig. 3.3 (a) The \mathbf{e}_t and \mathbf{e}_n elements of the Frenet triad for a plane curve with an inflection point. (b) One specification for the element \mathbf{B}_1 of the Bishop frame associated with the plane curve. (c) Another specification for the element \mathbf{B}_1 of the Bishop frame associated with the plane curve. The binormal vector $\mathbf{e}_b = \mathbf{e}_t \times \mathbf{e}_n$ and the normal vector $\mathbf{B}_2 = \mathbf{e}_t \times \mathbf{B}_1$ are not displayed. Expressions for the unit vectors can be found in Exercise 3.10.

The Bishop frame features the three vectors $\mathbf{e}_t = \mathbf{r}'$, \mathbf{B}_1 , and \mathbf{B}_2 and was introduced in a 1975 paper [28] authored by Bishop. This frame was first used with Kirchhoff's rod theory by Langer and Singer [196] and has since proven to be advantageous particularly in computer graphics (cf. Bergou et al. [22] and Hanson's marvelous book [155, Chapter 20]). Unlike the Frenet frame, Bishop's frame is not unique and is well defined even at points where the curvature of the curve vanishes (see Figure 3.3). To define the Bishop frame, a unit vector $\mathbf{B}_1(s_0)$ lying in the plane normal to \mathbf{e}_t at a chosen location $s = s_0$ on the space curve is chosen. This choice then determines a second unit vector: $\mathbf{B}_2(s_0) = \mathbf{e}_t(s_0) \times \mathbf{B}_1(s_0)$. The vectors $\mathbf{B}_1(s)$ and $\mathbf{B}_2(s)$ are assumed to only change in the direction of \mathbf{e}_t . That is, they are said to be relatively parallel to the space curve:

$$\frac{\partial \mathbf{B}_1}{\partial s} = -\kappa_{\mathbf{B}_1} \mathbf{e}_t, \quad \frac{\partial \mathbf{B}_2}{\partial s} = -\kappa_{\mathbf{B}_2} \mathbf{e}_t. \quad (3.5)$$

Here, the (Bishop) curvatures $\kappa_{\mathbf{B}_1}$ and $\kappa_{\mathbf{B}_2}$ are functions of s and they can have positive and negative values. Because \mathbf{B}_α is normal to $\frac{\partial \mathbf{B}_\alpha}{\partial s}$, the magnitude of the vectors \mathbf{B}_1 and \mathbf{B}_2 are preserved. For the Frenet triad, we note from Eqn. (3.2) that neither \mathbf{e}_n nor \mathbf{e}_b propagate in a relatively parallel manner along the curve unless the torsion $\tau = 0$. Using the identity $\mathbf{e}_t = \mathbf{B}_1 \times \mathbf{B}_2$, we find that

$$\frac{\partial \mathbf{e}_t}{\partial s} = \kappa_{\mathbf{B}_1} \mathbf{B}_1 + \kappa_{\mathbf{B}_2} \mathbf{B}_2. \quad (3.6)$$

Thus, we can define a vector

$$\boldsymbol{\omega}_B = \kappa_{\mathbf{B}_1} \mathbf{B}_2 - \kappa_{\mathbf{B}_2} \mathbf{B}_1, \quad (3.7)$$

where

$$\frac{\partial \mathbf{e}_t}{\partial s} = \boldsymbol{\omega}_B \times \mathbf{e}_t, \quad \frac{\partial \mathbf{B}_1}{\partial s} = \boldsymbol{\omega}_B \times \mathbf{B}_1, \quad \frac{\partial \mathbf{B}_2}{\partial s} = \boldsymbol{\omega}_B \times \mathbf{B}_2. \quad (3.8)$$

As with the Frenet triad, one can define a rotation tensor associated with the vector $\boldsymbol{\omega}_B$, but we do not pause to do so here.

As discussed in [28] and displayed in Figure 3.4, the Bishop frame can be related to the Frenet triad by defining an angle θ_B :

$$\begin{aligned} \mathbf{e}_n &= \cos(\theta_B) \mathbf{B}_1 + \sin(\theta_B) \mathbf{B}_2, \\ \mathbf{e}_b &= -\sin(\theta_B) \mathbf{B}_1 + \cos(\theta_B) \mathbf{B}_2. \end{aligned} \quad (3.9)$$

With the help of the Serret-Frenet relations (3.2) and assuming that $\kappa \neq 0$, it is straightforward to show how the curvatures $\kappa_{\mathbf{B}_1}$ and $\kappa_{\mathbf{B}_2}$ can be computed from κ and τ :

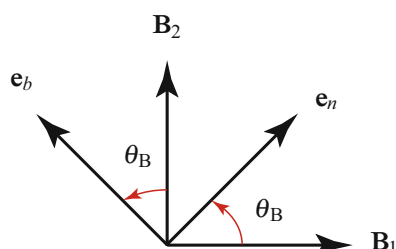


Fig. 3.4 The angle θ_B relating the two sets of normal vectors.

$$\kappa_{B_1} = \kappa \cos(\theta_B), \quad \kappa_{B_2} = \kappa \sin(\theta_B). \quad (3.10)$$

The angle θ_B is found by integrating the relation

$$\tau = \frac{\partial \theta_B}{\partial s}. \quad (3.11)$$

It is interesting to note that θ_B is thereby determined up to an arbitrary constant. Furthermore, the Darboux vector and the vector ω_B are related as follows:

$$\omega_B = \kappa_{B_1} B_2 - \kappa_{B_2} B_1 = \kappa e_b, \quad \omega_{SF} = \tau e_t + \omega_B. \quad (3.12)$$

An example of the computation of the Bishop frame for a plane curve is presented in Exercise 3.10. The results of this exercise are shown graphically in Figure 3.3 and they illustrate our earlier remarks about the nonuniqueness of the Bishop frame.

To illuminate additional features of the Bishop frame, we consider the example of a helical space curve shown in Figure 3.5. As discussed in Section 1.3.4, this curve has a nonvanishing curvature $\kappa = \frac{1}{R(1+\alpha^2)}$ and torsion $\tau = \alpha\kappa$. As a result, we can use an algorithm presented by Guggenheim [144] to compute the Bishop frame from the Frenet frame¹:

$$\begin{aligned} e_t &= \frac{1}{\sqrt{1+\alpha^2}} (\mathbf{e}_\theta + \alpha \mathbf{E}_3), \\ \mathbf{e}_n &= -\mathbf{e}_r, \\ \mathbf{e}_b &= \frac{1}{\sqrt{1+\alpha^2}} (-\alpha \mathbf{e}_\theta + \mathbf{E}_3). \end{aligned} \quad (3.13)$$

First, we compute θ_B using the identity $\tau = \frac{\partial \theta_B}{\partial s}$:

$$\begin{aligned} \theta_B(s) &= \int_{s_0}^s \alpha \kappa du + \theta_B(s_0) \\ &= \alpha \kappa (s - s_0) + \theta_B(s_0). \end{aligned} \quad (3.14)$$

Without loss of generality, we choose $s_0 = 0$ and $\theta_B(s_0) = 0$. Inverting the relations (3.9), and using the aforementioned results, we find that

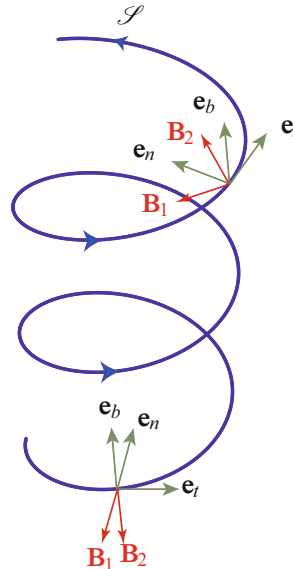


Fig. 3.5 Representative examples of the Frenet and Bishop frames at points on a helical space curve.

¹ We refer the reader to Bergou et al. [22] and Hanson [155, Chapter 20] for details on the numerical computation of the Bishop frame for space curves.

$$\begin{bmatrix} \mathbf{B}_1 \\ \mathbf{B}_2 \end{bmatrix} = \begin{bmatrix} \cos(\alpha\kappa s) & -\sin(\alpha\kappa s) \\ \sin(\alpha\kappa s) & \cos(\alpha\kappa s) \end{bmatrix} \begin{bmatrix} \mathbf{e}_n \\ \mathbf{e}_b \end{bmatrix}. \quad (3.15)$$

Observe that \mathbf{B}_1 and \mathbf{B}_2 revolve continuously relative to \mathbf{e}_n and \mathbf{e}_b . Furthermore, although κ and τ are constant, the curvatures $\kappa_{\mathbf{B}_1}$ and $\kappa_{\mathbf{B}_2}$ are continuously changing:

$$\kappa_{\mathbf{B}_1} = \kappa \cos(\alpha\kappa s), \quad \kappa_{\mathbf{B}_2} = \kappa \sin(\alpha\kappa s). \quad (3.16)$$

We leave it as an exercise to show that the Bishop frame obtained by choosing $\theta_B(s_0) \neq 0$ will differ from (3.15) by a rotation through an angle $\theta_B(s_0)$ about \mathbf{e}_t with concomitant changes to the curvatures $\kappa_{\mathbf{B}_1}$ and $\kappa_{\mathbf{B}_2}$. We close our discussion of the Bishop frame by noting that this frame is also known in the literature as the natural frame, the parallel transport frame, and the relatively parallel adapted frame (cf. [6, 28, 155]).

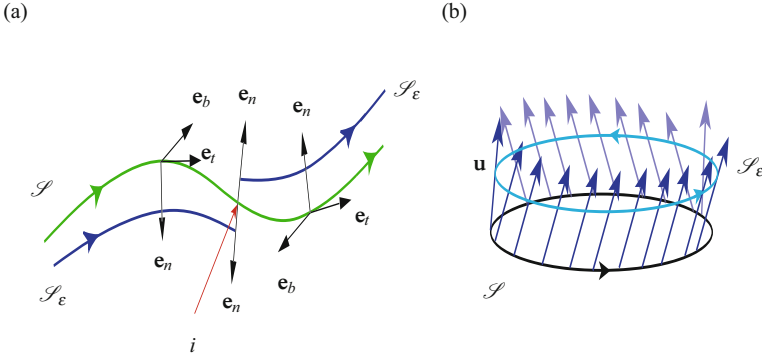


Fig. 3.6 Ribbons constructed from a space curve \mathcal{S} . (a) Ribbon constructed using the normal vector \mathbf{e}_n and (b) a ribbon constructed using a vector \mathbf{u} . Observe that the ribbon constructed using \mathbf{e}_n is poorly defined at a point of inflection i (where $\frac{\partial^2 \mathbf{r}}{\partial s^2} = \mathbf{0}$ or, equivalently, $\kappa = 0$). This well-known issue [42, 239] arises because \mathbf{e}_n suffers a discontinuity at i : $[\![\mathbf{e}_n]\!] \neq \mathbf{0}$.

3.2.1 Ribbons

The vector \mathbf{u} featuring in Eqn. (3.3) can be used to define another curve:

$$\mathcal{S}_\epsilon : \mathbf{r}_\epsilon = \mathbf{r}(s) + \epsilon \mathbf{u}(s). \quad (3.17)$$

If we consider the union of the points on \mathcal{S} , \mathcal{S}_ϵ , and the points along $\epsilon \mathbf{u}$ connecting them, then we will have defined a ruled surface (cf. Figure 3.6). In differential geometry, this surface is known as a ribbon and we shall assume in the sequel that ϵ is sufficiently small so that the two curves \mathcal{S} and \mathcal{S}_ϵ do not intersect. We also

note that if \mathcal{S} is closed and does not intersect itself, then we assume that \mathcal{S}_e is constructed to have these properties too. In many applications of the ideas presented in this chapter the pair of curves \mathcal{S} and \mathcal{S}_e model the sugar-phosphate backbone curves of DNA.

3.2.2 Gauss-Bonnet Theorem

It is often surprisingly useful to map the tangent vector to the space curve so that its tip describes a curve on a unit sphere S^2 . The associated curve is known as the tangent indicatrix or tantrix c_t and representative examples are shown in Figures 3.2 and 3.7. When c_t forms a closed curve on the sphere, then it also encloses a solid angle A .² The celebrated Gauss-Bonnet theorem, named after Carl F. Gauss (1777–1855) and Pierre O. Bonnet (1819–1892), we shall present relates this solid angle to properties of the tantrix. Dating to Kelvin and Tait [341, Section 123] in 1867, this theorem has also been used as a novel method to determine relative rotations of the cross sections of rods.

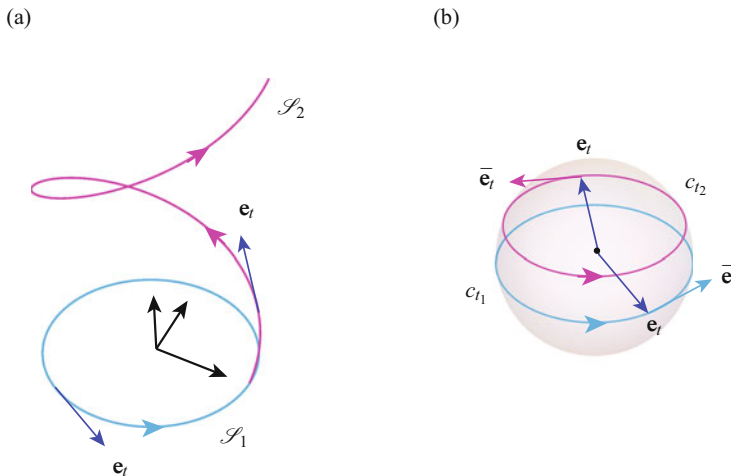


Fig. 3.7 A pair of space curves and their associated tangent indicatrices. In (a) the curves \mathcal{S}_1 is a circle and \mathcal{S}_2 is a helix. The respective tangent indicatrices c_{t_1} and c_{t_2} are shown in (b).

Consider the case where c_t forms a closed curve on S^2 and let us embed this sphere in \mathbb{E}^3 with \mathbf{E}_3 passing along the polar axis. We put coordinates on the sphere using a set of spherical polar coordinates $\{\phi_1 \in [0, 2\pi], \phi_2 \in [0, \pi]\}$ where $\phi_2 = 0$

² The total surface area of a unit sphere is 4π . In topology, the area A in Figure 3.2 is known as a solid angle.

and π at the north and south poles of the sphere, respectively. With this coordinate system in place, the tangent space at a point (ϕ_1, ϕ_2) on the sphere is spanned by the vectors \mathbf{e}_{ϕ_1} and \mathbf{e}_{ϕ_2} :

$$\begin{aligned}\mathbf{e}_{\phi_1} &= -\sin(\phi_1)\mathbf{E}_1 + \cos(\phi_1)\mathbf{E}_2, \\ \mathbf{e}_{\phi_2} &= \cos(\phi_2)\cos(\phi_1)\mathbf{E}_1 + \cos(\phi_2)\sin(\phi_1)\mathbf{E}_2 - \sin(\phi_2)\mathbf{E}_3,\end{aligned}\quad (3.18)$$

where

$$\mathbf{e}_t = \sin(\phi_2)\cos(\phi_1)\mathbf{E}_1 + \sin(\phi_2)\sin(\phi_1)\mathbf{E}_2 + \cos(\phi_2)\mathbf{E}_3. \quad (3.19)$$

Examining the rate of change of \mathbf{e}_t , we find that

$$\begin{aligned}\frac{\partial \mathbf{e}_t}{\partial s} &= \frac{\partial \phi_1}{\partial s} \sin(\phi_2) \mathbf{e}_{\phi_1} + \frac{\partial \phi_2}{\partial s} \mathbf{e}_{\phi_2}, \\ \kappa^2 &= \left(\frac{\partial \phi_2}{\partial s} \right)^2 + \left(\frac{\partial \phi_1}{\partial s} \right)^2 \sin^2(\phi_2).\end{aligned}\quad (3.20)$$

Thus, an expression for the unit tangent vector $\bar{\mathbf{e}}_t$ to c_t and the relation between the arc-length parameter s of \mathcal{S} and the arc-length parameter \bar{s} of c_t can be established:

$$\bar{\mathbf{e}}_t = \frac{1}{\kappa} \frac{\partial \mathbf{e}_t}{\partial s}, \quad \frac{ds}{d\bar{s}} = \frac{1}{\kappa}. \quad (3.21)$$

An expression for the curvature vector $\mathbf{k} = \frac{\partial \bar{\mathbf{e}}_t}{\partial \bar{s}}$ can also be computed. The geodesic curvature κ_g of c_t on S^2 is defined as the rate of change of $\bar{\mathbf{e}}_t$ in the tangent plane spanned by \mathbf{e}_{ϕ_1} and \mathbf{e}_{ϕ_2} . Using the properties of the scalar triple product and the definition (1.9) of the geometric torsion, we perform the following set of manipulations:

$$\begin{aligned}\kappa_g &= \left[\mathbf{e}_t, \bar{\mathbf{e}}_t, \frac{\partial \bar{\mathbf{e}}_t}{\partial \bar{s}} \right] \\ &= \left[\mathbf{e}_t, \frac{1}{\kappa} \frac{\partial \mathbf{e}_t}{\partial s}, \frac{1}{\kappa^2} \frac{\partial^2 \mathbf{e}_t}{\partial s^2} \right],\end{aligned}\quad (3.22)$$

and arrive at the conclusions that

$$\kappa_g = \frac{\tau}{\kappa}, \quad \kappa_g d\bar{s} = \tau ds. \quad (3.23)$$

In the event that the tangent indicatrix describes a great circle (which is the case if \mathcal{S} is a circle), then $\tau = 0$ and consequently $\kappa_g = 0$. This case illustrates the result that $\kappa_g = 0$ when c_t is a geodesic on S^2 .

Suppose that c_t is closed, then the Gauss-Bonnet theorem for this case states that the solid angle A enclosed by this curve satisfies the identity

$$\oint_{c_t} \kappa_g d\bar{s} + A = 2\pi \quad \text{modulo } 4\pi. \quad (3.24)$$

In the event that c_t has corners with exterior angles α_k ($k = 1, \dots, n$), then a term $\sum_{k=1}^n \alpha_k$ is added to the left-hand side of Eqn. (3.24) (cf., e.g., [234, Page 192, Exercise 15]). Although our interest in applications of the Gauss-Bonnet theorem is restricted to curves on the sphere S^2 , the theorem has a far broader range of application. We refer the reader to texts on differential geometry such as [188, 257] for details on more general forms of this classical theorem.

Let us now apply Eqn. (3.24) to the helix discussed earlier in Section 1.3.4. We recall that the curvature κ and torsion τ of the helix are

$$\kappa = \frac{1}{R(1+\alpha^2)} = \frac{1}{R} \cos^2(\zeta), \quad \tau = \frac{\alpha}{R(1+\alpha^2)} = \frac{1}{R} \cos(\zeta) \sin(\zeta), \quad (3.25)$$

where $\zeta = \arctan(\alpha)$ is the pitch angle of the helix. Thus, using the identity $\kappa_g = \tau/\kappa$, the geodesic curvature of the tangent indicatrix is

$$\kappa_g = \alpha. \quad (3.26)$$

If we examine the solid angle enclosed by the tantrix then it is easy to verify that Eqn. (3.24) holds. For the circle shown in Figure 3.7(a), c_{t_1} is a great circle with $\bar{s} \in [0, 2\pi]$ and so $\kappa_g = 0$. By inspection, the solid angle is 2π in agreement with Eqn. (3.24). On the other hand for the helix shown in Figure 3.7(a), $\kappa_g = \alpha$, $\bar{s} \in [0, 2\pi/\sqrt{1+\alpha^2}]$, and the solid angle A enclosed by c_{t_2} as given by Eqn. (3.24) and those obtained by directly computing the area of the spherical cap above c_{t_2} are in agreement: $A = 2\pi \left(1 - \alpha/\sqrt{1+\alpha^2}\right)$.

3.3 Gauss' Linking Number of Two Space Curves

The earliest measure of how much two curves wind around each other was developed in the early 19th century by Gauss. Although he first described this measure in his notebook in 1833, it was published posthumously in 1867. The derivation for Gauss' measure, which is known as the linking number, is not discussed in his notebook and the first derivation, motivated by his studies on electromagnetic induction, was supplied by James C. Maxwell (1831–1879) in 1867.³

Gauss' linking number pertains to two closed nonintersecting space curves \mathcal{S}_1 and \mathcal{S}_2 such as the pairs shown in Figures 3.1 and 3.8. If the curves are respectively parameterized by $s_1 \in [0, 2\pi]$ and $s_2 \in [0, 2\pi]$, then we can define the following unit vector \mathbf{e} which points from a point with position vector $\mathbf{r}_2(s_2)$ on \mathcal{S}_2 to a point on \mathcal{S}_1 with position vector $\mathbf{r}_1(s_1)$:

³ Our historical comments in this section are based entirely on the (recent) insightful papers by Epple [95, 96] and Ricca and Nipoti [301]. The latter paper contains a translation of the page in Gauss' notebook where Eqn. (3.28) is presented as well as copies of letters from Maxwell to Tait discussing the linking number.

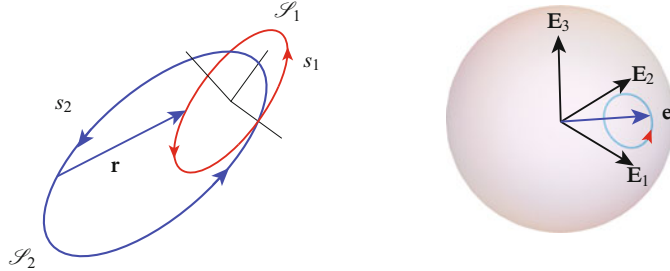


Fig. 3.8 An example of a pair of space curves \mathcal{S}_1 and \mathcal{S}_2 illustrating the vector $\mathbf{r} = \mathbf{r}_1(s_1) - \mathbf{r}_2(s_2)$ and the associated normalized unit vector $\mathbf{e} = \frac{\mathbf{r}}{\|\mathbf{r}\|}$. For the example shown in this figure, the space curves are defined by Eqn. (3.31) with $c = -1.5$. For the example of the Gauss map that is displayed, $s_2 = \frac{3\pi}{4}$ and s_1 varies from 0 to 2π .

$$\mathbf{e}(s_1, s_2) = \frac{\mathbf{r}_1(s_1) - \mathbf{r}_2(s_2)}{\|\mathbf{r}_1(s_1) - \mathbf{r}_2(s_2)\|}. \quad (3.27)$$

The linking number $L_k(\mathcal{S}_1, \mathcal{S}_2)$ between the two curves, which measures how much \mathcal{S}_1 winds around \mathcal{S}_2 , is then defined by the integral⁴

$$L_k(\mathcal{S}_1, \mathcal{S}_2) = \frac{1}{4\pi} \oint_{\mathcal{S}_1} \oint_{\mathcal{S}_2} f(s_1, s_2) ds_1 ds_2, \quad (3.28)$$

where

$$f(s_1, s_2) = \frac{(\mathbf{e}_{t_1}(s_1) \times \mathbf{e}_{t_2}(s_2)) \cdot \mathbf{e}(s_1, s_2)}{\|\mathbf{r}_1(s_1) - \mathbf{r}_2(s_2)\|^2}. \quad (3.29)$$

Here, \mathbf{e}_{t_1} is the unit tangent vector to \mathcal{S}_1 and \mathbf{e}_{t_2} is the unit tangent vector to \mathcal{S}_2 . As Gauss noted, and which we can also readily observe from the definition,

$$L_k(\mathcal{S}_1, \mathcal{S}_2) = L_k(\mathcal{S}_2, \mathcal{S}_1). \quad (3.30)$$

Gauss also noted (a remarkable result which is far from apparent) that $L_k(\mathcal{S}_1, \mathcal{S}_2)$ is integer-valued. The function \mathbf{e} is known as the Gauss map. As illustrated in Figure 3.8, its value can be visualized by plotting the locus of $\mathbf{e}(s_1, s_2)$ on the unit sphere.

To illuminate the linking number defined by Eqn. (3.28) let us consider the pair of ellipses shown in Figure 3.9:

$$\begin{aligned} \mathbf{r}_1(s_1) &= \cos(s_1) \mathbf{E}_1 + 2\sin(s_1) \mathbf{E}_2, \\ \mathbf{r}_2(s_1) &= (3\cos(s_1) + c) \mathbf{E}_2 + 2\sin(s_1) \mathbf{E}_3, \end{aligned} \quad (3.31)$$

⁴ Our convention for writing $L_k(\mathcal{S}_1, \mathcal{S}_2)$ is taken from Spivak [329, Problem 8.28, Page 402] and differs from Gauss' original prescription by a minus sign. As a result, our computations using Eqn. (3.28), such as the results shown in Figure 3.9, agree with those found by counting the signed crossings using Eqn. (3.34).

where c is a constant. We consider three cases: $c = -1.5$, $c = 0$, and $c = 1.5$. For the first and third of these cases, \mathcal{S}_2 can be considered to wind once around \mathcal{S}_1 while in the second case, the space curves do not cross. Numerically evaluating the double integral in Eqn. (3.28), we find the values of $L_k(\mathcal{S}_1, \mathcal{S}_2)$ predicted for the respective cases are 1, 0, and -1.

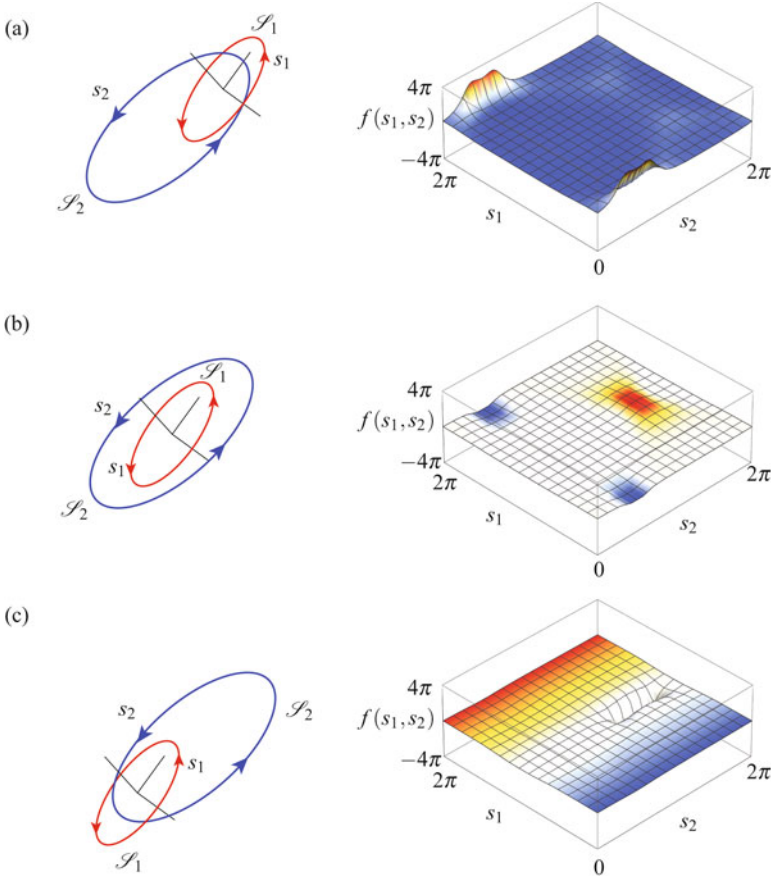


Fig. 3.9 Three examples of a pair of space curves \mathcal{S}_1 and \mathcal{S}_2 showing the behavior of the associated linking function $f(s_1, s_2)$ (cf. Eqn. (3.29)). For (a), $c = -1.5$ and $L_k(\mathcal{S}_1, \mathcal{S}_2) = 1$; for (b), $c = 0.0$ and $L_k(\mathcal{S}_1, \mathcal{S}_2) = 0$; and for (c), $c = 1.5$ and $L_k(\mathcal{S}_1, \mathcal{S}_2) = -1$. The linking number $L_k(\mathcal{S}_1, \mathcal{S}_2)$ is defined by Eqn. (3.28) and the constant c is used to specify the curve \mathcal{S}_2 (cf. Eqn. (3.31)).

While Gauss did not provide a derivation for L_k , Maxwell [233, Sections 417–422], who was working on establishing an expression for the work done by a magnetic pole while moving in a closed curve around a closed electric circuit, made several interesting observations. Among others, he noted that the integrand can be

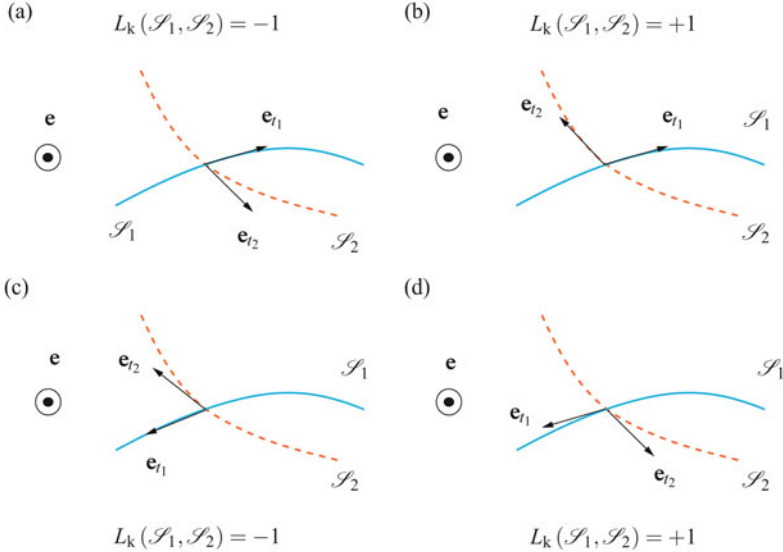


Fig. 3.10 The two distinct values of a signed crossing at a point of transversal crossing of two space curves and the pair of situations associated with each value. For (a) and (c), $L_k(\mathcal{S}_1, \mathcal{S}_2) = -1$ and $L_k(\mathcal{S}_1, \mathcal{S}_2) = +1$ for (b) and (d). In this figure, the dotted curve \mathcal{S}_2 is assumed to pass underneath the solid curve \mathcal{S}_1 at the crossing point, and, as a result, the vector \mathbf{e} (cf. Eqn. (3.27)) points out of the page. If the solid curve passes underneath the dashed curve, then the linking numbers shown in this figure would change sign.

viewed as the volume formed in part by the solid angle spanned by the partial derivatives of $\mathbf{e}(s_1, s_2)$:

$$-\mathbf{e} \cdot \left(\frac{\partial \mathbf{e}}{\partial s_1} \times \frac{\partial \mathbf{e}}{\partial s_2} \right) ds_1 ds_2 = \frac{(\mathbf{e}_{t_1}(s_1) \times \mathbf{e}_{t_2}(s_2)) \cdot \mathbf{e}(s_1, s_2)}{\|\mathbf{r}_1(s_1) - \mathbf{r}_2(s_2)\|^2} ds_1 ds_2. \quad (3.32)$$

As a result, the linking number (3.28) appears in studies on electromagnetism. Maxwell also noted a geometric method which can be used to evaluate the integrals in Eqn. (3.28). Before we discuss this method, we note that there are six other equivalent methods (up to a sign) of calculating $L_k(\mathcal{S}_1, \mathcal{S}_2)$.⁵

A geometric method for computing the linking number L_k uses signed crossings. Following [257, 294], suppose that the plane projection of the two curves \mathcal{S}_1 and \mathcal{S}_2 results in a point of crossing \mathcal{P} . This crossing corresponds to $\mathbf{r}_1(s_1)$ on \mathcal{S}_1 and $\mathbf{r}_2(s_2)$ on \mathcal{S}_2 . Suppose that \mathcal{S}_1 is above \mathcal{S}_2 at this crossing point (see Figure 3.10). We use the unit vector \mathbf{e} which points from \mathcal{S}_2 to \mathcal{S}_1 : Then, the index $J(\mathcal{P})$ at the crossing point \mathcal{P} is defined as

⁵ These methods are discussed in several places in the literature and summarized in Rolfsen's text [303, Chapter 5, Section D].

$$\begin{aligned} J(\mathcal{P}) &= 1 \text{ if } [\mathbf{e}_{t_1}(s_1), \mathbf{e}_{t_2}(s_2), \mathbf{e}] > 0, \\ J(\mathcal{P}) &= -1 \text{ if } [\mathbf{e}_{t_1}(s_1), \mathbf{e}_{t_2}(s_2), \mathbf{e}] < 0. \end{aligned} \quad (3.33)$$

The linking number of the curves is then defined as half the sum of the indices over all crossing points:

$$L_k(\mathcal{S}_1, \mathcal{S}_2) = \frac{1}{2} \sum_{\mathcal{P}} J(\mathcal{P}). \quad (3.34)$$

Notice that the linking number depends on the handedness of the triad $\{\mathbf{e}_{t_1}, \mathbf{e}_{t_2}, \mathbf{e}\}$. We leave it as an exercise to verify that Eqn. (3.34) agrees with the results found for the curves in Figure 3.9. The latter results were obtained by numerically integrating Eqn. (3.28).

The linking number of two closed curves which have no points of intersection has several properties which we now summarize:

- (i) The linking number is an integer ($\dots, -2, -1, 0, 1, 2, \dots$).
- (ii) $L_k(\mathcal{S}_1, \mathcal{S}_2) = L_k(\mathcal{S}_2, \mathcal{S}_1)$.
- (iii) If two curves are unlinked, then their linking number is zero.
- (iv) If we change the orientation of one of the curves then $L_k(\mathcal{S}_1, \mathcal{S}_2)$ will change sign. Changing the orientation of \mathcal{S}_1 can be achieved by reversing the direction of \mathbf{e}_{t_1} .
- (v) The linking number of two curves is invariant to continuous deformations of the curves as long as the two curves are not allowed to pass through each other. That is, the linking number is a topological invariant.

We remark that many of these properties are illustrated by the examples shown in Figures 3.1 and 3.9. For instance, we can continuously deform the ellipses to other ellipses in Figure 3.9(a) and not change the linking number (i.e., (v) above). Although the ellipse \mathcal{S}_2 shown in Figure 3.9(a) can be continuously transformed into the ellipse \mathcal{S}_2 shown in Figure 3.9(c), the orientation of the transformed ellipse will differ from that of \mathcal{S}_2 shown in Figure 3.9(c) and, as a result (from (iv) above), the linking number will differ by a sign. The difference in sign is in agreement with the numerical computations that used Eqn. (3.28). Cutting one of the ellipses and then gluing it back together so that the curves in Figure 3.9(a) transform to those in Figure 3.9(b) would result in a change in the linking number but such a possibility does not contradict (v). Property (iv) is the reason why the linking numbers in the caption for Figure 3.1 are given as \pm : for these pairs of curves the directions of \mathbf{e}_{t_1} and \mathbf{e}_{t_2} were not prescribed and so two values of the linking number are possible depending on the choices of \mathbf{e}_{t_1} and \mathbf{e}_{t_2} .

3.4 Total Geometric Torsion of a Space Curve and Total Twist of a Ribbon

Interest in the linking number of two space curves took on a new lease of life in the 1960s when a theorem by Călugăreanu showed that this quantity could be decomposed into the sum of two quantities known as twist and writhe. In preparation for discussing his wonderful theorem, we first pause to discuss measures of twist in space curves and rods.

To proceed, we recall that any space curve \mathcal{S} (which is not necessarily closed) can be endowed with a Frenet triad and that this triad has an associated Darboux vector. We define the total geometric torsion of a space curve of length ℓ as the integral of the geometric torsion:

$$T_w(\mathcal{S}, \mathbf{e}_n) = \frac{1}{2\pi} \int_0^\ell \omega_{SF} \cdot \mathbf{e}_t ds. \quad (3.35)$$

Here, s is the arc-length parameter of \mathcal{S} and this parameter varies from 0 to ℓ on \mathcal{S} . The division by 2π is a convention. With the help of the Serret-Frenet relations we note that the geometric torsion $\tau = \omega_{SF} \cdot \mathbf{e}_t$ and can be considered as the rate at which the normal vector \mathbf{e}_n rotates about the tangent vector \mathbf{e}_t .

Now suppose ℓ and \mathcal{S} are such that the tangent indicatrix c_t of the curve \mathcal{S} forms a closed curve on the unit sphere. From our earlier discussion on the Gauss-Bonnet theorem we are aware that (cf. Eqn. (3.24))

$$\oint_{c_t} \kappa_g d\bar{s} + A = 2\pi \quad \text{modulo } 4\pi. \quad (3.36)$$

However, we also showed previously (cf. Eqn. (3.23)) that $\kappa_g d\bar{s} = \tau ds$. Thus,

$$\int_0^\ell \tau ds + A = 2\pi \quad \text{modulo } 4\pi. \quad (3.37)$$

Whence, the total geometric torsion can be related to the spherical area enclosed by the tangent indicatrix:

$$T_w(\mathcal{S}, \mathbf{e}_n) + \frac{A}{2\pi} = 1 \quad \text{modulo } 2. \quad (3.38)$$

This relation was first recorded by Fuller [111, Eqn. (6.3)].⁶

Let us consider as an example a helical space curve⁷:

$$\kappa = \frac{1}{R(1+\alpha^2)} = \frac{1}{R} \cos^2(\zeta), \quad \tau = \frac{\alpha}{R(1+\alpha^2)} = \frac{1}{R} \cos(\zeta) \sin(\zeta), \quad (3.39)$$

⁶ Fuller's version of Eqn. (3.38) differs from ours in that $T_w(\mathcal{S}, \mathbf{e}_n)$ is replaced by the more general case $T_w(\mathcal{S}, \mathbf{u})$ in Eqn. (3.38). Alternative proofs of Fuller [111, Eqn. (6.3)] can be found in Aldinger et al. [7] and Kamien [176].

⁷ The parameters for this curve are discussed in Section 1.3.4.

where $\zeta = \arctan(\alpha)$ is the pitch angle of the helix. If we parameterize the helix with the angle ϕ , then

$$\frac{d\phi}{ds} = \frac{1}{R\sqrt{1+\alpha^2}} = \frac{\cos(\zeta)}{R}. \quad (3.40)$$

Consequently, for one segment of the helix,

$$\begin{aligned} T_w(\mathcal{S}, \mathbf{e}_n) &= \frac{1}{2\pi} \int_0^\ell \boldsymbol{\omega}_{SF} \cdot \mathbf{e}_t ds \\ &= \frac{1}{2\pi} \int_0^\ell \tau ds \\ &= \frac{1}{2\pi} \int_0^{2\pi} \tau R \sqrt{1+\alpha^2} d\phi \\ &= \frac{\alpha}{\sqrt{1+\alpha^2}} \\ &= \sin(\zeta). \end{aligned} \quad (3.41)$$

The total geometric torsion $T_w(\mathcal{S}, \mathbf{e}_n)$ is used to characterize configurations of double-stranded DNA. For the aforementioned segment of the helix, the tangent indicatrix forms a closed curve on the sphere. Thus, with the help of Fuller's identity (3.38), we find that the solid angle A enclosed by c_t is

$$A = 2\pi(1 - \sin(\zeta)), \quad (3.42)$$

a result that, as expected, is in agreement with our earlier calculation of this solid angle in Section 3.2.2.

The aforementioned integral of the rate at which \mathbf{e}_n rotates about \mathbf{e}_t can also be applied to the frame $\{\mathbf{e}_t, \mathbf{u}, \mathbf{e}_t \times \mathbf{u}\}$ that we previously used to generate a ribbon (cf. Page 98 and Figure 3.6). Following classic works in this area such as [110, 213], the resulting integral is known as the total twist and it depends on both \mathcal{S} and the choice of \mathbf{u} :

$$T_w(\mathcal{S}, \mathbf{u}) = \frac{1}{2\pi} \int_0^\ell \boldsymbol{\omega}_t \cdot \mathbf{e}_t ds. \quad (3.43)$$

When $\mathbf{u} = \mathbf{e}_n$, then the total twist corresponds to the total torsion $T_w(\mathcal{S}, \mathbf{e}_n)$ defined earlier. By way of comparison, if $\mathbf{u} = b_1 \mathbf{B}_1 + b_2 \mathbf{B}_2$ where $b_{1,2}$ are constants and $\mathbf{B}_{1,2}$ are the normal vectors associated with the Bishop frame, then

$$T_w(\mathcal{S}, b_1 \mathbf{B}_1 + b_2 \mathbf{B}_2) = \frac{1}{2\pi} \int_0^\ell \boldsymbol{\omega}_B \cdot \mathbf{e}_t ds = 0. \quad (3.44)$$

This result is the motivation for referring to the Bishop frame as a rotation minimizing frame. In the sequel, when specifying the twist, to avoid ambiguity where it might occur, we will specify the vector we are using to compute T_w .

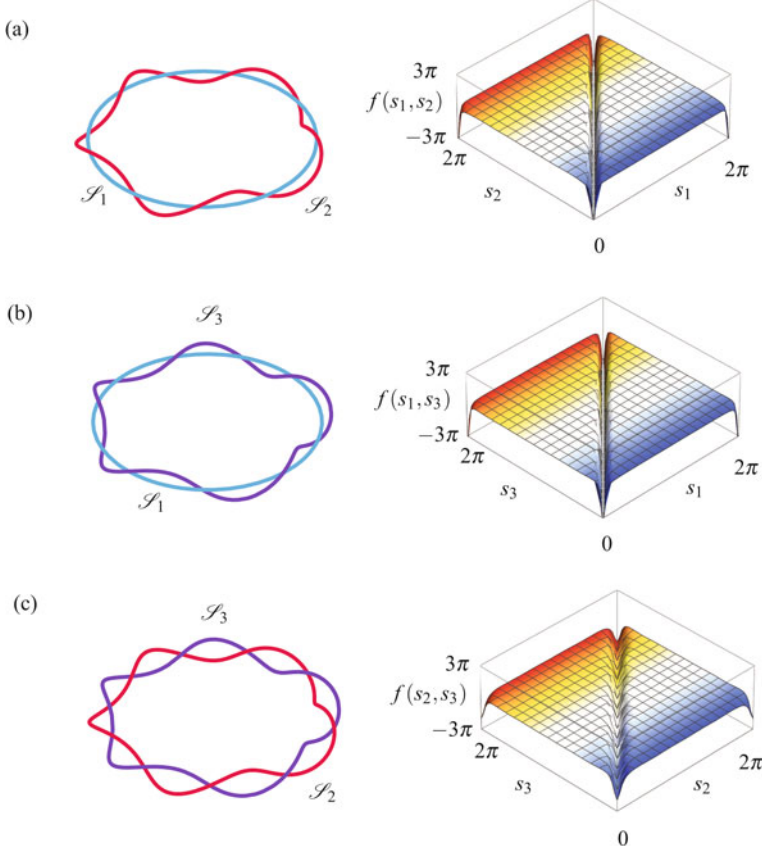


Fig. 3.11 Three distinct examples of a pair of space curves \mathcal{S} and \mathcal{S}_ϵ showing the behavior of the associated linking function $f(s_1, s_2)$ (cf. Eqn. (3.29)). For (a), $L_k(\mathcal{S} = \mathcal{S}_1, \mathcal{S}_\epsilon = \mathcal{S}_2) = -5$; for (b), $L_k(\mathcal{S} = \mathcal{S}_1, \mathcal{S}_\epsilon = \mathcal{S}_3) = -5$; and, for (c), $L_k(\mathcal{S} = \mathcal{S}_1, \mathcal{S}_\epsilon = \mathcal{S}_3) = -5$. The linking number $L_k(\mathcal{S}_1, \mathcal{S}_\epsilon)$ is defined by Eqn. (3.28). The curve \mathcal{S}_1 is a circle of radius 1 lying in the x - y plane. The curves \mathcal{S}_2 and \mathcal{S}_3 are constructed as ribbons using the unit normal vector to \mathcal{S}_1 (cf. Eqn. (3.52) with $n = 5$ and $\epsilon = 0.1$).

3.5 Călugăreanu's Theorem

Consider a closed ribbon formed from a pair of curves \mathcal{S} and \mathcal{S}_ϵ . As indicated by the three examples shown in Figure 3.11, the curve \mathcal{S}_ϵ is formed in the usual manner from the closed curve \mathcal{S} using a unit vector \mathbf{u} that is normal to \mathbf{e}_t and a number ϵ .⁸ Following standard practice, ϵ is considered to be sufficiently small so that the curves \mathcal{S} and \mathcal{S}_ϵ do not intersect. For such a ribbon, Călugăreanu [42–44]

⁸ The orientability condition on the ribbon is satisfied when $\mathbf{u}(s) = \mathbf{u}(s + \ell)$ where $s \in [0, \ell]$ on \mathcal{S} . Thus, the ribbon is not a Möbius strip.

showed that the linking number could be decomposed additively into the sum of a quantity known as the writhe and the total geometric torsion:

$$L_k(\mathcal{S}, \mathcal{S}_e) = W_r(\mathcal{S}) + T_w(\mathcal{S}, \mathbf{e}_n) + N(\mathcal{S}, \mathcal{S}_e). \quad (3.45)$$

In this equation,⁹

$$W_r = W_r(\mathcal{S}) = \frac{1}{4\pi} \oint_0^\ell \oint_0^\ell [\mathbf{e}_t(s_1) \times \mathbf{e}_t(s_2)] \cdot \frac{\mathbf{r}(s_1) - \mathbf{r}(s_2)}{\|\mathbf{r}(s_1) - \mathbf{r}(s_2)\|^3} ds_1 ds_2, \quad (3.46)$$

and $N(\mathcal{S}, \mathcal{S}_e)$ denotes the number of times \mathbf{u} revolves about \mathbf{e}_t . Thus, if we define an angle ψ ,

$$\mathbf{u} = \cos(\psi)\mathbf{e}_n + \sin(\psi)\mathbf{e}_b, \quad (3.47)$$

then, from [43],

$$N(\mathcal{S}, \mathcal{S}_e) = \frac{1}{2\pi} (\psi(\ell) - \psi(0)). \quad (3.48)$$

As noted by Moffatt and Ricca [239], the presence of $N(\mathcal{S}, \mathcal{S}_e)$ in Eqn. (3.45) accommodates the fact that the ribbon is formed with \mathbf{u} which is not necessarily equal to \mathbf{e}_n . We refer to Eqn. (3.45) as Călugăreanu's theorem.

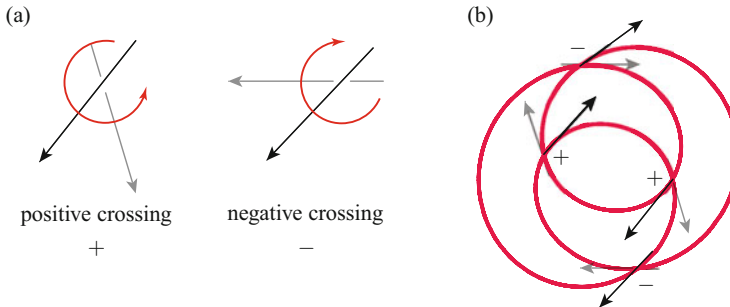


Fig. 3.12 (a) Conventions for the index $J_W(\mathcal{P})$ of the signed crossings of a curve with itself. These representations are a more compact version of the index conventions for $J(\mathcal{P})$ shown earlier in Figure 3.10. (b) Example of the use of the convention with a particular projection of a figure eight knot.

The writhing number $W_r(\mathcal{S})$ can be loosely interpreted as the number of times the curve \mathcal{S} folds or coils upon itself. Complementing this nonlocal behavior, $T_w(\mathcal{S}, \mathbf{e}_n) + N(\mathcal{S}, \mathcal{S}_e)$ is a measure of the twisting of the ribbon about \mathcal{S} . The beauty of Călugăreanu's theorem is that it states that the sum of these two quantities is equal to the (invariant) linking number of the two curves. Thus, any deformations of the ribbon performed that change $W_r(\mathcal{S})$ will induce an equal and opposite effect

⁹ As emphasized in [7], the domain of integration excludes those points $s_1 = s_2$ where the integrand becomes unbounded.

in $T_w(\mathcal{S}, \mathbf{e}_n) + N(\mathcal{S}, \mathcal{S}_\varepsilon)$. Thus, Eqn. (3.45) enables an intuitive understanding of the conversion of twist to writhe and vice versa that is often found in deformation of long slender bodies such as telephone cords and lengths of surgical tubing. Of course this perspective is gained after two material curves in the slender body are identified with \mathcal{S} and \mathcal{S}_ε . Such an identification is readily made in the case of double-stranded DNA where \mathcal{S} and \mathcal{S}_ε can be individually identified with one of the pair of sugar-phosphate backbone curves. Indeed, as evidenced by the works of Crick [77] and Pohl [293], it did not take long after Călugăreanu's work was published in the early 1960s for people to realize that his theorem could be applied to understand the coiling behavior of double-stranded DNA.

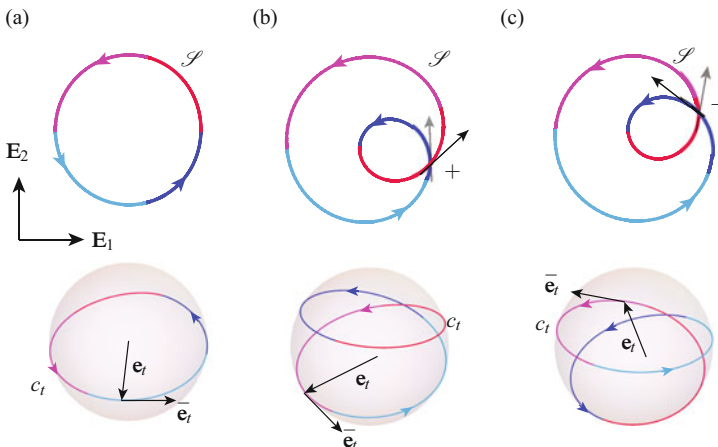


Fig. 3.13 Examples of calculations of $\mathcal{J}_W(\mathcal{P})$. (a), Closed curve with no crossings: $\mathcal{J}_W(\mathcal{P}) = 0$; (b), closed curve with a positive crossing: $\mathcal{J}_W(\mathcal{P}) = 1$; and (c), closed curve with a negative crossing: $\mathcal{J}_W(\mathcal{P}) = -1$. The tangent indicatrices c_t for each of the three curves are also shown. Observe from (b) and (c) that when over- and under-crossings are interchanged the index changes by a factor of 2. The parametric expressions for \mathcal{S} are taken from an example in [43] which is discussed further in Exercise 3.8.

In a highly cited paper that appeared in 1971, Fuller [110] introduced the term writhing number for $W_r(\mathcal{S})$ because the verb to writhe is defined as “to twist into coils or folds.” While the expression for the writhe integral has intriguing similarities to the definition (3.28) of the linking number of a pair of curves that was introduced earlier, it pertains only to the curve \mathcal{S} and can take non-integer values. Computing $W_r(\mathcal{S})$ has been the subject of many works since then. Several approaches can be found to this computation and each of them can offer a different perspective on $W_r(\mathcal{S})$ ¹⁰:

¹⁰ The primary reference for our summary of the methods used to compute the writhing number is [7]. We also recommend the later works [20, 21, 85, 169, 176] for helpful perspectives and insights on this topic.

- (i) Taking advantage of a parametric representation for \mathcal{S} , if it is available, the integrand in Eqn. (3.46) can be evaluated directly. In this context, we note that parametric expressions for trefoil, figure eight, and other knots are readily available. We also note that if \mathcal{S} is planar, then the triple product in the integrand in Eqn. (3.46) will be zero. Hence,

$$\text{For a planar curve } W_r = 0. \quad (3.49)$$

- (ii) Following Fuller [111], use Eqn. (3.45) to compute $W_r(\mathcal{S})$ by first computing $L_k(\mathcal{S}, \mathcal{S}_\varepsilon)$ and $T_w(\mathcal{S}, \mathbf{e}_n) + N(\mathcal{S}, \mathcal{S}_\varepsilon)$. The difference of these quantities then provides the sought after value of writhe:

$$W_r(\mathcal{S}) = L_k(\mathcal{S}, \mathcal{S}_\varepsilon) - T_w(\mathcal{S}, \mathbf{e}_n) - N(\mathcal{S}, \mathcal{S}_\varepsilon). \quad (3.50)$$

- (iii) Again following Fuller [111], one uses the Gauss-Bonnet theorem to establish a relation between $T_w(\mathcal{S}, \mathbf{e}_n)$ and the solid angle encircled by c_t (cf. Eqn. (3.38)). Then, after noting that $L_k(\mathcal{S}, \mathcal{S}_\varepsilon)$ is an integer, one appeals to Eqn. (3.45) to find

$$W_r(\mathcal{S}) = L_k(\mathcal{S}, \mathcal{S}_\varepsilon) - 1 + \frac{A}{2\pi} - N(\mathcal{S}, \mathcal{S}_\varepsilon) \quad \text{modulo 2}. \quad (3.51)$$

- (iv) As summarized in [21], $W_r(\mathcal{S})$ can be identified with the sum of the indices of the signed crossings of \mathcal{S} with itself averaged over all possible projection angles. The convention for the index $\mathcal{J}_w(\mathcal{P})$ of the crossings is shown in Figure 3.12. The curve with no self-crossings has zero writhe, while the closed curves in Figure 3.13(b) & (c) show that by twisting a loop through 360° , a change in the writhing number can be achieved. The trefoil knots discussed in Exercise 3.9 offer an illustration of the invariance of writhing number to the choice of the direction of increasing arc-length parameter s .

3.6 Examples of Computing Writhing Numbers

To illuminate our comments on writhing numbers, it is necessary to explore some examples. One of the few works that we found where explicit computations could be found is in a paper by White and Bauer [360] and our examples are inspired by their work. Pairs of the space curves in question form ribbons, examples of which are shown in Figure 3.11. The three space curves which form the ribbons have parametric representations in terms of the arc-length parameter s_1 of \mathcal{S}_1 ¹¹:

¹¹ The curves considered in [360] are discussed in Exercise 3.9.

$$\begin{aligned}\mathbf{r}_1(s_1) &= \cos(s_1)\mathbf{E}_1 + \sin(s_1)\mathbf{E}_2, \\ \mathbf{r}_2(s_1) &= \mathbf{r}_1 + \varepsilon(\cos(ns_1)\cos(s_1)\mathbf{E}_1 + \cos(ns_1)\sin(s_1)\mathbf{E}_2 + \sin(ns_1)\mathbf{E}_3), \\ \mathbf{r}_3(s_1) &= \mathbf{r}_1 - \varepsilon(\cos(ns_1)\cos(s_1)\mathbf{E}_1 + \cos(ns_1)\sin(s_1)\mathbf{E}_2 + \sin(ns_1)\mathbf{E}_3),\end{aligned}\quad (3.52)$$

where n and ε are constants. For the examples shown in Figure 3.11, $n = 5$ and $\varepsilon = 0.1$. Geometrically, the curves \mathcal{S}_2 and \mathcal{S}_3 wind counterclockwise about \mathcal{S}_1 . As s_1 ranges from 0 to 2π , \mathcal{S}_2 winds n times around \mathcal{S}_1 .

For the circle \mathcal{S}_1 , we have

$$\mathbf{e}_{t_1} = -\sin(s_1)\mathbf{E}_1 + \cos(s_1)\mathbf{E}_2, \quad \mathbf{e}_{n_1} = -\cos(s_1)\mathbf{E}_1 - \sin(s_1)\mathbf{E}_2, \quad \mathbf{e}_{b_1} = \mathbf{E}_3, \quad (3.53)$$

and

$$\kappa_1 = 1, \quad \tau_1 = 0. \quad (3.54)$$

For the helical spirals, some lengthy calculations reveal that

$$\begin{aligned}\frac{ds_2}{ds_1} &= \sqrt{\varepsilon^2 n^2 + (1 + \varepsilon \cos(ns_1))^2} = 1 + \varepsilon \cos(ns_1) + O(\varepsilon^2), \\ \kappa_2 &= 1 + \varepsilon(n^2 - 1)\cos(ns_1) + O(\varepsilon^2), \\ \tau_2 &= 0 + \varepsilon n(1 - n^2)\cos(ns_1) + \varepsilon^2 n(n^2 - 1 + (n^4 + 3n^2 - 1)\cos(2ns_1)) + O(\varepsilon^3), \\ \mathbf{e}_{t_2} &= \mathbf{e}_{t_1} + \varepsilon n(\sin(ns_1)\mathbf{e}_{n_1} + \cos(ns_1)\mathbf{e}_{b_1}) + O(\varepsilon^2), \\ \mathbf{e}_{n_2} &= \mathbf{e}_{n_1} - \varepsilon n(\mathbf{e}_{t_1} + n\mathbf{e}_{b_1})\sin(ns_1) + O(\varepsilon^2), \\ \mathbf{e}_{b_2} &= \mathbf{e}_{b_1} - \varepsilon n(\cos(ns_1)\mathbf{e}_{t_1} - n\sin(ns_1)\mathbf{e}_{n_1}) + O(\varepsilon^2).\end{aligned}\quad (3.55)$$

The corresponding results for \mathcal{S}_3 can be obtained from Eqn.(3.55) by setting $\varepsilon \rightarrow -\varepsilon$. Thus for the three ribbons shown in Figure 3.11, we have the respective normal vectors that are used to define the ribbons:

$$\begin{aligned}\mathbf{u}_1 &= -\cos(ns_1)\mathbf{e}_{n_1} + \sin(ns_1)\mathbf{e}_{b_1}, \\ \mathbf{u}_2 &= -\mathbf{u}_1, \\ \mathbf{u}_3 &= 2\mathbf{u}_2 + O(\varepsilon^2).\end{aligned}\quad (3.56)$$

The expressions (3.55) will now be used in conjunction with Eqn.(3.45) to obtain approximate expressions for the writhing numbers of the ribbons. For the third ribbon, extensive perturbation calculations are needed and we used a symbolic manipulation package for assistance.

To apply Călugăreanu's theorem (3.45), we compute using Eqns.(3.53) and (3.54) that

$$\begin{aligned}T_w(\mathcal{S}_1, \mathbf{e}_{n_1}) + N(\mathcal{S}_1, \mathcal{S}_2) &= N(\mathcal{S}_1, \mathcal{S}_2) = -n, \\ T_w(\mathcal{S}_1, \mathbf{e}_{n_1}) + N(\mathcal{S}_1, \mathcal{S}_3) &= N(\mathcal{S}_1, \mathcal{S}_3) = -n.\end{aligned}\quad (3.57)$$

By counting crossings and using Eqn. (3.34), we find that the linking numbers for these ribbons are also $-n$. Referring to Eqn. (3.50), this is consistent with the fact that the writhing number of the circle \mathcal{S}_1 is zero. Turning to the third ribbon, which is formed by \mathcal{S}_2 and \mathcal{S}_3 , we find that $L_k(\mathcal{S}_2, \mathcal{S}_3) = -n$, $N(\mathcal{S}_2, \mathcal{S}_3) = -n$, and

$$\begin{aligned} T_w(\mathcal{S}_2, \mathbf{e}_{n_2}) &= \frac{1}{2\pi} \int_0^{\ell_2} \tau_2 ds_2 \\ &= \frac{1}{2\pi} \int_0^{2\pi} \tau_2 \frac{ds_2}{ds_1} ds_1 \\ &= \frac{\varepsilon}{2\pi} \int_0^{2\pi} (1 - n^2) n \cos(ns_1) ds_1 \\ &\quad + \frac{\varepsilon^2 n}{4\pi} \int_0^{2\pi} n^2 - 1 + (2n^4 + 5n^2 - 1) \cos(2ns_1) ds_1 + O(\varepsilon^3) \\ &= \frac{\varepsilon^2 n}{2} (n^2 - 1) + O(\varepsilon^3). \end{aligned} \quad (3.58)$$

Consequently, using Călugăreanu's theorem (3.45), we compute the approximate expressions for the writhing numbers of the curves \mathcal{S}_2 and \mathcal{S}_3 :

$$\begin{aligned} W_r(\mathcal{S}_2) &= -\frac{\varepsilon^2 n}{2} (n^2 - 1) + O(\varepsilon^3), \\ W_r(\mathcal{S}_3) &= -\frac{\varepsilon^2 n}{2} (n^2 - 1) + O(\varepsilon^3). \end{aligned} \quad (3.59)$$

For the curves shown in Figure 3.11, $W_r(\mathcal{S}_2) \approx -1.2$.

The results of this analysis can be applied to circular strands of DNA (or DNA plasmids) that are discussed in the literature¹² provided the radius of the circular reference curve is used to non-dimensionalize the length scales. The radius R in this case is typically in the order of several hundred nanometers (nm) and εR is of the order of 1 nm.

3.7 Self-Linking of a Space Curve with Application to Strands of DNA

Restricting attention to curves with no points of inflection, Pohl [293] published the following identity for the self-linking number SL of the curve in 1968:

$$SL = W_r(\mathcal{S}) + T_w(\mathcal{S}, \mathbf{e}_n), \quad (3.60)$$

¹² See [169, 360] and references therein.

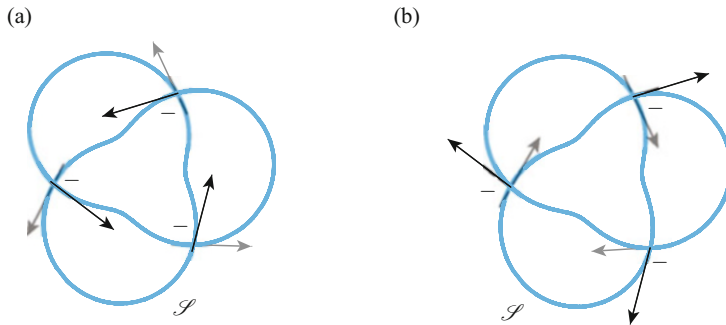


Fig. 3.14 A trefoil knot with a self-linking number $SL = -3$ showing the crossings for a given projection. (a) Computation of the crossing index using a given orientation of s and (b) computation by reversing the direction of s .

where SL is obtained from half the sum of the crossing indices $\mathcal{J}_W(\mathcal{P})$ of \mathcal{S} . As examples, $SL = -3$ for the trefoil knot shown in Figure 3.14, $SL = 0$ for the figure eight knot shown in Figure 3.12, and $SL = +1$ for the knot shown in Figure 3.13(c).

Pohl's student, White, subsequently extended Eqn. (3.60) in a well-cited paper [359]. In establishing Eqn. (3.60), Pohl was seeking to give “a new, clearer, and much simplified treatment of” Călugăreanu’s theorem as presented in [42–44]. It should be clear that Eqn. (3.60) is intimately related to Călugăreanu’s theorem (3.45). The identity (3.60) has also had an influential role in the literature on writhe and twist in rods and DNA.¹³ There are numerous papers (e.g., [68, 235, 294, 314, 335]) devoted to this topic and, in particular, calculating W_r and T_w for deformed strands of DNA.

As mentioned previously, one of the primary drivers for the spread of interest in Călugăreanu’s theorem (3.45) and Eqn. (3.60) has been an attempt to understand the supercoiling of DNA. To see how link, writhe, and twist can be applied to strands of double-stranded DNA (dsDNA), we recall that DNA can be modeled as two space curves \mathcal{S}_1 and \mathcal{S}_2 which are intertwined about a imaginary third curve \mathcal{S} which is known as the duplex or molecular axis. We can define a ribbon using \mathcal{S} and \mathcal{S}_1 (or \mathcal{S}_2). It is also interesting to note that dsDNA can also be found in closed configurations (called DNA circles or DNA plasmids). For example, the chromosome of the bacteria *E. Coli* is a DNA circle one millimeter in length, and has a linking number that is close to 300,000 [294].

The twisting number T_w of the DNA strand is calculated using the ribbon formed by \mathcal{S} and $\mathcal{S}_{1,2}$, and the linking number L_k is also determined using the two space curves. It is standard to then apply Călugăreanu’s theorem (3.45) to determine the writhe of the DNA strand.¹⁴

¹³ We refer the reader to [239] for a discussion of Călugăreanu’s legacy and the roles played by Călugăreanu’s theorem and Eqn. (3.60).

¹⁴ For examples, see [18, 360, 361].

For strands of DNA, one also defines the supercoiling density σ [83, 314]:

$$\sigma = \frac{L_k - L_{k_0}}{L_{k_0}}. \quad (3.61)$$

Here, L_{k_0} is the self-linking number of a strand of DNA where the molecular axis (duplex axis) is straight and unstressed. For B-DNA, there are 10.5 base pairs per turn of the helix, so when the molecular axis is straight and unstressed, $W_r = 0$ and

$$L_{k_0} = T_w = \frac{\text{Number of base pairs}}{10.5}. \quad (3.62)$$

For DNA in vivo, $\sigma = 0.5$ and $\sigma = -1.0$ for separated strands of double-stranded DNA. Strands of DNA, where $\sigma < 0 (> 0)$ are known as underwound (supercoiled).¹⁵

We emphasize that the twist T_w is the number of times that one sugar phosphate backbone wraps around the molecular axis \mathcal{S} and the writhe W_r is the average of the indices of the self-crossings of the double helix. In many of the recent experiments on DNA, one fixes L_k (i.e., σ) and varies T_w by extending the strands of DNA (see, e.g., [40, 314, 335]). In this way, L_k is a control parameter for their experiments. A lucid discussion on the importance of using L_k in this manner can be found in Pohl [294].

Because the linking number is a topological invariant, the only way to change it is to cut the DNA strands. This is precisely what some enzymes known as *topoisomers* perform [83, 241]. Indeed, there are two types of these enzymes, which either cut one strand (Type I) or two strands (Type II). The former enable changes in L_k of +1 while the latter enable changes of +2. An example of the latter phenomenon can be seen in Figure 3.13 where the self-linking number SL for two curves differs by a factor of 2.

3.8 Exercises

Exercise 3.1: Consider a plane curve $y = f(x)$. For this curve, compute the tangent indicatrix c_t and its geodesic curvature κ_g . Verify that c_t describes a geodesic (i.e., a curve of shortest distance between two points) on the sphere S^2 .

Exercise 3.2: Consider a left-handed circular helix ($\alpha < 0$) parameterized using a cylindrical polar coordinate system: $z = \alpha R\theta$. Compute the tangent indicatrix c_t for this helix and show that the Gauss-Bonnet theorem (3.24) can be used to compute the spherical area enclosed by c_t .

Exercise 3.3: While the linking number of two non-linked curves is zero (see, e.g., Figure 3.9(b)), the converse is not true. To see this fact, show that the linking number

¹⁵ Underwound is also termed negatively supercoiled in contrast to the case $\sigma > 0$ which is termed positively supercoiled.

for the pair of closed space curves forming a link variously known as “Maxwell’s link” or the “Whitehead link” has a linking number of 0.¹⁶

Exercise 3.4: Verify the computation of the linking number for the three pairs of curves shown in Figure 3.9 using the signed crossing formula (3.34). In your solution you might notice the difference in orientation between the curve labeled \mathcal{S}_2 that is shown in Figures 3.9(a) and 3.9(c).

Exercise 3.5: After suitably modifying the definition (3.28), compute the linking number of the following pair of curves which are defined parametrically by the respective position vectors:

$$\mathbf{r}_1 = \mathbf{r}_1(s_1) = s_1 \mathbf{E}_1 + \mathbf{E}_3, \quad \mathbf{r}_2 = \mathbf{r}_2(s_2) = s_2 \mathbf{E}_2. \quad (3.63)$$

Exercise 3.6: After suitably modifying the definition (3.28), show that the linking number of two parallel lines is zero.

Exercise 3.7: Verify the identity (3.32). The following tensor, which describes a combined projection and scaling, will be useful in your work:

$$\mathbf{A} = \frac{1}{\|\mathbf{r}_1(s_1) - \mathbf{r}_2(s_2)\|} (\mathbf{I} - \mathbf{e} \otimes \mathbf{e}). \quad (3.64)$$

Here, from Eqn. (3.27),

$$\mathbf{e}(s_1, s_2) = \frac{\mathbf{r}_1(s_1) - \mathbf{r}_2(s_2)}{\|\mathbf{r}_1(s_1) - \mathbf{r}_2(s_2)\|}. \quad (3.65)$$

You will also find that the adjugate, $\text{adj}(\mathbf{A})$, of the non-invertible tensor \mathbf{A} is

$$\text{adj}(\mathbf{A}) = \frac{1}{\|\mathbf{r}_1(s_1) - \mathbf{r}_2(s_2)\|^2} \mathbf{e} \otimes \mathbf{e}, \quad (3.66)$$

and plays a role in the derivation because of the identity

$$\text{adj}(\mathbf{A})(\mathbf{a} \times \mathbf{b}) = \mathbf{A}\mathbf{a} \times \mathbf{A}\mathbf{b}, \quad (3.67)$$

which holds for any pair of vectors \mathbf{a} and \mathbf{b} .

Exercise 3.8: Consider the following parametric equation for a closed space curve that appeared in Călugăreanu [43, Pages 616–617]:

$$x(t) = \cos(t) - \lambda \cos(2t), \quad y(t) = \sin(t) - \lambda \sin(2t), \quad z(t) = \alpha \lambda \sin(t). \quad (3.68)$$

In these expressions, the parameters $\lambda \geq 0$ and $\alpha = \pm 1$. Three examples of these curves are shown in Figure 3.13. Determine the unit tangent vector \mathbf{e}_t , arc-length parameter $s = s(t)$, curvature κ , and torsion τ for this space curve. In addition, show

¹⁶ This result was first established by Maxwell [95, 301].

that there are no self-crossings provided $0 \leq \lambda < 0.5$, while for $\lambda > 0.5$ show that there is a self-crossing which can change sign depending on the whether $\alpha = \pm 1$.

Exercise 3.9: Consider the following pair of curves that are discussed in White and Bauer [360, Eqn. (16)]:

$$\begin{aligned}\mathbf{r}_1(s_1) &= R_A \cos(s_1)\mathbf{E}_1 + R_A \sin(s_1)\mathbf{E}_2, \\ \mathbf{r}_2(s_1) &= \mathbf{r}_1 - r(\cos(ns_1)\cos(s_1)\mathbf{E}_1 + \cos(ns_1)\sin(s_1)\mathbf{E}_2 - \sin(ns_1)\mathbf{E}_3).\end{aligned}\tag{3.69}$$

Here, r and R_A are constants and n is an integer.¹⁷ As s_1 ranges from 0 to 2π , show that \mathcal{S}_2 winds n times around \mathcal{S}_1 . Using the results in Section 3.6 where appropriate, show that $L_k(\mathcal{S}_1, \mathcal{S}_2) = n$.

Exercise 3.10: As an alternative to the Frenet triad, Bishop [28] proposed a framing of the curve that is now known as the Bishop frame: $\{\mathbf{e}_t, \mathbf{B}_1, \mathbf{B}_2\}$. As discussed in Section 3.2, for this right-handed orthonormal frame \mathbf{B}_1 and $\mathbf{B}_2 = \mathbf{e}_t \times \mathbf{B}_1$ are chosen such that they only change in the direction of \mathbf{e}_t :

$$\frac{\partial \mathbf{B}_1}{\partial s} = -\kappa_{\mathbf{B}_1} \mathbf{e}_t, \quad \frac{\partial \mathbf{B}_2}{\partial s} = -\kappa_{\mathbf{B}_2} \mathbf{e}_t.\tag{3.70}$$

Here, the curvatures $\kappa_{\mathbf{B}_1}$ and $\kappa_{\mathbf{B}_2}$ are functions of s . The present exercise explores the Bishop frame for the plane curve

$$\mathbf{r} = x\mathbf{E}_1 + f(x)\mathbf{E}_2,\tag{3.71}$$

where f is a sufficiently smooth function of x . The results of the exercise will reveal the advantage of the Bishop frame when a curve has an inflection point, and the nonuniqueness of the vectors \mathbf{B}_1 and \mathbf{B}_2 .

- (a) Consider the plane curve $\mathbf{r} = x\mathbf{E}_1 + f(x)\mathbf{E}_2$ shown in Figure 3.3. For this curve, show that the unit tangent vector has the representation

$$\mathbf{e}_t = \frac{1}{\sqrt{1 + \frac{df}{dx} \frac{df}{dx}}} \left(\mathbf{E}_1 + \frac{df}{dx} \mathbf{E}_2 \right),\tag{3.72}$$

and the curvature κ is

$$\kappa = \frac{\left| \frac{d^2 f}{dx^2} \right|}{\left(\sqrt{1 + \frac{df}{dx} \frac{df}{dx}} \right)^3}.\tag{3.73}$$

- (b) For the plane curve, show that two possible choices of the Bishop frame are

$$\{\mathbf{e}_t, \mathbf{B}_1 = \mathbf{n}_1, \mathbf{B}_2 = \mathbf{E}_3\}, \quad \{\mathbf{e}_t, \mathbf{B}_1 = -\mathbf{n}_1, \mathbf{B}_2 = -\mathbf{E}_3\},\tag{3.74}$$

¹⁷ The curve \mathcal{S}_2 is not identical to the curve \mathcal{S}_2 that is defined in Eqn. (3.52)₂.

where the unit vector

$$\mathbf{n}_1 = \frac{1}{\sqrt{1 + \frac{df}{dx} \frac{df}{dx}}} \left(\mathbf{E}_2 - \frac{df}{dx} \mathbf{E}_1 \right). \quad (3.75)$$

For this pair of frames, show the respective results:

$$\kappa_{B_1} = \frac{\frac{d^2 f}{dx^2}}{\left(\sqrt{1 + \frac{df}{dx} \frac{df}{dx}} \right)^3}, \quad \kappa_{B_2} = 0, \quad (3.76)$$

and

$$\kappa_{B_1} = -\frac{\frac{d^2 f}{dx^2}}{\left(\sqrt{1 + \frac{df}{dx} \frac{df}{dx}} \right)^3}, \quad \kappa_{B_2} = 0. \quad (3.77)$$

In contrast to the Frenet triad, observe that each of these frames is defined even at points where the curvature $\kappa = 0$ (i.e., at a point of inflection). It is also interesting to note that, for both Bishop frames, the angle θ_B (defined by Eqn. (3.9)) is either 0° or 180° and switches between these values at points of inflection.

- (c) Show that

$$\mathbf{B}_1 = \cos(\theta_0) \mathbf{n}_1 + \sin(\theta_0) \mathbf{E}_3, \quad \mathbf{B}_2 = -\sin(\theta_0) \mathbf{n}_1 + \cos(\theta_0) \mathbf{E}_3, \quad (3.78)$$

where θ_0 is a constant, satisfy the conditions (3.70) with

$$\kappa_{B_1} = \frac{\frac{d^2 f}{dx^2} \cos(\theta_0)}{\left(\sqrt{1 + \frac{df}{dx} \frac{df}{dx}} \right)^3}, \quad \kappa_{B_2} = \frac{\frac{d^2 f}{dx^2} \sin(\theta_0)}{\left(\sqrt{1 + \frac{df}{dx} \frac{df}{dx}} \right)^3}. \quad (3.79)$$

These results demonstrate statements in Bishop [28, Section 3] that the Bishop frame is not unique and that κ_{B_1} and κ_{B_2} are determined up to a rotation.

- (d) Compute Bishop frames for a circular arc and compare the frames to the Frenet triad. Your results should be consistent with Eqn. (3.15).

Part II

Mechanics of Rods

Chapter 4

Theory of the Elastica and a Selection of Its Applications

“What Euler gives us first is a golden analysis of the forms an elastic band may assume. It is a treatise on the nature of certain elliptic integrals in which scarcely any integrals are evaluated.”

C. A. Truesdell [350, Page 216] commenting on Euler’s analysis of the elastica in [106].

4.1 Introduction

For many problems, the string model we discussed is inadequate. This is particularly the case if the body that the string is intended to model shows an ability to respond to applied moments. In this instance, the next member in the hierarchy of potential models is a rod theory. There are a wide range of rod theories and the simplest possible nonlinear theory is known as the elastica. The elastica originates in a seminal work [106] by Leonhard Euler (1707–1783) in 1744 and a linearized version of this theory produces the well-known Bernoulli-Euler beam model. As we shall see in Chapter 5, Euler’s theory of the elastica was extended to include torsion and nonplanar motions by Kirchhoff and others in the 19th century.

Over the course of three centuries since its initial development, Euler’s theory of the elastica has been extended to include dynamical effects, material momentum, adhesion, and growth, among others. The theory has also been extensively applied to model many important structural mechanics problems such as growth of tree stems, deflection and buckling of columns, and deformation of carbon nanotubes, among many others (cf. Figure 4.1). In this chapter, we can only touch on a small subset of these applications. In addition to discussing some of Euler’s extraordinary analysis of the equations for the elastica, we emphasize adhesion problems as they also illuminate the role of the balance of material momentum and examine Bosi et al.’s ingenious arm scale that they presented in [32]. Prior to solving problems, we first summarize the governing equations for a rod which is subject to terminal

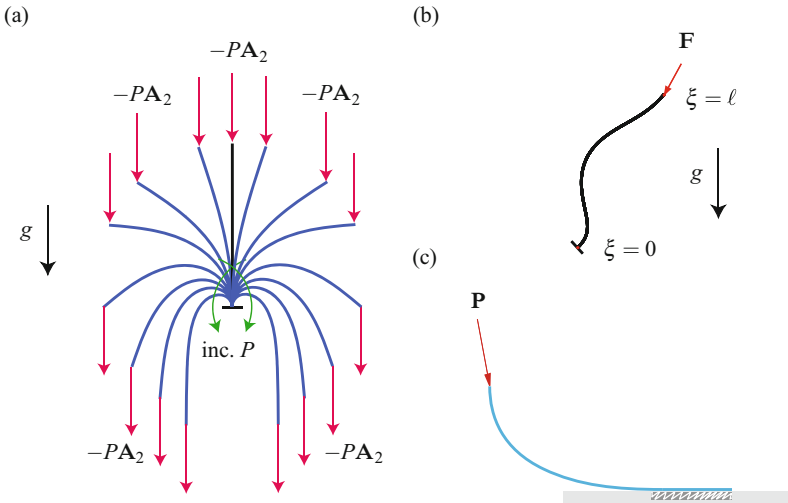


Fig. 4.1 A selection of problems that are analyzed using the elastica. (a) Buckling of an initially straight rod under the combined action of a terminal force $-PA_2$ and its own weight. The deformed configurations shown in this figure correspond to equilibrium configurations of the rod for values of the load P which are successively greater than the buckling load. (b) A simple rod-based model for the spine where the spine is fixed to the sacrum at $\xi = 0$ and to the head at $\xi = \ell$. The intrinsic curvature κ_0 of the elastica in this model mimics the intrinsic curvature of the spine. (c) A terminally loaded rod which has a portion adhered to a flat horizontal surface.

loadings, applied forces, and applied moments. Our development of the balance laws will have evident similarities to the corresponding developments for the theory of the string in Chapter 1.

After applying the theory to several problems, we then explore a variational formulation of the equations governing the elastica. This formulation enables us to establish nonlinear stability criteria for equilibrium configurations of the elastica and a short introduction to the calculus of variations needed for the formulation can be found in Chapter 9. While variational methods for rods can be found in Kirchhoff's seminal paper [185] from 1859, these methods for the elastica were taken to another level by Born in his dissertation [31] from 1906. We can only speculate as to how Born's work was inspired by the remarkable series of results on calculus of variations that were produced in Berlin and Göttingen at the end of the 19th century.¹ There has recently been a resurgence of interest (and new results) in stability criteria² and some of these developments appear in our discussion of stability criteria for buckled rods and adhered rods that occupy the closing sections of this chapter.

¹ These developments are discussed at length in Bolza's marvelous textbook [30].

² The interested reader is referred to the works of Bigoni et al. [26], Maddocks and his collaborators [169, 215, 224–226] and Majidi and his coworkers [219, 220, 268, 269] for discussions of, and references to, these results.

Our discussion of buckling and adhesional instabilities in this chapter relies heavily on the works by O'Reilly and Peters [268, 269] and Majidi, O'Reilly, and Williams [219, 220].

4.2 Kinematical Considerations

For the elastica, the rod is modeled with the assistance of a flexible material curve \mathcal{L} which resists bending. The classical treatment of this theory assumes that the material curve is inextensible, but we relax this assumption in the development of the theory and allow the material curve to stretch. The position vector of a point on the material curve in the present configuration \mathcal{C} is defined by the vector-valued function

$$\mathbf{r} = \mathbf{r}(\xi, t) = X(\xi, t)\mathbf{A}_1 + Y(\xi, t)\mathbf{A}_2. \quad (4.1)$$

Here, $\{\mathbf{A}_1, \mathbf{A}_2, \mathbf{A}_3 = \mathbf{A}_1 \times \mathbf{A}_2\}$ is a right-handed Cartesian basis for \mathbb{E}^3 . The convected coordinate ξ that is used to denote material points on the material curve is chosen to be the arc-length parameter of this curve in a fixed reference configuration. Thus, the arc-length parameter of the material curve in the present configuration and ξ are related:

$$\frac{\partial s}{\partial \xi} = \mu, \quad (4.2)$$

where μ is the stretch. We choose the parameterization s such that $\mu > 0$. For many statics problems where the material curve is assumed to be inextensible (i.e., $\mu = 1$), s and ξ are used interchangeably.

Referring to Figure 4.2, the material curve models the centerline of the planar rod-like body, and the rotation of a material curve which is orthogonal to the centerline can be defined using an angle $\theta = \theta(\xi, t)$. In this case,

$$\mathbf{r}' = \mu \mathbf{e}_t, \quad \mathbf{e}_t = \cos(\theta)\mathbf{A}_1 + \sin(\theta)\mathbf{A}_2, \quad \frac{\partial X}{\partial s} = \cos(\theta), \quad \frac{\partial Y}{\partial s} = \sin(\theta), \quad (4.3)$$

where $\mathbf{e}_t = \frac{\partial \mathbf{r}}{\partial s}$ is the unit tangent vector to the material curve in its present configuration and the prime denotes the partial derivative with respect to ξ .

Material fibers of the rod that are orthogonal to the centerline are assumed to remain orthogonal to the centerline. Consequently, the curvature κ of the centerline is related to θ :

$$\kappa = \frac{\partial \theta}{\partial s} = \frac{1}{\mu} \theta'. \quad (4.4)$$

In a state where neither forces nor moments act on the rod, we allow for the situation where the centerline can have a curvature and refer to this curvature as an intrinsic curvature $\kappa_0 = \kappa_0(\xi)$. An example of a rod with nonzero intrinsic curvature can be seen in the model for the spine shown in Figure 4.1(b). We also define an angular velocity vector and a strain vector $\mathbf{v} - \mathbf{v}_0$:

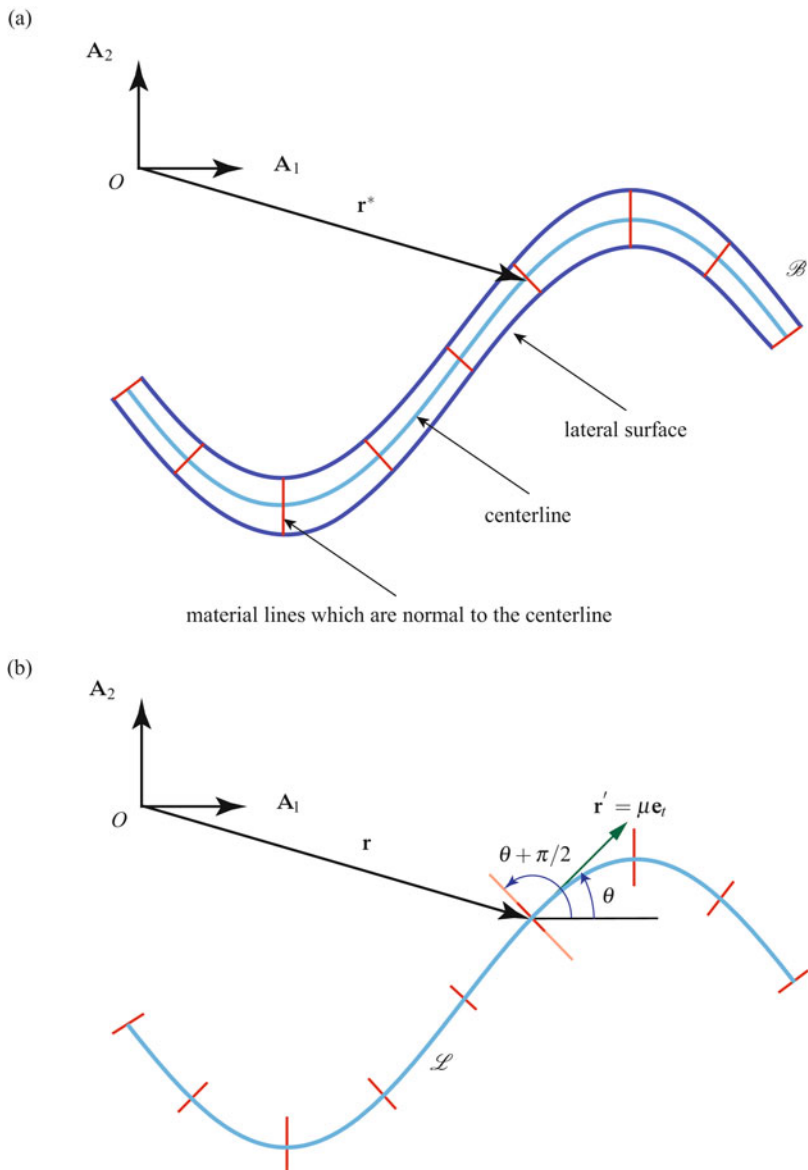


Fig. 4.2 (a) Schematic of the planar deformation of a three-dimensional body \mathcal{B} . The body is bounded by a lateral surface surrounding a centerline and bounding material lines. (b) The present configuration of the elastica used to model \mathcal{B} . Observe that the representative material lines displayed in \mathcal{B} are assumed to remain orthogonal to the material curve \mathcal{L} . The latter models the centerline of \mathcal{B} .

$$\omega = \dot{\theta} \mathbf{A}_3, \quad \mathbf{v} = \theta' \mathbf{A}_3 = \mu \kappa \mathbf{A}_3, \quad \mathbf{v}_0 = \kappa_0 \mathbf{A}_3. \quad (4.5)$$

In the sequel, $\kappa - \kappa_0$ will be known as the bending strain in the rod.

At a discontinuity, we have the jump conditions at a material point ξ associated with the kinematics of the curve. We assume that the position vector of the centerline is continuous and that the cross sections of the rod can be continuously related to the tangent vector:

$$[\![\mathbf{r}]\!]_{\xi} = \mathbf{0}, \quad [\![\theta]\!]_{\xi} = 0. \quad (4.6)$$

We leave it as an exercise for the reader to imagine situations where (4.6) are violated by \mathcal{L} being severed or a material fiber which is initially normal to \mathcal{L} being split into two pieces and pulled apart. Continuity of θ is synonymous with continuity of \mathbf{r}' . Thus, the centerline of the rod cannot exhibit kinks. By differentiating $\mathbf{r}(\gamma(t), t)$ and $\theta(\gamma(t), t)$ with respect to time at a point of discontinuity $\xi = \gamma$, we can show that

$$\mathbf{v}_{\gamma} = \left\{ \dot{\mathbf{r}} + \dot{\gamma} \mathbf{r}' \right\}_{\gamma}, \quad \left[\left[\dot{\mathbf{r}} + \dot{\gamma} \mathbf{r}' \right] \right]_{\gamma} = \mathbf{0}, \quad \omega_{\gamma} = \left\{ \dot{\theta} + \dot{\gamma} \theta' \right\}_{\gamma}, \quad \left[\left[\dot{\theta} + \dot{\gamma} \theta' \right] \right]_{\gamma} = 0, \quad (4.7)$$

where the angular velocity ω_{γ} is the sole component of $\omega_{\gamma} = \omega_{\gamma} \mathbf{A}_3$.

The linear momentum \mathbf{G} per unit length of ξ of the rod is defined by the expression

$$\mathbf{G} = \rho \mu \dot{\mathbf{r}}, \quad (4.8)$$

where $\rho = \rho(\xi, t)$ is the mass density per unit length of ξ , and μ is the stretch. In the sequel $\mu = 1$, but to facilitate comparisons with the string theory we do not impose this condition here. Further, the angular momentum density of the rod relative to O per unit length of ξ is

$$\mathbf{h}_O = \mathbf{r} \times \mathbf{G} + \rho \mu y^{22} \dot{\theta} \mathbf{A}_3, \quad (4.9)$$

where y^{22} is an inertia coefficient which has units of length squared and is related to the second moment of area I .³ For example, for a homogeneous rod whose cross section has a height h and a width b , $\rho_0 = \rho_0^* b h$, and $\rho_0 y^{22} = \rho_0^* I = \rho_0^* (bh^3/12)$. Hence, $y^{22} = h^2/12$. Supplementing this pair of momenta, the material momentum \mathbf{P} for the elastica is defined as

$$\mathbf{P} = -\rho \mu \mathbf{r}' \cdot \dot{\mathbf{r}} - \rho \mu y^{22} \dot{\theta} \theta'. \quad (4.10)$$

We also note that the kinetic energy density T of the elastica is

$$T = \frac{\rho \mu}{2} \dot{\mathbf{r}} \cdot \dot{\mathbf{r}} + \frac{\rho \mu y^{22}}{2} \dot{\theta}^2. \quad (4.11)$$

The evident parallels of this expression to that for the planar motion of a rigid body should be noted.

³ We shall give a prescription for this quantity later on in the related context of more general rod theories (cf. Eqns. (5.36)₃, (5.37), and (7.98)₃).

The theory of the inextensible elastica assumes that the strain energy function depends on the bending strain $\Delta\kappa = \theta' - \kappa_0 = \kappa - \kappa_0$. If the rod is nonhomogeneous, then the strain energy function ψ can also depend on the material coordinate ξ :

$$\rho\mu\psi = \rho\mu\psi(\theta' - \kappa_0, \xi). \quad (4.12)$$

For the constitutive relation proposed by Euler for the inextensible elastica,

$$\rho\mu\psi = \frac{EI}{2} (\theta' - \kappa_0)^2, \quad (4.13)$$

where the product of Young's modulus E and the second moment of area I , EI , is known as the flexural rigidity. Recently, modest generalizations of this constitutive relation have found application in elastica-based models for soft robot actuators (cf. [286, 372, 373] and references therein). For the extensible case, the strain energy function additionally depends on the stretch μ . One representation for this function is

$$\rho\mu\psi = \rho\mu\hat{\psi}(\theta' - \kappa_0, \mu, \xi). \quad (4.14)$$

For the extensible case, we note that $\theta' = \mu\kappa$. Alternatively, we could prescribe the functional representation

$$\rho\mu\psi = \rho\mu\tilde{\psi}(\kappa - \kappa_0, \mu, \xi), \quad (4.15)$$

where $\hat{\psi}(\mu\kappa - \kappa_0, \mu, \xi) = \tilde{\psi}(\kappa - \kappa_0, \mu, \xi)$.

If we consider two motions of the elastica which differ by a rigid body motion, then it is straightforward to use the results from Section 1.4.5 in Chapter 1 to show that

$$(\mathbf{r}^\perp)' = \mathbf{Q}\mathbf{r}', \quad \mu^\perp = \mu, \quad (\theta')^\perp = \theta'. \quad (4.16)$$

Because the motion of the elastica is planar, the rotation \mathbf{Q} has a fixed axis of rotation \mathbf{A}_3 . As a consequence of the relations (4.16), we can verify that the strain energy functions ψ and $\hat{\psi}$ that were discussed earlier (cf. Eqns. (4.12) and (4.14)) are invariant under superposed rigid body motions:

$$\begin{aligned} \psi^\perp &= \psi((\theta')^\perp - \kappa_0, \xi) = \psi(\theta' - \kappa_0, \xi), \\ \hat{\psi}^\perp &= \hat{\psi}((\theta')^\perp - \kappa_0, \mu^\perp, \xi) = \hat{\psi}(\theta' - \kappa_0, \mu, \xi). \end{aligned} \quad (4.17)$$

The importance of these results lies in our expectation that the strain energy of the elastica should not change if we rigidly move the elastica from one configuration to another.

4.3 Balance Laws

Preparatory to writing the conservation laws for the rod, we admit the following force fields for the theory of the elastica: a contact force, $\mathbf{n} = \mathbf{n}(\xi, t)$; a contact material force, $C = C(\xi, t)$,

$$C = \rho\mu\psi - \mathbf{n} \cdot \mathbf{r}' - \mathbf{m} \cdot \boldsymbol{\theta}' \mathbf{A}_3 - \frac{\rho\mu}{2} \dot{\mathbf{r}} \cdot \dot{\mathbf{r}} - \frac{\rho\mu y^{22}}{2} \dot{\theta}^2; \quad (4.18)$$

and a contact moment, $\mathbf{m} = \mathbf{m}(\xi, t)$. The body forces and surface tractions acting on the lateral surface of the three-dimensional body that the rod is modeling contribute to the assigned force, $\rho\mu\mathbf{f} = \rho\mu\mathbf{f}(\xi, t)$, and the assigned moment, $\mathbf{m}_a = \mathbf{m}_a(\xi, t) = M_a \mathbf{A}_3$, each per unit length ξ of the elastica. For the applications considered here, the prescriptions for \mathbf{f} and \mathbf{m}_a will be in agreement with more detailed treatments that are presented in Chapter 5 (cf. Eqns. (5.70) and (5.71)) and Section 7.6.1 in Chapter 7. Completing the assigned forces, we have the assigned material force b . As with the earlier developments of the theory of an elastic string, we are motivated by the works of Green and Naghdi [132] and Marshall and Naghdi [230], among others, and admit singular supplies of momentum, \mathbf{F}_γ , material momentum, \mathbf{B}_γ , angular momentum relative to O , \mathbf{M}_{O_γ} , and power, Φ_{E_γ} , at a specific material point $\xi = \gamma(t)$.⁴ It is useful to note that, in comparison to the string theory, the new quantities introduced here are moments and strains associated with the rotation θ of the tangent vector to \mathcal{L} .

We adopt the following balance laws for any fixed material segment (ξ_1, ξ_2) of the elastica. First, we record the conservations of mass and inertia:

$$\begin{aligned} \frac{d}{dt} \int_{\xi_1}^{\xi_2} \rho \mu d\xi &= 0, \\ \frac{d}{dt} \int_{\xi_1}^{\xi_2} \rho y^{22} \mu d\xi &= 0. \end{aligned} \quad (4.19)$$

The balance of linear momentum is

$$\frac{d}{dt} \int_{\xi_1}^{\xi_2} \rho \dot{\mathbf{r}} \mu d\xi = \int_{\xi_1}^{\xi_2} \rho \mu \mathbf{f} d\xi + [\mathbf{n}]_{\xi_1}^{\xi_2} + \int_{\xi_1}^{\xi_2} \mathbf{F}_\gamma \delta(\xi - \gamma) d\xi. \quad (4.20)$$

The balance of angular (or moment of) momentum relative to O is

$$\begin{aligned} \frac{d}{dt} \int_{\xi_1}^{\xi_2} \mathbf{h}_O d\xi &= [\mathbf{r} \times \mathbf{n} + \mathbf{m}]_{\xi_1}^{\xi_2} + \int_{\xi_1}^{\xi_2} (\mathbf{r} \times \rho \mu \mathbf{f} + \mathbf{m}_a) d\xi \\ &\quad + \int_{\xi_1}^{\xi_2} \mathbf{M}_{O_\gamma} \delta(\xi - \gamma) d\xi. \end{aligned} \quad (4.21)$$

⁴ As usual, for ease of exposition and without loss of generality, we assume that there is at most one such point.

As with the string, one has a balance of material momentum,

$$\frac{d}{dt} \int_{\xi_1}^{\xi_2} P d\xi = [C]_{\xi_1}^{\xi_2} + \int_{\xi_1}^{\xi_2} b d\xi + \int_{\xi_1}^{\xi_2} B_\gamma \delta(\xi - \gamma) d\xi. \quad (4.22)$$

One also has the balance of energy:

$$\begin{aligned} \frac{d}{dt} \int_{\xi_1}^{\xi_2} (\psi \rho \mu + T) d\xi &= [\mathbf{n} \cdot \mathbf{v} + \mathbf{m} \cdot \boldsymbol{\omega}]_{\xi_1}^{\xi_2} + \int_{\xi_1}^{\xi_2} (\rho \mu \mathbf{f} \cdot \mathbf{v} + \mathbf{m}_a \cdot \boldsymbol{\omega}) d\xi \\ &\quad + \int_{\xi_1}^{\xi_2} \Phi_{E_\gamma} \delta(\xi - \gamma) d\xi. \end{aligned} \quad (4.23)$$

The similarities in structure between these balance laws and those we presented earlier for a string should be recorded. In addition, you should notice the alterations made to the balances of energy, material momentum, and angular momentum to accommodate the moment fields.

As we shall see later in our discussion of the elastica arm scale, (4.22) will lead to a useful conservation law. We also take this opportunity to note that the balance of material momentum for a homogeneous rod, albeit in the absence of assigned forces and moments, has appeared as a conservation law of the form

$$\frac{d}{dt} \int_{\xi_0}^{\xi_1} P d\xi = [C]_{\xi_0}^{\xi_1} \quad (4.24)$$

in the literature (see [66, 182, 183] and references therein). Indeed for the static case, the conservation of C can be found in Love [213, Eqn. (7) in Sect. 262]. However, for the problems of interest in this chapter, we find that we need to allow for a nonzero b and a singular supply of material momentum B_γ .

4.3.1 Local Balance Laws and Constitutive Relations

For the elastica, we assume that the laws (4.19)–(4.23) hold for any material segment. With the help of the procedure used to localize the balance laws, we find the following balance laws should hold at a point $\xi \neq \gamma$ for the elastica. First, we have moment of inertia and mass conservations:

$$\rho_0 = \rho_0(\xi) = \rho \mu, \quad y^{22} = y^{22}(\xi). \quad (4.25)$$

Next, we find the balance laws for linear and angular momentum:

$$\rho_0 \ddot{\mathbf{r}} = \rho_0 \mathbf{f} + \frac{\partial \mathbf{n}}{\partial \xi}, \quad \rho_0 y^{22} \ddot{\theta} \mathbf{A}_3 = \mathbf{m}_a + \frac{\partial \mathbf{m}}{\partial \xi} + \frac{\partial \mathbf{r}}{\partial \xi} \times \mathbf{n}. \quad (4.26)$$

We also find local forms of the material momentum balance and energy balance:

$$\frac{\partial C}{\partial \xi} + b = \dot{P}, \quad (4.27)$$

and

$$\rho_0 \psi = \mathbf{m} \cdot \frac{\partial \omega}{\partial \xi} + \mathbf{n} \cdot \left(\frac{\partial \mathbf{v}}{\partial \xi} - \omega \times \frac{\partial \mathbf{r}}{\partial \xi} \right). \quad (4.28)$$

We have used Eqns. (4.25)–(4.26) to simplify the energy balance (4.28).

To establish a determinate system of governing equations for the elastica, we first need to establish constitutive relations for \mathbf{n} and \mathbf{m} . The methodology we use to establish these relations has parallels to the ones used earlier for strings in Section 1.6 of Chapter 1 and, in Section 8.6 of Chapter 8, for a three-dimensional continuum. We first consider the inextensible case: $\mu = 1$, $\frac{\partial \mathbf{v}}{\partial \xi} = \omega \times \frac{\partial \mathbf{r}}{\partial \xi}$, and the energy equation (4.28) simplifies dramatically:

$$\rho_0 \psi = \mathbf{m} \cdot \frac{\partial \omega}{\partial \xi}. \quad (4.29)$$

Additionally, it is assumed that

$$\rho_0 \psi = \rho_0 \psi(\Delta \kappa, \xi) \text{ where } \Delta \kappa = \kappa - \kappa_0. \quad (4.30)$$

Consequently,

$$\psi = \frac{\partial \psi}{\partial \Delta \kappa} \dot{\kappa} = \frac{\partial \psi}{\partial \Delta \kappa} \dot{\theta}'. \quad (4.31)$$

Next, we assume that the local form of the balance of energy (4.29) is identically satisfied by all motions of the elastica. Thus, we seek solutions \mathbf{m} and \mathbf{n} of Eqn. (4.29). Using a standard procedure, we find the desired constitutive relations:

$$\mathbf{m} = \rho_0 \frac{\partial \psi}{\partial \Delta \kappa} \mathbf{A}_3, \quad \mathbf{n} = n_1 \mathbf{A}_1 + n_2 \mathbf{A}_2, \quad (4.32)$$

where $n_1 = n_1(\xi, t)$ and $n_2 = n_2(\xi, t)$ must be determined from the balance laws. Use of the relations (4.32) implies that the local form of the energy balance is identically satisfied. We note that these relations include as a special case the Bernoulli-Euler relations for \mathbf{m} :

$$\mathbf{m} = EI \left(\theta' - \kappa_0 \right) \mathbf{A}_3, \quad (4.33)$$

where the strain energy function is prescribed as

$$\rho_0 \psi = \frac{EI}{2} \left(\theta' - \kappa_0 \right)^2 = \frac{EI}{2} (\kappa - \kappa_0)^2. \quad (4.34)$$

Observe that in contrast to the theory of the string, \mathbf{n} is no longer restricted to being parallel to \mathbf{r}' and now has a component in the normal direction \mathbf{e}_n to the material curve \mathcal{L} . This additional component can be interpreted as a shearing force.

The constitutive relations for the extensible elastica follow a similar line of argument with the strain energy function now being assumed to additionally depend on the stretch μ :

$$\rho_0 \psi = \rho_0 \hat{\psi} \left(\theta' - \kappa_0, \mu, \xi \right). \quad (4.35)$$

With the help of an identity,

$$\frac{\partial \mathbf{v}}{\partial \xi} = \boldsymbol{\omega} \times \frac{\partial \mathbf{r}}{\partial \xi} + \dot{\mu} \mathbf{e}_t, \quad (4.36)$$

the balance of energy (4.28) simplifies to

$$\rho_0 \dot{\psi} = \mathbf{m} \cdot \frac{\partial \boldsymbol{\omega}}{\partial \xi} + \mathbf{n} \cdot \dot{\mu} \mathbf{e}_t. \quad (4.37)$$

Whence, we find the constitutive relations

$$\begin{aligned} \mathbf{m} &= \rho_0 \frac{\partial \hat{\psi}}{\partial \theta'} \mathbf{A}_3, \\ \mathbf{n} &= \rho_0 \frac{\partial \hat{\psi}}{\partial \mu} \mathbf{e}_t + n_n \mathbf{e}_n, \end{aligned} \quad (4.38)$$

where the (shear) force $n_n \mathbf{e}_n$ must be determined from the balance laws. It is an interesting exercise to compare the constitutive relation for \mathbf{n} and its counterpart for an elastic string (cf. Eqn. (1.96)). Another interesting exercise is to compute the constitutive relations for \mathbf{m} and \mathbf{n} that arise when ψ is assumed to have the functional form $\rho \mu \tilde{\psi}(\kappa - \kappa_0, \mu, \xi)$ that was mentioned earlier.

For both the extensible and inextensible cases, we prescribe the assigned material force \mathbf{b} so that the local form of the material momentum balance law (4.27) is identically satisfied:

$$\mathbf{b}_p = -\rho_0 \mathbf{f} \cdot \mathbf{r}' - \mathbf{m}_a \cdot \theta' \mathbf{A}_3 - \left(\frac{\partial (\rho_0 \psi)}{\partial \xi} - \frac{\partial T}{\partial \xi} \right)_{\text{exp}}. \quad (4.39)$$

A similar prescription was used earlier with the theory of an elastic string and shall also be employed in the sequel with more elaborate rod theories.

4.3.2 Jump Conditions

Five jump conditions are obtained from the balance laws. The procedure is identical to that discussed in Section 1.5.3 in Chapter 1. Before presenting the conditions, we emphasize that they are supplemented by the compatibility conditions (4.6) and (4.7)_{2,4}:

$$[[\mathbf{r}]]_\xi = \mathbf{0}, \quad [[\theta]]_\xi = 0, \quad [[[\dot{\mathbf{r}} + \dot{\gamma} \mathbf{r}']]_\gamma = \mathbf{0}, \quad [[[\dot{\theta} + \dot{\gamma} \theta']]_\gamma = 0. \quad (4.40)$$

Turning to the jump conditions from the balance laws at a point $\xi = \gamma$, we find that

$$\begin{aligned} [[\rho_0]]_\gamma \dot{\gamma} &= 0, & [[[\rho_0 y^{22}]]]_\gamma \dot{\gamma} &= 0, \\ [[\mathbf{n} + \rho_0 \dot{\gamma} \mathbf{r}]]_\gamma + \mathbf{F}_\gamma &= \mathbf{0}, & [[\mathbf{C} + \dot{\gamma} \mathbf{P}]]_\gamma + \mathbf{B}_\gamma &= 0, \\ [[[\mathbf{m} + \rho_0 y^{22} \dot{\theta} \dot{\gamma} \mathbf{A}_3]]]_\gamma + \mathbf{M}_{O_\gamma} - \mathbf{r}(\gamma, t) \times \mathbf{F}_\gamma &= \mathbf{0}, \\ [[\rho_0 \psi + T]]_\gamma \dot{\gamma} + [[[\mathbf{n} \cdot \mathbf{v} + \mathbf{m} \cdot \boldsymbol{\omega}]]]_\gamma + \Phi_{E_\gamma} &= 0. \end{aligned} \quad (4.41)$$

It is convenient to define a moment \mathbf{M}_γ relative to the material point $\xi = \gamma$:

$$\mathbf{M}_\gamma = \mathbf{M}_{O_\gamma} - \mathbf{r}(\gamma, t) \times \mathbf{F}_\gamma. \quad (4.42)$$

The moment \mathbf{M}_γ will also prove to be convenient to use when dealing with boundary conditions.

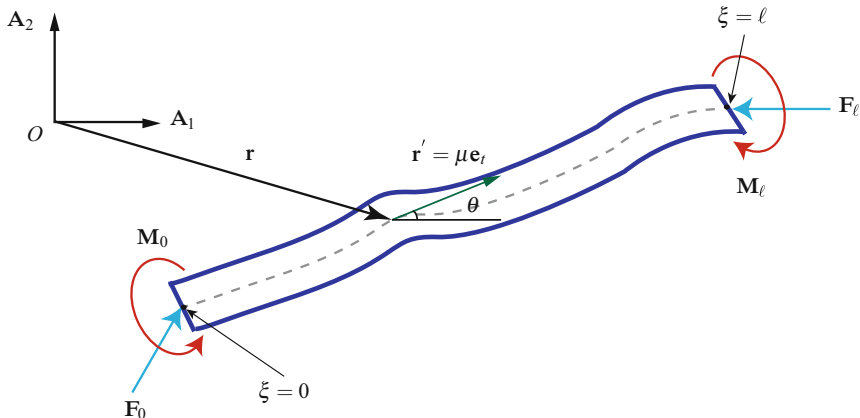


Fig. 4.3 Schematic of an elastica which is subject to terminal forces and moments.

The singular supplies in these jump conditions can be related by an identity which follows from the jump condition (4.41)₆ in a fashion similar to that used to establish (1.88)⁵:

$$\mathbf{B}_\gamma \dot{\gamma} + \mathbf{F}_\gamma \cdot \mathbf{v}_\gamma + \mathbf{M}_\gamma \cdot \boldsymbol{\omega}_\gamma \mathbf{A}_3 = \Phi_{E_\gamma}. \quad (4.43)$$

Note that the singular supplies are each associated with their conjugate velocity. Continuing a theme from earlier, we consider (4.43) to be an identity satisfied by the supplies and make no further mention of the jump condition (4.41)₆ from the energy balance.

As we have shown previously, the jump conditions are also helpful in establishing boundary conditions. For instance, for the situation shown in Figure 4.3, we can use

⁵ For additional details on this matter, see [263, 264] and Exercises 1.3 and 1.4.

the jump conditions to infer that $\mathbf{n}(0^+, t) = -\mathbf{F}_0$ and $\mathbf{m}(\ell^-, t) = \mathbf{M}_\ell$. In addition, in the absence of singular supplies and assuming that $\dot{\gamma} = 0$ (i.e., γ corresponds to a constant material point), the jump conditions yield

$$[\![\mathbf{n}]\!]_\gamma = \mathbf{0}, \quad [\![\mathbf{m}]\!]_\gamma = \mathbf{0}, \quad (4.44)$$

so \mathbf{n} and \mathbf{m} are continuous at such material points.

4.3.3 Summary of the Governing Equations

In the applications that follow, the material curve shall be assumed to be inextensible and the local forms of the balances of energy and material momentum are considered to be identically satisfied. In addition, the jump condition from the energy balance will be used to determine $\Phi_{E\gamma}$. Thus, the governing equations for the inextensible elastica that are used in the sequel are the differential equations (4.26) supplemented by the Bernoulli-Euler constitutive relations (4.33) and the jump conditions for linear momentum, material momentum, and moment of momentum (4.41)_{3,4,5}. We shall also appeal to the compatibility conditions (4.40).

4.4 A Terminally Loaded Elastica and the Kinetic Analogue

As a first application of the theory of the elastica, we consider the classical problem of a uniform rod of length ℓ which is subject to loadings at its ends. This problem, that of a terminally loaded rod, is the subject of Euler's celebrated work [106] and we will reproduce several of his results. For such a homogenous rod in the absence of assigned forces and moments, the equation governing the static equilibrium configuration can be found from Eqn. (4.26). The latter equations simplify dramatically to the following pair of results:

$$EI\theta'' + \left(\frac{\partial \mathbf{r}}{\partial \xi} \times \mathbf{n} \right) \cdot \mathbf{A}_3 = 0, \\ \mathbf{n} = \mathbf{n}_0 = n_0_1 \mathbf{A}_1 + n_0_2 \mathbf{A}_2, \quad (4.45)$$

where \mathbf{n}_0 is a constant. Here, the homogeneous rod is assumed to be subject to the following constant terminal loadings:

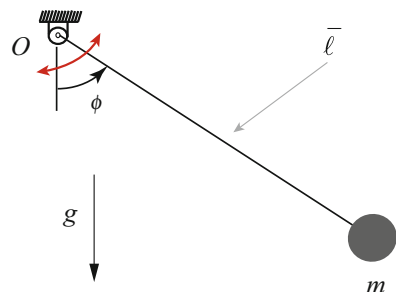


Fig. 4.4 A planar pendulum and the analogue model for an elastica. The simple pendulum of length $\bar{\ell}$ is free to rotate in a plane and is attached to a fixed point O by a pin joint.

$$\mathbf{F}_0 = P_1 \mathbf{A}_1 + P_2 \mathbf{A}_2, \quad \mathbf{F}_\ell = -P_1 \mathbf{A}_1 - P_2 \mathbf{A}_2, \quad \mathbf{M}_0 = M_0 \mathbf{A}_3, \quad \mathbf{M}_\ell = M_\ell \mathbf{A}_3, \quad (4.46)$$

and the Bernoulli-Euler constitutive relations, $\mathbf{m} = EI\theta' \mathbf{A}_3$, are assumed. Observe that Eqn. (4.46) implies that $\mathbf{n}_0 = -P_1 \mathbf{A}_1 - P_2 \mathbf{A}_2$. For the case where $P_2 = 0$, it should be apparent that if $P_1 > 0$ ($P_1 < 0$), then the rod is in compression (tension) if $\mathbf{r}'(0^+, t) \cdot \mathbf{A}_1 > 0$.

With some additional manipulations, the ordinary differential equation for $\theta(\xi)$ reduces to

$$EI\theta'' - P_2 \cos(\theta) + P_1 \sin(\theta) = 0. \quad (4.47)$$

Solutions to this equation which pertain to the boundary-value problem of interest must satisfy the boundary conditions:

$$\theta'(\xi = 0^+) = -\frac{M_0}{EI}, \quad \theta'(\xi = \ell^-) = \frac{M_\ell}{EI}. \quad (4.48)$$

This pair of conditions follow from Eqn. (4.46) and the jump condition (4.41)₅ from the balance of angular momentum.

We can express the differential equation (4.47) in an alternative form by defining a constant angle β :

$$\sin(\beta) = \frac{P_2}{\sqrt{P_1^2 + P_2^2}}, \quad \cos(\beta) = \frac{P_1}{\sqrt{P_1^2 + P_2^2}}. \quad (4.49)$$

Whence, Eqn. (4.47) becomes

$$EI(\theta - \beta)'' + \sqrt{P_1^2 + P_2^2} \sin(\theta - \beta) = 0. \quad (4.50)$$

Equivalently, one can choose \mathbf{A}_1 and \mathbf{A}_2 so that \mathbf{F}_0 and \mathbf{F}_ℓ have the simple representations $\mathbf{F}_0 = P\mathbf{A}_1$ and $\mathbf{F}_\ell = -P\mathbf{A}_1$. That is, one rotates \mathbf{A}_1 and \mathbf{A}_2 through an angle β about \mathbf{A}_3 so that $\mathbf{F}_0 = -\mathbf{F}_\ell$ are parallel to \mathbf{A}_1 . We choose to make such a selection, and so (4.47) simply becomes

$$EI\theta'' + P \sin(\theta) = 0. \quad (4.51)$$

A variety of pairs of suitable boundary conditions for $\theta(\xi)$ will be explored in the remainder of this chapter.

Dating to the 1800s, it was realized that the ordinary differential equation (4.51) is analogous to that governing the motion of a planar pendulum shown in Figure 4.4:

$$I_O \ddot{\phi} + mg\bar{l} \sin(\phi) = 0, \quad (4.52)$$

where the center of mass of the pendulum is located a distance \bar{l} from the pin-joint at O , and the mass moment of inertia of the pendulum about O is $I_O = m\bar{l}^2$. That is, the pendulum is analogous to the terminally loaded elastica: a correspondence that is known as the kinetic analogue. The advantage of the correspondence is that

it enables the use of known analytical solutions to Eqn. (4.52) to help develop an understanding of the solutions $\theta(\xi)$ to the differential equation (4.51) and analytical expressions for the corresponding $\mathbf{r}(\xi)$.

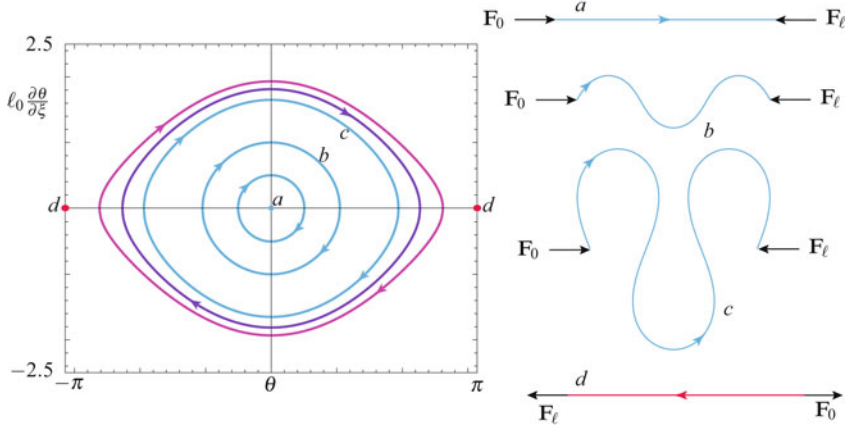


Fig. 4.5 A selection of some classic inflexional solutions $\theta'(\theta)$ and $\mathbf{r}(\xi)$ to the boundary-value problem (4.48) and (4.51) for a terminally loaded elastica where the length ℓ is varied and the loading parameter $\frac{P\ell_0^2}{EI}$ is held constant. The arrows on the graphs of $\theta'(\theta)$ and $\mathbf{r}(\xi)$ correspond to the direction of increasing ξ from 0 to ℓ . The solution labeled *a* corresponds to the straight compressed elastica (and the equilibrium $(\theta, \theta') = (0, 0)$); each one of the solutions labeled *b-c* correspond to elastic rods with points of inflection; and the solution labeled *d* is the solution corresponding to a tensile load (and the equilibrium $(\theta, \theta') = (\pi, 0)$). Observe that the rod in *a* is in compression, while the rod is in a state of tension in *d*.

To elaborate, consider a given boundary-value problem for a rod so that P_1 , P_2 , EI , and a length scale ℓ_0 are specified. Then, the correspondence between the pendulum equations of motion and those for the rod are found by first specifying the angle β (using Eqn. (4.49)), the length $\bar{\ell}$, and the scale T_0 (in seconds):

$$\frac{gT_0^2}{\bar{\ell}} = \frac{\ell_0^2}{EI} \sqrt{P_1^2 + P_2^2}. \quad (4.53)$$

Then, the solution to the equation of motion for the pendulum (4.52) which satisfies the boundary conditions (cf. Eqn. (4.48))

$$\dot{\phi}(t=0) = \frac{1}{T_0} \left(\frac{M_0 \ell_0}{EI} \right), \quad \dot{\phi}\left(t = \frac{\ell T_0}{\ell_0}\right) = \frac{1}{T_0} \left(\frac{M_\ell \ell_0}{EI} \right), \quad (4.54)$$

is analogous to the corresponding solution $\theta(\xi)$ to Eqn. (4.45).

As we shall see in several examples in Sections 4.5.3 and 4.6.4, the kinetic analogue enables one to obtain useful quantitative information on $\theta(\xi)$. However, in

order to determine the equilibrium configuration, this information must then be translated using the identities $\frac{\partial Y}{\partial \xi} = \sin(\theta)$ and $\frac{\partial X}{\partial \xi} = \cos(\theta)$ to provide the corresponding equation for the position vectors $\mathbf{r}(\xi)$ of points on the centerline of the rod (cf. Eqn. (4.3)_{2,3}). The most extraordinary examples of such calculations date to Euler [106] in the 18th century and Hess [168] among others in the 19th century.⁶ A discussion of these works can be found in Love's treatise [213, Sections 262–263] and Truesdell's epic commentary [350]. In addition to these works, the papers by Batista [17], Bigoni et al. [26], Coleman and Dill [65], and Domokos and Ruina [92] are recommended reading and resources for additional perspectives and references to works on the elastica.

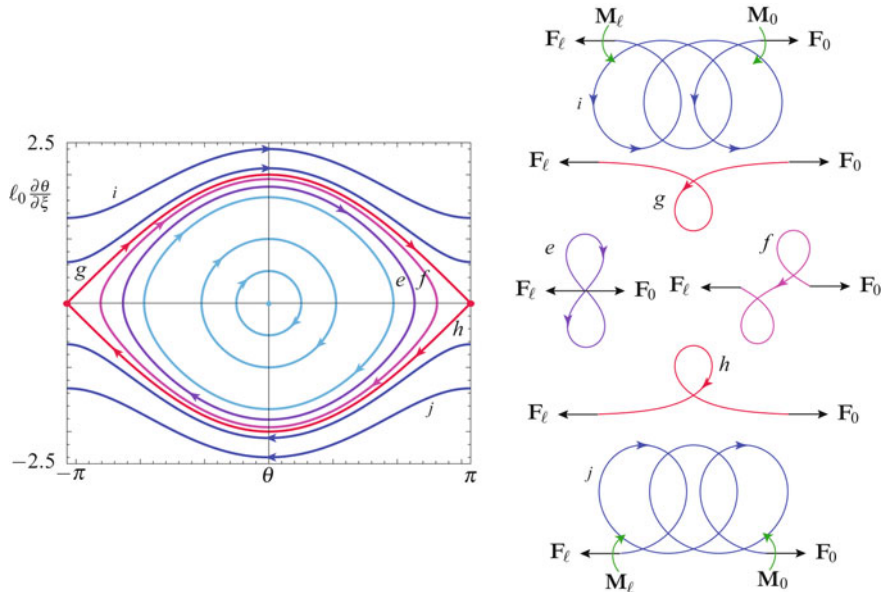


Fig. 4.6 An additional selection of some classic solutions $\theta'(\theta)$ and $\mathbf{r}(\xi)$ to the boundary-value problem (4.48) and (4.51) for a terminally loaded elastica where the length ℓ is varied and the loading parameter $\frac{P\ell_0^2}{EI}$ is held constant. The solutions labeled *e-h* are each examples of inflexional elastica and solutions labeled *i-j* are each examples of non-inflexional elastica. For the latter, terminal bending moments are always needed for equilibrium.

The solutions $\mathbf{r}(\xi)$ found by Euler [106] and documented further by Hess [168] and Love [213, Sections 262–263] are presented in Figures 4.5 and 4.6. To discuss the figures, we assume that \mathbf{A}_1 has been chosen so that $\beta = 0$ and the terminal load at $\xi = 0$ is simply $\mathbf{F}_0 = P\mathbf{A}_1$ with $P > 0$. We now comment on the

⁶ A translation of Euler's original work [106] is readily available and was published by Oldfather et al. [254].

solutions shown in the aforementioned figures. First, the equilibria of the equations $EI\theta'' + P_1 \sin(\theta) = 0$ correspond to straight equilibrium configurations of the rod. The equilibrium $(\theta, \theta') = (0, 0)$ corresponds to the compressed state, while the equilibrium $(\theta, \theta') = (\pi, 0)$ corresponds to the rod in tension. The reversal of the rod, which is akin to a reflection, that is evident in Figures 4.5 can be understood by examining the equilibrium configurations shown in this figure and the companion Figure 4.6.

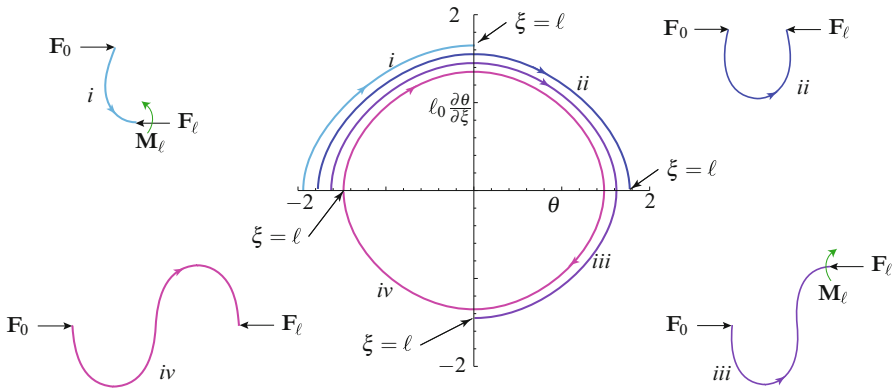


Fig. 4.7 A selection of some classic non-inflexional solutions $\theta'(\theta)$ and $\mathbf{r}(\xi)$ to the boundary-value problem (4.48) and (4.51) for a terminally loaded elastica where the length ℓ is varied and the loading parameter $\frac{P\ell^2}{EI}$ is held constant. It should be evident from these examples that, depending on the value of $\theta'(\xi = \ell)$, a terminal moment \mathbf{M}_ℓ may be required to maintain equilibrium. The arrows on the graphs of $\theta'(\theta)$ and $\mathbf{r}(\xi)$ correspond to the direction of increasing ξ from 0 to ℓ .

The solutions highlighted in Figure 4.5 each correspond to configurations of the elastica that are known as inflexional by Love [213]. These solutions, if ℓ is sufficiently large, contain points where the bending moment vanishes. Consequently, if ℓ is chosen appropriately, they can be supported by terminal forces only. This is the case for the solutions $\mathbf{r}(\xi)$ shown in Figure 4.5. By way of contrast, a family of inflexional solutions are shown in Figure 4.7 which are intended to further illuminate the correspondence between the trajectories in the phase portrait and the boundary conditions at the two ends of the rod.

The solutions labeled g and h in Figure 4.6 can be manifested in infinitely long rods by terminal forces alone. Each of the configurations for $\mathbf{r}(\xi)$ have a single loop and the corresponding solution curve $\theta'(\theta)$ in the phase portrait is known as a homoclinic orbit or separatrix. Two other types of solutions are shown in Figure 4.6. First, we find solutions where self-contact occurs. This occurs first for the solution labeled e and as one approaches the separatrix (labeled g and h), the centerline of

the elastica passes through itself and the reversal discussed earlier now becomes possible. With this reversal, the straight rod passes from a state of compression to one of tension.

Equilibrium configurations of the elastica that correspond to solutions of the form i and j shown in Figure 4.6 are classified by Love [213] as non-inflexional. Regardless of ℓ , these solutions require terminal moments in addition to terminal forces. If ℓ is sufficiently large, the space curve formed by $\mathbf{r}(\xi)$ inevitably involves self-contact of the rod at a discrete number of points. The self-contact phenomenon associated with the loop formation is technically challenging not least because we are assuming planar solutions yet an equilibrium configuration having a loop must be nonplanar. We shall return to this problem in Section 5.15.3 of Chapter 5 where a more sophisticated rod model is used to examine loop formation. Additional examples of the correspondence between solutions of the planar pendulum equation of motion and the shape of $\mathbf{r}(\xi)$ can also be found in Figure 5.16 and throughout the remainder of this chapter.

4.5 The Adhesion of a Rod

For the next set of applications of interest, we consider an elastic rod which is in partial contact with a horizontal surface (see Figure 4.8). Specifically, the portion $\xi \in (\gamma, \ell)$ is glued to the surface by a bond whose adhesive strength per unit length of rod is W_{ad} . This positive material constant is the work required to free a unit length of the rod from the horizontal surface.⁷ At the other end of the rod, a terminal force \mathbf{P} and a terminal moment \mathbf{M}_0 are applied at $\xi = 0$. The terminal loading can be used to peel the rod from the horizontal surface or maintain a state of adhesion. In addition to the deformed shape of the rod, one of the crucial unknowns in this problem is the value γ of the coordinate ξ where the adhesive bond is broken. The adhesion problem we are considering is sometimes referred to as the peeling problem or the peel test.

Our goal here is to show how to formulate and solve the adhesion problem. The method we present relies heavily on the jump condition from the balance of material momentum. This condition produces a boundary condition at the interface between the adhered and free segments of the rod.⁸ We model the rod as an elastica and note that such a model has received considerable attention in the literature⁹ in part because of its analytical tractability and in part because the system of interest is a prototype for studies of adhesion in peeling tape, Gecko setae [16], and carbon nanotubes [116, 117, 374].

⁷ Discussions on how to calculate this constant can be found in [172, 175].

⁸ Our emphasis of the key role played by the material momentum balance law in specifying the adhesion boundary condition is heavily influenced by the works [217, 219, 220, 264, 292].

⁹ See the papers [116, 117, 217, 219, 220, 290, 291, 364] and references therein.

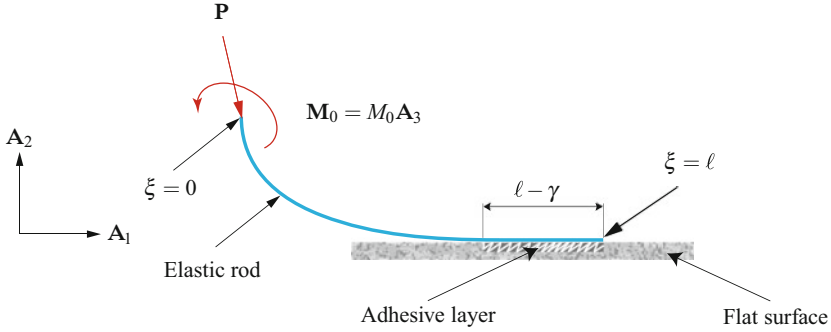


Fig. 4.8 Schematic of a terminally loaded rod of length ℓ where a portion of the rod has adhered to a horizontal surface.

4.5.1 General Considerations

We consider the simplest model for the adhesion problem and use the static version of the elastica theory. For convenience, we divide the rod into three sections: \mathcal{I}_1 : $0 < \xi < \gamma$, \mathcal{I}_{II} : $\xi = \gamma$, and \mathcal{I}_{III} : $\ell > \xi > \gamma$. On \mathcal{I}_1 , there are no body forces or surface tractions on the lateral surface, thus $\mathbf{m}_a = \mathbf{0}$ and $\mathbf{f} = \mathbf{0}$. This is in contrast to the situation on \mathcal{I}_{III} where surface tractions are present and $EI \frac{\partial \theta}{\partial \xi} = 0$. At $\xi = \gamma$, we have a discontinuity, a material momentum supply

$$B_\gamma = -W_{ad}. \quad (4.55)$$

and unknown momentum supplies \mathbf{F}_γ and \mathbf{M}_γ . As the problem is static and the centerline of the rod is inextensible, we will use s and ξ interchangeably. A variational formulation of this problem that is presented in Section 4.7.2.2 yields additional motivation for the prescription $B_\gamma = -W_{ad}$ and also demonstrates that the prescription (4.55) is in accord with other formulations of this adhesion problem.

Referring to Section 4.3, we recall the local form of the balance laws and constitutive relations for this theory:

$$\begin{aligned} \mathbf{n}' + \rho_0 \mathbf{f} &= \mathbf{0}, \\ \mathbf{m}' + \mathbf{r}' \times \mathbf{n} + \mathbf{m}_a &= \mathbf{0}, \\ C' + b &= 0, \\ \mathbf{m} = EI \frac{\partial \theta}{\partial \xi} \mathbf{A}_3, \quad C &= -\frac{EI}{2} \left(\frac{\partial \theta}{\partial \xi} \right)^2 - \mathbf{n} \cdot \mathbf{r}'. \end{aligned} \quad (4.56)$$

Here, we have specialized the prescription for C to the static case.

On \mathcal{I}_1 , we have the boundary conditions

$$\mathbf{n}(0^+) = -\mathbf{P}, \quad \mathbf{m}(0^+) = -\mathbf{M}_0 = -M_0 \mathbf{A}_3, \quad \mathbf{r}(\gamma^-) \cdot \mathbf{A}_2 = 0. \quad (4.57)$$

Correspondingly, on \mathcal{S}_{III} , we have the boundary conditions and contact conditions

$$\mathbf{n}(\ell^-) = \mathbf{0}, \quad \mathbf{r}(\xi) \cdot \mathbf{A}_2 = 0, \quad \frac{\partial \theta}{\partial \xi} = 0. \quad (4.58)$$

At $\xi = \gamma$, \mathbf{r} and θ are continuous,¹⁰ and we have the jump conditions

$$\begin{aligned} \mathbf{n}(\gamma^+) - \mathbf{n}(\gamma^-) + \mathbf{F}_\gamma &= \mathbf{0}, \\ -\mathbf{m}(\gamma^-) + \mathbf{M}_\gamma &= \mathbf{0}, \\ \mathbf{C}(\gamma^+) - \mathbf{C}(\gamma^-) + \mathbf{B}_\gamma &= 0. \end{aligned} \quad (4.59)$$

Note that we used the fact that $\mathbf{m}(\gamma^+) = \mathbf{0}$ in writing the second jump condition.

The governing equations for the boundary-value problem on \mathcal{S}_{I} yield the provisional solutions

$$\begin{aligned} \mathbf{n}(\xi) &= -\mathbf{P} = -P_1 \mathbf{A}_1 - P_2 \mathbf{A}_2, \\ EI \frac{\partial^2 \theta}{\partial \xi^2} - P_2 \cos(\theta) + P_1 \sin(\theta) &= 0. \end{aligned} \quad (4.60)$$

The differential equation (4.60)₂ needs to be solved subject to the boundary conditions

$$\theta(\gamma) = 0, \quad \frac{\partial \theta}{\partial \xi}(0) = -\frac{M_0}{EI}, \quad \frac{\partial \theta}{\partial \xi}(\gamma^-) = \theta'_-, \quad (4.61)$$

where θ'_- is presently unknown. For the boundary-value problem on \mathcal{S}_{III} , we find from the balance laws that

$$\mathbf{m}(\xi) = \mathbf{0}, \quad \mathbf{n}(\xi) = \mathbf{0}, \quad (4.62)$$

for $\xi \in (\gamma, \ell)$.

At the discontinuity, the jump conditions (4.59) can be explored in further detail. Substituting for the fields at γ^+ , we solve for \mathbf{F}_γ and \mathbf{M}_γ and specify $\frac{\partial \theta}{\partial \xi}(\gamma^-)$:

$$\begin{aligned} \mathbf{F}_\gamma &= \mathbf{n}(\gamma^-) = -\mathbf{P}, \\ \mathbf{M}_\gamma &= EI \theta'_- \mathbf{A}_3, \\ -W_{\text{ad}} &= -\frac{EI}{2} \left(\theta'_- \right)^2 + \mathbf{P} \cdot \mathbf{r}'(\gamma^-). \end{aligned} \quad (4.63)$$

These results are also displayed in Figure 4.9.

We remark that the equation (4.63)₃ for θ'_- , which is known as the adhesion boundary condition, arises from the material momentum balance law. In treatments of this problem where the material momentum balance law is not used, other assumptions are employed (cf. Majidi [217]). For instance, Glassmaker and Hui [117] postulate an energy balance in order to obtain an expression that is equivalent

¹⁰ See Eqn. (4.6).

to (4.63)₃. The interested reader is also referred to Section 4.7.2.2 where, as we mentioned previously, a variational formulation of the adhesion boundary condition is presented.

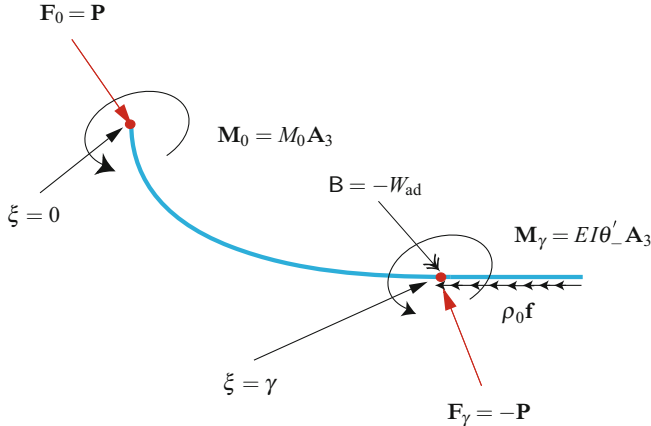


Fig. 4.9 Schematic of the singular supplies acting on the rod shown in Figure 4.8. The terminal moment \mathbf{M}_0 will appear in the examples considered in Sections 4.5.3.2 and 4.9.3.

4.5.2 Summary of the Solution Procedure

To solve the adhesion problem, we need to solve the differential equation (4.60)₂ subject to the boundary conditions (4.61) where θ'_- is determined from the equation

$$-W_{ad} = -\frac{EI}{2} (\theta'_-)^2 + P_1 \cos(\theta(\gamma)) + P_2 \sin(\theta(\gamma)). \quad (4.64)$$

The resulting solution of the boundary-value problem also provides the length γ .

The general solution to the differential equation (4.60)₂ can be obtained using classical methods and is aided by a graphical representation of the solutions that can be seen in Figure 4.10. Because there are no assigned forces acting on \mathcal{S}_1 of the rod, $b_p = 0$ and the local form of the balance of material momentum (4.56)₃ shows that C is conserved by the solutions to (4.60)₂:

$$C = -\frac{EI}{2} \left(\frac{\partial \theta}{\partial \xi} \right)^2 + \mathbf{P} \cdot \mathbf{r}'. \quad (4.65)$$

To examine the solutions to the boundary-value problem, it is first convenient to non-dimensionalize the differential equation using the variables

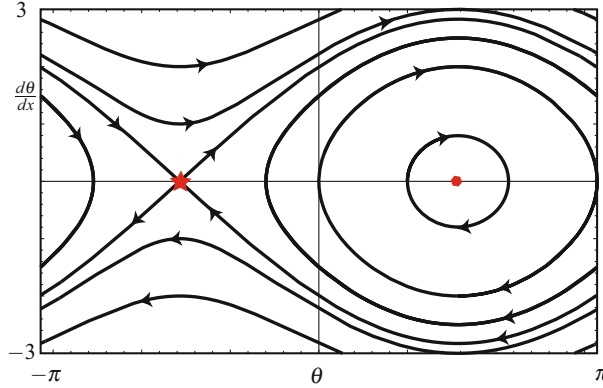


Fig. 4.10 The solutions of (4.60)₂ where $f_2 > 0$ and $f_1 = 0$. The equilibrium denoted by a hexagon is the equilibrium $\theta = \frac{\pi}{2}$, and the second equilibrium which is denoted by a star is the equilibrium $\theta = -\frac{\pi}{2}$. The arrows indicate the direction of increasing s .

$$x = \frac{\xi}{\ell}, \quad g = \frac{\gamma}{\ell}, \quad w = \frac{W_{ad}\ell^2}{EI}, \quad f_{1,2} = \frac{P_{1,2}\ell^2}{EI}, \quad \omega_0 = \frac{M_0\ell}{EI}. \quad (4.66)$$

With the help of these variables, we find that the first integral $-C$ of (4.60)₂ has the dimensionless representation

$$e_0 = -\frac{C\ell^2}{EI} = \frac{1}{2} \left(\frac{d\theta}{dx} \right)^2 - f_2 \sin(\theta) - f_1 \cos(\theta), \quad (4.67)$$

where e_0 is a constant determined by the boundary conditions.

Comparing the boundary condition (4.64) to the conservation (4.67), we find that

$$e_0 = \left(\frac{\ell^2}{EI} \right) W_{ad} = w_{ad}. \quad (4.68)$$

Thus the solution to the differential equation (4.60)₂ of interest to us is the integral curve corresponding to $e_0 = w_{ad}$. In addition, we notice that $e_0 = w_{ad}$ on \mathcal{S}_1 is consistent with the result that $C = 0$ throughout the segment \mathcal{S}_{III} . At the other end of the rod, we can use the fact that $e_0 = w_{ad}$ along with the boundary condition (4.61)₂ for $\frac{\partial\theta}{\partial\xi}$ to find an equation for $\theta_0 = \theta(\xi = 0)$ from the conservation (4.67):

$$w_{ad} = \frac{1}{2} \omega_0^2 - f_2 \sin(\theta_0) - f_1 \cos(\theta_0). \quad (4.69)$$

In addition to using this equation to determine θ_0 , the equation is also useful for finding allowable parameter ranges for adhesion (w_{ad}), terminal bending moment (ω_0), and terminal forces ($f_{1,2}$).

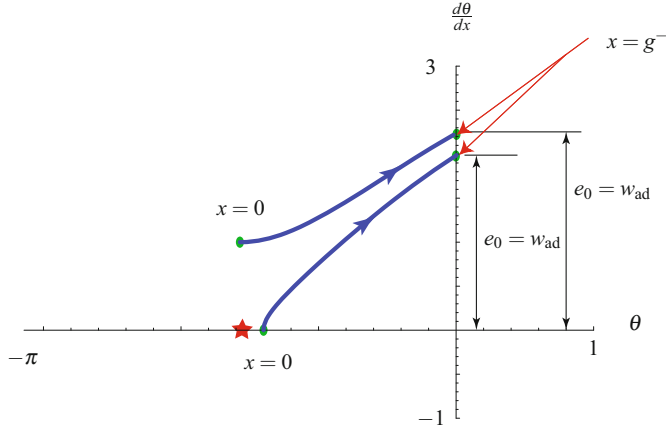


Fig. 4.11 Two representative solutions of (4.60)₂ where $f_2 > 0$ and $f_1 = 0$. The solution where $\frac{d\theta}{d\xi}(\xi = 0) = 0$ is discussed in Section 4.5.3.1, and the solution where $\frac{d\theta}{d\xi}(\xi = 0) > 0$ is discussed in Section 4.5.3.2. In the interests of clarity, the dimensionless adhesion energy w_{ad} has distinct values for the pair of solutions.

We can also use the integral (4.67) to obtain an analytical expression for $\theta(x)$:

$$\int_{x_0}^{x_1} du = \int_{\theta_0}^{\theta_1} \frac{d\theta}{\sqrt{2(e_0 + f_2 \sin(\theta) + f_1 \cos(\theta))}}, \quad (4.70)$$

where $x_0 = 0$. The integral on the right-hand side of this equation is an elliptic integral of the first kind, and an analytical solution for $\theta(x)$ can be developed.¹¹ We express this analytical solution symbolically as

$$\theta(x) = f(x, x_0, \theta_0, \theta_1, e_0, \omega_0, f_1, f_2). \quad (4.71)$$

The function f has four constants ($x_0 = 0$, e_0 , ω_0 , and θ_0) which need to be prescribed or are specified using Eqns. (4.68) and (4.69). A graphical summary of the aforementioned solution procedure can be seen in Figure 4.11 for two cases: one where $\omega_0 = 0$ and the other where $\omega_0 < 0$.

The identity (4.70) along with Eqns. (4.68) and (4.69) can also be used to determine the length of the adhered length $\ell - \gamma$ of the rod by setting $x_1 = \frac{\gamma}{\ell}$ and $\theta_1 = \theta(x = g) = 0$:

$$\frac{\gamma}{\ell} = \int_{\theta_0}^0 \frac{d\theta}{\sqrt{2(w_{ad} + f_2 \sin(\theta) + f_1 \cos(\theta))}}. \quad (4.72)$$

It is useful to note that the right-hand side of this equation can be evaluated without explicitly determining the shape of the deformed rod.

¹¹ For background on elliptic integrals and functions, Byrd and Friedman's classic handbook [41] and Lawden's concise textbook [200] are recommended. Integrals of the form (4.70) can also be evaluated using symbolic manipulation packages such as MATHEMATICA.

4.5.3 Examples

In the examples we now consider, we restrict attention to a rod where the force acting at one of the terminal points is $\mathbf{P} = P_2 \mathbf{A}_2$. In the first example, we assume that no moment acts at the point of application of the load. We find that this assumption leads to a very limited range of adhesive solutions. In the second example, we relax the boundary condition and assume that a terminal moment is applied. We then find a much wider range of situations where adhesion is possible. This is to be expected as the moment serves to press the rod onto the adhesive layer.

4.5.3.1 Pulling up or pushing down on the adhesive layer

To further illustrate the previous developments, consider the situation shown in Figure 4.8 with $\mathbf{P} = P_2 \mathbf{A}_2$. That is, $\mathbf{n}(\xi) = -P_2 \mathbf{A}_2$ on \mathcal{S}_1 . We next use the developments of the previous section. First, we use the boundary condition (4.61)₂ along with the conservation (4.67) to conclude that

$$e_0 = -f_2 \sin(\theta_0), \quad (4.73)$$

where $\theta_0 = \theta(x = x_0 = 0)$. As $e_0 = w_{\text{ad}}$, we can immediately see that the type of contact we are considering requires that the bond strength be less than the applied force: $w_{\text{ad}} \leq |f_2|$. That is, in terms of the dimensioned quantities, $W_{\text{ad}} \leq \|P_2 \mathbf{A}_2\|$.

The integral (4.70) reduces to

$$\int_{x_0}^{x_1} du = \int_{\theta_0}^{\theta_1} \frac{d\theta}{\sqrt{2f_2(\sin(\theta) - \sin(\theta_0))}}. \quad (4.74)$$

This integral can be expressed as the sum of two elliptic integrals of a well-known form.¹² We present our results for the case $f_2 > 0$, and can infer the results for $f_2 < 0$ where needed using symmetry arguments. Evaluating the right-hand side of (4.74), we find that

$$\sqrt{f_2}(x_1 - 0) = K(k) - F(\phi_1, k), \quad (4.75)$$

where $F(\phi, k)$ is an elliptic integral of the first kind and $K(k)$ is a complete elliptic integral of the first kind:

$$F(\phi, k) = \int_0^\phi \frac{dy}{\sqrt{1 - k^2 \sin^2(y)}}, \quad K = K(k) = F\left(\frac{\pi}{2}, k\right). \quad (4.76)$$

In (4.75), the modulus k and angle ϕ_1 are defined as

¹² See Example 288.50 for the integral $\int_{\psi}^{\frac{\pi}{2}} \frac{d\theta}{\sqrt{a + b \sin(\theta)}}$ where $b > |a| > 0$ in [41].

$$k^2 = \frac{1}{2} (1 - \sin(\theta_0)), \quad \phi_1 = \sin^{-1} \left(\sqrt{\frac{1 - \sin(\theta_1)}{1 - \sin(\theta_0)}} \right), \quad (4.77)$$

where $\theta_1 = \theta$ ($x = x_1$). With the help of our earlier observation that $e_0 = w_{\text{ad}}$ on \mathcal{S}_1 , we can easily obtain a pair of more illuminating expressions for k :

$$k^2 = \frac{1}{2} \left(1 + \frac{w_{\text{ad}}}{f_2} \right) = \frac{1}{2} \left(1 + \frac{W_{\text{ad}}}{P_2} \right). \quad (4.78)$$

The solution (4.75) can be used to determine the deformed shape of the rod once θ_0 and γ have been determined from the boundary conditions.

To determine the contact length $\ell - \gamma$, we invoke the boundary condition $\theta(\gamma) = 0$. Thus,

$$\frac{\gamma}{\ell} = \frac{1}{\sqrt{|f_2|}} (K(k) - F(\phi_g, k)), \quad (4.79)$$

where the angle ϕ_g corresponding to $\theta(\gamma) = 0$ is computed using Eqn. (4.77)₂:

$$\phi_g = \sin^{-1} \left(\sqrt{\frac{1}{1 - \sin(\theta_0)}} \right). \quad (4.80)$$

From Eqns. (4.73) and (4.79), we can determine the initial inclination θ_0 of the rod, and the length of the contact region for a given P_2 and $\frac{w_{\text{ad}}}{f_2} = \frac{W_{\text{ad}}}{P_2}$. The results are presented in Figure 4.12 and the corresponding solution curve of the ordinary differential equation can be seen in Figure 4.11.

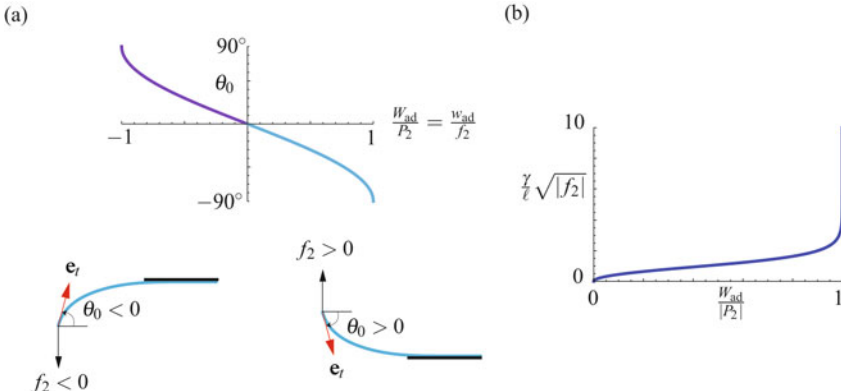


Fig. 4.12 Solutions to Eqns. (4.73) and (4.79) for (a) the angle θ_0 and (b) the contact point γ as functions of the adhesive strength $\frac{w_{\text{ad}}}{f_2} = \frac{W_{\text{ad}}}{P_2}$. When $\gamma = 0$, the entire rod is adhered to the surface.

Referring to Figure 4.12, several results can be concluded from (4.79). First, for the type of solutions we are seeking, the ratio of the adhesive strength W_{ad} to

the peeling force P_2 is restricted to lie in the range $-1 \leq \frac{w_{ad}}{P_2} \leq 1$. Outside of this range, either an adhesive solution is not possible, or the rod is entirely adhered to the surface. When P_2 is within the range needed for an adhesive solution, the precise amount of contact depends on P_2 and there will be a unique value of θ_0 for this solution. Figure 4.12(b) also illustrates that the contact length $\ell - \gamma$ increases as $\frac{w_{ad}}{|P_2|} = \frac{w_{ad}}{|f_2|}$ decreases. This seems contradictory until one realizes that as $\frac{w_{ad}}{|f_2|} \rightarrow 0$, the angle of inclination θ_0 at the tip of the rod also tends to 0. That is, it is not possible to vary P_2 and θ_0 independently without changing the contact length $\ell - \gamma$.

4.5.3.2 The Helpful Effects of a Terminal Moment M_0

We again consider the problem of the previous section, but replace the boundary condition $\frac{d\theta}{d\xi}(\xi = 0) = 0$ with the condition that $\theta(\xi = 0) = \theta_0 = -\frac{\pi}{2}$. For this case, there will be a terminal moment $\mathbf{M}_0 = -EI\frac{d\theta}{d\xi}(0^+) \mathbf{A}_3$ acting at $\xi = 0$ and $f_2 > 0$ (see Figure 4.9). The results for the case $\theta(\xi = 0) = \theta_0 = \frac{\pi}{2}$ and $f_2 < 0$ can be inferred using symmetry arguments.

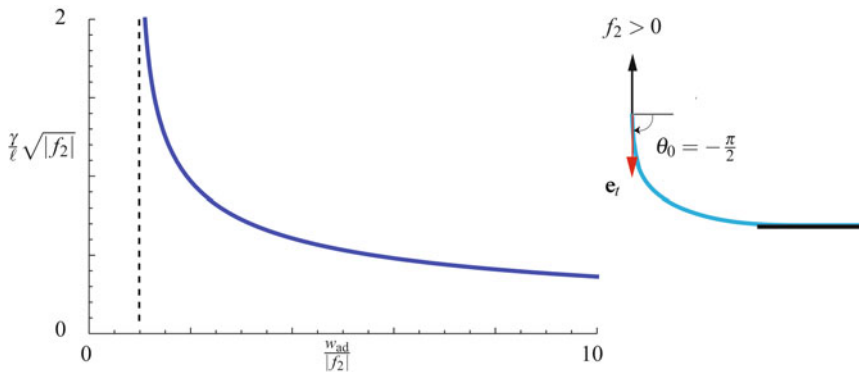


Fig. 4.13 The solution $\frac{\gamma}{\ell} \sqrt{|f_2|}$ as a function of $\frac{w_{ad}}{|f_2|}$ for the adhesion problem where the terminal end of the rod is constrained so that $\theta_0 = -\frac{\pi}{2}$ when $f_2 > 0$ and $\theta_0 = \frac{\pi}{2}$ when $f_2 < 0$. For these cases, a moment whose dimensionless form is $\mathbf{M}_0 = -\text{sgn}(f_2) \frac{EI}{\ell} \sqrt{w_{ad} - |f_2|} \mathbf{A}_3$ acts at $\xi = 0$.

We can use the analysis of the previous section with some slight modifications. As boundary conditions, we now have

$$\theta(x = g) = 0, \quad \theta(x = 0) = -\frac{\pi}{2}, \quad \frac{1}{2} \left(\frac{d\theta}{dx}(x = g^-) \right)^2 = w_{ad} + f_1. \quad (4.81)$$

The last condition is equivalent to $e_0 = w$. Applying (4.81)₂ to the conservation (4.67), we find that

$$\epsilon_0 = \frac{\omega_0^2}{2} + f_2, \quad (4.82)$$

where $-\omega_0 = \frac{d\theta}{dx}(x=0^+) > 0$. Thus, we have quickly found an expression for \mathbf{M}_0 :

$$\mathbf{M}_0 = -EI \frac{\partial \theta}{\partial \xi}(0^+) \mathbf{A}_3 = -\sqrt{2EI(W_{ad} - P_2)} \mathbf{A}_3, \quad P_2 > 0. \quad (4.83)$$

You will notice that the moment at $\xi = 0$ can improve the strength of the bond by increasing the range of allowable forces f_2 .

The solution of the governing differential equation we now seek is shown in Figure 4.11. It differs from the solution of the previous subsection in that $\frac{d\theta}{dx}(x=0) \neq 0$. The elliptic integral we now need to solve is

$$\int_0^{x_1} du = \int_{\theta_0}^{\theta_1} \frac{d\theta}{\sqrt{2(w_{ad} + f_2 \sin(\theta))}}. \quad (4.84)$$

Again, the integral on the right-hand side can be expressed in a canonical form¹³ and we can solve for x_1 . Evaluating the result when $x_1 = g$ and $\theta_1 = 0$, the contact point can be determined:

$$\frac{\gamma}{\ell} \sqrt{f_2} = \sqrt{\frac{2}{1 + \frac{w_{ad}}{f_2}}} \left(K(k) - F\left(\frac{\pi}{4}, k\right) \right), \quad k^2 = \frac{2}{1 + \frac{w_{ad}}{f_2}}. \quad (4.85)$$

For this case $\frac{w_{ad}}{f_2}$ ranges from 1 to ∞ , and, for a given value of this adhesion parameter, a contact length can be determined with the help of the solution (4.85). As can be inferred from Figure 4.13, for a given value of $\frac{w_{ad}}{f_2}$, we can determine the corresponding value of $\frac{\gamma}{\ell} \sqrt{f_2}$, and, based on the value of f_2 compute the contact length $\ell - \gamma$. As $\frac{w_{ad}}{f_2} \rightarrow \infty$, the contact length tends to ℓ .

Results for $f_2 < 0$ and $\theta_0 = \frac{\pi}{2}$ are also shown in Figure 4.13. These results can be easily inferred from the previous analysis using either a symmetry argument or by direct calculation. We note in particular that as $\omega_0 = -\frac{d\theta}{dx}(x=0^+) > 0$, the terminal moment in this case can be shown to have the representations

$$\mathbf{M}_0 = -EI \frac{\partial \theta}{\partial \xi}(0^+) \mathbf{A}_3 = \sqrt{2EI(W_{ad} + P_2)} \mathbf{A}_3, \quad P_2 < 0. \quad (4.86)$$

These expressions are notably consistent with our earlier results.

4.5.3.3 Closing Remarks

In conclusion, we have presented an analysis of the adhesion of a rod under terminal loading $\mathbf{P} = P_2 \mathbf{E}_2$ with a substrate. When the adhesive is weak, we found that the

¹³ See Example 288.00 for the integral $\int_{\psi}^{\frac{\pi}{2}} \frac{d\theta}{\sqrt{a+b \sin(\theta)}}$ where $a > b > 0$ in [41].

bond could be supported without the application of a terminal moment. However, for larger values of $\frac{W_{ad}}{|P_2|}$, application of a terminal moment helped to strengthen the bond.

4.6 The Elastica Arm Scale

In 2014, Bosi et al. [32] presented a novel measuring scale shown in Figure 4.14. The scale uses an elastic rod of length ℓ that is free to move inside a frictionless sleeve which is inclined at an angle α to the vertical. Weights P_1 and P_2 are attached to the respective ends of the lamella and, assuming that one of the weights and the slope of the tangent at the ends of the rod are known, the second weight can be determined from the relation

$$P_1 \cos(\theta(0) + \alpha) + P_2 \cos(\theta(\ell) + \alpha) = 0. \quad (4.87)$$

The device is referred to as an “elastica arm scale” and the inspiration for its design can be traced to the papers by Bigoni et al. [25, 27] on Eshelby-like forces in continua. We also refer the interested reader to Bigoni et al. [26] and Bosi et al. [33, 34] for related works and additional perspectives.

In this section of the book we will demonstrate how the scale operates by deriving the relation (4.87). In the process of the derivation, we find that we are able to extend Eqn. (4.87) to the case where the weight of the rod is considered and terminal moments can be applied to the ends (cf. Eqn. (4.115) on Page 154):

$$P_1 \cos(\theta(0) + \alpha) + P_2 \cos(\theta(\ell) + \alpha) = \rho_0 g \hat{\mathbf{g}} \cdot (\mathbf{r}(\ell) - \mathbf{r}(0)) + \frac{1}{2EI} (M_2^2 - M_1^2).$$

The analysis we employ, which is adapted from our recent paper [266], makes extensive use of the balance law for material momentum, shows that a conserved quantity $C - \rho_0 g \hat{\mathbf{g}} \cdot \mathbf{r}$ can be used to establish the relation (4.87), and includes the effects of terminal moments which were not considered in our earlier work. Our analysis complements the work of Bosi et al. [32]. These authors used a variational formulation to establish Eqn. (4.87) and they also include a nonlinear stability analysis of the equilibrium configurations of the rod.



Fig. 4.14 The elastica arm scale. Image courtesy of Davide Bigoni.

4.6.1 Background

The rod in this problem takes on static configurations that are shown schematically in Figure 4.15. The rod is assumed to be inextensible, and so we use the arc-length parameter s in place of ξ in the sequel. To enable easy comparisons with the literature on the arm scale, we define the following representation for the unit tangent to the curve:

$$\mathbf{r}' = \frac{\partial \mathbf{r}}{\partial s} = \cos(\theta) \mathbf{A}_2 - \sin(\theta) \mathbf{A}_1. \quad (4.88)$$

We note that for this problem θ represents the angle subtended by \mathbf{r}' with the \mathbf{A}_2 axis. The rod will be assumed to be homogeneous with a uniform mass density ρ_0 per unit length of s and the classic strain energy function $\rho_0 \psi = \frac{EI}{2} (\theta')^2$.

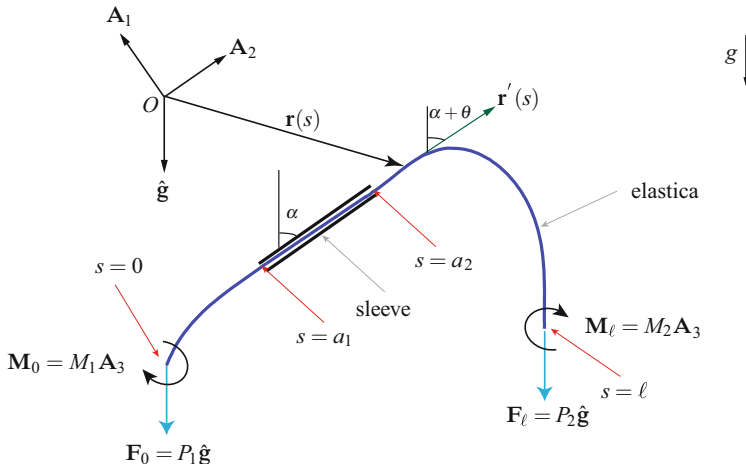


Fig. 4.15 Schematic representation of the Bosi et al.'s elastica arm scale. While neither the weight of the rod nor the presence of terminal moments is included in the original analysis of Bosi et al. [32], we show how they can be accommodated into their measurement device.

We are now in a position to recall from Section 4.3 the balance laws for forces, material forces, and moments for the elastica:

$$\begin{aligned} C' + b &= 0, \\ \mathbf{n}' + \rho_0 \mathbf{f} &= \mathbf{0}, \\ \mathbf{m}' + \mathbf{r}' \times \mathbf{n} &= \mathbf{0}. \end{aligned} \quad (4.89)$$

In these local forms, the force b is such that the material momentum balance law (4.89)₁ is identically satisfied and the force C is prescribed as

$$C = \rho_0 \psi - \mathbf{n} \cdot \mathbf{r}' - \mathbf{m} \cdot \theta' \mathbf{A}_3. \quad (4.90)$$

We thus find from Eqn. (4.39) that the assigned body force for the homogeneous rod is

$$\mathbf{b} = \mathbf{b}_p = -\rho_0 \mathbf{f} \cdot \mathbf{r}' . \quad (4.91)$$

The assigned body force $\rho_0 \mathbf{f}$ is not constant throughout the rod, so we refrain from simplifying this expression further at this stage in the analysis.

At a point of discontinuity $s = \gamma$, the following jump conditions hold:

$$\begin{aligned} [[C]]_\gamma + B_\gamma &= 0, \\ [[\mathbf{n}]]_\gamma + \mathbf{F}_\gamma &= \mathbf{0}, \\ [[\mathbf{m}]]_\gamma + \mathbf{M}_\gamma &= \mathbf{0}. \end{aligned} \quad (4.92)$$

As with many of the problems considered in this book, the latter pair of jump conditions are useful in establishing boundary conditions.

4.6.2 The Deformable Arm Scale

To analyze the arm scale it is convenient to consider three segments: the left freely hanging section, $s \in [0, a_1]$; the right freely hanging section, $s \in (a_2, \ell]$; and the section inside the smooth guide of length ℓ^* where

$$a_2 - a_1 = \ell^*. \quad (4.93)$$

Thus, in determining the equilibrium configuration of the deformed rod, it suffices to determine either a_1 or a_2 . The guide or sleeve is inclined at an angle α to the vertical.

4.6.2.1 The freely hanging segment $s \in [0, a_1]$

The first section of the rod we consider extends from the free end at $s = 0$ to the start of the guide at $s = a_1$. At the free end, we assume that a force $\mathbf{F}_0 = P_1 \hat{\mathbf{g}}$ along with a moment $\mathbf{M}_0 = M_1 \mathbf{A}_3$ act. Here, the unit vector $\hat{\mathbf{g}}$, which points downward, has the representation

$$\hat{\mathbf{g}} = -\cos(\alpha) \mathbf{A}_2 - \sin(\alpha) \mathbf{A}_1. \quad (4.94)$$

With the help of the jump conditions (4.92)_{2,3}, we find that

$$\mathbf{n}(0^+) = -\mathbf{F}_0 = -P_1 \hat{\mathbf{g}}, \quad \mathbf{m}(0^+) = -\mathbf{M}_0 = -M_1 \mathbf{A}_3. \quad (4.95)$$

With the help of the constitutive equations for \mathbf{m} and dropping the $^+$, we conclude that the boundary conditions on this section are

$$\theta(a_1^-) = 0, \quad \theta'(0) = -\frac{M_1}{EI}, \quad \mathbf{n}(0) = -P_1 \hat{\mathbf{g}}. \quad (4.96)$$

With the help of the balance laws for linear and angular momentum (4.89)_{2,3}, we find that

$$\begin{aligned}\mathbf{n}(s) &= -(P_1 + \rho_0 g s) \hat{\mathbf{g}}, \\ EI\theta'' &= (P_1 + \rho_0 g s) \sin(\theta + \alpha).\end{aligned}\quad (4.97)$$

From one of these results, expressions for the material force \mathbf{C} can be computed from Eqns. (4.90) and (4.96):

$$\begin{aligned}\mathbf{C}(s) &= -\frac{M^2(s)}{2EI} - \mathbf{n}(s) \cdot \mathbf{r}'(s) \\ &= -\frac{EI}{2} \theta'^2 - (P_1 + \rho_0 g s) \cos(\theta + \alpha), \\ \mathbf{C}(0) &= -\mathbf{n}(0) \cdot \mathbf{r}'(0) - \frac{M_1^2}{2EI}.\end{aligned}\quad (4.98)$$

In the first of these expressions for \mathbf{C} , we used the abbreviation $M(s) = \mathbf{m}(s) \cdot \mathbf{A}_3$. Because the rod is homogeneous, after computing \mathbf{b} using Eqn. (4.39), it is straightforward to find the following energy conservation law from the local form of the balance of material momentum (4.89)₁:

$$(\mathbf{C} - \rho_0 g \hat{\mathbf{g}} \cdot \mathbf{r})' = 0. \quad (4.99)$$

We note that $-\rho_0 g \hat{\mathbf{g}} \cdot \mathbf{r}$ is the gravitational potential energy for the material point located at \mathbf{r} on the rod. Thus, in the case where gravity is ignored and the terminal moment $M_1 \mathbf{A}_3$ is absent, the material force \mathbf{C} is constant throughout this segment of the rod: $\mathbf{C}(s) = \mathbf{C}(0) = -P_1 \hat{\mathbf{g}} \cdot \mathbf{r}'(0)$. This conservation is equivalent to the conservation law presented in Love [213, Eqn. (7) in Sect. 262] and is central to the analysis of the arm scale presented in Bosi et al. [32].

4.6.2.2 The freely hanging segment $s \in (a_2, \ell]$

The second segment of the rod of interest is terminally loaded at one end and extends to the sleeve at the other. At the free end, we assume that a force $\mathbf{F}_\ell = P_2 \hat{\mathbf{g}}$ along with a moment $\mathbf{M}_\ell = M_2 \mathbf{A}_3$ act. With the help of the jump conditions (4.92)_{2,3}, we find that

$$\mathbf{n}(\ell^-) = \mathbf{F}_\ell = P_2 \hat{\mathbf{g}}, \quad \mathbf{m}(\ell^-) = \mathbf{M}_\ell = M_2 \mathbf{A}_3. \quad (4.100)$$

Dropping the $-$, we conclude that for this portion of the rod, the boundary conditions are

$$\theta(a_2^+) = 0, \quad \theta'(\ell) = \frac{M_2}{EI}, \quad \mathbf{n}(\ell) = P_2 \hat{\mathbf{g}}. \quad (4.101)$$

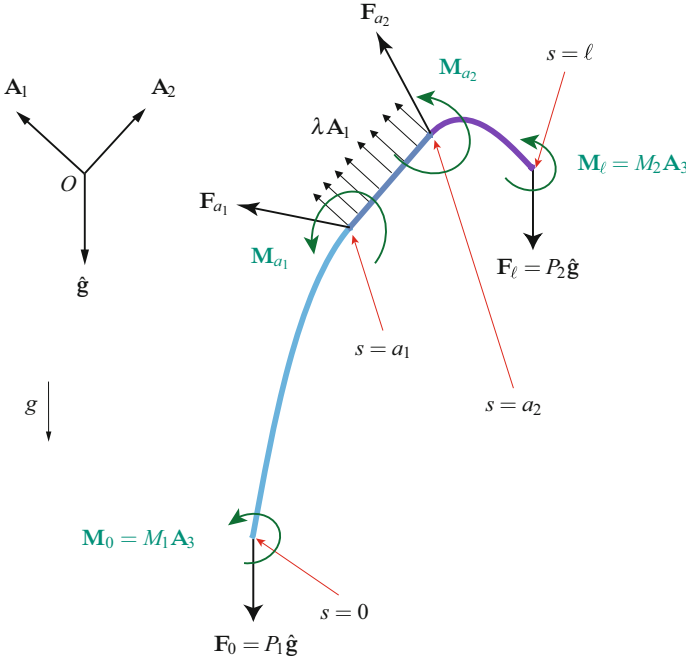


Fig. 4.16 Schematic showing the forces \mathbf{F}_{a_1} , \mathbf{F}_{a_2} , and $\lambda \mathbf{A}_1$, moments, \mathbf{M}_{a_1} and \mathbf{M}_{a_2} , and terminal loadings acting on the elastica arm scale. It is important to observe that there are no singular supplies of material momentum in this system: $\mathbf{B}_{a_1} = 0$ and $\mathbf{B}_{a_2} = 0$.

We parallel the developments in the previous section and compute that

$$\begin{aligned}\mathbf{n}(s) &= (P_2 + \rho_0 g(\ell - s)) \hat{\mathbf{g}}, \\ EI\theta'' &= -(P_2 + \rho_0 g(\ell - s)) \sin(\theta + \alpha).\end{aligned}\quad (4.102)$$

From these results and the balance of material forces, we again find a conservation law:

$$(C - \rho_0 g \hat{\mathbf{g}} \cdot \mathbf{r})' = 0. \quad (4.103)$$

For this segment of the rod, the material force has the representations

$$\begin{aligned}C(s) &= -\frac{EI}{2} (\theta')^2 + (P_2 + \rho_0 g(\ell - s)) \cos(\theta + \alpha) \\ &= -\frac{M^2(s)}{2EI} - \mathbf{n}(s) \cdot \mathbf{r}'(s), \\ C(\ell) &= -\mathbf{n}(\ell) \cdot \mathbf{r}'(\ell) - \frac{M_2^2}{2EI}.\end{aligned}\quad (4.104)$$

As in the previous section, if gravity and the terminal moment are ignored, then $C(s)$ is conserved along this segment of the rod where $C(\ell) = -P_2 \hat{\mathbf{g}} \cdot \mathbf{r}'(\ell)$.

4.6.2.3 The segment $s \in [a_1, a_2]$ of the rod in the smooth sleeve and the points of discontinuity

It is straightforward to show that the slope of the rod is continuous where the rod enters and exits the sleeve:

$$[\theta]_{a_1} = 0, \quad [\theta]_{a_2} = 0. \quad (4.105)$$

However, these results in no way imply that the curvature of the rod is continuous at these points. At $s = a_1$ and $s = a_2$, we assume that respective singular forces, \mathbf{F}_{a_1} and \mathbf{F}_{a_2} , and respective singular moments, \mathbf{M}_{a_1} and \mathbf{M}_{a_2} , act on the rod. In addition, for the segment of the rod in the frictionless guide, the assigned force acting on the rod can be decomposed into a gravitational force and a normal force $\lambda(s)\mathbf{A}_1$ (cf. Figure 4.16).

The balance of linear momentum for the portion of the rod in the sleeve reads

$$\mathbf{n}' + \rho_0 g \hat{\mathbf{g}} + \lambda \mathbf{A}_1 = \mathbf{0}, \quad s \in (a_1, a_2). \quad (4.106)$$

As $\theta = 0$ for this section of the rod, the balance of angular momentum reduces to

$$\mathbf{n}(s) = n_2(s)\mathbf{A}_2 = (n_2(a_1^+) + \rho_0 g \cos(\alpha)(s - a_1))\mathbf{A}_2. \quad (4.107)$$

That is, \mathbf{n} is tangent to the rod. We can now revisit the balance of linear momentum and solve for the normal force acting on the rod:

$$\lambda \mathbf{A}_1 = \rho_0 g \sin(\alpha) \mathbf{A}_1. \quad (4.108)$$

Furthermore, the contact material force C is simply

$$C = -n_2(a_1^+) - \rho_0 g \cos(\alpha)(s - a_1), \quad s \in (a_1, a_2). \quad (4.109)$$

In contrast to the other two segments of the rod, C decreases linearly with increasing s and the following material force b needs to be supplied to satisfy the material momentum balance law (4.89)₁ (cf. Eqn. (4.39)):

$$b = \rho_0 g \cos(\alpha). \quad (4.110)$$

Paralleling the developments in the previous segments of the rod, we again find that the energy $C - \rho_0 g \hat{\mathbf{r}} \cdot \mathbf{r}$ is conserved for this segment of the rod.

At $s = a_1$, we assume a vanishing singular supply $B_{a_1} = 0$ along with a singular force \mathbf{F}_{a_1} and singular moment \mathbf{M}_{a_1} acts. Thus, from the jump conditions (4.92),

$$\begin{aligned} \mathbf{F}_{a_1} &= \mathbf{n}(a_1^-) - \mathbf{n}(a_1^+), \\ \mathbf{M}_{a_1} &= \mathbf{m}(a_1^-) = EI\theta'(a_1^-)\mathbf{A}_3, \\ 0 &= C(a_1^-) - C(a_1^+). \end{aligned} \quad (4.111)$$

It is important to observe here that \mathbf{F}_{a_1} is an unknown reaction force while \mathbf{M}_{a_1} is prescribed by the solution to the boundary-value problem for the hanging segment $s \in [0, a_1]$. Noting that C is continuous at $s = a_1$, we use the jump condition (4.111)₃ to solve for $\mathbf{n}(a_1^+) \cdot \mathbf{A}_2$:

$$\mathbf{n}(a_1^+) \cdot \mathbf{A}_2 = \frac{M^2(a_1^-)}{2EI} + \mathbf{n}(a_1^-) \cdot \mathbf{A}_2. \quad (4.112)$$

The analysis at the exit point $s = a_2$ closely parallels the case for $s = a_1$. Again, we prescribe $B_{a_2} = 0$ and assume that a singular force \mathbf{F}_{a_2} and singular moment \mathbf{M}_{a_2} act at $s = a_2$. The jump condition associated with the material force balance yields continuity of C , and so we find

$$\mathbf{n}(a_2^-) = \left(\mathbf{n}(a_2^+) \cdot \mathbf{A}_2 + \frac{M^2(a_2^+)}{2EI} \right) \mathbf{A}_2. \quad (4.113)$$

It should be clear from the relations (4.112) and (4.113) that the axial component of the force \mathbf{n} experiences jumps at $s = a_1$ and $s = a_2$. However, because we assume that $B_{a_1} = 0$ and $B_{a_2} = 0$, C does not and this continuity serves to determine the jump in \mathbf{n} . Continuity of C and \mathbf{r} implies that the conserved quantity $C - \rho_0 g \hat{\mathbf{g}} \cdot \mathbf{r}$ is continuous at $s = a_1$ and $s = a_2$.

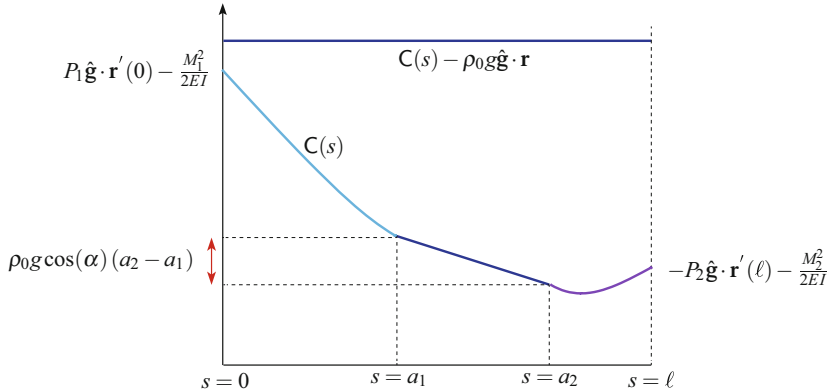


Fig. 4.17 Representative distributions of the material force C and the conserved energy $C - \rho_0 g \hat{\mathbf{g}} \cdot \mathbf{r}$ along the length of the deformable arm scale.

4.6.3 The Operation of the Arm Scale

With the help of Eqns.(4.98), (4.104), and (4.109), we are now in a position to examine the distributions of the material force C and the conserved quantity $C - \rho_0 g \hat{\mathbf{g}} \cdot \mathbf{r}$ along the rod. A summary of the results is presented in Figure 4.15.

The conservation of $C - \rho_0 g \hat{\mathbf{g}} \cdot \mathbf{r}$ provides the equation governing the operation of the arm scale. To see this, we use the expressions for C mentioned earlier to find that

$$\mathbf{n}(0) \cdot \mathbf{r}'(0) + \rho_0 g \hat{\mathbf{g}} \cdot \mathbf{r}(0) + \frac{M_1^2}{2EI} = \mathbf{n}(\ell) \cdot \mathbf{r}'(\ell) + \rho_0 g \hat{\mathbf{g}} \cdot \mathbf{r}(\ell) + \frac{M_2^2}{2EI}. \quad (4.114)$$

On substituting for \mathbf{r}' from Eqn. (4.88), $\mathbf{n}(0) = -P_1 \hat{\mathbf{g}}$, and $\mathbf{n}(\ell) = P_2 \hat{\mathbf{g}}$, it is straightforward to show that

$$P_1 \cos(\theta(0) + \alpha) + P_2 \cos(\theta(\ell) + \alpha) = \rho_0 g \hat{\mathbf{g}} \cdot (\mathbf{r}(\ell) - \mathbf{r}(0)) + \frac{1}{2EI} (M_2^2 - M_1^2). \quad (4.115)$$

This equation is the extension of the relation (4.87) when the weight of the rod is included and terminal moments are allowed. It is the operating principle for the arm scale: Given P_1 , M_1 , M_2 , α , the length of the sleeve, $\rho_0 g$, the difference in heights between the ends of the rod, and measurements of $\theta(0)$ and $\theta(\ell)$, P_2 can be determined.

We can use the jump conditions $\mathbf{F}_{a_1} + [\![\mathbf{n}]\!]_{a_1} = \mathbf{0}$ and $\mathbf{F}_{a_2} + [\![\mathbf{n}]\!]_{a_2} = \mathbf{0}$ to determine the reaction forces:

$$\begin{aligned} \mathbf{F}_{a_1} &= -\frac{M^2(a_1^-)}{2EI} \mathbf{A}_2 + (P_1 + \rho_0 g a_1) \sin(\alpha) \mathbf{A}_1 \\ &= \underbrace{-\frac{EI}{2} (\theta'(a_1^-))^2}_{\text{underbrace}} \mathbf{A}_2 + (P_1 + \rho_0 g a_1) \sin(\alpha) \mathbf{A}_1, \\ \mathbf{F}_{a_2} &= \frac{M^2(a_2^+)}{2EI} \mathbf{A}_2 + (P_2 + \rho_0 g (\ell - a_2)) \sin(\alpha) \mathbf{A}_1 \\ &= \underbrace{\frac{EI}{2} (\theta'(a_2^+))^2}_{\text{underbrace}} \mathbf{A}_2 + (P_2 + \rho_0 g (\ell - a_2)) \sin(\alpha) \mathbf{A}_1. \end{aligned} \quad (4.116)$$

Both of these forces are related to the bending moment (and bending strain) in the rod. In [32], the (underbraced) terms $\frac{M^2(a_1^+)}{2EI}$ and $\frac{M^2(a_2^-)}{2EI}$, which are the axial components of \mathbf{F}_{a_1} and \mathbf{F}_{a_2} , are called Eshelby-like forces. Here, and as displayed in Figure 4.16, we have shown how they manifest in reaction forces and how they can be explicitly attributed to the material force C .

4.6.4 Insights from a Pair of Pendula

To gain a different appreciation for the dramatic change in strain energy that occurs at $s = a_1$ and $s = a_2$ in the elastica arm scale, we ignore the weight of the elastica, set the terminal moments $\mathbf{M}_0 = \mathbf{M}_\ell = \mathbf{0}$, and consider a pair of pendula. The dimensionless time variable τ and important instances for the pendula are identified as follows:

$$\tau = \frac{s}{\ell}, \quad \tau_1 = \frac{a_1}{\ell} \quad \tau_2 = \frac{a_2}{\ell}. \quad (4.117)$$

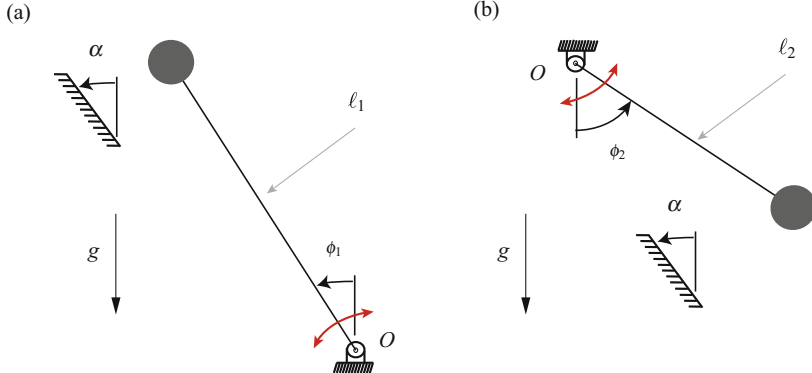


Fig. 4.18 The pair of pendula and the analogue model for the elastica arm scale. (a) The pendulum analogous to the segment $s \in (0, a_1^-)$ and (b) the pendulum analogous to the segment $s \in (a_2^+, \ell)$. The distinct lengths ℓ_1 and ℓ_2 of the pendula are defined in (4.124) and are respectively inversely proportional to the loads P_1 and P_2 .

Observe that as s ranges from $0 \rightarrow \ell$, τ ranges from $0 \rightarrow 1$. Here, we are modifying the classic kinetic analogue for a single elastica that we discussed in Section 4.4 to incorporate the unusual boundary conditions at $s = a_{1,2}$.

One of the pendula is analogous to the section $s \in [0, a_1^-)$ of the elastica. In the absence of terminal moments and ignoring the weight of the rod, the equation governing this section is (from Eqn. (4.97))

$$(\theta + \alpha)'' = \frac{P_1}{EI} \sin(\theta + \alpha), \quad \theta'(0) = 0, \quad \theta(a_1^-) = 0. \quad (4.118)$$

Thus, we can consider the motion of an analogous simple pendulum which oscillates about its downward equilibrium with a dimensionless frequency ω_1 :

$$\omega_1^2 = \frac{P_1 \ell^2}{EI}. \quad (4.119)$$

The equations of motion of this pendulum, which is shown in Figure 4.18, are

$$\frac{d^2\phi_1}{d\tau^2} = \omega_1^2 \sin(\phi_1), \quad \frac{d\phi_1}{d\tau}(0) = 0, \quad \phi_1(\tau_1) = \alpha. \quad (4.120)$$

The second pendulum models the segment of rod $s \in (a_2^+, \ell]$. For this segment of the rod we have (from Eqn. (4.102))

$$(\theta + \alpha)'' = -\frac{P_2}{EI} \sin(\theta + \alpha), \quad \theta'(\ell) = 0, \quad \theta(a_2^+) = 0. \quad (4.121)$$

Thus, we can consider the motion of an analogous simple pendulum which oscillates about its downward equilibrium with a dimensionless frequency ω_2 ,

$$\omega_2^2 = \frac{P_2 \ell^2}{EI}, \quad (4.122)$$

and whose equations of motion are described by

$$\frac{d^2\phi_2}{d\tau^2} = -\omega_2^2 \sin(\phi_2), \quad \frac{d\phi_2}{d\tau}(1) = 0, \quad \phi_2(\tau_2) = \alpha. \quad (4.123)$$

We refer to this pendulum as pendulum II and its counterpart of length ℓ_1 as pendulum I. If the dimensional measure t of time is given by $t = \beta \tau$ where β is a constant, then the lengths of pendulum I and pendulum II are

$$\begin{aligned} \ell_1 &= \beta^2 g \left(\frac{EI}{P_1 \ell^2} \right) = \frac{\beta^2 g}{\omega_1^2}, \\ \ell_2 &= \beta^2 g \left(\frac{EI}{P_2 \ell^2} \right) = \frac{\beta^2 g}{\omega_2^2}. \end{aligned} \quad (4.124)$$

With the help of Figure 4.19, we are now in a position to discuss the analogue model for the elastic arm scale. Consider pendulum I and assume that it is released from rest with $\phi_1(0) = \theta(0) + \alpha$. The pendulum falls as shown in Figure 4.19(b) and eventually collides with a surface in a perfectly plastic collision (cf. Figure 4.19(c)) wherein it loses all its kinetic energy. After a period $\frac{a_2 - a_1}{\ell}$ of no motion, pendulum II, which is at rest inclined at an angle $\phi_2 = \alpha$ to the vertical, is launched with a speed $\frac{d\phi_2}{d\tau}(\tau_2^+) > 0$ (cf. Figure 4.19(d)). The resulting motion of pendulum II persists until $\tau = 1$ where it eventually comes to a state of instantaneous rest (cf. Figure 4.19(e) & (f)). The counterpart of the material force C in this problem is the total energy of the individual pendula:

$$\begin{aligned} e_1 &= \frac{1}{2} \left(\frac{d\phi_1}{d\tau} \right)^2 + \omega_1^2 \cos(\phi_1), \\ e_2 &= \frac{1}{2} \left(\frac{d\phi_2}{d\tau} \right)^2 - \omega_2^2 \cos(\phi_2). \end{aligned} \quad (4.125)$$

We assume that the value of the total energies of both pendula are identical when they are in motion. This assumption prescribes $\frac{d\phi_2}{d\tau}(\tau_2^+)$:

$$\left(\frac{d\phi_2}{d\tau}(\tau_2^+) \right)^2 = \left(\frac{d\phi_1}{d\tau}(\tau_1^-) \right)^2 + 2(\omega_1^2 + \omega_2^2) \cos(\alpha). \quad (4.126)$$

In addition, the equality of the energies also implies that

$$\omega_1^2 \cos(\phi_1(0)) = -\omega_2^2 \cos(\phi_2(1)). \quad (4.127)$$

This identity is the counterpart to the relation (4.87) for the arm scale.

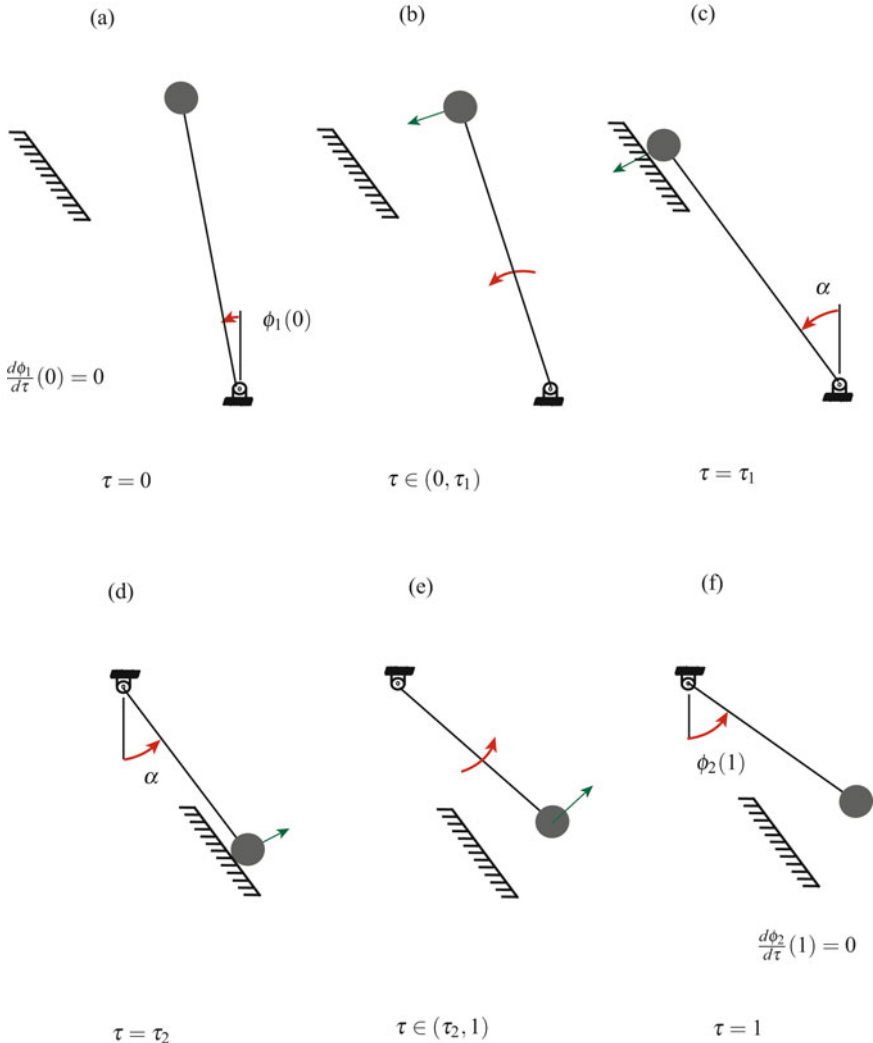


Fig. 4.19 Schematic of the motion of pendulum I ((a) - (c)) and the subsequent motion of pendulum II ((d) - (f)).

The kinetic analogue also sheds light on solving the boundary-value problem associated with the elastic arm (whose weight is ignored). For a given loading P_1 and P_2 on the elastica arm scale and a given length $a_2 - a_1$ of sleeve, ω_1 and ω_2 can be computed, and the phase portraits for both pendula can be constructed (cf. Figure 4.20). Now the solution shown in Figure 4.20(a) starts with a chosen $\phi_1(0)$. This value of $\phi_1(0)$ then determines the time of flight $\tau_1 = \frac{a_1}{\ell}$ to the impact event. This time of flight then prescribes the allowable time of flight $1 - \frac{a_2}{\ell}$ for pendulum II (cf. Figure 4.20(b)). The initial speed $\frac{d\phi_2}{d\tau}(\tau_2^+) > 0$ is prescribed by Eqn. (4.126)

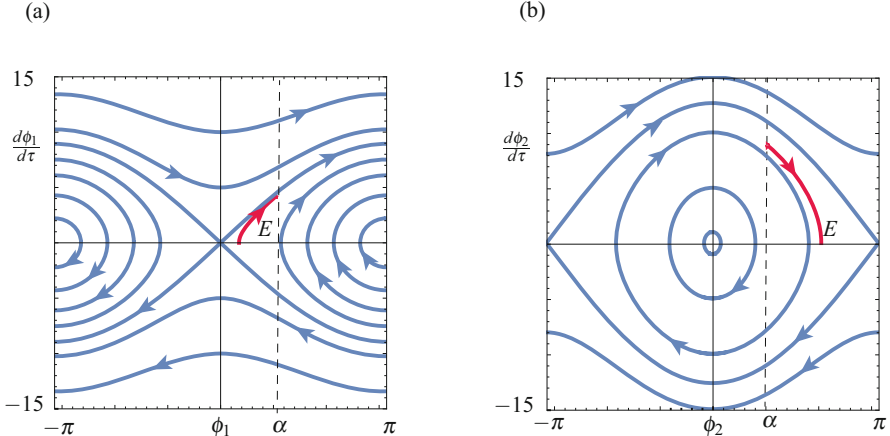


Fig. 4.20 Phase portraits for (a) pendulum I and (b) pendulum II. Referring to Eqns. (4.120) and (4.123), for the results shown in this figure, $\omega_1^2 = 20$, $\omega_2^2 = 40$, and $\alpha = 60^\circ$. The solution labeled E is discussed in the text and in Figure 4.21.

and then it remains to verify that ϕ_2 must transition to a state of instantaneous rest in $1 - \frac{a_2}{\ell}$ units of dimensionless time at a value of ϕ_2 given by Eqn. (4.127). Typically, for a given loading P_1 and P_2 on the elastica scale arm and a given length $a_1 - a_2$ of sleeve, it is necessary to iterate the values of $\phi_1(0)$ and a_1 so as to find a solution that satisfies Eqns. (4.126) and (4.127) given the time of flight $1 - \frac{a_2}{\ell}$ for pendulum II.

An example of a solution for prescribed values of ω_1 , ω_2 , and $a_2 - a_1$ is shown in Figure 4.21(a). The configuration of the elastic rod corresponding to this solution is constructed in Figure 4.21(b) after integrating Eqn. (4.88) to determine the position vector of the centerline \mathbf{r} . In computing the solution numerically, we found that

$$\frac{a_1}{\ell} = 0.4022, \quad \phi_1(0) = \frac{2\pi}{9}, \quad \frac{d\phi_2}{d\tau}(\tau_2^+) = 8.80633. \quad (4.128)$$

For the impact at $\tau = \tau_1 = \frac{a_1}{\ell}$, an energy

$$\frac{1}{2} \left(\frac{d\phi_1}{d\tau}(\tau_1^-) \right)^2 = \frac{1}{2} (4.19465)^2 \quad (4.129)$$

is lost by pendulum I. However for the launch at $\tau = \tau_2 = \frac{a_2}{\ell}$, an energy

$$\frac{1}{2} \left(\frac{d\phi_2}{d\tau}(\tau_2^+) \right)^2 = \frac{1}{2} (8.80633)^2 \quad (4.130)$$

is transferred to pendulum II. The plots of the total energies of the pendula shown in Figure 4.21(c) confirm conservation of energy during the pendulum motions while

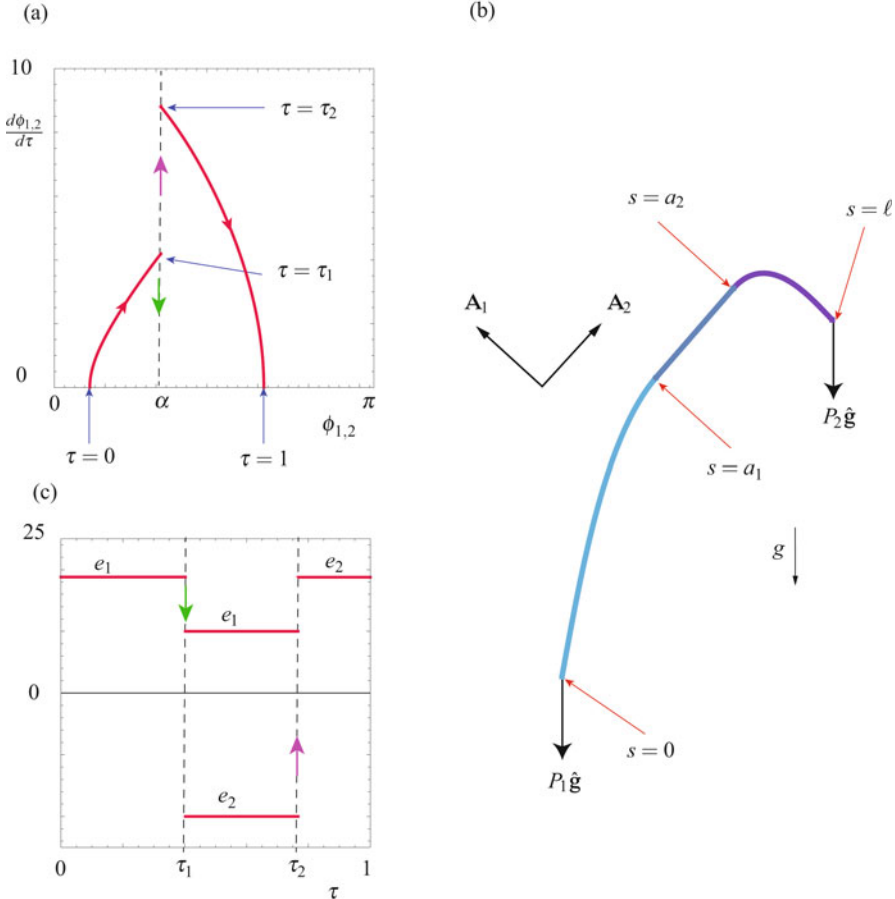


Fig. 4.21 (a) A solution to the pendulum equations of motion (4.120) and (4.123), (b) the corresponding elastica arm scale, and (c) the energy of the pendula during their motions. Referring to Eqns. (4.120) and (4.123), for the results shown in this figure, $\alpha = 60^\circ$, $\omega_1^2 = 20$, $\omega_2^2 = 40$, the sleeve is 36.44% of the length ℓ of the elastic rod, $\tau_1 = \frac{a_1}{\ell}$, and $\tau_2 = \frac{a_2}{\ell}$. The phase plane representation for the solution shown in (a) corresponds to the trajectory labeled E in Figure 4.20.

the pendula are moving - although the analogy we have presented breaks down when the pendula are stationary during the time interval $\tau \in (\tau_1, \tau_2)$.

When one of the terminal loads is zero, then it is possible to use a single pendulum to develop an analogue model for the deformable scale. In this case, say if $P_1 = 0$, then Eqn. (4.127) implies that $\theta(\ell) + \alpha = 90^\circ$. For pendulum II, we have $e_2 = 0$, $\phi_2(1 - \frac{a_2}{\ell}) = \alpha$, and $\phi_2(1) = 90^\circ$. Thus, it is possible to quickly arrive at a closed form expression for $\frac{a_2}{\ell}$ from Eqn. (4.125)₂¹⁴:

¹⁴ Eqn. (4.131) can also be inferred from [32, Eqn. (2.6)].

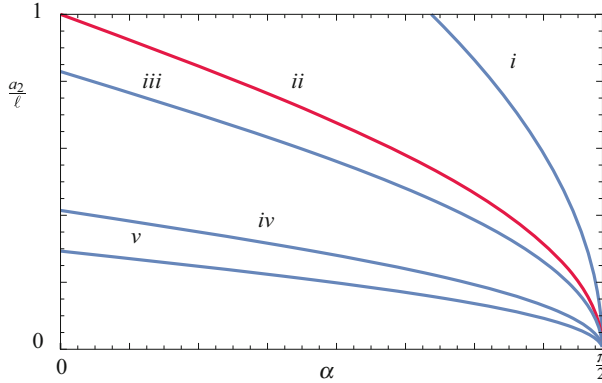


Fig. 4.22 The length $\frac{a_2}{\ell}$ as a function of α when $P_1 = 0$ for various values of P_2 . The results shown in this figure are calculated using Eqn. (4.131) with i , $\omega_2^2 = 1$; ii , $\omega_2^2 = K^2(\frac{1}{2}) \approx 3.43759$; iii , $\omega_2^2 = 5$; iv , $\omega_2^2 = 20$; and v , $\omega_2^2 = 40$.

$$\frac{a_2}{\ell} = f(\omega_2, \alpha) \quad \text{where} \quad f(\omega_2, \alpha) = \frac{1}{\omega_2} \left(K\left(\frac{1}{2}\right) - \sqrt{2}F\left(\frac{\alpha}{2}, 2\right) \right), \quad (4.131)$$

$K(x)$ is a complete elliptic integral of the first kind, and $F(x, m)$ is an elliptic integral of the first kind.¹⁵ The solutions $\frac{a_2}{\ell}$ to Eqn. (4.131) are shown in Figure 4.22.

Observe that for $\frac{P_2 \ell^2}{EI} > K^2(\frac{1}{2})$, the scale can be operated at all values of $\alpha \in (0, 90^\circ)$. In addition, the more vertical the sleeve (i.e., the smaller the value of α), the more sensitive the measurement $\frac{a_2}{\ell}$ is to changes in $\omega_2^2 = \frac{P_2 \ell^2}{EI}$. This result is evident from Figure 4.22 or $\ell \frac{\partial f}{\partial P_2}$ that can be calculated from Eqn. (4.131). Finally, we note that the range of values of α for which the scale operates is limited when $0 < \frac{P_2 \ell^2}{EI} < K^2(\frac{1}{2})$.

Our analysis of the arm scale assumes that

$$B_{a_1} = 0, \quad B_{a_2} = 0, \quad (4.132)$$

which in turn lead to a derivation of the relation Eqn. (4.87) for the operation of an arm scale (where the weight of the elastica was neglected). As with the chain problems, such as the chain fountain, discussed in Chapter 2, the prescriptions for the supplies of material momentum must be justified by experiment. To this end, we note that the relation Eqn. (4.87) governing the arm scale has been validated experimentally by Bosi et al. [32]. Their experiments justify the prescriptions we used for B_{a_1} and B_{a_2} .

¹⁵ As noted earlier, for background on elliptic integrals and functions, the handbook [41] and the textbook [200] are recommended.

4.7 Potential Energies and a Variational Formulation

For many problems that use the elastica as a model for a rod-like body, it is possible to use a variational principle to establish the equations of motion. A principal advantage of a variational formulation is that it also enables stability criteria to be established for the equilibrium configuration of the rod. Among others, these criteria enable the interpretation of buckling phenomena as instabilities. Central to any variational formulation is a potential energy functional Π and in this section we will be concerned with establishing such a function for a variety of boundary-value problems, a sample of which were shown earlier in Figure 4.1. Additional background on variational methods can be found in Chapter 9 and the references cited therein.

We restrict attention to rods which are terminally loaded with constant forces and constant moments. In the context of planar motions of the elastica, such forces and moments are conservative.¹⁶ We also assume that the assigned force $\rho_0\mathbf{f}$ is conservative; the prototypical example of such a force is gravitational: $\rho_0\mathbf{f} = -\rho_0 g \mathbf{A}_2$. In a second example, we allow for the fact that a portion of the rod may have adhered to a rigid surface.

4.7.1 A Terminally Loaded Rod Deforming Under a Conservative Assigned Force

As our first example, consider a rod which is fixed at $\xi = 0$ and loaded at $\xi = \ell$ by a terminal force and terminal moment:

$$\mathbf{F}_\ell = \mathbf{P} = P_1 \mathbf{A}_1 + P_2 \mathbf{A}_2, \quad \mathbf{M}_\ell = M_1 \mathbf{A}_3. \quad (4.133)$$

Examples of such rods can be seen in Figures 4.1(a) & (b). For these examples, we have the respective specifications:

$$\begin{aligned} \mathbf{F}_\ell &= -P \mathbf{A}_2, & \mathbf{M}_\ell &= \mathbf{0}, & \rho_0 \mathbf{f} &= -\rho_0 g \mathbf{A}_2, \\ \mathbf{F}_\ell &= P_1 \mathbf{A}_1 + P_2 \mathbf{A}_2, & \mathbf{M}_\ell &= \mathbf{0}, & \rho_0 \mathbf{f} &= -\rho_0 g \mathbf{A}_2. \end{aligned} \quad (4.134)$$

The example we consider in this section does not encompass the elastica arm scale or the adhered rod because the boundary condition at one end of the rod does not pertain to a fixed material point.

¹⁶ Referring the reader to [8, 163, 265, 375] for further details, it is known that a constant moment is not necessarily conservative.

The balance laws (4.26) and jump conditions (4.41)_{1,3} imply that

$$\begin{aligned}\mathbf{n}(\ell) &= \mathbf{P}, & EI\left(\theta'(\ell) - \kappa_0(\ell)\right) &= M_1, \\ \mathbf{n}(\xi) &= \mathbf{P} + \int_{\xi}^{\ell} \rho_0 \mathbf{f} ds, \\ \left(EI\left(\theta' - \kappa_0\right)\right)' + \left(\mathbf{A}_3 \times \mathbf{r}'\right) \cdot \left(\mathbf{P} + \int_{\xi}^{\ell} \rho_0 \mathbf{f} ds\right) &= 0.\end{aligned}\quad (4.135)$$

where we have dropped the $-$ ornamenting some of the ℓ s in these equations.

The total elastic strain energy Π_E of the elastica is

$$\Pi_E = \int_0^{\ell} \rho_0 \psi ds = \frac{1}{2} \int_0^{\ell} EI\left(\theta' - \kappa_0\right)^2 ds. \quad (4.136)$$

Noting that the potential energy of the terminal load is $-\mathbf{P} \cdot \mathbf{r}(\ell)$ and exploiting the constancy of \mathbf{P} , we find that this potential energy, which we denote by Π_P , can be represented as

$$\Pi_P = -\mathbf{P} \cdot \mathbf{r}(\ell) = -\int_0^{\ell} \mathbf{P} \cdot \mathbf{r}' ds - \mathbf{P} \cdot \mathbf{r}(0). \quad (4.137)$$

As the end $\xi = 0$ of the rod is fixed, we can ignore $\mathbf{P} \cdot \mathbf{r}(0)$ in much of the sequel. The contribution from the moment \mathbf{M}_{ℓ} can be expressed as

$$\Pi_{\mathbf{M}_{\ell}} = -\mathbf{M}_{\ell} \cdot \theta(\ell) \mathbf{A}_3 = -\int_0^{\ell} \mathbf{M}_{\ell} \cdot \theta' \mathbf{A}_3 ds - \mathbf{M}_{\ell} \cdot \theta(0) \mathbf{A}_3. \quad (4.138)$$

We have not found a discussion of $\Pi_{\mathbf{M}_{\ell}}$ in the literature, but note that it is crucial to assume in the establishment of the final representation that \mathbf{M}_{ℓ} is constant and parallel to the constant axis of rotation \mathbf{A}_3 . If either of these conditions are violated, then the moment will typically be nonconservative.

The potential energy Π_f of the assigned force $\rho_0 \mathbf{f}$ is simply the integral of $-\rho_0 \mathbf{f} \cdot \mathbf{r}$ over the length of the rod. However, to make this expression tractable to later analysis, we need to use the fundamental theorem of calculus and replace \mathbf{r} with the integral of \mathbf{r}' and then change the order of integration in the resulting integral.¹⁷ These manipulations are summarized in the following identities:

$$\begin{aligned}\Pi_f &= -\int_0^{\ell} \rho_0(s) \mathbf{f}(s) \cdot \mathbf{r}(s) ds \\ &= -\int_0^{\ell} \rho_0(s) \mathbf{f}(s) \cdot \left(\int_0^s \mathbf{r}'(u) du + \mathbf{r}(0)\right) ds \\ &= -\int_0^{\ell} \int_s^{\ell} \rho_0(u) \mathbf{f}(u) \cdot \mathbf{r}'(s) du ds - \int_0^{\ell} \rho_0(s) \mathbf{f}(s) \cdot \mathbf{r}(0).\end{aligned}\quad (4.139)$$

This completes the discussion of representations for the components of Π .

¹⁷ Our manipulations of Π_f are inspired by related work in a recent paper by Farjoun and Neu [108].

Combining the potential energy functions, we find the total potential energy of the rod:

$$\Pi = \int_0^\ell \left(\frac{EI}{2} (\theta' - \kappa_0)^2 - \left\{ \mathbf{P} + \int_s^\ell \rho_0(u) \mathbf{f}(u) du \right\} \cdot \mathbf{r}' - \mathbf{M}_\ell \cdot \theta' \mathbf{A}_3 \right) ds + C_0, \quad (4.140)$$

where the constant $C_0 = - \int_0^\ell \rho_0(s) \mathbf{f}(s) \cdot \mathbf{r}(0) ds - \mathbf{P} \cdot \mathbf{r}(0) - \mathbf{M}_\ell \cdot \theta(0) \mathbf{A}_3$. It is important to note that the term inside the curly brackets, which is equivalent to $\mathbf{n}(\xi = s)$, is a function of ξ and not \mathbf{r} .

After substituting for $\mathbf{r}' = \cos(\theta) \mathbf{A}_1 + \sin(\theta) \mathbf{A}_2$, we find that Π is a functional of the form $\Pi = \int_0^\ell f(\theta, \theta', \xi) ds$. We seek extremizers of Π using methods from the calculus of variations. To perform the variation, we let

$$\theta(\xi) = \theta^*(\xi) + \varepsilon \eta(\xi), \quad (4.141)$$

where the variation $\eta(\xi)$ satisfies the boundary condition

$$\eta(\xi = 0) = 0. \quad (4.142)$$

We substitute (4.141) into Π and then assume that $\lim_{\varepsilon \rightarrow 0} \frac{d\Pi}{d\varepsilon} = 0$. In other words, $\theta^*(\xi)$ extremizes Π . Using the standard methods from the calculus of variations¹⁸ we find a pair of necessary conditions for θ^* to extremize Π . The first of these conditions is the Euler-Lagrange necessary condition (cf. Eqn. (9.14)),

$$\frac{d}{d\xi} \left(\frac{\partial f}{\partial \theta'} \right) - \left(\frac{\partial f}{\partial \theta} \right) = 0, \quad (4.143)$$

where

$$\begin{aligned} \frac{d}{d\xi} \left(\frac{\partial f}{\partial \theta'} \right) &= \left(EI (\theta' - \kappa_0) - M_1 \right)' \\ &= \left(EI (\theta' - \kappa_0) \right)', \\ \frac{\partial f}{\partial \theta} &= - \left(\mathbf{P} + \int_\xi^\ell \rho_0(u) \mathbf{f}(u) du \right) \cdot (\cos(\theta) \mathbf{A}_2 - \sin(\theta) \mathbf{A}_1). \end{aligned} \quad (4.144)$$

In addition, the second condition is the natural boundary condition at $\xi = \ell$ (cf. Eqn. (9.12)):

$$EI (\theta'(\ell) - \kappa_0(\ell)) = M_1 = \mathbf{M}_\ell \cdot \mathbf{A}_3. \quad (4.145)$$

Upon inspection, we conclude that Eqns. (4.143) and (4.145) are identical to the governing equation (4.135)₄ and boundary condition (4.135)₂ we discussed earlier. We denote the solution to (4.143) with an asterisk. What is important to note is that the solution $\theta(\xi) = \theta^*(\xi)$ to either of these governing equations that satisfies the boundary conditions

¹⁸ These methods are discussed in Section 9.3 of Chapter 9.

$$\theta^*(\xi = 0) = \theta_0, \quad EI \left(\theta^{*'}(\ell) - \kappa_0(\ell) \right) = M_1, \quad (4.146)$$

satisfies a necessary condition for an extremizer of Π . Whether or not it is a minimizer or a maximizer can be partially ascertained by looking at the second variation of Π , a task we shall shortly examine.

The material we have just presented pertains to a rod where one end is clamped and the other is free. The corresponding developments where both ends are clamped or both ends are free are straightforward to deduce and we leave them as an exercise for the reader.

4.7.2 Application to an Adhesion Problem

Consider the problem shown in Figure 4.8 of a rod for which a portion $\ell - \gamma$ is contacting a rigid surface or the elastica arm scale shown in Figure 4.15. For these problems, additions are needed to our previous developments. The most significant of these amendments involves subdividing the potential energy functional into a set of piecewise potential energy functionals whose limits of integration are variable.

For a rod which is in contact with a rigid substrate, the total potential energy of the rod will be composed of the potential energy of terminal forces and moments, the integral of the strain energy per unit length, and the adhesion energy per unit length $-W_{ad}$. Many of the details, particularly for the segment of the rod $\xi \in [0, \gamma]$, are similar to those discussed earlier and so we focus on the differences. In particular for this rod, the balance of linear momentum can be used to show that

$$\begin{aligned} \mathbf{n}(0^+) &= -\mathbf{F}_0 = -\mathbf{P}, \\ \mathbf{n}(\xi) &= - \int_0^\xi \rho_0(u) \mathbf{f}(u) du - \mathbf{P}, \quad \xi \in [0, \gamma]. \end{aligned} \quad (4.147)$$

It is convenient to decompose the potential energy into the sum of the elastic potential energy in the noncontacting and contacting sections. Modulo an additive constant, the resulting expression for the total potential energy Π is¹⁹

$$\begin{aligned} \Pi &= \int_0^\gamma \left(\left\{ \frac{EI}{2} (\theta' - \kappa_0)^2 \right\} + \underbrace{\left(\int_0^s \rho_0(u) \mathbf{f}(u) du + \mathbf{P} \right)}_{=-\mathbf{n}} \cdot \mathbf{r}' + \mathbf{M}_0 \cdot \theta' \mathbf{A}_3 \right) d\xi \\ &\quad + \int_\gamma^\ell \left\{ \frac{EI}{2} \kappa_0^2 - \mathbf{n} \cdot \mathbf{A}_1 - W_{ad} \right\} d\xi + C_\gamma. \end{aligned} \quad (4.148)$$

¹⁹ The contribution of $\rho_0 \mathbf{f}$ to this expression follows from Eqn. (4.139) with some minor modifications to one of the limits of integration.

In writing Eqn. (4.148), we noted that $\mathbf{r}' = \mathbf{A}_1$ and $\theta = 0$ in the contact region and we defined an additive constant to Π :

$$C_\gamma = -\mathbf{P} \cdot \mathbf{r}(\gamma) - \mathbf{M}_0 \cdot \theta(\gamma) \mathbf{A}_3 - \int_0^\gamma \rho_0(s) \mathbf{f}(s) ds \cdot \mathbf{r}(\gamma). \quad (4.149)$$

The adhesion energy W_{ad} is subtracted from the penultimate term in Eqn. (4.148). This subtraction can be explained by the fact that W_{ad} is defined as the work of the adhesive and elastic restoring forces during interfacial detachment.²⁰

In the sequel, the behavior of the functional (4.148) with respect to variations in θ and γ will be computed:

$$\theta = \theta(\xi, \varepsilon) = \theta^*(\xi) + \varepsilon \eta(\xi), \quad \gamma = \gamma(\varepsilon) = \gamma^* + \varepsilon \mu. \quad (4.150)$$

In terms of a more classic notation, the respective variations in θ and γ are $\delta\theta = \varepsilon\eta$ and $\delta\gamma = \varepsilon\mu$. In the region where the rod is adhering to the horizontal surface, θ is prescribed and so

$$\eta(\xi) = 0 \quad \forall \xi \in (\gamma, \ell]. \quad (4.151)$$

It is known that the variations of θ and γ are not independent and must satisfy compatibility conditions.²¹ To find these conditions we compute the first and second derivatives of $\theta(\xi = \gamma^* + \varepsilon\mu, \varepsilon)$ with respect to ε evaluated at $\varepsilon = 0$. The desired set of compatibility conditions are obtained by taking the first and second derivatives of Eqn. (4.150)₁ with respect to ε and then setting $\varepsilon \rightarrow 0$:

$$\left[[\mu \theta^{*\prime} + \eta] \right]_\gamma = 0, \quad \left[[\mu^2 \theta^{*\prime\prime} + 2\mu \eta'] \right]_\gamma = 0. \quad (4.152)$$

These conditions prove remarkably useful when simplifying expressions for the first and second variations of Π .

4.7.2.1 Static Balance Laws

By considering variations of the form (4.150)₁ and keeping γ fixed, we find that the equation $\frac{d\Pi}{d\varepsilon}|_{\varepsilon=0} = 0$ leads, as anticipated, to a differential equation which is identical to that obtained using the balances of linear and angular momentum:

$$\frac{\partial}{\partial \xi} \left(EI \left(\theta^{*\prime} - \kappa_0 \right) \right) + \mathbf{n} \cdot (\cos(\theta^*) \mathbf{A}_2 - \sin(\theta^*) \mathbf{A}_1) = 0, \quad (4.153)$$

where $\xi \in (0, \gamma)$. This differential equation is often known as the Euler-Lagrange equation because it is intimately related to the Euler-Lagrange necessary condition.

²⁰ Alternatively, the adhesion may be represented as a surface potential by also adding $W_{ad}\ell$ to Π . This is accomplished by eliminating W_{ad} in the second integrand and adding it to the first integrand.

²¹ Compatibility conditions of the form (4.152) for adhesion problems can be found in [219] and [318] and for problems where the rod passes through a sleeve, as in the elastica arm scale, in [27, 32]. They express the restrictions that variations in $\theta(\gamma^\pm)$ and γ are not always independent.

We also obtain the boundary conditions at $\xi = 0$ and $\xi = \gamma^{*-}$:

$$EI\left(\theta^{*'}(0) - \kappa_0\right) = -\mathbf{M}_0 \cdot \mathbf{A}_3, \quad \theta^*(\gamma^{*-}) = 0. \quad (4.154)$$

In the condition (4.153), we identified the term comprised of \mathbf{P} and $\rho_0 \mathbf{f}$ with the contact force \mathbf{n} (cf. Eqn. (4.147)).

4.7.2.2 Adhesion Boundary Conditions

To consider the variations of γ , we need to use the Leibniz rule. You may recall that we used this rule earlier in Chapter 1 (cf. Eqn. (1.48)) to obtain jump conditions from the integral form of the balance laws. In the present context, this rule takes the form

$$\frac{d}{d\varepsilon} \int_{g(\varepsilon)}^{f(\varepsilon)} \mathbf{a}(u, \varepsilon) du = \int_{g(\varepsilon)}^{f(\varepsilon)} \frac{d}{d\varepsilon} \mathbf{a}(u, \varepsilon) du + \mathbf{a}(f(\varepsilon), \varepsilon) \frac{df}{d\varepsilon} - \mathbf{a}(g(\varepsilon), \varepsilon) \frac{dg}{d\varepsilon}. \quad (4.155)$$

The natural boundary condition at the edge of the region of adhesive contact is obtained by applying the variations (4.150). After differentiating the expression for the functional Π with respect to ε , using the Leibniz rule (4.155), taking the limit $\varepsilon \rightarrow 0$, using Eqns. (4.153) and (4.154), and then setting the resulting expression to 0, we find that

$$\left(\left[\left[\frac{EI}{2} \left(\theta^{*'} - \kappa_0 \right)^2 - \mathbf{n} \cdot \mathbf{r}' \right] \right]_\gamma - W_{ad} \right) \mu = 0. \quad (4.156)$$

The condition (4.156) must hold for all μ . Whence, we find the adhesion boundary condition²²

$$\left[\left[\frac{EI}{2} \left(\theta^{*'} - \kappa_0 \right)^2 - \mathbf{n} \cdot \mathbf{r}' \right] \right]_\gamma = W_{ad}. \quad (4.157)$$

This boundary condition can be further simplified by noting that (because θ is a continuous function of ξ) $\left[\left[\mathbf{r}' \right] \right]_\gamma = \mathbf{0}$. Thus, we can use Eqn. (4.41)₁ to write

$$\left[\left[\frac{EI}{2} \left(\theta^{*'} - \kappa_0 \right)^2 \right] \right]_\gamma + \mathbf{F}_\gamma \cdot \mathbf{E}_1 = W_{ad}. \quad (4.158)$$

In the absence of shear adhesion (i.e., \mathbf{F}_γ is normal to the surface and so $\mathbf{F}_\gamma \cdot \mathbf{E}_1 = 0$) or when the shear traction is distributed along the interface between the rod and the surface, the boundary condition (4.158) is the same natural boundary condition previously derived in [217] and [318] and corresponds to the jump in material

²² If the rod were extensible, then $\left[\left[\mathbf{n} \cdot \mathbf{r}' \right] \right]_\gamma$ would be due to the jump in the stretch of the centerline across the discontinuity. For examples where this situation arises, see [181] and [218].

momentum (4.41)₂ with $B_\gamma = -W_{\text{ad}}$. When adhesion is absent, as it is in the elastica arm scale, then $W_{\text{ad}} = 0$ and the condition corresponding to Eqn. (4.158) is discussed and exploited in [27, 32].

In addition to a force \mathbf{F}_γ and material force B_γ at the edge of the region of adhesive contact, a moment \mathbf{M}_γ can also be present. This moment is computed from Eqn. (4.41)₃:

$$\mathbf{M}_\gamma = \left(EI\theta^{*\prime}(\gamma^{*-}) - EI\theta^{*\prime}(\gamma^{*+}) \right) \mathbf{A}_3. \quad (4.159)$$

An example of \mathbf{M}_γ can be seen in Figure 4.9. Moments of this type also appear in the elastica arm scale (cf. Eqn. (4.111)) and are similar to the adhesion moment discussed in the literature (cf. [282]).

Where no confusion should arise, in the sequel we will drop the $*$ ornamenting the solutions $\theta^*(\xi)$ and γ^* of the boundary-value problem.

4.8 Conditions for Stability from the Second Variation

We now turn to examining stability conditions for the equilibrium configurations discussed in the previous sections. The central idea here is to consider an expansion of Π about $\varepsilon = 0$:

$$\Pi(\varepsilon) = \Pi(\varepsilon = 0) + \frac{d\Pi}{d\varepsilon} \Big|_{\varepsilon=0} \varepsilon + \frac{1}{2} \frac{d^2\Pi}{d\varepsilon^2} \Big|_{\varepsilon=\varepsilon_0} \varepsilon^2, \quad (4.160)$$

where $\varepsilon_0 \in [0, \varepsilon]$. Now for an equilibrium configuration the first variation of Π is zero:

$$\delta\Pi = \frac{d\Pi}{d\varepsilon} \Big|_{\varepsilon=0} \varepsilon = 0, \quad (4.161)$$

and, after assuming that $\frac{d^2\Pi}{d\varepsilon^2}$ is continuous in a neighborhood of $\varepsilon = 0$, we can conclude that

$$\Pi(\varepsilon) - \Pi(\varepsilon = 0) = \frac{1}{2} \frac{d^2\Pi}{d\varepsilon^2} \Big|_{\varepsilon=\varepsilon_0} \varepsilon^2 \approx \frac{1}{2} \frac{d^2\Pi}{d\varepsilon^2} \Big|_{\varepsilon=0} \varepsilon^2. \quad (4.162)$$

The latter term is known as the second variation $\delta^2\Pi$ of Π :

$$\delta^2\Pi = \frac{1}{2} \frac{d^2\Pi}{d\varepsilon^2} \Big|_{\varepsilon=0} \varepsilon^2. \quad (4.163)$$

Thus, if $\frac{d^2\Pi}{d\varepsilon^2} \Big|_{\varepsilon=0} \geq 0$, then the potential energy functional is minimized at an equilibrium configuration. This nonnegativity of the second variation enables us to conclude that the configuration satisfies a necessary condition for stability. If the stronger condition $\frac{d^2\Pi}{d\varepsilon^2} \Big|_{\varepsilon=0} > 0$ holds, then we can conclude that the configuration

satisfies a sufficient condition for stability and we classify the configuration as stable. By way of contrast, if we can show that $\frac{d^2\Pi}{d\varepsilon^2}\Big|_{\varepsilon=0} < 0$, then the necessary condition for stability is not satisfied and we conclude that the equilibrium configuration is unstable.

We now explore conditions that can be used to determine the sign of $\frac{d^2\Pi}{d\varepsilon^2}\Big|_{\varepsilon=0}$ and use them to establish a necessary condition, which we denote as N1, for stability. For some cases, we are able to establish a pair of sufficiency conditions, which are referred to as B1 and S1, for stability. For the purposes of exposition, it is convenient to first consider the adhesion problem in Section 4.7.2. Our presentation is based on the works of Majidi, O'Reilly, and Williams [219, 220].

4.8.1 A Representation for the Second Variation

We return to the adhesion problem shown in Figure 4.8 and discussed in Section 4.7.2. For this problem, the potential energy functional to be examined was presented in Eqn. (4.148) and we reproduce it here for convenience:

$$\begin{aligned}\Pi = \int_0^\gamma & \left\{ \frac{EI}{2} (\theta' - \kappa_0)^2 \right\} - \mathbf{n} \cdot \mathbf{r}' + \mathbf{M}_0 \cdot \theta' \mathbf{A}_3 d\xi + C_\gamma \\ & + \int_\gamma^\ell \left\{ \frac{EI}{2} \kappa_0^2 - \mathbf{n} \cdot \mathbf{A}_1 - W_{\text{ad}} \right\} d\xi.\end{aligned}\quad (4.164)$$

We consider variations of θ and γ of the form (4.150) and evaluate $\frac{d^2\Pi}{d\varepsilon^2}\Big|_{\varepsilon=0}$. After some rearranging, we find that this derivative has a simple additive decomposition:

$$\begin{aligned}\frac{d^2\Pi}{d\varepsilon^2}\Big|_{\varepsilon=0} = & \int_0^\gamma (EI\eta'\eta' + P\eta^2) d\xi \\ & - \left[\left[(EI(\theta^{*'} - \kappa_0))'(\theta^{*'} - \kappa_0) - \mathbf{n}' \cdot \mathbf{r}' - \frac{(EI)'}{2} (\theta^{*'} - \kappa_0)^2 \right] \right]_\gamma \mu^2 \\ & - \left[[2EI(\theta^{*'} - \kappa_0)\eta' - S(\mu\theta^{*'} + 2\eta)] \right]_\gamma \mu,\end{aligned}\quad (4.165)$$

where

$$\begin{aligned}P &= \mathbf{n} \cdot (\cos(\theta^*) \mathbf{A}_1 + \sin(\theta^*) \mathbf{A}_2), \\ S &= (\mathbf{r}' \times \mathbf{n}) \cdot \mathbf{A}_3 = \mathbf{n} \cdot (-\sin(\theta^*) \mathbf{A}_1 + \cos(\theta^*) \mathbf{A}_2).\end{aligned}\quad (4.166)$$

To start to simplify this expression, we first invoke the compatibility conditions (4.152):

$$0 = \mu\theta^{*'}(\gamma^-) + \eta(\gamma^-), \quad 0 = \mu\theta^{*''}(\gamma^-) + 2\eta'(\gamma^-). \quad (4.167)$$

This helps to eliminate η' and η from the expression (4.165):

$$\begin{aligned} \frac{d^2\Pi}{d\varepsilon^2}\Big|_{\varepsilon=0} &= \int_0^\gamma \left(EI\eta'\eta' + P\eta^2 \right) d\xi \\ &\quad - \left[\left[\left(EI(\theta^{*'} - \kappa_0) \right)' (\theta^{*'} - \kappa_0) - \mathbf{n}' \cdot \mathbf{r}' - \frac{(EI)'}{2} (\theta^{*'} - \kappa_0)^2 \right] \right]_\gamma \mu^2 \\ &\quad + \left[\left[EI(\theta^{*'} - \kappa_0) \theta^{*''} + S\theta^{*''} \right] \right]_\gamma \mu^2. \end{aligned} \quad (4.168)$$

We next appeal to the balance laws for the two segments of the rod:

$$\begin{aligned} \left(EI(\theta^{*'} - \kappa_0) \right)' + S &= 0, & \mathbf{n}' + \rho_0 \mathbf{f} &= \mathbf{0}, & \xi \in (0, \gamma), \\ \left(EI(\theta^{*'} - \kappa_0) \right)' + \mathbf{n} \cdot \mathbf{A}_2 &= 0, & \mathbf{n}' + \rho_0 \mathbf{f} + \lambda \mathbf{A}_2 &= \mathbf{0}, & \xi \in (\gamma, \ell), \end{aligned} \quad (4.169)$$

where $\lambda \mathbf{A}_2$ is the normal force exerted by the horizontal surface on the rod. Omitting details, the end result of the manipulations is that the expression for $\frac{d^2\Pi}{d\varepsilon^2}\Big|_{\varepsilon=0}$ reduces to a desirable decoupled form:

$$\begin{aligned} J = \frac{d^2\Pi}{d\varepsilon^2}\Big|_{\varepsilon=0} &= \int_0^\gamma \left(EI\eta'\eta' + P\eta^2 \right) d\xi \\ &\quad - \left[\left[S\theta^{*'} + \rho_0 \mathbf{f} \cdot \mathbf{r}' + \frac{(EI)'}{2} (\theta^{*'} - \kappa_0)^2 \right] \right]_\gamma \mu^2 \\ &\quad + \left[\left[EI(\theta^{*'} - \kappa_0) \kappa_0' \right] \right]_\gamma \mu^2. \end{aligned} \quad (4.170)$$

The terms associated with μ^2 can be simplified further by appealing to the fact that the segment of the rod in contact with the flat surface has a constant $\theta^* = 0$, however we do not pause to do this here. We also note that for many problems with homogeneous rods in the absence of intrinsic curvature and gravitational loading, the simplifications to the right-hand side of Eqn. (4.170) are extensive and reduce the term associated with μ to a single term: $+ \mu^2 S(\gamma^-) \theta^*(\gamma^-)$.

It is important to notice that the integral term in Eqn. (4.170) may not be positive because we are uncertain as to the contribution of the term $P\eta^2 = (\mathbf{n} \cdot \mathbf{r}') \eta^2$. This is particularly the case when the rod is in compression (and we anticipate that possible buckling instabilities might be present). To proceed, we follow an idea dating to the French mathematician Adrien-Marie Legendre (1752–1833) in 1786 and add the following term to Eqn. (4.170)²³:

²³ Further background on Legendre's treatment of the second variation can be found in the superb texts by Bolza [30] and Gelfand and Fomin [113].

$$\int_0^\gamma \frac{\partial}{\partial \xi} (\eta^2 w) d\xi - [\eta^2 w]_0^\gamma = 0. \quad (4.171)$$

Manipulating the resulting expression for J from Eqn. (4.170), we find that

$$\begin{aligned} J &= \int_0^\gamma EI \left\{ \eta' + \left(\frac{w}{EI} \right) \eta \right\}^2 + \left(w' + P - \frac{w^2}{EI} \right) \eta^2 d\xi \\ &\quad - \left[\left[S\theta^{*'} + \rho_0 \mathbf{f} \cdot \mathbf{r}' + \frac{(EI)'}{2} (\theta^{*'} - \kappa_0)^2 \right] \right]_\gamma \mu^2 \\ &\quad + \left[\left[EI (\theta^{*'} - \kappa_0) \kappa'_0 \right] \right]_\gamma \mu^2 - [\eta^2 w]_0^\gamma. \end{aligned} \quad (4.172)$$

It is useful to note that

$$\begin{aligned} -[\eta^2 w]_0^\gamma &= \eta^2(0)w(0) - \eta^2(\gamma^-)w(\gamma^-) \\ &= \eta^2(0)w(0) - \mu^2 (\theta^{*'}(\gamma^-))^2 w(\gamma^-). \end{aligned} \quad (4.173)$$

Thus, provided a solution $w(\xi)$ to the following Riccati equation can be found,

$$\frac{\partial w}{\partial \xi} + P - \frac{w^2}{EI} = 0, \quad (4.174)$$

we can then express J in its final desired form:

$$J = J_1 + J_2, \quad (4.175)$$

where

$$\begin{aligned} J_1 &= \int_0^\gamma EI \left\{ \eta' + \left(\frac{w}{EI} \right) \eta \right\}^2 d\xi, \\ J_2 &= - \left[\left[S\theta^{*'} + \rho_0 \mathbf{f} \cdot \mathbf{r}' + \frac{(EI)'}{2} (\theta^{*'} - \kappa_0)^2 \right] \right]_\gamma \mu^2 \\ &\quad + \left[\left[EI (\theta^{*'} - \kappa_0) \kappa'_0 \right] \right]_\gamma \mu^2 + \eta^2(0)w(0) - \mu^2 (\theta^{*'}(\gamma^-))^2 w(\gamma^-). \end{aligned} \quad (4.176)$$

Observe that adding the identity (4.171) to J succeeds in making the integrand a positive semi-definite function of η (provided we can find a bounded solution $w(\xi)$ to the Riccati equation). It is also interesting to observe that we have some freedom in choosing the initial conditions for $w(\xi)$ and this freedom will be exploited in the sequel.

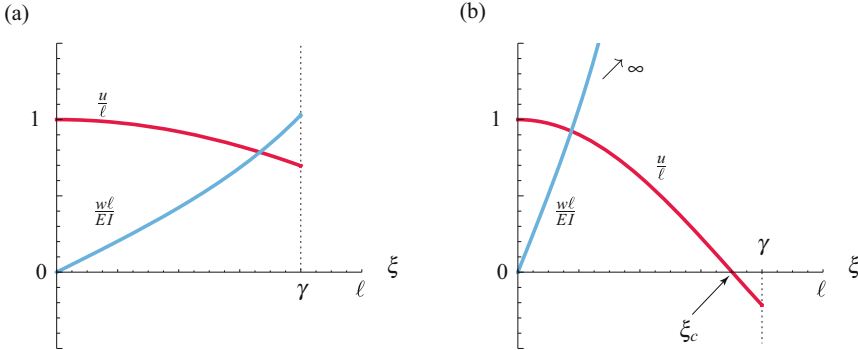


Fig. 4.23 Schematic of solutions $u(\xi)$ to a Jacobi equation (4.178) and the corresponding solutions $w(\xi)$ to a Riccati equation (4.174). In (a) there is no conjugate point to $\xi = 0$ in the interval $[0, \gamma]$ and in (b) there is a conjugate point ξ_c to $\xi = 0$ in the interval $[\gamma, \ell]$ where $w(\xi) \nearrow \infty$ as $\xi \nearrow \xi_c$ and $w(\xi) \searrow -\infty$ as $\xi \searrow \xi_c$. For the examples shown in (a), $\frac{P\ell^2}{EI} = -1$ and $\gamma = 0.8\ell$. Correspondingly for (b), the parameter values are $\frac{P\ell^2}{EI} = -5$ and $\gamma = 0.8\ell$ and, as a result, $\xi_c \approx 0.70248\ell$.

4.8.2 Conjugate Points and the Riccati and Jacobi Equations

For many problems seeking a bounded solution $w(\xi)$ to the Riccati equation is challenging. Part of the challenge is to distinguish parameter regimes where the solution becomes unbounded from their bounded counterparts. Fortunately, a remedy is at hand that is attributed to the German mathematician Carl Jacobi (1804–1851). The solution is to employ a Jacobi transformation which relates the function $w(\xi)$ to another function $u(\xi)$:

$$w = -EI \frac{u'}{u}. \quad (4.177)$$

Substituting for $w(\xi)$ in the Riccati equation (4.174), one finds that this transformation produces a Jacobi differential equation for $u(\xi)$ from Eqn. (4.174):

$$EIu'' - Pu = 0. \quad (4.178)$$

We consider solutions $u(\xi) \forall \xi \in [0, \gamma]$ to Eqn. (4.178) which satisfy the initial conditions

$$u(\xi = 0) = 1, \quad u'(\xi = 0) = 0. \quad (4.179)$$

Note that this pair of initial conditions is equivalent to $w(0) = 0$. If the solution $u(\xi_c) = 0$ for some ξ_c , then the point ξ_c is said to be conjugate to $\xi = 0$.²⁴

²⁴ Our definition of the conjugate point differs from the traditional definition as the latter applies to the case where the rod is clamped at both of its ends.

To relate unbounded solutions of the Riccati equation to conjugate points, we recall a theorem that can be found in [298]:

Bounded solutions to the Riccati equation (4.174) for $w(\xi)$ on a given interval exist if, and only if, a solution $u(\xi)$ for the corresponding Jacobi differential equation (4.178) exists on the same interval with $u(\xi) \neq 0$ and w given by (4.177). We use this theorem to conclude that the solution to the Riccati equation becomes unbounded at a conjugate point: $\lim_{\xi \rightarrow \xi_c} |w(\xi)| = \infty$ (see Figure 4.23(b)). On the other hand, and as demonstrated in Figure 4.23(a), the existence of a bounded solution $w(\xi) \forall \xi \in [\gamma, \ell]$ is equivalent to the nonexistence of conjugate points to $\xi = \ell$ in the interval $[\gamma, \ell]$ for the solution $u(\xi)$ to the Jacobi equation (4.178).

4.8.3 The Criterion N1

We have now compiled all the needed background to state the necessary condition for stability which we denote by N1. Part of this criterion pertains to the buckling instability of the rod. The second part of the criterion is intimately related to the kinematics at the adhesion point $\xi = \gamma$.

CRITERION N1: *If a solution $\{\theta^*(\xi), \gamma^*\}$ to the boundary-value problem (4.153), (4.154), and (4.158) minimizes Π then the solution $w(\xi) \forall \xi \in [0, \gamma^*]$ to the boundary-value problem*

$$\frac{\partial w}{\partial \xi} + P - \frac{w^2}{EI} = 0, \quad w(0) = 0, \quad (4.180)$$

cannot become unbounded in the interval $[0, \gamma^]$ and the following inequality must be satisfied:*

$$\begin{aligned} & \left[\left[EI \left(\theta^{*'} - \kappa_0 \right) \kappa_0' \right] \right]_\gamma - \left[\left[S \theta^{*'} + \rho_0 \mathbf{f} \cdot \mathbf{r}' + \frac{(EI)'}{2} \left(\theta^{*'} - \kappa_0 \right)^2 \right] \right]_\gamma \\ & \geq \left(\theta^{*'} (\gamma^-) \right)^2 w(\gamma^-). \end{aligned} \quad (4.181)$$

We sketch a proof of the criterion as follows. First, if a solution $w(\xi)$ to the Riccati equation (4.180) can be found, then we can decompose J into the sum of J_1 and J_2 as shown in (4.175). Further, J_1 will be positive semi-definite (cf. Eqn. (4.176)). Simplifying J_2 using the fact that $w(0) = 0$, we find that it is sufficient for Eqn. (4.181) to hold in order for $J_2 \geq 0$. This completes the proof.

The adhesion boundary condition (4.158) can often be used to express $\theta^{*'}(\gamma^+)$ in terms of W_{ad} . In this instance, the condition (4.181) can then be interpreted as a condition on the relative work of the adhesion to that of loading P_1 . On the other hand, the existence of a solution to the Riccati equation (4.180) implies that the rod has not buckled.

4.8.4 The Criterion B1

Many of the buckling problems of interest involve rods where one end is free and the other is clamped at $\xi = \ell$. To examine stability for these cases, it suffices to examine J and ignore the effects of γ . To ignore the effects of changing γ , one simply sets $\mu = 0$ in the expression for J shown in Eqn. (4.175). In this case, we can establish a very useful sufficient condition for stability by choosing the initial condition $w(0) = 0$ and appealing to some known results from the calculus of variations.²⁵ We label the resulting criterion B1.

CRITERION B1: Consider the case of a terminally loaded rod which is clamped at $\xi = \ell$ and subject to a conservative assigned body force. If a solution $\{\theta^*(\xi)\}$ to the boundary-value problem

$$\begin{aligned} \frac{\partial}{\partial \xi} \left(EI \left(\theta^{*\prime} - \kappa_0 \right) \right) + \mathbf{n} \cdot (\cos(\theta^*) \mathbf{A}_2 - \sin(\theta^*) \mathbf{A}_1) &= 0, \\ EI \left(\theta^{*\prime}(0) - \kappa_0 \right) &= -\mathbf{M}_0 \cdot \mathbf{A}_3, \quad \theta^*(\ell) = \theta_\ell, \end{aligned} \quad (4.182)$$

results in a solution $u(\xi) \forall \xi \in [0, \ell]$ to Eqns. (4.178) and (4.179) with no conjugate points in $\xi \in [0, \ell]$ then the equilibrium configuration defined by $\theta^*(\xi)$ is stable.

This stability criterion is classical and equivalent statements can be found in many papers on stability of rods featuring variational methods. The criterion can also be stated in terms of the Riccati differential equation. However, because of the simplicity of J_2 (i.e., $J_2 = 0$) it is more convenient to state the result using the Jacobi differential equation. We shall explore an application of B1 in Section 4.9.

4.8.5 The Criterion S1

For some applications featuring adhered rods, the geometry of the adhesive interface as well as the constitutive properties of the rod conspire so that the boundary term J_2 defined in Eqn. (4.176) can be set to zero by simply choosing the initial condition

$$w(0) = 0. \quad (4.183)$$

One example of such a situation arises when the rod is homogeneous, has no intrinsic curvature and $\theta^{*\prime}(\gamma^\pm) = 0$. In this case, we can strengthen N1 to yield a sufficient condition, which we denote by S1, for stability. Because $J_2 = 0$, the forthcoming criterion only pertains to perturbations in θ : perturbations to γ need not be considered.

²⁵ See, in particular, [113, Theorem 3 in Section 26]. Choosing $w(0) = 0$ implies that the boundary term J_2 defined in Eqn. (4.176) will vanish.

Referring to Theorem 3 in [113, Section 26], we can now readily establish a sufficient condition for positive definiteness of J and, hence, a sufficient condition for stability.²⁶ In the interests of brevity, we merely state the criterion:

CRITERION S1: Consider the case $\theta^*(\gamma^+) = 0$. If a solution $\{\theta^*(\xi), \gamma^*\}$ to the boundary-value problem is such that either

- (i) a bounded solution $w(\xi) \forall \xi \in [\gamma^*, \ell]$ to Eqn. (4.174) can be found where $w(\ell) = 0$, or
 - (ii) there are no points conjugate to $\xi = \ell$ in the interval $[\gamma^*, \ell]$,
- then $\{\theta^*(\xi), \gamma^*\}$ is stable.

Clearly, the development of a stability criterion in this case is identical in all but one respect to the case of a rod fixed at one end and subject to a terminal load \mathbf{P} at the other.²⁷ The distinction from this classical problem is that the length $\ell - \gamma$ of the beam is typically a (nonlinear) function of \mathbf{P} , EI , and W_{ad} .

4.9 Simple Examples of Buckling

We now consider a series of examples designed to illustrate the conditions established in the previous section.

4.9.1 Compressing an Adhered Rod

To illuminate the criteria N1 and S1, consider the rod shown in Figure 4.24.²⁸ The rod of length ℓ has a section of length γ which is restrained by friction from moving on a horizontal surface. The contact between the rod and the surface can be maintained with $W_{ad} = 0$. An applied force $F\mathbf{A}_1$ acts at the material point $\xi = 0$. Clearly, if the applied force F is too large then the unattached section of the rod will buckle. This buckling instability will be revealed using the criterion S1.

To analyze this problem, we first solve the balance laws with the help of the appropriate boundary conditions and find the trivial solution

$$\mathbf{n}(\xi) = -F\mathbf{A}_1, \quad \theta^*(\xi) = 0. \quad (4.184)$$

²⁶ Gelfand and Fomin's proof in [113] pertains to the fixed-fixed case. It requires some minor modifications to deal with the fixed-free case of interest here and these modifications are outlined in [289].

²⁷ That is, the problem of a terminally loaded fixed-free strut.

²⁸ This example is adopted from [219]. It is the simplest illustrative example of a buckling problem featuring adhesion that we could find.

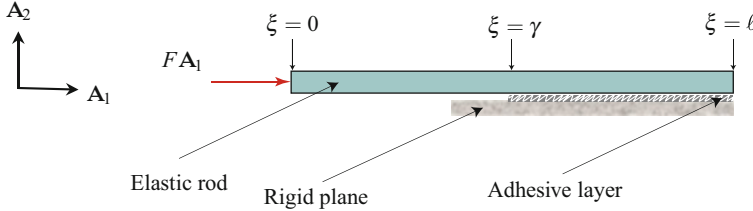


Fig. 4.24 An axially loaded elastic rod of length ℓ . A portion of the rod $\xi \in (\gamma, \ell]$ has adhered to the rigid horizontal plane.

This solution is statically admissible for all values of F and all adhesion lengths $\gamma > 0$. To examine the possibility of buckling, we establish the appropriate single Riccati and Jacobi equations, from Eqns. (4.174) and (4.178):

$$\frac{\partial w}{\partial \xi} = F + \frac{w^2}{EI}, \quad EIw'' + Fu = 0, \quad \xi \in [0, \gamma]. \quad (4.185)$$

The boundary conditions for these differential equations are, respectively,

$$w(\xi = 0) = 0, \quad u(\xi = 0) = 1, \quad u'(\xi = 0) = 0. \quad (4.186)$$

The solutions of the pair of boundary-value problems are

$$u(\xi) = \cos \left(\sqrt{\frac{F}{EI}} \xi \right), \quad w(\xi) = -\sqrt{FEI} \tan \left(\sqrt{\frac{F}{EI}} \xi \right). \quad (4.187)$$

Using the solutions (4.187), it is straightforward to show that the Riccati equation (4.185)₁ has a bounded solution and, equivalently, there are no conjugate points to $\xi = 0$ in the interval $[0, \gamma]$ provided $F < F_{\text{crit}}$ ²⁹:

$$F_{\text{crit}} = \frac{\pi^2 EI}{4\gamma^2}. \quad (4.188)$$

We conclude with the help of S1 that the straight configuration $\theta^* = 0$ is stable provided $F < F_{\text{crit}}$ and unstable otherwise. Notice that instability occurs when the rod buckles and is independent of the adhesive.

Now suppose that $F > F_{\text{crit}}$. It follows that $u(\xi_c) = 0$ for $\xi = \xi_c$. That is, $\xi = \xi_c$ is the conjugate point to $\xi = 0$. We observe from the solutions (4.187) that $w(\xi) \nearrow \infty$ as $\xi \searrow \xi_c$ as expected from our earlier discussion in Section 4.8.2. We can thus appeal to the criterion N1 to conclude that the equilibrium configuration in this case is unstable.

²⁹ This is equivalent to the classical result for the buckling load of a fixed-free strut.

4.9.2 Buckling of a Clamped Rod

We now examine the classic problem of a straight uniform rod which is clamped at $\xi = \ell$, subjected to a vertical force $-F\mathbf{A}_2$ at the free end $\xi = 0$, and must support its own weight (see Figure 4.25). Initially the rod is straight, but as F increases this straight configuration will eventually become unstable, and the rod will then buckle into one of either two configurations (which turn out to be stable). Examples of the buckled states are shown in Figure 4.26. This buckling problem has a celebrated history and we refer the reader to the discussions in Love's textbook [213], a paper by Maddocks [215], Timoshenko and Gere's textbook on elastic stability [345, Chapter 2], and a seminal historical review by Truesdell [350]. By way of additional applications, a closely related analysis applied to understanding the stability of the human spine in the sagittal plane can be found in [211].

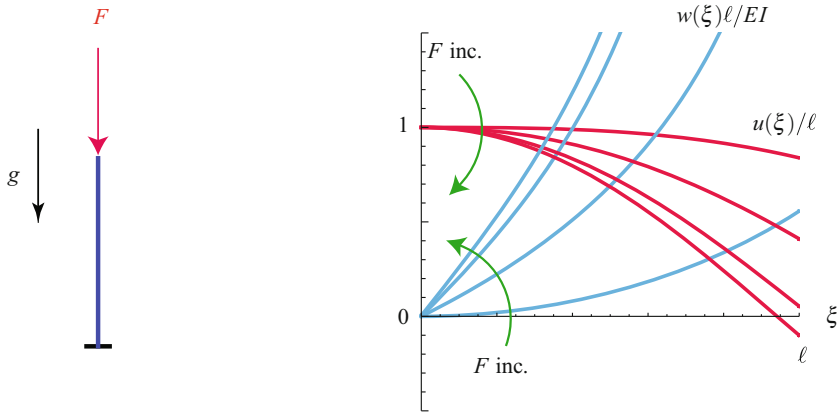


Fig. 4.25 Solutions $u(\xi)$ to the Jacobi equation (4.191)₂ and $w(\xi)$ to the Riccati equation (4.191)₃ for the straight strut. For the examples shown, $\alpha = 1.0$, $\beta_{\text{crit}} \approx 2.16$, and the values of $\beta = \frac{F\ell^2}{EI}$ are 0.0, 1.0, 2.0, and 2.5.

For the problem at hand,

$$\kappa_0 = 0, \quad \mathbf{F}_0 = -F\mathbf{A}_2, \quad \rho_0 \mathbf{f} = -\rho_0 g \mathbf{A}_2. \quad (4.189)$$

It follows that

$$P = \mathbf{n} \cdot \mathbf{r}' = (F + \rho_0 g \xi) \sin(\theta^*). \quad (4.190)$$

The Euler-Lagrange, Jacobi, and Riccati equations for this problem can be deduced from Eqns. (4.153)₁, (4.178), and (4.174), respectively:

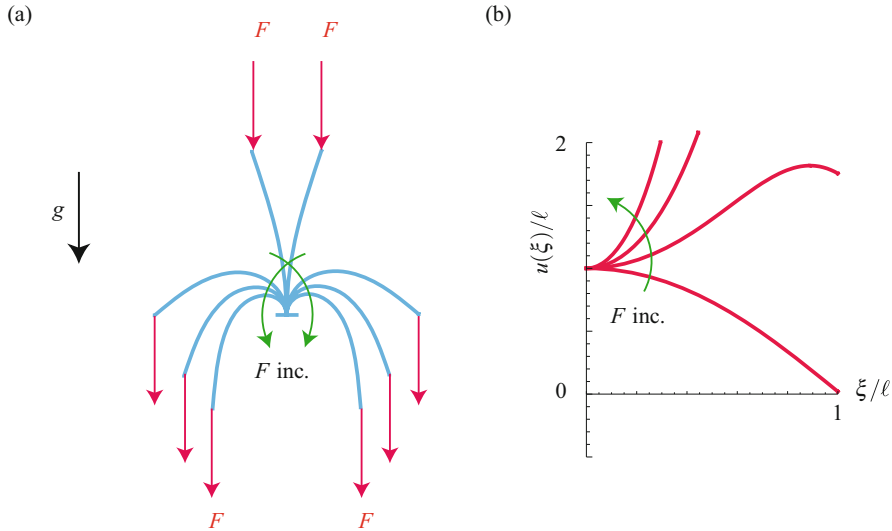


Fig. 4.26 (a) Schematic of the buckled states of a heavy terminally loaded strut elastica which is subject to a terminal load $-F\mathbf{A}_2$. (b) The solution of the Jacobi equation (4.191)₂ for the buckled strut as β increases from β_{crit} . For the examples shown, $\alpha = 1.0$, $\beta_{\text{crit}} \approx 2.16$, and the values of $\beta = \frac{F\ell^2}{EI}$ used in (a) and (b) are 2.2, 5, 10, and 20.

$$\begin{aligned} EI \frac{\partial^2 \theta^*}{\partial \xi^2} &= -(F + \rho_0 g \xi) \cos(\theta^*), \\ EI u'' &= (F + \rho_0 g \xi) \sin(\theta^*) u, \\ \frac{\partial w}{\partial \xi} - \frac{w^2}{EI} &= -(F + \rho_0 g \xi) \sin(\theta^*) u. \end{aligned} \quad (4.191)$$

The solutions to these equations are subject to the following boundary conditions:

$$\begin{aligned} \theta^*(\xi = \ell) &= -90^\circ, & \frac{\partial \theta^*}{\partial \xi}(\xi = 0) &= 0, \\ w(\xi = 0) &= 0, & u(\xi = 0) &= 1, & u'(\xi = 0) &= 0. \end{aligned} \quad (4.192)$$

In the sequel, we shall fix the dimensionless weight parameter $\alpha = \frac{\rho_0 g \ell^3}{EI}$ and vary the terminal load parameter $\beta = \frac{F\ell^2}{EI}$.

Examining the solution to the Euler-Lagrange equation (4.191)₁, we observe that the straight strut (i.e., $\theta^* = -90^\circ$) is a solution for all F and $\rho_0 g$. Assuming that α is sufficiently small, we find that the Riccati equation (4.191)₃ for the straight strut has a bounded solution provided β is smaller than a critical value β_{crit} .³⁰

³⁰ An analytic expression, featuring Airy functions, for $w(\xi)$ can be established for Eqn. (4.191)₃ when $\theta^* = -90^\circ$.

A representative sample of w for varying β is shown in Figure 4.26(b). When $\beta \geq \beta_{\text{crit}}$, then Eqn. (4.191)₃ does not have a solution. We conclude with the help of S1 that the straight strut is stable for $\beta < \beta_{\text{crit}}$ and, using B1, that the straight strut is unstable for $\beta \geq \beta_{\text{crit}}$. For $\beta > \beta_{\text{crit}}$, the Euler-Lagrange equation (4.191)₁ admits two nontrivial solutions (or buckled states) which are mirror images of each other. The evolution of these solutions as F is increased beyond its critical value $F_{\text{crit}} = EI\beta_{\text{crit}}/\ell^2$ is shown in Figure 4.26(a). We note that, as F is increased, the strut shows considerable deflection from the vertical. It suffices to examine a single Riccati equation (4.191)₃ to determine the stability of both buckled solutions. Referring to Figure 4.26(b), we find that the Riccati equation (4.191)₃ possess bounded solutions for each one of the pair of buckled states and conclude, with the help of the criterion S1, that the buckled states are stable.

4.9.3 Stability of Peeling

The third class of problems we examine involves a rod which is partially adhered to a rigid surface. Examples of this class of problem were considered in Section 4.5 and, for the reader's convenience, we rapidly recall some of these developments here. The example discussed here is adapted from [219].

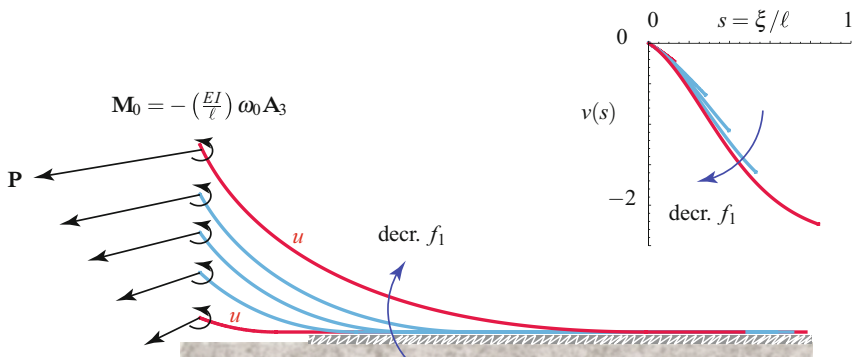


Fig. 4.27 Deformed configurations of the terminally loaded rod for various values of $f_1: -2, -3, -4, -5$, and -5.9 . The corresponding values of Γ (which is defined in Eqn. (4.205)) for these solutions are -1.03053 , 1.37988 , 2.3106 , 1.76842 , and -0.000105 , respectively. The inset image shows the corresponding solutions $v(s)$ for the Riccati equation (4.204). Unlike the other three solutions shown, the solutions displayed for $f_1 = -2$ and $f_1 = -5.9$, which are labeled u , do not satisfy (4.205) and are unstable. The remaining parameters for the solutions shown are $f_2 = -1$, $\omega_0 = -3$, and $w_{\text{ad}} = 6$.

Referring to Figures 4.8 and 4.27, we assume that the rod is terminally loaded at $\xi = 0$ by a force $\mathbf{F}_0 = \mathbf{P} = P_1 \mathbf{A}_1 + P_2 \mathbf{A}_2$ and a terminal moment $\mathbf{M}_0 = M_0 \mathbf{A}_3$. At $\xi = \gamma$, the rod adheres to the flat horizontal surface with the aid of a dry adhesion

mechanism. Paralleling our previous developments it can be shown that the ordinary differential equation governing $\theta(\xi)$ for $\xi \in [0, \gamma]$ is

$$EI \frac{\partial^2 \theta}{\partial \xi^2} - P_2 \cos(\theta) + P_1 \sin(\theta) = 0, \quad (4.193)$$

where

$$\theta(\gamma) = 0, \quad \frac{\partial \theta}{\partial \xi}(0) = -\frac{M_0}{EI}, \quad \frac{\partial \theta}{\partial \xi}(\gamma^-) = \theta'_-. \quad (4.194)$$

As part of the solution process, θ'_- , $\theta(\xi = 0) = \theta_0$, and γ will be determined. At $\xi = \gamma$, the adhesion boundary condition holds:

$$-W_{\text{ad}} = -\frac{EI}{2} \left(\theta'_- \right)^2 + \mathbf{P} \cdot \mathbf{r}'(\gamma^-), \quad (4.195)$$

and owing to the conservation of C on $(0, \gamma)$, we can relate the adhesion energy at $\xi = \gamma$ to the configuration of the rod (cf. Eqn. (4.67)):

$$W_{\text{ad}} = \frac{EI}{2} \left(\frac{\partial \theta}{\partial \xi} \right)^2 - P_2 \sin(\theta) - P_1 \cos(\theta). \quad (4.196)$$

At this stage, it is convenient to reintroduce several dimensionless quantities,

$$x = \frac{\xi}{\ell}, \quad v = \frac{w}{\ell}, \quad \bar{g} = \frac{\gamma}{\ell}, \quad (4.197)$$

and loading parameters,

$$f_1 = \frac{P_1 \ell^2}{EI}, \quad f_2 = \frac{P_2 \ell^2}{EI}, \quad \omega_0 = -\frac{M_0 \ell}{EI}, \quad w_{\text{ad}} = \frac{W_{\text{ad}} \ell^2}{EI}. \quad (4.198)$$

Note that we have dropped the $*$ ornamenting the solutions θ^* and γ^* to the boundary-value problem.

Solving the boundary-value problem is greatly facilitated by noting that γ can be determined using the conservation of C and the adhesion boundary condition. To elaborate, at $x = \bar{g} = \gamma/\ell$ we find that

$$e_0 = -\frac{C \ell^2}{EI} = \left(\frac{\ell^2}{EI} \right) W_{\text{ad}} = w_{\text{ad}}. \quad (4.199)$$

Applying the conservation to the other end of the rod (at $\xi = 0$) permits us to conclude that

$$e_0 = -f_2 \sin(\theta_0) - f_1 \cos(\theta_0) + \frac{\omega_0^2}{2}, \quad (4.200)$$

where $\theta_0 = \theta(\xi = 0)$. Thus,

$$\begin{aligned} w_{\text{ad}} - \frac{\omega_0^2}{2} &= -f_2 \sin(\theta_0) - f_1 \cos(\theta_0), \\ \frac{1}{2} \left(\frac{\partial \theta}{\partial s} \right)^2 &= w_{\text{ad}} + f_2 \sin(\theta) + f_1 \cos(\theta). \end{aligned} \quad (4.201)$$

The first of these equations can be used to determine θ_0 . It can also be used to show a necessary restriction on some of the parameters of the system:

$$1 \geq \frac{w_{\text{ad}} - \frac{\omega_0^2}{2}}{\sqrt{f_1^2 + f_2^2}} \geq -1. \quad (4.202)$$

We observe from this equation that the stronger the dry adhesive, the greater the magnitude of the terminal force needed to ensure an adhered state. Further, for a given terminal force, a terminal moment can be introduced to ensure the necessary condition (4.202) is satisfied.

The second of the conditions (4.201) can be used to solve for γ :

$$\frac{\gamma}{\ell} = \int_{\theta_0}^0 \frac{d\theta}{\sqrt{2(w_{\text{ad}} + f_2 \sin(\theta) + f_1 \cos(\theta))}}. \quad (4.203)$$

Once γ has been determined using the identity (4.203), it is then straightforward to solve the initial-value problem consisting of the ordinary differential equation (4.193) subject to the boundary conditions $\theta(0) = \theta_0$ and $\theta'(0) = -M_0/EI$ in order to determine $\theta(\xi) = \theta^*(\xi)$. With the assistance of Eqn. (4.203), we take this opportunity to note the expected result that, for a given loading f_1 and f_2 , the adhered length of the rod ($\ell - \gamma$) increases with increasing w_{ad} .

The solution $\{\theta^*(\xi), \gamma^*\}$ to the boundary-value problem is then interrogated using Criterion N1 to determine stability. We recall from Section 4.8.3:

CRITERION N1: If a solution $\{\theta^*(\xi), \gamma^*\}$ to the boundary-value problem (4.193) minimizes Π then the solution $v(x) \forall x \in [0, \gamma^*/\ell]$ to the Riccati equation

$$\frac{\partial v}{\partial x} - f_1 \cos(\theta^*) - f_2 \sin(\theta^*) - v^2 = 0, \quad v(0) = 0, \quad (4.204)$$

cannot become unbounded in the interval $[0, \gamma^*/\ell]$ and the following inequality must be satisfied at the point $x = \bar{g} = \gamma^*/\ell$:

$$\begin{aligned} \Gamma &= (f_2 \cos(\theta^*(\gamma^{*-})) - f_1 \sin(\theta^*(\gamma^{*-}))) \frac{\partial \theta^*}{\partial s}(\gamma^{*-}) \\ &\quad - \left(\frac{\partial \theta^*}{\partial s}(\gamma^{*-}) \right)^2 v(\gamma^{*-}) \geq 0. \end{aligned} \quad (4.205)$$

As discussed in [219, 220], the presence of the bounded solution to the Riccati equation indicates stability of the rod. This existence result is identical to the more familiar use of an equivalent Jacobi equation in studies on buckling that can be found in the literature. The condition (4.205) is intimately related to the work of the adhesion W_{ad} at $\xi = \gamma$.

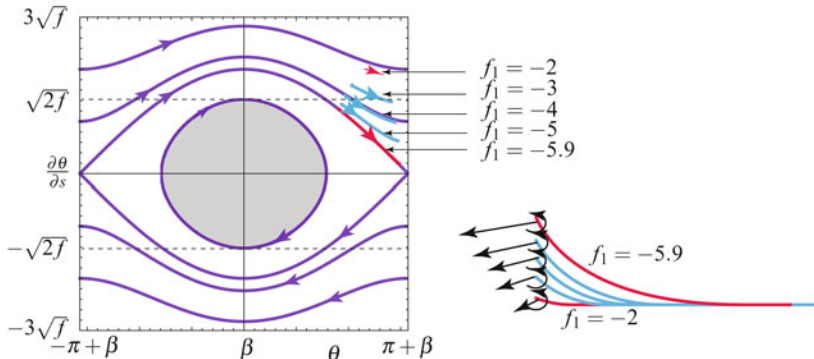


Fig. 4.28 Phase portrait of the ordinary differential equation (4.207). The shaded region containing the point $(\theta, \frac{\partial \theta}{\partial s}) = (\beta, 0)$ is bounded by the level-set corresponding to $w_{\text{ad}} = 0$ and does not contain solutions to the adhesion boundary-value problem. The trajectories labeled with values of f_1 correspond to the solutions shown in the inset image in this figure and in (additional detail in) Figure 4.27.

While the solution space of $EI\theta'' + P_1 \sin(\theta) - P_2 \cos(\theta) = 0$ has a wealth of solutions, most of them are not applicable to the adhesion problem of interest. To elaborate further on this, we define the angle β subtended by \mathbf{P} with the horizontal:

$$f = \sqrt{f_1^2 + f_2^2}, \quad \cos(\beta) = \frac{f_1}{f}, \quad \sin(\beta) = \frac{f_2}{f}. \quad (4.206)$$

The solutions $\theta(s)$ of interest are those that satisfy

$$\frac{\partial^2}{\partial s^2}(\theta - \beta) + f \sin(\theta - \beta) = 0 \quad (4.207)$$

with

$$\frac{1}{2} \left(\frac{\partial}{\partial s}(\theta - \beta) \right)^2 - f \cos(\theta - \beta) = w_{\text{ad}} > 0. \quad (4.208)$$

Thus the set of admissible solutions excludes the region in state space from the fixed point at $\theta = \beta$ (where $w_{\text{ad}} = f$) to the level set of $\theta - \frac{\partial \theta}{\partial s}$ where $w_{\text{ad}} = 0$ (see Figure 4.28).

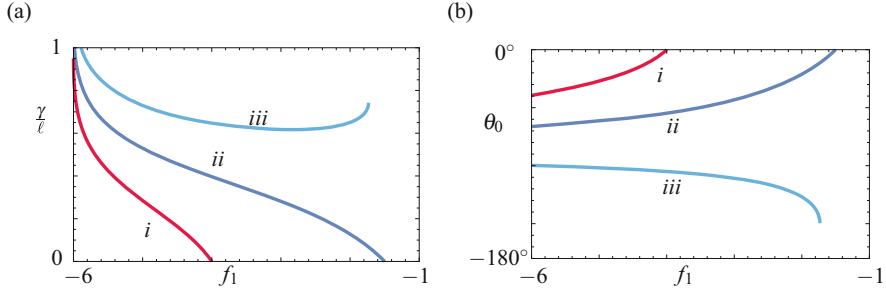


Fig. 4.29 The dimensionless length γ/ℓ and angle θ_0 computed using (4.203) and (4.201)₁, respectively, as a function of the dimensionless shear force $f_1 = \left(\frac{\ell^2}{EI}\right) \mathbf{P} \cdot \mathbf{A}_1$ for three values of ω_0 : *i*, $\omega_0 = -2.0$; *ii*, $\omega_0 = -3.0$; and *iii*, $\omega_0 = -4.0$. The remaining parameters for the solution shown are $f_2 = -1$ and $w_{ad} = 6$.

4.9.3.1 An Example

We now consider a numerical example to illustrate the previous developments. After a parameter search, we select a rod with a preload in the normal direction and an applied moment on the end:

$$f_2 = -1, \quad w_{ad} = 6, \quad \omega_0 = -3. \quad (4.209)$$

We now vary the (dimensionless) shear force f_2 . Arbitrary values of f_2 are not possible, and our first check is to examine the existence of a physically realistic γ using Eqn. (4.203). Some of the numerical results are shown in Figure 4.29(a). We see from this figure that $-1.5 > f_2 > \approx -5.986$ in order for γ to be realizable. That is, $\gamma \in (0, \ell)$. We also observe that changing ω_0 changes the adhered length of the rod, and, from Figure 4.29(b), how the angle of inclination θ_0 at the free end also changes.

For each of the solutions computed, we next calculate Γ using Eqn. (4.205). After checking the sign of Γ , we then appeal to Criterion N1 to ascertain instability. As summarized in Figure 4.27, the configurations with $f_1 = -2$ and $f_1 = -5.9$ are unstable. Because a bounded solution to the appropriate Riccati equation (4.204) exists for all the configurations shown, this instability can be attributed entirely to adhesion.

4.10 Additional Areas of Application of the Elastica

Euler's elastica, being the simplest nonlinear rod theory, has been applied to a wealth of problems and space precludes us from giving full justice to all these works. Among many others, the areas of application include flexible risers in ocean

environments [312, 313], folding of thin sheets [216], soft robot gripping and locomotion mechanisms [372, 373], the buckling of rods in constrained environments [91] and in carbon nanotube bundles [374], and the growth and dynamics of plant stems. The application of the elastica to plant growth has several interesting aspects including an intermediate growth configuration, branching and tree-like structures, a time-evolving intrinsic curvature and constitutive relations that change with time. This area of application was championed by the works by Silk and her coworkers [322–324] and further promoted by Goldstein and Goriely’s work [118] on evolving constitutive relations. We refer the reader to [109, 121, 122, 145, 269, 273, 274, 368] for additional references and perspectives on this interesting area of application and close this chapter with the hope that we have given the reader the relevant background to comprehend, critique, and appreciate the aforementioned works.

4.11 Exercises

Exercise 4.1: Suppose a rod (of length ℓ) is subject to terminal forces $\mathbf{F}_0 = R\mathbf{A}_1$ and $\mathbf{F}_\ell = -R\mathbf{A}_1$. Show that \mathbf{n} is constant and that Eqn. (4.26) reduces to an ordinary differential equation for θ :

$$EI \frac{\partial^2 \theta}{\partial \xi^2} + R \sin(\theta) = 0. \quad (4.210)$$

What are the boundary conditions for $\theta'(\xi = 0^+)$ and $\theta'(\xi = \ell^-)$? Show that Eqn. (4.210) is equivalent to the equation of motion of a simple pendulum in a gravitational field. By non-dimensionalizing this equation, numerically determine its solutions for three values (say -5 , 0 , and 5) of the parameter

$$\beta = \frac{R\ell^2}{EI}. \quad (4.211)$$

It is a good idea to plot the solutions on the plane $\theta - \frac{\partial \theta}{\partial u}$ where $u = \frac{\xi}{\ell}$. You should also verify that your solutions conserve the energy

$$e(u) = \frac{1}{2} \left(\frac{\partial \theta}{\partial u} \right)^2 - \beta \cos(\theta). \quad (4.212)$$

Exercise 4.2: Determine the shape $\mathbf{r}(\xi)$ of the elastica corresponding to the trajectories you found in Exercise 4.1. For your solutions, it is convenient to choose $\mathbf{r}(\xi = 0) = \mathbf{0}$.

- (a) Determine the terminal moments \mathbf{M}_0 and \mathbf{M}_ℓ needed to support these solutions.
- (b) For the case $\beta = 0$, give an interpretation for the presence of an infinite number of equilibria of (4.210). In addition, show that the space curve formed by $\mathbf{r}(\xi)$ is either a straight line or the arc of a circle.

- (c) Discuss the distinction between the cases $\beta > 0$ and $\beta < 0$.
- (d) For the case $\beta > 0$, compare your results to Hess's which date to 1885 and can be found in Love's book [213, Page 404]. You should comment on the "apparent" change in the boundary conditions between Figures 51–53 and 54 of [213]. In addition, discuss why terminal moments are needed to capture all the solutions shown on [213, Page 404].

Exercise 4.3: Consider an elastica of length ℓ which is horizontal and subject to terminal forces:

$$\begin{aligned}\mathbf{n}(\xi = 0^+) &= -R\mathbf{A}_1, & \mathbf{M}(\xi = 0^+) &= \mathbf{0}, \\ \mathbf{n}(\xi = \ell^-) &= -R\mathbf{A}_1, & \mathbf{M}(\xi = \ell^-) &= \mathbf{0}.\end{aligned}\quad (4.213)$$

Show that if $R = R_{cn}$ for some integer n where

$$R_{cn} = \left(\frac{n\pi}{\ell}\right)^2 EI, \quad (4.214)$$

then, in addition to the trivial solution $\theta = 0$, another solution is possible. The existence of this other solution is known as a *buckling instability* and R_{cn} is known as a buckling load. Give an interpretation of the buckling phenomenon using the phase portrait similar to that shown in Figure 4.10. You should also notice that by fixing R , buckling can also be achieved by varying the length ℓ .³¹

Exercise 4.4: For the case where $\beta > 0$ and assuming that θ is small, show that Eqn. (4.210) reduces to the equation for a Bernoulli-Euler beam subject to a terminal loading³²:

$$EI \frac{d^4y}{dx^4} + R \frac{d^2y}{dx^2} = 0. \quad (4.215)$$

What is the analytical solution to this equation and how many boundary conditions are needed to uniquely prescribe a solution?

Exercise 4.5: Using the non-dimensionalizations (4.66), verify that Eqn. (4.60)₂ can be written in the form

$$\frac{d^2\theta}{dx^2} - f_2 \cos(\theta) + f_1 \sin(\theta) = 0. \quad (4.216)$$

Using a change of variables, show that this equation can be simplified to

$$\frac{d^2\Theta}{dx^2} - \sqrt{f_2^2 + f_1^2} \cos(\Theta) = 0, \quad (4.217)$$

³¹ Additional perspectives on buckling can be found in Section 5.17 of Chapter 5. We also refer the reader to the seminal text by Timoshenko and Gere [345, Chapter 2].

³² The interested reader is referred to the works of Eshelby [102, Page 142] and Kienzler and Herrmann [182, 183] for discussions on material forces in the context of Bernoulli-Euler beam theory.

where

$$\Theta = \theta + \beta, \quad \cos(\beta) = \frac{f_2}{\sqrt{f_1^2 + f_2^2}}, \quad \sin(\beta) = \frac{f_1}{\sqrt{f_1^2 + f_2^2}}. \quad (4.218)$$

Argue that Eqn. (4.217) can also be obtained by suitably rotating the basis vectors \mathbf{A}_1 and \mathbf{A}_2 about \mathbf{A}_3 . Establish a first integral of Eqn. (4.217).

Exercise 4.6: Consider the adhesion problem discussed in Section 4.5.3.1. Using Eqn. (4.75), establish an expression for θ as a function of $\frac{\xi}{\ell} \sqrt{-f_2}$. With the help of these expressions and Eqn. (4.79), determine $\mathbf{r}(\xi)$ using either numerical or analytical techniques.

Exercise 4.7: Consider the adhesion problem discussed in Section 4.5.3.2. Using elliptic functions, establish an expression for θ as a function of $\frac{\xi}{\ell} \sqrt{-f_2}$. With the help of these expressions and Eqn. (4.85), determine $\mathbf{r}(\xi)$ using either numerical or analytical techniques.

Exercise 4.8: Suppose a variant of the adhesion problems discussed in Sections 4.5.3.1 and 4.5.3.2 is considered where $f_1 \neq 0$. Show that by using the results of Exercise 4.5 it is possible to solve the adhesion problem with a small amount of modifications to the analyses presented in these subsections.

Exercise 4.9: Consider the Johnson-Kendall-Robert's (JKR) theory of adhesion [175] applied to the adhesion problems discussed in Section 4.5.3. In this theory, one solves the problem by seeking minimizers (γ and $\theta(\xi)$) of the potential energy functional

$$\Pi = \int_{\xi=0}^{\xi=\gamma} \left(\mathbf{P} \cdot \mathbf{r}' + \frac{EI}{2} \left(\frac{d\theta}{d\xi} \right)^2 \right) d\xi + \int_{\xi=\gamma}^{\xi=\ell} \left(\frac{EI}{2} \left(\frac{d\theta}{d\xi} \right)^2 - W_{ad} \right) d\xi, \quad (4.219)$$

subject to the condition that $\theta(\xi) = 0$ for $\xi \in [\gamma, \ell]$. Show that the Euler-Lagrange necessary condition for an extremizer yields the differential equation (4.60)₂, and the Weierstrass corner condition (9.25) yields the boundary condition (4.64).³³ From these results, you should be able to conclude that the solution γ found earlier is such that the potential energy of the system is extremized.

³³ As can be seen from Section 9.3.2, the variations used to establish the corner condition (9.25) correspond to varying γ . For further details on calculus of variations problems of this type see [30, Section 10].

Chapter 5

Kirchhoff's Rod Theory

“A new idea, supple in application to a variety of mechanical theories and formalisms, was proposed by DUHEM [1893, 1, Ch. II]: A body is to be regarded as a collection not only of points but also of *directions associated with the points*: These vectors, which we shall call the *directors* of the body, are susceptible of rotations and stretches *independent* of the deformation of material elements.”

J. L. Ericksen and C. A. Truesdell [100, Page. 297] commenting on Pierre Duhem’s (1861–1916) contribution in [94] to the historical development of theories for rods and shells.

5.1 Introduction

The modeling capabilities of inextensible and elastic strings are limited to situations where complete flexibility is assumed. To develop a model capable of resisting bending and torsion, one needs to put additional structure on the theory of a string. The added ingredients we use are a deformable set of vectors which are associated with each point of the material curve. These vectors are known as directors.¹ In the simplest such rod theory, which we present in this chapter, the two directors, \mathbf{d}_1 and \mathbf{d}_2 , deform rigidly and their projections onto the tangent vector \mathbf{e}_t to the material curve remain constant: $(\mathbf{d}_1 \times \mathbf{d}_2) \cdot \mathbf{e}_t = \text{constant}$. We assume that $\{\mathbf{d}_1, \mathbf{d}_2, \mathbf{e}_t\}$ can be considered as an orthonormal triad which varies with the point of the material curve to which it is associated. It may also be helpful to visualize the vectors \mathbf{d}_1 and \mathbf{d}_2 remaining parallel to material fibers in the cross section as the rod is deformed.

¹ The terminology “director” was introduced in a seminal paper [100] by Ericksen and Truesdell in 1958. For further discussion on the historical developments following the publication of this paper, see [12, 243, 245].

In a seminal work [185] published in 1859, Gustav Kirchhoff (1824–1887) proposed a rod theory capable of modeling bending and torsion. The theory is discussed at length in Love's influential treatise [213]. Although Kirchhoff's treatment differs from the modern one we discuss here, the rod theory we present is known as Kirchhoff's rod theory in recognition of his contribution. In the early years of the 20th century, the Cosserat brothers, Eugène (1866–1931) and François (1852–1914), influenced by Duhem [94], formulated Kirchhoff's rod theory using what are now known as directors in [71, 72]. Consequently, the rod theory is also considered as an example of a Cosserat rod theory. Kirchhoff's rod theory is arguably the most popular three-dimensional rod theory in use and has been the subject of a large number of works since the mid-1950s. It has been applied to a wide range of problems including configurations of DNA minicircles (see, e.g., [317, 319, 320]), tendril persion and vine attachment in plants (see, e.g., [122, 235]), torsional buckling (see, e.g., [164]), and chaotic vibrations of an elastic rod (see, e.g., [78, 79]), among many others. Works on these applications have also been supplemented by an ever increasing body of work, such as [221, 222, 224, 226], examining the linear and nonlinear stability of the equilibrium configurations of the rod and works in computer graphics where this rod theory is used to model strands of hair (see [22, 281, 355] and references therein).

Our exposition of the theory benefits greatly from the aforementioned research and, in particular, the works of Antman [10, 12], Green and Laws [130], and Naghdi and Rubin [246]. In the first part of this chapter, we examine how the introduction of the directors captures the torsional and bending strains. We then explore the types of discontinuities that this rod theory can reproduce. Following our developments with the string, the balance laws are first postulated and then the local forms and jump conditions are derived. Our treatment of this matter parallels the developments for strings and consequently many of the arguments are presented with minimal detail.

Once the balance laws and jump conditions are established, the process of prescribing constitutive relations and examining which of these conditions are non-trivial begins. You will find that the theory promptly reduces to a tractable set of equations which are highly amenable to applications and simplifications. For example, we readily find Euler's theory of the elastica as a special case of the rod theory. In addition, for static configurations of a Kirchhoff rod, the governing ordinary differential equations can often be placed in one-to-one correspondence with the equations governing the attitude of a rigid body.

The chapter concludes with a range of applications of the theory to studying the deformed shape of rods subject to terminal loads. While we cover a spectrum of works on some classic problems, we need to limit our scope to a small fraction of the work that has used Kirchhoff's rod theory. Our hope is that we will have provided the necessary background and a sufficient number of applications for the reader to be able to continue their own exploration and enjoyment of the vast literature discussing applications of this popular rod theory.

5.2 The Directed Curve

Thus far, we have introduced two different types of curves: space curves and material curves. A directed curve is a material curve \mathcal{L} to which at each point a set of directors are defined. The directors represent kinematical quantities pertaining to the cross sections of a rod-like body. Hence, the directed curve serves as a model for a rod-like body. Following the seminal work of the Cosserat brothers in the early 1900s, a directed curve is often known as a Cosserat curve.

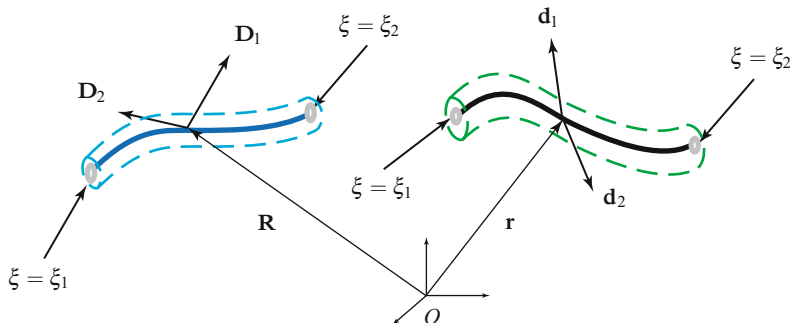


Fig. 5.1 The curve $\mathbf{r}(\xi, t)$ and the vector fields $\mathbf{d}_\alpha(\xi, t)$ at a point along its length. The reference configuration \mathcal{R}_0 of the Cosserat (or directed) curve is also shown in this figure.

Referring to Figure 5.1, in its present configuration \mathcal{R} , the directed curve is defined by the vector-valued functions $\mathbf{r} = \mathbf{r}(\xi, t)$ and $\mathbf{d}_\alpha = \mathbf{d}_\alpha(\xi, t)$ where $\alpha = 1, 2$. Here, ξ is a convected coordinate along the material curve and \mathbf{r} is the position vector of a material point of the curve with respect to a fixed origin. As mentioned previously, the vectors \mathbf{d}_1 and \mathbf{d}_2 are known as directors.

A reference configuration \mathcal{R}_0 of the directed curve is defined by the vector fields $\mathbf{R} = \mathbf{R}(\xi)$ and $\mathbf{D}_\alpha = \mathbf{D}_\alpha(\xi)$. For convenience, we shall assume that ξ is the arc-length parameter of the reference configuration of the material curve. It should be clear that we are assuming that the reference configuration is fixed.

In many treatments, it is common to denote $\frac{\partial \mathbf{r}}{\partial \xi}$ by \mathbf{d}_3 . This is especially the case with the papers of Green, Naghdi, and Rubin [245, 309]. Similarly, $\frac{\partial \mathbf{R}}{\partial \xi}$ is denoted by \mathbf{D}_3 . Alternatively, following Antman [12], one defines $\mathbf{d}_3 = \mathbf{d}_1 \times \mathbf{d}_2$ and $\mathbf{D}_3 = \mathbf{D}_1 \times \mathbf{D}_2$. For the rod theory presented in this chapter, it is convenient to use Antman's definition.

5.2.1 An Approximation

Our conception of a rod is primarily as an approximation to a three-dimensional body. In this context, the need to relate quantities associated with the three-dimensional body to the corresponding quantities associated with the rod is crucial

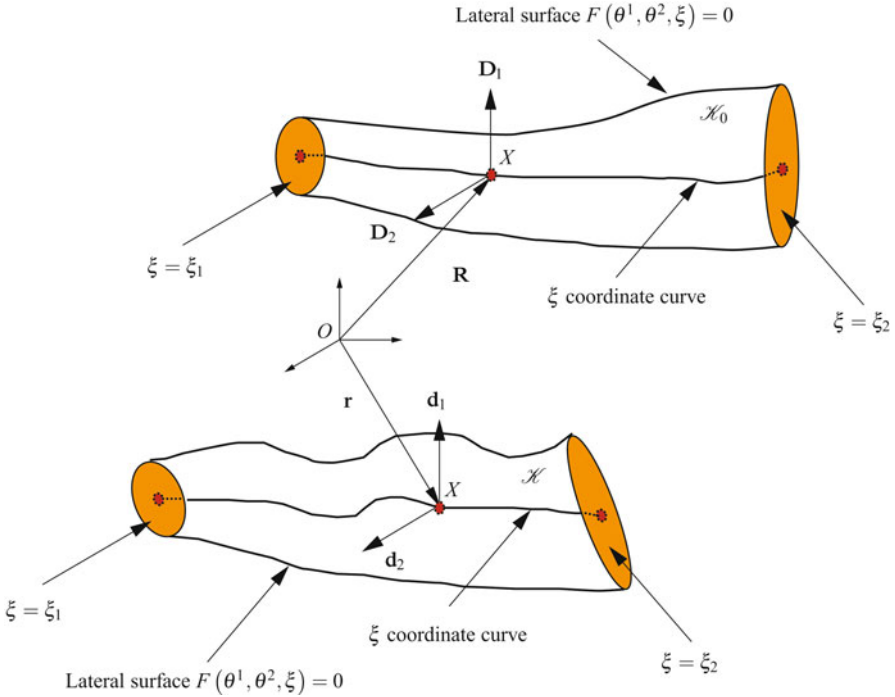


Fig. 5.2 Schematic of the reference \mathcal{K}_0 and present \mathcal{K} configurations of a three-dimensional rod-like body whose reference configuration is parameterized using a curvilinear coordinate system. The ends of the body are described by $\theta^3 = \xi$ coordinate surfaces, the centerline is described by a ξ coordinate curve where $\theta^1 = \theta^2 = 0$, and the lateral surface of the body is described using the function $F(\theta^1, \theta^2, \xi)$.

in applications. Fortunately, there has been a wealth of work performed on the correspondences between fields associated with the rod theory and those associated with the three-dimensional body that it is modeling. Of particular relevance is the work of Green, Naghdi, and their coworkers [131, 137], which we will now employ.

Consider a three-dimensional rod-like body \mathcal{B} and assign to it a set of curvilinear coordinates θ^i . If we were to model this body using a directed curve, then the following identifications would be made:

$$\xi = \theta^3, \quad \mathbf{R}^* = \mathbf{R}(\xi) + \sum_{\alpha=1}^2 \theta^\alpha \mathbf{D}_\alpha(\xi). \quad (5.1)$$

Here, \mathbf{R}^* is the position vector of the material point identified using θ^i (see Figure 5.2). In the present configuration, these choices imply the following approximation:

$$\mathbf{r}^* = \mathbf{r}^*(\theta^i, t) \approx \mathbf{r}(\xi, t) + \sum_{\alpha=1}^2 \theta^\alpha \mathbf{d}_\alpha(\xi, t). \quad (5.2)$$

This result will be very useful in prescribing kinematical quantities in the sequel.

5.3 Kinematics of Kirchhoff's Rod Theory

For Kirchhoff's rod theory, the material curve \mathcal{L} is assumed to be inextensible: $\frac{\partial \mathbf{r}}{\partial \xi} = \mathbf{e}_t$. Further the cross sections are assumed to remain plane, and the projection of the normal vector to the cross section onto \mathbf{e}_t remains constant. Torsion is accommodated by a rotation of the directors about \mathbf{e}_t . To render these statements into a mathematically tractable form, we assume that \mathbf{D}_1 , \mathbf{D}_2 , and \mathbf{D}_3 define a right-handed orthonormal triad at each ξ :

$$[\mathbf{D}_1, \mathbf{D}_2, \mathbf{D}_3] = 1. \quad (5.3)$$

If we denote a fixed right-handed basis for \mathbb{E}^3 by $\{\mathbf{E}_1, \mathbf{E}_2, \mathbf{E}_3\}$, then we can define a rotation tensor \mathbf{P}_0 :

$$\mathbf{P}_0 = \mathbf{D}_1 \otimes \mathbf{E}_1 + \mathbf{D}_2 \otimes \mathbf{E}_2 + \mathbf{D}_3 \otimes \mathbf{E}_3. \quad (5.4)$$

That is, $\mathbf{D}_i = \mathbf{P}_0 \mathbf{E}_i$. For many reference configurations, we can choose \mathbf{D}_i such that $\mathbf{P}_0 = \mathbf{I}$; some exceptions are for what Love [213] refers to as initially curved rods.

Under a motion of the directed curve, the vectors \mathbf{d}_i retain their relative orientation and magnitude. Consequently,

$$\mathbf{d}_i = \mathbf{P} \mathbf{D}_i, \quad (i = 1, 2, 3), \quad (5.5)$$

where \mathbf{P} is a rotation tensor.² You should notice that

$$\mathbf{d}_\alpha = \mathbf{P} \mathbf{P}_0 \mathbf{E}_\alpha, \quad \frac{\partial \mathbf{r}}{\partial \xi} = \mathbf{P} \frac{\partial \mathbf{R}}{\partial \xi}, \quad (\alpha = 1, 2). \quad (5.6)$$

These two equations define the constraints on the rod. They are often known as "Kirchhoff's constraints."

The constraints (5.6) imply that

$$\mathbf{d}'_\alpha = (\mathbf{P}(\mathbf{v} + \mathbf{v}_0)) \times \mathbf{d}_\alpha. \quad (5.7)$$

Here, the prime denotes the partial derivative with respect to ξ , and \mathbf{v} and \mathbf{v}_0 are axial vectors of skew-symmetric tensors³:

$$\mathbf{v} = \text{ax}(\mathbf{K}), \quad \mathbf{K} = \mathbf{P}^T \mathbf{P}', \quad \mathbf{v}_0 = \text{ax}(\mathbf{K}_0), \quad \mathbf{K}_0 = \mathbf{P}'_0 \mathbf{P}_0^T. \quad (5.8)$$

² Recall that an orthogonal tensor \mathbf{Q} has the property that $\mathbf{Q}\mathbf{Q}^T = \mathbf{I}$ and so $\det(\mathbf{Q}) = \pm 1$. A proper-orthogonal tensor \mathbf{Q} has a determinant of 1. From Euler's theorem in rigid body dynamics, proper-orthogonal tensors and rotation tensors are synonymous.

³ Recall that the axial vector \mathbf{b} of any skew-symmetric tensor $\mathbf{B} = -\mathbf{B}^T$ has the property that $\mathbf{b} \times \mathbf{c} = \mathbf{B}\mathbf{c}$ for any vector \mathbf{c} . As a skew-symmetric tensor has three independent components, there is a one-to-one correspondence between \mathbf{B} and its axial vector \mathbf{b} (cf. Eqns. (1.17) and (1.18)).

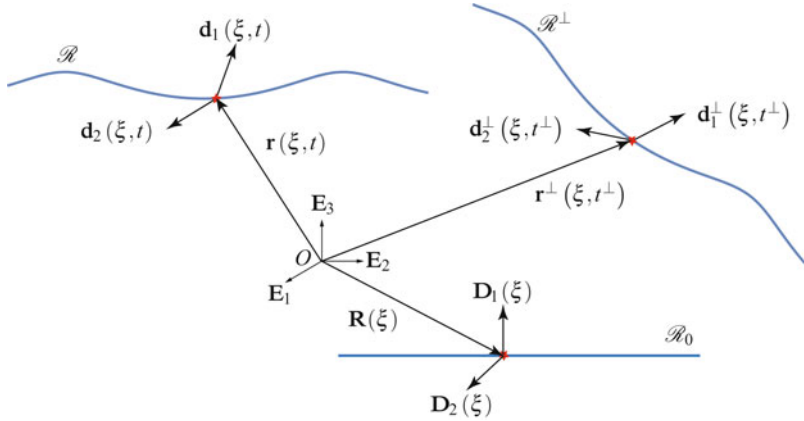


Fig. 5.3 An example of two motions of a directed curve which differ by a rigid body motion. Observe that both motions are relative to the same reference configuration \mathcal{R}_0 .

The axial vector \mathbf{v} will play a key role in the sequel. We note that the identity

$$\text{ax}(\mathbf{QBQ}^T) = \det(\mathbf{Q}) \mathbf{Q} \text{ax}(\mathbf{B}), \quad (5.9)$$

which holds for all orthogonal tensors \mathbf{Q} and all skew-symmetric tensors \mathbf{B} , was used to establish (5.7) from (5.6).

Referring to Figure 5.3, we now consider two motions of a directed curve which differ by a rigid body motion:

$$\begin{aligned} \mathbf{r}^\perp(\xi, t^\perp) &= \mathbf{Q}(t) \mathbf{r}(\xi, t) + \mathbf{q}(t), \\ \mathbf{d}_1^\perp(\xi, t^\perp) &= \mathbf{Q}(t) \mathbf{d}_1(\xi, t), \quad \mathbf{d}_2^\perp(\xi, t^\perp) = \mathbf{Q}(t) \mathbf{d}_2(\xi, t). \end{aligned} \quad (5.10)$$

As with the previous developments in the theory of a string, \mathbf{Q} is a proper-orthogonal tensor-valued function of time, $\mathbf{q}(t)$ is a vector-valued function of time, and $t^\perp = t + a$ with a being constant. It follows that

$$\mathbf{P}^\perp(\xi, t^\perp) = \mathbf{Q}(t) \mathbf{P}(\xi, t). \quad (5.11)$$

An easy calculation shows that the tensor \mathbf{K} and its associated axial vector \mathbf{v} are identical at the same material point of the present configurations \mathcal{R} and \mathcal{R}^\perp :

$$\mathbf{K}^\perp(\xi, t^\perp) = \mathbf{K}(\xi, t), \quad \mathbf{v}^\perp(\xi, t^\perp) = \mathbf{v}(\xi, t). \quad (5.12)$$

Consequently, \mathbf{v} is used in the sequel as a strain measure. We invite the reader to examine how our remarks pertain to the strain measures $\frac{\partial \theta}{\partial \xi}$ and μ for the extensible elastica.

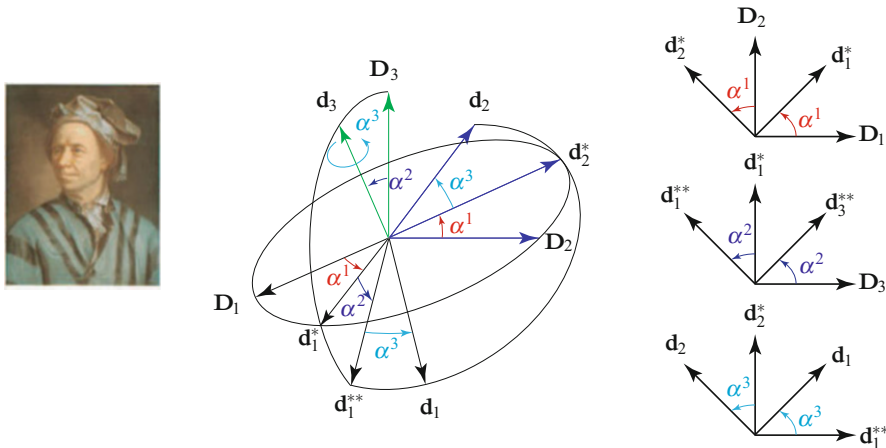


Fig. 5.4 Schematic of a set of 3-2-3 Euler angles that are used to parameterize a rotation from the basis $\{\mathbf{D}_1, \mathbf{D}_2, \mathbf{D}_3\}$ to the basis $\{\mathbf{d}_1, \mathbf{d}_2, \mathbf{d}_3\}$. The three axes of rotation are $\mathbf{e}_1 = \mathbf{D}_3 = \mathbf{d}_3^*$, $\mathbf{e}_2 = \mathbf{d}_2^{**} = \mathbf{d}_2^*$, and $\mathbf{e}_3 = \mathbf{d}_3^{**} = \mathbf{d}_3$ and the inset image is a Handmann's portrait of Leonhard Euler (1707–1783) from 1753. For details on the intermediate bases used to construct the figure, see Eqn. (5.17).

5.3.1 Parameterizations of the Rotation Tensor

To parameterize the rotation tensor \mathbf{P} we follow classic treatments and use a set of Euler angles. Specifically, we incorporate Love's exposition in [213] and, from the 12 possible choices of Euler angles, use a set of 3-2-3 Euler angles to parameterize \mathbf{P} .⁴ We also supplement Love's exposition with a more modern treatment of the Euler angles from the textbook [265]. Complementing our discussion of the 3-2-3 set of Euler angles, the corresponding developments for a set of 3-2-1 Euler angles are presented in Exercise 5.6 at the end of this chapter.⁵ This set of Euler angles is more suited to examining linearized versions of the rod theory presented in this chapter. We also take this opportunity to note that Euler angles are not the sole parameterization for \mathbf{P} in Kirchhoff's rod theory in the literature. Recently, Maddocks and his coworkers [86, 178] have ingeniously used quaternions (also known as the Euler-Rodrigues parameters) to parameterize \mathbf{P} while Simo and Vu-Quoc [327] have used the exponential map. For a discussion of these parameterizations and several others, the interested reader is referred to Shuster's authoritative review [321] on rotations.

⁴ The 3-2-3 set of Euler angles is also used in several texts, for example, Ginsberg [115, Section 4.2], Kelvin and Tait [180], Routh [305, 306], and Whittaker [362].

⁵ The 3-2-1 set of Euler angles are sometimes known as the Tait-Bryan angles and are prominent in aircraft and vehicle dynamics. The first instance of their development and use dates to the seminal work of Fick and Helmholtz [166, 167] on the kinematics of the eye (see [156, 253] and references therein) in the mid-1800s and Tait's work [336] on rigid body dynamics in 1868.

In the 3-2-3 set of Euler angles, the tensor \mathbf{P} is decomposed into the product of three simple rotations:

$$\mathbf{P} = \mathbf{Q}_E(\alpha^3, \mathbf{e}_3) \mathbf{Q}_E(\alpha^2, \mathbf{e}_2) \mathbf{Q}_E(\alpha^1, \mathbf{e}_1), \quad (5.13)$$

where the function $\mathbf{Q}_E(\theta, \mathbf{i})$ describes a rotation about an axis described by a unit vector \mathbf{i} through a counterclockwise angle θ ⁶:

$$\mathbf{Q}_E(\theta, \mathbf{i}) = \cos(\theta)(\mathbf{I} - \mathbf{i} \otimes \mathbf{i}) + \sin(\theta)\text{skew}(\mathbf{i}) + \mathbf{i} \otimes \mathbf{i}. \quad (5.14)$$

The basis $\{\mathbf{e}_1, \mathbf{e}_2, \mathbf{e}_3\}$ is known as the Euler basis. This basis is not orthogonal, and, for the 3-2-3 set of interest here,

$$\begin{aligned} \mathbf{e}_1 &= \mathbf{D}_3 \\ &= \cos(\alpha^2) \mathbf{d}_3 - \sin(\alpha^2) (\cos(\alpha^3) \mathbf{d}_1 - \sin(\alpha^3) \mathbf{d}_2), \\ \mathbf{e}_2 &= \cos(\alpha^1) \mathbf{D}_2 - \sin(\alpha^1) \mathbf{D}_1 \\ &= \cos(\alpha^3) \mathbf{d}_2 + \sin(\alpha^3) \mathbf{d}_1, \\ \mathbf{e}_3 &= \cos(\alpha^2) \mathbf{D}_3 + \sin(\alpha^2) (\cos(\alpha^1) \mathbf{D}_1 + \sin(\alpha^1) \mathbf{D}_2) \\ &= \mathbf{d}_3. \end{aligned} \quad (5.15)$$

The angles α^1 and α^3 range from 0 to 2π . Because

$$[\mathbf{e}_1, \mathbf{e}_2, \mathbf{e}_3] = -\sin(\alpha^2), \quad (5.16)$$

in order to ensure that the Euler basis is a basis for \mathbb{E}^3 , we restrict the second angle $\alpha^2 \in (0, \pi)$. Other perspectives on the singularity when $\alpha^2 = 0, \pi$ might be helpful. First, we note that α^1 and α^2 are polar coordinates for the axis of rotation $\mathbf{e}_3 = \mathbf{d}_3$. Thus, the singularity arises when, for a single value of α^2 , multiple values of α^1 are possible. We shall examine two other perspectives shortly.

Referring to Figure 5.4, it is straightforward to transform from \mathbf{d}_i to \mathbf{D}_i and vice versa with the help of two pairs of intermediate bases $\{\mathbf{d}_1^*, \mathbf{d}_2^*, \mathbf{d}_3^*\}$ and $\{\mathbf{d}_1^{**}, \mathbf{d}_2^{**}, \mathbf{d}_3^{**}\}$:

$$\begin{aligned} \begin{bmatrix} \mathbf{d}_1^* \\ \mathbf{d}_2^* \\ \mathbf{d}_3^* \end{bmatrix} &= \begin{bmatrix} \cos(\alpha^1) & \sin(\alpha^1) & 0 \\ -\sin(\alpha^1) & \cos(\alpha^1) & 0 \\ 0 & 0 & 1 \end{bmatrix} \begin{bmatrix} \mathbf{D}_1 \\ \mathbf{D}_2 \\ \mathbf{D}_3 \end{bmatrix}, \\ \begin{bmatrix} \mathbf{d}_1^{**} \\ \mathbf{d}_2^{**} \\ \mathbf{d}_3^{**} \end{bmatrix} &= \begin{bmatrix} \cos(\alpha^2) & 0 & -\sin(\alpha^2) \\ 0 & 1 & 0 \\ \sin(\alpha^2) & 0 & \cos(\alpha^2) \end{bmatrix} \begin{bmatrix} \mathbf{d}_1^* \\ \mathbf{d}_2^* \\ \mathbf{d}_3^* \end{bmatrix}, \\ \begin{bmatrix} \mathbf{d}_1 \\ \mathbf{d}_2 \\ \mathbf{d}_3 \end{bmatrix} &= \begin{bmatrix} \cos(\alpha^3) & \sin(\alpha^3) & 0 \\ -\sin(\alpha^3) & \cos(\alpha^3) & 0 \\ 0 & 0 & 1 \end{bmatrix} \begin{bmatrix} \mathbf{d}_1^{**} \\ \mathbf{d}_2^{**} \\ \mathbf{d}_3^{**} \end{bmatrix}. \end{aligned} \quad (5.17)$$

⁶ The operator $\text{skew}(\mathbf{i})$ transforms \mathbf{i} into a skew-symmetric tensor such that $\mathbf{i} \times \mathbf{b} = \text{skew}(\mathbf{i})\mathbf{b}$ for any vector \mathbf{b} (cf. Eqn. (1.19)).

After recalling that \mathbf{P} has several representations, including

$$\mathbf{P} = \sum_{i=1}^3 \mathbf{d}_i \otimes \mathbf{D}_i = \sum_{i=1}^3 \sum_{k=1}^3 P_{ik} \mathbf{D}_i \otimes \mathbf{D}_k = \sum_{i=1}^3 \sum_{k=1}^3 P_{ik} \mathbf{d}_i \otimes \mathbf{d}_k, \quad (5.18)$$

we note that the three matrices in Eqn. (5.17) can be combined to provide expressions for the components $P_{ik} = (\mathbf{P} \mathbf{D}_k) \cdot \mathbf{D}_i$ of \mathbf{P} :

$$\begin{bmatrix} P_{11} & P_{12} & P_{13} \\ P_{21} & P_{22} & P_{23} \\ P_{31} & P_{32} & P_{33} \end{bmatrix} = \begin{bmatrix} c_1 c_2 c_3 - s_1 s_3 & -c_3 s_1 - c_1 c_2 s_3 & c_1 s_2 \\ c_2 c_3 s_1 + c_1 s_3 & c_1 c_3 - c_2 s_1 s_3 & s_1 s_2 \\ -c_3 s_2 & s_2 s_3 & c_2 \end{bmatrix}. \quad (5.19)$$

In writing expressions for the components P_{ik} , we have used the helpful abbreviations $c_k = \cos(\alpha^k)$ and $s_k = \sin(\alpha^k)$.

It is natural to choose a reference configuration so that $\mathbf{P} = \mathbf{I}$ in an undeformed configuration. However, as we now show, when the 3-2-3 set of Euler angles is used to parameterize \mathbf{P} such a selection is problematic. To proceed, we examine the conditions by which the components of \mathbf{P} in Eqn. (5.19) reduce to $P_{ik} = \delta_{ik}$. It is straightforward to see that these conditions are simply

$$\alpha^2 = 0, \quad \alpha^1 + \alpha^3 = n\pi, \quad n = 0, 1, 2, 3, 4. \quad (5.20)$$

Thus, there is no one-to-one correspondence between the 3-2-3 set of Euler angles and the identity tensor. In addition, in order to use the 3-2-3 set of Euler angles to parameterize $\mathbf{P} = \mathbf{I}$ we must set α^2 to one of its singular values and this will present other problems.

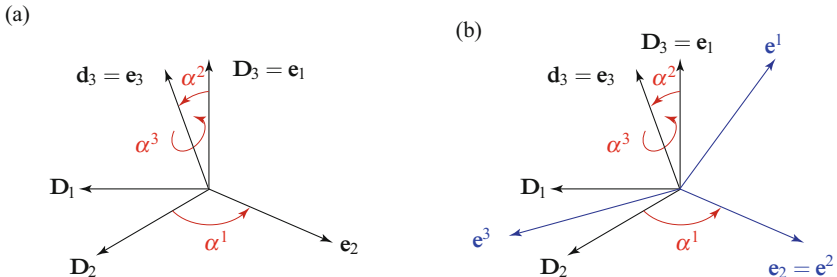


Fig. 5.5 Schematic of the Euler and dual Euler basis vectors associated with a 3-2-3 set of Euler angles. (a) The Euler basis vectors, \mathbf{e}_1 , \mathbf{e}_2 , and \mathbf{e}_3 , and their relation to the Euler angles (cf. Eqn. (5.15)) and (b) the corresponding dual Euler basis vectors, \mathbf{e}^1 , \mathbf{e}^2 , and \mathbf{e}^3 , (cf. Eqn. (5.23)).

In addition to the Euler basis, we also have a companion dual Euler basis. The latter basis has application to representations of moment vectors [262, 270, 271] and we shall exploit this in the sequel. We also note that there is a direct correspondence between the Euler and dual Euler basis sets and covariant and contravariant sets of basis vectors in differential geometry. Given an Euler basis, the corresponding dual

Euler basis vectors are defined by the nine relations

$$\mathbf{e}^k \cdot \mathbf{e}_i = \delta_i^k \quad (i = 1, 2, 3, \text{ and } k = 1, 2, 3), \quad (5.21)$$

where δ_i^k is the Kronecker delta: $\delta_i^k = 1$ if $i = k$ and is otherwise 0. The solution to these nine equations is known in differential geometry (see, e.g., [140, Eqn. (1.9.13)] or [325, Exercise 2.11]):

$$\mathbf{e}^1 = \frac{\mathbf{e}_2 \times \mathbf{e}_3}{(\mathbf{e}_1 \times \mathbf{e}_2) \cdot \mathbf{e}_3}, \quad \mathbf{e}^2 = \mathbf{e}_2, \quad \mathbf{e}^3 = \frac{\mathbf{e}_1 \times \mathbf{e}_2}{(\mathbf{e}_1 \times \mathbf{e}_2) \cdot \mathbf{e}_3}. \quad (5.22)$$

The expression for \mathbf{e}^2 is greatly simplified because this Euler basis vector is perpendicular to the other two: $\mathbf{e}_1 \perp \mathbf{e}_2$ and $\mathbf{e}_3 \perp \mathbf{e}_2$. With the help of Eqn. (5.22), we now compute the dual Euler basis vectors for the 3-2-3 set of Euler angles:

$$\begin{aligned} \mathbf{e}^1 &= \frac{\mathbf{e}_2 \times \mathbf{e}_3}{[\mathbf{e}_1, \mathbf{e}_2, \mathbf{e}_3]} = \operatorname{cosec}(\alpha^2) (\sin(\alpha^3) \mathbf{d}_2 - \cos(\alpha^3) \mathbf{d}_1), \\ \mathbf{e}^2 &= \frac{\mathbf{e}_3 \times \mathbf{e}_1}{[\mathbf{e}_1, \mathbf{e}_2, \mathbf{e}_3]} = \mathbf{e}_2 = \cos(\alpha^3) \mathbf{d}_2 + \sin(\alpha^3) \mathbf{d}_1, \\ \mathbf{e}^3 &= \frac{\mathbf{e}_1 \times \mathbf{e}_2}{[\mathbf{e}_1, \mathbf{e}_2, \mathbf{e}_3]} = \cot(\alpha^2) (\cos(\alpha^3) \mathbf{d}_1 - \sin(\alpha^3) \mathbf{d}_2) + \mathbf{d}_3. \end{aligned} \quad (5.23)$$

The Euler and dual Euler bases are sketched in Figure 5.5. As a third and final perspective on the Euler angle singularity, we observe from Eqn. (5.23) that the dual Euler basis vectors are not defined when $\alpha^2 = 0, \pi$.

For future reference, we note that the axial vector associated with $\dot{\mathbf{P}}\mathbf{P}^T$ has a simple representation⁷:

$$\boldsymbol{\omega} = \operatorname{ax}(\dot{\mathbf{P}}\mathbf{P}^T) = \dot{\alpha}^3 \mathbf{e}_3 + \dot{\alpha}^2 \mathbf{e}_2 + \dot{\alpha}^1 \mathbf{e}_1. \quad (5.24)$$

In addition, referring to Eqn. (5.7), we find that

$$\mathbf{P}(\mathbf{v} + \mathbf{v}_0) = \frac{\partial \alpha^3}{\partial \xi} \mathbf{e}_3 + \frac{\partial \alpha^2}{\partial \xi} \mathbf{e}_2 + \frac{\partial \alpha^1}{\partial \xi} \mathbf{e}_1 + \mathbf{P}\mathbf{v}_0. \quad (5.25)$$

Using the representations for \mathbf{e}_i in terms of \mathbf{d}_k given in Eqn. (5.15), it is straightforward to compute $\mathbf{P}^T \mathbf{e}_i$ and arrive at a representation for $\mathbf{v} + \mathbf{v}_0$.

⁷ The axial vectors in Eqns. (5.24) and (5.25) can be computed by direct differentiation of the tensor \mathbf{P} or using the relative angular velocity vector proposed by Casey and Lam [51]. Applications of Casey and Lam's relative angular velocity vector can be found in the textbook [265, Sections 6.7 and 6.8].

5.3.2 Strains

The components of $\mathbf{P}\mathbf{v}$ with respect to the basis $\{\mathbf{d}_1, \mathbf{d}_2, \mathbf{d}_3 = \mathbf{d}_1 \times \mathbf{d}_2\}$ define three strain measures:

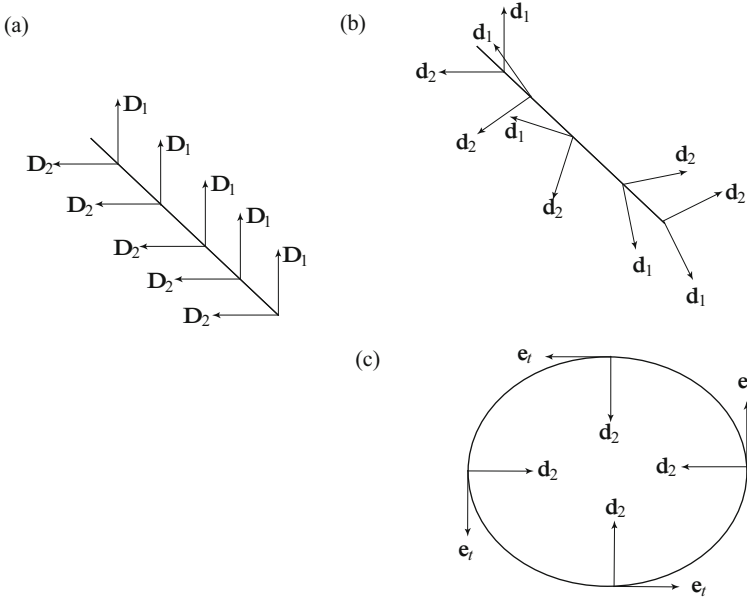


Fig. 5.6 Illustration of the strains for the Kirchhoff rod theory. (a), The reference configuration \mathcal{R}_0 of a straight rod; (b), pure torsion ($v_1 = 0, v_2 = 0, v_3 \neq 0$) of the rod; and (c), pure bending ($v_1 \neq 0, v_2 = 0, v_3 = 0$) of the rod so that its material curve forms a circle in the present configuration \mathcal{R} .

$$\mathbf{v} = v_1 \mathbf{D}_1 + v_2 \mathbf{D}_2 + v_3 \mathbf{D}_3. \quad (5.26)$$

An alternative set of strain measures are the components of $\mathbf{P}(\mathbf{v} + \mathbf{v}_0)$ with respect to the basis $\{\mathbf{d}_1, \mathbf{d}_2, \mathbf{d}_3 = \mathbf{d}_1 \times \mathbf{d}_2\}$:

$$\mathbf{v} + \mathbf{v}_0 = (v_1 + v_{01}) \mathbf{D}_1 + (v_2 + v_{02}) \mathbf{D}_2 + (v_3 + v_{03}) \mathbf{D}_3. \quad (5.27)$$

This set of strains could be considered as taken relative to a reference configuration where the centerline was straight and the directors were constant. Some authors use \mathbf{v} as a strain measure: particularly for rod models of double-stranded DNA where $\mathbf{v}_0 = v_{03} \mathbf{E}_3$ (see, e.g., [158, 199, 228]).

The strains v_1 and v_2 are associated with the curvature of the centerline and are commonly referred to as curvatures. The question “why are there two curvatures when a space curve only has one?” shall be answered shortly. In addition, v_3

is known as the torsion. This torsion should not be confused with the geometric torsion τ . We illustrate these bending and torsional strains in Figure 5.6. For the reference configuration \mathcal{R}_0 shown in this figure, the intrinsic strains v_{0k} are zero.

If a set of 3-2-3 Euler angles are used to parameterize \mathbf{P} , then, computing the components $\mathbf{Pv} \cdot \mathbf{d}_k$ with the help of Eqns. (5.15), (5.25), and (5.26), we find that⁸

$$\begin{bmatrix} v_1 \\ v_2 \\ v_3 \end{bmatrix} = \begin{bmatrix} -\sin(\alpha^2) \cos(\alpha^3) & \sin(\alpha^3) & 0 \\ \sin(\alpha^2) \sin(\alpha^3) & \cos(\alpha^3) & 0 \\ \cos(\alpha^2) & 0 & 1 \end{bmatrix} \begin{bmatrix} \frac{\partial \alpha^1}{\partial \xi} \\ \frac{\partial \alpha^2}{\partial \xi} \\ \frac{\partial \alpha^3}{\partial \xi} \end{bmatrix}. \quad (5.28)$$

Inverting the matrix in the above equation or, equivalently, computing $\mathbf{Pv} \cdot \mathbf{e}^k$ with the help of Eqns. (5.23), (5.25), and (5.26), yields expressions for the spatial rates of change of the Euler angles in terms of the strains v_i :

$$\begin{bmatrix} \frac{\partial \alpha^1}{\partial \xi} \\ \frac{\partial \alpha^2}{\partial \xi} \\ \frac{\partial \alpha^3}{\partial \xi} \end{bmatrix} = \begin{bmatrix} -\text{cosec}(\alpha^2) \cos(\alpha^3) & \text{cosec}(\alpha^2) \sin(\alpha^3) & 0 \\ \sin(\alpha^3) & \cos(\alpha^3) & 0 \\ \cot(\alpha^2) \cos(\alpha^3) & -\cot(\alpha^2) \sin(\alpha^3) & 1 \end{bmatrix} \begin{bmatrix} v_1 \\ v_2 \\ v_3 \end{bmatrix}. \quad (5.29)$$

It should be transparent from the above equations that, while it is easy to correlate the rotation of the directors to the changes in Euler angles, correlating $\frac{\partial \alpha^k}{\partial \xi}$ to the rod strains v_i is nontrivial and, moreover, is impossible when $\alpha^2 = 0, \pi$.

5.3.2.1 An Example

As an illustrative example, we consider the helically plied structures shown in Figure 5.7. Suppose we wish to model the helical plies and the cylindrical structure about which they are wrapped as a single rod. We are then faced with the issue of a choice of reference configuration for such a structure and, with that, a choice of the directors \mathbf{D}_1 and \mathbf{D}_2 . Here, we consider one possible choice where these directors “follow” the helical strand. We emphasize that $\mathbf{R}(\xi)$ for all the three structures shown in Figure 5.7 is the position vector of material points located on the centerline of the cylindrical body. A closely related application will be discussed in Section 5.18 when helical springs, such as the one shown in Figure 5.27, are analyzed using Kirchhoff's rod theory.

To proceed, we choose a fixed unit vector \mathbf{E}_3 which is parallel to the axis of the rod in its reference configuration⁹:

$$\mathbf{R}(\xi) = \xi \mathbf{E}_3. \quad (5.30)$$

⁸ For the reader comparing our treatment to Love's classic work, the relations (5.28) are identical to [213, Eqn. (8), Page 386].

⁹ You may wish to look at our earlier discussion of the helix in Section 3.4.

We assume that the pitch angle of the helix is β , and the equation of the centerline of the helical strand is parameterized using a polar angle ϕ :

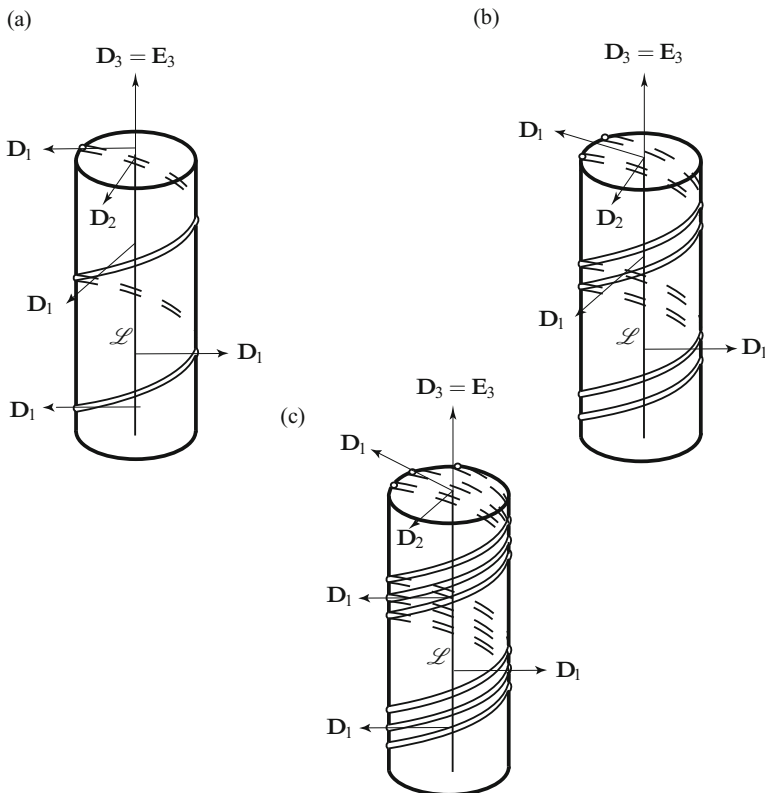


Fig. 5.7 Examples of reference configurations of a cylindrical body with helical plies wound on its lateral surface. Representatives of the referential values of the directors \mathbf{D}_1 and \mathbf{D}_2 associated with the Cosserat rod that can be used to model the body are also shown in this figure. The material curve \mathcal{L} associated with the rod is the centerline of the cylindrical body. In (a), a single ply; in (b), a two-ply; and in (c), a triple-ply. The two-ply is similar to double-stranded DNA. This figure is adapted from [199].

$$\mathbf{x} = R(\cos(\phi)\mathbf{E}_1 + \sin(\phi)\mathbf{E}_2) + R\tan(\beta)\phi\mathbf{E}_3. \quad (5.31)$$

Here, R and $\beta \neq 0$ are constants, and

$$\xi = R\tan(\beta)\phi. \quad (5.32)$$

We next prescribe the referential directors:

$$\begin{aligned}\mathbf{D}_1(\xi) &= \cos\left(\frac{\xi}{R\tan(\beta)}\right)\mathbf{E}_1 + \sin\left(\frac{\xi}{R\tan(\beta)}\right)\mathbf{E}_2, \\ \mathbf{D}_2(\xi) &= -\sin\left(\frac{\xi}{R\tan(\beta)}\right)\mathbf{E}_1 + \cos\left(\frac{\xi}{R\tan(\beta)}\right)\mathbf{E}_2, \\ \mathbf{D}_3(\xi) &= \mathbf{E}_3.\end{aligned}\quad (5.33)$$

With this choice, the material coordinate ξ is chosen to be the arc-length parameter for the reference configuration where $\xi = 0$ when $\phi = 0$. Notice that we can express the representation (5.31) for \mathbf{x} in the compact form

$$\mathbf{x}(\xi) = R\mathbf{D}_1(\xi) + \mathbf{R}(\xi). \quad (5.34)$$

It is straightforward to see that the rotation tensor $\mathbf{P}_0 = \sum_{k=1}^3 \mathbf{D}_k \otimes \mathbf{E}_k$ corresponds to a rotation about \mathbf{E}_3 through an angle $\frac{\xi}{R\tan(\beta)}$. Consequently, the axial vector of $\mathbf{P}'_0 \mathbf{P}_0^T$ is

$$\mathbf{v}_0 = v_0 \mathbf{E}_3 = \frac{\cot(\beta)}{R} \mathbf{E}_3. \quad (5.35)$$

Thus, the reference configuration of the rod has a constant pretwist $v_0 = \frac{\cot(\beta)}{R}$. This pretwist is often known as the intrinsic twist and can be compared to the geometric torsion $\tau = \frac{\alpha}{R(1+\alpha^2)} = \frac{1}{R} \cos(\beta) \sin(\beta)$ of a helical space curve and the total torsion $T_w(\mathcal{S}, \mathbf{e}_n) = \sin(\beta)$ of a turn of a helical space curve that were discussed in Section 3.4.

5.3.3 Inertias

We suppose that the three-dimensional body that the directed curve is modeling has a mass density per unit volume in a fixed reference configuration of $\rho_0^* = \rho_0^*(\xi, \theta^1, \theta^2)$. The directed curve has a mass per unit length in its reference configuration of $\rho_0 = \rho_0(\xi)$. We prescribe this density and five distinct inertias as follows¹⁰:

$$\begin{aligned}\rho_0 &= \int_{\mathcal{A}} \rho_0^* da, \\ \rho_0 y^{0\alpha} &= \int_{\mathcal{A}} \theta^\alpha \rho_0^* da, \\ \rho_0 y^{\alpha\beta} &= \int_{\mathcal{A}} \theta^\alpha \theta^\beta \rho_0^* da,\end{aligned}\quad (5.36)$$

where $\alpha, \beta = 1, 2$ and $da = \sqrt{Gd\theta^1 d\theta^2}$. We observe that $y^{12} = y^{21}$ and this symmetry is assumed in the sequel.

¹⁰ A derivation of these results was first presented in [137]. The developments used in [137] can also be found in the text [309].

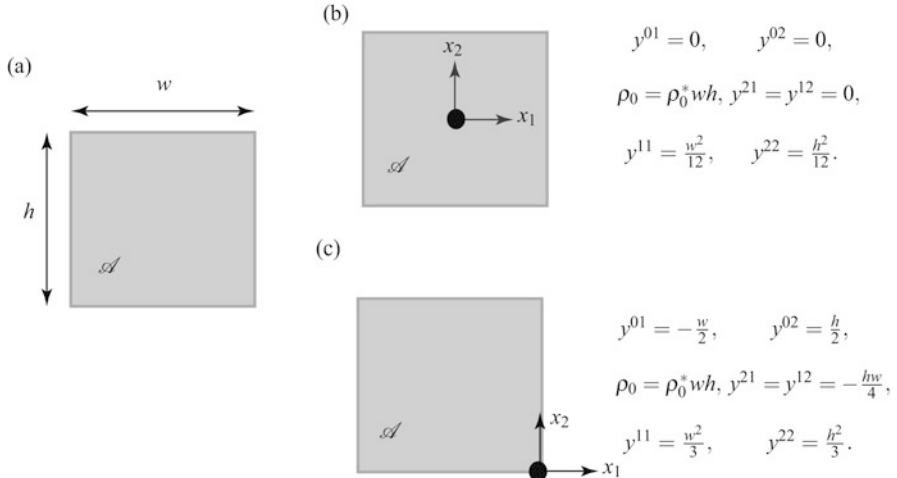


Fig. 5.8 Computation of the coefficients $y^{0\alpha}$ and $y^{\alpha\beta}$ using Eqn. (5.36) for a homogeneous rod with rectangular cross sections in the reference configuration \mathcal{R}_0 . (a), Geometry of the cross section; (b), the case where the centerline is chosen to pass through the center of the cross section; and (c), the case where the centerline is chosen to pass through a corner point.

The integrals in Eqn. (5.36) are taken over the cross section \mathcal{A} of the reference configuration of the rod-like body that the directed curve is modeling. These cross sections correspond to $\theta^3 = \xi$ coordinate surfaces. That is, θ^1 and θ^2 are curvilinear coordinates which parameterize the cross sections of the rod (see Section 5.2.1 and Figure 5.2), and the point $(\theta^1, \theta^2) = (0, 0)$ on each section corresponds to the material point of the directed curve.

Suppose a set of Cartesian coordinates are used to parameterize the reference configuration of the rod-like body: $\theta^1 = x_1$, $\theta^2 = x_2$, $\theta^3 = x_3$, $\sqrt{G} = 1$, and $da = dx_1 dx_2$. As shown in Figure 5.8(b), if we assume that the centerline is the line at the intersection of the planes $x_1 = 0$ and $x_2 = 0$, then, for the case of a homogeneous rod with a rectangular cross section of width w and height h ,

$$\begin{aligned} \rho_0 &= \rho_0^* wh, \quad y^{0\alpha} = 0, \quad y^{12} = 0, \\ \rho_0 y^{11} &= \rho_0^* I_2 = \rho_0^* \left(\frac{hw^3}{12} \right), \quad \rho_0 y^{22} = \rho_0^* I_1 = \rho_0^* \left(\frac{wh^3}{12} \right). \end{aligned} \quad (5.37)$$

Here, I_2 is the second moment of area of the cross section about the x_2 axis. You should notice that if the centerline is chosen to pass through one of the corners of the cross section, then this will alter the values of $y^{0\alpha}$ and $y^{\alpha\beta}$. We refer the interested

reader to Figure 5.8(c) for an example of a situation where the centerline is chosen to pass through one of the corners on the lower lateral surface of a rod-like body with a rectangular cross section.¹¹

5.4 Further Kinematics and Discontinuities

Because the directors in Kirchhoff's rod theory behave as part of an orthonormal triad, the kinematics in this rod theory are particularly rich in representations. For example, differentiating Eqn. (5.6)₁ with respect to t , we find that

$$\dot{\mathbf{d}}_\alpha = \boldsymbol{\omega} \times \mathbf{d}_\alpha. \quad (5.38)$$

Here, $\boldsymbol{\omega}$ is the axial vector of a skew-symmetric tensor:

$$\boldsymbol{\omega} = \omega_1 \mathbf{d}_1 + \omega_2 \mathbf{d}_2 + \omega_3 \mathbf{d}_3 = \mathbf{ax}(\dot{\mathbf{P}} \mathbf{P}^T). \quad (5.39)$$

Concerning the vector \mathbf{v} , it is interesting (and not surprising) to note that the time derivative of \mathbf{v} and the arc-length derivative of $\boldsymbol{\omega}$ are related:

$$\dot{\mathbf{v}} = \mathbf{P}^T \boldsymbol{\omega}', \quad \boldsymbol{\omega}' = \mathbf{P} \dot{\mathbf{v}}. \quad (5.40)$$

To establish these compatibility relations, one uses Eqn. (5.9), the fact that $\dot{\mathbf{v}}_0 = \mathbf{0}$, and the skew-symmetries of $\mathbf{P}^T \dot{\mathbf{P}}$ and $\mathbf{P}^T \mathbf{P}'$. The relations (5.40) will be used later to help establish constitutive relations for the rod.

The discontinuities that are inherent in the rod theory can be categorized as those associated with the translation of the material curve and those associated with the rotation of the cross sections. The former are considered by examining the discontinuities in the time- and ξ -derivatives of \mathbf{r} while the latter are encompassed by discontinuities in the time- and ξ -derivatives of the rotation tensor \mathbf{PP}_0 . To proceed, we first assume that \mathbf{r} and \mathbf{d}_α are continuous functions of ξ :

$$[\![\mathbf{r}]\!]_\gamma = \mathbf{0}, \quad [\![\mathbf{d}_1]\!]_\gamma = \mathbf{0}, \quad [\![\mathbf{d}_2]\!]_\gamma = \mathbf{0}. \quad (5.41)$$

That is, the centerline of the rod has no breaks and the directors vary continuously with ξ . As a consequence of the continuity of \mathbf{d}_1 and \mathbf{d}_2 , it follows that \mathbf{d}_3 and \mathbf{P} are also continuous:

$$[\![\mathbf{d}_3]\!]_\gamma = \mathbf{0}, \quad [\![\mathbf{P}]\!]_\gamma = \mathbf{0}. \quad (5.42)$$

Thus, the centerline of the rod cannot have any kinks.

For rods, we have the velocity \mathbf{v}_γ , which is identical to one presented earlier for strings:

¹¹ As discussed by Naghdi [244], the freedom to make such a selection can be advantageous for formulating contact problems. It can also be advantageous when attempting to develop rod models for deformable bodies as in [286].

$$\begin{aligned}\mathbf{v}_\gamma &= \lim_{\sigma \rightarrow 0} \left(\frac{d}{dt} \mathbf{r}(\gamma(t) \pm \sigma, t) \right) = \mathbf{v}^+ + \dot{\gamma} \mathbf{r}'^+ \\ &= \mathbf{v}^- + \dot{\gamma} \mathbf{r}'^-, \end{aligned}\quad (5.43)$$

where $\sigma > 0$. That is,

$$\mathbf{v}_\gamma = \left\{ \mathbf{v} + \dot{\gamma} \mathbf{r}' \right\}_\gamma. \quad (5.44)$$

This velocity vector describes the shock speed experienced by the material curve relative to a fixed observer.

The velocity vector of the directors and the derivatives \mathbf{d}'_α can also experience discontinuities. Such behavior can be associated with the deformation of the cross sections of the rod, as opposed to the centerline of the rod. The discontinuities in $\dot{\mathbf{d}}_\alpha$ and \mathbf{d}'_α are not independent. As with the vector \mathbf{r} , we correlate left-sided and right-sided calculations of $\dot{\mathbf{d}}_\alpha$ and \mathbf{d}'_α to find two equivalent representations for each of the vectors $\mathbf{w}_{1\gamma}$ and $\mathbf{w}_{2\gamma}$. For instance,

$$\begin{aligned}\mathbf{w}_{1\gamma} &= \lim_{\sigma \rightarrow 0} \left(\frac{d}{dt} \mathbf{d}_1(\gamma(t) \pm \sigma, t) \right) = \dot{\mathbf{d}}_1^+ + \dot{\gamma} \mathbf{d}'_1^+ \\ &= \dot{\mathbf{d}}_1^- + \dot{\gamma} \mathbf{d}'_1^-. \end{aligned}\quad (5.45)$$

That is,

$$\begin{aligned}\mathbf{w}_{1\gamma} &= \left\{ \dot{\mathbf{d}}_1 + \dot{\gamma} \mathbf{d}'_1 \right\}_\gamma \\ &= \{(\boldsymbol{\omega} + \dot{\gamma} \mathbf{P}(\mathbf{v} + \mathbf{v}_0)) \times \mathbf{d}_1\}_\gamma. \end{aligned}\quad (5.46)$$

In arriving at the final expression, we used Eqn. (5.38) and the identity $\mathbf{d}'_1 = (\mathbf{P}(\mathbf{v} + \mathbf{v}_0)) \times \mathbf{d}_1$.

Although $[\![\mathbf{d}_\alpha]\!]_\gamma = \mathbf{0}$ implies that $[\![\mathbf{P}\mathbf{P}_0\mathbf{E}_\alpha]\!]_\gamma = \mathbf{0}$, we cannot expect \mathbf{v} and $\boldsymbol{\omega}$ to be continuous at a point of discontinuity. Indeed, it is possible, and useful, to calculate the velocity $\boldsymbol{\omega}_\gamma$ by examining the time derivative of $\mathbf{P}(\xi = \gamma(t), t) \mathbf{P}_0(\xi = \gamma(t))$:

$$\begin{aligned}\boldsymbol{\omega}_\gamma &= \text{ax} \left(\left(\left(\dot{\mathbf{P}}\mathbf{P}_0 + \dot{\gamma} \left(\mathbf{P}'\mathbf{P}_0 + \mathbf{P}\mathbf{P}'_0 \right) \right) \mathbf{P}_0^T \mathbf{P}^T \right)^+ \right) \\ &= \text{ax} \left(\left(\left(\dot{\mathbf{P}}\mathbf{P}_0 + \dot{\gamma} \left(\mathbf{P}'\mathbf{P}_0 + \mathbf{P}\mathbf{P}'_0 \right) \right) \mathbf{P}_0^T \mathbf{P}^T \right)^- \right) \\ &= (\boldsymbol{\omega} + \dot{\gamma} \det(\mathbf{P}) \mathbf{P}(\mathbf{v} + \mathbf{v}_0))^+ \\ &= (\boldsymbol{\omega} + \dot{\gamma} \det(\mathbf{P}) \mathbf{P}(\mathbf{v} + \mathbf{v}_0))^-, \end{aligned}\quad (5.47)$$

where we used the definitions (5.8)_{1,2} and (5.38) and the identity (5.9). It can be concluded from Eqn. (5.47) that

$$\boldsymbol{\omega}_\gamma = \{ \boldsymbol{\omega} + \dot{\gamma} \mathbf{P}(\mathbf{v} + \mathbf{v}_0) \}_\gamma,$$

$$\boldsymbol{\omega}^+ + \dot{\gamma}(\mathbf{P}(\mathbf{v} + \mathbf{v}_0))^+ = \boldsymbol{\omega}^- + \dot{\gamma}(\mathbf{P}(\mathbf{v} + \mathbf{v}_0))^- . \quad (5.48)$$

These results clearly parallel those we found for \mathbf{v}_γ , $\mathbf{w}_{1\gamma}$, and $\mathbf{w}_{2\gamma}$. We also observe the useful identities

$$\mathbf{w}_{1\gamma} = \boldsymbol{\omega}_\gamma \times \mathbf{d}_1(\gamma, t), \quad \mathbf{w}_{2\gamma} = \boldsymbol{\omega}_\gamma \times \mathbf{d}_2(\gamma, t). \quad (5.49)$$

To establish these results from Eqn. (5.46), the facts that $\{\mathbf{d}_\alpha\} = \mathbf{d}_\alpha(\gamma, t)$ were used. It follows from the definitions of the velocity \mathbf{v}_γ and angular velocity $\boldsymbol{\omega}_\gamma$ that

$$[\![\mathbf{v}]\!]_\gamma = - \left[\left[\mathbf{r}' \right] \right]_\gamma \dot{\gamma}, \quad [\![\boldsymbol{\omega}]\!]_\gamma = - [\![\mathbf{P}(\mathbf{v} + \mathbf{v}_0)]\!]_\gamma \dot{\gamma}. \quad (5.50)$$

These conditions are crucial in establishing an alternative form of the jump condition arising from the balance of energy.

5.5 Momenta and Kinetic Energy

We define the linear momentum \mathbf{G} per unit length of ξ of the rod by the expression

$$\mathbf{G} = \rho \mu \left(\dot{\mathbf{r}} + \sum_{\alpha=1}^2 y^{0\alpha} \dot{\mathbf{d}}_\alpha \right). \quad (5.51)$$

Supplementing this momentum, we define the two director momenta per unit length of ξ :

$$\begin{aligned} \mathbf{L}^1 &= \rho \mu \left(y^{01} \dot{\mathbf{r}} + \sum_{\alpha=1}^2 y^{1\alpha} \dot{\mathbf{d}}_\alpha \right), \\ \mathbf{L}^2 &= \rho \mu \left(y^{02} \dot{\mathbf{r}} + \sum_{\alpha=1}^2 y^{2\alpha} \dot{\mathbf{d}}_\alpha \right). \end{aligned} \quad (5.52)$$

To examine the physical interpretations of these three momenta, we can, without loss in generality, set $y^{0\alpha} = 0$. Then, \mathbf{G} can be identified as the linear momentum of the material curve, and \mathbf{L}^α can be identified as the linear momenta of the cross sections of the rod.

The material momentum of a segment (ξ_1, ξ_2) of the directed curve is defined as the integral of the material momentum \mathbf{P} , $\int_{\xi_1}^{\xi_2} \mathbf{P} d\xi$, where

$$\mathbf{P} = - \left(\mathbf{r}' \cdot \mathbf{G} + \mathbf{d}_1' \cdot \mathbf{L}^1 + \mathbf{d}_2' \cdot \mathbf{L}^2 \right). \quad (5.53)$$

This momentum is sometimes referred to as the pseudomomentum and first appeared in the literature in [264]. You should notice how the expression for \mathbf{P} simplifies to that presented earlier for a string (see Eqn. (1.44)).

The kinetic energy of a segment (ξ_1, ξ_2) of the directed curve is defined as $\int_{\xi_1}^{\xi_2} T d\xi$ where the kinetic energy density T is

$$T = \frac{1}{2} (\dot{\mathbf{r}} \cdot \mathbf{G} + \dot{\mathbf{d}}_1 \cdot \mathbf{L}^1 + \dot{\mathbf{d}}_2 \cdot \mathbf{L}^2). \quad (5.54)$$

Note that we are not imposing inextensibility here, so we leave μ arbitrary.

The angular momentum relative to O of a segment (ξ_1, ξ_2) of the directed curve is

$$\mathbf{h}_O = \int_{\xi_1}^{\xi_2} \mathbf{h}_O d\xi, \quad (5.55)$$

where

$$\mathbf{h}_O = \mathbf{r} \times \mathbf{G} + \mathbf{d}_1 \times \mathbf{L}^1 + \mathbf{d}_2 \times \mathbf{L}^2. \quad (5.56)$$

Because, $\dot{\mathbf{d}}_\alpha = \boldsymbol{\omega} \times \mathbf{d}_\alpha$, we can also define inertia tensors \mathbf{J}_R and \mathbf{J}_{R_0} :

$$\begin{aligned} \mathbf{J}_{R_0} &= \rho \mu (y^{11} + y^{22}) \mathbf{I} - \sum_{\alpha=1}^2 \sum_{\beta=1}^2 \rho \mu y^{\alpha\beta} \mathbf{D}_\alpha \otimes \mathbf{D}_\beta, \\ \mathbf{J}_R &= \rho \mu (y^{11} + y^{22}) \mathbf{I} - \sum_{\alpha=1}^2 \sum_{\beta=1}^2 \rho \mu y^{\alpha\beta} \mathbf{d}_\alpha \otimes \mathbf{d}_\beta. \end{aligned} \quad (5.57)$$

It should be noted that

$$\mathbf{J}_R = \mathbf{P} \mathbf{J}_{R_0} \mathbf{P}^T, \quad (5.58)$$

a result which parallels that for the inertia tensors of a rigid body (cf., e.g., [48]). We also note that the inertia tensor can be used to write a compact expression for a portion of the kinetic energy density of the rod:

$$\sum_{\alpha=1}^2 \sum_{\beta=1}^2 \rho \mu y^{\alpha\beta} \mathbf{d}_\alpha \cdot \dot{\mathbf{d}}_\beta = \mathbf{J}_R \boldsymbol{\omega} \cdot \boldsymbol{\omega}. \quad (5.59)$$

The inertia tensor \mathbf{J}_R is equivalent to that for a lamella with $\mathbf{d}_1 \times \mathbf{d}_2$ normal to the plane of this infinitesimally thin body. It is left as an exercise to show how T and \mathbf{h}_O can be partially expressed in terms of \mathbf{J}_R .

5.6 A Strain Energy Function

The directed curve associated with the Kirchhoff rod theory is capable of resisting bending in two directions and torsion. We use the skew-symmetric tensor \mathbf{K} to help define the associated strains. As a consequence, the strain energy function per unit mass is assumed to be a function of the three strains v_i and (if the rod is not homogeneous) possibly ξ :

$$\psi = \psi(v_1, v_2, v_3, \xi). \quad (5.60)$$

It is important to note that the material time derivative of this function has the following representations:

$$\begin{aligned}\dot{\psi} &= \sum_{i=1}^3 \frac{\partial \psi}{\partial v_i} \dot{v}_i \\ &= \frac{\partial \psi}{\partial \mathbf{v}} \cdot \dot{\mathbf{v}} \\ &= \left(\mathbf{P} \frac{\partial \psi}{\partial \mathbf{v}} \right) \cdot \frac{\partial \boldsymbol{\omega}}{\partial \xi}.\end{aligned}\quad (5.61)$$

We used the notation $\frac{\partial \psi}{\partial \mathbf{v}} = \sum_{i=1}^3 \frac{\partial \psi}{\partial v_i} \mathbf{D}_i$ and the identity (5.40)₁ to obtain these representations. They will play an important role when we find constitutive equations. Calculation of a representation for $\rho_0 \dot{\psi}$ where

$$\psi = \hat{\psi}(v_1 - v_{01}, v_2 - v_{02}, v_3 - v_{03}, \xi) \quad (5.62)$$

and a proof that $\hat{\psi}$ is invariant under superposed rigid body motions are left as exercises.

It is common to consider Taylor series expansions of ψ about the reference configuration $v_i = 0$:

$$\begin{aligned}2\rho_0 \psi(v_1, v_2, v_3, \xi) &= 2\rho_0 \psi(0, 0, 0, \xi) + \sum_{i=1}^3 \sum_{k=1}^3 A_{ik}(\xi) v_i v_k \\ &\quad + \sum_{i=1}^3 \sum_{k=1}^3 \sum_{r=1}^3 B_{ikr}(\xi) v_i v_k v_r + \dots\end{aligned}\quad (5.63)$$

The coefficients A_{ik} and B_{ikr} will depend both on the geometric properties of the cross sections and the constitution of the rod-like body that the rod is modeling. It is standard to invoke material symmetry arguments, such as those presented in [12, 158, 198, 228], to reduce the number of coefficients. These arguments along with the assumptions that the rod-like body is isotropic, linearly elastic, that the reference configuration is straight and unstressed, and that the directors $\mathbf{D}_{1,2}$ are chosen to be parallel to the principal axis of the area moment of inertia tensor for the cross section, are used to motivate the most popular form of the expansion of $\rho_0 \psi$ in the literature which dates to Kirchhoff in 1859 [185]:

$$2\rho_0 \psi = EI_1 v_1^2 + EI_2 v_2^2 + \mathcal{D} v_3^2. \quad (5.64)$$

In this equation, E is Young's modulus, I_α are second moments of area, and \mathcal{D} is the torsional rigidity. Rods whose strain energy function are given by Eqn. (5.64) with $I_1 = I_2$ are sometimes referred to as (transversely) isotropic.¹²

¹² We discuss this matter in additional detail in Section 6.4.3 of Chapter 6.

It is convenient to recall the parameters EI_α and \mathcal{D} for a selection of geometries that can be found in the literature on linear elasticity [328]. First, for a straight rod with a circular cross section of radius r , it is known that

$$EI_1 = EI_2 = \frac{\pi Er^4}{4}, \quad \mathcal{D} = \frac{EI_1}{1+\nu}. \quad (5.65)$$

For a straight rod with an elliptical cross section of semi-axes a and b ,

$$EI_1 = \frac{\pi Eab^3}{4}, \quad EI_2 = \frac{\pi Eb a^3}{4}, \quad \mathcal{D} = \left(\frac{E}{2(1+\nu)} \right) \frac{\pi a^3 b^3}{a^2 + b^2}. \quad (5.66)$$

Finally, for a straight rod with a square cross section of width w ,

$$EI_1 = EI_2 = \frac{Ew^4}{12}, \quad \mathcal{D} \approx \frac{27EI_1}{32(1+\nu)}. \quad (5.67)$$

In general, closed-form solutions for \mathcal{D} are only available for a limited number of cross sections.

5.7 Balance Laws for the Rod Theory

Preparatory to writing the conservation laws for the directed curve, we record some additional notation. Associated with the inertia of \mathcal{R} is its mass density $\rho = \rho(\xi, t)$. Pertaining to forces, $\mathbf{n} = \mathbf{n}(\xi, t)$ is the contact force, $\mathbf{m} = \mathbf{m}(\xi, t)$ is the contact moment, and $\mathbf{f} = \mathbf{f}(\xi, t)$ and $\mathbf{l}^\beta = \mathbf{l}^\beta(\xi, t)$ are the respective assigned force and assigned director forces per unit mass. We also define the contact material force C and assigned material force b . For the prescription of the former,¹³

$$C = \rho \mu \psi - \mathbf{n} \cdot \mathbf{r}' - \mathbf{m} \cdot (\mathbf{P}(\mathbf{v} + \mathbf{v}_0)) - T. \quad (5.68)$$

If we ignore the directors and set $\mathbf{m} = \mathbf{0}$, then this prescription reduces to the one we presented earlier for a string (see Eqn. (1.69)). We also remark that for static problems involving rods where $\rho \mu \psi$ has the classic quadratic form (5.64), C is identical to an energy integral used to establish solutions for boundary-value problems.¹⁴

¹³ The prescription (5.68) is a generalization of Eqn. (56)₁ in [264] to the case of an intrinsically curved rod.

¹⁴ See, e.g., [213, Eqn. (3), Section 260] or the more recent work [164, Eqn. (20)].

5.7.1 Assigned Forces, Assigned Director Forces, and Assigned Moments

It is convenient to be able to prescribe the assigned force fields in terms of the three-dimensional body force $\rho_0^* \mathbf{b}$ acting on the rod and surface tractions \mathbf{t} acting on the lateral surface of the rod.¹⁵ The prescriptions are, with evident parallels to the prescriptions (5.36) for the inertia coefficients,

$$\begin{aligned}\rho_0 \mathbf{f} &= \int_{\mathcal{A}} \mathbf{b} \rho_0^* da + \oint_{\partial \mathcal{A}} \mathbf{t} du, \\ \rho_0 \mathbf{l}^\alpha &= \int_{\mathcal{A}} \mathbf{b} \theta^\alpha \rho_0^* da + \oint_{\partial \mathcal{A}} \mathbf{t} \theta^\alpha du.\end{aligned}\quad (5.69)$$

Here, $\partial \mathcal{A}$ is the boundary of the cross section, ρ_0^* is the mass density per unit volume, and u is the arc-length parameter on this boundary.

The force $\rho_0 \mathbf{f}$ is the resultant of the body force and surface traction at a value of ξ (i.e., at a particular cross section). You should also notice that

$$\begin{aligned}\sum_{\alpha=1}^2 \mathbf{d}_\alpha \times \rho_0 \mathbf{l}^\alpha &= \sum_{\alpha=1}^2 \mathbf{d}_\alpha \times \int_{\mathcal{A}} \mathbf{b} \theta^\alpha \rho_0^* da + \sum_{\alpha=1}^2 \mathbf{d}_\alpha \times \oint_{\partial \mathcal{A}} \mathbf{t} \theta^\alpha du \\ &= \sum_{\alpha=1}^2 \int_{\mathcal{A}} \theta^\alpha \mathbf{d}_\alpha \times \mathbf{b} \rho_0^* da + \sum_{\alpha=1}^2 \oint_{\partial \mathcal{A}} \theta^\alpha \mathbf{d}_\alpha \times \mathbf{t} du.\end{aligned}\quad (5.70)$$

Consequently, we can consider $\sum_{\alpha=1}^2 \mathbf{d}_\alpha \times \rho_0 \mathbf{l}^\alpha$ as the moment (relative to the material point ξ on the centerline) of the body force and surface tractions acting on rod-like body (see Section 5.2.1 and Eqn. (5.2)). That is,

$$\mathbf{m}_a = \sum_{\alpha=1}^2 \mathbf{d}_\alpha \times \rho_0 \mathbf{l}^\alpha,\quad (5.71)$$

where \mathbf{m}_a denotes the applied or assigned moment.

A selection of three examples where $\rho_0 \mathbf{f}$ and $\rho_0 \mathbf{l}^\alpha$ are computed using the prescriptions (5.69) are shown in Figure 5.9. In these examples, the tractions \mathbf{t}_A , \mathbf{t}_B , and \mathbf{t}_C are applied to lateral surface of a rod whose cross section in the present configuration is assumed to be a rectangle of height h and width w . In this situation, $\theta^1 = x_1$ and $\theta^2 = x_2$. The line integrals $\oint_{\partial \mathcal{A}} \mathbf{t} du$ and $\oint_{\partial \mathcal{A}} \mathbf{t} \theta^\alpha du$ are evaluated by taking the path in a counterclockwise manner around the perimeter of the rectangle:

¹⁵ A derivation of these results was first presented in [137] and is based on the approximation (5.2): $\mathbf{r}^* = \mathbf{r}(\xi, t) + \sum_{\alpha=1}^2 \theta^\alpha \mathbf{d}_\alpha(\xi, t)$. However, the derivation is difficult to follow. A recent treatment by [309] is far more transparent (see also [260] and Section 7.12 in Chapter 7).

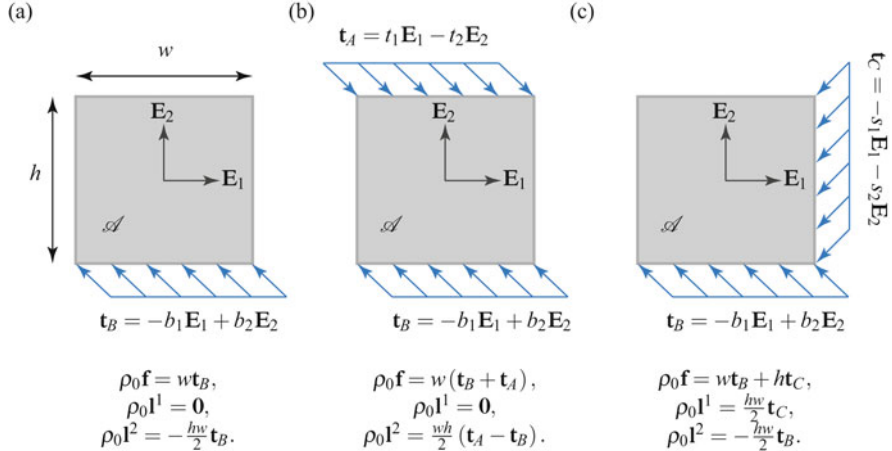


Fig. 5.9 Three examples of the computation of $\rho_0 \mathbf{f}$ and $\rho_0 \mathbf{l}^\alpha$ using Eqn. (5.69) (or, equivalently, Eqn. (7.38)). The cross section \mathcal{A} of the rod in the present configuration is assumed to be rectangular in shape with $\mathbf{d}_1 = \mathbf{E}_1$ and $\mathbf{d}_2 = \mathbf{E}_2$ in the examples shown. The corresponding moments \mathbf{m}_a are presented in Eqn. (5.74).

$$\oint_{\partial \mathcal{A}} \mathbf{q} du = \int_{-w/2}^{w/2} \mathbf{q} dx_1 + \int_{-h/2}^{h/2} \mathbf{q} dx_2 - \int_{w/2}^{-w/2} \mathbf{q} dx_1 - \int_{h/2}^{-h/2} \mathbf{q} dx_2 \\ = \int_{-w/2}^{w/2} \mathbf{q} dx_1 + \int_{-h/2}^{h/2} \mathbf{q} dx_2 + \int_{-w/2}^{w/2} \mathbf{q} dx_1 + \int_{-h/2}^{h/2} \mathbf{q} dx_2, \quad (5.72)$$

where \mathbf{q} is an arbitrary integrable function and the arc-length parameter $du = \pm dx_1$ or $du = \pm dx_2$. For all three examples shown in Figure 5.9, suppose a gravitational force in the $-\mathbf{E}_2$ direction acts on the rod, then the corresponding assigned forces are

$$\rho_0 \mathbf{f} = -\rho_0 g \mathbf{E}_2, \quad \rho_0 \mathbf{l}^1 = \mathbf{0}, \quad \rho_0 \mathbf{l}^2 = \mathbf{0}. \quad (5.73)$$

We take this opportunity to note that prescriptions for $\rho_0 \mathbf{f}$ of the type presented here were previously used in the examples discussed in Chapter 2 for strings. Other instances of the prescriptions (5.69) can be found in the application of Green and Naghdi's rod theory to contact problems in [247, 251].

For the moment \mathbf{m}_a associated with the assigned force and assigned director forces in Figure 5.9, we assume for simplicity that the present configurations are such that $\mathbf{d}_1 = \mathbf{E}_1$ and $\mathbf{d}_2 = \mathbf{E}_2$. Then, using the prescription (5.71) for \mathbf{m}_a , we find for the respective examples that

$$\begin{aligned} \mathbf{m}_a &= -\frac{1}{2} h w b_1 \mathbf{E}_3, \\ \mathbf{m}_a &= -\frac{1}{2} h w (b_1 + t_1) \mathbf{E}_3, \\ \mathbf{m}_a &= -\frac{1}{2} h w (b_1 + s_2) \mathbf{E}_3. \end{aligned} \quad (5.74)$$

As expected these moments are clockwise. It is also comforting to observe that if the applied tractions in Figure 5.9(b) are such that $t_1 = -b_1$, then the assigned moment will vanish (as expected).

As with the earlier developments of the theory of an elastic string, here we are motivated by the works of Green and Naghdi [132] and Marshall and Naghdi [230], among others, and admit singular supplies at a specific material point $\xi = \gamma(t)$.¹⁶ The four supplies are those for momentum, \mathbf{F}_γ , material momentum, \mathbf{B}_γ , angular momentum relative to O , \mathbf{M}_{O_γ} , and energy rate, Φ_{E_γ} . For a rod theory incorporating growth or decay, one could also consider supplies of mass and inertia but we do not consider these here.

5.7.2 Conservation Laws

We adopt the following balance laws for any fixed material segment (ξ_1, ξ_2) of the material curve. First, we record the conservations of mass and inertia:

$$\begin{aligned} \frac{d}{dt} \int_{\xi_1}^{\xi_2} \rho \mu d\xi &= 0, \\ \frac{d}{dt} \int_{\xi_1}^{\xi_2} \rho y^{0\alpha} \mu d\xi &= 0, \\ \frac{d}{dt} \int_{\xi_1}^{\xi_2} \rho y^{\alpha\beta} \mu d\xi &= 0. \end{aligned} \quad (5.75)$$

The balance of linear momentum is

$$\frac{d}{dt} \int_{\xi_1}^{\xi_2} \rho (\dot{\mathbf{r}} + y^{0\alpha} \dot{\mathbf{d}}_\alpha) \mu d\xi = \int_{\xi_1}^{\xi_2} \rho \mu \mathbf{f} d\xi + [\mathbf{n}]_{\xi_1}^{\xi_2} + \int_{\xi_1}^{\xi_2} \mathbf{F}_\gamma \delta(\xi - \gamma) d\xi, \quad (5.76)$$

where $\delta(\cdot)$ is the Dirac delta distribution. The balance of angular (or moment of) momentum relative to O is

$$\begin{aligned} \frac{d\mathbf{H}_O}{dt} &= [\mathbf{r} \times \mathbf{n} + \mathbf{m}]_{\xi_1}^{\xi_2} + \int_{\xi_1}^{\xi_2} (\mathbf{r} \times \mathbf{f} + \mathbf{d}_\alpha \times \mathbf{l}^\alpha) \rho \mu d\xi \\ &\quad + \int_{\xi_1}^{\xi_2} \mathbf{M}_{O_\gamma} \delta(\xi - \gamma) d\xi. \end{aligned} \quad (5.77)$$

As with the string, one has a balance of material momentum:

$$\frac{d}{dt} \int_{\xi_1}^{\xi_2} \mathbf{P} d\xi = [\mathbf{C}]_{\xi_1}^{\xi_2} + \int_{\xi_1}^{\xi_2} \mathbf{b} d\xi + \int_{\xi_1}^{\xi_2} \mathbf{B}_\gamma \delta(\xi - \gamma) d\xi. \quad (5.78)$$

¹⁶ For ease of exposition and without loss of generality, we assume that there is at most one such point.

One also has the balance of energy:

$$\begin{aligned} \frac{d}{dt} \int_{\xi_1}^{\xi_2} (\psi \rho \mu + T) d\xi &= [\mathbf{n} \cdot \mathbf{v} + \mathbf{m} \cdot \boldsymbol{\omega}]_{\xi_1}^{\xi_2} + \int_{\xi_1}^{\xi_2} (\mathbf{f} \cdot \mathbf{v} + \mathbf{l}^\alpha \cdot \dot{\mathbf{d}}_\alpha) \rho \mu d\xi \\ &\quad + \int_{\xi_1}^{\xi_2} \Phi_{E_\gamma} \delta(\xi - \gamma) d\xi. \end{aligned} \quad (5.79)$$

The similarities in structure between these balance laws and those we presented earlier for a string and the elastica should be noted.

5.8 Local Balance Laws and Jump Conditions

In the balance laws, we assume that there is one point of discontinuity. Consequently, with the help of the Leibnitz rule, we can follow the procedure discussed in Section 1.5.3 and establish local forms of the balance laws and jump conditions.

5.8.1 Local Balance Laws

In the interests of brevity, and because the procedure is so similar to the one we used for the string, we do not give details here of the procedure discussed to establish the following local forms of the balance laws from Eqns. (5.75)–(5.79). Instead, we just quote the final results:

$$\begin{aligned} \rho_0 &= \rho_0(\xi) = \rho \mu, \\ y^{0\alpha} &= y^{0\alpha}(\xi), \\ y^{\alpha\beta} &= y^{\alpha\beta}(\xi), \\ \rho_0 \ddot{\mathbf{r}} + \rho_0 y^{0\alpha} \ddot{\mathbf{d}}_\alpha &= \rho_0 \mathbf{f} + \frac{\partial \mathbf{n}}{\partial \xi}, \\ \mathbf{d}_1 \times \dot{\mathbf{L}}^1 + \mathbf{d}_2 \times \dot{\mathbf{L}}^2 &= \mathbf{m}_a + \frac{\partial \mathbf{m}}{\partial \xi} + \frac{\partial \mathbf{r}}{\partial \xi} \times \mathbf{n}, \\ \dot{\mathbf{P}} &= C' + \mathbf{b}, \\ \rho_0 \dot{\psi} &= \mathbf{m} \cdot \frac{\partial \boldsymbol{\omega}}{\partial \xi} + \mathbf{n} \cdot \left(\frac{\partial \mathbf{v}}{\partial \xi} - \boldsymbol{\omega} \times \frac{\partial \mathbf{r}}{\partial \xi} \right). \end{aligned} \quad (5.80)$$

To establish these laws, we used mass conservation and the linear and angular momentum balances to simplify the local form of the energy balance.¹⁷ We also used the identity $\dot{\mathbf{d}}_\alpha \cdot \mathbf{a} = (\boldsymbol{\omega} \times \mathbf{d}_\alpha) \cdot \mathbf{a} = (\mathbf{d}_\alpha \times \mathbf{a}) \cdot \boldsymbol{\omega}$ for any vector \mathbf{a} .

¹⁷ Some of the details and manipulations involved are outlined in Exercises 5.2 and 5.3.

5.8.2 Jump Conditions

From the balance laws (5.75)–(5.79), we find that the following jump conditions must hold at $\xi = \gamma(t)$:

$$\begin{aligned} [[\rho_0]]_\gamma \dot{\gamma} &= 0, \\ [[[\rho_0 y^{0\alpha}]]]_\gamma \dot{\gamma} &= 0, \\ [[[\rho_0 y^{\alpha\beta}]]]_\gamma \dot{\gamma} &= 0, \\ [[\mathbf{n} + \dot{\gamma}\mathbf{G}]]_\gamma + \mathbf{F}_\gamma &= \mathbf{0}, \\ [[[\mathbf{r} \times \mathbf{n} + \mathbf{m}]]]_\gamma + [[[\mathbf{h}_O]]]_\gamma \dot{\gamma} + \mathbf{M}_{O\gamma} &= \mathbf{0}, \\ [[[\mathbf{C} + \mathbf{P}\dot{\gamma}]]]_\gamma + \mathbf{B}_\gamma &= 0, \\ [[[\mathbf{n} \cdot \mathbf{v} + \mathbf{m} \cdot \boldsymbol{\omega}]]]_\gamma + [[[\mathbf{T} + \rho_0 \boldsymbol{\psi}]]]_\gamma \dot{\gamma} + \Phi_{E\gamma} &= 0. \end{aligned} \quad (5.81)$$

Notice that it was assumed that $[[\mathbf{r}]]_\gamma = \mathbf{0}$ and $[[\mathbf{d}_\alpha]]_\gamma = \mathbf{0}$.

We can also invoke some of the jump conditions in order to simplify those associated with momentum and energy. For example, using the identity

$$\begin{aligned} [[[\mathbf{h}_O]]]_\gamma &= [[[\mathbf{r} \times \mathbf{G} + \mathbf{d}_1 \times \mathbf{L}^1 + \mathbf{d}_2 \times \mathbf{L}^2]]]_\gamma \\ &= \mathbf{r}(\gamma, t) \times [[[\mathbf{G}]]]_\gamma + [[[\mathbf{d}_1 \times \mathbf{L}^1 + \mathbf{d}_2 \times \mathbf{L}^2]]]_\gamma, \end{aligned} \quad (5.82)$$

we can use the jump condition $[[\mathbf{n}]]_\gamma + [[[\mathbf{G}]]]_\gamma \dot{\gamma} + \mathbf{F}_\gamma = \mathbf{0}$ to express the jump condition associated with the balance of angular momentum as

$$[[[\mathbf{m}]]]_\gamma + [[[\mathbf{d}_1 \times \mathbf{L}^1 + \mathbf{d}_2 \times \mathbf{L}^2]]]_\gamma \dot{\gamma} + \mathbf{M}_{O\gamma} - \mathbf{r}(\gamma, t) \times \mathbf{F}_\gamma = \mathbf{0}. \quad (5.83)$$

The moment $\mathbf{M}_{O\gamma} - \mathbf{r}(\gamma, t) \times \mathbf{F}_\gamma$ can be interpreted as a moment relative to the point $\xi = \gamma$ on the material curve as opposed to the moment $\mathbf{M}_{O\gamma}$ relative to O .¹⁸ Consequently, we define

$$\mathbf{M}_\gamma = \mathbf{M}_{O\gamma} - \mathbf{r}(\gamma, t) \times \mathbf{F}_\gamma, \quad (5.84)$$

which is the singular supply of angular momentum relative to the material point $\xi = \gamma$ on the material curve. As with $\mathbf{M}_{O\gamma}$, the supply \mathbf{M}_γ can also be interpreted as a moment.

To simplify the jump condition arising from the energy balance, we use the jump conditions from the balances of material momentum, linear momentum, and angular momentum to show that

¹⁸ As we saw earlier for a string, the jump condition (5.83) simplifies to $\mathbf{M}_{O\gamma} - \mathbf{r}(\gamma, t) \times \mathbf{F}_\gamma = \mathbf{0}$ (i.e., $\mathbf{M}_\gamma = \mathbf{0}$ when the directors are ignored (cf. Eqn. (1.87))). As mentioned in an earlier chapter, the physical interpretation of this result is that a string can neither transmit nor resist a moment, so application of a nonzero \mathbf{M}_γ at $\xi = \gamma$ is not feasible.

$$\begin{aligned} \mathbf{B}_\gamma \dot{\gamma} + \mathbf{F}_\gamma \cdot \mathbf{v}_\gamma + \mathbf{M}_\gamma \cdot \boldsymbol{\omega}_\gamma &= -[\mathbb{P}\dot{\gamma} + \mathbf{C}]_\gamma \dot{\gamma} - [\mathbb{n} + \dot{\gamma}\mathbf{G}]_\gamma \cdot \mathbf{v}_\gamma \\ &\quad - [\mathbf{m} + (\mathbf{d}_1 \times \mathbf{L}^1 + \mathbf{d}_2 \times \mathbf{L}^2) \dot{\gamma}]_\gamma \cdot \boldsymbol{\omega}_\gamma. \end{aligned} \quad (5.85)$$

Using the definition of \mathbf{C} and repeated use of the identities (1.58) and (5.50), the right-hand side simplifies dramatically and we arrive at the identity¹⁹

$$\mathbf{B}_\gamma \dot{\gamma} + \mathbf{F}_\gamma \cdot \mathbf{v}_\gamma + \mathbf{M}_\gamma \cdot \boldsymbol{\omega}_\gamma = -[\mathbf{n} \cdot \mathbf{v} + \mathbf{m} \cdot \boldsymbol{\omega}]_\gamma - [T + \rho_0 \psi]_\gamma \dot{\gamma}. \quad (5.86)$$

With this identity, it is easy to see that the jump condition (5.81)₇ is equivalent to

$$\mathbf{B}_\gamma \dot{\gamma} + \mathbf{F}_\gamma \cdot \mathbf{v}_\gamma + \mathbf{M}_\gamma \cdot \boldsymbol{\omega}_\gamma = \Phi_{E_\gamma}. \quad (5.87)$$

As expected, if we ignore the moment term in this equation, then we arrive at the form of this identity that we found in an earlier chapter for a string.

5.9 Constitutive Relations

For the elastic rod (elastic directed curve), the constitutive relations for \mathbf{m} and \mathbf{n} are obtained by assuming that the local balance of energy (5.80)₆ is identically satisfied. The procedure we use has evident parallels to the ones used for strings in Section 1.6 of Chapter 1, for the elastica in Section 4.3.1 of Chapter 4, and, in Section 8.6 of Chapter 8, for a three-dimensional continuum.

The local form of the energy balance is

$$\rho_0 \dot{\psi} = \mathbf{m} \cdot \frac{\partial \boldsymbol{\omega}}{\partial \xi} + \mathbf{n} \cdot \left(\frac{\partial \mathbf{v}}{\partial \xi} - \boldsymbol{\omega} \times \frac{\partial \mathbf{r}}{\partial \xi} \right). \quad (5.88)$$

We also need to use the fact that $\frac{\partial \mathbf{r}}{\partial \xi}$ is the unit tangent vector which is perpendicular to \mathbf{d}_α . These facts are expressed in the constraint (5.6)₂. Differentiating this constraint we would find that

$$\frac{\partial \mathbf{v}}{\partial \xi} = \boldsymbol{\omega} \times \frac{\partial \mathbf{r}}{\partial \xi}. \quad (5.89)$$

Using our previous expression for $\dot{\psi}$ (see Eqn. (5.61)), we find that

$$\left(\rho_0 \mathbf{P} \frac{\partial \psi}{\partial \mathbf{v}} - \mathbf{m} \right) \cdot \frac{\partial \boldsymbol{\omega}}{\partial \xi} = 0. \quad (5.90)$$

¹⁹ A key calculation used to arrive at the simplification is discussed in Exercise 5.7.

Assuming that \mathbf{m} is independent of $\frac{\partial \omega}{\partial \xi}$, and that the above equation holds for all $\frac{\partial \omega}{\partial \xi}$, we conclude that

$$\mathbf{m} = \rho_0 \mathbf{P} \frac{\partial \psi}{\partial \mathbf{v}} = \sum_{i=1}^3 \rho_0 \frac{\partial \psi}{\partial v_i} \mathbf{d}_i, \quad \mathbf{n} = \sum_{i=1}^3 n_i \mathbf{d}_i, \quad (5.91)$$

where $n_i = n_i(\xi, t)$. Observe that \mathbf{n} is absent from Eqn. (5.90) and this explains why the constitutive relations for \mathbf{n} are independent of the partial derivatives of the strain energy function. The components n_k of \mathbf{n} can be considered as constraint responses whose function is to ensure that the constraints that the centerline of the rod is inextensible, and the cross sections of the rod retain their orientation relative to the centerline. We shall explore this interpretation in further detail in Section 7.11 of Chapter 7.

For the special strain energy function discussed earlier,

$$2\rho_0 \psi = EI_1 v_1^2 + EI_2 v_2^2 + \mathcal{D} v_3^2, \quad (5.92)$$

the constitutive relations for the contact moment are

$$\mathbf{m} = EI_1 v_1 \mathbf{d}_1 + EI_2 v_2 \mathbf{d}_2 + \mathcal{D} v_3 \mathbf{d}_3. \quad (5.93)$$

When the rod is undeformed in its reference configuration ($\mathbf{D}_i = \mathbf{E}_i$, and $v_{0i} = 0$), then the constitutive equations (5.93) are those discussed in Kirchhoff [185] and repeated in Love [213]. If $v_{0i} \neq 0$, then Eqn. (5.93) can also be used, provided it is understood that the total strain (relative to an undeformed reference configuration) is $v_i + v_{0i}$. When the rod has a so-called kinetic symmetry $I_1 = I_2$, the relations (5.93) simplify - this often happens for rods with circular or square cross sections.

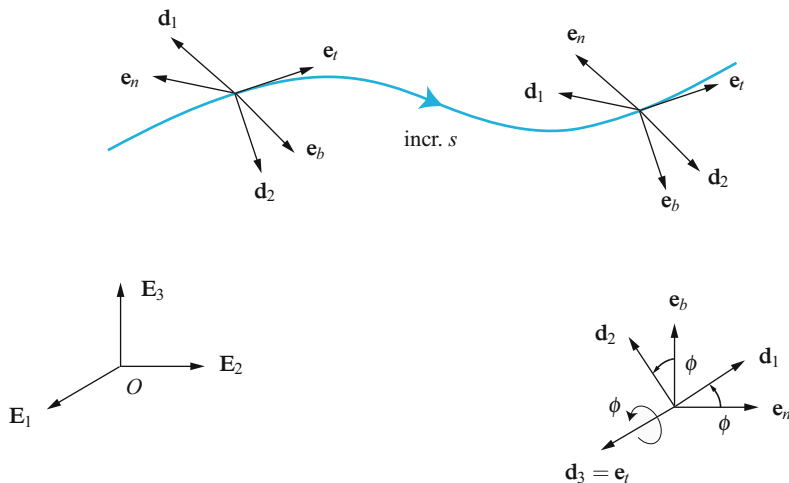


Fig. 5.10 Illustration of the evolution of the Frenet triad and the directors \mathbf{d}_1 and \mathbf{d}_2 along a directed curve.

5.10 Twist, Torsion, and Tortuosity

The material curve associated with the directed curve can, at each instant, be associated with a space curve \mathcal{S} . It is natural to question how $\mathbf{v} + \mathbf{v}_0$ and $\mathbf{P}\mathbf{P}_0$ for the directed curve is related to $\boldsymbol{\omega}_{SF}$, $\boldsymbol{\omega}_B$, and \mathbf{Q}_{SF} for \mathcal{S} . We turn to discussing these matters here.

Recall that for a space curve \mathcal{S} in Euclidean three-dimensional space \mathbb{E}^3 (see Figure 5.10), we can define the position vector of a point on the curve:

$$\mathbf{r} = \mathbf{r}(s) = x_1(s)\mathbf{E}_1 + x_2(s)\mathbf{E}_2 + x_3(s)\mathbf{E}_3. \quad (5.94)$$

The Frenet triad to this curve is the set of three vectors $\{\mathbf{e}_t, \mathbf{e}_n, \mathbf{e}_b\}$. These vectors satisfy the Serret-Frenet relations (1.2). Another set of vectors that can be defined at each point on the curve is the Bishop frame $\{\mathbf{e}_t, \mathbf{B}_1, \mathbf{B}_2\}$. You may also recall that using the Darboux vector $\boldsymbol{\omega}_{SF} = \tau\mathbf{e}_t + \kappa\mathbf{e}_b$, the Serret-Frenet relations can be expressed in a compact form. Here, τ is the geometric torsion of the space curve and κ is the curvature. The corresponding angular velocity vector associated with the Bishop frame is $\boldsymbol{\omega}_B = \kappa_{B_1}\mathbf{B}_2 - \kappa_{B_2}\mathbf{B}_1 = \kappa\mathbf{e}_b$ (cf. Eqn. (3.7)).

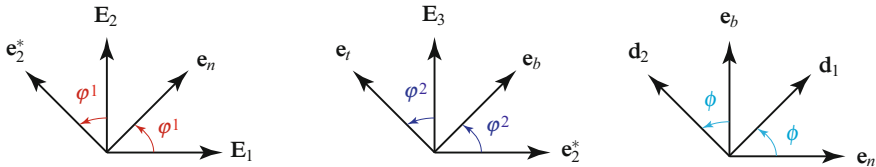


Fig. 5.11 Schematic of the three rotations used to parameterize \mathbf{Q}_{SF} and \mathbf{Q}_t (cf. Eqn. (5.97)). The unit vector $\mathbf{e}_2^* = \cos(\varphi^1)\mathbf{E}_2 - \sin(\varphi^1)\mathbf{E}_1$. The rotations used in the parameterization are equivalent to the parameterization of the compound rotation $\mathbf{Q}_t\mathbf{Q}_{SF}$ using a set of 3-1-3 Euler angles.

Now, the directors associated with (Kirchhoff's) directed curve remain tangent to the centerline: $\frac{\partial \mathbf{r}}{\partial \xi} = \mathbf{e}_t$. Consequently, \mathbf{e}_n and \mathbf{e}_b are coplanar with \mathbf{d}_1 and \mathbf{d}_2 . We can therefore deduce that

$$\mathbf{d}_1 = \mathbf{Q}_t \mathbf{e}_n, \quad \mathbf{d}_2 = \mathbf{Q}_t \mathbf{e}_b, \quad (5.95)$$

where \mathbf{Q}_t is a rotation tensor corresponding to a rotation about the unit tangent vector \mathbf{e}_t through an angle ϕ . This rotation tensor has multiple equivalent representations:

$$\begin{aligned} \mathbf{Q}_t &= \mathbf{Q}_E(\phi, \mathbf{e}_t) \\ &= \mathbf{d}_1 \otimes \mathbf{e}_n + \mathbf{d}_2 \otimes \mathbf{e}_b + \mathbf{d}_3 \otimes \mathbf{e}_t \\ &= \cos(\phi)(\mathbf{d}_1 \otimes \mathbf{d}_1 + \mathbf{d}_2 \otimes \mathbf{d}_2) + \sin(\phi)(\mathbf{d}_2 \otimes \mathbf{d}_1 - \mathbf{d}_1 \otimes \mathbf{d}_2) + \mathbf{d}_3 \otimes \mathbf{d}_3 \\ &= \cos(\phi)(\mathbf{e}_n \otimes \mathbf{e}_n + \mathbf{e}_b \otimes \mathbf{e}_b) + \sin(\phi)(\mathbf{e}_b \otimes \mathbf{e}_n - \mathbf{e}_n \otimes \mathbf{e}_b) + \mathbf{e}_t \otimes \mathbf{e}_t. \end{aligned} \quad (5.96)$$

Here, ϕ is a counterclockwise angle of rotation and the function \mathbf{Q}_E was defined earlier in Eqn. (5.14).

Several results now follow immediately:

$$\mathbf{P}\mathbf{P}_0 = \mathbf{Q}_t\mathbf{Q}_{SF}, \quad (5.97)$$

where

$$\mathbf{Q}_{SF} = \mathbf{e}_t \otimes \mathbf{E}_3 + \mathbf{e}_n \otimes \mathbf{E}_1 + \mathbf{e}_b \otimes \mathbf{E}_2. \quad (5.98)$$

We parameterize \mathbf{Q}_{SF} with a pair of rotations illustrated in Figure 5.11:

$$\mathbf{Q}_{SF} = \mathbf{Q}_E(\varphi^2, \mathbf{e}_n) \mathbf{Q}_E(\varphi^1, \mathbf{E}_3), \quad (5.99)$$

where

$$\mathbf{e}_n = \cos(\varphi^1) \mathbf{E}_1 + \sin(\varphi^1) \mathbf{E}_2. \quad (5.100)$$

Further, using methods similar to what was used earlier with the 3-2-3 set of Euler angles, we can conclude that

$$\mathbf{P}(\mathbf{v} + \mathbf{v}_0) = \boldsymbol{\omega}_{SF} + \frac{\partial \phi}{\partial s} \mathbf{e}_t = \boldsymbol{\omega}_B + \left(\tau + \frac{\partial \phi}{\partial s} \right) \mathbf{e}_t. \quad (5.101)$$

Hence,

$$\begin{aligned} v_3 + v_{0_3} &= \tau + \frac{\partial \phi}{\partial s} = \frac{\partial \varphi^1}{\partial s} \cos(\varphi^2) + \frac{\partial \phi}{\partial s}, \\ v_1 + v_{0_1} &= \kappa \sin(\phi) = \frac{\partial \varphi^1}{\partial s} \sin(\varphi^2) \sin(\phi) + \frac{\partial \varphi^2}{\partial s} \cos(\phi), \\ v_2 + v_{0_2} &= \kappa \cos(\phi) = \frac{\partial \varphi^1}{\partial s} \sin(\varphi^2) \cos(\phi) - \frac{\partial \varphi^2}{\partial s} \sin(\phi). \end{aligned} \quad (5.102)$$

In the context of the differential geometry of curves on surfaces, the relations (5.102) are known as Bonnet's theorem and Meusnier's theorem, respectively (see [188]). For Kirchhoff's rod theory, they were first written down by Love in 1892 (see [213, Section 253]). Here, we have supplemented his relations with a representation using φ^1 and φ^2 . We observe from the relation (5.102)₁ that if $v_3 + v_{0_3} = 0$, then the frame $\{\mathbf{e}_t, \mathbf{d}_1, \mathbf{d}_2\}$ can be considered a Bishop frame.

It is a common error to assume that $\tau = v_3 + v_{0_3}$. We follow Love and call ϕ the angle of twist. To interpret ϕ in this manner, imagine a straight rod ($\tau = 0$) and twist it between its ends. Possibly to avoid confusion with (geometric) torsion, Love defines the tortuosity Σ as $\Sigma = \frac{1}{\tau}$ and uses Σ exclusively (see Table 5.1).

Referring to our earlier discussion in Section 1.3.4 from Chapter 1, φ^2 will be constant for a helix:

$$\cos(\varphi^2) = R\alpha \frac{\partial \theta}{\partial s} = R \tan(\gamma) \frac{\partial \theta}{\partial s}. \quad (5.103)$$

Table 5.1 The notation of Love [213, Chapter XVIII] and its correlation to the notation used in this book.

Love's notation	Our notation	Terminology
Σ	$\frac{1}{t}$	tortuosity
f	$\phi - \frac{3\pi}{2} + 2n\pi$	angle of twist
ψ	α^1	Euler angle
θ	α^2	Euler angle
ϕ	α^3	Euler angle
κ	v_1	bending strain
κ'	v_2	bending strain
τ	v_3	torsional strain
ρ	$\frac{1}{\kappa}$	radius of curvature
N	$\mathbf{n} \cdot \mathbf{d}_1$	shear force
N'	$\mathbf{n} \cdot \mathbf{d}_2$	shear force
T	$\mathbf{n} \cdot \mathbf{e}_t$	tension
A, B , and C	EI_2, EI_1 , and \mathcal{D}	rigidities

In addition, from the relations (5.102) and the earlier representation (1.34) for ω_{SF} , we conclude that

$$\kappa = \frac{\partial \varphi^1}{\partial s} \sin(\varphi^2), \quad \tau = \frac{\partial \varphi^1}{\partial s} \cos(\varphi^2), \quad \frac{\partial \theta}{\partial s} = \frac{\partial \varphi^1}{\partial s}. \quad (5.104)$$

The angle θ in this discussion was used in the representation $\mathbf{r} = R\mathbf{e}_r + R\alpha\theta\mathbf{E}_3$ that appeared throughout Chapter 1.

5.11 Summary of the Governing Equations for Kirchhoff's Rod Theory

To summarize the equations governing Kirchhoff's rod theory, we have the following jump conditions:

$$\begin{aligned} [[\mathbf{r}]]_\gamma &= \mathbf{0}, & [[\mathbf{P}\mathbf{P}_0]]_\gamma &= \mathbf{0}, \\ [[\rho_0]]_\gamma \dot{\gamma} &= 0, & [[[\rho_0 y^{0\alpha}]]_\gamma \dot{\gamma}] &= 0, & [[[\rho_0 y^{\alpha\beta}]]_\gamma \dot{\gamma}] &= 0, \\ [[\mathbf{n} + \mathbf{G}\dot{\gamma}]]_\gamma + \mathbf{F}_\gamma &= \mathbf{0}, \\ [[\mathbf{C} + \mathbf{P}\dot{\gamma}]]_\gamma + \mathbf{B}_\gamma &= 0, \\ [[\mathbf{m}]]_\gamma + [[[\mathbf{d}_1 \times \mathbf{L}^1 + \mathbf{d}_2 \times \mathbf{L}^2]]_\gamma \dot{\gamma}] + \mathbf{M}_\gamma &= \mathbf{0}. \end{aligned} \quad (5.105)$$

These are supplemented by the partial differential equations

$$\dot{\mathbf{G}} = \rho_0 \mathbf{f} + \frac{\partial \mathbf{n}}{\partial \xi},$$

$$\rho_0 \left(\sum_{\alpha=1}^2 \mathbf{d}_\alpha \times y^{0\alpha} \ddot{\mathbf{r}} + \sum_{\alpha=1}^2 \sum_{\beta=1}^2 \mathbf{d}_\alpha \times y^{\alpha\beta} \ddot{\mathbf{d}}_\beta \right) = \mathbf{m}_a + \frac{\partial \mathbf{m}}{\partial \xi} + \frac{\partial \mathbf{r}}{\partial \xi} \times \mathbf{n}. \quad (5.106)$$

To close this system of equations, constitutive relations for \mathbf{m} need to be supplied while \mathbf{n} is considered to be indeterminate:

$$\mathbf{m} = \rho_0 \mathbf{P} \frac{\partial \psi}{\partial \mathbf{v}} = \sum_{i=1}^3 \rho_0 \frac{\partial \psi}{\partial v_i} \mathbf{d}_i, \quad \mathbf{n} = \sum_{i=1}^3 n_i \mathbf{d}_i. \quad (5.107)$$

The jump condition arising from the energy balance is not listed above as it is used to relate the mechanical powers of the singular supplies:

$$\mathbf{B}_\gamma \dot{\gamma} + \mathbf{F}_\gamma \cdot \mathbf{v}_\gamma + \mathbf{M}_\gamma \cdot \boldsymbol{\omega}_\gamma = \Phi_{E_\gamma}. \quad (5.108)$$

Given the appropriate boundary and initial conditions, the preceding equations serve to enable the calculation of \mathbf{r} and \mathbf{P} (or equivalently \mathbf{d}_α) for a directed curve.

5.12 Relation to the Theory of the Elastica

We may consider the elastica as a restricted theory. The adjective “restricted” is used here in the sense that the rod’s motion is planar and torsional deformations, among others, are not accommodated. An alternative viewpoint is to consider the theory as a member of a hierarchy of constrained theories. From this perspective, we note that the theory of the elastica presented in Chapter 4 can also be obtained from Kirchhoff’s theory by assuming that the motion of the material curve is planar, $\mathbf{r} = x\mathbf{E}_1 + z\mathbf{E}_3$, that the rotation tensor $\mathbf{P}_0 = \mathbf{I}$, and that the rotation tensor \mathbf{P} corresponds to a rotation about $\mathbf{E}_2 = \mathbf{D}_2$ through an angle θ :

$$\begin{aligned} \mathbf{P} &= \mathbf{d}_1 \otimes \mathbf{E}_1 + \mathbf{d}_2 \otimes \mathbf{E}_2 + \mathbf{d}_3 \otimes \mathbf{E}_3 \\ &= \cos(\theta) (\mathbf{d}_1 \otimes \mathbf{d}_1 + \mathbf{d}_3 \otimes \mathbf{d}_3) + \sin(\theta) (\mathbf{d}_1 \otimes \mathbf{d}_3 - \mathbf{d}_3 \otimes \mathbf{d}_1) + \mathbf{d}_2 \otimes \mathbf{d}_2. \end{aligned} \quad (5.109)$$

One also needs to make the identifications $\mathbf{E}_1 \rightarrow \mathbf{A}_2$, $\mathbf{E}_2 \rightarrow \mathbf{A}_3$, and $\mathbf{E}_3 \rightarrow \mathbf{A}_1$. The vectors associated with the rotation \mathbf{P} are

$$\boldsymbol{\omega} = \dot{\theta} \mathbf{E}_2, \quad \mathbf{P}\mathbf{v} = v_2 \mathbf{E}_2 = \theta' \mathbf{E}_2. \quad (5.110)$$

Further, the inertias $y^{0\alpha}$ and $y^{12} = y^{21}$ are set to zero.

It is interesting to note that when the motion of the Kirchhoff rod is planar, then the frame $\{\mathbf{e}_i, \mathbf{d}_1, \mathbf{d}_2\}$ is a Bishop frame with $\kappa_{B_1} = \theta'$ and $\kappa_{B_2} = 0$ for the space curve \mathcal{S} occupied by the material curve \mathcal{L} in the present configuration.

5.13 A Terminally Loaded Rod and a Kinetic Analogue

As a first application of the rod theory, we consider a stationary inextensible rod of length ℓ which is loaded by forces at its ends²⁰:

$$\mathbf{n}(0^+, t) = -\mathbf{F}_0, \quad \mathbf{n}(\ell^-, t) = -\mathbf{F}_0, \quad (5.111)$$

where \mathbf{F}_0 is constant. Supplementing these conditions are three independent conditions from the following twelve boundary values:

$$\alpha^k(0^+, t), \quad \alpha^k(\ell^-, t), \quad v_k(0^+, t), \quad v_k(\ell^-, t). \quad (5.112)$$

For example, if a rod is clamped at $\xi = 0$ and free from external moments at $\xi = \ell$, then $\alpha^k(0^+, t)$ are prescribed, and, with the possible help of constitutive relations (5.91), $v_k(\ell^-, t)$ are prescribed. Alternatively, if a moment \mathbf{M}_ℓ is applied at $\xi = \ell$, then $\mathbf{m}(\ell^-, t) = \mathbf{M}_\ell$ and Eqn. (5.91) are used to prescribe $v_k(\ell^-, t)$.

In the absence of assigned body forces and moments (i.e., $\mathbf{f} = \mathbf{0}$ and $\mathbf{m}_a = \mathbf{0}$) and assuming the problem at hand remains static, we can solve for \mathbf{n} from the local form of the balance of linear momentum (5.106)₁:

$$\mathbf{n}(\xi) = -\mathbf{F}_0, \quad \xi \in (0, \ell). \quad (5.113)$$

The local form of the balance of angular momentum (5.106)₂ reduces to

$$\frac{\partial \mathbf{m}}{\partial \xi} = \frac{\partial \mathbf{r}}{\partial \xi} \times \mathbf{F}_0. \quad (5.114)$$

Indeed, the balance laws (5.106) both yield conservations:

$$\mathbf{n}' = \mathbf{0}, \quad (\mathbf{m} + \mathbf{r} \times \mathbf{n})' = \mathbf{0}. \quad (5.115)$$

That is, the contact force \mathbf{n} and the contact moment relative to a fixed point O are both constant functions of ξ . If the rod is homogeneous, as shown in Exercise 5.5, $b_p = 0$, and we have the additional conservation

$$C' = 0, \text{ where } C = \rho_0 \psi - \mathbf{n} \cdot \mathbf{r}' - \mathbf{m} \cdot (\mathbf{P}(\mathbf{v} + \mathbf{v}_0)). \quad (5.116)$$

We emphasize that the conservations (5.115) apply independently of the form of the strain energy function $\rho_0 \psi$.

Assuming that the strain energy function of the rod is (cf. Eqn. (5.64))

$$2\rho_0 \psi = EI_1 v_1^2 + EI_2 v_2^2 + \mathcal{D} v_3^2, \quad (5.117)$$

we find using Eqn. (5.107)₁ that

$$\mathbf{m} = EI_1 v_1 \mathbf{d}_1 + EI_2 v_2 \mathbf{d}_2 + \mathcal{D} v_3 \mathbf{d}_3. \quad (5.118)$$

²⁰ The jump conditions $[\![\mathbf{n}]\!]_\gamma + \mathbf{F}_\gamma = \mathbf{0}$ and $[\![\mathbf{m}]\!]_\gamma + \mathbf{M}_\gamma = \mathbf{0}$ where $\gamma = 0$ and $\gamma = \ell$ are used to compute the boundary conditions on \mathbf{n} and \mathbf{m} .

Taking the \mathbf{d}_i components of the balance of angular momentum leads to three scalar equations for $v_k(\xi)$:

$$\begin{aligned} (EI_1 v_1)' - (EI_2 - \mathcal{D}) v_2 v_3 &= -\mathbf{F}_0 \cdot \mathbf{d}_2, \\ (EI_2 v_2)' - (\mathcal{D} - EI_1) v_3 v_1 &= \mathbf{F}_0 \cdot \mathbf{d}_1, \\ (\mathcal{D} v_3)' - (EI_1 - EI_2) v_1 v_2 &= 0. \end{aligned} \quad (5.119)$$

To determine the deformed state of the rod, the differential equations (5.119) are supplemented by an appropriate combination of six boundary conditions on the Euler angles α^k and the strains v_k , an Euler angle parameterization of the rotation tensor \mathbf{P} , and a description of the reference configuration of the rod. For instance, if a 3-2-3 set of Euler angles are used to parameterize \mathbf{P} then the differential equations (5.119) are supplemented by the ordinary differential equations (5.29) relating v_k to the rates of change of the Euler angles.

5.13.1 Kirchhoff's Kinetic Analogue

The equations (5.119) are identical in form to Euler's equations for the motion of a rigid body which is free to rotate about a fixed point O where the body is subject to a force \mathbf{F}_0 acting at the center of mass \bar{X} and the position of the center of mass is a unit length along one of the principal axes of the rigid body. This correspondence is known as the kinetic analogue and was first noted by Kirchhoff in his seminal paper [185] from 1859. It has enabled researchers, such as the authors of [164, 170, 178, 319], to leverage the considerable body of work on rigid body dynamics problems such as the Lagrange top, the asymmetric top, and the moment-free motion of a rigid body to gain insight into $\mathbf{d}_k(\xi)$ (see Figure 5.12). Indeed, in some of the applications considered in the remainder of this chapter, the kinetic analogue will play a prominent role.

As with the corresponding analogue for the elastica that was discussed in Section 4.4 of Chapter 4, once \mathbf{P} is known, it remains to integrate $\mathbf{r}' = \mathbf{d}_3$ with respect to ξ to determine the shape $\mathbf{r}(\xi)$ of the deformed material curve. Recently, it has come to be appreciated that this integration is greatly facilitated by conservation laws.²¹ To elaborate, \mathbf{n} is constant for the terminally loaded rod and so the local form of the balance of angular momentum (5.115)₂ can be integrated:

$$\mathbf{m} - \mathbf{r} \times \mathbf{F}_0 = \mathbf{c}, \quad (5.120)$$

²¹ The reader is referred to Kehrbaum and Maddocks [178] for a lucid discussion of this integration along with commentary on the works of Ilyukhin [170], Langer and Singer [196], and Shi and Hearst [319].

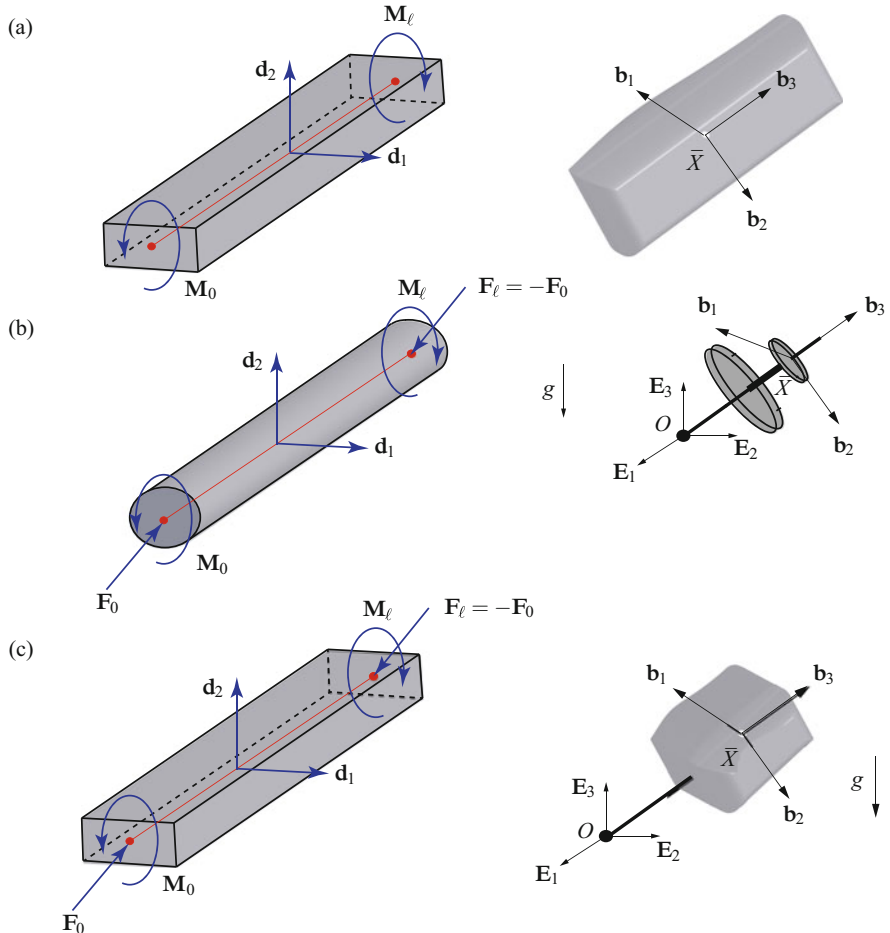


Fig. 5.12 Three cases of Kirchhoff's kinetic analogue: (a), moment-free motion of a rigid body is analogous to a rod deformed by the action of (terminally applied) moments; (b), motion of a heavy symmetric top (Lagrange top) that is connected to a fixed point O by a ball and socket joint and is subject to a gravitational loading is analogous to a rod with $I_1 = I_2$ deformed by terminally applied forces and moments; and (c), motion of an asymmetric heavy rigid body that is connected to a fixed point O by a ball and socket joint and is subject to a gravitational loading is analogous to a terminally loaded rod which has distinct flexural and torsional stiffnesses. The body-fixed basis $\{\mathbf{b}_1, \mathbf{b}_2, \mathbf{b}_3\}$ corotates with the rigid body. In Kirchhoff's kinetic analogue, the behavior of $\mathbf{b}_k(t)$ is placed in one-to-one correspondence with the vectors \mathbf{d}_i ; $\mathbf{b}_i = \mathbf{d}_i$ and $\xi = t$.

where \mathbf{c} is a constant. If we temporarily choose the fixed right-handed orthogonal basis $\{\mathbf{A}_1, \mathbf{A}_2, \mathbf{A}_3\}$ such that $\mathbf{F}_0 = -n\mathbf{A}_3$, then

$$X = \mathbf{r} \cdot \mathbf{A}_1 = \frac{1}{n} (\mathbf{m} - \mathbf{c}) \cdot \mathbf{A}_2, \quad Y = \mathbf{r} \cdot \mathbf{A}_2 = -\frac{1}{n} (\mathbf{m} - \mathbf{c}) \cdot \mathbf{A}_1. \quad (5.121)$$

Whence, if $\mathbf{m}(\xi)$ is known, then the plane projection of \mathbf{r} can be determined immediately. By way of contrast, the \mathbf{A}_3 component of \mathbf{r} is then obtained by integrating $\mathbf{r}' \cdot \mathbf{A}_3$ with respect to ξ . In applications of the rod theory to terminally loaded rods where $\rho_0 \psi$ is given by the classic functional form (5.64) with $EI_1 = EI_2$, the relations (5.121) are used to explain why the planar projection of \mathbf{r} is bounded to lie in a circular domain (cf. [319, Page 5191]).

5.14 The Simplest Problem: Bending and Torquing into a Helical Shape

As one of our first applications of Kirchhoff's rod theory, let us consider a homogeneous, linearly elastic, inextensible rod where $I_1 = I_2$. The rod is loaded at its ends by a pair of constant moments:

$$\mathbf{F}_0 = -\mathbf{0}, \quad \mathbf{M}_0 = -\mathbf{M}_A, \quad \mathbf{F}_\ell = \mathbf{0}, \quad \mathbf{M}_\ell = \mathbf{M}_B. \quad (5.122)$$

It is preferable at this point not to provide any additional details on $\mathbf{M}_{A,B}$. We now proceed to establish the classic result that the deformed shape of the centerline of the rod is a helical space curve and the rod has a constant twist. This result is a natural extension to the corresponding result for an elastica: the centerline of an elastica loaded at its ends with equal and opposite applied moments will have the shape of a circular arc.²²

The assumption that $EI_1 = EI_2 = EI$ enables the governing equations for $v_k(\xi)$ to simplify dramatically from (5.119):

$$\begin{aligned} v'_1 - (1 - \beta) v_2 v_3 &= 0, \\ v'_2 - (\beta - 1) v_3 v_1 &= 0, \\ v'_3 &= 0. \end{aligned} \quad (5.123)$$

We have introduced a parameter

$$\beta = \frac{\mathcal{D}}{EI}, \quad (5.124)$$

which is the ratio of torsional to bending stiffnesses in the rod. For a rod with a circular cross section of radius r , $\mathcal{D} = \frac{EI}{2(1+\nu)}$ where ν is Poisson's ratio and $I = \frac{\pi r^4}{2}$, and so $\beta \leq 0.5$.

The equations (5.123) have an exact solution:

$$\begin{bmatrix} v_1(\xi) \\ v_2(\xi) \end{bmatrix} = \begin{bmatrix} \cos(\delta\xi) & \sin(\delta\xi) \\ -\sin(\delta\xi) & \cos(\delta\xi) \end{bmatrix} \begin{bmatrix} v_1(0) \\ v_2(0) \end{bmatrix}, \quad (5.125)$$

²² See the discussion pertaining to Exercise 4.2 on Page 183.

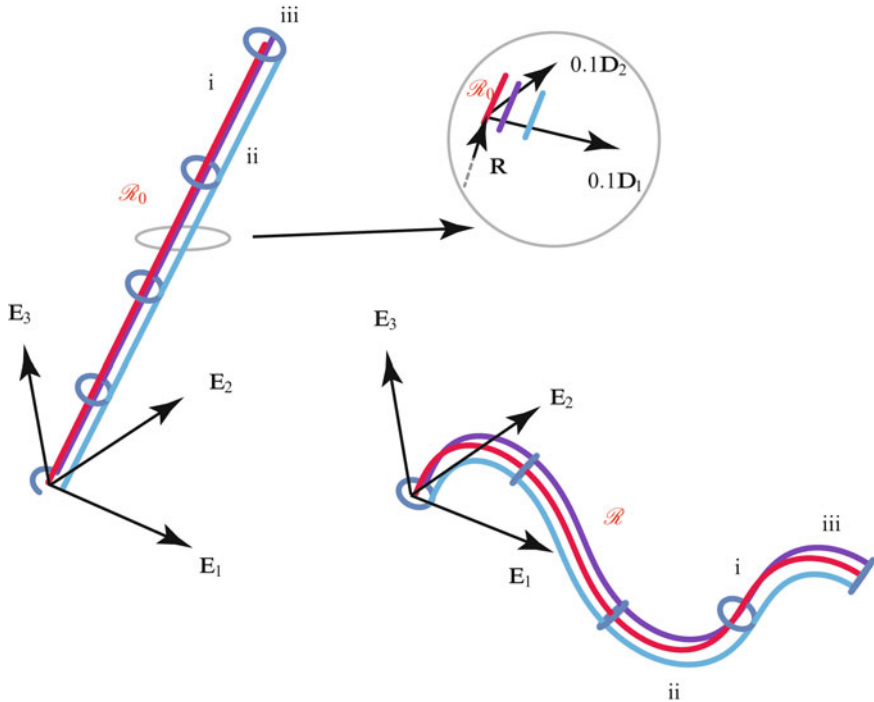


Fig. 5.13 Representative examples of the deformation of material curves from the bending and twisting of a rod with terminal moments. Reference and present configurations of three material curves are shown: (i) $\mathbf{R}(\xi)$, (ii) $\mathbf{R} + 0.1\mathbf{D}_1$, and (iii) $\mathbf{R} + 0.1\mathbf{D}_2$ are the chosen curves in the reference configuration. Their counterparts in the present configuration are (i) $\mathbf{r}(\xi)$, (ii) $\mathbf{r} + 0.1\mathbf{d}_1$, and (iii) $\mathbf{r} + 0.1\mathbf{d}_2$. The inset image shows the directors in the reference configuration \mathcal{R}_0 shows the material curve \mathcal{L} in the reference configuration \mathcal{R}_0 is deformed into a helical curve in the present configuration.

where

$$v_3(\xi) = v_3(0), \quad \delta = (1 - \beta) v_3(0). \quad (5.126)$$

To interpret the resulting shape of the material line, we first rewrite the solutions for $v_\alpha(\xi)$ as

$$\begin{aligned} v_1(\xi) &= \sqrt{v_1^2(0) + v_2^2(0)} \sin(\delta\xi + \varphi_0), \\ v_2(\xi) &= \sqrt{v_1^2(0) + v_2^2(0)} \cos(\delta\xi + \varphi_0), \end{aligned} \quad (5.127)$$

where the angle φ_0 is given by

$$\tan(\varphi_0) = \frac{v_1(0)}{v_2(0)}. \quad (5.128)$$

Appealing to Bonnet and Meusnier's theorems (5.102) from Section 5.10, we conclude that the space curve formed by the material curve is a helix with a curvature κ and torsion τ which are given by the following expressions:

$$\begin{aligned}\kappa &= \sqrt{v_1^2(\xi) + v_2^2(\xi)} = \sqrt{v_1^2(0) + v_2^2(0)}, \\ \tau &= v_3(\xi) - \frac{\partial \phi}{\partial \xi} = \beta v_3(0) = \left(\frac{\mathcal{D}}{EI} \right) v_3(0).\end{aligned}\quad (5.129)$$

In addition, the angle of twist of the rod is

$$\phi(\xi) = \delta\xi + \phi(0) = \left(1 - \frac{\mathcal{D}}{EI} \right) v_3(0)\xi + \phi(0), \quad \phi_0 = \phi(0). \quad (5.130)$$

Thus, under terminal moments, the centerline of the rod deforms into a circular helix and the directors twist about the helical curve at a constant rate. The torques needed to achieve this state can be computed with the help of the constitutive relations:

$$\begin{aligned}\mathbf{M}_A &= -EI(v_1(0)\mathbf{d}_1(0) + v_2(0)\mathbf{d}_2(0)) - \mathcal{D}v_3(0)\mathbf{d}_3(0), \\ \mathbf{M}_B &= EI(v_1(\ell)\mathbf{d}_1(\ell) + v_2(\ell)\mathbf{d}_2(\ell)) + \mathcal{D}v_3(0)\mathbf{d}_3(\ell).\end{aligned}\quad (5.131)$$

The radius R and parameter α for the helical curve formed by the centerline can be found from Eqn. (5.129) with the help of Eqn. (1.35): we leave this as an exercise for the interested reader.

As an example of a rod twisted into a helical form, consider the initially straight rod shown in Figure 5.13. The rod in question is assumed to have the material properties

$$\beta = \frac{\mathcal{D}}{EI} = 0.5, \quad \ell = 4. \quad (5.132)$$

To avoid singularities in the 3-2-3 Euler angles that are used to parameterize $\mathbf{d}_k(\xi)$, the reference configuration is chosen so that $\mathbf{R}(\xi)$ describes a straight line, $\mathbf{P}_0 = \mathbf{I}$, and the rotation tensor \mathbf{P} is a constant rotation with $\alpha^1 = \alpha^3 = 0$ and $\alpha^2 = \frac{\pi}{8}$. The end $\xi = 0$ is subject to an applied moment,

$$\mathbf{M}_A = -3EI\mathbf{d}_1(0) - 3\mathcal{D}\mathbf{d}_3(0), \quad (5.133)$$

and the directors are assumed to have the initial values

$$\begin{aligned}\mathbf{d}_1(0) &= \cos\left(\frac{\pi}{8}\right)\mathbf{E}_1 - \sin\left(\frac{\pi}{8}\right)\mathbf{E}_3, \\ \mathbf{d}_2(0) &= \mathbf{E}_2, \\ \mathbf{d}_3(0) &= \cos\left(\frac{\pi}{8}\right)\mathbf{E}_3 + \sin\left(\frac{\pi}{8}\right)\mathbf{E}_1.\end{aligned}\quad (5.134)$$

Integrating (5.29) and (5.123), the Euler angles α^k and, with the help of (5.19), the directors $\mathbf{d}_\alpha(\xi)$ and the tangent vector $\mathbf{r}'(\xi) = \mathbf{d}_3(\xi)$ can be computed. An additional integration of $\mathbf{d}_3(\xi)$ provides $\mathbf{r}(\xi)$. An applied moment \mathbf{M}_B at $\xi = \ell$ is

needed for equilibrium and this moment can be determined from the computed values of $v^k(\ell^-)$ and $\mathbf{d}_k(\ell^-)$. The results of these computations are displayed in Figure 5.13. In addition, to the shape of the deformed material curve \mathcal{L} , the deformed shape of two other material curves, $\mathbf{r} + 0.1\mathbf{d}_1$ and $\mathbf{r} + 0.1\mathbf{d}_2$, and five circular cross sections are shown.

It is natural to ask if helical solutions are possible for rods modeled using Kirchhoff's rod theory where the symmetry $I_1 = I_2$ is absent? The affirmative answer to this question can be found in a recent paper by Chouaieb et al. [60] where the search for helical solutions, that was initiated by Kirchhoff, is completed.

5.15 Hockling of Cables, Loop Formation, and Localized Buckling

The next set of problems we consider pertain to an initially straight rod which has the symmetry $EI_1 = EI_2$. In addition to the terminal moments that deformed the rod in the previous section, the rod is also subject to terminal forces. For this rod, depending on the loading and boundary conditions, we will find some of the helical solutions just discussed as well as more complex spatial shapes of the material curve such as those shown in Figure 5.14. These solutions find application to a wide range of models for problems including the looping and hockling of marine cables [75] and the supercoiling of DNA [319, 320]. The model we present is nonlinear. However, as discussed in Love [213, Section 272(d)] the model can be linearized to provide a model for the vibration of a shaft of finite length that is subject to combined thrust and torsion. Such a model was famously employed by Greenhill [141] in 1883 to examine the buckling instability in the driveshafts of ships.

We assume that the terminal loading is given by Eqn. (5.111), the strain energy function is prescribed as in the classic functional form (5.64), and the reference configuration is chosen so that $\mathbf{D}_i = \mathbf{E}_i$ with \mathbf{E}_3 taken to be parallel to the direction of the terminal loading:

$$\mathbf{F}_0 = F_0 \mathbf{E}_3, \quad \mathbf{F}_\ell = F_\ell \mathbf{E}_3, \quad F_0 = -F_\ell. \quad (5.135)$$

The kinetic analogue for this problem is a symmetric rigid body which is free to rotate about a fixed point O and is subject to a gravitational force (see Figure 5.12(b)). In recognition of the seminal work performed on this problem in the 1780s by Joseph-Louis Lagrange (1736–1813), the rigid body dynamics problem is known as the Lagrange top.²³ The gravitational force is analogous to the terminal load $F_\ell \mathbf{E}_3$ and the pair of conserved angular momenta are analogous to conserved components of the contact moment \mathbf{m} in the rod.

²³ Lagrange's original work is presented in [191, 192, Sections IX.34–IX.41]. Other treatments of this problem can be found in Arnold [15, Section 30], Lewis et al. [205], Marsden and Ratiu [229, Chapter 1], and Whittaker [362, Sections 71–73].

The highlights of the analysis of this example include the demonstration of buckling of a twisted, initially straight rod subject to tensile end loads and terminal moments into a pair of helical forms. We also show the evolution of the handedness of the helical forms as a loading parameter is varied and discuss the presence of a localized buckling solution corresponding to a homoclinic orbit in the state space of a reduced system governing the evolution of the Euler angle $\alpha^2(\xi)$. We are fortunate to be able to leverage a large literature on this problem and shall cite several works in the sequel. However, two aspects of our analysis are novel. First, the discussion of the changing handedness of the helical forms has not been discussed in the literature. Second, we show how the dual Euler basis can be used to obtain physically meaningful representations for the contact moment \mathbf{m} in the rod and asymptotic estimates for the terminal moments \mathbf{M}_0 and \mathbf{M}_ℓ .

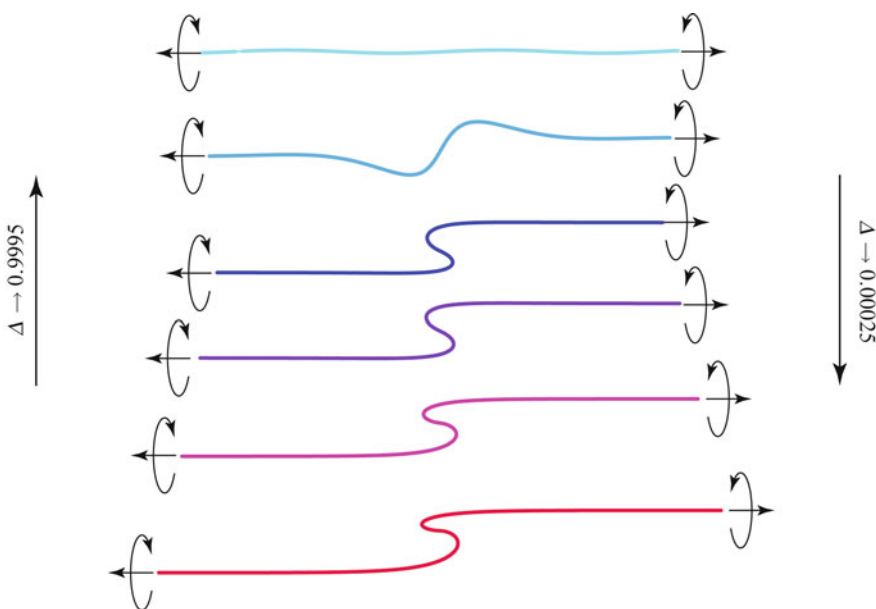


Fig. 5.14 Deformation of a twisted, initially straight rod as the terminal forces $\mathbf{F}_\ell = F_\ell \mathbf{E}_3 = -\mathbf{F}_0$ and terminal moments (proportional to a parameter c) are varied in a particular manner. The variation of the loading is captured by a dimensionless parameter $\Delta = \frac{c^2}{4F_\ell EI}$ which is decreased from 0.9995 to 0.00025 for the results shown. The planar projections of the deformed centerlines are shown in additional detail in Figure 5.18.

5.15.1 Development of the Reduced Dynamical System

The strains v_k of the rod are again governed by the differential equations (5.119) supplemented by the ordinary differential equations (5.29). However, this formulation of the equations governing the rod is not very amenable to analysis and it is more convenient to consider the components of $\frac{\partial \mathbf{m}}{\partial \xi} = -\frac{\partial \mathbf{r}}{\partial \xi} \times \mathbf{F}_\ell$ projected onto the Euler basis for the 3-2-3 set of Euler angles:

$$\{\mathbf{e}_1 = \mathbf{E}_3, \mathbf{e}_2 = \cos(\alpha^3) \mathbf{d}_2 + \sin(\alpha^3) \mathbf{d}_1, \mathbf{e}_3 = \mathbf{d}_3\}. \quad (5.136)$$

That is,

$$\begin{aligned} \frac{\partial}{\partial \xi} (\mathbf{m} \cdot \mathbf{E}_3) &= -(\mathbf{d}_3 \times F_\ell \mathbf{E}_3) \cdot \mathbf{E}_3, \\ \frac{\partial}{\partial \xi} (\mathbf{m} \cdot \mathbf{e}_2) - \mathbf{m} \cdot \mathbf{e}'_2 &= -(\mathbf{d}_3 \times F_\ell \mathbf{E}_3) \cdot \mathbf{e}_2, \\ \frac{\partial}{\partial \xi} (\mathbf{m} \cdot \mathbf{d}_3) - \mathbf{m} \cdot \mathbf{d}'_3 &= -(\mathbf{d}_3 \times F_\ell \mathbf{E}_3) \cdot \mathbf{d}_3. \end{aligned} \quad (5.137)$$

The resulting three second-order differential equations for the Euler angles are equivalent to Lagrange's equations of motion.²⁴ Expanding the components of \mathbf{m} in the above equations, one finds that

$$\begin{aligned} \frac{\partial}{\partial \xi} \left((\mathcal{D} \cos^2(\alpha^2) + EI \sin^2(\alpha^2)) \frac{\partial \alpha^1}{\partial \xi} + \mathcal{D} \cos(\alpha^2) \frac{\partial \alpha^3}{\partial \xi} \right) &= 0, \\ EI \frac{\partial^2 \alpha^2}{\partial \xi^2} + \mathcal{D} \frac{\partial \alpha^1}{\partial \xi} \frac{\partial \alpha^3}{\partial \xi} \sin(\alpha^2) + \left(\frac{\mathcal{D} - EI}{2} \right) \frac{\partial \alpha^1}{\partial \xi} \frac{\partial \alpha^1}{\partial \xi} \sin(2\alpha^2) &= F_\ell \sin(\alpha^2), \\ \frac{\partial}{\partial \xi} \left(\mathcal{D} \left(\frac{\partial \alpha^1}{\partial \xi} \cos(\alpha^2) + \frac{\partial \alpha^3}{\partial \xi} \right) \right) &= 0. \end{aligned} \quad (5.138)$$

The first and third of these equations lead to the conclusion that the following pair of components of the contact moment \mathbf{m} are conserved along the rod:

$$\begin{bmatrix} c_F = \mathbf{m} \cdot \mathbf{E}_3 \\ c_S = \mathbf{m} \cdot \mathbf{d}_3 \end{bmatrix} = \begin{bmatrix} \mathcal{D} \cos^2(\alpha^2) + EI \sin^2(\alpha^2) & \mathcal{D} \cos(\alpha^2) \\ \mathcal{D} \cos(\alpha^2) & \mathcal{D} \end{bmatrix} \begin{bmatrix} \frac{\partial \alpha^1}{\partial \xi} \\ \frac{\partial \alpha^3}{\partial \xi} \end{bmatrix}, \quad (5.139)$$

where c_F and c_S are constants. That is, the component of \mathbf{m} in the direction of \mathbf{F}_ℓ is conserved, the component of \mathbf{m} along the axis of symmetry \mathbf{d}_3 of the rod is conserved, and the moment vector \mathbf{m} has the representation²⁵

$$\mathbf{m} = c_F \mathbf{e}^1 + c_S \mathbf{e}^3 + m_2 \mathbf{e}^2, \quad (5.140)$$

²⁴ See Exercise 5.8 for further details on the Lagrangian and the specific form of Lagrange's equations of interest here.

²⁵ The application here of the dual Euler basis vectors to explain the terminal loading on the rod is novel and, to the best of our knowledge, has not appeared previously in the vast literature on terminally loaded rods.

where expressions for the dual Euler basis vectors can be found in Eqn. (5.23). Observe that the only component of \mathbf{m} that varies along the rod is in the $\mathbf{e}^2 = \mathbf{e}_2 = \cos(\alpha^3)\mathbf{d}_2 + \sin(\alpha^3)\mathbf{d}_1$ direction. It is interesting to also note that \mathbf{e}_2 is perpendicular to the axis of symmetry \mathbf{d}_3 and the applied forces $\mathbf{F}_0 = F_0\mathbf{E}_3$ and $\mathbf{F}_\ell = F_\ell\mathbf{E}_3$. As noted previously, these conservations are precisely analogous to the conservation of two distinct components of the angular momentum of a symmetric rigid body freely rotating about a fixed point while subject to a gravitational force.

Of particular interest in the sequel is the limiting behavior of the moment $c\mathbf{e}^1 + c\mathbf{e}^3$ as the angle α^2 approaches 0. As c is a constant, it suffices to compute the limiting value of the sum of the dual Euler basis vectors:

$$\lim_{\alpha^2 \rightarrow 0} (\mathbf{e}^1 + \mathbf{e}^3) = \lim_{\alpha^2 \rightarrow 0} \left(\mathbf{d}_3 - \frac{1 - \cos(\alpha^2)}{\sin(\alpha^2)} (\cos(\alpha^3)\mathbf{d}_1 - \sin(\alpha^3)\mathbf{d}_2) \right). \quad (5.141)$$

That is,

$$\lim_{\alpha^2 \rightarrow 0} (\mathbf{e}^1 + \mathbf{e}^3) = \mathbf{E}_3. \quad (5.142)$$

We shall use this result in the sequel to explore asymptotic limits of terminal moments applied to the rod.

The expressions for the conservations (5.139) can be inverted to yield $\frac{\partial \alpha^1}{\partial \xi}$ and $\frac{\partial \alpha^3}{\partial \xi}$ as functions of α^2 , \mathcal{D} , EI , c_S , and c_F :

$$\begin{bmatrix} \frac{\partial \alpha^1}{\partial \xi} \\ \frac{\partial \alpha^3}{\partial \xi} \end{bmatrix} = \begin{bmatrix} \frac{\text{cosec}^2(\alpha^2)}{EI} & -\frac{\cot(\alpha^2)\text{cosec}(\alpha^2)}{EI} \\ -\frac{\cot(\alpha^2)\text{cosec}(\alpha^2)}{EI} & \frac{1}{\mathcal{D}} + \frac{\cot^2(\alpha^2)}{EI} \end{bmatrix} \begin{bmatrix} c_F = \mathbf{m} \cdot \mathbf{E}_3 \\ c_S = \mathbf{m} \cdot \mathbf{d}_3 \end{bmatrix}. \quad (5.143)$$

Observe that once $\alpha^2(\xi)$ is known, then (5.143) can be integrated (often numerically) to determine $\alpha^1(\xi)$ and $\alpha^3(\xi)$.

To find the differential equation governing $\alpha^2(\xi)$ that accommodates the conservations of $\mathbf{m} \cdot \mathbf{E}_3$ and $\mathbf{m} \cdot \mathbf{d}_3$, we follow a classic procedure developed by Routh [305] which is known as Routhian reduction. The first step of the reduction is to use the pair of conservations (5.143) to eliminate $\frac{\partial \alpha^1}{\partial \xi}$ and $\frac{\partial \alpha^3}{\partial \xi}$ from the differential equation (5.138)₂. After some rearranging and algebraic manipulations, the following two-parameter family of ordinary differential equations for $\alpha^2(\xi)$ is obtained:

$$EI \frac{\partial^2 \alpha^2}{\partial \xi^2} + \frac{(c_F c_S (1 + \cos^2(\alpha^2)) - (c_F^2 + c_S^2) \cos(\alpha^2))}{EI \sin^3(\alpha^2)} = F_\ell \sin(\alpha^2). \quad (5.144)$$

This set of differential equations can be expressed in the compact form²⁶

$$EI \frac{\partial^2 \alpha^2}{\partial \xi^2} = -\frac{\partial U}{\partial \alpha^2}, \quad (5.145)$$

where the function

$$U = U(c_S, c_F, \alpha^2) = \frac{(c_F - c_S \cos(\alpha^2))^2}{2EI \sin^2(\alpha^2)} + F_\ell \cos(\alpha^2). \quad (5.146)$$

Analysis of Eqn. (5.144) is facilitated in the sequel both with the help of dimensionless variables,

$$x = \frac{\xi}{\hat{\ell}}, \quad \hat{c}_F = \frac{c_F \hat{\ell}}{EI}, \quad \hat{c}_S = \frac{c_S \hat{\ell}}{EI}, \quad \hat{F}_\ell = \frac{F_\ell \hat{\ell}^2}{EI}, \quad (5.147)$$

and the extensive body of work that has been performed on the corresponding differential equations for the Lagrange top. In order to accommodate rods of infinite length and to enable simplification of differential equations in the sequel, the length scale $\hat{\ell}$ will not necessarily be chosen to equal the length ℓ of the rod.

We henceforth consider instances where $c_S = c_F = c$. In this case, the moment components in the directions of \mathbf{d}_3 and \mathbf{F}_0 are equal and the differential equation (5.144) simplifies dramatically:

$$EI \frac{\partial^2 \alpha^2}{\partial \xi^2} + \frac{c^2 (1 - \cos(\alpha^2))^2}{EI \sin^3(\alpha^2)} = F_\ell \sin(\alpha^2). \quad (5.148)$$

The differential equation (5.148) is analogous to the reduced dynamical system used to demonstrate the well-known stabilization of a vertical upright top (sleeping top) as it is spun at successively faster speeds. The forthcoming bifurcation as c^2 increases corresponds to this stabilization.

5.15.2 The Straight Rod and a Pair of Rods Bent into a Helical Form

After examining the conditions governing the equilibria $(\alpha^2 = \alpha_0^2, \frac{\partial \alpha^2}{\partial \xi} = 0)$ of Eqn. (5.148), it can be shown that for $c^2 > 4F_\ell EI$ only one equilibrium is present, while for $c^2 < 4F_\ell EI$, three equilibria are present²⁷:

²⁶ This classic result can be used to show that the solutions to the second-order differential equation (5.144) conserve $\frac{EI}{2} \left(\frac{\partial \alpha^2}{\partial \xi} \right)^2 + U$ and can be expressed in terms of Weierstrassian elliptic functions. For further details on this integration and the Routhian reduction procedure that can be used to establish Eqn. (5.144), the exposition in Whittaker [362, Section 71] is highly recommended.

²⁷ For details on this calculation, see Exercise 5.9.

$$\alpha_0^2 = 0, \quad \alpha_0^2 = \pm \arccos \left(-1 + 2\sqrt{\Delta} \right). \quad (5.149)$$

Here, we have found it convenient to define a parameter Δ :

$$\Delta = \frac{c^2}{4F_\ell EI}. \quad (5.150)$$

For the equilibria where $\alpha_0^2 \neq 0$, we note from Eqn. (5.143) that $\frac{\partial \alpha^1}{\partial \xi}$ and $\frac{\partial \alpha^3}{\partial \xi}$ are constant throughout the equilibrium state of the rod:

$$\frac{\partial \alpha^1}{\partial \xi} = \alpha_0^{1'} = \frac{c}{2EI} \frac{1}{\sqrt{\Delta}}, \quad \frac{\partial \alpha^3}{\partial \xi} = \alpha_0^{3'} = \frac{c}{\mathcal{D}} - \frac{c}{EI} \left(1 - \frac{1}{2\sqrt{\Delta}} \right). \quad (5.151)$$

Referring to Figure 5.15 where the solutions are plotted, it is obvious that when $4F_\ell EI = c^2$ a (pitchfork) bifurcation occurs. For both types of equilibria, $\mathbf{n} = F_\ell \mathbf{E}_3$, and, as $\mathbf{m} \cdot \mathbf{e}_2 = EI \frac{\partial \alpha^2}{\partial \xi}$, the moment component $\mathbf{m} \cdot \mathbf{e}^2 = \mathbf{m} \cdot \mathbf{e}_2 = 0$.

For the first type of equilibrium $\mathbf{d}_3 = \mathbf{E}_3$ and the centerline of the rod is straight with $\alpha_0^2 = 0$. Invoking the identity (5.142), we conclude that the terminal moments at the ends of the rod are $\mp c \mathbf{E}_3$. We also observe that these moments are parallel to the terminal forces $\mathbf{F}_0 = -F_\ell \mathbf{E}_3 = -\mathbf{F}_\ell$. The bifurcation of this solution as Δ drops below 1 has close similarities to Greenhill's famed buckling formula for a straight rod of finite length ℓ .²⁸ Here, however, we also have the unusual situation that the terminal loadings of the rod are tensile. In other words, a combination of tensile loads and torque can produce buckling in a straight rod.

With the help of the relations (5.15) for the Euler basis vectors, for the second type of equilibrium we find that

$$\begin{aligned} \mathbf{Pv} &= \alpha_0^{1'} \mathbf{E}_3 + \alpha_0^{3'} \mathbf{d}_3 \\ &= -\alpha_0^{1'} \sin(\alpha_0^2) \cos(\alpha^3) \mathbf{d}_1 + \alpha_0^{1'} \sin(\alpha_0^2) \sin(\alpha^3) \mathbf{d}_2 \\ &\quad + \left(\alpha_0^{3'} + \cos(\alpha_0^2) \alpha_0^{1'} \right) \mathbf{d}_3. \end{aligned} \quad (5.152)$$

Invoking Bonnet and Meusnier's theorems (5.102) from Section 5.10, using the fact that

$$1 + \cos(\alpha_0^2) = 2\sqrt{\Delta} = \sqrt{\frac{c^2}{F_\ell EI}}, \quad (5.153)$$

and employing the relations (5.139), it can be shown that the centerline of the rod has constant curvature and constant torsion and that the directors twist at a constant rate about this centerline:

²⁸ Greenhill's development of [141, Eqn.(1)] forms the basis for Exercise 5.12 at the end of this chapter. We note that the bifurcation at hand cannot be predicted as a limit of his criterion (see Eqn. (5.252)) when the length of the rod $\ell \rightarrow \infty$.

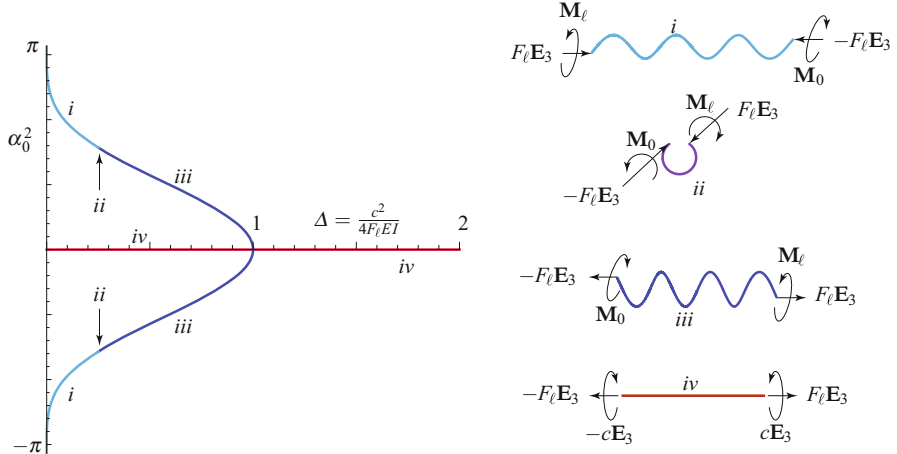


Fig. 5.15 The equilibria α_0^2 of Eqn. (5.148) as a function of the dimensionless parameter $\Delta = \frac{c^2}{4F_\ell EI}$ when $c = c_S = c_F$. The trivial branch corresponds to the straight equilibrium of the rod (labeled *iv* in the figure). For $\Delta < 1/4$, the nontrivial branches correspond to rods whose centerlines are helical curves (labeled *i* in the figure). As $\Delta = 1/4$, the centerlines of these rods become plane circles (labeled *ii* in the figure), and we observe that the helical curves (labeled *iii* in the figure) now change handedness as Δ increases past $1/4$. The parameter value $\Delta = 1/4$ corresponds to the force parameter $F_\ell = c^2/EI$ and $\alpha_0^2 = \pm\frac{\pi}{2}$.

$$\begin{aligned}\phi &= \alpha^3 - \operatorname{sgn} \left(\alpha_0^{1'} \sin(\alpha_0^2) \right) \frac{\pi}{2}, \\ \kappa &= \left| \alpha_0^{1'} \sin(\alpha_0^2) \right| = \left| \left(\frac{\sin(\alpha_0^2)}{1 + \cos(\alpha_0^2)} \right) \frac{c}{EI} \right|, \\ \tau &= \alpha_0^{1'} \cos(\alpha_0^2) = \left(\frac{\cos(\alpha_0^2)}{1 + \cos(\alpha_0^2)} \right) \frac{c}{EI}.\end{aligned}\quad (5.154)$$

That is, the centerline of the rod is bent into a helix. We can use the identity (5.101) with Eqn. (5.154) to show that the axis of the helix is parallel to the terminal loadings $\mathbf{F}_\ell = -\mathbf{F}_0 = F_\ell \mathbf{E}_3$:

$$\begin{aligned}\mathbf{\omega}_{SF} &= \mathbf{Pv} - \frac{\partial \phi}{\partial s} \mathbf{e}_t \\ &= \alpha_0^{1'} (-\sin(\alpha_0^2) \cos(\alpha^3) \mathbf{d}_1 + \sin(\alpha_0^2) \sin(\alpha^3) \mathbf{d}_2 + \cos(\alpha_0^2) \mathbf{d}_3) \\ &= \alpha_0^{1'} \mathbf{E}_3 \\ &= \sqrt{\frac{F_\ell}{EI}} \mathbf{E}_3.\end{aligned}\quad (5.155)$$

The rod in this case is said to have been bent into a helical form [213, Section 271].

With the help of the expression (5.154)₃ for τ , it can be shown that for values of $\Delta < 1/4$ that the helical forms are left handed (right handed) if $c > 0$ ($c < 0$). In the limiting case as $\Delta \searrow 0$, the curvature of the helical forms tends to zero and the centerline of the rod straightens. When $\Delta = 1/4$, $\tau = 0$, $\alpha_0^2 = \pm\pi/2$, and the torsion of the helical forms vanishes, so the centerline of the rod now has the shape of a circular arc of radius EI/c . It is also interesting to note that, for this value of Δ , $EIf_\ell = c^2$. For $1/4 < \Delta < 1$, the helical forms change handedness from their earlier counterparts: the helical forms are now right handed (left handed) if $c > 0$ ($c < 0$).²⁹ As recorded in Figure 5.15, observe that the terminal loadings change as Δ passes through $1/4$ in a manner reminiscent of a similar transition observed in the elastica (cf. Figures 4.5 and 4.6).

The moment \mathbf{m} in these twisted helical states is not constant. Rather, it varies throughout the rod and has components along the tangent to the centerline of the rod as well as in the cross section:

$$\begin{aligned}\mathbf{m} &= c\mathbf{e}^1 + c\mathbf{e}^3 \\ &= c \left(\mathbf{d}_3 - \frac{1 - \cos(\alpha_0^2)}{\sin(\alpha_0^2)} (\cos(\alpha^3)\mathbf{d}_1 - \sin(\alpha^3)\mathbf{d}_2) \right) \\ &= c \left(\mathbf{E}_3 + \frac{1 - \cos(\alpha_0^2)}{\sin(\alpha_0^2)} (\cos(\alpha^1)\mathbf{E}_1 + \sin(\alpha^1)\mathbf{E}_2) \right).\end{aligned}\quad (5.156)$$

These representations can be used to determine the moments \mathbf{M}_0 and \mathbf{M}_ℓ applied to the ends of the rod. With the help of the identity (5.142), we are able to conclude that the moment in the twisted helical states asymptotes to the moment in the straight rod. While this result is satisfying on physical grounds, given the singularity in the Euler angle parameterization when $\alpha^2 = 0, \pi$, it is also surprising. For the case when $\Delta = 1/4$ and the helical forms have no torsion, the contact moment in the rod can be found from the expression (5.156):

$$\mathbf{m} = c\mathbf{E}_3 + c\sin(\alpha_0^2)(\cos(\alpha^1)\mathbf{E}_1 + \sin(\alpha^1)\mathbf{E}_2). \quad (5.157)$$

Observe that the circular arc formed by $\mathbf{r}(\xi)$ lies in the $X - Y$ plane and the moment \mathbf{m} will have a component in the $X - Y$ plane. This component is needed to balance the moment due to terminal loadings $\mathbf{F}_\ell = F_\ell\mathbf{E}_3 = -\mathbf{F}_0$.

In summary, if $\Delta < 1$, then 3 types of equilibria are possible. As shown in Figure 5.15, one of equilibria corresponds to the straight rod, while the second and third correspond to a pair of helical forms whose handedness depends on the sign of $c = \mathbf{m} \cdot \mathbf{E}_3 = \mathbf{m} \cdot \mathbf{d}_3$ and the value of Δ . When $\Delta = 1/4$, the helical forms degenerate to circular forms (i.e., the centerline of the rod forms a circular arc). What distinguishes the two twisted helical rods is a phase offset in their twist angles (see Eqn. (5.154)₁). For a given value of Δ , these twisted helical states have a value of

²⁹ This observation on the change in handedness as Δ varies does not appear to have been previously recorded in the literature.

the energy function U that is lower than their straight counterpart and this suggests that the straight configuration for a rod of infinite length becomes unstable as Δ decreases past 1 and can be said to have buckled.

Much of what we have just described on the equilibrium states of the top and their correspondence to straight and twisted helical rods dates to Kirchhoff's seminal work from 1859. Our exposition has been heavily influenced by Love [213, Section 270] and the more recent work on this topic by Coyne [75] and Thompson and his coworkers [164, 340]. With the help of numerical integration capabilities that were not available to Love et al., the latter authors were able to examine the nonequilibrium solutions of (5.148) and discuss the corresponding deformed configurations of a rod. The picture they present, and which we will presently examine, is one with a remarkably rich range of deformed rod shapes.

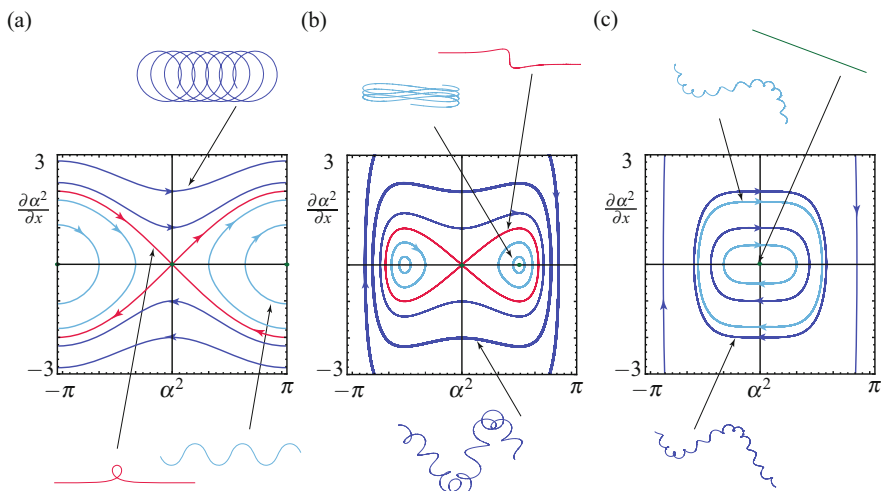


Fig. 5.16 Phase portraits of the differential equation (5.159) for three different values of the parameter $\frac{F_\ell EI}{c^2}$. In (a), $c^2 = 0$; in (b), $c^2 = 0.50F_\ell EI$; and in (c), $c^2 = 8F_\ell EI$. The inset images correspond to the deformed material curve of a terminally loaded rod of finite length where $\alpha^2(\xi)$ corresponds to a portion of a trajectory in the phase portrait. For the pair of nontrivial equilibria in (b), the corresponding helical forms of the centerline of the rod are shown in Figure 5.15. The case $c^2 = 0$ corresponds to the terminally loaded planar elastica discussed in Section 4.4 of Chapter 4.

5.15.3 Nontrivial and Localized Equilibrium States of the Rod

To explore additional solutions to the terminally loaded rod beyond the straight and helical forms discussed earlier, we non-dimensionalize the differential equations (5.148) using Eqn. (5.147) by choosing $\hat{\ell}$ so that $\hat{F}_\ell = 1$:

$$\hat{\ell} = \sqrt{\frac{EI}{F_\ell}}. \quad (5.158)$$

The resulting dimensionless form of the differential equation (5.148) is

$$\frac{\partial^2 \alpha^2}{\partial x^2} + \frac{4\Delta((1 - \cos(\alpha^2))^2)}{\sin^3(\alpha^2)} = \sin(\alpha^2). \quad (5.159)$$

The bifurcation shown in Figure 5.15 is evident in changes to the phase portrait of the second-order differential equation (5.159) as $\frac{F_\ell EI}{c^2}$ is varied that are observed in Figure 5.16. The solutions shown in these phase portraits can be classified as fixed points (corresponding to the solutions discussed in the previous section), closed orbits, a figure ∞ loop that contains the origin, and a pair of orbits that asymptote to the fixed point in Figure 5.16(a). The figure ∞ loop and the latter orbit are pairs of homoclinic orbits.

Representative examples of $\mathbf{r}(\xi)$ corresponding to portions of the orbits and fixed points are shown in Figure 5.16. As evident from the deformed shapes of the centerline of the rod, there is a rich variety of solutions. While some recent progress has been made to establish a classification for all these solutions³⁰ we focus attention here on those solutions which correspond to the homoclinic orbits. Explicit solutions for $\alpha^2(x)$ for the homoclinic orbits can be found using conservation of an energy-like function e :

$$e = \frac{1}{2} \left(\frac{\partial \alpha^2}{\partial x} \right)^2 + \frac{2\Delta(1 - \cos(\alpha^2))}{(1 + \cos(\alpha^2))} + \cos(\alpha^2). \quad (5.160)$$

This energy-like function is inferred from the differential equation (5.145) by non-dimensionalizing U : $U \rightarrow U/F_\ell \hat{\ell}$. We can easily compute the value of the level set of the energy-like function e that passes through the origin in the phase plane to find that it is $e = 1$. Thus,

$$\int_{x_1}^{x_2} dv = \int_{\alpha_1^2}^{\alpha_2^2} \frac{\sin(\chi)}{\sqrt{(2 - 2\cos(\chi))\sin^2(\chi) - 4\Delta(1 - \cos(\chi))^2}} d\chi. \quad (5.161)$$

Using the change of variables, $u = \cos(\chi)$, the integral on the right-hand side of this equation simplifies and can be evaluated:

$$\begin{aligned} x_2 - x_1 &= - \int_{u_2}^{u_1} \frac{du}{\sqrt{2(1-u)\sqrt{1-2\Delta+u}}} \\ &= \frac{1}{\sqrt{1-\Delta}} \operatorname{Arctanh} \left(\sqrt{\frac{1+u-2\Delta}{2(1-\Delta)}} \right) \Big|_{u_1}^{u_2}, \end{aligned} \quad (5.162)$$

³⁰ See the works of Goriely [222, 249], Maddocks [86, 169, 178], Thompson [164, 340], and their coworkers.

where $u_\beta = \cos(\alpha_\beta^2)$. We choose $u_1 = \cos(\alpha_0^2) = 2\sqrt{\Delta} - 1$ and $x_1 = 0$.³¹ Whence,

$$\cos(\alpha^2(x)) = 2\Delta - 1 + 2(1 - \Delta) \tanh^2 \left(x\sqrt{1 - \Delta} + \operatorname{Arctanh} \left(\sqrt{\frac{\sqrt{\Delta} - \Delta}{1 - \Delta}} \right) \right). \quad (5.163)$$

This expression can be used to determine $\alpha^1(x)$ and $\alpha^3(x)$ by integrating the differential equations (5.143). A further integration of an expression for \mathbf{d}_3 in terms of the Euler angles (see Eqn. (5.15)) provides the deformed shape $\mathbf{r}(\xi)$ of the centerline:

$$\frac{\partial \mathbf{r}}{\partial \xi} = \cos(\alpha^2(\xi)) \mathbf{E}_3 + \sin(\alpha^2(\xi)) (\cos(\alpha^1(\xi)) \mathbf{E}_1 + \sin(\alpha^1(\xi)) \mathbf{E}_2). \quad (5.164)$$

Observe that as $\xi \rightarrow \pm\infty$, $\alpha^2(\xi) \rightarrow 0$ and $\mathbf{d}_3 = \frac{\partial \mathbf{r}}{\partial \xi} \rightarrow \mathbf{E}_3$. It is also helpful to recall that $\xi = \sqrt{\frac{EI}{F_\ell}}x$ when interpreting these results.

A pair of examples of computing the deformed shapes of the rod corresponding to the homoclinic orbits is presented in Figure 5.17. For these examples, the parameter $\Delta = 0.25$ and the solutions are integrated numerically using the initial values $\cos(\alpha_0^2) = 2\sqrt{\Delta} - 1$ and $\frac{\partial \alpha^2}{\partial x}(x=0) = 2(1 - \sqrt{\Delta})$. In its entirety, each orbit pertains to a rod of infinite length, so only a portion of the centerline corresponding to each orbit is shown. Different initial values of $\mathbf{r}(x=0)$ are chosen to distinguish the two sets of results. As can be seen from the figure, \mathbf{d}_3 asymptotes to \mathbf{E}_3 , as expected. We also note that the twist angle $\phi(x) = \alpha^3(x)$ increases monotonically throughout the length of the deformed rod. For a rod of finite length $x \in (x_1, x_2)$, if the loading parameters and boundary conditions are chosen so that $\alpha^2(x)$ lies on the homoclinic orbit, then, in addition to terminal forces $\mathbf{F}_\ell = F_\ell \mathbf{E}_3 = -\mathbf{F}_0$, moments

$$\begin{aligned} \mathbf{M}_A &= -\mathbf{m}(\xi_1^+) = -c(\mathbf{e}^1(\xi_1^+) + \mathbf{e}^3(\xi_1^+)) - EI \frac{\partial \alpha^2}{\partial \xi}(\xi_1^+) \mathbf{e}_2(\xi_1^+), \\ \mathbf{M}_B &= \mathbf{m}(\xi_2^-) = c(\mathbf{e}^1(\xi_2^-) + \mathbf{e}^3(\xi_2^-)) + EI \frac{\partial \alpha^2}{\partial \xi}(\xi_2^-) \mathbf{e}_2(\xi_2^-), \end{aligned} \quad (5.165)$$

must be applied at the respective ends of the rod. If the rod has an infinite length, then, after invoking the limit (5.142), we would find that the terminal moments needed are $\mathbf{M}_{-\infty} = -c\mathbf{E}_3$ and $\mathbf{M}_\infty = c\mathbf{E}_3$.

The problem of looping and hockling of cables prompted Coyne [75] to examine the deformed shape of an infinitely long rod subject to combined torsion and thrust. He made the important observation that as Δ decreased below 1, the deformed shapes of the rod corresponding to the homoclinic orbits that arise exhibited loops. These loops are easiest to see in the $Y-Z$ projections of the deformed shapes and examples are shown in Figure 5.18 and are similar to the planar loops found by

³¹ It is useful to note that this choice implies that $\frac{\partial \alpha^2}{\partial x}(x=x_1=0) = \pm 2(1 - \sqrt{\Delta})$. To see this result, it suffices to set $e = 1$ in Eqn. (5.160) and then solve for $\frac{\partial \alpha^2}{\partial x}$ when $\cos(\alpha_0^2) = 2\sqrt{\Delta} - 1$.

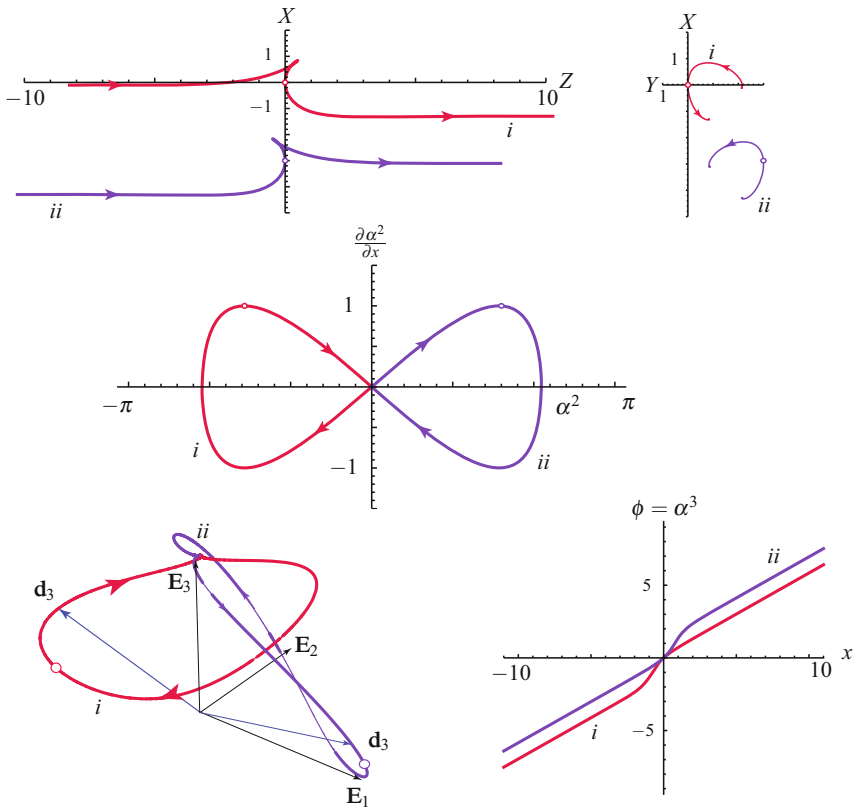


Fig. 5.17 The pair (*i* and *ii*) of homoclinic orbits of the differential equation (5.159) for values of the parameters $\Delta = \frac{c^2}{4F_\ell EI} = 0.250$ and $\frac{EI}{\mathcal{D}} = 1.3$. Corresponding to each of the orbits, the inset images show plots of the twist angle $\phi(\xi) = \alpha^3(\xi)$, the tangent indicatrices of \mathbf{d}_3 , and the components of the position vector $\mathbf{r}(x) = X(x)\mathbf{E}_1 + Y(x)\mathbf{E}_2 + Z(x)\mathbf{E}_3$ for a finite section of a rod of infinite length that is loaded at its ends by forces and moments. The circle in the images is intended to help indicate the correspondence between points on the various graphs and the arrows indicate the direction of increasing ξ .

Euler in 1744 that we discussed in Section 4.4 of Chapter 4. Coyne then noted that, because a rod has a given diameter, self-contacting of the rod during this loop formation might be possible. Trying to remove the loop in marine cables by changing F_ℓ or c is problematic and often leads to a smaller loop with large permanent strains which damage the marine cable - a process known as hockling.

To explore the onset of the loop formation, we examine an infinitely long rod which is subject to terminal forces $\mathbf{F}_\ell = -\mathbf{F}_0 = F_\ell \mathbf{E}_3$ and moments $\mathbf{M}_\ell = -\mathbf{M}_0 = c \mathbf{E}_3$ and assume that the loading is such that $\Delta < 1$ and $\alpha^2(x)$ and its derivative trace out a homoclinic orbit in the phase plane. The displacement of the ends of the rod can be found using Eqn. (5.163) and used to calculate the shortening s_ℓ of the rod as Δ varies:

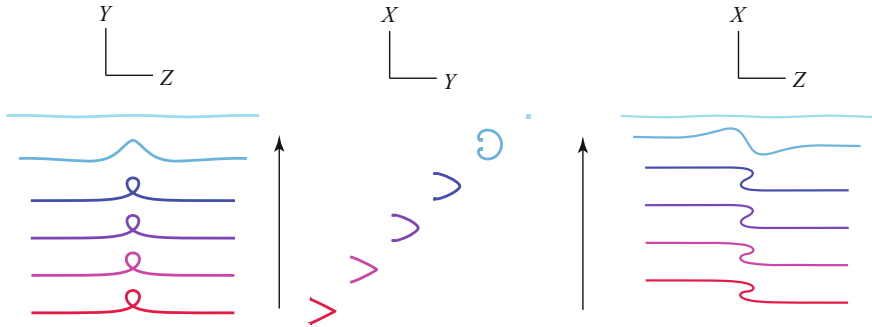


Fig. 5.18 Planar projections of the deformed centerline of the rod shown in Figure 5.14. For these projections, $\Delta = 0.00025, 0.0025, 0.025, 0.25, 0.75, 0.9995$, and $\frac{EI}{\mathcal{G}} = 1.3$. The arrow indicates the direction of decreasing Δ . The initial values of $\mathbf{r}(x=0)$ are chosen to be different for each of the curves in order to distinguish the solutions, and $\alpha^2(0) = -\arccos(-1 + 2\sqrt{\Delta})$, $\frac{\partial \alpha^2}{\partial x}(x=0) = 0$. The variable $x \in [-10, 10]$ for all the solutions and the behavior of the twist angle $\phi(x)$ and strain $v_2(x)$ for these solutions are shown in Figure 5.19.

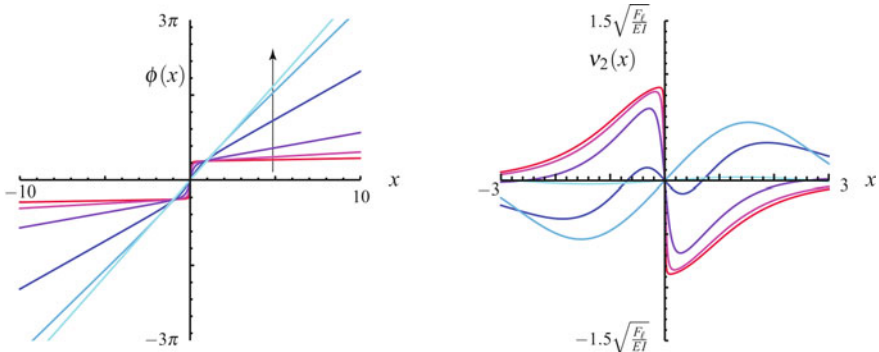


Fig. 5.19 The twist angle $\phi = \phi(x)$ and strain $v_2(x)$ for the deformed rods whose centerlines are shown in Figure 5.14. The arrow indicates the direction of decreasing Δ . In contrast to the bending strain v_2 (and v_1), because of the conservation, $\mathbf{m} \cdot \mathbf{d}_3 = c_s$, the strain v_3 is uniform throughout the rod.

$$\begin{aligned}
 s_\ell &= 2 \int_0^\infty (1 - \cos(\alpha^2(\xi))) d\xi \\
 &= 2\hat{\ell} \int_0^\infty (1 - \cos(\alpha^2(x))) dx \\
 &= 4\sqrt{\frac{EI}{F_\ell}} \sqrt{1-\Delta} \left[1 - \sqrt{\frac{\sqrt{\Delta}}{1+\sqrt{\Delta}}} \right]. \tag{5.166}
 \end{aligned}$$

From the final expression, with some rearranging, we can write the change in length as a function of the terminal loadings as

$$s_\ell = 8 \left(\frac{EI}{c} \right) \sqrt{\Delta - \Delta^2} \left[1 - \sqrt{\frac{\sqrt{\Delta}}{1 + \sqrt{\Delta}}} \right]. \quad (5.167)$$

This expression is used to determine the shortening s_ℓ as a function of Δ for various values of c . The results are shown in Figure 5.20.

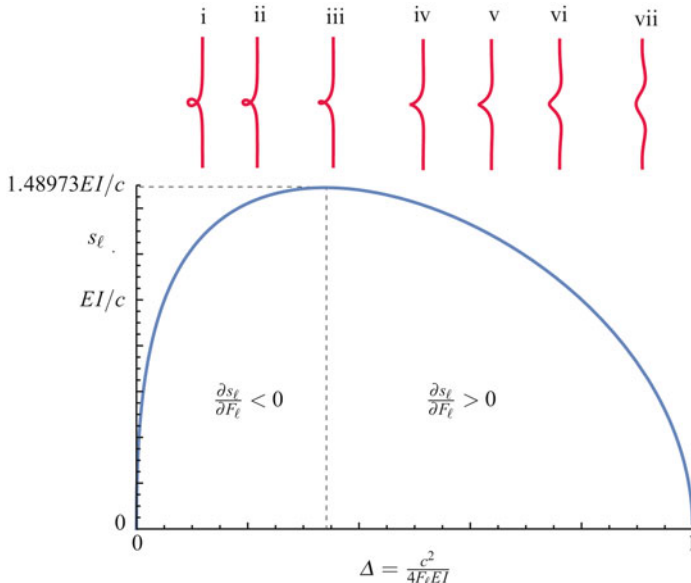


Fig. 5.20 The shortening s_ℓ of a rod of infinite length as a function of the loading parameter Δ as described by Eqn. (5.167). The inset images are projections on the $Y-Z$ plane of a portion of the deformed centerline $\mathbf{r}(\xi)$: (i), $\Delta = 0.1$; (ii), $\Delta = 0.2$; (iii), $\Delta \approx 0.3389388$; (iv), $\Delta = 0.5$; (v), $\Delta = 0.6$; (vi), $\Delta = 0.75$; and (vii), $\Delta = 0.90$. The maximum shortening $s_\ell \approx 1.48973 \frac{EI}{c}$ occurs when $\Delta \approx 0.3389388$.

To see why the loop formation can be problematic, suppose we impose terminal forces $\mathbf{F}_\ell = F_\ell \mathbf{E}_3$ and $\mathbf{F}_0 = -F_0 \mathbf{E}_3$ and terminal moments $\mathbf{M}_\ell = -\mathbf{M}_0 = c \mathbf{E}_3$ on the infinitely long rod.³² Initially, we assume that the rod is straight and twisted and that $\Delta > 1$. We now increase F_0 so that Δ becomes smaller than 1 and assume that the rod deforms so that $\alpha^2(\xi)$ and its derivative lie on one of the homoclinic orbits (and remain there as this orbit changes with changing F_0). Referring to Figure 5.20, eventually, as Δ decreases past 0.5 the rod will develop a loop. Because of the thickness

³² Our discussion here, while also based on the behavior of s_ℓ as F_0 varies, is different from Coyne's. In particular, his discussion has statements on stability and instability that we have not been able to follow.

of the rod, self-contact becomes possible. This may lead to the rod supercoiling but our model is insufficient to predict this phenomenon. Ignoring the possibility of self-contact, as F_ℓ is increased further so that $\Delta < 0.3389388$, the shortening starts to decrease and the loop (in the $Y - Z$ plane) grows. As can be seen from Figure 5.19, the rate of change in the angle of twist of the rod also increases and becomes unbounded at $\xi = 0$ as $\Delta \rightarrow 0$. However, the strain v_3 remains constant, while the bending strains v_1 and v_2 increase dramatically as F_0 increases. The concomitant large strains in the rod render our model unrealistic because plastic deformation (or hockling) now becomes likely.

5.15.4 Comments

While a configuration of the rod having a loop is present for the infinitely long rod where $\alpha^2(\xi)$ and its derivative describe a homoclinic orbit, other configurations, many with multiple loops, are also present and can be seen in Figure 5.16(b)-(c). These configurations have not received as much attention in the literature in part because analytical solutions for $\mathbf{r}(\xi)$ (which can be found in [319]) are not as tractable as those for the homoclinic case (cf. Eqn. (5.163)). While analytical solutions for $\mathbf{r}(\xi)$ are available in a handful of the aforementioned special cases and have proven to be very helpful in categorizing the rich array of possible shapes $\mathbf{r}(\xi)$, in general one cannot expect such good fortune. Indeed, it has been recently shown by Mielke and Holmes [238] that small perturbations in the form of terminal forces or inhomogeneities to the case of a rod with $EI_1 \neq EI_2$ that is terminally loaded by end moments (such as discussed in Section 5.14) can lead to spatially complex (chaotic) $\mathbf{r}(\xi)$. Examples of such complex shapes can be seen in a work by Davies and Moon [84] that was inspired by [238]. A recent perspective on, and extensions to, [238] can be found in [165].

Hopefully, a sufficient variety of spatial forms for $\mathbf{r}(\xi)$ have been presented in this chapter for the reader to appreciate the richness of the problem of a terminally loaded rod. What we have not touched upon is the manner in which $\mathbf{r}(\xi)$ changes (even in a quasistatic manner) as the loading parameters are varied. Several works, such as [340], present experiments on these transitions and there are papers such as [75, 162, 164] which discuss the transitions from an analytical perspective using a quasistatic analysis. Motivated in part by the additional application to DNA supercoiling, the papers by Bergou et al. [22], Clauvelin et al. [61], van der Heijden et al. [162], and Jawed et al. [173] also include the effects of self-contact. The results in [162] (and others) have been explored using numerical methods (and including dynamical effects) by Goyal et al. [124–126]. The analyses of Coleman et al. [67, 68] on closed loops of rod as models for DNA minicircles are also noteworthy. Despite the large body of work on the application of rod theory to looping, hockling, physical knots, and the related problem of DNA supercoiling, much remains to be discovered in this rich application of rod theory.

5.16 Rods with Intrinsic Curvature: Tendril Perversion, Helical Solutions, and Buckling

Throughout the literature one finds a large focus on the analysis of twisted rods where the centerline is in the form of a helix. These analyses are frequently motivated by the use of rod-based models to determine the static behavior of double-stranded DNA molecules. Another biomechanical application of rod theories occurs in studies on the static behavior of plant tendrils and branches. In this area of application, one finds segments of the plant tendril which are in the form both of left-handed and right-handed helices. An example of such a situation is shown in Figure 5.21 which is reproduced from Charles Darwin's (1809–1882) celebrated and lucid work [81] on climbing plants. The tendril connecting the helices of opposite handedness is known, following Goriely and Tabor [123], as a perversion and the phenomenon of the changing handedness of the helical structures formed by the tendril is known as tendril perversion.³³ For instance, referring to Figure 5.21, the tendril connects the plant stem to a support and has three perversions, a pair of left-handed helices, and a pair of right-handed helices. Related examples where a rod-like body has segments of its length taking on helical structures with varying handedness occur in telephone cords, umbilical cords, and embryonic heart loops.³⁴

The rod model used to examine tendril perversions consists of an intrinsically curved rod where $v_{01} = 1/R$. That is, the reference configuration of the centerline of the rod is circular. An easy visualization of such a reference configuration is to imagine a slinky of infinitesimal thickness. By applying forces, the slinky expands out into a helical shape that is similar to a telephone cord. In plant stems, it is well known that intrinsic curvatures of the type $v_{01} = 1/R$ are induced by differential growth where one side of the plant stems grows at a faster rate than the other. The growth-induced intrinsic curvature assists in enabling plant stems to retain their form in the presence of gravitational and wind loading.³⁵ This intrinsic curvature can also be induced in the laboratory by stretching strips of rubber



Fig. 5.21 Examples of tendril perversion in the plant *Bryonia dioica*. This figure is copied with permission from Darwin [81, Figure 13].

³³ The terminology is based on the use of the word perversion (or “Verkehrung” (= reversal)) by the famed topologist Johann B. Listing (1808–1882) for a transformation that changes the handedness of a helix (see [208, Page 22]).

³⁴ For additional discussions on tendril perversion, the reader is referred to Domokos and Healey [90], Keller [179], Männer [223], and McMillen and Goriely [235].

³⁵ For additional references on this topic, the reader is referred to [121, 273, 295, 323, 365] and references therein.

of different initial length to the same length and then gluing them together.³⁶ In this section, we explore various problems associated with intrinsically curved rods. These range from simple deformation of the rod to buckling instabilities and perversions. First, we examine various representations of the balance laws.

5.16.1 Balance Laws for an Intrinsically Curved Rod

We consider a terminally loaded elastic rod where $\mathbf{v}_0 \neq \mathbf{0}$. To explore some of the issues of interest it is useful to express the balance laws for this rod using the Frenet triad $\{\mathbf{e}_t, \mathbf{e}_n, \mathbf{e}_b\}$:

$$\mathbf{n} = n_t \mathbf{e}_t + n_n \mathbf{e}_n + n_b \mathbf{e}_b, \quad \mathbf{m} = m_t \mathbf{e}_t + m_n \mathbf{e}_n + m_b \mathbf{e}_b. \quad (5.168)$$

Thus, the balance laws, $\mathbf{n}' = \mathbf{0}$ and $\mathbf{m}' + \mathbf{r}' \times \mathbf{n} = \mathbf{0}$, can be expressed as six first-order differential equations:

$$\begin{aligned} \begin{bmatrix} n_t' \\ n_n' \\ n_b' \end{bmatrix} &= \begin{bmatrix} 0 & \kappa & 0 \\ -\kappa & 0 & \tau \\ 0 & -\tau & 0 \end{bmatrix} \begin{bmatrix} n_t \\ n_n \\ n_b \end{bmatrix}, \\ \begin{bmatrix} m_t' \\ m_n' \\ m_b' \end{bmatrix} &= \begin{bmatrix} 0 & \kappa & 0 \\ -\kappa & 0 & \tau \\ 0 & -\tau & 0 \end{bmatrix} \begin{bmatrix} m_t \\ m_n \\ m_b \end{bmatrix} + \begin{bmatrix} 0 \\ n_b \\ -n_n \end{bmatrix}. \end{aligned} \quad (5.169)$$

To establish these equations, the Serret-Frenet relations (1.13) were used. It is also convenient to recall the definition of the Darboux vector $\boldsymbol{\omega}_{SF} = \tau \mathbf{e}_t + \kappa \mathbf{e}_b$.

The representation (5.169) will prove useful for some, but not all, of the subsequent developments. Indeed two other representations will appear in the sequel: (5.270) which projects the balance laws onto the \mathbf{d}_i basis vectors, and (5.194) which is the linearization of the balance laws about an equilibrium configuration. For the latter, a set of 1-2-3 Euler angles are used to parameterize the rotation tensor \mathbf{P} .³⁷

5.16.2 Helical Solutions: Solving for the Geometric Torsion, Curvature, and Angle of Twist

Tacitly ignoring boundary conditions and constitutive relations for the present, we seek equilibria of Eqn. (5.169). That is, solutions to these equations where the

³⁶ The interested reader is referred to the paper by Liu et al. [209] where an example of such an intrinsically curved body is used to help analyze perversions.

³⁷ In the interests of brevity, the developments of these two representations of the balance laws are discussed in Exercises 5.14 and 5.15.

components of \mathbf{n} and \mathbf{m} in terms of the Frenet triad are constant: $n'_t = n'_n = n'_b = 0$ and $m'_t = m'_n = m'_b = 0$. Based on the recent works of Goriely et al. [123, 235], we show that two solutions are present: a straight possibly twisted configuration and a configuration where the centerline takes the shape of a helix and the rod is twistless.³⁸

We first consider solutions where the centerline is straight: $\kappa = 0$ and $\tau = 0$. Thus, we find the expected results that $\mathbf{n} = n\mathbf{e}_t$ and \mathbf{m} is constant. For the more interesting case where $\kappa \neq 0$, we find that κ and τ are constants and that

$$n_n = 0, \quad \kappa n_t = \tau n_b, \quad m_n = 0, \quad \kappa m_t - \tau m_b = n_b. \quad (5.170)$$

Thus, the centerline of the rod is in the form of a helical space curve. In addition, we can also conclude that \mathbf{n} is parallel to the Darboux vector:

$$\begin{aligned} \mathbf{n} &= n_t \mathbf{e}_t + n_b \mathbf{e}_b \\ &= n_b \left(\frac{\tau}{\kappa} \mathbf{e}_t + \mathbf{e}_b \right) \\ &= (\kappa m_t - \tau m_b) \left(\mathbf{e}_b + \frac{\tau}{\kappa} \mathbf{e}_t \right) \\ &= \left(m_t - \frac{\tau}{\kappa} m_b \right) \boldsymbol{\omega}_{SF}. \end{aligned} \quad (5.171)$$

For a circular helix, the Darboux vector is parallel to the axis of the helix.³⁹ If we assume that the rod has end points at $\xi = \pm\ell$, then, as \mathbf{n} is constant throughout the rod, the terminal loadings define the axis of the helix:

$$\mathbf{F}_{-\ell} = F_0 \mathbf{E}, \quad \mathbf{F}_\ell = -F_0 \mathbf{E}, \quad \mathbf{n}(\xi) = -F_0 \mathbf{E}, \quad (5.172)$$

where \mathbf{E} is a unit vector that is parallel to $\boldsymbol{\omega}_{SF}$. In general, terminal moments will also need to be applied to the rod and we leave it as an exercise for the reader to determine these moments.

To proceed further, we need to make some assumptions about the constitution of the rod. We assume that the rod has a nontrivial intrinsic curvature $\mathbf{v}_0 = v_{0_1} \mathbf{D}_1 + v_{0_2} \mathbf{D}_2 + v_{0_3} \mathbf{D}_3$ and a strain energy function

$$2\rho_0 \psi = EI_1 v_1^2 + EI_2 v_2^2 + \mathcal{D} v_3^2. \quad (5.173)$$

We presume that v_{0_k} and the moduli EI_1 , EI_2 , and \mathcal{D} are constants. With the help of the constitutive relations (5.93) and the Bonnet-Meusnier relations (5.102) we find that

³⁸ A complementary perspective on solutions of this type can be found in the discussion of Erickson's uniform states in Section 6.6 in Chapter 6.

³⁹ This result was discussed in an earlier chapter of this text and the reader is referred to Eqn. (1.34) for details.

$$\mathbf{m} = \mathcal{D} \left(\tau + \frac{\partial \phi}{\partial s} - v_{0_3} \right) \mathbf{e}_t + (EI_1 v_1 \cos(\phi) - EI_2 v_2 \sin(\phi)) \mathbf{e}_n + (EI_1 v_1 \sin(\phi) + EI_2 v_2 \cos(\phi)) \mathbf{e}_b, \quad (5.174)$$

where

$$v_1 = \kappa \sin(\phi) - v_{0_1}, \quad v_2 = \kappa \cos(\phi) - v_{0_2}. \quad (5.175)$$

The condition $m_n = 0$ is satisfied if

$$(EI_1 - EI_2) \kappa \sin(\phi) \cos(\phi) = EI_1 v_{1_0} \cos(\phi) - EI_2 v_{2_0} \sin(\phi). \quad (5.176)$$

This can be considered as an equation for the twist angle ϕ . Except for the trivial case where the rod is symmetric ($EI_1 = EI_2$) and $v_{0_1} = v_{0_2} = 0$, this angle must be a constant. We henceforth assume that ϕ is constant: $\phi = \phi_0$. With the help of Eqns. (5.172) and (5.174), we see that the remaining condition (5.170)₄ yields the identity

$$\left(\mathcal{D}(\tau - v_{0_3}) - \frac{\tau}{\kappa} (EI_1 v_1 \sin(\phi_0) + EI_2 v_2 \cos(\phi_0)) \right) \omega_{SF} \cdot \mathbf{E} = -F_0. \quad (5.177)$$

In conclusion, we have two equations, Eqns. (5.176) and (5.177), for the unknown parameters κ , ϕ_0 , and τ of the rod solution.

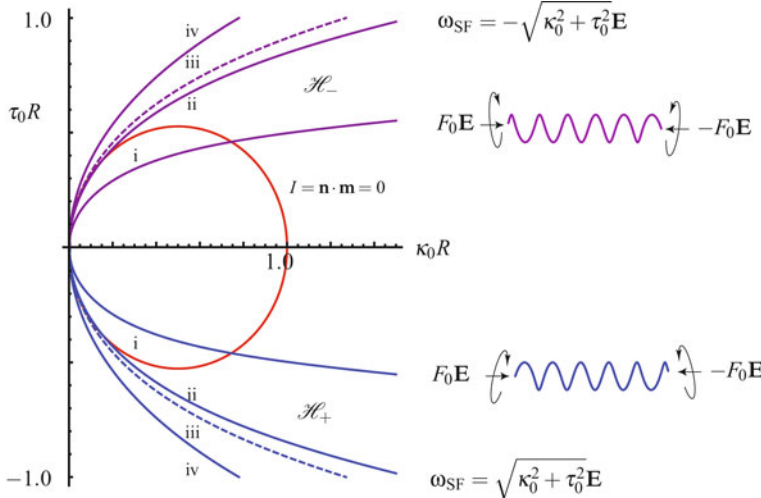


Fig. 5.22 Solutions (κ_0, τ_0) of Eqn. (5.180) with the angle of twist $\phi = \phi_0 = \frac{\pi}{2}$ for various values of $f_0 = \frac{F_0 R^2}{EI_1}$. For the solutions shown, $\frac{\mathcal{D}}{EI_1} = 0.9$ and a critical value of $f_0 = 1/\mathcal{D}$: (i), $f_0 = 0.5$; (ii), $f_0 = 1.0$; (iii), $f_0 = 1/0.9$; and (iv), $f_0 = 1.5$. The zero level set of the integral $I = \mathbf{n} \cdot \mathbf{m}$ is also shown.

To illustrate the above solution procedure, we follow the literature on tendril perversion models and assume that the rod is curved into a constant radius circle in

its reference configuration (cf. [90, 123, 235]):

$$v_{01} = \frac{1}{R}, \quad v_{02} = 0, \quad v_{03} = 0. \quad (5.178)$$

In this case, the condition (5.174) is identically satisfied when⁴⁰

$$\phi_0 = \pm \frac{\pi}{2}. \quad (5.179)$$

Finally, we find an equation for κ and τ from Eqn. (5.176):

$$\left(\mathcal{D} - \frac{EI_1 \sin(\phi_0)}{\kappa} \left(\kappa \sin(\phi_0) - \frac{1}{R} \right) \right) (\tau \omega_{SF}) \cdot \mathbf{E} = -F_0. \quad (5.180)$$

Given $\frac{F_0 R^2}{EI_1}$, $\frac{\mathcal{D}}{EI_1}$, and ϕ_0 , we can solve Eqn. (5.180) for the pair (τ_0, κ_0) . We denote a solution to Eqn. (5.180) by the pair (τ_0, κ_0) and representative cases for a range of values of F_0 are shown in Figure 5.22. Because of the possibilities

$$\omega_{SF} = \pm \sqrt{\kappa^2 + \tau^2} \mathbf{E}, \quad (5.181)$$

each solution (τ_0, κ_0) with $\omega_{SF} = \sqrt{\kappa_0^2 + \tau_0^2} \mathbf{E}$ has a counterpart $(-\tau_0, \kappa_0)$ with $\omega_{SF} = -\sqrt{\kappa_0^2 + \tau_0^2} \mathbf{E}$. This pair of helical solutions, which we respectively denote by \mathcal{H}_+ and \mathcal{H}_- , will have opposite handedness. While the terminal forces on these solutions will be identical, it is straightforward to show that the terminal moments will be different.

5.16.2.1 Tendril Perversion in an Infinitely Long Rod

We conclude from the analysis that was just discussed that, for a given rod and applied force F_0 , a pair of helical solutions, \mathcal{H}_+ and \mathcal{H}_- , can be found which, apart from their handedness, are qualitatively identical. If a solution to the differential equations (5.169) can be found that connects the pair, then the corresponding solution corresponds to a perversion. Goriely et al. [123, 235] assumed that the rod is of infinite length and so they sought the so-called heteroclinic orbits that connect the pairs of fixed points corresponding to \mathcal{H}_+ and \mathcal{H}_- . To help find the solution, they cleverly exploited the fact that the solutions to (5.169) conserve $I = \mathbf{n} \cdot \mathbf{m}$. Evaluating this integral of motion at one end of the orbit, say at \mathcal{H}_+ , we would find, after imposing the conditions (5.170), (5.174), and (5.179), that

$$\mathbf{n} \cdot \mathbf{m} = \left(\frac{\mathcal{D} \tau_0^2}{\kappa_0} + m_b \right) (\mathcal{D} \kappa_0 - m_b) \tau_0, \quad (5.182)$$

⁴⁰ In the sequel, our numerical results pertain to $\phi_0 = \frac{\pi}{2}$. We found that the solutions of Eqn. (5.180) for $\phi_0 = -\frac{\pi}{2}$ are qualitatively similar and so, in the interests of brevity, they are not mentioned.

where $m_b = EI_1 \left(\kappa_0 \sin(\phi_0) - \frac{1}{R} \right) \sin(\phi_0)$. On the other hand, evaluating $\mathbf{n} \cdot \mathbf{m}$ at the other end of the orbit, we find that

$$\mathbf{n} \cdot \mathbf{m} = - \left(\frac{\mathcal{D}\tau_0^2}{\kappa_0} + m_b \right) (\mathcal{D}\kappa_0 - m_b) \tau_0. \quad (5.183)$$

Consequently, $I = \mathbf{n} \cdot \mathbf{m} = 0$ on the heteroclinic orbit. That is, remarkably, the force and moment are orthogonal along the orbit. For fixed points with $\phi_0 = \frac{\pi}{2}$, if $0 < F_0 \leq (EI_1)^2 / \mathcal{D}R^2$, then we can always find a pair of fixed points for a given F_0 and $I = 0$ at both points (cf. Figure 5.23).⁴¹ When $\phi_0 = -\frac{\pi}{2}$, the set of suitable fixed points with $I = 0$ is empty and these solutions are not discussed any further.

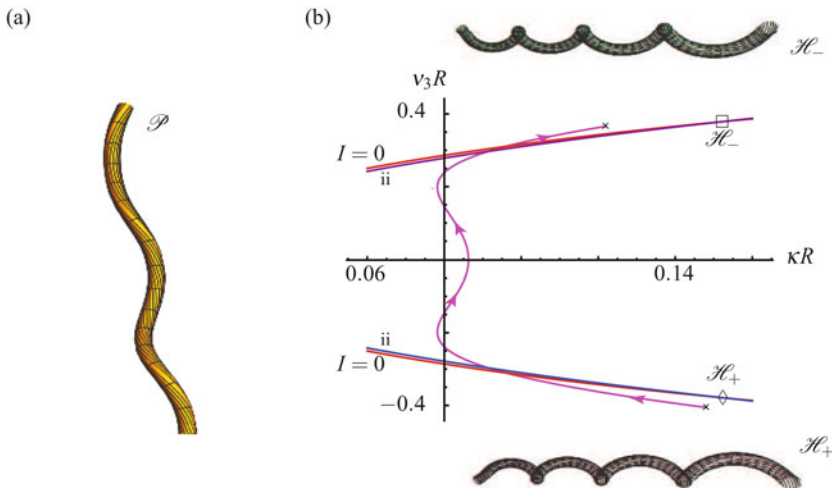


Fig. 5.23 (a) The deformed rod corresponding to an approximation \mathcal{P} to the perversion connecting a pair of helical solutions \mathcal{H}_+ and \mathcal{H}_- . The pair of solutions \mathcal{H}_+ and \mathcal{H}_- satisfy Eqn. (5.180) with the angle of twist $\phi = \phi_0 = \frac{\pi}{2}$ for a given value of $f_0 = \frac{F_0 R^2}{EI_1} = 1$ and have a value of the integral $I = \mathbf{n} \cdot \mathbf{m} = 0$. (b) The evolution of $\kappa(\xi)$ and $v_3(\xi)$ along \mathcal{P} . The level set $I = 0$ of the integral $\mathbf{n} \cdot \mathbf{m}$ in the $\kappa - v_3$ parameter plane and the points \mathcal{H}_+ (labeled with a \diamond) and \mathcal{H}_- (labeled with a \square) are also shown. The parameter values and labels are identical to those for Figure 5.22.

For a given F_0 , and a pair \mathcal{H}_\pm , the next task is to see if there is a solution to the differential equations (5.169) that connects the pair of fixed points. To progress, the form (5.169) is not convenient to use. Instead, we use the \mathbf{d}_i components of the balances of linear and angular momenta.⁴² The resulting set of eighteen first-order

⁴¹ Whence our reference to the critical value $f_0 = \frac{1}{\mathcal{D}}$ in the caption for Figure 5.22.

⁴² The derivation of this form of $\mathbf{m}' + \mathbf{r}' \times \mathbf{n} = \mathbf{0}$ is similar to the derivation of Eqn. (5.119) and is discussed in Exercise 5.14.

differential equations are⁴³

$$\begin{aligned}\mathbf{r}' &= \mathbf{d}_3, & \mathbf{d}_1' &= v_3 \mathbf{d}_2 - v_2 \mathbf{d}_3, & \mathbf{d}_2' &= -v_3 \mathbf{d}_1 + \left(v_1 + \frac{1}{R}\right) \mathbf{d}_3, \\ \mathbf{d}_3' &= v_2 \mathbf{d}_1 - \left(v_1 + \frac{1}{R}\right) \mathbf{d}_2,\end{aligned}\quad (5.184)$$

and

$$n_1' = -v_2 n_3 + v_3 n_2, \quad n_2' = -v_3 n_1 + \left(v_1 + \frac{1}{R}\right) n_3,$$

$$n_3' = -\left(v_1 + \frac{1}{R}\right) n_2 + v_2 n_1,$$

$$\begin{aligned}EI_1 v_1' - EI_2 v_2 v_3 + \mathcal{D} v_2 v_3 &= n_2, \\ EI_2 v_2' - \mathcal{D} \left(v_1 + \frac{1}{R}\right) v_3 + EI_1 v_3 v_1 &= -n_1, \\ \mathcal{D} v_3' - EI_1 v_2 v_1 + EI_2 \left(v_1 + \frac{1}{R}\right) v_2 &= 0.\end{aligned}\quad (5.185)$$

In these equations,

$$\mathbf{n} = n_1 \mathbf{d}_1 + n_2 \mathbf{d}_2 + n_3 \mathbf{d}_3 = -F_0 \mathbf{E}. \quad (5.186)$$

Subject to the appropriate boundary conditions, we then solve the six first-order differential equations (5.185) to determine the heteroclinic orbit connecting the fixed points \mathcal{H}_+ ,

$$\begin{aligned}v_1(-\infty) &= \kappa_0 - \frac{1}{R}, & v_2(-\infty) &= 0, & v_3(-\infty) &= \tau_0, \\ \mathbf{n}(-\infty) &= \left(\mathcal{D}\tau_0 - EI\left(\frac{\tau_0}{\kappa_0}\right)\left(\kappa_0 - \frac{1}{R}\right)\right)(\mathbf{d}_1(-\infty) + \tau_0 \mathbf{d}_3(-\infty)),\end{aligned}\quad (5.187)$$

and \mathcal{H}_- ,

$$\begin{aligned}v_1(\infty) &= \kappa_0 - \frac{1}{R}, & v_2(\infty) &= 0, & v_3(\infty) &= -\tau_0, \\ \mathbf{n}(\infty) &= \left(-\mathcal{D}\tau_0 + EI\left(\frac{\tau_0}{\kappa_0}\right)\left(\kappa_0 - \frac{1}{R}\right)\right)(\mathbf{d}_1(-\infty) - \tau_0 \mathbf{d}_3(-\infty)).\end{aligned}\quad (5.188)$$

We have restricted attention to an isotropic rod, i.e., $I = I_1 = I_2$, in writing the above expressions for the fixed points. One can choose $\mathbf{d}_j(-\infty) = \mathbf{E}_j$. If an orbit can be found connecting these two fixed points, then this orbit will correspond to a

⁴³ Note that we can express each of the vector equations $\mathbf{d}_i' = (\mathbf{P}(\mathbf{v} + \mathbf{v}_0)) \times \mathbf{d}_i$ in terms of their \mathbf{E}_k components to form three first-order differential equations. However, in the interests of brevity, we refrain from writing out the components.

perversion connecting two helical solutions with opposite handedness. These orbits can only be found numerically, and the numerical computations are challenging.

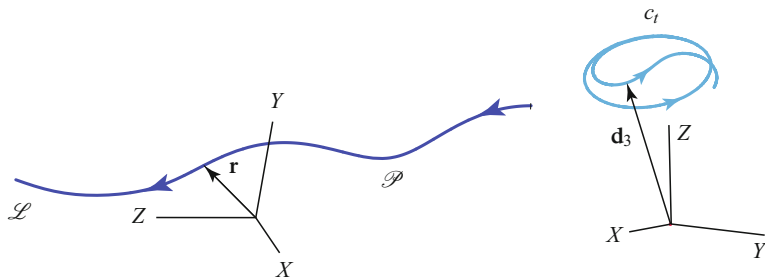


Fig. 5.24 The centerline $\mathbf{r}(\xi)$ and tangent indicatrix c_t for the approximation \mathcal{P} to a perversions that is shown in Figure 5.23. The arrows indicate the direction of increasing ξ .

An example of an approximation to the heteroclinic orbit is shown in Figure 5.23(a). The procedure used to compute this solution is taken from [235].⁴⁴ The solution is supposed to connect the point $(\kappa_0, \tau_0) \approx (0.15193, -0.37837)$ to the point $(\kappa_0, \tau_0) \approx (0.15193, +0.37837)$. However, owing to the approximation procedure used, the solution asymptotes to and from points in the $\kappa - v_3$ parameter plane that are distinct from \mathcal{H}_{\pm} . The centerline $\mathbf{r}(\xi)$ and the tangent indicatrix c_t corresponding to \mathcal{P} are shown in Figure 5.24. Observe that the tangent indicatrix starts off as a circle (as expected for a helical space curve⁴⁵) but does not quite transition to a circle (for the tangent indicatrix corresponding to \mathcal{H}_{-}). The behavior of the indicatrix is also in stark contrast to the seemingly straight shape of the centerline. Indeed, the approximate perversions \mathcal{P} found by McMillen and Goriely's method are surprisingly straight given that they connect two helices of opposite handedness (cf. the examples shown in [235, Figure 16]). However, examining the perversions in Figure 5.21, this also appears to be the case for tendril perversions.

5.17 Buckling of a Clamped Rod

The work we have just discussed on tendril perversions suffers from the deficiencies that it applies only to infinitely long rods and only a single perversions is found. In nature, just as in telephone cords, multiple perversions are present in rods of finite length. To address this problem, Domokos and Healey [90] examined the problem of a rod of finite length, say ℓ , that has a constant intrinsic curvature v_{01} . The ends of the rod are clamped and with the appropriate terminal moments and an arbitrary

⁴⁴ We are grateful to Tyler McMillen and Alain Goriely for generously supplying the code needed to construct the solutions shown in Figures 5.23 and 5.24.

⁴⁵ See Figure 3.7 on Page 99 in Chapter 3.

force, the rod is straightened (cf. Figure 5.25). It is then of interest to examine what happens to the rod when the force is varied. As noted in [90] and also demonstrated in the experiments in Liu et al. [209] it is not unusual to find multiple perversions. In [90], it is shown explicitly how these perversions are related to bifurcations from the straight configuration. Subsequent work by Healey and his students in [159, 190] addressed the stability of some of these solutions.

While we do not explore the bifurcations, we examine the linearized buckling modes found by Domokos and Healey in [90]. Central to the analysis is the establishment of a set of equations governing supposedly small perturbations to a static deformed configuration of the rod. These developments fall into the category of “small-on-large” in the continuum mechanics literature. As we shall see, when we confine our work to the case where the rod is initially straight (i.e., $v_{0_1} = 0$), then we would recover a pair of familiar differential equations for the flexural perturbations and an equation for the twist. These three equations correspond to the linearized equations for Kirchhoff's rod theory and the (expected) decoupling will also appear in other linearized theories from Green et al. [131, 138] that we present in Chapter 7.

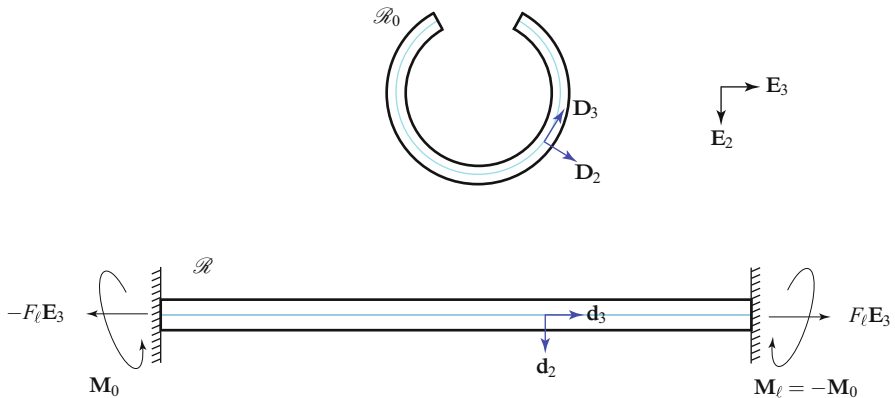


Fig. 5.25 Reference \mathcal{R}_0 and present \mathcal{R} configurations of an intrinsically curved rod with $v_{0_1} = \frac{1}{R} > 0$. The centerline of the rod has a length ℓ and the rod is deformed by terminal moments into a straight line. The ends of the rod are then clamped as shown and subject to a pair of balanced terminal loadings.

We return to the intrinsically curved rod of the previous section but now assume that it is of finite length ℓ . As shown in Figure 5.25, we presume the rod is straightened by the application of terminal moments,

$$\mathbf{M}_0 = M_0 \mathbf{D}_1 = EI_1 v_{1_0} \mathbf{E}_1, \quad \mathbf{M}_\ell = -M_0 \mathbf{D}_1 = -EI_1 v_{1_0} \mathbf{E}_1, \quad (5.189)$$

and the ends of the rod are then clamped:

$$\begin{aligned}\mathbf{r}(\xi = 0) &= \mathbf{0}, & \mathbf{r}(\xi = \ell) \cdot \mathbf{E}_1 &= 0, & \mathbf{r}(\xi = \ell) \cdot \mathbf{E}_2 &= 0, \\ \mathbf{d}_k(\xi = 0) &= \mathbf{E}_k, & \mathbf{d}_k(\xi = \ell) &= \mathbf{E}_k, & \mathbf{n}(\xi = \ell) &= F_\ell \mathbf{E}_3.\end{aligned}\quad (5.190)$$

Note that $\mathbf{P}(\xi = 0) = \mathbf{P}_0^T(\xi = 0)$ and $\mathbf{P}(\xi = \ell) = \mathbf{P}_0^T(\xi = 0)$. We shall use a set of 1-2-3 Euler angles to parameterize \mathbf{P} :

$$\begin{aligned}\mathbf{P}\mathbf{P}_0 &= \sum_{i=1}^3 \mathbf{d}_i \otimes \mathbf{E}_i = \mathbf{Q}_E(\vartheta^3, \mathbf{e}_3) \mathbf{Q}_E(\vartheta^2, \mathbf{e}_2) \mathbf{Q}_E(\vartheta^1, \mathbf{e}_1) \mathbf{Q}_E(\vartheta^0, \mathbf{D}_1), \\ \mathbf{P}_0 &= \sum_{i=1}^3 \mathbf{D}_i \otimes \mathbf{E}_i = \cos(\vartheta^0)(\mathbf{I} - \mathbf{E}_1 \otimes \mathbf{E}_1) + \sin(\vartheta^0) \text{skew}(\mathbf{E}_1) + \mathbf{E}_1 \otimes \mathbf{E}_1.\end{aligned}\quad (5.191)$$

Further details on these angles are presented in Exercise 5.15. It should be apparent from the reference configuration shown in Figure 5.25 that $\vartheta_0' = v_{01} = \frac{1}{R} > 0$.

The straight configuration \mathcal{R} shown in Figure 5.25 is defined by $\mathbf{r} = \xi \mathbf{E}_3$, $\mathbf{n} = F_\ell \mathbf{E}_3$, and $\mathbf{m} = -M_0 \mathbf{E}_1$. We leave it as an exercise to show that the balance laws are satisfied. We next consider perturbations to this configuration while preserving the boundary conditions (5.190):

$$\begin{aligned}\mathbf{r} &= \xi \mathbf{E}_3 + \varepsilon u_1 \mathbf{E}_1 + \varepsilon u_2 \mathbf{E}_2 + \varepsilon u_3 \mathbf{E}_3, \\ \vartheta^1 &= -\vartheta^0 + \varepsilon \bar{\theta}_1, & \vartheta^2 &= 0 + \varepsilon \bar{\theta}_2, & \vartheta^3 &= 0 + \varepsilon \bar{\theta}_3, \\ n_1 &= 0 + \varepsilon \bar{n}_1, & n_2 &= 0 + \varepsilon \bar{n}_2, & n_3 &= F_\ell + \varepsilon \bar{n}_3,\end{aligned}\quad (5.192)$$

where ε is assumed to be small. Evaluating \mathbf{v} and \mathbf{P} with the help of Eqns. (5.274) and (5.278), we find that

$$\begin{aligned}v_1 &= -v_{01} + \varepsilon \bar{\theta}_1', & v_2 &= \varepsilon \bar{\theta}_2', & v_3 &= \varepsilon \bar{\theta}_3', \\ \mathbf{d}_1 &= \mathbf{E}_1 + \varepsilon \bar{\theta}_3 \mathbf{E}_2 - \varepsilon \bar{\theta}_2 \mathbf{E}_3, & \mathbf{d}_2 &= \mathbf{E}_2 - \varepsilon \bar{\theta}_3 \mathbf{E}_1 + \varepsilon \bar{\theta}_1 \mathbf{E}_3, \\ \mathbf{d}_3 &= \mathbf{E}_3 + \varepsilon \bar{\theta}_2 \mathbf{E}_1 - \varepsilon \bar{\theta}_1 \mathbf{E}_2 = \left(1 + \varepsilon u_3'\right) \mathbf{E}_3 + \varepsilon u_1' \mathbf{E}_1 + \varepsilon u_2' \mathbf{E}_2.\end{aligned}\quad (5.193)$$

While $\|\mathbf{d}_3\| = 1$, this inextensibility constraint is only approximately satisfied to $\mathcal{O}(\varepsilon)$. Substituting the ansatzen (5.193) into the balance law (5.185) and ignoring terms of $\mathcal{O}(\varepsilon^2)$ we find the following differential equations:

$$\left. \begin{aligned}\bar{\theta}_1 &= -u_2', \\ EI_1 \bar{\theta}_1'' &= F_\ell \bar{\theta}_1,\end{aligned}\right\} \leftarrow \text{flexural modes}$$

$$\left. \begin{aligned}\bar{\theta}_2 &= u_1', \\ EI_2 \bar{\theta}_2'' - M_0 \bar{\theta}_3' &= F_\ell \bar{\theta}_2, \\ \mathcal{D} \bar{\theta}_3'' + M_0 \bar{\theta}_2' &= 0.\end{aligned}\right\} \leftarrow \text{flexural-torsional modes}\quad (5.194)$$

The boundary conditions associated with these equations are

$$u_\alpha(\xi = 0) = 0, \quad u_\alpha(\xi = \ell) = 0, \quad \bar{\theta}_\alpha(\xi = 0) = 0, \quad \bar{\theta}_\alpha(\xi = \ell) = 0, \quad (5.195)$$

where $\alpha = 1, 2$. Observe that the flexural (or bending) modes described by u_2 are uncoupled from the flexural-torsional modes $u_1 - \bar{\theta}_3$.

By differentiating Eqn. (5.194)₂ once and then using Eqn. (5.194)₁, we arrive at a canonical equation for u_2 . Similarly, by differentiating Eqn. (5.194)₄ once, eliminating $\bar{\theta}_3$ using Eqn. (5.194)₅, and then using Eqn. (5.194)₃, we arrive at an equation for u_1 . The respective equations and their associated boundary conditions are

$$\begin{aligned} u_2''' - \frac{F_\ell}{EI_1} u_2'' &= 0, \quad u_2(\xi = 0, \ell) = 0, \quad u_2'(\xi = 0, \ell) = 0, \\ u_1''' + \left(\frac{M_0^2}{\mathcal{D}EI_2} - \frac{F_\ell}{EI_2} \right) u_1'' &= 0, \quad u_1(\xi = 0, \ell) = 0, \quad u_1'(\xi = 0, \ell) = 0. \end{aligned} \quad (5.196)$$

The general solution $u(\xi)$ to this pair of differential equations, associated characteristic equation (5.200) and modes (5.201) can be found in classic texts on elastic stability (see [345, Section 2.2]):

$$u = A_1 \cos(v\xi) + A_2 \sin(v\xi) + A_3\xi + A_4, \quad (5.197)$$

where $v^2 = -\frac{F_\ell}{EI_1}$ or $\left(\frac{M_0^2}{\mathcal{D}EI_2} - \frac{F_\ell}{EI_2} \right)$, and $A_{1,2,3,4}$ are determined by the boundary and initial conditions.

The coupled torsional-flexural modes can be solely attributed to the nonvanishing intrinsic curvature. Indeed, if we set $v_{01} = 0$, then we find three sets of equations for the pair of flexures u_1 and u_2 and the torsion $\bar{\theta}_3$ about a straight undeformed equilibrium configuration:

$$EI_1 u_2''' = F_\ell u_2'', \quad EI_2 u_1''' = F_\ell u_1'', \quad \mathcal{D}\bar{\theta}_3'' = 0. \quad (5.198)$$

This decoupling is also a consequence of the choice of constitutive relations and the geometry of the undeformed rod. Later, in Chapter 7, we shall find an instance of a similar decoupling for extensional, torsional, and flexural deformations in a more general rod theory. In all of these instances, if appropriate geometric and constitutive symmetries are imposed, then the linearized equations for flexure reduce to those for a strut that were first proposed by Euler [106] and occupy a prominent place in texts on elastic stability.⁴⁶

Imposing the four boundary conditions on $u_{1,2}$ and their derivatives produces the following set of linear equations for $A_{1,2,3,4}$:

⁴⁶ A translation of Euler's comments on stability can be found in [254, Pages 102–103]. Timoshenko and Gere [345, Chapter 2] contains a comprehensive discussion of the buckling of a strut and the dependency of the critical loads on the boundary conditions. The text by Ziegler [375] is also highly recommended.

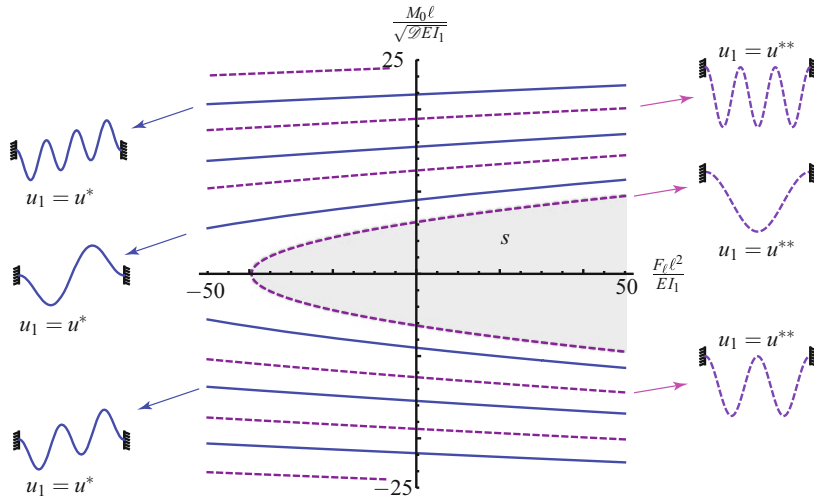


Fig. 5.26 Solutions to the characteristic equations $\tan\left(\frac{v\ell}{2}\right) = \frac{v\ell}{2}$ (dashed lines) and $\sin\left(\frac{v\ell}{2}\right) = 0$ (solid lines) in the $\frac{F_\ell \ell^2}{EI_1} - \frac{M_0 \ell}{\sqrt{D E I_1}}$ parameter plane. The associated modes shapes, from Eqns. (5.201) and (5.202), for the flexural components $u_1(\xi)$ (and the readily inferred torsional components $\bar{\theta}_3(\xi) = -\frac{M_0}{D} u_1(\xi)$) of the associated coupled flexural-torsional modes are also shown.

$$\begin{bmatrix} 1 & 0 & 0 & 1 \\ \cos(v\ell) & \sin(v\ell) & \ell & 1 \\ 0 & v & 1 & 0 \\ -v \sin(v\ell) & v \cos(v\ell) & 1 & 0 \end{bmatrix} \begin{bmatrix} A_1 \\ A_2 \\ A_3 \\ A_4 \end{bmatrix} = \begin{bmatrix} 0 \\ 0 \\ 0 \\ 0 \end{bmatrix}. \quad (5.199)$$

For nontrivial solutions, the determinant of the matrix in this equation must be zero. The resulting equation, which will be solved for $v\ell$, is known as the characteristic equation:

$$\sin\left(\frac{v\ell}{2}\right) \left(\cos\left(\frac{v\ell}{2}\right) - \frac{2}{v\ell} \sin\left(\frac{v\ell}{2}\right) \right) = 0. \quad (5.200)$$

Observe that this equation can be split into a pair of equations for $v\ell$: $\sin(v\ell/2) = 0$ and $\tan(v\ell/2) = v\ell/2$. In addition, we can solve for $A_{2,3,4}$ in terms of A_1 to find that

$$u(\xi) = \begin{cases} u^*(\xi) = A_1 (\cos(v\xi) - 1 + \cot(\frac{v\ell}{2}) (v\xi - \sin(v\xi))) \text{ when} \\ \tan(\frac{v\ell}{2}) = \frac{v\ell}{2} \neq 0, \\ u^{**}(\xi) = A_1 (\cos(v\xi) - 1) \text{ when } \sin(\frac{v\ell}{2}) = 0. \end{cases} \quad (5.201)$$

For the case (5.194)₂ involving coupled flexure and torsion, we find the surprisingly simple results

$$\bar{\theta}_3(\xi) = \begin{cases} \bar{\theta}_3^*(\xi) = -\frac{M_0}{\mathcal{D}} u^*(\xi) = -v_{01} u^*(\xi) \text{ when } \tan\left(\frac{v\ell}{2}\right) = \frac{v\ell}{2} \neq 0, \\ \bar{\theta}_3^{**}(\xi) = -\frac{M_0}{\mathcal{D}} u^{**}(\xi) = -v_{01} u^*(\xi) \text{ when } \sin\left(\frac{v\ell}{2}\right) = 0. \end{cases} \quad (5.202)$$

For the rod shown in Figure 5.25, $v_{01} = +1/R$ and so we have $\bar{\theta}_3 = -u_1/R$. The results (5.201) enable us to return to the equations (5.196)₁ for the flexural perturbations in the \mathbf{E}_2 direction and find the buckling loads F_ℓ for the rods. The results are similar to those we presented earlier in Chapter 4 (see Section 4.9.2 in particular) and are not mentioned any further.

For the coupled flexural-torsion modes, the characteristic equation (5.200) provides two sets of values for $v\ell$ (one of which is $v\ell = 2\pi, 4\pi, \dots$) and two sets of modes (cf. Eqns. (5.201) and (5.202)). Referring to Figure 5.26, we solve the equations $\tan(v\ell/2) = v\ell/2$ and $\sin(v\ell/2) = 0$ for the corresponding values of M_0 and F_ℓ . Based on this linearized analysis, buckling of the clamped rod is said to have occurred when the pairing $M_0 - F_\ell$ are such that they no longer lie in the shaded region labeled s in this figure. When $M_0 = 0$, the associated critical value of the compressive load $F_\ell = -4\pi^2 EI_1/\ell^2$ is well known.⁴⁷ When the rod has an intrinsic curvature (i.e., $M_0 \neq 0$), then it is easy to see from Figure 5.26 an observation made by Domokos and Healey in [90]: the rod can buckle even when $F_\ell > 0$ (i.e., the rod is in tension) if $v_{01} = \pm 1/R$ is sufficiently large.

5.18 Spiral Springs and a Stiffness Matrix

A natural extension to the analysis just presented would be to consider a rod whose centerline in its undeformed state has the shape of a circular helix. Such an analysis is needed to determine the behavior of a helical spring under external loading. The simplest model for such a spring is to consider a thin circular inextensible rod of length ℓ whose centerline forms a circular helix of radius R and pitch angle ς (cf. Figure 5.27):

$$\mathbf{R}(\xi) = R\mathbf{e}_{\theta_0} + R\theta_0(\xi) \tan(\varsigma) \mathbf{E}_3, \quad (5.203)$$

where $\mathbf{e}_{\theta_0} = \cos(\theta_0(\xi))\mathbf{E}_1 + \sin(\theta_0(\xi))\mathbf{E}_2$. This configuration is chosen as the reference configuration of the rod and we assume that $\theta'_0 > 0$. The rod is loaded at its ends by a force and moment combination that is known as a wrench:

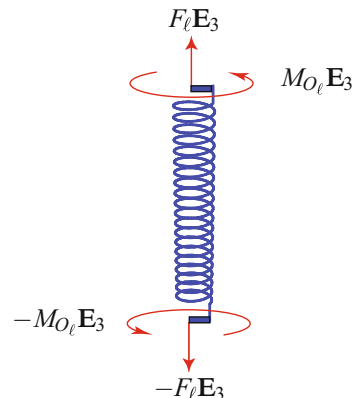


Fig. 5.27 A helical spring loaded by a terminal force $\mathbf{F}_\ell = F_\ell \mathbf{E}_3$ and a terminal moment $\mathbf{M}_{O_\ell} = M_{O_\ell} \mathbf{E}_3 = \mathbf{M}_\ell + \mathbf{r}(\ell) \times \mathbf{F}_\ell$.

⁴⁷ See [213, Section 264] or [345, Chapter 2].

$$\mathbf{n}(\ell^-) = F_\ell \mathbf{E}_3, \quad \mathbf{m}(\ell^-) = M_{O_\ell} \mathbf{E}_3 - \mathbf{r}(\ell^-) \times F_\ell \mathbf{E}_3. \quad (5.204)$$

For such combinations, the force \mathbf{F}_ℓ and moment \mathbf{M}_{O_ℓ} are parallel. As shown in Figure 5.27, rigid attachments can be added to the ends of the spring so that an applied force and an applied moment which act in the same direction can be applied to the spring. Following the classical theory of spiral (helical) springs that is discussed in Love [213, Section 271], we seek to determine expressions for the change in height of the spring and the change in a cylindrical polar angle. These changes determine the gross extensional and torsional stiffnesses of the spring - the microscopic stiffnesses for these effects would be infinity and \mathcal{D} .

The model we discuss here dates to the 19th century. However, as has been recently pointed out by Đurićković et al. [89] it serves as a very useful model for studying the twist-stretch coupling observed in experiments on DNA strands that we shall discuss in Section 6.5 of Chapter 6.

5.18.1 The Reference Configuration

In the reference configuration \mathcal{R}_0 the position vector of a point on the centerline of the rod is assumed to have a representation (5.203). We choose the directors \mathbf{D}_1 and \mathbf{D}_2 so the rod is untwisted in its reference state. The rotation tensor \mathbf{P}_0 can be decomposed into the product of two simple rotations⁴⁸:

$$\mathbf{P}_0 = \mathbf{Q}_E(\varphi^2, \cos(\varphi^1) \mathbf{E}_1 + \sin(\varphi^1) \mathbf{E}_2) \mathbf{Q}_E(\varphi^1, \mathbf{E}_3), \quad (5.205)$$

where

$$\theta_0(\xi) = \varphi^1(\xi) - \pi, \quad \varsigma = \frac{\pi}{2} - \varphi^2. \quad (5.206)$$

A quick calculation shows that the intrinsic strains for the rod are

$$\mathbf{v}_0 = v_{0_2} \mathbf{D}_2 + v_{0_3} \mathbf{D}_3 = \frac{\partial \varphi^1}{\partial \xi} \cos(\varphi^2) \mathbf{D}_3 + \frac{\partial \varphi^1}{\partial \xi} \sin(\varphi^2) \mathbf{D}_2. \quad (5.207)$$

Using Eqn. (1.33), it can be shown that the strains are related to the curvature κ_0 and torsion τ_0 of the helical space curve defined by $\mathbf{R}(\xi)$:

$$\kappa_0 = \frac{\cos^2(\varsigma)}{R} = \frac{\partial \varphi^1}{\partial \xi} \sin(\varphi^2), \quad \tau_0 = \frac{\cos(\varsigma) \sin(\varsigma)}{R} = \frac{\partial \varphi^1}{\partial \xi} \cos(\varphi^2). \quad (5.208)$$

The following identities will be particularly useful in the sequel:

$$\tau_0^2 + \kappa_0^2 = \frac{\kappa_0}{R}, \quad \tan(\varsigma) \kappa_0 = \tau_0. \quad (5.209)$$

⁴⁸ Our comments here are intimately related to the discussion on \mathbf{Q}_{SF} and \mathbf{o}_{SF} in Section 5.10.

For the helical space curve defined by $\mathbf{R}(\xi)$, the corresponding tangent vector \mathbf{e}_{t_0} , normal vector \mathbf{e}_{n_0} , and binormal vector \mathbf{e}_{b_0} are

$$\mathbf{e}_{t_0} = \mathbf{D}_3, \quad \mathbf{e}_{n_0} = \mathbf{D}_1, \quad \mathbf{e}_{b_0} = \mathbf{D}_2. \quad (5.210)$$

Helpful expressions for the Frenet triad basis vectors can be found in Eqn. (1.31).

5.18.2 The Balance Laws

We assume that the cross sections of the rod are circular, $I_1 = I_2 = I$, and that the strain energy function of the rod is

$$2\rho_0\psi = EIv_1^2 + EIv_2^2 + \mathcal{D}v_3^2. \quad (5.211)$$

The balance laws for the rod are $\mathbf{n}' = \mathbf{0}$ and $\mathbf{m}' + \mathbf{r}' \times \mathbf{n} = \mathbf{0}$. With the help of the terminal loading conditions,

$$\mathbf{n}(\ell^-) = F_\ell \mathbf{E}_3, \quad \mathbf{m}(\ell^-) = M_{O_\ell} \mathbf{E}_3 - \mathbf{r}(\ell^-) \times F_\ell \mathbf{E}_3, \quad (5.212)$$

we find that the contact force and a moment are parallel to \mathbf{E}_3 throughout the length of the spring:

$$\mathbf{n}(\xi) = F_\ell \mathbf{E}_3, \quad \mathbf{m}(\xi) + \mathbf{r}(\xi) \times \mathbf{n}(\xi) = M_{O_\ell} \mathbf{E}_3. \quad (5.213)$$

Projecting the balance of angular momentum onto the basis vectors $\{\mathbf{d}_1, \mathbf{d}_2, \mathbf{d}_3\}$ and using the constitutive relations for \mathbf{m} , the following differential equations can be established⁴⁹:

$$\begin{aligned} EIv'_1 - EIv_2(v_3 + v_{0_3}) + \mathcal{D}(v_2 + v_{0_2})v_3 &= \mathbf{d}_2 \cdot F_\ell \mathbf{E}_3, \\ EIv'_2 - \mathcal{D}v_1v_3 + EI(v_3 + v_{0_3})v_1 &= -\mathbf{d}_1 \cdot F_\ell \mathbf{E}_3, \\ \mathcal{D}v'_3 EIv_{0_2}v_1 &= 0. \end{aligned} \quad (5.214)$$

In writing this form of the equations we have exploited the symmetry $EI_1 = EI_2$ and the fact that $v_{0_1} = 0$.

We seek solutions to Eqn. (5.214) where the centerline of the deformed rod forms a helical space curve:

$$\mathbf{r}(\xi) = r(\cos(\theta(\xi))\mathbf{E}_1 + \sin(\theta(\xi))\mathbf{E}_2) + r\theta(\xi)\tan(\sigma)\mathbf{E}_3, \quad (5.215)$$

with $\theta' > 0$. The directors lie in the osculating plane,

$$\mathbf{e}_t = \mathbf{d}_3, \quad \mathbf{e}_n = \mathbf{d}_1, \quad \mathbf{e}_b = \mathbf{d}_2, \quad (5.216)$$

⁴⁹ Further details on the procedure to establish equations of this form are discussed in Exercise 5.14.

and the strains v_k are related to the curvature, $\kappa = \frac{\cos^2(\sigma)}{r}$, and torsion, $\tau = \frac{\cos(\sigma)\sin(\sigma)}{r}$, of the curve formed by the centerline in \mathcal{R} in the following manner:

$$v_1 = 0, \quad v_2 = \kappa - v_{0_2} = \kappa - \kappa_0, \quad v_3 = \tau - v_{0_3} = \tau - \tau_0. \quad (5.217)$$

For the sought-after solution,

$$\mathbf{P}\mathbf{P}_0 = \mathbf{Q}_{\mathbf{E}} \left(\frac{\pi}{2} - \sigma, \cos(\theta + \pi) \mathbf{E}_1 + \sin(\theta + \pi) \mathbf{E}_2 \right) \mathbf{Q}_{\mathbf{E}} (\theta + \pi, \mathbf{E}_3). \quad (5.218)$$

This tensor, just like its counterpart for the reference configuration, is an example of the tensor \mathbf{Q}_{SF} .

Setting $v'_1 = 0$, $v'_2 = 0$, and $v'_3 = 0$ in Eqn. (5.214), we see that this balance law is satisfied provided

$$\begin{aligned} \mathbf{d}_1 \cdot F_{\ell} \mathbf{E}_3 &= 0, & v_1 &= 0, \\ EI_2 v_2 (v_3 + v_{0_3}) - \mathcal{D}(v_2 + v_{0_2}) v_3 + \mathbf{e}_b \cdot F_{\ell} \mathbf{E}_3 &= 0. \end{aligned} \quad (5.219)$$

The first two of these equations are trivially satisfied and the third simplifies to

$$\cos(\sigma) F_{\ell} = \mathcal{D} \kappa (\tau - \tau_0) - EI \tau (\kappa - \kappa_0). \quad (5.220)$$

The contact moment in the rod is

$$\mathbf{m} = EI(\kappa - \kappa_0) \mathbf{d}_2 + \mathcal{D}(\tau - \tau_0) \mathbf{d}_3. \quad (5.221)$$

Using the boundary condition (5.212)₂ and Eqn. (1.31), we find that

$$M_{O_{\ell}} = EI(\kappa - \kappa_0) \cos(\sigma) + \mathcal{D}(\tau - \tau_0) \sin(\sigma). \quad (5.222)$$

The relations (5.220) and (5.222) provide equations to determine the moment and force needed to generate a given helical centerline and a twistless rod.

5.18.3 A Stiffness Matrix

Consider applying the wrench $(F_{\ell} \mathbf{E}_3, M_{O_{\ell}} \mathbf{E}_3)$ to the rod in its reference state. The deformation of the rod as a result of this system deforms the rod's centerline into a helix and the twist of the rod remains 0. Changes in the scalars F_{ℓ} and $M_{O_{\ell}}$ alter the radius r and pitch angle σ of the helix and the position vector $\mathbf{r}(\xi = \ell)$:

$$\begin{aligned} \Delta \theta &= \theta(\xi = \ell) - \theta_0(\xi = \ell) = \ell \left(\frac{\cos(\sigma)}{r} - \frac{\cos(\varsigma)}{R} \right), \\ \Delta z &= z(\xi = \ell) - z_0(\xi = \ell) = \ell (\sin(\sigma) - \sin(\varsigma)). \end{aligned} \quad (5.223)$$

We define the following perturbations:

$$\Delta\sigma = \sigma - \varsigma, \quad \Delta r = r - R, \quad \Delta\kappa = \kappa - \kappa_0, \quad \Delta\tau = \tau - \tau_0, \quad (5.224)$$

and define the concomitant changes to F_ℓ and M_{O_ℓ} :

$$F_\ell = 0 + \Delta F_\ell, \quad M_{O_\ell} = 0 + \Delta M_{O_\ell}. \quad (5.225)$$

By considering Taylor series expansions of κ and τ and assuming that all quantities of the form $\Delta\kappa, \Delta r, \dots$ are small, it should not be difficult to verify that⁵⁰

$$\begin{aligned} \begin{bmatrix} \Delta\kappa \\ \Delta\tau \end{bmatrix} &= \begin{bmatrix} -\kappa_0 & -2\tau_0 \\ -\tau_0 & 2\kappa_0 - \frac{1}{R} \end{bmatrix} \begin{bmatrix} \frac{\Delta r}{R} \\ \Delta\sigma \end{bmatrix}, \\ \begin{bmatrix} \frac{\Delta z}{R} \\ \Delta\theta \end{bmatrix} &= \frac{\ell}{R} \begin{bmatrix} 0 & \cos(\varsigma) \\ -\cos(\varsigma) & -\sin(\varsigma) \end{bmatrix} \begin{bmatrix} \frac{\Delta r}{R} \\ \Delta\sigma \end{bmatrix}. \end{aligned} \quad (5.226)$$

Combining these two results, one finds that

$$\begin{bmatrix} \Delta\kappa \\ \Delta\tau \end{bmatrix} = \frac{R \sec(\varsigma)}{\ell} \begin{bmatrix} -\tau_0 & \kappa_0 \\ \kappa_0 & \tau_0 \end{bmatrix} \begin{bmatrix} \frac{\Delta z}{R} \\ \Delta\theta \end{bmatrix}. \quad (5.227)$$

These expressions can be used to quantify changes to the end point of any helical space curve as the torsion and curvature are varied.

Expanding the expressions (5.220) and (5.222) for F_ℓ and M_{O_ℓ} about their equilibrium values of 0 as functions of changing κ, τ , and σ , using Eqn. (5.227) and performing some minor rearranging, we find that the changes to these quantities can be related to the geometric changes at the end $\xi = \ell$ by a symmetric stiffness matrix:

$$\begin{bmatrix} \frac{\Delta F_\ell R^2}{EI} \\ \frac{\Delta M_{O_\ell} R}{EI} \end{bmatrix} = \begin{bmatrix} k_{11} & k_{12} \\ k_{12} & k_{22} \end{bmatrix} \begin{bmatrix} \frac{\Delta z}{R} \\ \Delta\theta \end{bmatrix}. \quad (5.228)$$

The components $k_{\alpha\beta}$ of the stiffness matrix have the compact representations

$$\begin{aligned} \begin{bmatrix} k_{11} & k_{12} \\ k_{12} & k_{22} \end{bmatrix} &= \frac{R^2}{\ell} \begin{bmatrix} \frac{\mathcal{D}}{EI} \kappa_0 + \frac{\tau_0^2}{\kappa_0} & \left(\frac{\mathcal{D}}{EI} - 1 \right) \tau_0 \\ \left(\frac{\mathcal{D}}{EI} - 1 \right) \tau_0 & \frac{\mathcal{D}}{EI} \frac{\tau_0^2}{\kappa_0} + \kappa_0 \end{bmatrix} \\ &= \frac{R^2}{\ell} \begin{bmatrix} -\frac{\tau_0}{\kappa_0} & \frac{\mathcal{D}}{EI} \\ 1 & \frac{\mathcal{D}}{EI} \frac{\tau_0}{\kappa_0} \end{bmatrix} \begin{bmatrix} -\tau_0 & \kappa_0 \\ \kappa_0 & \tau_0 \end{bmatrix}. \end{aligned} \quad (5.229)$$

As discussed in Love [213, Section 271], relations of the form (5.228) are classic and can be found in Kelvin and Tait [180, Section 607].⁵¹ We emphasize that the stiffness matrix pertains to small perturbations from the trivial equilibrium

⁵⁰ The identities (5.209) are particularly helpful in establishing several of the results which follow and enabling comparisons with [89, Eqns. (9) and (10)].

⁵¹ The representation (5.228) is a dimensionless form of [213, Eqn. (42), Section 271].

configuration. If perturbations from another helical configuration are of interest, then the components of this matrix are expected to change and it is a straightforward exercise to establish the stiffness matrix in this case.

Observe that the components of the stiffness matrix are combinations of the geometric (κ_0 , τ_0 , I , R , ℓ) and material (E and ν) properties of the rod. The stiffness matrix is symmetric, has a determinant $\frac{\mathcal{D}R^2}{EI\ell^2}$, and is positive definite. Indeed, it is possible to form an energy function E_{spring} consisting of a quadratic form composed of $\Delta\theta$, $\frac{\Delta z}{R}$ and the following stiffness matrix:

$$E_{\text{spring}} = \frac{1}{2} k_{11} \left(\frac{\Delta z}{R} \right)^2 + k_{12} \frac{\Delta z}{R} \Delta\theta + \frac{1}{2} k_{22} \Delta\theta^2. \quad (5.230)$$

Functions of this type would appear in rigid body dynamics problems when the spring is treated as a discrete element. As astutely discussed by Đuričković et al. [89] such a function provides a model to interpret recent works, such as [120, 177, 207, 227], on the twist-stretch coupling in the mechanical testing of DNA strands. Particular focus is placed on a term that is equivalent to k_{12} in these works. Remarkably, Gore et al. [120] have been able to quantify this term for strands of B-DNA and estimate this quantity in the range of -90×10^{-21} Nm.

We can invert the linear relations (5.228) to find the useful results

$$\begin{bmatrix} \frac{\Delta z}{R} \\ \Delta\theta \end{bmatrix} = \frac{EI\ell}{\mathcal{D}} \begin{bmatrix} \frac{\mathcal{D}}{EI} \frac{\tau_0^2}{\kappa_0} + \kappa_0 & -\left(\frac{\mathcal{D}}{EI} - 1\right) \tau_0 \\ -\left(\frac{\mathcal{D}}{EI} - 1\right) \tau_0 & \frac{\mathcal{D}}{EI} \kappa_0 + \frac{\tau_0^2}{\kappa_0} \end{bmatrix} \begin{bmatrix} \frac{\Delta F_\ell R^2}{EI} \\ \frac{\Delta M_{O_\ell} R}{EI} \end{bmatrix} \\ = 2\pi \begin{bmatrix} \frac{\sin(\zeta)}{\cos^2(\zeta)} + \frac{EI}{\mathcal{D}} \cos(\zeta) & \left(\frac{EI}{\mathcal{D}} - 1\right) \sin(\zeta) \\ \left(\frac{EI}{\mathcal{D}} - 1\right) \sin(\zeta) & \cos(\zeta) + \frac{EI}{\mathcal{D}} \frac{\sin(\zeta)}{\cos^2(\zeta)} \end{bmatrix} \begin{bmatrix} \frac{\Delta F_\ell R^2}{EI} \\ \frac{\Delta M_{O_\ell} R}{EI} \end{bmatrix}. \quad (5.231)$$

For rods with circular cross sections, $\frac{EI}{\mathcal{D}} = 1 + \nu$, where ν is Poisson's ratio. Thus, $EI > \mathcal{D}$. Consequently, we can attribute twist-stretch coupling to the helical nature of the spring: if the spring were circular, $\zeta = 0$ and this coupling would be absent. It is easy to see from Eqn. (5.231) that the application of a positive increment ΔF_ℓ to the force acting on the end will result in a positive Δz and, assuming $\tau_0 > 0$, a positive $\Delta\theta$. Thus the spring will appear to overwind (as opposed to underwind for $\Delta\theta < 0$).⁵² In addition, we can also conclude with the help of the relations (5.228)₂ that the radius of the helix will shrink ($\Delta r < 0$). This shrinkage is in compliance with the fact that the centerline of the helical rod is inextensible (and so $\ell = 2\pi r \sec(\sigma) = 2\pi R \sec(\zeta)$).

Our discussion has been limited to the case considered in the classic work of Kelvin and Tait. Recently, Đuričković et al. [89] have extended this analysis to consider helical springs where $EI_1 \neq EI_2$ and linearized stiffness matrices for more general cases than the one we have presented.

⁵² The terminology we use here is from the literature on DNA testing (cf. Đuričković et al. [89]).

5.19 Closing Remarks

We have only the space and opportunity to touch upon a small fraction of the work that has been published on the terminally loaded rod where $EI_1 = EI_2$. To do full justice to these works would fill hundreds of pages. In addition, many of the problems considered in the earlier chapters have nonplanar counterparts where bending and torsion are significant which remain to be explored. If this chapter has both motivated the reader to further explore some of the papers mentioned (and the works they inspired) and provided sufficient background to read and appreciate these works, then it will have achieved one of its primary purposes.

5.20 Exercises

Exercise 5.1: Recall the expression (5.54) for the kinetic energy T of the rod. Using the symmetries $y^{\alpha\beta} = y^{\beta\alpha}$, show that

$$\dot{T} = \dot{\mathbf{r}} \cdot \dot{\mathbf{G}} + \dot{\mathbf{d}}_1 \cdot \dot{\mathbf{L}}^1 + \dot{\mathbf{d}}_2 \cdot \dot{\mathbf{L}}^2. \quad (5.232)$$

In a similar fashion, starting from (5.56), show that

$$\dot{\mathbf{h}}_O = \mathbf{r} \times \dot{\mathbf{G}} + \dot{\mathbf{d}}_1 \times \dot{\mathbf{L}}^1 + \dot{\mathbf{d}}_2 \times \dot{\mathbf{L}}^2. \quad (5.233)$$

Exercise 5.2: Show that the local form of (5.77) reduces to (5.80)₅ with the help of (5.233).

Exercise 5.3: Show that the local form of (5.79) reduces to (5.80)₇ with the help of (5.232).

Exercise 5.4: Consider the jump condition associated with the balance of material momentum for a rod. Show that this jump condition has the representation

$$\begin{aligned} \{\mathbf{n}\} \cdot [\mathbf{r}']_\gamma + \{\mathbf{m}\}_\gamma \cdot [\mathbf{P}(\mathbf{v} + \mathbf{v}_0)]_\gamma - [\rho_0 \psi]_\gamma &= \mathbf{M}_\gamma \cdot \{\mathbf{P}(\mathbf{v} + \mathbf{v}_0)\}_\gamma \\ &\quad + \mathbf{F}_\gamma \cdot \{\mathbf{r}'\}_\gamma + \mathbf{B}_\gamma. \end{aligned} \quad (5.234)$$

Exercise 5.5: Consider the local form of the balance of material momentum for a rod where $\mathbf{v}_0 = \mathbf{0}$. Show that this law is identically satisfied if $\mathbf{b} = \mathbf{b}_p$ where

$$\mathbf{b}_p = -\rho_0 \mathbf{f} \cdot \mathbf{r}' - \mathbf{m}_a \cdot (\mathbf{P}\mathbf{v}) - \left(\frac{\partial(\rho_0 \psi)}{\partial \xi} - \frac{\partial T}{\partial \xi} \right)_{\text{exp}}. \quad (5.235)$$

This result is used to help demonstrate when C is conserved in static boundary-value problems.

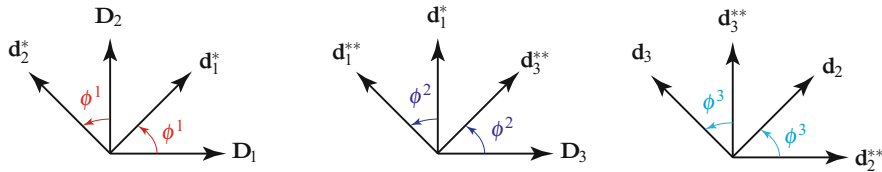


Fig. 5.28 Schematic of the three rotations used to define the 3-2-1 set of Euler angles (cf. Eqn. (5.236)).

Exercise 5.6: Consider the case where a set of 3-2-1 Euler angles are used to parameterize the rotation tensor $\mathbf{P} = \sum_{i=1}^3 \mathbf{d}_i \otimes \mathbf{D}_i$:

$$\mathbf{P} = \mathbf{Q}_{\mathbf{E}}(\phi^3, \mathbf{e}_3) \mathbf{Q}_{\mathbf{E}}(\phi^2, \mathbf{e}_2) \mathbf{Q}_{\mathbf{E}}(\phi^1, \mathbf{e}_1). \quad (5.236)$$

- (a) With the help of the intermediate results shown in Figure 5.28, show that the Euler basis vectors for the 3-2-1 set of Euler angles have the representations

$$\begin{aligned} \mathbf{e}_1 &= \mathbf{D}_3 \\ &= \cos(\phi^2) \cos(\phi^3) \mathbf{d}_3 + \cos(\phi^2) \sin(\phi^3) \mathbf{d}_2 - \sin(\phi^2) \mathbf{d}_1, \\ \mathbf{e}_2 &= \cos(\phi^1) \mathbf{D}_2 - \sin(\phi^1) \mathbf{D}_1 \\ &= \cos(\phi^3) \mathbf{d}_2 - \sin(\phi^3) \mathbf{d}_3, \\ \mathbf{e}_3 &= \cos(\phi^2) \cos(\phi^1) \mathbf{D}_1 + \cos(\phi^2) \sin(\phi^1) \mathbf{D}_2 - \sin(\phi^2) \mathbf{D}_3 \\ &= \mathbf{d}_1. \end{aligned} \quad (5.237)$$

- (b) Why is this set of Euler angles subject to the restrictions $\phi^1 \in [0, 2\pi]$, $\phi^2 \in (-\pi/2, \pi/2)$, and $\phi^3 \in [0, 2\pi)$?

- (c) Show that the components $P_{ik} = (\mathbf{P} \mathbf{D}_k) \cdot \mathbf{D}_i$ of \mathbf{P} have the representations

$$\begin{bmatrix} P_{11} & P_{12} & P_{13} \\ P_{21} & P_{22} & P_{23} \\ P_{31} & P_{32} & P_{33} \end{bmatrix} = \begin{bmatrix} c_2 c_1 & -c_3 s_1 - c_1 s_2 s_3 & -c_1 c_3 s_2 + s_1 s_3 \\ c_2 s_1 & c_3 c_1 - s_1 s_2 s_3 & -c_3 s_1 s_2 - c_1 s_3 \\ s_2 & c_2 s_3 & c_2 c_3 \end{bmatrix}. \quad (5.238)$$

In writing expressions for the components P_{ik} , we have employed the abbreviations $c_k = \cos(\phi^k)$ and $s_k = \sin(\phi^k)$.

- (d) Show that the dual Euler basis vectors for the 3-2-1 set of Euler angles have the representations

$$\begin{bmatrix} \mathbf{e}^1 \\ \mathbf{e}^2 \\ \mathbf{e}^3 \end{bmatrix} = \begin{bmatrix} 0 & \sin(\phi^3) \sec(\phi^2) & \cos(\phi^3) \sec(\phi^2) \\ 0 & \cos(\phi^3) & -\sin(\phi^3) \\ 1 & \sin(\phi^3) \tan(\phi^2) & \cos(\phi^3) \tan(\phi^2) \end{bmatrix} \begin{bmatrix} \mathbf{d}_1 \\ \mathbf{d}_2 \\ \mathbf{d}_3 \end{bmatrix}. \quad (5.239)$$

Establish the corresponding representations for \mathbf{e}^k in terms of \mathbf{D}_1 , \mathbf{D}_2 , and \mathbf{D}_3 .

- (e) Show that the components $v_i = \mathbf{v} \cdot \mathbf{D}_i$ of the strain vector $\mathbf{Pv} = \sum_{i=1}^3 v_i \mathbf{d}_i$ have the following representations in terms of the 3-2-1 set of Euler angles:

$$\begin{bmatrix} v_1 \\ v_2 \\ v_3 \end{bmatrix} = \begin{bmatrix} -\sin(\phi^2) & 0 & 1 \\ \cos(\phi^2)\sin(\phi^3) & \cos(\phi^3) & 0 \\ \cos(\phi^2)\cos(\phi^3) & -\sin(\phi^3) & 0 \end{bmatrix} \begin{bmatrix} \frac{\partial \phi^1}{\partial \xi} \\ \frac{\partial \phi^2}{\partial \xi} \\ \frac{\partial \phi^3}{\partial \xi} \end{bmatrix}. \quad (5.240)$$

In addition, show that the inverses of these relations are

$$\begin{bmatrix} \frac{\partial \phi^1}{\partial \xi} \\ \frac{\partial \phi^2}{\partial \xi} \\ \frac{\partial \phi^3}{\partial \xi} \end{bmatrix} = \begin{bmatrix} 0 & \sin(\phi^3)\sec(\phi^2) & \cos(\phi^3)\sec(\phi^2) \\ 0 & \cos(\phi^3) & -\sin(\phi_3) \\ 1 & \sin(\phi^3)\tan(\phi^2) & \cos(\phi^3)\tan(\phi^2) \end{bmatrix} \begin{bmatrix} v_1 \\ v_2 \\ v_3 \end{bmatrix}. \quad (5.241)$$

- (f) Show that the vector $\mathbf{d}_3 = \mathbf{r}'$ has the representation

$$\mathbf{d}_3 = \sin(\phi^2) \mathbf{D}_1 + \cos(\phi^2) \sin(\phi^3) \mathbf{D}_2 + \cos(\phi^2) \cos(\phi^3) \mathbf{D}_3. \quad (5.242)$$

With the help of this expression for \mathbf{r}' , compute representations for the curvature κ and torsion τ of the centerline of a rod whose rotation tensor \mathbf{P} is parameterized using a set of 3-2-1 Euler angles.

- (g) Consider an initially straight homogeneous rod which is subject to terminal moments and terminal forces and deforms into a twisted rod whose centerline remains straight (see Figure 5.6(b)). For this rod, we assume that $\mathbf{P} = \mathbf{Q}_{\mathbf{E}}(\phi_0, \mathbf{E}_3)$ where $\frac{\partial \phi_0}{\partial \xi}$ is a constant and choose $\mathbf{D}_k = \mathbf{E}_k$. To examine the stability of the deformed configuration, we consider perturbations to the straight twisted state:

$$\mathbf{P} = \mathbf{Q}_{\mathbf{E}}(\delta\phi^3, \mathbf{e}_3) \mathbf{Q}_{\mathbf{E}}(\delta\phi^2, \mathbf{e}_2) \mathbf{Q}_{\mathbf{E}}(\delta\phi^1, \mathbf{e}_1) \mathbf{Q}_{\mathbf{E}}(\phi_0, \mathbf{E}_3), \quad (5.243)$$

where $\delta\phi^k$ are assumed to be small.⁵³ Show that

$$\mathbf{P}\mathbf{v} \approx \frac{\partial \delta\phi^3}{\partial \xi} \mathbf{i}_1 + \frac{\partial \delta\phi^2}{\partial \xi} \mathbf{i}_2 + \left(\frac{\partial \delta\phi^1}{\partial \xi} + \frac{\partial \phi_0}{\partial \xi} \right) \mathbf{E}_3, \quad (5.244)$$

where $\mathbf{i}_1 = \mathbf{Q}_{\mathbf{E}}(\phi_0, \mathbf{E}_3) \mathbf{E}_1$ and $\mathbf{i}_2 = \mathbf{Q}_{\mathbf{E}}(\phi_0, \mathbf{E}_3) \mathbf{E}_2$. By considering the deformed centerline of the rod, show that the following identifications can be made:

$$\delta\phi^2 \approx \frac{\partial \hat{X}}{\partial s}, \quad \delta\phi^3 \approx \frac{\partial \hat{Y}}{\partial s}, \quad \frac{\partial Z}{\partial s} \approx 1, \quad (5.245)$$

where $\mathbf{r} = \hat{X}\mathbf{i}_1 + \hat{Y}\mathbf{i}_2 + Z\mathbf{E}_3$.

- (h) Suppose \mathbf{P} is given by Eqn. (5.243). Show that

$$\mathbf{r}' \times \mathbf{r}'' = \mathbf{d}_3 \times \mathbf{d}_3' \approx -\frac{\partial \delta\phi^3}{\partial \xi} \mathbf{i}_1 + \frac{\partial \delta\phi^2}{\partial \xi} \mathbf{i}_2. \quad (5.246)$$

⁵³ That is, we are considering a set of three infinitesimal rotations superposed on a finite rotation.

Noting that $\kappa \mathbf{e}_b = \mathbf{r}' \times \mathbf{r}''$, give an interpretation of the perturbation that the infinitesimal rotations $\delta\phi^k$ provide.

- (i) Suppose the strain energy function of the rod is given by Eqn. (5.64). Determine an expression for the moment \mathbf{m} in the rod when \mathbf{P} is given by Eqn. (5.243).

Exercise 5.7: To establish the alternative form (5.87) of the jump condition (5.81)₇ a variety of identities were employed. To this end, show that

$$[\![\mathbf{G}]\!]_\gamma \cdot \mathbf{v}_\gamma = [\![\mathbf{G} \cdot (\dot{\mathbf{r}} + \dot{\gamma}\mathbf{r}')]\!]_\gamma,$$

and that

$$[\![[\mathbf{d}_\beta \times \mathbf{L}^\beta]]]_\gamma \cdot \mathbf{w}_\gamma = [\![((\mathbf{w} + \dot{\gamma}\mathbf{P}(\mathbf{v} + \mathbf{v}_0)) \times \mathbf{d}_\beta) \times \mathbf{L}^\beta]\!]_\gamma, \quad (\beta = 1, 2). \quad (5.247)$$

With the help of the preceding results, show that

$$[\![2T]\!]_\gamma \dot{\gamma} = [\![\mathbf{P}\dot{\gamma}]\!]_\gamma \dot{\gamma} + [\![\mathbf{G}\dot{\gamma}]\!]_\gamma \cdot \mathbf{v}_\gamma + [\![[\mathbf{d}_1 \times \mathbf{L}^1 + \mathbf{d}_2 \times \mathbf{L}^2]]]\!]_\gamma \cdot \mathbf{w}_\gamma. \quad (5.248)$$

The continuity of \mathbf{d}_1 and \mathbf{d}_2 as well as the identities (1.58) and (5.50) should be used to arrive at your solution.

Exercise 5.8: Verify that the equations (5.138) for the rod problem discussed in Section 5.15 are equivalent to Lagrange's equations of motion,

$$\frac{\partial}{\partial \xi} \left(\frac{\partial L}{\partial \alpha^{k'}} \right) - \frac{\partial L}{\partial \alpha^k} = 0, \quad (k = 1, 2, 3), \quad (5.249)$$

where

$$L = \frac{EI}{2} \left(\frac{\partial \alpha^2}{\partial \xi} \frac{\partial \alpha^2}{\partial \xi} + \frac{\partial \alpha^1}{\partial \xi} \frac{\partial \alpha^1}{\partial \xi} \sin^2(\alpha^2) \right) + \frac{\mathcal{D}}{2} \left(\frac{\partial \alpha^1}{\partial \xi} \cos(\alpha^2) + \frac{\partial \alpha^3}{\partial \xi} \right)^2 - F_\ell \cos(\alpha^2). \quad (5.250)$$

Exercise 5.9: Consider the differential equation (5.148) discussed in Section 5.15. Show that the equilibria $(\alpha^2 = \alpha_0^2, \frac{\partial \alpha^2}{\partial \xi} = 0)$ of this equation are governed by a quartic equation for $\cos(\alpha_0^2)$. For $\frac{F_\ell EI}{c^2} > \frac{1}{4}$, show that 3 equilibria are present and for $\frac{F_\ell EI}{c^2} < \frac{1}{4}$ the only equilibrium present is $\alpha_0^2 = 0$. In contrast, show that the differential equation (5.251) has a single equilibrium $(\alpha^2 = \alpha_0^2 = \pi, \frac{\partial \alpha^2}{\partial \xi} = 0)$ for all nonzero values of $\frac{F_\ell EI}{c^2}$.

Exercise 5.10: Consider the analytical expression (5.163) for $\alpha^2(\xi)$ corresponding to the homoclinic orbit. With the help of Eqns. (5.163) and (5.164) and the representations (5.15) for the Euler basis vectors, determine analytical expressions for the centerline of the deformed rod. Show how the shape of this centerline and the

tangent indicatrix changes as Δ increases from 0 to 1. As a check on your answers, examples of $\mathbf{r}(\xi)$ and $\mathbf{d}_3(\xi)$ can be seen in Figures 10–12 in [164].

Exercise 5.11: Consider the case of a rod where $EI_1 = EI_2$ which is loaded at its ends by terminal force and moments as in Section 5.15. Suppose that $c_S = -c_F = c$. In this case, the moment components in the directions of \mathbf{d}_3 and \mathbf{F}_0 are equal and opposite. Show that the differential equation (5.144) simplifies to

$$EI \frac{\partial^2 \alpha^2}{\partial \xi^2} - \frac{c^2((1 + \cos(\alpha^2))^2)}{EI \sin^3(\alpha^2)} = F_\ell \sin(\alpha^2). \quad (5.251)$$

The differential equation (5.251) is analogous to the equation used to demonstrate the stability of a downward pointing top (sleeping top) for any spin speed. Classify the solutions to Eqn. (5.251), show that the sole equilibrium corresponds to a twisted rod whose centerline is straight, and show that the remaining deformed shapes of the rod's centerline are qualitatively similar.

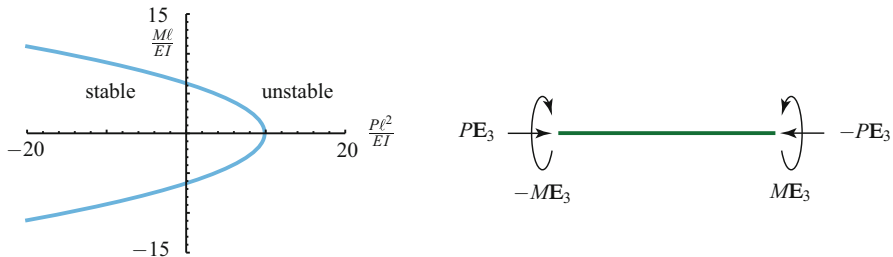


Fig. 5.29 Greenhill's stability criterion (5.252) for a straight terminally loaded rod of length ℓ . The development of the criterion was motivated by possible buckling instabilities in the drive shafts (propeller shafts) of ships some of which were over 150 feet long and close to 2 feet in diameter.

Exercise 5.12: In Greenhill [141], the following criterion for stability of a rod of length ℓ where $EI = EI_1 = EI_2$ which is subject to a thrust force P and an applied moment M was established⁵⁴:

$$\frac{M^2}{4EI} + P \leq \frac{\pi^2 EI}{\ell^2}. \quad (5.252)$$

The criterion is shown in Figure 5.29. The terminal loadings on the rod are $\mathbf{F}_0 = P\mathbf{E}_3$, $\mathbf{F}_\ell = -P\mathbf{E}_3$, $\mathbf{M}_0 = -M\mathbf{E}_3$, and $\mathbf{M}_\ell = M\mathbf{E}_3$. Thus, when $P > 0$, the rod is in compression. To establish his criterion, Greenhill derived the following pair of linearized equations for the transverse deflections u_1 and u_2 of the rod:

⁵⁴ Additional discussions of this criterion can be found in [213, Section 272] and [345, Pages 156–157]. Ziegler's delightful introductory text [375, Chapter 5, Section 3] has an informative discussion of the case where $P = 0$.

$$\begin{bmatrix} \frac{\partial^2 u_1}{\partial x^2} \\ \frac{\partial^2 u_2}{\partial x^2} \end{bmatrix} + \begin{bmatrix} 0 & \frac{M}{EI} \\ -\frac{M}{EI} & 0 \end{bmatrix} \begin{bmatrix} \frac{\partial u_1}{\partial x} \\ \frac{\partial u_2}{\partial x} \end{bmatrix} + \begin{bmatrix} \frac{P}{EI} & 0 \\ 0 & \frac{P}{EI} \end{bmatrix} \begin{bmatrix} u_1 \\ u_2 \end{bmatrix} = \begin{bmatrix} 0 \\ 0 \end{bmatrix}. \quad (5.253)$$

Here, x is the axial coordinate and the deflections u_1 and u_2 are subject to the boundary conditions

$$u_1(x=0) = 0, \quad u_2(x=0) = 0, \quad u_1(x=\ell) = 0, \quad u_2(x=\ell) = 0. \quad (5.254)$$

- (a) Show that $u_1(x)$ is governed by the differential equation

$$\frac{\partial^4 u_1}{\partial x^4} + \left(\left(\frac{M}{EI} \right)^2 + \frac{2P}{EI} \right) \frac{\partial^2 u_1}{\partial x^2} + \left(\frac{P}{EI} \right)^2 u_1 = 0. \quad (5.255)$$

- (b) Verify that the general solution to Eqn. (5.253) is

$$\begin{aligned} u_1 &= A_1 \sin(\omega_1 x) + A_2 \cos(\omega_1 x) + A_3 \sin(\omega_2 x) + A_4 \cos(\omega_2 x), \\ u_2 &= B_1 \sin(\omega_1 x) + B_2 \cos(\omega_1 x) + B_3 \sin(\omega_2 x) + B_4 \cos(\omega_2 x), \end{aligned} \quad (5.256)$$

where $A_{1,2,3,4}$ and $B_{1,2,3,4}$ are constants, and $\omega_{1,2}$ are the roots of

$$\left(\omega^2 - \frac{P}{EI} \right)^2 - \left(\frac{M}{EI} \right)^2 \omega^2 = 0. \quad (5.257)$$

That is,

$$\omega_{1,2} = \frac{M}{2EI} \pm \sqrt{\left(\frac{M}{2EI} \right)^2 + \frac{P}{EI}}. \quad (5.258)$$

- (c) Assuming $M \neq 0$, with the help of Eqn. (5.253), show that

$$B_1 = -f_1 A_2, \quad B_2 = f_1 A_1, \quad B_3 = -f_2 A_4, \quad B_4 = f_2 A_3, \quad (5.259)$$

where

$$\begin{aligned} f_1 &= \left(-\omega_1^2 + \frac{P}{EI} \right) \left(\omega_1 \frac{M}{EI} \right)^{-1} = 1, \\ f_2 &= \left(-\omega_2^2 + \frac{P}{EI} \right) \left(\omega_2 \frac{M}{EI} \right)^{-1} = 1. \end{aligned} \quad (5.260)$$

- (d) By forming a matrix equation for $A_{1,2,3,4}$ using the boundary conditions (5.254) and examining the determinant of the resulting matrix, show that nonzero solutions to the boundary-value problem are possible when the following equation is satisfied:

$$\sin\left(\frac{\ell}{2}(\omega_1 - \omega_2)\right) = 0. \quad (5.261)$$

Show that this equation implies Greenhill's stability criterion (5.252).

- (e) Consider the case $M = 0$. Show that $\omega_1 = \omega_2 = \sqrt{\frac{P}{EI}}$ and, in order for a non-trivial solution to the boundary-value problem to exist, that

$$\sin\left(\sqrt{\frac{P}{EI}}\ell\right) = 0. \quad (5.262)$$

Verify that this condition is equivalent to the classic Euler buckling formula $\frac{P\ell^2}{EI} = \pi^2$. Why cannot this result be directly found from Eqn. (5.261)?

- (f) Consider the case $P = 0$. Show that $\omega_2 = 0$ and $\omega_1 = \frac{M}{EI}$ and, in order for a nontrivial solution to the boundary-value problem to exist, that

$$\cos\left(\frac{M\ell}{EI}\right) = 1. \quad (5.263)$$

Verify that this condition is equivalent to the classic torsional instability criterion $\frac{M\ell}{EI} = 2\pi$.

- (g) After non-dimensionalizing P and M , numerically determine the solutions $\frac{P\ell^2}{EI}$ and $\frac{M\ell}{EI}$ to Eqn. (5.261) such that nonzero solutions to the boundary-value can be found. It is prudent to verify that the limiting cases of your results are the solutions discussed in Eqn. (5.252) and the earlier parts (e) and (f) of this exercise. Plot representative values of the solutions $u_1(x)$ and $u_2(x)$ corresponding to the buckling modes of the shaft. For certain instances, these modes should reduce to the classic buckling modes discussed in (e) and (f).
- (h) Using your results from (g), show that if the rod is in tension ($P < 0$), then by choosing P appropriately it is possible for the rod to support an arbitrarily large moment M without becoming unstable.

Exercise 5.13: Greenhill's development of the linearized equations (5.253) in [141] starts with a model for an initially straight homogenous rod whose strain energy function is given by Eqn. (5.64).

- (a) For this rod show that, under loading by terminal forces $\pm PE_3$ and moments $\mp ME_3$ and assuming that the centerline remains straight, the angle of twist changes at a constant rate along the length of the rod.
- (b) Consider an order ε perturbation to the straight state:

$$\mathbf{r} = X\mathbf{E}_1 + Y\mathbf{E}_2 + Z\mathbf{E}_3 = z\mathbf{E}_3 + \varepsilon(u_1\mathbf{E}_1 + u_2\mathbf{E}_2 + u_3\mathbf{E}_3). \quad (5.264)$$

Show that

$$\frac{\partial z}{\partial s} = 1 + \mathcal{O}(\varepsilon), \quad \frac{\partial u_1}{\partial s} = \frac{\partial u_1}{\partial z} + \mathcal{O}(\varepsilon), \quad \frac{\partial u_2}{\partial s} = \frac{\partial u_2}{\partial z} + \mathcal{O}(\varepsilon). \quad (5.265)$$

- (c) Starting from the ansatz (5.264) and using the results (5.265), show that

$$\begin{aligned}\kappa \mathbf{e}_b &= \mathbf{r}' \times \mathbf{r}'' \\ &= -\epsilon \frac{\partial^2 u_2}{\partial z^2} \mathbf{E}_1 + \epsilon \frac{\partial^2 u_1}{\partial z^2} \mathbf{E}_2 + \mathcal{O}(\epsilon^2).\end{aligned}\quad (5.266)$$

If the perturbation to the straight twisted state is such that

$$EI\kappa \mathbf{e}_b + M\mathbf{r}' - \mathbf{r} \times P\mathbf{E}_3 = \text{constant}, \quad (5.267)$$

then show how Eqn. (5.267) leads to the differential equations (5.253).

- (d) Show how Eqn. (5.267) can be partially motivated by the balance laws $\mathbf{n}' = \mathbf{0}$ and $(\mathbf{m} + \mathbf{r} \times \mathbf{n})' = \mathbf{0}$ along with the appropriate boundary conditions. For assistance with this problem, the results of Exercise 5.6(g)-(i) may prove to be helpful.

Exercise 5.14: This exercise outlines the establishment of the following extension to Kirchhoff's kinetic analogue that was proposed by Joseph Larmor (1857–1942) [197, Section 8]: "That the motion of a gyroscopic pendulum (i.e., a solid rotating about a fixed point with a revolving fly-wheel mounted on an axis fixed in it) is exactly analogous to the form assumed by a wire originally helical, when deformed by any distribution of forces applied to its extremities."⁵⁵ Larmor's extension is helpful when analyzing the deformed shapes of plant tendrils and wires that have intrinsic curvatures, geometric torsion, and twist.

- (a) Consider a rod which has an intrinsic curvature $\mathbf{v}_0 = v_{01}\mathbf{D}_1 + v_{02}\mathbf{D}_2 + v_{03}\mathbf{D}_3$. Under which conditions does the rod correspond to a twisted rod with a straight centerline, a twisted rod with a circular centerline, and a twisted rod where the centerline is bent into a circular helix?
- (b) Show that
- $$\mathbf{d}'_k = \left(\sum_{i=1}^3 (v_i + v_{0i}) \mathbf{d}_i \right) \times \mathbf{d}_k. \quad (5.268)$$
- (c) Suppose the rod is bent by application of terminal forces $\pm \mathbf{F}_0$ and terminal moments. Using balances of linear and angular momentum, $\mathbf{n}' = \mathbf{0}$ and $\mathbf{m}' + \mathbf{r}' \times \mathbf{n} = \mathbf{0}$, and assuming a constitutive relation

$$2\rho_0\psi = EI_1 v_1^2 + EI_2 v_2^2 + \mathcal{D}v_3^2, \quad (5.269)$$

establish the equations governing $v_k(\xi)$:

$$\begin{aligned}EI_1 v'_1 - EI_2 v_2 (v_3 + v_{03}) + \mathcal{D}(v_2 + v_{02}) v_3 &= -\mathbf{d}_2 \cdot \mathbf{F}_0, \\ EI_2 v'_2 - \mathcal{D}(v_1 + v_{01}) v_3 + EI_1 (v_3 + v_{03}) v_1 &= \mathbf{d}_1 \cdot \mathbf{F}_0, \\ \mathcal{D}v'_3 - EI_1 (v_2 + v_{02}) v_1 + EI_2 (v_1 + v_{01}) v_2 &= 0.\end{aligned}\quad (5.270)$$

⁵⁵ This extension is presented in far greater detail in Love [213, Section 261] than in Larmor's original work [197, Section 8].

The constitutive parameters EI_1 , EI_2 , and \mathcal{D} are assumed to be constant. HINT: the derivation of Eqn. (5.270) closely follows the developments of Eqns. (5.119).

- (d) Using the conservations (5.115) and (5.116), show that the following three quantities are conserved along the length of the rod:

$$\mathbf{n} \cdot \mathbf{m}, \quad C, \quad \mathbf{n} \cdot \mathbf{n}. \quad (5.271)$$

For the conservation of C , it is necessary to assume that v_{k_0} are constant. This assumption is adopted for the remainder of this exercise.

- (e) Show that the equations you found in (c) correspond to those for the orientation of a gyrostat which is free to rotate about a fixed point O . Give a sketch of the gyrostat and discuss how the orientation of the flywheel relative to the outer rigid casing is related to v_{0_k} , EI_1 , EI_2 , \mathcal{D} , and the moment of inertia I of the flywheel about its axis of symmetry.

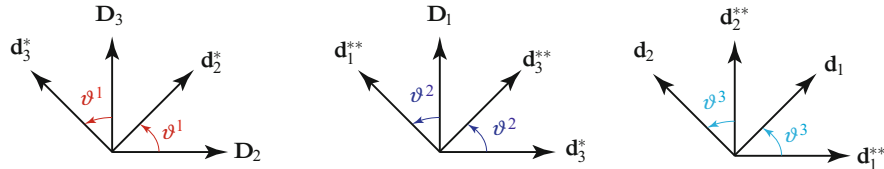


Fig. 5.30 Schematic of the three rotations used to define the 1-2-3 set of Euler angles (cf. Eqn. (5.272)).

Exercise 5.15: In many applications of rods theories, the rod has an intrinsic curvature v_{0_1} . For these situations, it is convenient to use a 1-2-3 set of Euler angles to parameterize $\mathbf{P} = \sum_{i=1}^3 \mathbf{d}_i \otimes \mathbf{D}_i$ (cf. Figure 5.30). Whence,⁵⁶

$$\begin{aligned} \mathbf{P}\mathbf{P}_0 &= \sum_{i=1}^3 \mathbf{d}_i \otimes \mathbf{E}_i = \mathbf{Q}_E(\vartheta^3, \mathbf{e}_3) \mathbf{Q}_E(\vartheta^2, \mathbf{e}_2) \mathbf{Q}_E(\vartheta^1, \mathbf{e}_1) \mathbf{Q}_E(\vartheta^0, \mathbf{D}_1), \\ \mathbf{P}_0 &= \sum_{i=1}^3 \mathbf{D}_i \otimes \mathbf{E}_i = \cos(\vartheta^0) (\mathbf{I} - \mathbf{E}_1 \otimes \mathbf{E}_1) + \sin(\vartheta^0) \text{skew}(\mathbf{E}_1) + \mathbf{E}_1 \otimes \mathbf{E}_1. \end{aligned} \quad (5.272)$$

Here, the angle ϑ^0 is intimately related to the sole nonvanishing intrinsic curvature:

$$v_{0_1} = \frac{\partial \vartheta^0}{\partial \xi}. \quad (5.273)$$

⁵⁶ Parameterizations of this type are sometimes used in studies on the dynamics of satellites in orbit. See, for example, Rumenantsev [311] and articles such as [272, 333] citing this work.

- (a) Show that the components $P_{ik} = (\mathbf{P}\mathbf{D}_k) \cdot \mathbf{D}_i$ of \mathbf{P} have the representations

$$\begin{bmatrix} P_{11} & P_{12} & P_{13} \\ P_{21} & P_{22} & P_{23} \\ P_{31} & P_{32} & P_{33} \end{bmatrix} = \begin{bmatrix} c_2c_3 & -c_2s_3 & s_2 \\ c_3s_1s_2 + c_1s_3 & c_1c_3 - s_1s_2s_3 & -c_2s_1 \\ -c_1c_3s_2 + s_1s_3 & c_3s_1 + c_1s_2s_3 & c_1c_2 \end{bmatrix}. \quad (5.274)$$

In writing expressions for the components P_{ik} , we have employed the abbreviations $c_k = \cos(\vartheta^k)$ and $s_k = \sin(\vartheta^k)$.

- (b) Show that the Euler basis vectors used in the representations (5.272) for the rotation tensors \mathbf{P} and \mathbf{P}_0 have the representations

$$\begin{aligned} \mathbf{e}_1 &= \mathbf{E}_1 = \mathbf{D}_1 \\ &= \cos(\vartheta^2)\cos(\vartheta^3)\mathbf{d}_1 - \cos(\vartheta^2)\sin(\vartheta^3)\mathbf{d}_2 + \sin(\vartheta^2)\mathbf{d}_3, \\ \mathbf{e}_2 &= \cos(\vartheta^1)\mathbf{D}_2 + \sin(\vartheta^1)\mathbf{D}_3 \\ &= \cos(\vartheta^3)\mathbf{d}_2 + \sin(\vartheta^3)\mathbf{d}_1, \\ \mathbf{e}_3 &= \sin(\vartheta^2)\mathbf{D}_1 - \cos(\vartheta^2)\sin(\vartheta^1)\mathbf{D}_2 + \cos(\vartheta^2)\cos(\vartheta^1)\mathbf{D}_3 \\ &= \mathbf{d}_3 = \mathbf{e}_l. \end{aligned} \quad (5.275)$$

In addition, show that

$$\begin{aligned} \mathbf{E}_3 &= (-\cos(\vartheta^1 + \vartheta^0)\sin(\vartheta^2)\cos(\vartheta^3) + \sin(\vartheta^1 + \vartheta^0)\sin(\vartheta^3))\mathbf{d}_1 \\ &\quad + (\cos(\vartheta^1 + \vartheta^0)\sin(\vartheta^2)\sin(\vartheta^3) + \sin(\vartheta^1 + \vartheta^0)\cos(\vartheta^3))\mathbf{d}_2 \\ &\quad + \cos(\vartheta^1 + \vartheta^0)\cos(\vartheta^2)\mathbf{d}_3. \end{aligned} \quad (5.276)$$

- (c) Why are the Euler angles subject to the restrictions $\vartheta^1 \in [0, 2\pi]$, $\vartheta^2 \in (-\pi/2, \pi/2)$, and $\vartheta^3 \in [0, 2\pi]$? Suppose the reference configuration of the centerline of the rod lies in the $\mathbf{E}_2 - \mathbf{E}_3$. Show that the Euler angles in this configuration are not close to the singularities associated with ϑ^2 . Could the same statement be made if a set of 1-2-1 Euler angles were used to parameterize \mathbf{P} ?

- (d) Show that the dual Euler basis vectors have the following representations:

$$\begin{bmatrix} \mathbf{e}^1 \\ \mathbf{e}^2 \\ \mathbf{e}^3 \end{bmatrix} = \begin{bmatrix} \sec(\vartheta^2)\cos(\vartheta^3) & -\sec(\vartheta^2)\sin(\vartheta^3) & 0 \\ \sin(\vartheta^3) & \cos(\vartheta^3) & 0 \\ -\tan(\vartheta^2)\cos(\vartheta^3) & \tan(\vartheta^2)\sin(\vartheta^3) & 1 \end{bmatrix} \begin{bmatrix} \mathbf{d}_1 \\ \mathbf{d}_2 \\ \mathbf{d}_3 \end{bmatrix}. \quad (5.277)$$

Establish the corresponding representations for \mathbf{e}^k in terms of the two set of basis vectors $\{\mathbf{E}_1, \mathbf{E}_2, \mathbf{E}_3\}$ and $\{\mathbf{D}_1, \mathbf{D}_2, \mathbf{D}_3\}$.

- (e) Show that the components $v_i = \mathbf{v} \cdot \mathbf{D}_i$ of the strain vector $\mathbf{P}\mathbf{v} = \sum_{i=1}^3 v_i \mathbf{d}_i$ have the following representations:

$$\begin{bmatrix} v_1 \\ v_2 \\ v_3 \end{bmatrix} = \begin{bmatrix} \cos(\vartheta^2)\cos(\vartheta^3) & \sin(\vartheta^3) & 0 \\ -\cos(\vartheta^2)\sin(\vartheta^3) & \cos(\vartheta^3) & 0 \\ \sin(\vartheta^2) & 0 & 1 \end{bmatrix} \begin{bmatrix} \frac{\partial \vartheta^1}{\partial \xi} \\ \frac{\partial \vartheta^2}{\partial \xi} \\ \frac{\partial \vartheta^3}{\partial \xi} \end{bmatrix}. \quad (5.278)$$

In addition, show that the inverses of these relations are

$$\begin{bmatrix} \frac{\partial \vartheta^1}{\partial \xi} \\ \frac{\partial \vartheta^2}{\partial \xi} \\ \frac{\partial \vartheta^3}{\partial \xi} \end{bmatrix} = \begin{bmatrix} \cos(\vartheta^3) \sec(\vartheta^2) & -\sin(\vartheta^3) \sec(\vartheta^2) & 0 \\ \sin(\vartheta^3) & \cos(\vartheta^3) & 0 \\ -\cos(\vartheta^3) \tan(\vartheta^2) & \sin(\vartheta^3) \tan(\vartheta^2) & 1 \end{bmatrix} \begin{bmatrix} v_1 \\ v_2 \\ v_3 \end{bmatrix}. \quad (5.279)$$

(f) With the help of the Bonnet-Meusnier relations (5.102) and the representations

$$\begin{aligned} \mathbf{D}'_2 &= v_{01} \mathbf{D}_3, \\ \mathbf{D}'_3 &= -v_{01} \mathbf{D}_2, \\ \mathbf{d}_3' &= \mathbf{r}' = \mathbf{e}_t \\ &= \sin(\vartheta^2) \mathbf{D}_1 - \sin(\vartheta^1) \cos(\vartheta^2) \mathbf{D}_2 + \cos(\vartheta^2) \cos(\vartheta^1) \mathbf{D}_3, \end{aligned} \quad (5.280)$$

show that

$$\kappa^2 = \left(\frac{\partial \vartheta^0}{\partial \xi} + \frac{\partial \vartheta^1}{\partial \xi} \right)^2 \cos^2(\vartheta^2) + \left(\frac{\partial \vartheta^2}{\partial \xi} \right)^2. \quad (5.281)$$

With the help of this result, derive expressions for the torsion τ of the centerline and rate of change of the angle of twist $\frac{\partial \phi}{\partial s}$ of a rod whose rotation tensor \mathbf{P} is parameterized using a set of 1-2-3 Euler angles. Give a physical interpretation of the conditions whereby $\frac{\partial \phi}{\partial s} = \frac{\partial \vartheta^3}{\partial s}$.

Chapter 6

Theory of an Elastic Rod with Extension and Shear

“In this way, one arrives at the kinematical model of a rod consisting of a one-dimensional continuum M^1 and a set of two vector fields $\left(\begin{smallmatrix} \mathbf{d}_1^i(\xi, t) \\ \mathbf{d}_2^i(\xi, t) \end{smallmatrix}\right)$ in M^1 whose values fix a homogeneous deformation of the cross section of the rod through the point ξ . ”

R. A. Toupin’s discussion in [348, Page 90] of a model for a rod as a material curve with a set of directors.

6.1 Introduction

For many of the applications analyzed using Kirchhoff’s rod theory one cannot help but ask about the influence of extensibility of the centerline. This is particularly true for the telephone cord that is often used to demonstrate perversions. In attempting to use a rod theory to analyze the twisting and bending of a length of surgical tubing, the possibility for relaxing some of the assumptions associated with the deformation of the cross sections in Kirchhoff’s rod theory also appears to be desirable. Two paths are available to develop the resulting rod theory. One avenue is to establish the theory as an approximate solution for a three-dimensional continuum. A second avenue, popularized by Ericksen and Truesdell’s paper [100] on directors in 1958, is to model the rod as a directed (or Cosserat) curve – that is, as a material curve with a set of deformable vectors (directors) associated with each point on this curve. While the resulting rod theory stands alone as a separate theory, many of the parameters in the models produced by this theory, such as mass density per unit length and stiffnesses, are identified by directly comparing the predictions of the rod theory to corresponding problems from the three-dimensional theory. In the early 1970s several researchers, including Antman [10], Green and Laws [130], and Reissner [299, 300], extended Kirchhoff’s theory to include extension of the centerline and

rotation of the cross sections relative to the centerline. The latter effect is known as transverse shear. As shall be shown in an exercise at the end of this chapter, a linearized version of the rod theory provides Stephen P. Timoshenko's (1878–1972) celebrated beam theory [344]. The extensions to Kirchhoff's original theory were neither free from controversy nor recriminations and many contributions on the topic have largely been forgotten.

Primarily because of Antman's seminal book [12] and papers, the most popular form of the theory in the recent literature is the one which he presents. His formulation has inspired a numerical implementation of the theory in an influential paper [327] written by Simo and Vu-Quoc. In addition, partially because both \mathbf{n} and \mathbf{m} are prescribed by constitutive relations involving six strains, the theory has enabled several teams of researcher to propose a range of Hamiltonian formulations using notions from geometric mechanics (cf. [86, 178, 238, 326]).

Antman [12] is the primary resource for the analyses of problems describing the rod theory discussed in this chapter. Our developments will be closely aligned with [12, Chapter 8] and include an explicit discussion of material momentum and recent treatments of material symmetry for elastic rods. We present a limited discussion of applications and refer the reader to [12] for examples and analyses. One application that we do consider is motivated by a remarkable series of recent works where strands of DNA molecules are subject to mechanical testing (see the review [40]). From these tests, it has become apparent that a twist-bend coupling [228] and a stretch-twist coupling [177, 227] is present. While the twist-bend coupling can be modeled using Kirchhoff's rod theory by incorporating the strains $v_1 v_3$ and $v_2 v_3$ in the strain energy function, the latter coupling requires an extensible rod theory of the type considered in this chapter. Further, as demonstrated by Healey [158], the theory discussed in the present chapter is ideal for wire ropes which possess an inherent helical symmetry. The second application we consider is an analysis of static solutions for the rod theory that is based on Ericksen's notion of uniform states for rods.

6.2 Kinematical Considerations

For the rod theory of interest in this chapter, the rod is modeled as a material curve \mathcal{L} to which at each point a pair of directors \mathbf{d}_1 and \mathbf{d}_2 are defined. As in the previous chapter, the material curve with its associated directors is known as a Cosserat or directed curve. Variants of the rod theory discussed here were proposed by Antman [10] and Green and Laws [130], among others, and it is often known, following [12], as a special Cosserat rod theory.

In the reference configuration \mathcal{R}_0 and present configuration \mathcal{R} of the directed curve, the directors are denoted by $\mathbf{D}_\alpha = \mathbf{D}_\alpha(\xi)$ and $\mathbf{d}_\alpha(\xi, t)$, where $\alpha = 1, 2$. The locations of material points in the two configurations are defined by the vector-valued functions $\mathbf{R}(\xi)$ and $\mathbf{r}(\xi, t)$, respectively. The configuration \mathcal{R}_0 of the directed curve is defined by the triple $\mathbf{R}(\xi)$ and $\mathbf{D}_\alpha(\xi)$ and the configuration \mathcal{R} of the directed curve is defined by the triple $\mathbf{r}(\xi, t)$ and $\mathbf{d}_\alpha(\xi, t)$.

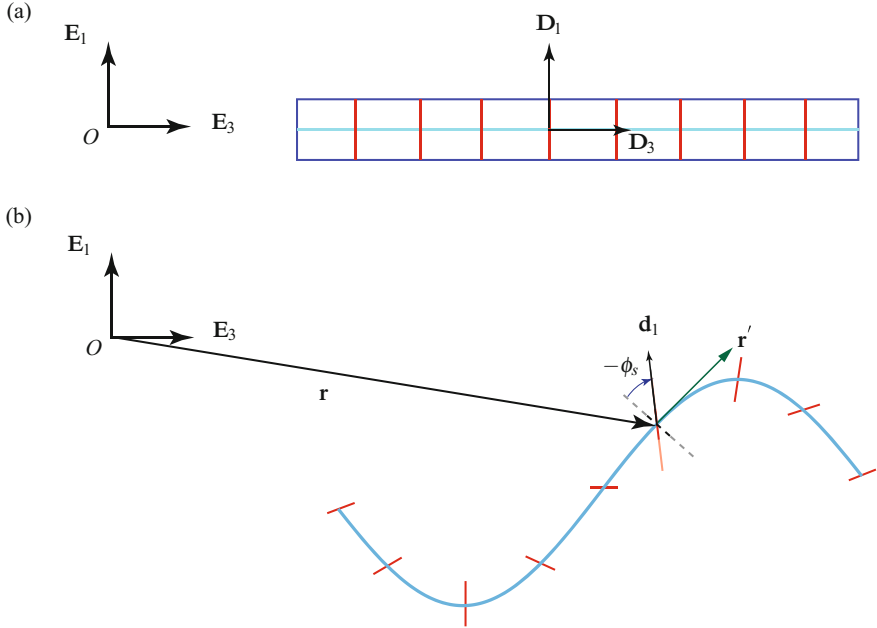


Fig. 6.1 (a) Schematic of the reference configuration for a straight rod. (b) The present configuration of the rod. Note that the cross sections of the rod are not constrained to remain normal to the tangent vector \mathbf{r}' .

For the rod theory of interest, the directors retain their magnitude and relative orientation:

$$\mathbf{d}_\alpha(\xi, t) = \mathbf{P}(\xi, t)\mathbf{D}_\alpha(\xi), \quad \mathbf{D}_\alpha(\xi) = \mathbf{P}_0(\xi)\mathbf{E}_\alpha. \quad (6.1)$$

Here, as in the previous chapter, \mathbf{P} and \mathbf{P}_0 are rotation tensors and $\{\mathbf{E}_1, \mathbf{E}_2, \mathbf{E}_3\}$ are a set of fixed, right-handed orthonormal basis vectors. We recall the definitions of the skew-symmetric tensors

$$\mathbf{K} = \mathbf{P}^T \mathbf{P}', \quad \mathbf{K}_0 = \mathbf{P}_0^T \mathbf{P}_0', \quad (6.2)$$

and their respective axial vectors \mathbf{v} and \mathbf{v}_0 :

$$\mathbf{v} = \text{ax}(\mathbf{K}), \quad \mathbf{v}_0 = \text{ax}(\mathbf{K}_0). \quad (6.3)$$

Differentiating Eqn. (6.1)₁ and using the identity (5.9), we find a familiar result:

$$\mathbf{d}'_\alpha = (\mathbf{P}(\mathbf{v} + \mathbf{v}_0)) \times \mathbf{d}_\alpha. \quad (6.4)$$

It is crucial to note here that we are not assuming that $\mathbf{d}_1 \times \mathbf{d}_2 \parallel \mathbf{r}'$. That is, we are allowing transverse shearing of the cross sections of the rod that may initially be normal to the tangent vector \mathcal{L} (cf. Fig. 6.1).

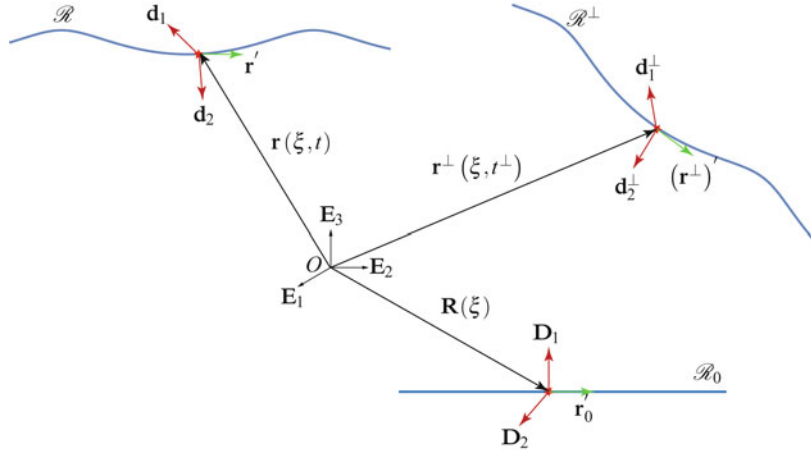


Fig. 6.2 Schematic of a pair of motions of a directed curve which differ by a rigid body motion. Observe that both motions are relative to the same reference configuration \mathcal{R}_0 .

A pair of motions $(\mathbf{r}(\xi, t), \mathbf{d}_\alpha(\xi, t))$ and $(\mathbf{r}^\perp(\xi, t^\perp), \mathbf{d}_\alpha^\perp(\xi, t^\perp))$ of a directed curve differ by a rigid body motion if

$$\begin{aligned}\mathbf{r}^\perp(\xi, t^\perp) &= \mathbf{Q}(t)\mathbf{r}(\xi, t) + \mathbf{q}(t), \\ \mathbf{d}_1^\perp(\xi, t^\perp) &= \mathbf{Q}(t)\mathbf{d}_1(\xi, t), \\ \mathbf{d}_2^\perp(\xi, t^\perp) &= \mathbf{Q}(t)\mathbf{d}_2(\xi, t).\end{aligned}\quad (6.5)$$

Here, \mathbf{Q} is a proper-orthogonal tensor-valued function of time, $\mathbf{q}(t)$ is a vector-valued function of time, and $t^\perp = t + a$ with a being constant (cf. Figure 6.2). Observe that

$$\mathbf{P}^\perp(\xi, t^\perp) = \mathbf{Q}(t)\mathbf{P}(\xi, t), \quad (\mathbf{P}^\perp(\xi, t^\perp))' = \mathbf{Q}(t)\mathbf{P}'(\xi, t). \quad (6.6)$$

With the help of the identities $\mathbf{a} \cdot (\mathbf{Ab}) = \mathbf{b} \cdot (\mathbf{A}^T \mathbf{a})$ for all second-order tensors \mathbf{A} and $\mathbf{Q}(\mathbf{a} \times \mathbf{b}) = (\mathbf{Qa}) \times (\mathbf{Qb})$ for all proper-orthogonal tensors \mathbf{Q} , it should be easy to see that the inner products $\mathbf{r}' \cdot \mathbf{r}', \mathbf{r}' \cdot \mathbf{d}_\alpha$, and $\mathbf{d}_\alpha \cdot \mathbf{d}_\beta$ remain invariant under superposed rigid body motions whereas $\mathbf{r} \cdot \mathbf{r}$ or $\mathbf{r} \cdot \mathbf{d}_\alpha$ are not the same for a motion and another motion which differs from it by a rigid body motion.

The components of \mathbf{Pv} and $\mathbf{r}' - \mathbf{PR}'$ with respect to the basis $\{\mathbf{d}_1, \mathbf{d}_2, \mathbf{d}_3 = \mathbf{d}_1 \times \mathbf{d}_2\}$ define the six strain measures:

$$\begin{aligned}\boldsymbol{\eta} &= \mathbf{P}^T \mathbf{r}' - \mathbf{R}' = \eta_1 \mathbf{D}_1 + \eta_2 \mathbf{D}_2 + \eta_3 \mathbf{D}_3, \\ \mathbf{v} &= v_1 \mathbf{D}_1 + v_2 \mathbf{D}_2 + v_3 \mathbf{D}_3.\end{aligned}\quad (6.7)$$

Here, $\mathbf{D}_3 = \mathbf{D}_1 \times \mathbf{D}_2$ and neither \mathbf{d}_3 nor \mathbf{D}_3 should be confused with the unit tangent vector to the centerline of the rod. We leave it as an exercise to verify that

$$\boldsymbol{\eta}^\perp(\xi, t^\perp) = \boldsymbol{\eta}(\xi, t), \quad \mathbf{v}^\perp(\xi, t^\perp) = \mathbf{v}(\xi, t). \quad (6.8)$$

That is, the vectors \mathbf{v} and $\boldsymbol{\eta}$ are suitable candidates for strain measures for the rod theory. If we identify \mathbf{d}_1 and \mathbf{d}_2 with the cross section of the rod-like body that the directed curve is modeling, then v_1 and v_2 can be identified as flexural (bending) strains, and v_3 is the torsional strain of the cross section. The strains η_1 and η_2 measure the change in the \mathbf{d}_1 and \mathbf{d}_2 components of \mathbf{r}' and are considered to be shearing strains:

$$\eta_\beta = (\mathbf{P}^T \mathbf{r}' - \mathbf{R}') \cdot \mathbf{D}_\beta = \mathbf{r}' \cdot \mathbf{d}_\beta - \mathbf{R}' \cdot \mathbf{D}_\beta. \quad (6.9)$$

The sixth strain measure η_3 provides a measure of the change in the volume $\mathbf{r}' \cdot (\mathbf{d}_1 \times \mathbf{d}_2)$:

$$\eta_3 = (\mathbf{P}^T \mathbf{r}' - \mathbf{R}') \cdot \mathbf{D}_3 = \mathbf{r}' \cdot \mathbf{d}_3 - \mathbf{R}' \cdot \mathbf{D}_3. \quad (6.10)$$

Only in exceptional instances is η_3 equal to the extension (stretch) squared of the centerline.

6.3 Summary of the Governing Equations for the Rod Theory

The balances laws for the theory are identical to those for the Kirchhoff rod theory that we presented in Section 5.7.2 of Chapter 5. The primary differences are the constitutive relations for \mathbf{n} and \mathbf{m} and the fact that $\mathbf{r}' \neq \mathbf{d}_1 \times \mathbf{d}_2$. These differences were anticipated in writing Chapter 5 so that much of the material could be recycled in the present chapter. As a consequence our discussion here is brief.

The conservation laws (5.75)–(5.79) are postulated and the local forms and jump conditions are established in the usual manner. Omitting details, we find the following jump conditions:

$$\begin{aligned} [[\mathbf{r}]]_\gamma &= \mathbf{0}, & [[\mathbf{PP}_0]]_\gamma &= \mathbf{0}, \\ [[\rho_0]]_\gamma \dot{\gamma} &= 0, & [[[\rho_0 y^{0\alpha}]]_\gamma \dot{\gamma}] &= 0, & [[[\rho_0 y^{\alpha\beta}]]_\gamma \dot{\gamma}] &= 0, \\ [[\mathbf{n}]]_\gamma + [[\mathbf{G}]]_\gamma \dot{\gamma} + \mathbf{F}_\gamma &= \mathbf{0}, \\ [[\mathbf{C}]]_\gamma + [[\mathbf{P}]]_\gamma \dot{\gamma} + \mathbf{B}_\gamma &= 0, \\ [[\mathbf{m}]]_\gamma + [[[\mathbf{d}_1 \times \mathbf{L}^1 + \mathbf{d}_2 \times \mathbf{L}^2]]_\gamma \dot{\gamma} + \mathbf{M}_{O_\gamma} - \mathbf{r}(\gamma, t) \times \mathbf{F}] &= \mathbf{0}. \end{aligned} \quad (6.11)$$

Here, the linear momentum \mathbf{G} and director momenta \mathbf{L}^β have the familiar forms

$$\mathbf{G} = \rho_0 \dot{\mathbf{r}} + \rho_0 \sum_{\alpha=1}^2 y^{0\alpha} \dot{\mathbf{d}}_\alpha, \quad \mathbf{L}^\beta = \rho_0 y^{0\beta} \dot{\mathbf{r}} + \rho_0 \sum_{\alpha=1}^2 y^{\beta\alpha} \dot{\mathbf{d}}_\alpha. \quad (6.12)$$

The jump conditions are supplemented by the pair of partial differential equations and the local form of the balance of energy:

$$\begin{aligned}\dot{\mathbf{G}} &= \rho_0 \mathbf{f} + \frac{\partial \mathbf{n}}{\partial \xi}, \\ \rho_0 \left(\sum_{\alpha=1}^2 \mathbf{d}_\alpha \times y^{0\alpha} \ddot{\mathbf{r}} + \sum_{\alpha=1}^2 \sum_{\beta=1}^2 \mathbf{d}_\alpha \times y^{\alpha\beta} \ddot{\mathbf{d}}_\beta \right) &= \mathbf{m}_a + \frac{\partial \mathbf{m}}{\partial \xi} + \frac{\partial \mathbf{r}}{\partial \xi} \times \mathbf{n}, \\ \rho_0 \psi &= \mathbf{n} \cdot \left(\frac{\partial \mathbf{v}}{\partial \xi} - \boldsymbol{\omega} \times \frac{\partial \mathbf{r}}{\partial \xi} \right) + \mathbf{m} \cdot \frac{\partial \boldsymbol{\omega}}{\partial \xi}. \end{aligned}\quad (6.13)$$

Observe that $\frac{\partial \mathbf{v}}{\partial \xi} - \boldsymbol{\omega} \times \frac{\partial \mathbf{r}}{\partial \xi}$ is the corotational rate of $\frac{\partial \mathbf{r}}{\partial \xi}$.

The jump condition arising from the energy balance (5.79) is not listed above. As with the theories of strings and rods we have discussed previously, this jump condition is used to relate the mechanical powers of the singular supplies:

$$B_\gamma \dot{\gamma} + \mathbf{F}_\gamma \cdot \mathbf{v}_\gamma + \mathbf{M}_\gamma \cdot \boldsymbol{\omega}_\gamma = \Phi_{E_\gamma}, \quad (6.14)$$

where the resultant moment \mathbf{M}_γ is defined by the identity

$$\mathbf{M}_\gamma = \mathbf{M}_{O_\gamma} - \mathbf{r}(\gamma, t) \times \mathbf{F}_\gamma. \quad (6.15)$$

Given the appropriate boundary conditions, constitutive relations, and initial conditions, the preceding equations serve to enable the calculation of \mathbf{r} and \mathbf{P} (or equivalently \mathbf{d}_α) for a directed curve.

6.3.1 Constitutive Relations for \mathbf{n} and \mathbf{m}

Using the strains \mathbf{v} and $\boldsymbol{\eta}$, the strain energy function of the rod is assumed to have the representations

$$\begin{aligned}\rho_0 \psi &= \rho_0 \psi \left(\boldsymbol{\eta}(\xi), \mathbf{v}(\xi), \mathbf{v}_0(\xi), \mathbf{R}'(\xi), \xi \right) \\ &= \rho_0 \hat{\psi}(\eta_i, v_k, \xi). \end{aligned}\quad (6.16)$$

In the second of these representations, $\eta_i = \boldsymbol{\eta}(\xi) \cdot \mathbf{D}_i(\xi)$ and $v_k = \mathbf{v}(\xi) \cdot \mathbf{D}_k(\xi)$. Observe that both representations of $\rho_0 \psi$ are invariant under superposed rigid body motions of the directed curve: $\psi^\perp = \psi$. Later, we shall use the local form of the balance of energy to specify constitutive relations for \mathbf{n} and \mathbf{m} using ψ .

We can parallel our earlier developments in Section 5.4 of Chapter 5 to find that

$$\dot{\mathbf{d}}_\alpha = \boldsymbol{\omega} \times \mathbf{d}_\alpha, \quad \boldsymbol{\omega} = \mathbf{ax}(\dot{\mathbf{P}} \mathbf{P}^T). \quad (6.17)$$

In addition, the derivatives of \mathbf{P} with respect to ξ and t are related (cf. Eqn. (5.40)):

$$\boldsymbol{\omega}' = \mathbf{P} \dot{\mathbf{v}}. \quad (6.18)$$

Given any vector \mathbf{b} , say, where

$$\mathbf{b} = b_1 \mathbf{d}_1 + b_2 \mathbf{d}_2 + b_3 (\mathbf{d}_1 \times \mathbf{d}_2), \quad (6.19)$$

then the corotational rate of \mathbf{b} has the representations

$$\dot{\mathbf{b}} - \boldsymbol{\omega} \times \mathbf{b} = \dot{b}_1 \mathbf{d}_1 + \dot{b}_2 \mathbf{d}_2 + \dot{b}_3 (\mathbf{d}_1 \times \mathbf{d}_2). \quad (6.20)$$

This identity is helpful for interpreting representations for the derivatives of strain energy functions. For instance, differentiating $\boldsymbol{\eta}$ with respect to time and noting that the axial vector of $\mathbf{P}\dot{\mathbf{P}}^T$ is $-\boldsymbol{\omega}$, we find that

$$\dot{\boldsymbol{\eta}} = \mathbf{P}^T (\mathbf{v}' - \boldsymbol{\omega} \times \mathbf{r}'). \quad (6.21)$$

The identities (6.18) and (6.21) can also be considered as compatibility equations for the material time and ξ derivatives.

The material time derivative of $\rho_0 \psi$ has several representations:

$$\begin{aligned} \rho_0 \dot{\psi} &= \rho_0 \sum_{k=1}^3 \frac{\partial \hat{\psi}}{\partial \eta_k} \dot{\eta}_k + \rho_0 \sum_{k=1}^3 \frac{\partial \hat{\psi}}{\partial v_k} \dot{v}_k \\ &= \left(\rho_0 \sum_{k=1}^3 \frac{\partial \hat{\psi}}{\partial \eta_k} \mathbf{D}_k \right) \cdot \dot{\boldsymbol{\eta}} + \left(\rho_0 \sum_{k=1}^3 \frac{\partial \hat{\psi}}{\partial v_k} \mathbf{D}_k \right) \cdot \dot{\mathbf{v}} \\ &= \mathbf{P} \rho_0 \frac{\partial \hat{\psi}}{\partial \mathbf{v}} \cdot \boldsymbol{\omega}' + \mathbf{P} \rho_0 \frac{\partial \hat{\psi}}{\partial \boldsymbol{\eta}} \cdot (\mathbf{v}' - \boldsymbol{\omega} \times \mathbf{r}'), \end{aligned} \quad (6.22)$$

where we used the identities (6.18) and (6.21) and defined the following pair of vectors:

$$\frac{\partial \hat{\psi}}{\partial \mathbf{v}} = \sum_{k=1}^3 \frac{\partial \hat{\psi}}{\partial v_k} \mathbf{D}_k, \quad \frac{\partial \hat{\psi}}{\partial \boldsymbol{\eta}} = \sum_{k=1}^3 \frac{\partial \hat{\psi}}{\partial \eta_k} \mathbf{D}_k. \quad (6.23)$$

The role played by \mathbf{P} in establishing the last of the relations (6.22) is to change the basis from \mathbf{D}_k to \mathbf{d}_k in the vectors $\frac{\partial \hat{\psi}}{\partial \mathbf{v}}$ and $\frac{\partial \hat{\psi}}{\partial \boldsymbol{\eta}}$.

The constitutive relations for the rod are found by considering the local form of the balance of energy:

$$\rho_0 \dot{\psi} = \mathbf{m} \cdot \frac{\partial \boldsymbol{\omega}}{\partial \xi} + \mathbf{n} \cdot \left(\frac{\partial \mathbf{v}}{\partial \xi} - \boldsymbol{\omega} \times \frac{\partial \mathbf{r}}{\partial \xi} \right). \quad (6.24)$$

Following the procedure we have used several times previously, we now introduce the representation (6.22)₃ for $\rho_0 \dot{\psi}$ and rearrange the local form of the balance of energy:

$$\left(\mathbf{m} - \mathbf{P} \rho_0 \frac{\partial \hat{\psi}}{\partial \mathbf{v}} \right) \cdot \boldsymbol{\omega}' + \left(\mathbf{n} - \mathbf{P} \rho_0 \frac{\partial \hat{\psi}}{\partial \boldsymbol{\eta}} \right) \cdot (\mathbf{v}' - \boldsymbol{\omega} \times \mathbf{r}') = 0. \quad (6.25)$$

Assuming this equation holds for all motions of the rod and that \mathbf{n} and \mathbf{m} are independent of $\dot{\eta}_k$ and \dot{v}_i , it follows that

$$\begin{aligned}\mathbf{n} &= \mathbf{P}\rho_0 \frac{\partial \hat{\psi}}{\partial \boldsymbol{\eta}} \\ &= \rho_0 \frac{\partial \hat{\psi}}{\partial \eta_1} \mathbf{d}_1 + \rho_0 \frac{\partial \hat{\psi}}{\partial \eta_2} \mathbf{d}_2 + \rho_0 \frac{\partial \hat{\psi}}{\partial \eta_3} (\mathbf{d}_1 \times \mathbf{d}_2), \\ \mathbf{m} &= \mathbf{P}\rho_0 \frac{\partial \hat{\psi}}{\partial \mathbf{v}} \\ &= \rho_0 \frac{\partial \hat{\psi}}{\partial v_1} \mathbf{d}_1 + \rho_0 \frac{\partial \hat{\psi}}{\partial v_2} \mathbf{d}_2 + \rho_0 \frac{\partial \hat{\psi}}{\partial v_3} (\mathbf{d}_1 \times \mathbf{d}_2).\end{aligned}\quad (6.26)$$

Thus, in contrast to the constitutive relations Eqn. (5.91) for the Kirchhoff theory, \mathbf{n} is completely described by constitutive relations. It may be helpful to note that we are no longer imposing the constraint $\mathbf{r}' = \mathbf{d}_1 \times \mathbf{d}_2$. Consequently, the shear forces $\mathbf{n} \cdot \mathbf{d}_\alpha$ can be loosely interpreted as being responsible for deforming (shearing) \mathbf{d}_α in the tangential direction to the material curve.

The reference configuration \mathcal{R}_0 is said to be a natural configuration if $\mathbf{n} = \mathbf{0}$ and $\mathbf{m} = \mathbf{0}$ when $\mathbf{v} = \mathbf{0}$ and $\boldsymbol{\eta} = \mathbf{0}$:

$$\frac{\partial \hat{\psi}}{\partial \mathbf{v}} (\mathbf{v} = \mathbf{0}, \boldsymbol{\eta} = \mathbf{0}, \xi) = \mathbf{0}, \quad \frac{\partial \hat{\psi}}{\partial \boldsymbol{\eta}} (\mathbf{v} = \mathbf{0}, \boldsymbol{\eta} = \mathbf{0}, \xi) = \mathbf{0}. \quad (6.27)$$

Such a directed curve can be held in equilibrium without the application of external forces $\rho_0 \mathbf{f}$ or moments \mathbf{m}_a , or terminal forces and moments at its boundary.

We consider linearizations of $\rho_0 \psi$ so these functions are expressed as quadratic functions of the components of \mathbf{v} and $\boldsymbol{\eta}$. Thus, if the reference configuration is a natural configuration, we find the canonical form

$$\rho_0 \psi = \frac{1}{2} \mathbf{g}^T \mathbf{A} \mathbf{g} + \mathbf{v}^T \mathbf{C} \mathbf{g} + \frac{1}{2} \mathbf{v}^T \mathbf{B} \mathbf{v}, \quad (6.28)$$

where

$$\mathbf{g} = \begin{bmatrix} \eta_1 \\ \eta_2 \\ \eta_3 \end{bmatrix}, \quad \mathbf{v} = \begin{bmatrix} v_1 \\ v_2 \\ v_3 \end{bmatrix}, \quad (6.29)$$

and

$$\mathbf{A} = \begin{bmatrix} a_{11} & a_{12} & a_{13} \\ a_{12} & a_{22} & a_{23} \\ a_{13} & a_{23} & a_{33} \end{bmatrix}, \quad \mathbf{B} = \begin{bmatrix} b_{11} & b_{12} & b_{13} \\ b_{12} & b_{22} & b_{23} \\ b_{13} & b_{23} & b_{33} \end{bmatrix}, \quad \mathbf{C} = \begin{bmatrix} c_{11} & c_{12} & c_{13} \\ c_{21} & c_{22} & c_{23} \\ c_{31} & c_{32} & c_{33} \end{bmatrix}. \quad (6.30)$$

The coefficients a_{ik} , b_{ik} , and c_{ik} may depend on ξ , the intrinsic strains v_{0j} , and $\mathbf{R} \cdot \mathbf{E}_k$. Material symmetry conditions are often imposed to reduce the number of coefficients a_{ik} , b_{ik} , and c_{ik} from 21. These conditions will be discussed shortly and the most dramatic of them will reduce the number of coefficients from 21 to four. In a

geometrically nonlinear theory with a quadratic strain energy function, the constitutive relations for \mathbf{n} and \mathbf{m} have the forms

$$\mathbf{n} = \sum_{i=1}^3 n_i \mathbf{d}_i, \quad \mathbf{m} = \sum_{i=1}^3 m_i \mathbf{d}_i, \quad (6.31)$$

where

$$\begin{bmatrix} n_1 \\ n_2 \\ n_3 \end{bmatrix} = \mathbf{A}\mathbf{g} + \mathbf{C}\mathbf{v}, \quad \begin{bmatrix} m_1 \\ m_2 \\ m_3 \end{bmatrix} = \mathbf{C}\mathbf{g} + \mathbf{B}\mathbf{v}. \quad (6.32)$$

For a linearized theory, the strains η_i and v_i are linearized about a reference configuration, and \mathbf{n} and \mathbf{m} are expressed in terms of the \mathbf{D}_i basis, e.g., $\mathbf{n} \approx \sum_{k=1}^3 n_k \mathbf{D}_k$.

6.4 Treatments of Material Symmetry

In contrast to three-dimensional continua, the strain energy function of an elastic rod depends not only on the constitution of the rod but also on its geometry. For Kirchhoff's rod theory, the most well-known example of the geometry dependence lies in the simplification to the strain energy function $\rho_0 \psi = \frac{EI_1}{2} v_1^2 + \frac{EI_2}{2} v_2^2 + \frac{G}{2} v_3^2$ that occurs when the cross section of the rod is either circular or square (i.e., $I_1 = I_2$). In the more elaborate rod theory under consideration in this chapter the number of strains has risen to six and it is natural to ask if there are conditions under which the strain energy function contains coupling terms between, say, torsion v_3 and dilation η_3 ? To explore this question, it is necessary to establish restrictions on the function $\rho_0 \psi$ that manifest because of material symmetry.

The notion of material symmetry employed here is broader than the one used in three-dimensional continuum mechanics because it must account not only for the constitution of the continuum composing the rod but also for the geometry of the rod. For instance, consider a rod composed of an isotropic linearly elastic material. The material symmetry of the rod will depend on the geometry of the cross section. For instance, a rod with a rectangular cross section is expected to behave differently than one with a circular cross section and this will be reflected in the strain energy function of the rod and the inertial coefficients $y^{\alpha\beta}$.

Several treatments of material symmetry for rods can be found in the literature. The first class of treatments considers the invariance of a strain energy function under specific orthogonal transformations of a reference configuration (see, e.g., Antman [12, Section 8.11], Cohen [62], Green and Naghdi [133, Section 9], Green, Naghdi, and Wenner [138, Section 8], and Lauderdale and O'Reilly [198]). The resulting set of transformations forms what is known as the material symmetry group of the rod. Two generalizations of these treatments can also be found in the literature. The first generalization includes transformations of the coordinate ξ in parallel with an orthogonal transformation. This treatment is motivated by the use of rod theories to model rod-like bodies, such as wire rope and DNA strands, that possess

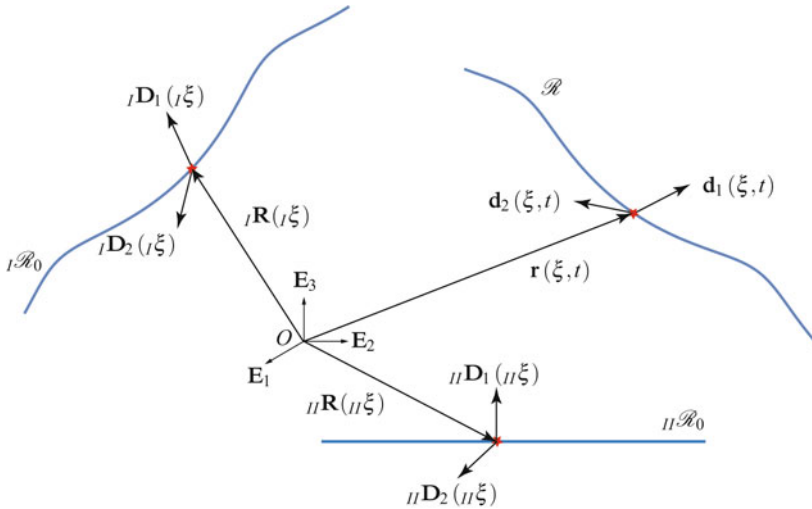


Fig. 6.3 The pair of reference configurations $I\mathcal{R}_0$ and $II\mathcal{R}_0$ of a directed curve and the present configuration \mathcal{R} .

helical microstructures. The seminal work on this type of treatment is a recent paper by Healey [158]. The second generalization considers orthogonal transformations which are functions of ξ and transformations of the coordinate ξ and can be found in the recent papers [199, 214]. In this chapter, we only consider the simplest treatment and refer the reader to the literature for details on the more general treatments.

6.4.1 The Case of a Constant Transformation \mathbf{Q}

For the treatment of material symmetry that we present, we consider a pair of reference configurations of the directed curve (cf. Figure 6.3). The pair of configurations are denoted by $I\mathcal{R}_0$ and $II\mathcal{R}_0$, respectively. The material coordinates in these configurations are denoted by $I\xi$ and $II\xi$, respectively, and are presumed to be identical:

$$\xi = II\xi = I\xi. \quad (6.33)$$

We suppose that the directors and tangent vectors in $I\mathcal{R}_0$ and $II\mathcal{R}_0$ can be related by a *constant* orthogonal transformation \mathbf{Q} :

$$\begin{aligned} II\mathbf{D}_\beta(II\xi) &= \mathbf{Q}_I \mathbf{D}_\beta(I\xi), \\ \frac{\partial II\mathbf{R}}{\partial II\xi}(II\xi) &= \mathbf{Q}_I \mathbf{R}'(I\xi), \\ II\mathbf{P}_0(II\xi) &= \mathbf{Q}_I \mathbf{P}_0(I\xi). \end{aligned} \quad (6.34)$$

Here, the prime denotes the partial derivative with respect to $I\xi$. Representative examples of proper- and improper-orthogonal transformations elements of the material symmetry groups are shown in Figure 6.4.

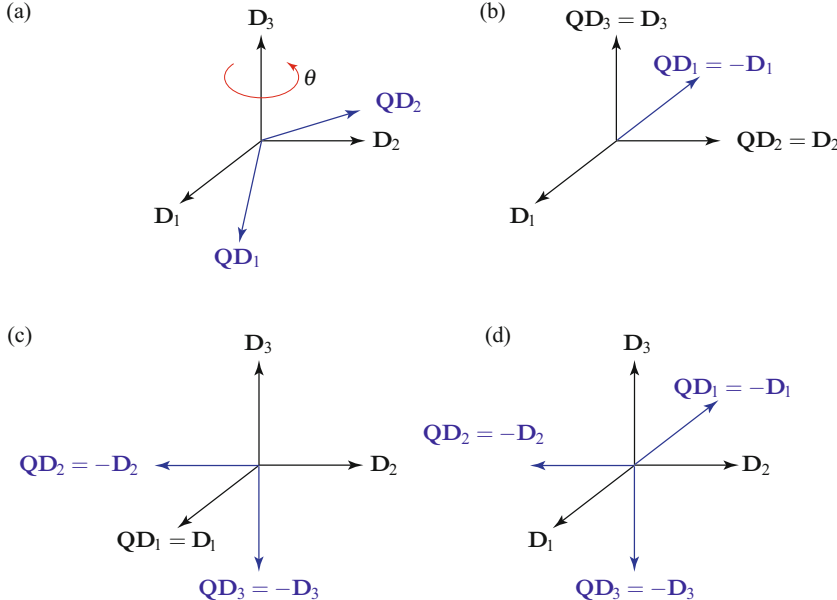


Fig. 6.4 The orthogonal transformations that are elements in the transverse isotropy material symmetry groups: (a), a rotation about \mathbf{D}_3 : $\mathbf{Q} = \mathbf{Q}_E(\theta, \mathbf{D}_3)$; (b), a reflection in the $\mathbf{D}_2 - \mathbf{D}_3$ plane: $\mathbf{Q} = \mathbf{R}_{\mathbf{D}_1}$; (c), a rotation about \mathbf{D}_1 through an angle of 180° : $\mathbf{Q} = -\mathbf{R}_{\mathbf{D}_1}$; and (d), an inversion: $\mathbf{Q} = -\mathbf{I}$.

It follows from the relations (6.34) that

$$II\mathbf{P}(II\xi) = I\mathbf{P}(I\xi)\mathbf{Q}^T, \quad II\mathbf{\eta}(II\xi) = \mathbf{Q}_I\mathbf{\eta}(I\xi), \quad (6.35)$$

and

$$II\mathbf{K}(II\xi) = \mathbf{Q}_I\mathbf{K}(I\xi)\mathbf{Q}^T, \quad II\mathbf{v}(II\xi) = \mathbf{Q}^A_I\mathbf{v}(I\xi). \quad (6.36)$$

In these equations, $\mathbf{Q}^A = \det(\mathbf{Q})\mathbf{Q}$ is the adjugate of \mathbf{Q} . We recall that the adjugate \mathbf{B}^A of a tensor \mathbf{B} has the property that $\mathbf{B}^A(\mathbf{a} \times \mathbf{b}) = \mathbf{B}\mathbf{a} \times \mathbf{B}\mathbf{b}$. For an invertible tensor \mathbf{B} , $\mathbf{B}^A = \det(\mathbf{B})(\mathbf{B}^{-1})^T$. Using the adjugate, it can be shown that

$$(\mathbf{B}^A \mathbf{c}) \times \mathbf{b} = (\mathbf{B}\mathbf{C}\mathbf{B}^T) \mathbf{b}, \quad (6.37)$$

for all vectors \mathbf{b} and skew-symmetric tensors $\mathbf{C} = -\mathbf{C}^T$ where $\mathbf{c} = \mathbf{a} \times (\mathbf{C})$. This property of the adjugate is used to establish Eqn. (6.36)₂ from Eqn. (6.36)₁ and it is repeatedly used throughout Section 6.6.

For the same present configuration $(\mathbf{r}, \mathbf{d}_\alpha)$ and the *same* material point, the strain energy functions of the rod relative to the two reference configurations are, respectively,

$$\begin{aligned}\rho_0 \psi &= {}_I \rho_{0I} \psi({}_I \boldsymbol{\eta}({}_I \xi), {}_I \mathbf{v}({}_I \xi), {}_I \xi) \\ &= {}_{II} \rho_{0II} \psi({}_{II} \boldsymbol{\eta}({}_{II} \xi), {}_{II} \mathbf{v}({}_{II} \xi), {}_{II} \xi).\end{aligned}\quad (6.38)$$

For notational simplicity, the possible dependency of the strain energy functions on $\boldsymbol{\nu}_0(\xi)$ and $\mathbf{R}'(\xi)$ have been lumped into the dependency on ξ . We find, with the help of the relations (6.34)–(6.36), that

$$\begin{aligned}\psi &= {}_{II} \rho_{0II} \psi({}_{II} \boldsymbol{\eta}({}_{II} \xi), {}_{II} \mathbf{v}({}_{II} \xi), {}_{II} \xi) \\ &= {}_I \rho_{0I} \psi\left(\mathbf{Q}^T {}_{II} \boldsymbol{\eta}({}_{B\xi}), (\mathbf{Q}^A)^{-1} {}_{II} \mathbf{v}({}_{II} \xi), {}_{II} \xi\right).\end{aligned}\quad (6.39)$$

The specific point where ${}_{II} \mathbf{v}$ and ${}_{II} \boldsymbol{\eta}$ are evaluated in ${}_I \psi$ is important to note.

We define two reference configurations of the rod to be material symmetry related if, for all motions with the same \mathbf{v} and $\boldsymbol{\eta}$, and the same value of the material coordinates, ${}_I \xi = \xi$ and ${}_{II} \xi = \xi$,

$${}_I \rho_{0I} \psi(\boldsymbol{\eta}(\xi), \mathbf{v}(\xi), \xi) = {}_{II} \rho_{0II} \psi(\boldsymbol{\eta}(\xi), \mathbf{v}(\xi), \xi). \quad (6.40)$$

With the assistance of Eqn. (6.39), we can express the condition (6.40) in terms of the strain energy function ${}_I \psi$:

$$\begin{aligned}\rho_0 \psi(\boldsymbol{\eta}(\xi), \mathbf{v}(\xi), \xi) &= \rho_0 \psi(\mathbf{Q}^T \boldsymbol{\eta}(\xi), \det(\mathbf{Q}) \mathbf{Q}^T \mathbf{v}(\xi), \xi), \\ &= \rho_0 \tilde{\psi}(\mathbf{Q}^T \boldsymbol{\eta}(\xi), \mathbf{Q}^T \mathbf{K}(\xi) \mathbf{Q}, \xi).\end{aligned}\quad (6.41)$$

For convenience, we have dropped the left-subscript I and made some other obvious simplifications in notation. The function $\tilde{\psi}$ has been introduced for future convenience so we can easily exploit results from the literature.

In part because the product of two orthogonal transformations is an orthogonal transformation and the identity \mathbf{I} is an orthogonal transformation, the group structure associated with the symmetry condition (6.41) can readily be developed. Elements \mathfrak{g} of the group \mathfrak{G} will be orthogonal transformations, $\mathfrak{g} = (\mathbf{Q})$. The group operation $\mathfrak{g}_2 \circ \mathfrak{g}_1 = (\mathbf{Q}_2 \mathbf{Q}_1)$ yields another element $\mathbf{Q}_2 \mathbf{Q}_1$ of the group. It is easy to see that the group operation is associative: $\mathfrak{g}_3 \circ (\mathfrak{g}_2 \circ \mathfrak{g}_1) = (\mathfrak{g}_3 \circ \mathfrak{g}_2) \circ \mathfrak{g}_1 = (\mathbf{Q}_3 \mathbf{Q}_2 \mathbf{Q}_1)$. In addition, the identity and inverse elements are

$$\mathfrak{i} = (\mathbf{I}), \quad \mathfrak{g}^{-1} = (\mathbf{Q}^T). \quad (6.42)$$

The group \mathfrak{G} is known as the material symmetry group of the rod.

Table 6.1 Invariants in irreducible function bases for the five different transverse isotropies. The function bases are taken from Zheng [371, Tables 12 and 14] for scalar functions of a vector η and a skew-symmetric tensor $\mathbf{K} = \text{skew}(\mathbf{v})$.

Material Symmetry Group \mathfrak{G}	Elements \mathfrak{g} of \mathfrak{G}	Irreducible function bases
\mathcal{C}_∞	$\{\mathbf{Q}_E(\theta, \mathbf{D}_3), \theta \in [0, 2\pi]\}$	$\mathbf{v} \cdot \mathbf{v}, \quad \eta \cdot \eta,$ $\eta \cdot \mathbf{D}_3, \quad \mathbf{v} \cdot \mathbf{D}_3,$ $\mathbf{v} \cdot \eta, \quad \mathbf{D}_3 \cdot (\eta \times \mathbf{v}).$
$\mathcal{C}_{\infty h}$	$\{-\mathbf{I}, \mathbf{Q}_E(\theta, \mathbf{D}_3), \theta \in [0, 2\pi]\}$	$\mathbf{v} \cdot \mathbf{v}, \quad \eta \cdot \eta,$ $(\eta \cdot \mathbf{D}_3)^2, \quad \mathbf{v} \cdot \mathbf{D}_3,$ $(\mathbf{v} \times \eta) \cdot (\mathbf{v} \times \eta), \quad \mathbf{D}_3 \cdot (\eta \times (\mathbf{v} \times \eta)),$ $\mathbf{D}_3 \cdot (\eta \times (\mathbf{v} \times (\mathbf{v} \times \eta))),$ $(\mathbf{D}_3 \cdot \eta)(\mathbf{D}_3 \cdot (\eta \times \mathbf{v})).$
$\mathcal{C}_{\infty v}$	$\{\mathbf{R}\mathbf{e}_{\mathbf{D}_1}, \mathbf{Q}_E(\theta, \mathbf{D}_3), \theta \in [0, 2\pi]\}$	$\mathbf{v} \cdot \mathbf{v}, \quad \eta \cdot \eta,$ $\eta \cdot \mathbf{D}_3, \quad (\mathbf{v} \cdot \mathbf{D}_3)^2,$ $\mathbf{D}_3 \cdot (\eta \times \mathbf{v}),$ $\mathbf{D}_3 \cdot (\mathbf{v} \times (\mathbf{v} \times \eta)).$
$\mathcal{D}_{\infty h}$	$\{-\mathbf{R}\mathbf{e}_{\mathbf{D}_1}, \mathbf{Q}_E(\theta, \mathbf{D}_3), \theta \in [0, 2\pi]\}$	$\mathbf{v} \cdot \mathbf{v}, \quad \eta \cdot \eta,$ $(\eta \cdot \mathbf{D}_3)^2, \quad (\mathbf{v} \cdot \mathbf{D}_3)^2,$ $(\mathbf{v} \times \eta) \cdot (\mathbf{v} \times \eta), \quad (\mathbf{D}_3 \cdot \eta)(\mathbf{D}_3 \cdot (\mathbf{v} \times \eta)),$ $(\mathbf{D}_3 \cdot (\mathbf{v} \times \eta))(\mathbf{D}_3 \cdot (\mathbf{v} \times (\mathbf{v} \times \eta))).$
\mathcal{D}_∞	$\{-\mathbf{I}, \mathbf{R}\mathbf{e}_{\mathbf{D}_1}, \mathbf{Q}_E(\theta, \mathbf{D}_3), \theta \in [0, 2\pi]\}$	$\mathbf{v} \cdot \mathbf{v}, \quad \eta \cdot \eta,$ $(\eta \cdot \mathbf{D}_3)^2, \quad (\mathbf{v} \cdot \mathbf{D}_3)^2,$ $\mathbf{v} \cdot \eta, \quad (\mathbf{D}_3 \cdot \eta)(\mathbf{D}_3 \cdot \mathbf{v}),$ $(\mathbf{D}_3 \cdot (\eta \times \mathbf{v}))(\mathbf{D}_3 \cdot \mathbf{v}),$ $(\mathbf{D}_3 \cdot \eta)(\mathbf{D}_3 \cdot (\mathbf{v} \times \eta)).$

6.4.2 Transverse Isotropy and Transverse Hemitropy

For many rod-like bodies modeled using rod theory, the structure of the continuum has a material symmetry and this symmetry is reflected in the constitutive relations for the rod. One prominent example arises when the body has a unique preferred direction and the material is said to be transversely isotropic. If this body is modeled as a rod with a circular cross section and the preferred direction is aligned with the axis of the rod, then the rod inherits this material symmetry. An example of this situation lies in modeling an insulated electrical cord using a rod theory. A second example arises when the elastic rod-like body is isotropic. If the cross sections are circular, then the resulting rod is said to be transversely isotropic or, more commonly, isotropic.

For a three-dimensional continua there are five distinct types of transverse isotropy and, depending on the rod's strain energy function, some of them may be indistinguishable.¹ The five groups, along with their elements, are as follows:

$$\text{Rotational symmetry : } \mathcal{C}_\infty = \{\mathbf{Q}_E(\theta, \mathbf{D}_3), \theta \in [0, 2\pi]\},$$

$$\text{Rotational symmetry : } \mathcal{C}_{\infty h} = \mathcal{C}_\infty \cup \{-\mathbf{I}\},$$

$$\text{Rotational symmetry : } \mathcal{C}_{\infty v} = \mathcal{C}_\infty \cup \{\mathbf{R}\mathbf{e}_{\mathbf{D}_1}\},$$

$$\text{Transverse hemitropy : } \mathcal{D}_{\infty h} = \mathcal{C}_\infty \cup \{-\mathbf{R}\mathbf{e}_{\mathbf{D}_1}\},$$

$$\text{Transverse isotropy : } \mathcal{D}_\infty = \mathcal{C}_\infty \cup \{-\mathbf{I}, \mathbf{R}\mathbf{e}_{\mathbf{D}_1}\}.$$

In these groups,

$$\mathbf{R}\mathbf{e}_{\mathbf{D}_1} = \mathbf{I} - 2\mathbf{D}_1 \otimes \mathbf{D}_1 \quad (6.43)$$

is a reflection about the plane perpendicular to \mathbf{D}_1 and $\mathbf{Q}_E(\theta, \mathbf{D}_3)$ is a rotation about the axis \mathbf{D}_3 through an angle θ (cf. Figure 6.4). We also note that

$$-\mathbf{R}\mathbf{e}_{\mathbf{D}_1} = 2\mathbf{D}_1 \otimes \mathbf{D}_1 - \mathbf{I} = \mathbf{Q}_E(\pi, \mathbf{D}_1). \quad (6.44)$$

For the rod-like body, we assume that the preferred direction is chosen to coincide with the axis \mathbf{D}_3 in the reference configuration \mathcal{R}_0 . In addition, we assume that this configuration is straight and natural with $\mathbf{v}_0 = \mathbf{0}$. Motivated by the correspondence between the rod theory and the three-dimensional theory of a continuum, we adopt the definitions above for the rod theory. We next seek the most general forms of the strain energy function for the rod which has one of the aforementioned five material symmetry groups.

The most general form of a function compatible with the material symmetry condition (6.41) is determined by an irreducible set of functions. The members of the irreducible set of functions are invariant under the elements of the rod's material symmetry group. For example, $\mathbf{v} \cdot \mathbf{v} = (\mathbf{Q}\mathbf{v} \cdot \mathbf{Q}\mathbf{v})$ and so the function $\mathbf{v} \cdot \mathbf{v}$ is invariant under orthogonal transformations while $\mathbf{v} \cdot \mathbf{E}_3$ (which transforms to $\mathbf{Q}\mathbf{v} \cdot \mathbf{E}_3$) does not possess this invariance. Following seminal work by Ronald S. Rivlin (1905–1995) and others, Zheng et al. (see [369–371] and references therein) have compiled the smallest (irreducible) sets of invariant functions for a wide range of strain energy functions. Their results for functions of a vector and a skew-symmetric tensor are presented in Table 6.1. For the five material symmetry groups of the rod, we use these results to establish the simplest functional forms of the strain energy function $\rho_0\psi$ which satisfy the material symmetry condition (6.41) for each of the groups. Specifically, using the results from [371, Tables 12 and 14] which are summarized in Table 6.1, we find that

$$\rho_0\psi = F(A, \mathbf{v}_0(\xi), \xi), \quad (6.45)$$

¹ By way of additional background, we also note that if a function is invariant only under proper-orthogonal transformations (i.e., rotations) then it is said to be hemitropic. The adjective isotropic pertains to the case where the function is invariant under orthogonal transformations.

where the arguments A can be read from Table 6.1. The linearized (quadratic) strain energy function can also be readily determined by restricting attention to quadratic elements of the irreducible function basis.

For instance, consider the transverse isotropy $\mathcal{D}_{\infty h}$. As we shall see, this type of symmetry is synonymous with the notion of an isotropic rod. We can infer from Table 6.1 that the most general functional form of $\rho_0 \psi$ that is compatible with the material symmetry condition for all of the elements of $\mathcal{D}_{\infty h}$ is

$$\rho_0 \psi = F(v_1^2 + v_2^2, v_3^2, \eta_1^2 + \eta_2^2, \eta_3^2, i_1, i_2, i_3, \mathbf{v}_0(\xi), \xi), \quad (6.46)$$

where the quartic, cubic, and quintic terms are

$$\begin{aligned} i_1 &= (\mathbf{v} \times \boldsymbol{\eta}) \cdot (\mathbf{v} \times \boldsymbol{\eta}), \\ i_2 &= (\mathbf{D}_3 \cdot \boldsymbol{\eta})(\mathbf{D}_3 \cdot (\mathbf{v} \times \boldsymbol{\eta})), \\ i_3 &= (\mathbf{D}_3 \cdot (\mathbf{v} \times \boldsymbol{\eta}))(\mathbf{D}_3 \cdot (\mathbf{v} \times (\mathbf{v} \times \boldsymbol{\eta}))). \end{aligned} \quad (6.47)$$

For the quadratic strain energy function (6.28) these restrictions imply that the most general quadratic strain energy function that is compatible with the transverse isotropy material symmetry group $\mathcal{D}_{\infty h}$ is

$$\rho_0 \psi = \frac{a_{11}}{2} (\eta_1^2 + \eta_2^2) + \frac{b_{11}}{2} (v_1^2 + v_2^2) + \frac{a_{33}}{2} \eta_3^2 + \frac{b_{33}}{2} v_3^2. \quad (6.48)$$

Whence, the number of coefficients has been reduced from 21 to four. We leave it as an exercise for the reader to show that the quadratic strain energy functions for the material symmetry groups associated with \mathcal{C}_{∞} and $\mathcal{D}_{\infty h}$ are identical to the function (6.48).

A rod whose material symmetry group is \mathcal{C}_{∞} is aptly termed transversely hemitropic by Healey [158]. For such a rod, we can infer the most general form of the strain energy function that is compatible with the material symmetry group using Table 6.1:

$$\rho_0 \psi = F(v_1^2 + v_2^2, v_3, \eta_1^2 + \eta_2^2, \eta_3, \eta_1 v_1 + \eta_2 v_2, (\eta_1 v_2 - v_1 \eta_2)). \quad (6.49)$$

The quadratic strain energy function for such a rod is readily inferred:

$$\begin{aligned} \rho_0 \psi &= \frac{a_{11}}{2} (\eta_1^2 + \eta_2^2) + \frac{b_{11}}{2} (v_1^2 + v_2^2) + \frac{a_{33}}{2} \eta_3^2 + \frac{b_{33}}{2} v_3^2 \\ &\quad + \underbrace{c_{11}(\eta_1 v_1 + \eta_2 v_2) + c_{33} \eta_3 v_3 + c_{12}(\eta_1 v_2 - v_1 \eta_2)}. \end{aligned} \quad (6.50)$$

The underbraced terms in this equation are the differences between the quadratic strain energy functions for the isotropic and hemitropic cases. We also note that a nonvanishing c_{33} in this expression implies that there will be coupling between extension and torsion in a straight rod. As discussed in Healey [158], the strain energy function (6.50) with $c_{12} = 0$ is suitable for modeling some rods whose microstructure has a helical symmetry.

6.4.3 Application to Kirchhoff's Rod Theory

The strain energy function for a homogenous rod modeled using Kirchhoff's rod theory with $\mathbf{v}_0 = \mathbf{0}$ has the functional form

$$\rho_0 \psi = \rho_0 \psi(\mathbf{v}). \quad (6.51)$$

It is straightforward to develop a material symmetry condition akin to the condition (6.41) for such a rod. For the material symmetry groups \mathcal{C}_∞ and $\mathcal{C}_{\infty h}$, we can use the previous developments to show that the strain energy function has the invariant form

$$\rho_0 \psi = F(v_1^2 + v_2^2, v_3). \quad (6.52)$$

By way of contrast, for the material symmetry groups \mathcal{D}_∞ , $\mathcal{D}_{\infty h}$, and $\mathcal{C}_{\infty v}$, the invariant form of the strain energy function is

$$\rho_0 \psi = F(v_1^2 + v_2^2, v_3^2). \quad (6.53)$$

Thus, these three material symmetry groups are commonly associated with the notion of an isotropic Kirchhoff rod. Furthermore, for all five material symmetry groups, the quadratic form of the strain energy function is the familiar

$$\rho_0 \psi = \frac{b_{11}}{2} (v_1^2 + v_2^2) + \frac{b_{33}}{2} v_3^2. \quad (6.54)$$

By comparing solutions of the Kirchhoff rod theory to the solutions to the corresponding problems in three-dimensional linear elasticity, the identifications $b_{11} = EI$ and $b_{33} = \mathcal{D}$ can be made.

6.5 Application to Torsion and Extension

In many recent experiments on segments of double-stranded DNA, one end of the single molecule of DNA is attached to a fixed surface, while the other end is subject to a force $F_\ell \mathbf{E}_3$ and a moment $M_\ell \mathbf{E}_3$. These effects are simulated using optical tweezers, hydrodynamic drag, or magnetic fields. A schematic of one such experiment is shown in Figure 6.5(a) and reviews of the experiments are presented in [40, 120]. A coupling between stretching and twisting is observed in many of these experiments. In the sequel, we explore how this effect can be explained by modeling the strand of DNA as an initially straight rod with a helical microstructure. As emphasized in Đurićković et al. [89], one can also model the DNA strand as a helical spring and observe the same couplings reported in the biophysics literature.

Referring to Figures 5.7(b) and 6.5(b), we use the material curve to model the duplex (molecular) axis and choose the directors to follow the phosphate backbone strands of DNA:

$$\mathbf{D}_1 = \cos(\phi_h) \mathbf{E}_1 + \sin(\phi_h) \mathbf{E}_2, \quad \mathbf{D}_2 = \cos(\phi_h) \mathbf{E}_2 - \sin(\phi_h) \mathbf{E}_1, \quad \mathbf{D}_3 = \mathbf{E}_3, \quad (6.55)$$

where the angle ϕ_h is a function of the coordinate ξ . Hence,

$$\mathbf{v}_0 = v_{03} \mathbf{E}_3 = \frac{\partial \phi_h}{\partial \xi} \mathbf{E}_3, \quad (6.56)$$

and \mathbf{v}_0 is constant.

We will model the single molecule of DNA using a rod whose strain energy function $\rho_0 \psi$ is

$$2\rho_0 \psi = b_{11} v_1^2 + b_{22} v_2^2 + b_{33} v_3^2 + a_{11} (\eta_1^2 + \eta_2^2) + a_{33} \eta_3^2 + 2c_{33} \eta_3 v_3. \quad (6.57)$$

Here c_{33} is a coefficient responsible for the coupling of torsion and extension. The constants in this strain energy function must be identified by experiments or comparison to models based on worm-like chains used in the biophysics literature. By way of illustration, the radius of the rod will be approximately 10 Å and $v_{03} \approx 0.185$ radians/Å [228]. Using data from [35], the bending moduli $b_{11} = b_{22} \approx 2 \times 10^{-28}$ Nm² and the torsional modulus $b_{33} \approx 2 - 4 \times 10^{-28}$ Nm². Gore et al. [120] have measured $c_{33} \approx -90 \times 10^{-21}$ Nm. With the help of the identities (6.26), we conclude that

$$\begin{aligned} \mathbf{n} &= a_{11} (\eta_1 \mathbf{d}_1 + \eta_2 \mathbf{d}_2) + (a_{33} \eta_3 + c_{33} v_3) \mathbf{d}_3, \\ \mathbf{m} &= b_{11} v_1 \mathbf{d}_1 + b_{22} v_2 \mathbf{d}_2 + (b_{33} v_3 + c_{33} \eta_3) \mathbf{d}_3. \end{aligned} \quad (6.58)$$

From this pair of constitutive relations observe that, if $\mathbf{v} = \mathbf{0}$, a nonzero η_3 will induce a moment in the rod and, if $\mathbf{n} = \mathbf{0}$, a nonzero torsion v_3 will induce a force in the rod.

We suppose that the DNA strands are subject to negligible external body forces and negligible surface tractions on the lateral surfaces, $\rho_0 \mathbf{f} = \mathbf{0}$ and $\mathbf{l}^\alpha = \mathbf{0}$, and we restrict attention to static solutions. Starting from the balance laws,

$$\frac{\partial \mathbf{n}}{\partial \xi} = \mathbf{0}, \quad \frac{\partial \mathbf{m}}{\partial \xi} + \frac{\partial \mathbf{r}}{\partial \xi} \times \mathbf{n} = \mathbf{0}, \quad (6.59)$$

using the appropriate constitutive relations for \mathbf{n} and \mathbf{m} , and taking the components of the balance laws (6.59) relative to the basis $\{\mathbf{d}_1, \mathbf{d}_2, \mathbf{d}_1 \times \mathbf{d}_2\}$, we can establish the ordinary differential equations governing the shape of the material curve and the behavior of \mathbf{d}_α .

The boundary conditions for the problem of interest are

$$\begin{aligned} \mathbf{r}(0, t) &= \mathbf{0}, & \mathbf{d}_1(0, t) &= \mathbf{E}_1, & \mathbf{d}_2(0, t) &= \mathbf{E}_2, \\ \mathbf{n}(\ell, t) &= F_\ell \mathbf{E}_3, & \mathbf{m}(\ell, t) &= M_\ell \mathbf{E}_3, \end{aligned} \quad (6.60)$$

where F_ℓ and M_ℓ are constants.

From the balance laws, we find that \mathbf{n} is constant. Assuming that the centerline remains straight, $\mathbf{r}' \parallel \mathbf{E}_3$, then we also find that \mathbf{m} is constant. Consequently,

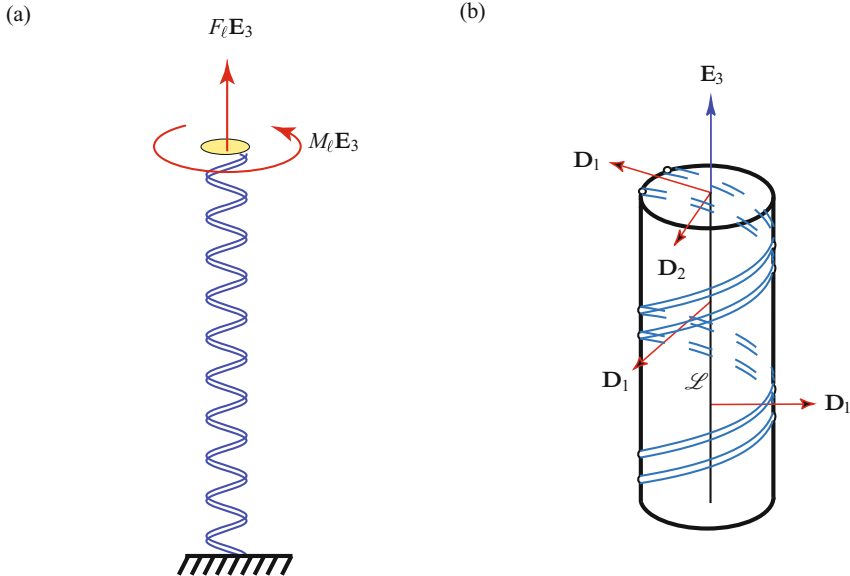


Fig. 6.5 (a) Schematic of a strand of DNA being stretched and torqued. One end of the strand is fixed while the other end is affixed to a bead which is used to transmit the applied torque and force. In experiments on DNA in the literature, the force F_ℓ ranges from 0 to 70 picoNewtons. (b) A portion of the reference configuration \mathcal{R}_0 for a rod model of the DNA strand.

$$\begin{bmatrix} F_\ell \\ M_\ell \end{bmatrix} = \begin{bmatrix} a_{33} & c_{33} \\ c_{33} & b_{33} \end{bmatrix} \begin{bmatrix} \eta_3 \\ v_3 \end{bmatrix}. \quad (6.61)$$

For the simple deformation being considered here, we can express η_3 and v_3 in terms of the displacement $\Delta z \approx \mathbf{r}(\ell) \cdot \mathbf{E}_3 - \mathbf{r}(0) \cdot \mathbf{E}_3 - \ell$ and the change in the angle of twist at the top of the structure: $\Delta \theta \approx v_3 \ell$. In these expressions,

$$\ell = \mathbf{R}(\ell) \cdot \mathbf{E}_3 - \mathbf{R}(0) \cdot \mathbf{E}_3 \quad (6.62)$$

is the initial height of the helical structure. Inverting the linear equations (6.61), we find that

$$\begin{aligned} \frac{\Delta z}{\ell} \approx \eta_3 &= \frac{1}{a_{33}b_{33} - c_{33}^2} (b_{33}F_\ell - c_{33}M_\ell), \\ \frac{\Delta \theta}{\ell} \approx v_3 &= \frac{1}{a_{33}b_{33} - c_{33}^2} (a_{33}M_\ell - c_{33}F_\ell). \end{aligned} \quad (6.63)$$

After assuming that the strain energy function is positive definite,² we observe that if $c_{33} > 0 (< 0)$ then application of a clockwise moment alone can stretch (compress)

² Necessary conditions for the positive definiteness of the strain energy function (6.57) include $a_{33} > 0$, $b_{33} > 0$, and $a_{33}b_{33} - c_{33}^2 > 0$.

the rod and application of a tensile force alone can cause it to rotate in the clockwise (counterclockwise) direction. The linear relations (6.63) can be used to identify the parameters a_{33} , b_{33} , and c_{33} from tests where F_ℓ and M_ℓ are controlled and $\frac{\Delta z}{\ell}$ and $\frac{\Delta \theta}{\ell}$ are measured.

We take this opportunity to note that relations which are similar to (6.61) appear in studies on the extension and twist of wire ropes [73, Chapter 4]. Indeed, we encountered related work earlier in Chapter 5 when we examined the coupling between twist and extension in a helical spring (cf. Eqn. (5.228)). If we now identify the stiffnesses for both models, we will find the identifications

$$\begin{aligned} a_{33} &= \frac{\mathcal{D}\kappa_0}{R} + \frac{EI}{R} \frac{\tau_0^2}{\kappa_0}, \\ b_{33} &= \mathcal{D}R\tau_0^2 + EIR\kappa_0, \\ c_{33} &= (\mathcal{D} - EI)\tau_0. \end{aligned} \quad (6.64)$$

We note that the coupling coefficient $c_{33} < 0$ for right-handed helices which agrees with the experimental results of Gore et al. [120] who examined the twist-stretch coupling of strands of DNA.

6.6 Ericksen's Uniform States

In a remarkable paper, Ericksen [97] proposed a static solution for a wide range of rod theories where the centerline of the rod describes a helical space curve, a straight line, or a circular arc, and the directors form constant angles with the normal and binormal vectors to this curve (cf. Figure 6.6). We now explore Ericksen's so-called uniform states for initially straight homogeneous rods where $\mathbf{D}_i = \mathbf{E}_i$. The deformed shape of the rod in a uniform state is specified by a rotation tensor \mathbf{Q} as follows:

$$\begin{aligned} \mathbf{r}'(\xi) &= \mathbf{Q}(\xi)\mathbf{r}'(0), \\ \mathbf{d}_\beta(\xi) &= \mathbf{Q}(\xi)\mathbf{d}_\beta(0), \\ \mathbf{d}_\alpha'(\xi) &= \mathbf{Q}(\xi)\mathbf{d}_\alpha'(0). \end{aligned} \quad (6.65)$$

The axial vector associated with the skew-symmetric tensor $\mathbf{Q}'\mathbf{Q}^T$ is denoted by \mathbf{v}_Q and we shall find that it is a constant throughout the length of the rod.³ We also note that Ericksen's analysis provides a transparent proof that wrenches are needed to maintain the deformed rod and the axis of the wrench coincides with the axis of the helical space curve. His analysis can be applied to rods modeled using Kirchhoff's rod theory and, to this end, we invite the reader to revisit Sections 5.14 and 5.16.2 of the previous chapter.

³ Our use of the symbol \mathbf{Q} to denote the rotation tensor associated with the uniform state should not be confused with the use of the same symbol to denote an orthogonal transformation in an earlier section of this chapter.

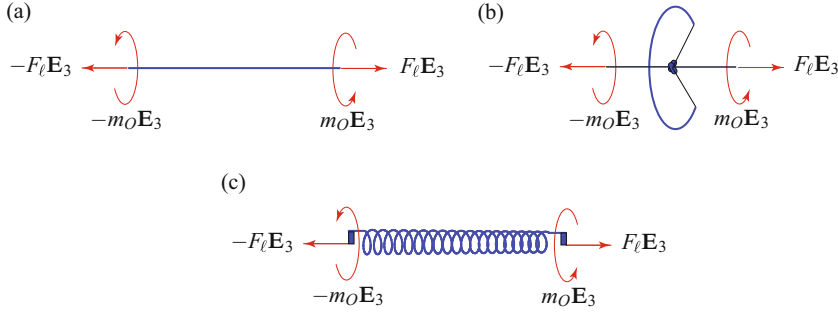


Fig. 6.6 Ericksen's uniform states of a rod where the centerline $\mathbf{r}(\xi)$ takes the form of (a), a straight line, (b), a circular arc, and (c), a circular helix. The deformed state of the rod is maintained by a wrench in all three cases. Rigid appendages are added to the ends of the rod to enable the wrench loading.

6.6.1 Kinematical Considerations

Taking the derivative of Eqn. (6.65)₂ and comparing the result to Eqn. (6.65)₃, we are lead to the compatibility condition

$$\mathbf{Q}'(\xi)\mathbf{Q}^T(\xi) = \mathbf{Q}(\xi) \left(\mathbf{Q}'(0)\mathbf{Q}^T(0) \right) \mathbf{Q}^T(\xi). \quad (6.66)$$

Whence,

$$\mathbf{v}_Q(\xi) = \mathbf{Q}(\xi)\mathbf{v}_Q(0). \quad (6.67)$$

It follows from this relation that the vector $\mathbf{v}_Q(\xi)$ is constant throughout the rod:

$$\mathbf{v}_Q'(\xi) = \mathbf{Q}'(\xi)\mathbf{v}_Q(0) = \mathbf{Q}'(\xi)\mathbf{Q}^T(\xi)\mathbf{v}_Q(\xi) = \mathbf{v}_Q(\xi) \times \mathbf{v}_Q(\xi) = \mathbf{0}. \quad (6.68)$$

That is, the rotation \mathbf{Q} has a constant angular rate. Because $\mathbf{Q}(\xi = 0) = \mathbf{I}$, the axis of rotation of \mathbf{Q} is parallel to $\mathbf{v}_Q(\xi)$.⁴ We choose the axis of rotation to be \mathbf{E}_3 without loss in generality. We also define the scalar v_Q :

$$\mathbf{v}_Q(\xi) = v_Q \mathbf{E}_3. \quad (6.69)$$

The identity $\mathbf{QE}_3 = \mathbf{E}_3$ will be exploited numerous times in the sequel.

Differentiating the equation $\mathbf{r}'(\xi) = \mathbf{Q}(\xi)\mathbf{r}'(0)$, we find that

$$\mathbf{r}''(\xi) = \mathbf{v}_Q(\xi) \times \mathbf{r}'(\xi). \quad (6.70)$$

Integrating this equation, we find the results

$$\mathbf{r}'(\xi) = \mathbf{v}_Q(\xi) \times \mathbf{r}(\xi) + \mathbf{c}_h, \quad \mathbf{r}(\xi) = \mathbf{Q}(\xi)\mathbf{r}(0) + \xi\mathbf{c}_h, \quad (6.71)$$

⁴ A proof of this result can be found in [267].

where \mathbf{c}_h is a constant. It is convenient to choose the origin so that

$$\mathbf{c}_h = \Upsilon v_Q \mathbf{E}_3, \quad (6.72)$$

where Υ is a constant. Thus, the centerline of the rod has the shape of a circular helix, or, if $\Upsilon = 0$, a circle, or, if $v_Q = 0$, a straight line. The centerline is in a state of uniform stretch:

$$\mu = \left\| \mathbf{r}'(\xi) \right\| = \left\| \mathbf{r}'(0) \right\|. \quad (6.73)$$

Consequently, the arc-length parameter s for the centerline and the material coordinate ξ are not identical:

$$\mu = \frac{\partial s}{\partial \xi}. \quad (6.74)$$

With the help of Eqn. (1.33), we can identify the parameters of the circular helix:

$$R = \sqrt{(\mathbf{r}(0) \cdot \mathbf{E}_1)^2 + (\mathbf{r}(0) \cdot \mathbf{E}_2)^2}, \quad \tau = \frac{\Upsilon}{R^2 + \Upsilon^2}, \quad \kappa = \frac{R}{R^2 + \Upsilon^2}. \quad (6.75)$$

When $\Upsilon = 0$, the centerline is a circular arc of radius R .

With regards to the rotation tensor $\mathbf{P}(\xi)$, we find that

$$\mathbf{Q}(\xi) = \mathbf{P}(\xi) \mathbf{P}^T(0), \quad \mathbf{P}(\xi) = \mathbf{Q}(\xi) \mathbf{P}(0). \quad (6.76)$$

Consequently,

$$\begin{aligned} \mathbf{v}(\xi) &= \text{ax} \left(\mathbf{P}^T(\xi) \mathbf{P}'(\xi) \right) \\ &= \text{ax} \left(\mathbf{P}^T(0) \mathbf{Q}^T(\xi) \mathbf{Q}'(\xi) \mathbf{P}(0) \right) \\ &= \mathbf{P}^T(0) \mathbf{Q}^T(\xi) \mathbf{v}_Q(\xi) \\ &= \mathbf{P}^T(0) \mathbf{v}_Q(0). \end{aligned} \quad (6.77)$$

For the uniform states, we can quickly find that the strain measure $\boldsymbol{\eta}$ is also a constant throughout the rod:

$$\begin{aligned} \boldsymbol{\eta}(\xi) &= \mathbf{P}^T(\xi) \mathbf{r}'(\xi) - \mathbf{E}_3 \\ &= \mathbf{P}^T(0) \mathbf{r}'(0) - \mathbf{E}_3 \\ &= \boldsymbol{\eta}(0). \end{aligned} \quad (6.78)$$

The constancy of the strains \mathbf{v} and $\boldsymbol{\eta}$ throughout the rod is the motivation for Ericksen's choice of the term "uniform state." Because the rotation tensor for the tangent vector is identical to those for the directors, the deformed state of the rod will be twistless.

6.6.2 Forces and Moments

With the help of the constitutive relations (6.26) for \mathbf{n} and \mathbf{m} and the assumptions (6.65), it is straightforward to see that

$$\mathbf{n}(\xi) = \mathbf{Q}(\xi)\mathbf{n}(0), \quad \mathbf{m}(\xi) = \mathbf{Q}(\xi)\mathbf{m}(0). \quad (6.79)$$

We assume the rod is maintained in equilibrium solely by terminal loadings:

$$\mathbf{n}(0^+) = -\mathbf{F}_0, \quad \mathbf{n}(\ell^-) = \mathbf{F}_\ell, \quad \mathbf{m}(0^+) = -\mathbf{M}_0, \quad \mathbf{m}(\ell^-) = \mathbf{M}_\ell, \quad (6.80)$$

where we will drop the + ornamenting 0 and – ornamenting ℓ in the sequel. The equilibrium equations yield

$$\mathbf{n}' = \mathbf{0}, \quad (\mathbf{m} + \mathbf{r} \times \mathbf{n})' = \mathbf{0}. \quad (6.81)$$

It follows that \mathbf{F}_0 and \mathbf{F}_ℓ are equal and opposite and both are parallel to the axis of rotation of \mathbf{Q} :

$$\mathbf{F}_\ell = -\mathbf{F}_0 = F_\ell \mathbf{E}_3. \quad (6.82)$$

The second conservation implies that

$$\mathbf{m}(\xi) + \mathbf{r}(\xi) \times \mathbf{n}(\xi) = \mathbf{m}_O, \quad (6.83)$$

where \mathbf{m}_O is a constant. Substituting for $\mathbf{r}(\xi)$ and using the fact that $\mathbf{n} \parallel \mathbf{E}_3$, we find that

$$\mathbf{m}(\xi) + \mathbf{r}(\xi) \times \mathbf{n}(\xi) = \mathbf{Q}(\xi)(\mathbf{m}(0) + \mathbf{r}(0) \times \mathbf{n}(0)). \quad (6.84)$$

This implies that $\mathbf{Q}(\xi)\mathbf{m}_O = \mathbf{m}_O$. Consequently, either $\mathbf{m}_O = \mathbf{0}$ or $\mathbf{m}_O = m_O \mathbf{E}_3$ where m_O is a scalar. We can now conclude that the terminal moments on the rod are

$$\mathbf{M}_0 = -m_O \mathbf{E}_3 + \mathbf{r}(0) \times F_\ell \mathbf{E}_3, \quad \mathbf{M}_\ell = m_O \mathbf{E}_3 - \mathbf{r}(\ell) \times F_\ell \mathbf{E}_3. \quad (6.85)$$

The fact that \mathbf{F}_ℓ and the moment relative to O , \mathbf{m}_O , are parallel to \mathbf{E}_3 constitutes a type of loading known in the literature as a wrench (cf. Figure 6.6).

Thus Ericksen's ingenious perspective demonstrates the ubiquitous nature of helical forms and shows how they are supported by a wrench in the rod theory of interest here. An alternative derivation of this result can be found in Antman [12, Section 9.2]. It remains to solve for the deformed shape of the rod and we refer the interested reader to [12, Section 9.2] for a discussion of the solution procedure.

6.7 Closing Comments

The rod theory we have just discussed is capable of accommodating extensibility, transverse shear, torsion, and flexure. It is also the first theory we have considered since the elastic string where the contact forces and moments are completely

prescribed by constitutive relations. Consequently, the governing equations lead to partial differential equations for the components of \mathbf{r} and \mathbf{d}_α . For most problems, these governing equations are provided in a noncontroversial manner by the balance of linear momentum and balance of angular momentum. If we relax the assumption that the directors are unit vectors and allow their magnitudes to vary, then we can in principle capture the contraction and expansion of the cross sections of the rod. However, the source of the extra equations needed to describe the evolution of these magnitudes is not obvious. Before turning to an exploration of one solution to this problem, we note that many of the problems analyzed using Kirchhoff's rod theory remain to be explored using the more sophisticated theory discussed in the present chapter. Some progress towards this end has been made. For instance, Stump analyzed the hocking problem in [334]. However, many problems remain to be examined.

6.8 Exercises

Exercise 6.1: Consider a rod whose strain energy function is given by the expression

$$2\rho_0\psi = EI_1v_1^2 + EI_2v_2^2 + \mathcal{D}v_3^2 + \frac{kEA}{2(1+\nu)}(\eta_1^2 + \eta_2^2) + EA\eta_3^2, \quad (6.86)$$

where k is known as the shear correction factor.⁵ Numerically determine the static equilibria of a uniform, homogeneous rod of length ℓ which is subject to equal and opposite end forces $\mathbf{n}_0 = -\mathbf{n}(0,t) = \mathbf{n}(\ell,t)$, and end moments $\mathbf{m}(0,t)$ and $\mathbf{m}(\ell,t)$. You should assume that there are no body forces and no surface tractions on the rod-like body that the rod is modeling. For the material properties, use those for steel or aluminum.

Exercise 6.2: Consider an infinitely long, homogeneous rod undergoing a steady axial motion. Show that the equations governing the deformed shape of the rod are similar to those governing a static equilibrium.⁶

Exercise 6.3: Consider the static equilibrium of a homogeneous rod in the absence of assigned forces and moments. Under which conditions is the material contact force C constant throughout the rod?

⁵ The shear correction factor is a constant in beam theory that is used to match static and dynamic solutions of the three-dimensional theory to those for the rod theory. The factor depends on the geometry of the cross section and the type of comparisons used (cf. [74, 93, 143, 310] and references therein). For a square cross section of a linearly elastic isotropic rod-like body with $\nu = 0.3$, $k \approx 0.85$ (0.822) if a comparison based on a static (dynamic) solution is employed (cf. [93, Table 3]).

⁶ An analysis of the resulting equations can be found in Antman and Liu [13]. We also refer the reader to the paper by Coleman et al. [66] for a related analysis for a planar rod theory.

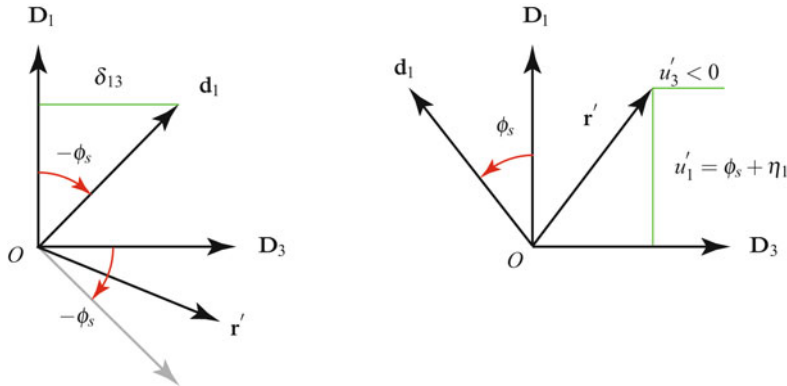


Fig. 6.7 The kinematic measures u_1 , u_3 , ϕ_s , and δ_{13} associated with a linearized theory known as Timoshenko beam theory [344]. It is important to notice that \mathbf{r}' and \mathbf{d}_1 are not constrained to be orthogonal in the rod theory of interest here.

Exercise 6.4: Consider the homogeneous rod which is straight in an undeformed natural configuration, $\mathbf{P}_0 = \mathbf{I}$, that is shown in Figure 6.1. The strain energy function of the rod has the representation

$$\rho_0 \psi = \frac{EI_1}{2} v_1^2 + \frac{EI_2}{2} v_2^2 + \frac{\mathcal{D}}{2} v_2^3 + \frac{kEA}{4(1+\nu)} (\eta_1^2 + \eta_2^2) + \frac{EA}{2} \eta_2^3, \quad (6.87)$$

where k is known as the shear correction factor. We consider small amplitude, planar, flexural deformations of this rod⁷:

$$\begin{aligned} \mathbf{R} &= z\mathbf{E}_3, \\ \mathbf{r} &= u_1\mathbf{E}_1 + u_3\mathbf{E}_3 + \mathbf{R} + \mathcal{O}(\varepsilon^2), \\ \mathbf{d}_1 &= \mathbf{E}_1 + \delta_{13}\mathbf{E}_3 + \mathcal{O}(\varepsilon^2), \\ \mathbf{d}_2 &= \mathbf{E}_2, \end{aligned} \quad (6.88)$$

where ε is a small number.

- (a) For the deformations of interest, the rotation tensor \mathbf{P} has the representation $\mathbf{P} = \mathbf{Q}_E(\phi_s, \mathbf{E}_2)$. Show that

$$\mathbf{P}\mathbf{v} = \frac{\partial \phi_s}{\partial z} \mathbf{E}_2. \quad (6.89)$$

With the help of the identity $\mathbf{d}_1 = \mathbf{P}\mathbf{D}_1$ and Figure 6.7, show that

$$\phi_s \approx -\delta_{13}. \quad (6.90)$$

⁷ The reader is also referred to the closely related Exercises 5.6 and 7.4.

- (b) Show that the nontrivial strains of the rod are, to $\mathcal{O}(\varepsilon^2)$,

$$\eta_1 = \frac{\partial u_1}{\partial z} + \delta_{13}, \quad \eta_3 = \frac{\partial u_3}{\partial z}, \quad v_2 = \frac{\partial \phi_s}{\partial z} = -\frac{\partial \delta_{13}}{\partial z}. \quad (6.91)$$

Explain why $\frac{\partial u_1}{\partial z} + \delta_{13}$ is known as the transverse shearing strain of the rod. Show that the contact force \mathbf{n} and contact moment \mathbf{m} have the representations

$$\mathbf{n} = \left(\frac{kEA}{2(1+\nu)} \right) \eta_1 \mathbf{E}_1 + EA \eta_3 \mathbf{E}_3, \quad \mathbf{m} = EI_2 v_2 \mathbf{E}_2. \quad (6.92)$$

- (c) Argue that the equations governing the motion of the rod reduce to the three differential equations

$$\begin{aligned} & \left. \begin{aligned} \frac{\partial}{\partial z} \left(EA \frac{\partial u_3}{\partial z} \right) + \rho_0 \mathbf{f} \cdot \mathbf{E}_3 &= \rho_0 \frac{\partial^2 u_3}{\partial t^2}, \\ \frac{\partial}{\partial z} \left(\frac{kEA}{2(1+\nu)} \left(\frac{\partial u_1}{\partial z} - \phi_s \right) \right) + \rho_0 \mathbf{f} \cdot \mathbf{E}_1 &= \rho_0 \frac{\partial^2 u_1}{\partial t^2}, \\ \frac{\partial}{\partial z} \left(EI_2 \frac{\partial \phi_s}{\partial z} \right) + \frac{kEA}{2(1+\nu)} \left(\frac{\partial u_1}{\partial z} - \phi_s \right) + \mathbf{m}_a \cdot \mathbf{E}_2 &= \rho_0 y^{11} \frac{\partial^2 \phi_s}{\partial t^2}. \end{aligned} \right\} \xrightarrow{\text{Extension/Contraction}} \\ & \left. \begin{aligned} \end{aligned} \right\} \xrightarrow{\text{Flexure}} \end{aligned} \quad (6.93)$$

Here, $y^{11} = I_2/A$, $\mathbf{n} \cdot \mathbf{E}_1$ is known as a shear force, and $\mathbf{m} \cdot \mathbf{E}_2$ is known as the bending moment.

- (d) Show that the flexural equations (6.93)_{2,3} correspond to those for a Timoshenko beam [344] that can be found in the literature (cf. [152, 204, 275, 310] and references therein). You should observe that the extensional equations are identical to those for the longitudinal vibration of a bar. We also note that an alternative derivation of the Timoshenko beam equations is discussed in the forthcoming Exercise 7.4.

Chapter 7

Green and Naghdi's Rod Theory

“As often happens in the history of science, the simple ideas are the hardest to achieve; simplicity does not come of itself but must be created.”

C. A. Truesdell [350, Page 251].

7.1 A Hierarchy of Rod Theories

The rod theory discussed in this chapter originated in a paper by Green and Laws in 1966 [128]. In this theory, the material curve is extensible, and the directors \mathbf{d}_α can change their length and relative orientation. That is, the directors can deform in an arbitrary manner. The rod theory was further developed in a series of papers by Green, Naghdi, and several of their coworkers. They also showed how it could be established by integrating the three-dimensional equations of continuum mechanics. In this chapter, this theory is presented in the most general form for an elastic rod with two directors and possible discontinuities. The presentation also enables us to examine prescriptions for fields associated with a variety of rod theories and the theory of a string.

As discussed in Section 7.11 below, we can consider the rod theory discussed in this chapter as one which subsumes the recently discussed Cosserat rod theory, Kirchhoff rod theory and Euler's elastica as constrained theories. Furthermore, as emphasized in the exercises at the end of this chapter, a linearized version of the rod theory yields, as special cases, the classical Timoshenko beam and Bernoulli-Euler beam theories.¹ We also note that the theory was extended by Green and Naghdi [134, 135] to encompass an arbitrary number of directors and has been applied to

¹ For more information on this matter, see [127, 131, 137, 186, 247, 309].

a variety of liquid jet and fluid flow problems [19, 129, 134, 247]. As can be appreciated from Naghdi's 1982 review article [245] and Rubin's recent book [309], closely related theories have been developed for shells and plates. We also refer the interested reader to these two works for other perspectives on the rod theory that is discussed in this chapter.

There are two philosophies on the use of rod theories. The first, known as a direct approach, considers the rod theory as a self-contained theory that provides a mechanical model for a rod. We have emphasized this approach throughout this book. A complementary perspective is to consider the rod to be an approximate theory for a three-dimensional continuum. As discussed in Section 7.12, such an approach also provides an approximate correspondence between the fields associated with the rod theory and their three-dimensional counterparts. While we have emphasized the direct approach throughout this book, these correspondences enable us to show how the body force and tractions acting on the lateral surface of a rod-like body manifest in assigned forces, assigned director forces, assigned material forces, and boundary conditions for a rod. Indeed, the correspondences are used throughout this book when solving specific problems.

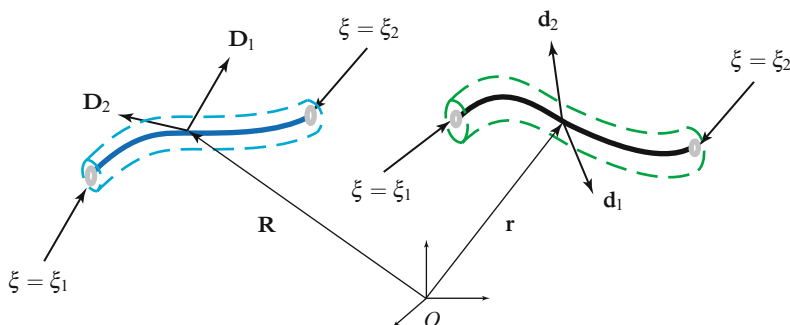


Fig. 7.1 The curve $\mathbf{r}(\xi, t)$ and the vector fields $\mathbf{d}_\alpha(\xi, t)$ at a point along its length. The reference configuration of the Cosserat (or directed) curve is also shown in this figure.

7.2 Kinematics of Green and Naghdi's Rod Theory

We follow many of the developments discussed in Chapter 5 for the kinematics of the Kirchhoff rod theory and recall that a directed curve is a material curve to which at each point a set of deformable directors is defined (see Figure 7.1). In the most primitive version of Green and Naghdi's rod theory, there are two directors and the material curve associated with the directed curve is assumed to be extensible: $\frac{\partial \mathbf{r}}{\partial \xi} = \mu \mathbf{e}_t$. In the present configuration of the directed curve, we denote the tangent vector by $\frac{\partial \mathbf{r}}{\partial \xi} = \mathbf{d}_3$, and, as usual, the directors are denoted by \mathbf{d}_1 and \mathbf{d}_2 .

As before, we define a reference configuration of the directed curve by the vector fields $\mathbf{R} = \mathbf{R}(\xi)$ and $\mathbf{D}_\alpha = \mathbf{D}_\alpha(\xi)$. For convenience, we shall assume that ξ is the arc-length parameter of the fixed reference configuration of the material curve. It is also convenient to define the displacement vectors:

$$\mathbf{u} = \mathbf{r} - \mathbf{R}, \quad \mathbf{d}_1 = \mathbf{d}_1 - \mathbf{D}_1, \quad \mathbf{d}_2 = \mathbf{d}_2 - \mathbf{D}_2. \quad (7.1)$$

These vectors are used in a linear theory for the rod which will be discussed shortly.

Although the cross sections of the rod-like body that the directed curve is modeling are assumed to remain plane, in the rod theory of interest the directors do not necessarily retain their orientation relative to the centerline. To render this assumption into a mathematically tractable form, we only assume that the referential vectors \mathbf{D}_1 , \mathbf{D}_2 , and \mathbf{D}_3 define a right-handed basis at each ξ :

$$[\mathbf{D}_1, \mathbf{D}_2, \mathbf{D}_3] > 0. \quad (7.2)$$

Denoting, as usual, a fixed right-handed basis for \mathbb{E}^3 by $\{\mathbf{E}_1, \mathbf{E}_2, \mathbf{E}_3\}$, we define a linear transformation \mathbf{F}_0 :

$$\mathbf{F}_0 = \mathbf{D}_1 \otimes \mathbf{E}_1 + \mathbf{D}_2 \otimes \mathbf{E}_2 + \mathbf{D}_3 \otimes \mathbf{E}_3. \quad (7.3)$$

That is, $\mathbf{D}_i = \mathbf{F}_0 \mathbf{E}_i$. For many reference configurations, we can choose \mathbf{D}_i such that $\mathbf{F}_0 = \mathbf{I}$.

Under a motion of the directed curve, the vectors \mathbf{d}_i can change their relative orientation and magnitude. Consequently,

$$\mathbf{d}_i = \mathbf{F}_1 \mathbf{D}_i, \quad (i = 1, 2, 3), \quad (7.4)$$

where $\mathbf{F}_1 = \mathbf{F}_1(\xi, t)$ is a linear transformation. You should notice that

$$\mathbf{d}_\alpha = \mathbf{F}_1 \mathbf{F}_0 \mathbf{E}_\alpha, \quad \frac{\partial \mathbf{r}}{\partial \xi} = \mathbf{F}_1 \frac{\partial \mathbf{R}}{\partial \xi}, \quad (\alpha = 1, 2). \quad (7.5)$$

If we restrict \mathbf{F}_1 and \mathbf{F}_0 to be proper-orthogonal (i.e., rotation) tensors, then we recover Antman's rod theory [10, 12] and a later theory of Green and Laws [130]. If, in addition, we restrict $\mathbf{d}_3 = \mathbf{F}_1 \mathbf{F}_0 \mathbf{E}_3$ (that is, $\mathbf{d}_3 = \frac{\partial \mathbf{r}}{\partial \xi} = \mathbf{e}_t$ and $\mathbf{d}_\alpha \cdot \mathbf{d}_3 = 0$), then we recover Kirchhoff's rod theory.

Because $[\mathbf{D}_1, \mathbf{D}_2, \mathbf{D}_3] > 0$ and it is assumed that $[\mathbf{d}_1, \mathbf{d}_2, \mathbf{d}_3] > 0$, we can define reciprocal (dual) vectors \mathbf{D}^k and \mathbf{d}^k :

$$\mathbf{D}^1 = \frac{\mathbf{D}_2 \times \mathbf{D}_3}{[\mathbf{D}_1, \mathbf{D}_2, \mathbf{D}_3]}, \quad \mathbf{D}^2 = \frac{\mathbf{D}_3 \times \mathbf{D}_1}{[\mathbf{D}_1, \mathbf{D}_2, \mathbf{D}_3]}, \quad \mathbf{D}^3 = \frac{\mathbf{D}_1 \times \mathbf{D}_2}{[\mathbf{D}_1, \mathbf{D}_2, \mathbf{D}_3]}, \quad (7.6)$$

and

$$\mathbf{d}^1 = \frac{\mathbf{d}_2 \times \mathbf{d}_3}{[\mathbf{d}_1, \mathbf{d}_2, \mathbf{d}_3]}, \quad \mathbf{d}^2 = \frac{\mathbf{d}_3 \times \mathbf{d}_1}{[\mathbf{d}_1, \mathbf{d}_2, \mathbf{d}_3]}, \quad \mathbf{d}^3 = \frac{\mathbf{d}_1 \times \mathbf{d}_2}{[\mathbf{d}_1, \mathbf{d}_2, \mathbf{d}_3]}. \quad (7.7)$$

It is straightforward to verify that

$$\mathbf{D}^k \cdot \mathbf{D}_i = \delta_i^k, \quad \mathbf{d}^k \cdot \mathbf{d}_i = \delta_i^k. \quad (7.8)$$

Using these sets of vectors, it is easy to establish the representation

$$\mathbf{F}_1 = \mathbf{d}_1 \otimes \mathbf{D}^1 + \mathbf{d}_2 \otimes \mathbf{D}^2 + \mathbf{d}_3 \otimes \mathbf{D}^3. \quad (7.9)$$

This tensor is similar to the deformation gradient in continuum mechanics. It was introduced, in the context of the present rod theory, by Naghdi [245] in the early 1980s.

As with the rod theories discussed in the previous two chapters, a pair of motions $(\mathbf{r}(\xi, t), \mathbf{d}_\alpha(\xi, t))$ and $(\mathbf{r}^\perp(\xi, t^\perp), \mathbf{d}_\alpha^\perp(\xi, t^\perp))$ of a directed curve differ by a rigid body motion if

$$\begin{aligned} \mathbf{r}^\perp(\xi, t^\perp) &= \mathbf{Q}(t) \mathbf{r}(\xi, t) + \mathbf{q}(t), \\ \mathbf{d}_1^\perp(\xi, t^\perp) &= \mathbf{Q}(t) \mathbf{d}_1(\xi, t), \\ \mathbf{d}_2^\perp(\xi, t^\perp) &= \mathbf{Q}(t) \mathbf{d}_2(\xi, t). \end{aligned} \quad (7.10)$$

Here, \mathbf{Q} is a proper-orthogonal tensor-valued function of time, $\mathbf{q}(t)$ is a vector-valued function of time, and $t^\perp = t + a$ with a being constant (cf. Figure 6.2).

7.2.1 Three-Dimensional Considerations

For the rod-like body that the rod is modeling, we parallel the developments of Section 5.2.1 for the Kirchhoff rod theory. That is, we prescribe a convected coordinate system θ^i such that

$$\xi = \theta^3, \quad \mathbf{R}^* = \mathbf{R}^*(\theta^i) = \mathbf{R}(\xi) + \sum_{\alpha=1}^2 \theta^\alpha \mathbf{D}_\alpha(\xi), \quad (7.11)$$

where \mathbf{R}^* is the position vector in the reference configuration of the material point identified using θ^i (see Figure 5.2). The position vector of the same material point in the present configuration is then approximated by

$$\mathbf{r}^* = \mathbf{r}^*(\theta^i, t) \approx \mathbf{r}(\xi, t) + \sum_{\alpha=1}^2 \theta^\alpha \mathbf{d}_\alpha(\xi, t). \quad (7.12)$$

We will use (7.11) and (7.12) in the sequel to motivate several identifications.

7.3 Strains

In contrast to Euler's elastica, which had two strain measures, and Kirchhoff's rod theory, which has three strain measures, Green and Naghdi's rod theory has twelve strains. Six of these strain measures, which are denoted by γ_{ik} , capture the changes

to the three components of the pair of directors. The other six strain measures, which are denoted by $\kappa_{\alpha j}$, capture the components of the rate of change of the directors. Thus,

$$\begin{aligned}\gamma_{ik} &= \mathbf{d}_i \cdot \mathbf{d}_k - \mathbf{D}_i \cdot \mathbf{D}_k, \\ \kappa_{\alpha k} &= \frac{\partial \mathbf{d}_\alpha}{\partial \xi} \cdot \mathbf{d}_k - \frac{\partial \mathbf{D}_\alpha}{\partial \xi} \cdot \mathbf{D}_k.\end{aligned}\quad (7.13)$$

It is an interesting exercise to verify the following calculations that were first recorded in [245]:

$$\mathbf{F}_1^T \mathbf{F}_1 - \mathbf{F}_0^T \mathbf{F}_0 = \sum_{i=1}^3 \sum_{k=1}^3 \gamma_{ik} \mathbf{D}^i \otimes \mathbf{D}^k, \quad \mathbf{F}_1^T \mathbf{G}_\alpha - {}_0 \mathbf{G}_\alpha = \sum_{k=1}^3 \kappa_{\alpha k} \mathbf{D}^k \otimes \mathbf{D}^3. \quad (7.14)$$

Here,

$$\mathbf{G}_\alpha = \frac{\partial \mathbf{d}_\alpha}{\partial \xi} \otimes \mathbf{D}^3, \quad {}_0 \mathbf{G}_\alpha = \frac{\partial \mathbf{D}_\alpha}{\partial \xi} \otimes \mathbf{D}^3. \quad (7.15)$$

We could also define three additional strains:

$$\kappa_{3k} = \frac{\partial^2 \mathbf{r}}{\partial \xi^2} \cdot \mathbf{d}_k - \frac{\partial^2 \mathbf{R}}{\partial \xi^2} \cdot \mathbf{D}_k = \frac{\partial \mathbf{d}_3}{\partial \xi} \cdot \mathbf{d}_k - \frac{\partial \mathbf{D}_3}{\partial \xi} \cdot \mathbf{D}_k. \quad (7.16)$$

However, it can be shown that this is unnecessary.²

7.3.1 Infinitesimal Strains

In the linear theory for a rod whose reference configuration is straight and prismatic, we identify

$$x_3 = \xi, \quad \mathbf{D}_\alpha = \mathbf{E}_\alpha, \quad \mathbf{R} = x_3 \mathbf{E}_3, \quad \mathbf{D}_3 = \mathbf{E}_3. \quad (7.17)$$

Implicit in the linear theory are the assumptions that the displacements

$$\mathbf{u} = \mathbf{r} - \mathbf{R}, \quad \boldsymbol{\delta}_\alpha = \mathbf{d}_\alpha - \mathbf{D}_\alpha, \quad (7.18)$$

and their derivatives $\frac{\partial \mathbf{u}}{\partial \xi} = \boldsymbol{\delta}_3$ and $\frac{\partial \boldsymbol{\delta}_\alpha}{\partial \xi}$ are small.

Following [137, 138, 247] and using Eqns. (7.11) and (7.12), the definitions of the displacement vectors (7.1), the prescription $\mathbf{R}^* = \mathbf{R} + \sum_{\beta=1}^2 x_\beta \mathbf{E}_\beta$, and the approximation $\mathbf{r}^* \approx \mathbf{r} + \sum_{\beta=1}^2 x_\beta \mathbf{d}_\beta$ allows us to make the following correspondences:

² See Exercise 7.1.

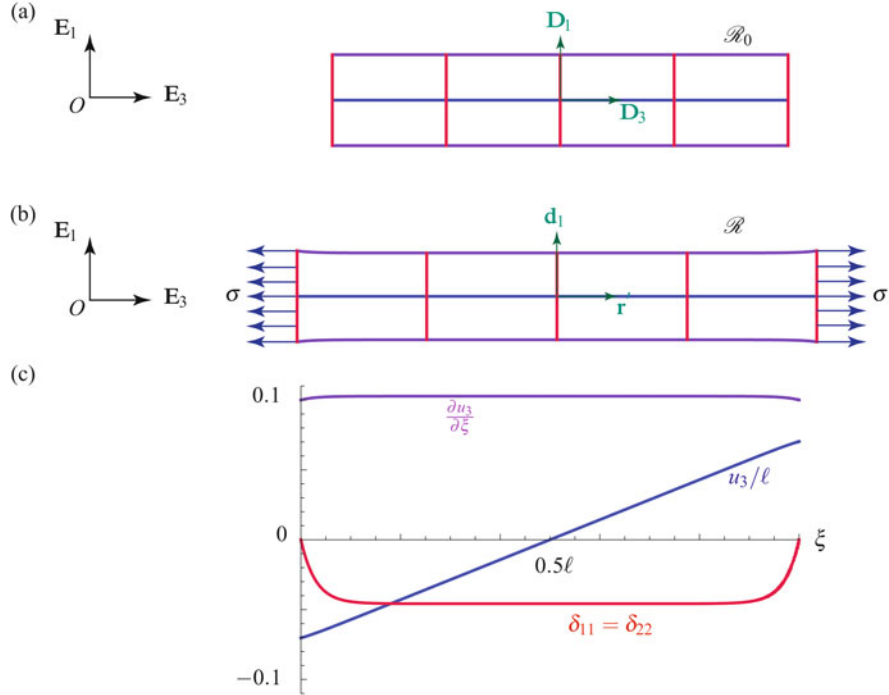


Fig. 7.2 Axial extension and lateral contraction of a rod. (a) Schematic of the reference configuration \mathcal{R}_0 for a straight rod with a square cross section. (b) The present configuration \mathcal{R} of the rod which is subject to tractions on its ends. (c) The displacements u_3 and $\delta_{11} = \delta_{22}$ and strain $\frac{\partial u_3}{\partial \xi}$. For illustrative purposes, the traction field σ is such that $\frac{n_3}{4k_3} = 0.1$, $\nu = 0.32$, and the width-to-length ratio of the rod is 0.1.

lateral extensions : $\delta_{11} = \mathbf{d}_1 \cdot \mathbf{E}_1, \quad \delta_{22} = \mathbf{d}_2 \cdot \mathbf{E}_2,$

axial extension : $u_3 = \mathbf{u} \cdot \mathbf{E}_3,$

flexural deformations in the $x_1 - x_3$ plane : $\delta_{13} = \mathbf{d}_1 \cdot \mathbf{E}_3, \quad u_1 = \mathbf{u} \cdot \mathbf{E}_1,$

flexural deformations in the $x_2 - x_3$ plane : $\delta_{23} = \mathbf{d}_2 \cdot \mathbf{E}_3, \quad u_2 = \mathbf{u} \cdot \mathbf{E}_2,$

torsional deformations : $\delta_{12} = \mathbf{d}_1 \cdot \mathbf{E}_2, \quad \delta_{21} = \mathbf{d}_2 \cdot \mathbf{E}_1.$

Depending on the geometry of the rod and its constitution, one can find that the equations governing flexure, torsion, and extension decouple. In such instances, the linearized equations can be solved separately for these deformation modes. An example of such an instance arises in the application of the linearized theory to the expansion and lateral contraction of an isotropic, linearly elastic rod with a square cross section. The deformation of this rod when it is subject to terminal loadings is shown in Figure 7.2 and is based on the exact solution for the linearized theory

that was developed by Green et al. [138, Section 9].³ It is interesting to observe the contraction of the rod that is synonymous with the Poisson effect. The linearized theory for flexure reduces in many cases to Timoshenko's celebrated beam theory and some results for the flexure of a beam under its own weight are presented in Figure 7.3.

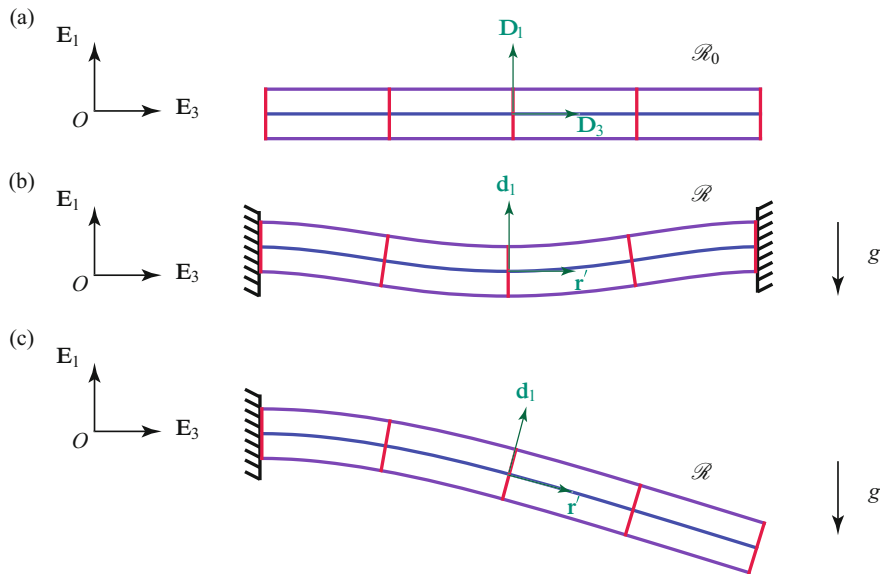


Fig. 7.3 Bending of a beam under a gravitational loading. (a) Schematic of the reference configuration \mathcal{R}_0 for a straight rod. (b) The present configuration \mathcal{R} of a clamped rod loaded under its self weight. (c) The present configuration \mathcal{R} of a cantilevered rod loaded under its self weight. For illustrative purposes, the displacements u_1 and δ_{13} have been magnified by factors of 10000 and 1000 in (b) and (c).

The expressions for the strains associated with the directed curve also simplify when interest is restricted to a theory with infinitesimal strains:

$$\begin{aligned}
 \gamma_j &= \mathbf{d}_i \cdot \mathbf{d}_j - \mathbf{D}_i \cdot \mathbf{D}_j \\
 &= \boldsymbol{\delta}_i \cdot \boldsymbol{\delta}_j + \boldsymbol{\delta}_i \cdot \mathbf{D}_j + \boldsymbol{\delta}_j \cdot \mathbf{D}_i \\
 &= \boldsymbol{\delta}_i \cdot \mathbf{E}_j + \boldsymbol{\delta}_j \cdot \mathbf{E}_i + \boldsymbol{\delta}_i \cdot \boldsymbol{\delta}_j \\
 &\approx \delta_{ij} + \delta_{ji},
 \end{aligned} \tag{7.19}$$

and

³ This problem is discussed in further detail in Exercise 7.3.

$$\begin{aligned}
\kappa_{\alpha i} &= \mathbf{d}'_\alpha \cdot \mathbf{d}_i - \mathbf{D}'_\alpha \cdot \mathbf{D}_i \\
&= (\mathbf{\delta}'_\alpha + \mathbf{D}'_\alpha) \cdot (\mathbf{\delta}_i + \mathbf{D}_i) \\
&= (\mathbf{\delta}'_\alpha + \mathbf{0}) \cdot (\mathbf{\delta}_i + \mathbf{E}_i) \\
&\approx \mathbf{\delta}'_\alpha \cdot \mathbf{E}_i = \delta'_{\alpha i}.
\end{aligned} \tag{7.20}$$

Here, the prime denotes partial differentiation with respect to ξ and $\delta_{ij} = \mathbf{\delta}_i \cdot \mathbf{E}_j$. Thus we find the following identifications for the strains⁴:

$$\begin{aligned}
\text{lateral and axial extensions : } &\gamma_{11}, \quad \gamma_{22}, \quad \gamma_{33}, \quad \kappa_{11}, \quad \kappa_{22}, \\
\text{flexural deformations in the } x_1 - x_3 \text{ plane : } &\gamma_{13}, \quad \kappa_{13}, \\
\text{flexural deformations in the } x_2 - x_3 \text{ plane : } &\gamma_{23}, \quad \kappa_{23}, \\
\text{torsional deformations : } &\gamma_{12}, \quad \kappa_{12}, \quad \kappa_{21}.
\end{aligned}$$

The linearized equations governing these strains for a variety of classical problems are discussed in the exercises at the end of this chapter. The reader is also referred to [127, 186, 258] for discussions on linearized theories that arise from considering small deformations superposed on large deformations of an elastic rod.

7.4 Momenta and Kinetic Energy

Because the directors in Green and Naghdi's rod theory do not necessarily behave as part of an orthonormal triad, the kinematics in this rod theory are fairly straightforward to describe.

As with the Kirchhoff rod theory, we define six inertias $y^{0\alpha}$ and $y^{\alpha\beta}$ and a pair of mass densities: ρ per unit length of the directed curve in the present configuration and ρ_0 per unit length of ξ in the reference configuration. The linear momentum \mathbf{G} per unit length of ξ of the rod is

$$\mathbf{G} = \rho \mu \left(\dot{\mathbf{r}} + \sum_{\alpha=1}^2 y^{0\alpha} \dot{\mathbf{d}}_\alpha \right). \tag{7.21}$$

Supplementing this momentum, we define the pair of director momenta per unit length of ξ :

$$\mathbf{L}^1 = \rho \mu \left(y^{01} \dot{\mathbf{r}} + \sum_{\alpha=1}^2 y^{1\alpha} \dot{\mathbf{d}}_\alpha \right), \quad \mathbf{L}^2 = \rho \mu \left(y^{02} \dot{\mathbf{r}} + \sum_{\alpha=1}^2 y^{2\alpha} \dot{\mathbf{d}}_\alpha \right). \tag{7.22}$$

⁴ When the transverse shears γ_{13} and γ_{23} are constrained to be identically zero, the equations governing flexure often reduce to those for the classic Bernoulli-Euler beam.

As before, to examine the physical interpretations of these three momenta, we can, without loss in generality, set $y^{0\alpha} = 0$. Then \mathbf{G} can be identified as the linear momentum of the material curve, and \mathbf{L}^α can be identified as the momenta of the cross sections of the rod.

The material momentum of a segment (ξ_1, ξ_2) of the directed curve is defined as the integral of the material momentum P , $\int_{\xi_1}^{\xi_2} P d\xi$, where

$$P = - \left(\mathbf{r}' \cdot \mathbf{G} + \mathbf{d}_1' \cdot \mathbf{L}^1 + \mathbf{d}_2' \cdot \mathbf{L}^2 \right). \quad (7.23)$$

This momentum is sometimes referred to as the pseudomomentum and first appeared in the literature in [264]. You should notice how the expression for P is similar to the one we defined earlier for the Kirchhoff rod theory (see Eqn. (5.53)), and that it simplifies to that presented earlier for a string (see Eqn. (1.44)). The angular momentum relative to O of a segment (ξ_1, ξ_2) of the directed curve is

$$\mathbf{H}_O = \int_{\xi_1}^{\xi_2} \mathbf{h}_O d\xi, \quad (7.24)$$

where

$$\mathbf{h}_O = \mathbf{r} \times \mathbf{G} + \mathbf{d}_1 \times \mathbf{L}^1 + \mathbf{d}_2 \times \mathbf{L}^2. \quad (7.25)$$

The kinetic energy of a segment (ξ_1, ξ_2) of the directed curve is defined as $\int_{\xi_1}^{\xi_2} T d\xi$ where the kinetic energy density T is

$$T = \frac{1}{2} \left(\dot{\mathbf{r}} \cdot \mathbf{G} + \dot{\mathbf{d}}_1 \cdot \mathbf{L}^1 + \dot{\mathbf{d}}_2 \cdot \mathbf{L}^2 \right). \quad (7.26)$$

Note that we are not imposing inextensibility here, so we have left μ arbitrary in all of our definitions for the momenta and kinetic energy. Furthermore, because the directors do not behave as part of an orthonormal triad, further simplification of the expressions for the momenta and kinetic energy is not possible.

7.5 The Strain Energy Function

The directed curve in this case resists bending, extension, lateral contractions and expansions, and torsion. Motivated by the terms on the right-hand side of the forthcoming energy balance (7.57), one assumes that

$$\rho_0 \psi = \rho_0 \bar{\psi} \left(\mathbf{d}_\alpha, \mathbf{r}', \mathbf{d}_\beta', \xi \right). \quad (7.27)$$

However, the strain energy function should be invariant under superposed rigid body motions. Hence, the identity

$$\bar{\psi} \left(\mathbf{d}_\alpha, \mathbf{r}', \mathbf{d}_\beta', \xi \right) = \bar{\psi} \left(\mathbf{Q} \mathbf{d}_\alpha, \mathbf{Q} \mathbf{r}', \mathbf{Q} \mathbf{d}_\beta', \xi \right) \quad (7.28)$$

should hold for all proper-orthogonal tensors \mathbf{Q} . As discussed in Green, Naghdi, and Wenner [138, Section 7], Cauchy's representation theorem for hemitropic functions⁵ can be used to show that the strain energy function ψ depends on the twelve inner products of $\mathbf{d}_i \cdot \mathbf{d}_k$ and $\mathbf{d}'_\alpha \cdot \mathbf{d}_k$ where $\mathbf{r}' = \mathbf{d}_3$. Normalizing the strains so they vanish in a present configuration where these products are identical to the referential values we find that the strain energy function per unit mass can be expressed as a function of the twelve strains γ_{ik} and $\kappa_{\beta j}$ and (if the rod is not homogeneous) possibly ξ :

$$\psi = \psi(\gamma_{ik}, \kappa_{\alpha j}, \xi). \quad (7.29)$$

It is helpful to note that the material time derivative of this function has the representations

$$\begin{aligned} \dot{\psi} &= \sum_{i=1}^3 \sum_{k=1}^3 \frac{\partial \psi}{\partial \gamma_{ik}} \dot{\gamma}_{ik} + \sum_{\alpha=1}^2 \sum_{k=1}^3 \frac{\partial \psi}{\partial \kappa_{\alpha k}} \dot{\kappa}_{\alpha k} \\ &= \sum_{i=1}^3 \frac{\partial \psi}{\partial \mathbf{d}_i} \cdot \dot{\mathbf{d}}_i + \sum_{\alpha=1}^2 \frac{\partial \psi}{\partial \frac{\partial \mathbf{d}_\alpha}{\partial \xi}} \cdot \frac{\partial \dot{\mathbf{d}}_\alpha}{\partial \xi}. \end{aligned} \quad (7.30)$$

Because $\psi = \psi(\gamma_{ik}, \kappa_{\beta j}, \xi)$, the previous representations follow in a straightforward manner from the chain rule:

$$\begin{aligned} \frac{\partial \psi}{\partial \frac{\partial \mathbf{d}_\alpha}{\partial \xi}} &= \sum_{i=1}^3 \frac{\partial \psi}{\partial \kappa_{\alpha i}} \mathbf{d}_i, \\ \frac{\partial \psi}{\partial \mathbf{d}_k} &= \sum_{\alpha=1}^2 \frac{\partial \psi}{\partial \kappa_{\alpha k}} \frac{\partial \mathbf{d}_\alpha}{\partial \xi} + 2 \sum_{i=1}^3 \frac{\partial \psi}{\partial \gamma_{ki}} \mathbf{d}_i. \end{aligned} \quad (7.31)$$

For future purposes, note that Eqn. (7.31) implies that

$$\mathbf{d}_1 \times \frac{\partial \psi}{\partial \mathbf{d}_1} + \mathbf{d}_2 \times \frac{\partial \psi}{\partial \mathbf{d}_2} + \mathbf{d}_3 \times \frac{\partial \psi}{\partial \mathbf{d}_3} + \mathbf{d}'_1 \times \frac{\partial \psi}{\partial \frac{\partial \mathbf{d}_1}{\partial \xi}} + \mathbf{d}'_2 \times \frac{\partial \psi}{\partial \frac{\partial \mathbf{d}_2}{\partial \xi}} = \mathbf{0}. \quad (7.32)$$

This identity will be used in Section 7.8. In anticipation of the forthcoming discussion, observe that if we restrict attention to the theory of an elastic string, then Eqn. (7.32) reduces to $\mathbf{d}_3 \times \frac{\partial \psi}{\partial \mathbf{d}_3} = \mathbf{0}$. This identity implies that $\mathbf{n} = \rho_0 \frac{\partial \psi}{\partial \mathbf{d}_3}$ is parallel to the tangent vector $\mathbf{r}' = \mathbf{d}_3$.

⁵ Cauchy's representation theorem for a function $f = f(\mathbf{a}, \mathbf{b}, \mathbf{c})$ states that if $f(\mathbf{a}, \mathbf{b}, \mathbf{c}) = f(\mathbf{Q}\mathbf{a}, \mathbf{Q}\mathbf{b}, \mathbf{Q}\mathbf{c})$ for all possible rotations \mathbf{Q} , then f can be expressed as a function of the inner products $\mathbf{a} \cdot \mathbf{a}$, $\mathbf{b} \cdot \mathbf{b}$, $\mathbf{c} \cdot \mathbf{c}$, $\mathbf{a} \cdot \mathbf{b}$, $\mathbf{b} \cdot \mathbf{c}$, and $\mathbf{a} \cdot \mathbf{c}$, and the triple product $[\mathbf{a}, \mathbf{b}, \mathbf{c}]$. Discussions of Cauchy's theorem can be found in Antman [12, Section 7.8] and Truesdell and Noll [351, Section 11].

7.5.1 Infinitesimal Theory

It is common to consider Taylor series expansions of ψ about a reference configuration where $\gamma_{ik} = 0$ and $\kappa_{\alpha k} = 0$. Assuming that the reference configuration has no residual forces, a strain energy function applicable to this case was given to quadratic approximation by Green, Laws, and Naghdi in 1967 [131]:

$$\begin{aligned} 2\rho_0 \psi = & k_1 \gamma_{11}^2 + k_2 \gamma_{22}^2 + k_3 \gamma_{33}^2 + k_7 \gamma_{11} \gamma_{22} + k_8 \gamma_{11} \gamma_{33} + k_9 \gamma_{22} \gamma_{33} \\ & + \frac{k_4}{4} (\gamma_{12} + \gamma_{21})^2 + k_5 \gamma_{23}^2 + k_6 \gamma_{13}^2 + k_{10} \kappa_{11}^2 + k_{11} \kappa_{22}^2 \\ & + k_{12} \kappa_{12}^2 + k_{13} \kappa_{21}^2 + k_{14} \kappa_{12} \kappa_{21} + k_{15} \kappa_{23}^2 \\ & + k_{16} \kappa_{13}^2 + k_{17} \kappa_{11} \kappa_{22}. \end{aligned} \quad (7.33)$$

This strain energy function has 17 unknown coefficients k_1, \dots, k_{17} which need to be prescribed in order to apply the rod theory.

The identification of the 17 coefficients is a nontrivial task and requires comparison of exact solutions from the three-dimensional theory of elasticity with exact solutions of the rod theory. For the general nonlinear theory, this feat has not been accomplished. What has been achieved was done in a remarkable series of works [131, 133, 137, 138].⁶ A rod composed of an isotropic, linearly elastic material was considered and the reference centerline of this rod was assumed to be straight:

$$\theta^1 = x_1, \quad \theta^2 = x_2, \quad \theta^3 = x_3, \quad \mathbf{D}_i = \mathbf{E}_i. \quad (7.34)$$

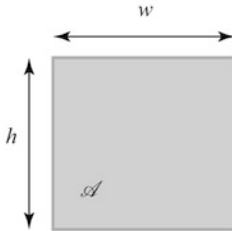
The strains were assumed to be infinitesimal (cf. Eqns. (7.19) and (7.20)) and exact solutions for the deformed rod, such as the pair shown in Figure 7.3, were developed. Then, the constants k_1, \dots, k_{17} for various rods were determined by comparing exact solutions of the rod theory to corresponding solutions from three-dimensional linear elasticity. The resulting values of the constants are functions of Poisson's ratio ν , Young's modulus E , and the geometric properties of the undeformed three-dimensional rod-like body that the rod theory is modeling.

Consider a homogeneous rod composed of an isotropic, linearly elastic material, which has a rectangular cross section of height h (in the \mathbf{E}_2 direction) and a width w (in the \mathbf{E}_1 direction). We choose the centerline to pass through the geometric center of the cross section (cf. Figure 7.4(a)).⁷ For such a rod, Green and Naghdi [133] showed that

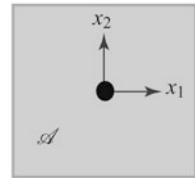
⁶ This series of works was summarized and critiqued in the paper [260].

⁷ Some of the consequences of selecting a different centerline can be seen in Figure 5.8 on Page 201.

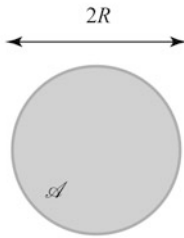
(a)



$$\begin{aligned} y^{01} &= 0, & y^{02} &= 0, \\ \rho_0 &= \rho_0^* wh, & y^{21} &= y^{12} = 0, \\ y^{11} &= \frac{w^2}{12}, & y^{22} &= \frac{h^2}{12}, \\ \rho_0 y^{11} &= \rho_0^* I_2, & \rho_0 y^{22} &= \rho_0^* I_1. \end{aligned}$$



(b)



$$\begin{aligned} y^{01} &= 0, & y^{02} &= 0, \\ \rho_0 &= \rho_0^* \pi R^2, & y^{21} &= y^{12} = 0, \\ y^{11} &= \frac{R^2}{2}, & y^{22} &= \frac{R^2}{2}, \\ \rho_0 y^{11} &= \rho_0 y^{22} = \rho_0^* I, & I &= \frac{\pi R^4}{4}. \end{aligned}$$

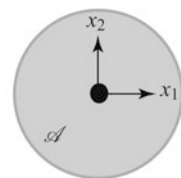


Fig. 7.4 The coefficients $y^{0\alpha}$ and $y^{\alpha\beta}$ computed using Eqn. (5.36) for a homogeneous rod. In (a), the rod has a rectangular cross section in the reference configuration \mathcal{R}_0 and, in (b), the rod has a circular cross section in the reference configuration \mathcal{R}_0 . The centerline is chosen to pass through the center of the cross section in both instances.

$$\begin{aligned} k_1 &= k_2 = k_3 = \frac{EA(1-\nu)}{4(1+\nu)(1-2\nu)}, \\ k_4 &= \frac{EA}{2(1+\nu)}, & k_5 &= k_6 = k \left(\frac{EA}{2(1+\nu)} \right), \\ k_7 &= k_8 = k_9 = \frac{2\nu}{1-\nu} k_1, \\ k_{10} &= \frac{EI_2}{2(1+\nu)}, & k_{11} &= \frac{EI_1}{2(1+\nu)}, & k_{12} &= k_{13}, \\ 2k_{12} + k_{14} &= \frac{E(I_1 + I_2)}{2(1+\nu)}, & 2k_{12} - k_{14} &= \mathcal{D}, \\ k_{15} &= EI_1, & k_{16} &= EI_2, & k_{17} &= 0. \end{aligned} \tag{7.35}$$

Here, k is the shear correction factor and \mathcal{D} is the torsional rigidity. The area A and areal moments of inertia are

$$A = wh, \quad I_1 = \int_{\mathcal{A}} x_2^2 dx_1 dx_2 = \frac{h^3 w}{12}, \quad I_2 = \int_{\mathcal{A}} x_1^2 dx_1 dx_2 = \frac{w^3 h}{12}. \tag{7.36}$$

The corresponding area and areal moments for a rod with a circular cross section are recorded in Figure 7.4(b). As regards the shear correction factor, Green and Naghdi

[133] found that $k = \frac{5}{6}$ while Rubin [309] argues that it should be 1. In addition, alternative prescriptions can be found elsewhere in the literature (cf., e.g., [93]). We note for future purposes that, for a circular rod of radius R , $\mathcal{D} = \frac{1}{2} \left(\frac{E}{2(1+\nu)} \right) \pi R^4$ (see Green, Naghdi, and Wenner [137, 138]). The prescriptions (7.35) are used extensively in the exercises at the end of this chapter.

Additional prescriptions for the strain energy functions of a rod modeling an orthotropic elastic body can be found in [133] and a rod modeling a tapered cylindrical body composed of an isotropic linearly elastic material can be found in [138].

7.6 Conservation Laws for the Rod Theory

Preparatory to writing the conservation laws for the material curve, we record some additional notation. Pertaining to forces, we have

$$\begin{aligned}
\text{contact force : } & \mathbf{n} = \mathbf{n}(\xi, t), \\
\text{contact director forces : } & \mathbf{m}^1 = \mathbf{m}^1(\xi, t), \quad \mathbf{m}^2 = \mathbf{m}^2(\xi, t), \\
\text{contact material force : } & C = C(\xi, t), \\
\text{intrinsic director forces : } & \mathbf{k}^1 = \mathbf{k}^1(\xi, t), \quad \mathbf{k}^2 = \mathbf{k}^2(\xi, t), \\
\text{assigned force per unit mass : } & \mathbf{f} = \mathbf{f}(\xi, t), \\
\text{assigned director forces per unit mass : } & \mathbf{l}^1 = \mathbf{l}^1(\xi, t), \quad \mathbf{l}^2 = \mathbf{l}^2(\xi, t), \\
\text{assigned material force per unit length of } \xi : & b = b(\xi, t).
\end{aligned}$$

From [264], the contact material force for this rod theory can be defined as

$$C = \rho \mu \psi - \mathbf{n} \cdot \mathbf{r}' - \mathbf{m}^1 \cdot \mathbf{d}_1' - \mathbf{m}^2 \cdot \mathbf{d}_2' - T. \quad (7.37)$$

If we ignore the directors, then this prescription reduces to the one we presented earlier for a string (see Eqn. (1.69)). The prescription (5.68) for the Kirchhoff rod theory can be obtained from Eqn. (7.37) by noting that $\mathbf{d}_\alpha' = (\mathbf{P}(\mathbf{v} + \mathbf{v}_0)) \times \mathbf{d}_\alpha$ and the moment $\mathbf{m} = \mathbf{d}_1 \times \mathbf{m}^1 + \mathbf{d}_2 \times \mathbf{m}^2$ in Kirchhoff's theory.

7.6.1 Assigned Forces and Director Forces

It is often convenient to be able to prescribe the assigned forces in terms of the three-dimensional body force $\rho_0^* \mathbf{b}$ acting on the rod and surface tractions \mathbf{t} acting on the lateral surface of the rod (see Figure 7.5). These prescriptions are from [138, 309], parallel the prescriptions (5.36), and shall be motivated in further detail in Section 7.12:

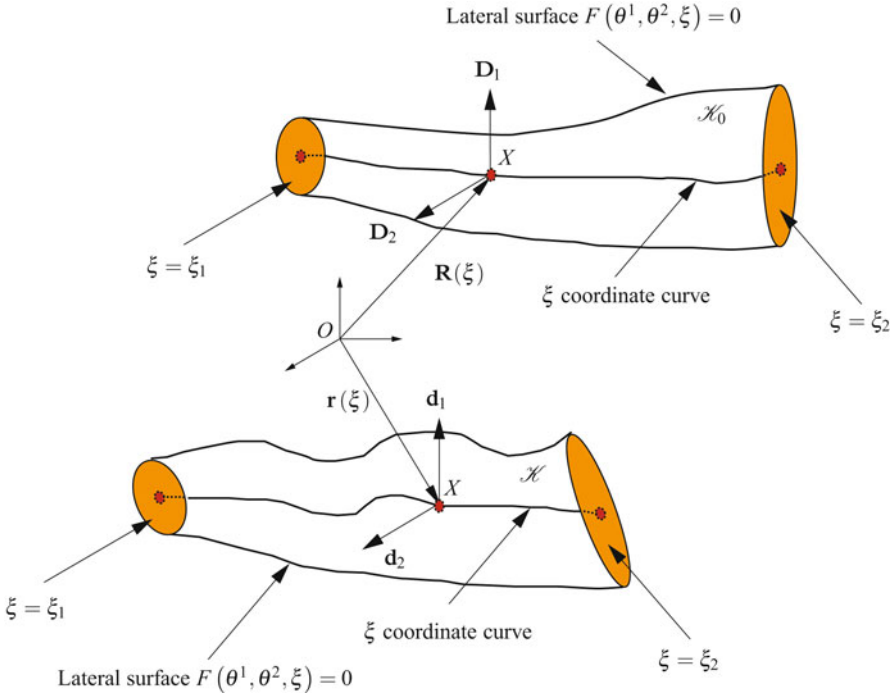


Fig. 7.5 Schematic of the reference \mathcal{K}_0 and present \mathcal{K} configurations of a rod-like body whose reference configuration is parameterized using a curvilinear coordinate system. The ends of the body are described by $\theta^3 = \xi$ coordinate surfaces, the centerline is described by a ξ coordinate curve where $\theta^1 = \theta^2 = 0$, and the lateral surface of the body is described using the function $F(\theta^1, \theta^2, \xi) = 0$.

$$\begin{aligned}\rho_0 \mathbf{f} &= \int_{\mathcal{A}} \mathbf{b} \rho_0^* da + \oint_{\partial \mathcal{A}} \mathbf{t} du, \\ \rho_0 \mathbf{l}^\alpha &= \int_{\mathcal{A}} \mathbf{b} \theta^\alpha \rho_0^* da + \oint_{\partial \mathcal{A}} \mathbf{t} \theta^\alpha du.\end{aligned}\quad (7.38)$$

Here, $\partial \mathcal{A}$ is the boundary of the cross section and u is the arc-length parameter on this boundary. The force $\rho_0 \mathbf{f}$ is the resultant of the body force and surface traction at a value of ξ (i.e., at a particular cross section). For completeness, we note the following prescription for the assigned moment \mathbf{m}_a which appears in the balance laws for the earlier rod theories (cf., e.g., Eqn. (5.80)₅):

$$\begin{aligned}\mathbf{m}_a &= \sum_{\alpha=1}^2 \mathbf{d}_\alpha \times \rho_0 \mathbf{l}^\alpha \\ &= \sum_{\alpha=1}^2 \int_{\mathcal{A}} \theta^\alpha \mathbf{d}_\alpha \times \mathbf{b} \rho_0^* da + \sum_{\alpha=1}^2 \oint_{\partial \mathcal{A}} \theta^\alpha \mathbf{d}_\alpha \times \mathbf{t} du.\end{aligned}\quad (7.39)$$

This prescription can be inferred from Eqn. (7.38) with the help of Green and Laws [130] (cf. [276, Section 4]). The prescriptions (7.38) and (7.39) are identical to those we presented earlier for Kirchhoff's rod theory (cf. Eqns. (5.69) and (5.71)) and we refer the reader to our earlier discussion on Page 209 for examples.

7.6.2 Singular Supplies

Motivated by applications in the literature, we admit singular supplies of momentum \mathbf{F}_γ , material momentum B_γ , director momenta \mathbf{F}_γ^1 and \mathbf{F}_γ^2 , angular momentum \mathbf{M}_{O_γ} , and power Φ_{E_γ} at a specific material point $\xi = \gamma(t)$.⁸ In the sequel, and paralleling the situations we encountered previously, we shall find that \mathbf{M}_{O_γ} and Φ_{E_γ} are given by identities involving \mathbf{F}_γ , B_γ , \mathbf{F}_γ^1 , and \mathbf{F}_γ^2 .

The supply B_γ is related to changes in energy, such as the adhesion boundary condition discussed in Section 4.5 of Chapter 4, and can be related to the driving traction found in theories of phase transitions [2, 3]. The primary examples of singular supplies \mathbf{F}_γ thus far have arisen in the elastica arm scale (see Eqn. (4.116) on Page 154) and the problem of the chain falling off the edge of a table (see Eqn. (2.56) on Page 66). For these problems, \mathbf{F}_γ is a reaction force exerted by an object on the rod or chain. In a complementary manner, the prescriptions (7.38) for $\rho_0 \mathbf{f}$ and $\rho_0 \boldsymbol{\ell}^\alpha$ can be used to develop prescriptions for the supplies \mathbf{F}_γ and \mathbf{F}_γ^α :

$$\begin{aligned}\mathbf{F}_\gamma &= \lim_{\chi \rightarrow 0} \int_{\gamma-\chi}^{\gamma+\chi} \left(\int_{\mathcal{A}} \mathbf{b} \rho_0^* da + \oint_{\partial \mathcal{A}} \mathbf{t} du \right) d\xi, \\ \mathbf{F}_\gamma^\alpha &= \lim_{\chi \rightarrow 0} \int_{\gamma-\chi}^{\gamma+\chi} \left(\int_{\mathcal{A}} \mathbf{b} \theta^\alpha \rho_0^* da + \oint_{\partial \mathcal{A}} \mathbf{t} \theta^\alpha du \right) d\xi.\end{aligned}\quad (7.40)$$

We also note for completeness that the forthcoming expression (7.129)₃ for b_p can be used to motivate a prescription for B_γ :

$$\begin{aligned}B_\gamma &= - \lim_{\chi \rightarrow 0} \int_{\gamma-\chi}^{\gamma+\chi} \int_{\mathcal{A}} \rho_0^* \mathbf{b} \cdot \left(\mathbf{r}' + \sum_{\beta=1}^2 \theta^\beta \mathbf{d}'_\beta \right) dAd\xi \\ &\quad - \lim_{\chi \rightarrow 0} \int_{\gamma-\chi}^{\gamma+\chi} \int_{\mathcal{A}} \left(\frac{\partial}{\partial \theta^3} \left(\rho_0^* \psi^* - \frac{1}{2} \rho_0^* \mathbf{v}^* \cdot \mathbf{v}^* \right) \right)_{\text{exp}} dAd\xi \\ &\quad + \lim_{\chi \rightarrow 0} \int_{\gamma-\chi}^{\gamma+\chi} \oint_{\partial \mathcal{A}(\xi)} \left(\mathbf{r}' \cdot \mathbf{t} + \theta^1 \mathbf{d}'_1 \cdot \mathbf{t} + \theta^2 \mathbf{d}'_2 \cdot \mathbf{t} \right) du d\xi.\end{aligned}\quad (7.41)$$

This prescription for B_γ is difficult to implement because \mathbf{r}' and \mathbf{d}'_β are not necessarily continuous at $\xi = \gamma$. As a result, in applications to date, nontrivial selections for

⁸ As usual, for ease of exposition and without loss of generality, we assume that there is at most one such point.

B_γ have not attempted to correlate this energy supply to the corresponding quantities in three-dimensional continuum mechanics.

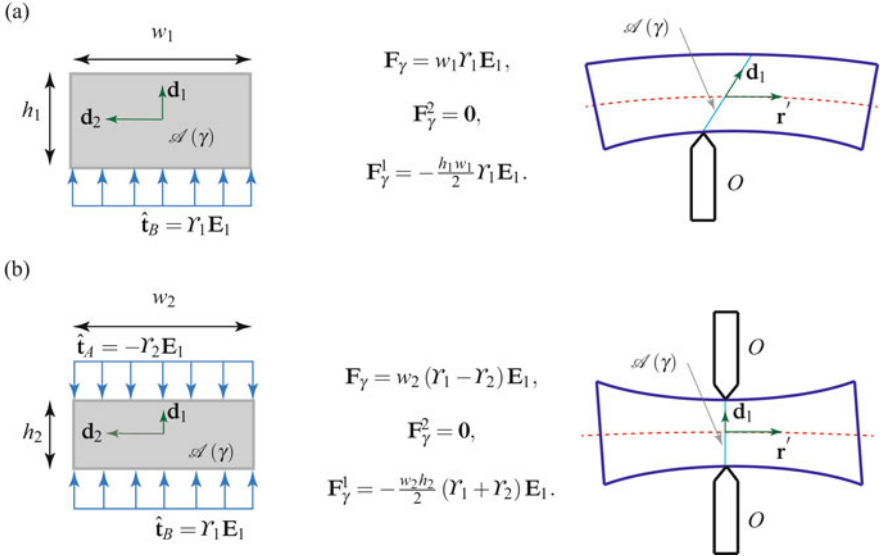


Fig. 7.6 Contact of a rod with (a) a single rigid, knife-edged object O and (b) a pair of rigid, knife-edged objects O . The contact induces singular forces \mathbf{F}_γ and director forces \mathbf{F}_γ^β on the rod at the material point $\xi = \gamma$. These forces can be computed using the prescriptions (7.40). The cross sections $\mathcal{A}(\gamma)$ of the rod in the present configurations are assumed to be rectangular in shape.

The body force \mathbf{b} is usually a continuous bounded function, so the integral terms containing this force vanish from the right-hand side of the prescriptions for \mathbf{F}_γ and \mathbf{F}_γ^β . We find it convenient to define a force field per unit length:

$$\hat{\mathbf{t}} = \hat{\mathbf{t}}(u) = \lim_{\chi \rightarrow 0} \int_{-\chi}^{\gamma+\chi} \mathbf{t} d\xi. \quad (7.42)$$

The units of \mathbf{t} are N/m² while those for $\hat{\mathbf{t}}$ are Nm. The prescriptions for \mathbf{F}_γ and \mathbf{F}_γ^α simplify to

$$\begin{aligned} \mathbf{F}_\gamma &= \oint_{\partial \mathcal{A}} \hat{\mathbf{t}} du, \\ \mathbf{F}_\gamma^\alpha &= \oint_{\partial \mathcal{A}} \hat{\mathbf{t}} \theta^\alpha du. \end{aligned} \quad (7.43)$$

Observe that the units of \mathbf{F}_γ are in Newtons while those of \mathbf{F}_γ^α are in Newton meters. To illustrate the prescriptions (7.43), consider a rod in contact with a sharp rigid knife-edged object (cf. Figure 7.6). In a fixed reference configuration, the cross section is assumed to be rectangular with a height h and width w . The contact of the rod

with the knife edge produces a force field $\hat{\mathbf{t}}$ per unit width at a point on the lateral surface of the rod. For illustrative purposes, we assume for the examples shown in the figure that the shape of the deformed cross section at $\xi = \gamma$ is that of a rectangle, and the force field induced by the contact is uniformly distributed along the width of the rod. In the first example, shown in Figure 7.6(a), the rod is in contact with the object along a material line ($\xi = \gamma, \theta_1 = -h/2$) on its lateral surface. The contact induces nonzero supplies \mathbf{F}_γ and \mathbf{F}_γ^1 proportional to the magnitude of the force Y_1 and, among other strains, these forces induce shearing and contraction of the rod. In the second example, the rod is in contact with a pair of knife edges along the respective material lines ($\xi = \gamma, \theta_1 = \mp h/2$) on its lateral surface (cf. Figure 7.6(b)). The force \mathbf{F}_γ in this case represents a squeezing force on the rod and the average of the squeezing action on the upper and lower surfaces is reflected in the force \mathbf{F}_γ^1 . For additional examples of the prescriptions (7.43) in applications with rods contacting sharp objects, the reader is referred to [251].

7.6.3 Conservation Laws

We adopt the following balance laws for any fixed material segment (ξ_1, ξ_2) of the material curve. First, we record the conservations of mass and inertia:

$$\begin{aligned} \frac{d}{dt} \int_{\xi_1}^{\xi_2} \rho \mu d\xi &= 0, \\ \frac{d}{dt} \int_{\xi_1}^{\xi_2} \rho y^{0\alpha} \mu d\xi &= 0, \\ \frac{d}{dt} \int_{\xi_1}^{\xi_2} \rho y^{\alpha\beta} \mu d\xi &= 0. \end{aligned} \quad (7.44)$$

Here, the six inertia coefficients $\rho y^{0\alpha}$ and $\rho y^{\alpha\beta}$ have units of kg and kg m, respectively. The balance of linear momentum is

$$\frac{d}{dt} \int_{\xi_1}^{\xi_2} \mathbf{G} d\xi = [\mathbf{n}]_{\xi_1}^{\xi_2} + \int_{\xi_1}^{\xi_2} \rho \mu \mathbf{f} d\xi + \int_{\xi_1}^{\xi_2} \mathbf{F}_\gamma \delta(\xi - \gamma) d\xi, \quad (7.45)$$

where $\delta(\cdot)$ is the Dirac delta distribution. The balance of material momentum is

$$\frac{d}{dt} \int_{\xi_1}^{\xi_2} \mathbf{P} d\xi = [\mathbf{C}]_{\xi_1}^{\xi_2} + \int_{\xi_1}^{\xi_2} \mathbf{b} d\xi + \int_{\xi_1}^{\xi_2} \mathbf{B}_\gamma \delta(\xi - \gamma) d\xi. \quad (7.46)$$

The pair of balances of director momentum are

$$\begin{aligned} \frac{d}{dt} \int_{\xi_1}^{\xi_2} \mathbf{L}^1 d\xi &= [\mathbf{m}^1]_{\xi_1}^{\xi_2} + \int_{\xi_1}^{\xi_2} \rho \mu \mathbf{l}^1 - \mathbf{k}^1 d\xi + \int_{\xi_1}^{\xi_2} \mathbf{F}_\gamma^1 \delta(\xi - \gamma) d\xi, \\ \frac{d}{dt} \int_{\xi_1}^{\xi_2} \mathbf{L}^2 d\xi &= [\mathbf{m}^2]_{\xi_1}^{\xi_2} + \int_{\xi_1}^{\xi_2} \rho \mu \mathbf{l}^2 - \mathbf{k}^2 d\xi + \int_{\xi_1}^{\xi_2} \mathbf{F}_\gamma^2 \delta(\xi - \gamma) d\xi. \end{aligned} \quad (7.47)$$

The balance of angular momentum is

$$\begin{aligned} \frac{d\mathbf{H}_O}{dt} = & \left[\mathbf{r} \times \mathbf{n} + \sum_{\alpha=1}^2 \mathbf{d}_\alpha \times \mathbf{m}^\alpha \right]_{\xi_1}^{\xi_2} + \int_{\xi_1}^{\xi_2} \left(\mathbf{r} \times \mathbf{f} + \sum_{\alpha=1}^2 \mathbf{d}_\alpha \times \mathbf{l}^\alpha \right) \rho \mu d\xi \\ & + \int_{\xi_1}^{\xi_2} \mathbf{M}_{O\gamma} \delta(\xi - \gamma) d\xi. \end{aligned} \quad (7.48)$$

One also has the balance of energy:

$$\begin{aligned} \frac{d}{dt} \int_{\xi_1}^{\xi_2} T + \rho \mu \psi d\xi = & \left[\mathbf{n} \cdot \mathbf{v} + \sum_{\alpha=1}^2 \mathbf{m}^\alpha \cdot \dot{\mathbf{d}}_\alpha \right]_{\xi_1}^{\xi_2} + \int_{\xi_1}^{\xi_2} \left(\mathbf{f} \cdot \mathbf{v} + \sum_{\alpha=1}^2 \mathbf{l}^\alpha \cdot \dot{\mathbf{d}}_\alpha \right) \rho \mu d\xi \\ & + \int_{\xi_1}^{\xi_2} \Phi_{E\gamma} \delta(\xi - \gamma) d\xi. \end{aligned} \quad (7.49)$$

Prior to deducing local forms of these laws and the associated jump conditions, we pause to note that the two director momentum balance laws here are unique. The balance laws for the earlier rod theories discussed in this book can be formulated using conservations of mass, inertia, linear momentum, angular momentum, and energy. However, for Green and Naghdi's rod theory, the pair of balances of director momentum are needed to provide a closed set of equations for the rod theory. The (somewhat tentative) manner in which this pair of balance laws was introduced in Green and Laws [128, Eqn. (3.17)] differs from the later works such as [138, Eqn. (6.16)] where they are clearly introduced as balance laws on a comparable level with linear momentum and energy. The other rod theories we have discussed in this book can be considered as special constrained theories that follow from Green and Naghdi's theory. The reader interested in examining this perspective on the Cosserat theory discussed in Chapter 6 and Kirchhoff's rod theory is referred to [64, 246, 276, 308] and Section 7.11 below.

7.7 Local Balance Laws and Jump Conditions

In the balance laws, we assume that there is one point of discontinuity. Consequently, with the help of the Leibnitz rule, we can follow the procedure discussed in Section 1.5.3 and establish local forms of the balance laws and jump conditions.

7.7.1 Local Balance Laws

In the interests of brevity, and because the procedure is so similar to the one we used for the string, we do not give details here on how to establish the following

local forms of the balance laws from Eqns. (7.44)–(7.49). Instead, we just quote the final results:

$$\begin{aligned}
 \rho_0 &= \rho_0(\xi) = \rho \mu, \\
 y^{0\alpha} &= y^{0\alpha}(\xi), \\
 y^{\alpha\beta} &= y^{\alpha\beta}(\xi), \\
 \rho_0 \ddot{\mathbf{r}} + \sum_{\alpha=1}^2 \rho_0 y^{0\alpha} \ddot{\mathbf{d}}_\alpha &= \rho_0 \mathbf{f} + \frac{\partial \mathbf{n}}{\partial \xi}, \\
 \rho_0 y^{0\alpha} \ddot{\mathbf{r}} + \sum_{\beta=1}^2 \rho_0 y^{\alpha\beta} \ddot{\mathbf{d}}_\beta &= \rho_0 \mathbf{l}^\alpha - \mathbf{k}^\alpha + \frac{\partial \mathbf{m}^\alpha}{\partial \xi}, \\
 \mathbf{0} &= \sum_{\alpha=1}^2 \mathbf{d}_\alpha \times \mathbf{k}^\alpha + \sum_{\beta=1}^2 \frac{\partial \mathbf{d}_\beta}{\partial \xi} \times \mathbf{m}^\beta + \frac{\partial \mathbf{r}}{\partial \xi} \times \mathbf{n}, \\
 \dot{\mathbf{P}} &= \mathbf{b} + \mathbf{C}', \\
 \rho_0 \dot{\psi} &= \sum_{\beta=1}^2 \mathbf{m}^\beta \cdot \frac{\partial \mathbf{d}_\beta}{\partial \xi} + \mathbf{n} \cdot \frac{\partial \mathbf{v}}{\partial \xi} + \sum_{\alpha=1}^2 \mathbf{k}^\alpha \cdot \dot{\mathbf{d}}_\alpha. \tag{7.50}
 \end{aligned}$$

To establish these laws, we used mass conservation, the balance of linear momentum, and the director momentum balances to simplify the local form of the energy balance (7.50)₈.

To establish the final form of the balance of angular momentum, we started with

$$\begin{aligned}
 \sum_{\alpha=1}^2 \rho_0 \left(\mathbf{d}_\alpha \times y^{0\alpha} \ddot{\mathbf{r}} + \sum_{\beta=1}^2 \mathbf{d}_\alpha \times y^{\alpha\beta} \ddot{\mathbf{d}}_\beta \right) &= \sum_{\alpha=1}^2 \mathbf{d}_\alpha \times \rho_0 \mathbf{l}^\alpha + \underbrace{\sum_{\alpha=1}^2 \mathbf{d}_\alpha \times \frac{\partial \mathbf{m}^\alpha}{\partial \xi}}_{\text{underbrace}} \\
 &\quad + \sum_{\alpha=1}^2 \frac{\partial \mathbf{d}_\alpha}{\partial \xi} \times \mathbf{m}^\alpha + \frac{\partial \mathbf{r}}{\partial \xi} \times \mathbf{n}. \tag{7.51}
 \end{aligned}$$

Substituting for the underbraced term $\frac{\partial \mathbf{m}^\alpha}{\partial \xi}$ from the balances of director momentum (7.50)₅ then allowed us to eliminate the inertial terms and the assigned director forces $\rho_0 \mathbf{l}^\alpha$, and obtain the balance law (7.50)₆. This form of the balance law is analogous to the moment of momentum balance law in continuum mechanics (which states that the Cauchy stress tensor \mathbf{T} is symmetric).

As with the earlier theories, we assume that \mathbf{b} is prescribed as \mathbf{b}_p so that the local form of the balance of material momentum (7.50)₇ is identically satisfied. Following a standard procedure, one finds that

$$\mathbf{b}_p = -\rho_0 \mathbf{f} \cdot \mathbf{r}' - \rho_0 \mathbf{l}^1 \cdot \mathbf{d}'_1 - \rho_0 \mathbf{l}^2 \cdot \mathbf{d}'_2 - \left(\frac{\partial}{\partial \xi} (\rho_0 \psi - T) \right)_{\text{exp}}. \tag{7.52}$$

In the event that the rod is homogeneous and assigned forces and assigned director forces are absent, this prescription can be used to show that C is conserved for static problems.

7.7.2 Jump Conditions

From the balance laws (7.44)–(7.49), we find that the following jump conditions must hold at $\xi = \gamma(t)$:

$$\begin{aligned} [[\rho_0]]_\gamma \dot{\gamma} &= 0, \\ [[[\rho_0 y^{0\alpha}]]]_\gamma \dot{\gamma} &= 0, \\ [[[\rho_0 y^{\alpha\beta}]]]_\gamma \dot{\gamma} &= 0, \\ [[\mathbf{n}]]_\gamma + [[\mathbf{G}]]_\gamma \dot{\gamma} + \mathbf{F}_\gamma &= \mathbf{0}, \\ [[\mathbf{m}^\alpha]]_\gamma + [[\mathbf{L}^\alpha]]_\gamma \dot{\gamma} + \mathbf{F}_\gamma^\alpha &= \mathbf{0}, \\ \mathbf{r}(\gamma, t) \times \mathbf{F}_\gamma + \mathbf{d}_1(\gamma, t) \times \mathbf{F}_\gamma^1 + \mathbf{d}_2(\gamma, t) \times \mathbf{F}_\gamma^2 - \mathbf{M}_{O\gamma} &= \mathbf{0}, \\ [[C]]_\gamma + [[P]]_\gamma \dot{\gamma} + B_\gamma &= 0, \\ [[[\mathbf{n} \cdot \mathbf{v} + \mathbf{m}^1 \cdot \dot{\mathbf{d}}_1 + \mathbf{m}^2 \cdot \dot{\mathbf{d}}_2]]]_\gamma + [[\rho_0 \psi + T]]_\gamma \dot{\gamma} + \Phi_{E\gamma} &= 0. \end{aligned} \quad (7.53)$$

Notice that the assumptions $[[\mathbf{r}]] = \mathbf{0}$ and $[[\mathbf{d}_\alpha]] = \mathbf{0}$ have been extensively employed to simplify the jump conditions.

We can also invoke some of the jump conditions in order to simplify the condition that is associated with the jump in energy. In particular, paralleling the developments in Exercise 5.7, we find that Eqn. (7.53)₈ reduces to

$$\Phi_{E\gamma} = \mathbf{F}_\gamma \cdot \mathbf{v}_\gamma + \mathbf{F}_\gamma^1 \cdot \mathbf{w}_{1\gamma} + \mathbf{F}_\gamma^2 \cdot \mathbf{w}_{2\gamma} + B_\gamma \dot{\gamma}. \quad (7.54)$$

Thus, we view the energy jump condition (7.54) as an identity for $\Phi_{E\gamma}$ in terms of the supplies of the singular forces. The velocities in this equation were defined earlier in Section 5.4.

The jump condition for the balance of angular momentum was simplified considerably with the help of (7.53)_{1,...,5}. First, we started with

$$\left[\left[\mathbf{r} \times \mathbf{n} + \sum_{\beta=1}^2 \mathbf{d}_\beta \times \mathbf{m}^\beta \right] \right]_\gamma + \left[\left[\mathbf{r} \times \mathbf{G} + \sum_{\beta=1}^2 \mathbf{d}_\beta \times \mathbf{L}^\beta \right] \right]_\gamma \dot{\gamma} = -\mathbf{M}_{O\gamma}. \quad (7.55)$$

Continuity of \mathbf{r} and \mathbf{d}_α allowed us to write this equation as

$$\mathbf{r}(\gamma, t) \times [[\mathbf{n} + \dot{\gamma} \mathbf{G}]]_\gamma + \sum_{\beta=1}^2 \mathbf{d}_\beta(\gamma, t) \times \left[\left[\mathbf{m}^\beta + \dot{\gamma} \mathbf{L}^\beta \right] \right]_\gamma = -\mathbf{M}_{O\gamma}. \quad (7.56)$$

Using (7.53)_{4,5}, we then easily found the final desired form:

$$\mathbf{M}_{O_\gamma} = \mathbf{r}(\gamma, t) \times \mathbf{F}_\gamma + \mathbf{d}_1(\gamma, t) \times \mathbf{F}_\gamma^1 + \mathbf{d}_2(\gamma, t) \times \mathbf{F}_\gamma^2.$$

Consequently, the moment \mathbf{M}_{O_γ} is *not* an independent quantity. This parallels the situation we encountered earlier with an elastic string.

7.8 Constitutive Relations

For the elastic rod (elastic directed curve), the constitutive relations for \mathbf{m}^α , \mathbf{k}^α , and \mathbf{n} are obtained by assuming that the local balance of energy (7.50)₈ is identically satisfied subject to the restriction that the local form of the balance of angular momentum (7.50)₆ is also satisfied. That is, we need to solve the equation

$$\rho_0 \psi = \sum_{\beta=1}^2 \mathbf{m}^\beta \cdot \frac{\partial \mathbf{d}_\beta}{\partial \xi} + \mathbf{n} \cdot \frac{\partial \mathbf{v}}{\partial \xi} + \sum_{\alpha=1}^2 \mathbf{k}^\alpha \cdot \dot{\mathbf{d}}_\alpha \quad (7.57)$$

for \mathbf{m}^α , \mathbf{k}^α , and \mathbf{n} , subject to the restriction

$$\mathbf{0} = \sum_{\alpha=1}^2 \mathbf{d}_\alpha \times \mathbf{k}^\alpha + \sum_{\alpha=1}^2 \frac{\partial \mathbf{d}_\alpha}{\partial \xi} \times \mathbf{m}^\alpha + \frac{\partial \mathbf{r}}{\partial \xi} \times \mathbf{n}. \quad (7.58)$$

This restriction is surprisingly easy to satisfy provided the strain energy function has a certain functional form.⁹

Motivated by the arguments leading to Eqn. (7.29), we assume that

$$\psi = \psi(\gamma_{ik}, \kappa_{\alpha j}, \xi). \quad (7.59)$$

Using the representation (7.30) for ψ , we can express the balance of energy (7.57) as

$$\begin{aligned} & \left(\rho_0 \frac{\partial \psi}{\partial \mathbf{d}_3} - \mathbf{n} \right) \cdot \dot{\mathbf{d}}_3 + \sum_{\beta=1}^2 \left(\rho_0 \frac{\partial \psi}{\partial \mathbf{d}_\beta} - \mathbf{k}^\beta \right) \cdot \dot{\mathbf{d}}_\beta \\ & + \sum_{\beta=1}^2 \left(\rho_0 \frac{\partial \psi}{\partial \mathbf{d}'_\beta} - \mathbf{m}^\beta \right) \cdot \dot{\mathbf{d}}'_\beta \\ & = 0. \end{aligned} \quad (7.60)$$

⁹ As summarized in Section 8.6, a parallel situation arises in the three-dimensional theory. That is, the constitutive relations for the stress tensor of a hyperelastic continuum automatically satisfy the local form of the balance of angular momentum provided the strain energy function is properly invariant under superposed rigid body motions.

For this equation to hold for all $\dot{\mathbf{d}}_i$ and $\dot{\mathbf{d}}'_\alpha$, we assume that the terms inside the parentheses are independent of $\dot{\mathbf{d}}_i$ and $\dot{\mathbf{d}}'_\alpha$ and conclude that

$$\mathbf{n} = \rho_0 \frac{\partial \psi}{\partial \mathbf{d}_3}, \quad \mathbf{k}^\beta = \rho_0 \frac{\partial \psi}{\partial \mathbf{d}_\beta}, \quad \mathbf{m}^\beta = \rho_0 \frac{\partial \psi}{\partial \mathbf{d}'_\beta}. \quad (7.61)$$

Noting that $\psi = \psi(\gamma_{ik}, \kappa_{\alpha j}, \xi)$, we can use the representations (7.31) for $\rho_0 \frac{\partial \psi}{\partial \mathbf{d}_i}$ and $\rho_0 \frac{\partial \psi}{\partial \mathbf{d}'_\beta}$ combined with the constitutive relations (7.61) to show that the local form of the balance of angular momentum (7.58) is identically satisfied (cf. Eqn. (7.32)).

7.8.1 Constrained Elastic Rods

There are a variety of perspectives one can take on Kirchhoff's rod theory, Euler's elastica, and the Cosserat rod theory discussed in the previous chapters. First, each one of these theories can be considered as a separate stand-alone theory. Alternatively, each theory can be considered as an approximation to a three-dimensional rod-like body. A third perspective is to consider each one of these theories as an example of the rod theory discussed in the present chapter subject to a set of constraints. In this instance, the previous arguments on constitutive relations need to be altered in the manner we are about to present. Before doing so we note that Naghdi and Rubin [246] were the first to present a comprehensive treatment of this topic in the context of Green and Naghdi's rod theory. While our discussion is greatly influenced by their work, we employ an argument used in [276] to simplify some of their results. In particular, we assume that the constraint is invariant under superposed rigid body motions and this allows us to invoke the identity (7.63)₂ below. Consequently, and paralleling the unconstrained case, the local form of the balance of angular momentum is identically satisfied by the response functions for \mathbf{n} , \mathbf{m}^β , and \mathbf{k}^β .

We suppose that the rod has a strain energy function $\rho_0 \psi$ as before, but we now assume that the motion of the rod is subject to a constraint $\phi = 0$. We assume that the constraint function is invariant under superposed rigid body motions of the rod, thus

$$\phi = \phi(\gamma_{ik}, \kappa_{\alpha j}, \xi). \quad (7.62)$$

Paralleling our earlier developments with the strain energy function, it can be shown that

$$\begin{aligned} \dot{\phi} &= \frac{\partial \phi}{\partial \mathbf{r}'} \cdot \mathbf{v}' + \sum_{\beta=1}^2 \frac{\partial \phi}{\partial \mathbf{d}'_\beta} \cdot \dot{\mathbf{d}}'_\beta + \sum_{\alpha=1}^2 \frac{\partial \phi}{\partial \mathbf{d}_\alpha} \cdot \dot{\mathbf{d}}_\alpha, \\ \mathbf{0} &= \mathbf{r}' \times \frac{\partial \phi}{\partial \mathbf{r}'} + \sum_{\alpha=1}^2 \mathbf{d}_\alpha \times \frac{\partial \phi}{\partial \mathbf{d}_\alpha} + \sum_{\beta=1}^2 \mathbf{d}'_\beta \times \frac{\partial \phi}{\partial \mathbf{d}'_\beta}. \end{aligned} \quad (7.63)$$

The fact that $\phi = 0$ for all times and motions also implies that $\dot{\phi} = 0$. The partial derivatives of ψ with respect to \mathbf{d}_i and $\dot{\mathbf{d}}_\beta'$ can be expressed in terms of the strains using identities of the form (7.31) but we do not pause to do this here.

To prescribe constitutive relations for \mathbf{n} , \mathbf{m}^β , and \mathbf{k}^α , we seek solutions to the local form of the energy balance subject to the constraint $\phi = 0$. That is, we seek solutions \mathbf{n} , \mathbf{m}^β , and \mathbf{k}^α to

$$\rho_0 \dot{\psi} = \sum_{\beta=1}^2 \mathbf{m}^\beta \cdot \dot{\mathbf{d}}_\beta' + \mathbf{n} \cdot \mathbf{v}' + \sum_{\alpha=1}^2 \mathbf{k}^\alpha \cdot \dot{\mathbf{d}}_\alpha, \quad (7.64)$$

subject to the constraint

$$\frac{\partial \phi}{\partial \mathbf{r}'} \cdot \mathbf{v}' + \sum_{\beta=1}^2 \frac{\partial \phi}{\partial \mathbf{d}_\beta'} \cdot \dot{\mathbf{d}}_\beta' + \sum_{\alpha=1}^2 \frac{\partial \phi}{\partial \mathbf{d}_\alpha} \cdot \dot{\mathbf{d}}_\alpha = 0. \quad (7.65)$$

Assuming that \mathbf{n} , \mathbf{m}^β , and \mathbf{k}^α are independent of the rates \mathbf{v}' , $\dot{\mathbf{d}}_\alpha$, and $\dot{\mathbf{d}}_\beta'$, we conclude that

$$\begin{aligned} \mathbf{n} &= \rho_0 \frac{\partial \psi}{\partial \mathbf{d}_3} + \lambda \frac{\partial \phi}{\partial \mathbf{d}_3}, \\ \mathbf{k}^\beta &= \rho_0 \frac{\partial \psi}{\partial \mathbf{d}_\beta} + \lambda \frac{\partial \phi}{\partial \mathbf{d}_\beta}, \\ \mathbf{m}^\beta &= \rho_0 \frac{\partial \psi}{\partial \mathbf{d}_\beta'} + \lambda \frac{\partial \phi}{\partial \mathbf{d}_\beta'}, \end{aligned} \quad (7.66)$$

where $\lambda = \lambda(\xi, t)$. The terms associated with λ in the constitutive relations can be termed reactive forces or constraint responses. Their role is to ensure that the constraint $\phi = 0$ is enforced. The value of the function $\lambda(\xi, t)$ needed to ensure that the constraint is enforced is determined as part of the solution to the boundary-value problem associated with the rod.

In the absence of constraints, the relations (7.66) simplify to the relations (7.61) as expected. Because ψ and ϕ are invariant under superposed rigid body motions, we can use the identities (7.32) and (7.63)₂ to show that the local form of the balance of angular momentum is identically satisfied. We note that the procedure we have just used parallels the corresponding procedure in continuum mechanics.¹⁰ As can be seen in the example discussed in Section 7.11 below, extensions of the aforementioned procedures to the case of multiple constraints is trivial.

The derivatives of $\rho_0 \psi$ assume that the constraint is imposed after the derivatives have been evaluated. Alternatively, as discussed in [46, 47, 50], one can impose the constraint $\phi = 0$ on the strain energy function $\rho_0 \psi$ to produce a constrained strain energy function $\rho_0 \psi_c$. The resulting constitutive relations for \mathbf{n} , \mathbf{m}^β , and \mathbf{k}^α in terms of ψ_c are identical to the relations (7.66) with ψ being replaced by its constrained

¹⁰ The developments for three-dimensional continua subject to internal constraints are discussed in Section 8.6 of Chapter 8 and in Exercise 8.4 that can be found on Page 373.

counterpart ψ_c provided any differences are subsumed into the λ s. As an illustrative example, suppose that the strain energy functions and the constraint are

$$\rho_0 \psi = \frac{\alpha_1}{2} \gamma_{33}^2 + \alpha_2 \gamma_{33} \gamma_{13}, \quad \rho_0 \psi_c = \frac{\alpha_1}{2} \gamma_{33}^2, \quad \phi = \gamma_{13}, \quad (7.67)$$

where α_1 and α_2 are constants. For this (admittedly artificial) example where the shear strain γ_{13} is constrained to be zero, we find the following constitutive relations for \mathbf{n} :

$$\begin{aligned} \mathbf{n} &= \rho_0 \frac{\partial \psi}{\partial \mathbf{d}_3} + \lambda \frac{\partial \phi}{\partial \mathbf{d}_3} \\ &= \left(2\alpha_1 \gamma_{33} + 2\alpha_2 \underbrace{\gamma_{13}}_{=0} \right) \mathbf{d}_3 + \alpha_2 \gamma_{33} \mathbf{d}_1 + \lambda \mathbf{d}_1, \\ &= 2\alpha_1 \gamma_{33} \mathbf{d}_3 + (\lambda + \alpha_2 \gamma_{33}) \mathbf{d}_1. \end{aligned} \quad (7.68)$$

Alternatively, using the constrained strain energy function $\rho_0 \psi_c$, we find that

$$\begin{aligned} \mathbf{n} &= \rho_0 \frac{\partial \psi_c}{\partial \mathbf{d}_3} + \hat{\lambda} \frac{\partial \phi}{\partial \mathbf{d}_3} \\ &= 2\alpha_1 \gamma_{33} \mathbf{d}_3 + \hat{\lambda} \mathbf{d}_1. \end{aligned} \quad (7.69)$$

Clearly, this constitutive relation is equivalent to the earlier representation $\mathbf{n} = 2\alpha_1 \gamma_{33} \mathbf{d}_3 + \lambda \mathbf{d}_1$ provided we equate

$$\hat{\lambda} = \lambda + \alpha_2 \gamma_{33}. \quad (7.70)$$

That is, we subsume $\alpha_2 \gamma_{33}$ into the function λ and define a new function $\hat{\lambda}$.

7.9 Summary of the Governing Equations for an Elastic Rod

We take this opportunity to summarize the governing equations for the rod theory. Based on the previous developments, the nontrivial balance laws and jump conditions are

$$[\![\rho_0]\!]_\gamma \dot{\gamma} = 0, \quad [\![\rho_0 y^{0\alpha}]\!]_\gamma \dot{\gamma} = 0, \quad [\![\rho_0 y^{\alpha\beta}]\!]_\gamma \dot{\gamma} = 0,$$

$$\rho_0 = \rho_0(\xi) = \rho \mu, \quad y^{0\alpha} = y^{0\alpha}(\xi), \quad y^{\alpha\beta} = y^{\alpha\beta}(\xi),$$

$$[\![\mathbf{n}]\!]_\gamma + [\![\mathbf{G}]\!]_\gamma \dot{\gamma} + \mathbf{F}_\gamma = \mathbf{0},$$

$$[\![\mathbf{m}^\alpha]\!]_\gamma + [\![\mathbf{L}^\alpha]\!]_\gamma \dot{\gamma} + \mathbf{F}_\gamma^\alpha = \mathbf{0},$$

$$[\![\mathbf{C}]\!]_\gamma + [\![\mathbf{P}]\!]_\gamma \dot{\gamma} + \mathbf{B}_\gamma = 0,$$

$$\begin{aligned}\rho_0 \ddot{\mathbf{r}} + \sum_{\beta=1}^2 \rho_0 y^{0\beta} \ddot{\mathbf{d}}_\beta &= \rho_0 \mathbf{f} + \frac{\partial \mathbf{n}}{\partial \xi}, \\ \rho_0 y^{0\alpha} \ddot{\mathbf{r}} + \sum_{\beta=1}^2 \rho_0 y^{\alpha\beta} \ddot{\mathbf{d}}_\beta &= \rho_0 \mathbf{l}^\alpha - \mathbf{k}^\alpha + \frac{\partial \mathbf{m}^\alpha}{\partial \xi}. \end{aligned} \quad (7.71)$$

The local forms of the balances of linear and director momenta provide nine partial differential equations for the nine fields $\mathbf{r}(\xi, t)$ and $\mathbf{d}_\alpha(\xi, t)$.

For an elastic rod, the equations (7.71) are supplemented by the constitutive relations

$$\mathbf{n} = \rho_0 \frac{\partial \psi}{\partial \mathbf{d}_3}, \quad \mathbf{k}^\beta = \rho_0 \frac{\partial \psi}{\partial \mathbf{d}_\beta}, \quad \mathbf{m}^\beta = \rho_0 \frac{\partial \psi}{\partial \mathbf{d}_\beta}, \quad (7.72)$$

where $\psi = \psi(\gamma_{ik}, \kappa_{\alpha k}, \xi)$. For an elastic rod subject to a constraint $\phi = 0$, these constitutive relations are replaced by the relations (7.66) and the balance laws are supplemented by the constraint. In addition, we have the identities

$$\begin{aligned}\mathbf{M}_{O_\gamma} &= \mathbf{r}(\gamma, t) \times \mathbf{F}_\gamma + \mathbf{d}_1(\gamma, t) \times \mathbf{F}_\gamma^1 + \mathbf{d}_2(\gamma, t) \times \mathbf{F}_\gamma^2, \\ \Phi_{E_\gamma} &= \mathbf{F}_\gamma \cdot \mathbf{v}_\gamma + \mathbf{F}_\gamma^1 \cdot \mathbf{w}_{1\gamma} + \mathbf{F}_\gamma^2 \cdot \mathbf{w}_{2\gamma} + \mathbf{B}_\gamma \dot{\gamma}, \end{aligned} \quad (7.73)$$

that can be used to define the moment \mathbf{M}_{O_γ} and power Φ_{E_γ} .

7.10 Boundary Conditions

Boundary conditions pertaining to displacements are easy to formulate. Suppose, for instance, that one end of a rod (corresponding to $\xi = 0$, say) is fixed. The boundary conditions are then

$$\mathbf{r}(0, t) = \mathbf{0}, \quad \mathbf{d}_\alpha(0, t) = \mathbf{0}. \quad (7.74)$$

If the other end of the rod, say at $\xi = \ell$ is free of external tractions, then the boundary conditions are

$$\mathbf{n}(\ell, t) = \mathbf{0}, \quad \mathbf{m}^\alpha(\ell, t) = \mathbf{0}. \quad (7.75)$$

Using the constitutive relations (7.72), we can express these conditions in terms of $\mathbf{d}_i(\ell, t)$ and $\mathbf{d}'_\alpha(\ell, t)$.

For more complex boundary conditions, it is often convenient to use the following identifications with the three-dimensional theory:

$$\begin{aligned}\mathbf{n} &= \int_{\mathcal{A}} \mathbf{T}^3 d\theta^1 d\theta^2, \\ \mathbf{k}^\alpha &= \int_{\mathcal{A}} \mathbf{T}^\alpha d\theta^1 d\theta^2, \\ \mathbf{m}^\beta &= \int_{\mathcal{A}} \theta^\beta \mathbf{T}^3 d\theta^1 d\theta^2. \end{aligned} \quad (7.76)$$

As shall be discussed in Sections 7.12.5 and 7.12.6, $\mathbf{T}^i = \sqrt{g}\mathbf{T}\mathbf{g}^{*i}$ are tractions defined in terms of the three-dimensional Cauchy stress tensor \mathbf{T} . Note that

$$da = \sqrt{g}d\theta^1 d\theta^2. \quad (7.77)$$

For static problems, when we prescribe forces (or traction fields) on the end surfaces of the rod, we can calculate $\mathbf{T}\mathbf{g}^{*i}$ and then use the prescriptions (7.76) to determine \mathbf{n} and \mathbf{m}^β .¹¹ Equivalently, one can employ the jump conditions

$$[\![\mathbf{n}]\!]_\gamma + [\![\mathbf{G}]\!]_\gamma \dot{\gamma} = -\mathbf{F}_\gamma, \quad [\![\mathbf{m}^\alpha]\!]_\gamma + [\![\mathbf{L}^\alpha]\!]_\gamma \dot{\gamma} = -\mathbf{F}_\gamma^\alpha, \quad (7.78)$$

to prescribe the terminal conditions on the contact forces \mathbf{n} and \mathbf{m}^α given \mathbf{F}_γ and \mathbf{F}_γ^α .

7.11 Kirchhoff's Rod Theory as a Constrained Rod Theory

There are a variety of perspectives one can take on Kirchhoff's rod theory. First, as we did in Chapter 5, the theory can be considered as a separate stand-alone theory. Alternatively, the theory can be considered as an approximation to a three-dimensional rod-like body. A third perspective is to consider Kirchhoff's rod theory as an example of the rod theory discussed in the present chapter subject to six independent constraints. We now explore this third perspective in greater detail and note that our developments can also be applied to the rod theory discussed in Chapter 6. Our exposition in this section is based on the works of Green and Laws [130] and O'Reilly and Turcotte [276].

Recalling the developments in Section 7.8.1, the constraints of interest here are assumed to be expressible in terms of the strains γ_{ij} and $\kappa_{\beta k}$. For Kirchhoff's rod theory, we recall with the help of the relations (5.7) that $\mathbf{d}_i = \mathbf{P}\mathbf{D}_i = \mathbf{P}\mathbf{P}_0\mathbf{E}_i$ and $\mathbf{d}'_\alpha = \mathbf{P}(\mathbf{v} + \mathbf{v}_0)\mathbf{d}_\alpha$. These conditions imply that nine of the twelve strain measures are identically zero. Thus, the Kirchhoff rod theory can be considered as a constrained theory where the vectors \mathbf{d}_i are subject to the following constraints:

$$\phi_1 = 0, \quad \phi_2 = 0, \quad \phi_3 = 0, \quad \phi_4 = 0, \quad \phi_5 = 0, \quad \phi_6 = 0, \quad (7.79)$$

where

$$\begin{aligned} \phi_1 &= \gamma_{11}, & \phi_2 &= \gamma_{22}, & \phi_3 &= \gamma_{33}, \\ \phi_4 &= \gamma_{12}, & \phi_5 &= \gamma_{13}, & \phi_6 &= \gamma_{23}. \end{aligned} \quad (7.80)$$

These constraints imply that $\kappa_{11} = 0$, $\kappa_{22} = 0$, and $\kappa_{12} + \kappa_{21} = 0$. It is easy to check that each of the six constraints is invariant under superposed rigid body motions of

¹¹ Equations (7.76)_{1,3} were first presented in [137] and, for the reasons discussed in [260], are only useful on the end surfaces. For a linear theory, it is shown in Exercise 7.2 that the identifications (7.76) simplify considerably.

the directed curve. We also note that the nonzero strains associated with this theory pertain to torsion (κ_3) and flexure (κ_1 and κ_2):

$$\kappa_{12} = -\kappa_{21} = \nu_3, \quad \kappa_{13} = -\nu_2, \quad \kappa_{23} = \nu_1, \quad (7.81)$$

where the components $\nu_k = \mathbf{v} \cdot \mathbf{D}_k$. Here, the vector \mathbf{v} is the axial vector of the skew-symmetric tensor $\mathbf{K} = \mathbf{P}^T \mathbf{P}'$.

The strain energy function for this constrained theory simplifies:

$$\rho_0 \psi = \rho_0 \psi_c. \quad (7.82)$$

The function ψ_c is the restriction of ψ to the case where the six constraints are imposed:

$$\rho_0 \psi_c = \rho_0 \psi_c (\kappa_{12} = \nu_3, \kappa_{13} = -\nu_2, \kappa_{23} = \nu_1, \xi). \quad (7.83)$$

The function ψ_c is sometimes known as the constrained strain energy function [47, 50]. The constitutive relations in this case are obtained from the relations (7.66) with some obvious modifications to accommodate multiple constraints:

$$\begin{aligned} \mathbf{n} &= \rho_0 \frac{\partial \psi_c}{\partial \mathbf{d}_3} + \lambda_3 \frac{\partial \phi_3}{\partial \mathbf{d}_3} + \lambda_5 \frac{\partial \phi_5}{\partial \mathbf{d}_3} + \lambda_6 \frac{\partial \phi_6}{\partial \mathbf{d}_3} \\ &= \rho_0 \frac{\partial \psi_c}{\partial \mathbf{d}_3} + 2\lambda_3 \mathbf{d}_3 + \lambda_5 \mathbf{d}_1 + \lambda_6 \mathbf{d}_2, \\ \mathbf{k}^1 &= \rho_0 \frac{\partial \psi_c}{\partial \mathbf{d}_1} + \lambda_1 \frac{\partial \phi_1}{\partial \mathbf{d}_1} + \lambda_4 \frac{\partial \phi_4}{\partial \mathbf{d}_1} + \lambda_5 \frac{\partial \phi_5}{\partial \mathbf{d}_1} \\ &= \rho_0 \frac{\partial \psi_c}{\partial \mathbf{d}_1} + 2\lambda_1 \mathbf{d}_1 + \lambda_4 \mathbf{d}_2 + \lambda_5 \mathbf{d}_3, \\ \mathbf{k}^2 &= \rho_0 \frac{\partial \psi_c}{\partial \mathbf{d}_2} + \lambda_2 \frac{\partial \phi_2}{\partial \mathbf{d}_2} + \lambda_4 \frac{\partial \phi_4}{\partial \mathbf{d}_2} + \lambda_6 \frac{\partial \phi_6}{\partial \mathbf{d}_2} \\ &= \rho_0 \frac{\partial \psi_c}{\partial \mathbf{d}_2} + 2\lambda_2 \mathbf{d}_2 + \lambda_4 \mathbf{d}_1 + \lambda_6 \mathbf{d}_3, \\ \mathbf{m}^\beta &= \rho_0 \frac{\partial \psi_c}{\partial \mathbf{d}'_\beta}. \end{aligned} \quad (7.84)$$

In these expressions,

$$\begin{aligned} \rho_0 \frac{\partial \psi_c}{\partial \mathbf{d}_1} &= \mathbf{0}, & \rho_0 \frac{\partial \psi_c}{\partial \mathbf{d}_2} &= \rho_0 \frac{\partial \psi_c}{\partial \kappa_{12}} \mathbf{d}'_1, \\ \rho_0 \frac{\partial \psi_c}{\partial \mathbf{d}_3} &= \rho_0 \frac{\partial \psi_c}{\partial \kappa_{13}} \mathbf{d}'_1 + \rho_0 \frac{\partial \psi_c}{\partial \kappa_{23}} \mathbf{d}'_2. \end{aligned} \quad (7.85)$$

Because the vectors \mathbf{d}_i form a basis, $\rho_0 \frac{\partial \psi_c}{\partial \mathbf{d}_3}$ can be subsumed into λ_3 , λ_5 , and λ_6 :

$$\mathbf{n} = 2\tilde{\lambda}_3 \mathbf{d}_3 + \tilde{\lambda}_5 \mathbf{d}_1 + \tilde{\lambda}_6 \mathbf{d}_2, \quad (7.86)$$

Whence, \mathbf{n} is composed entirely of constraint (or reactive) components. By way of contrast, the bending moment \mathbf{m} is completely prescribed by the strain energy function:

$$\begin{aligned}\mathbf{m} &= \mathbf{d}_1 \times \mathbf{m}^1 + \mathbf{d}_2 \times \mathbf{m}^2 \\ &= \mathbf{d}_1 \times \rho_0 \frac{\partial \psi_c}{\partial \mathbf{d}'_1} + \mathbf{d}_2 \times \rho_0 \frac{\partial \psi_c}{\partial \mathbf{d}'_2} \\ &= \rho_0 \frac{\partial \psi_c}{\partial \kappa_{23}} \mathbf{d}_1 - \rho_0 \frac{\partial \psi_c}{\partial \kappa_{13}} \mathbf{d}_2 + \rho_0 \frac{\partial \psi_c}{\partial \kappa_{12}} \mathbf{d}_3.\end{aligned}\quad (7.87)$$

As expected, the constitutive relations for \mathbf{m} agree with their counterpart (5.91). The constitutive relations for \mathbf{n} are equivalent to those employed in the Kirchhoff rod theory when the terms involving the derivatives of the strain energy function are subsumed into the functions λ_3 , λ_5 , and λ_6 .

For this constrained theory, the balances of linear and director momenta along with the constitutive relations (7.84) provide a determinate system of equations for \mathbf{r} , \mathbf{d}_α , and the six scalar-valued functions $\lambda_1, \dots, \lambda_6$. For instance, the balance of linear momentum,

$$\mathbf{n}' + \rho_0 \mathbf{f} = \rho_0 \ddot{\mathbf{r}} + \sum_{\beta=1}^2 y^{0\beta} \ddot{\mathbf{d}}_\beta, \quad (7.88)$$

can be used to determine $\tilde{\lambda}_3$, $\tilde{\lambda}_5$, and $\tilde{\lambda}_6$, i.e., the tangential and shear components of \mathbf{n} . The helpful series of identities¹²

$$\begin{aligned}\mathbf{m}' &= \mathbf{d}'_1 \times \mathbf{m}^1 + \mathbf{d}'_2 \times \mathbf{m}^2 + \mathbf{d}_1 \times (\mathbf{m}^1)' + \mathbf{d}_2 \times (\mathbf{m}^2)' \\ &= \mathbf{d}_1 \times ((\mathbf{m}^1)' - \mathbf{k}^1) + \mathbf{d}_2 \times ((\mathbf{m}^2)' - \mathbf{k}^2) - \mathbf{r}' \times \mathbf{n} \\ &= \mathbf{d}_1 \times (\dot{\mathbf{L}}^1 - \rho_0 \mathbf{l}^1) + \mathbf{d}_2 \times (\dot{\mathbf{L}}^2 - \rho_0 \mathbf{l}^2) - \mathbf{r}' \times \mathbf{n},\end{aligned}\quad (7.89)$$

can be used to show that the balance of angular momentum for Kirchhoff's rod theory (cf. Eqn. (5.106)),

$$\mathbf{m}' + \mathbf{r}' \times \mathbf{n} + \mathbf{m}_a = \mathbf{d}_1 \times \dot{\mathbf{L}}^1 + \mathbf{d}_2 \times \dot{\mathbf{L}}^2, \quad (7.90)$$

is equivalent to the sum of the cross products of \mathbf{d}_β with their respective balance of director momentum (7.71)₁₁. That is, by combining the balances of director momentum in this manner we generate an equation that is free from the functions $\lambda_1, \dots, \lambda_6$.

Of the six scalar equations that constitute the balances of director momenta, three distinct linear combinations of these equations provide the balance of angular momentum for the constrained rod and another three linear combinations provide equations for λ_1 , λ_2 , and λ_4 . To elaborate, once Eqns. (7.88) and (7.90) have been used to determine the motion (\mathbf{r} , \mathbf{d}_1 , and \mathbf{d}_2) of the rod, we can return to the balances of director momenta to determine the remaining unknown functions λ_1 , λ_2 , and λ_4 :

¹² The local form of the balance of angular momentum (7.50)₆ is used to establish this identity.

$$\begin{aligned}\lambda_1 &= \rho_0 \mathbf{l}^1 \cdot \mathbf{d}_1 - \dot{\mathbf{L}}^1 \cdot \mathbf{d}_1 + (\mathbf{m}^1)' \cdot \mathbf{d}_1 - \rho_0 \frac{\partial \psi_c}{\partial \mathbf{d}_1} \cdot \mathbf{d}_1, \\ \lambda_2 &= \rho_0 \mathbf{l}^2 \cdot \mathbf{d}_2 - \dot{\mathbf{L}}^2 \cdot \mathbf{d}_2 + (\mathbf{m}^2)' \cdot \mathbf{d}_2 - \rho_0 \frac{\partial \psi_c}{\partial \mathbf{d}_2} \cdot \mathbf{d}_2, \\ \lambda_4 &= \rho_0 \mathbf{l}^1 \cdot \mathbf{d}_2 - \dot{\mathbf{L}}^1 \cdot \mathbf{d}_2 + (\mathbf{m}^1)' \cdot \mathbf{d}_2 - \rho_0 \frac{\partial \psi_c}{\partial \mathbf{d}_1} \cdot \mathbf{d}_2.\end{aligned}\quad (7.91)$$

These expressions can be simplified using Eqn. (7.85) but we leave this matter here in the hopes we have convinced the reader that Kirchhoff's rod theory can also be considered as a constrained theory from the perspective of Green and Naghdi's rod theory (and the Cosserat theory discussed in the previous chapter). In addition, as discussed in Rubin [308], if the constraint $\phi_3 = 0$ is not imposed in the previous developments, then a constrained rod theory where the centerline is extensible and the rod resists torsion and bending is obtained (i.e., a Kirchhoff rod theory with an extensible centerline).

7.12 Prescriptions and Three-Dimensional Considerations

The balance laws for Green and Naghdi's rod theory can be motivated directly from the balance laws for a three-dimensional continuum. The resulting correspondences have been used throughout this book (see, e.g., Eqns. (5.2) and (7.76)) for the balances of energy, linear momentum, and angular momentum. We now examine them in more detail. Our discussion follows Green, Naghdi, and Wenner [137] with the help of some added insights from [260, 309]. Additional background on curvilinear coordinates and three-dimensional continuum mechanics can be found in Chapter 8. By restricting attention to special cases, such as a string and a rod where the directors are orthogonal, prescriptions for the quantities appearing in the balance laws for the string and rod theories discussed in the earlier chapters of this book can be established using the procedures discussed below. For the latter theories, the director momentum balance laws are not needed.¹³

To avoid confusion where it may arise, quantities associated with the three-dimensional body are sometimes ornamented with an asterisk. For example, \mathbf{r}^* , ρ_0^* , and \mathbf{v}^* denote kinematical quantities associated with the rod-like body and \mathbf{r} , ρ_0 , and \mathbf{v} denote quantities associated with the rod.

7.12.1 Kinematical Considerations

Consider a rod-like body \mathcal{B} and assign to it a set of convected curvilinear coordinates θ^i . Let \mathbf{R}^* and \mathbf{r}^* denote the position vectors of material points in the reference

¹³ See, for example, the derivation of the balance laws for Kirchhoff's rod theory presented in [285].

\mathcal{K}_0 and present \mathcal{K} configurations, respectively (cf. Figure 7.5). Associated with the coordinate systems, we can define covariant and contravariant basis vectors:

$$\mathbf{G}_i^* = \frac{\partial \mathbf{R}^*}{\partial \theta^i}, \quad \mathbf{G}^{*k} \cdot \mathbf{G}_i^* = \delta_i^k, \quad \mathbf{g}_i^* = \frac{\partial \mathbf{r}^*}{\partial \theta^i}, \quad \mathbf{g}^{*k} \cdot \mathbf{g}_i^* = \delta_i^k. \quad (7.92)$$

The deformation gradient \mathbf{F}^* has the representation

$$\mathbf{F}^* = \sum_{i=1}^3 \mathbf{g}_i^* \otimes \mathbf{G}^{*i}. \quad (7.93)$$

Clearly, $\mathbf{g}_i^* = \mathbf{F}^* \mathbf{G}_i^*$.

To model this body using a directed curve, we make the following identifications:

$$\xi = \theta^3, \quad \mathbf{R}^* = \mathbf{R}^*(\theta^i) = \mathbf{R}(\xi) + \sum_{\alpha=1}^2 \theta^\alpha \mathbf{D}_\alpha(\xi). \quad (7.94)$$

In the present configuration, these choices imply the following approximation:

$$\mathbf{r}^* = \mathbf{r}^*(\theta^i, t) \approx \mathbf{r}(\xi, t) + \sum_{\alpha=1}^2 \theta^\alpha \mathbf{d}_\alpha(\xi, t). \quad (7.95)$$

It is a good exercise to calculate the corresponding approximate expression for \mathbf{F}^* :

$$\mathbf{F}^* \approx \mathbf{F}_1 \mathbf{A}, \quad (7.96)$$

where

$$\begin{aligned} \mathbf{F}_1 &= \sum_{i=1}^3 \mathbf{d}_i \otimes \mathbf{D}^i, \\ \boldsymbol{\lambda}_\alpha &= \mathbf{F}_0^{-1} \mathbf{G}_\alpha = \sum_{i=1}^3 \left(\frac{\partial \mathbf{d}_\alpha}{\partial \xi} \cdot \mathbf{d}^i \right) \mathbf{D}_i \otimes \mathbf{D}^3, \\ \mathbf{A} &= \left(\mathbf{I} + \sum_{\sigma=1}^2 \theta^\sigma \boldsymbol{\lambda}_\sigma \right) \left(\mathbf{I} + \sum_{\alpha=1}^2 \theta^\alpha {}_0 \mathbf{G}_\alpha \right)^{-1}. \end{aligned} \quad (7.97)$$

The tensors $\mathbf{G}_\alpha = \frac{\partial \mathbf{d}_\alpha}{\partial \xi} \otimes \mathbf{D}^3$ and ${}_0 \mathbf{G}_\alpha = \frac{\partial \mathbf{d}_\alpha}{\partial \xi} \otimes \mathbf{D}^3$ were introduced previously in Section 7.3. Some of the notations we have just introduced are from Naghdi's review article [245, Section 13]. He introduced these notations in an effort to draw comparisons between the rod theory and the three-dimensional continuum theory. Subsequently, his ideas were expanded by other researchers (see [19, 258, 307]) to explore applications of the theory to liquid jets, problems where a small deformation is superposed on a large deformation, and constitutive restrictions for elastic rods.

7.12.2 Inertias

We suppose that the three-dimensional body \mathcal{B} that the directed curve is modeling has a mass density per unit volume in a fixed reference configuration of $\rho_0^* = \rho_0^*(\theta^1, \theta^2, \xi)$. The directed curve has a mass per unit length in its reference configuration of $\rho_0 = \rho_0(\xi)$. We prescribe this density and five inertias in the usual manner¹⁴:

$$\begin{aligned}\rho_0 &= \int_{\mathcal{A}} \rho_0^* da, \\ \rho_0 y^{0\alpha} &= \int_{\mathcal{A}} \theta^\alpha \rho_0^* da, \\ \rho_0 y^{\alpha\beta} &= \int_{\mathcal{A}} \theta^\alpha \theta^\beta \rho_0^* da,\end{aligned}\tag{7.98}$$

where $\alpha, \beta = 1, 2$. The integrals in these expressions are taken over the cross section \mathcal{A} of the reference configuration of the rod-like body that the curve is modeling. These cross sections correspond to $\theta^3 = \xi$ coordinate surfaces. That is, θ^1 and θ^2 are curvilinear coordinates which parameterize the cross sections of the rod (see Section 5.2.1), and the point $\theta^\alpha = 0$ on each section corresponds to the material point of the directed curve.

7.12.3 Preliminary Identities Pertaining to Volume Integrals

The divergence theorem plays a prominent role in the developments we are about to discuss. To this end, we take this opportunity to collect several results involving this theorem. Our interest is in integrating functions for a body \mathcal{B} whose volume is bounded by a lateral surface and a pair of end sections (see Figure 7.5). We suppose that the body of interest \mathcal{B} has a mass density per unit volume in its reference configuration of ρ_0^* and ρ^* in its present configuration and recall that volume elements in the reference and present configurations respectively are

$$dV = \sqrt{G} d\theta^1 d\theta^2 d\theta^3, \quad dv = \sqrt{g} d\theta^1 d\theta^2 d\theta^3, \tag{7.99}$$

where

$$\sqrt{G} = (\mathbf{G}_1^* \times \mathbf{G}_2^*) \cdot \mathbf{G}_3^*, \quad \sqrt{g} = (\mathbf{g}_1^* \times \mathbf{g}_2^*) \cdot \mathbf{g}_3^*. \tag{7.100}$$

Mass conservation dictates that

$$\sqrt{G} \rho_0^* = \sqrt{g} \rho^*. \tag{7.101}$$

We assume that the body is bounded by the lateral surface

$$F = F(\theta^1, \theta^2, \xi) = 0 \tag{7.102}$$

¹⁴ See Eqn. (5.36).

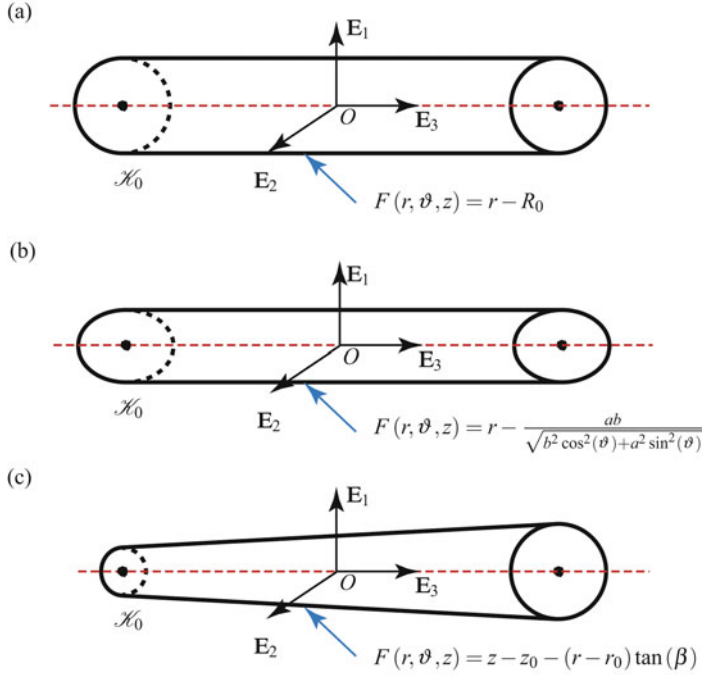


Fig. 7.7 Examples of the function $F = F(\theta^1, \theta^2, \xi) = 0$ for the lateral surface of the reference configuration \mathcal{H}_0 : (a) a rod-like body with a circular cross section; (b) a rod-like body with an elliptical cross section; and (c) a rod-like body shaped as a truncated, tapered cone. In this figure, R_0 , β , a , b , r_0 , and z_0 are constants, and r , ϑ , and z are a standard set of cylindrical polar coordinates.

and the end sections $\xi = \xi_1$ and $\xi = \xi_2$. Three examples of this surface and the associated three-dimensional bodies are shown in Figure 7.7.

Using the divergence theorem for tensor-valued functions, it can be shown that¹⁵

$$\begin{aligned} \int_{\xi_1}^{\xi_2} \int_{\mathcal{A}(\xi)} f \operatorname{Div}(\mathbf{P}) dV &= - \int_{\xi_1}^{\xi_2} \int_{\mathcal{A}(\xi)} \sum_{r=1}^3 \mathbf{P} \mathbf{G}^{*r} \frac{\partial f}{\partial \theta^r} dV + \int_{\xi_1}^{\xi_2} \oint_{\partial \mathcal{A}(\xi)} f \mathbf{P} \mathbf{N} dA \\ &\quad + \int_{\mathcal{A}(\xi_2)} f \mathbf{P} \mathbf{G}^{*3} \sqrt{G} d\theta^1 d\theta^2 - \int_{\mathcal{A}(\xi_1)} f \mathbf{P} \mathbf{G}^{*3} \sqrt{G} d\theta^1 d\theta^2, \end{aligned} \quad (7.103)$$

where $f = f(\theta^1, \theta^2, \xi)$ and \mathbf{N} is the unit outward normal to the lateral surface $F = 0$. Employing results of the form (8.43) and (8.44), we find that $\sqrt{G} \mathbf{P} \mathbf{G}^{*3} = \mathbf{T}^3$ and $\mathbf{P} \mathbf{N} dA = \mathbf{t} dA$. Thus,

¹⁵ We refer the reader to Eqn. (8.46) on Page 356 for further details on the divergence of \mathbf{P} . Our development of Eqn. (7.106) was inspired by the treatment in Rubin [307].

$$\begin{aligned} \int_{\xi_1}^{\xi_2} \int_{\mathcal{A}(\xi)} f \operatorname{Div}(\mathbf{P}) dV &= - \int_{\xi_1}^{\xi_2} \int_{\mathcal{A}(\xi)} \sum_{r=1}^3 \mathbf{P} \mathbf{G}^{*r} \frac{\partial f}{\partial \theta^r} dV + \int_{\xi_1}^{\xi_2} \oint_{\partial \mathcal{A}(\xi)} f \mathbf{t} da \\ &\quad + \int_{\mathcal{A}(\xi_2)} f \mathbf{T}^3 d\theta^1 d\theta^2 - \int_{\mathcal{A}(\xi_1)} f \mathbf{T}^3 d\theta^1 d\theta^2. \end{aligned} \quad (7.104)$$

We assume that the lateral surface can be parameterized by the coordinates ξ and u , so that

$$\int_{\xi_1}^{\xi_2} \oint_{\partial \mathcal{A}(\xi)} f \mathbf{t} da = \int_{\xi_1}^{\xi_2} \oint_{\partial \mathcal{A}(\xi)} f \mathbf{t} du d\xi. \quad (7.105)$$

That is, the coordinate u parameterizes the boundary of \mathcal{A} . We thus arrive at the final desired form of the identity for the volume integral:

$$\begin{aligned} \int_{\xi_1}^{\xi_2} \int_{\mathcal{A}(\xi)} f \operatorname{Div}(\mathbf{P}) dV &= - \int_{\xi_1}^{\xi_2} \int_{\mathcal{A}(\xi)} \sum_{r=1}^3 \mathbf{T}^r \frac{\partial f}{\partial \theta^r} \sqrt{G} d\theta^1 d\theta^2 d\xi \\ &\quad + \int_{\xi_1}^{\xi_2} \oint_{\partial \mathcal{A}(\xi)} f \mathbf{t} du d\xi \\ &\quad + \int_{\mathcal{A}(\xi_2)} f \mathbf{T}^3 d\theta^1 d\theta^2 \\ &\quad - \int_{\mathcal{A}(\xi_1)} f \mathbf{T}^3 d\theta^1 d\theta^2. \end{aligned} \quad (7.106)$$

When $f = 1$ this identity will be used to motivate the balance of linear momentum for the rod, and, when $f = \theta^1$ and $f = \theta^2$, the balances of director momenta.

The second type of volume integral pertains to the balance of material momentum. Here, we will be taking the \mathbf{G}_3^* component of a balance law. The identity of interest is

$$\begin{aligned} \int_{\xi_1}^{\xi_2} \int_{\mathcal{A}(\xi)} \operatorname{Div}(\mathbf{o}^*) \cdot \mathbf{G}_3^* dV &= \int_{\xi_1}^{\xi_2} \int_{\mathcal{A}(\xi)} -\operatorname{Div}(\mathbf{P}^T \mathbf{F}^* \mathbf{G}_3^*) - \frac{\partial L^*}{\partial \theta^3} dV \\ &\quad + \int_{\xi_1}^{\xi_2} \int_{\mathcal{A}(\xi)} \sum_{r=1}^3 (\mathbf{F}^{*T} \mathbf{P} \mathbf{G}^{*r}) \cdot \frac{\partial \mathbf{G}_3^*}{\partial \theta^r} dV. \end{aligned} \quad (7.107)$$

In these integrands, the energy-momentum tensor \mathbf{o}^* and Lagrangian density L^* are

$$\begin{aligned} \mathbf{o}^* &= -L^* \mathbf{I} - \mathbf{F}^{*T} \mathbf{P}, \\ L^* &= \frac{1}{2} \rho_0^* \mathbf{v}^* \cdot \mathbf{v}^* - \rho_0^* \psi^*. \end{aligned} \quad (7.108)$$

Applying the divergence theorem to the term $\operatorname{Div}(\mathbf{P}^T \mathbf{F}^* \mathbf{G}_3^*) = \operatorname{Div}(\mathbf{P}^T \mathbf{g}_3^*)$ and using the identity $\mathbf{T}^r = \sqrt{G} \mathbf{P} \mathbf{G}^{*r}$, we find

$$\begin{aligned}
\int_{\xi_1}^{\xi_2} \int_{\mathcal{A}(\xi)} \operatorname{Div}(\mathbf{\sigma}^*) \cdot \mathbf{G}_3^* dV &= - \int_{\xi_1}^{\xi_2} \oint_{\partial \mathcal{A}(\xi)} \mathbf{g}_3^* \cdot \mathbf{P} \mathbf{N} dA \\
&\quad - \int_{\mathcal{A}(\xi_2)} \mathbf{T}^3 \cdot \mathbf{g}_3^* d\theta^1 d\theta^2 - \int_{\mathcal{A}(\xi_2)} L^* \sqrt{G} d\theta^1 d\theta^2 \\
&\quad + \int_{\mathcal{A}(\xi_1)} \mathbf{T}^3 \cdot \mathbf{g}_3^* d\theta^1 d\theta^2 + \int_{\mathcal{A}(\xi_1)} L^* \sqrt{G} d\theta^1 d\theta^2 \\
&\quad + \int_{\xi_1}^{\xi_2} \int_{\mathcal{A}(\xi)} \sum_{r=1}^3 \mathbf{T}^r \cdot \left(\mathbf{F}^* \frac{\partial \mathbf{G}_3^*}{\partial \theta^r} \right) d\theta^1 d\theta^2 d\xi.
\end{aligned} \tag{7.109}$$

Observe that the term with $\frac{\partial \mathbf{G}_3^*}{\partial \theta^r}$ will vanish if the reference configuration is such that $\mathbf{R}'' = \mathbf{0}$ and $\mathbf{D}'_\alpha = \mathbf{0}$.

7.12.4 Integrating the Balance of Linear Momentum

The local balance laws and constitutive relations for the body are

$$\underbrace{\sum_{i=1}^3 \left(\frac{\partial \mathbf{F}^* \mathbf{S}^*}{\partial \theta^i} \right) \mathbf{G}^{*i} + \rho_0^* \mathbf{b}}_{=\operatorname{Div}(\mathbf{P})} = \rho_0^* \ddot{\mathbf{r}}^*, \quad \mathbf{S}^* = (\mathbf{S}^*)^T, \quad \mathbf{S}^* = \rho_0^* \frac{\partial \psi^*}{\partial \mathbf{C}^*}, \tag{7.110}$$

where $\mathbf{C}^* = (\mathbf{F}^*)^T \mathbf{F}^*$, \mathbf{b} is the body force per unit mass, \mathbf{S}^* is the second Piola-Kirchhoff stress tensor, and ψ^* is the three-dimensional strain energy function.

We now substitute the approximation $\mathbf{F}^* = \mathbf{F}_1 \mathbf{A}$ (see Eqn. (7.96)) into Eqn. (7.110)₁ and multiply by \sqrt{G} and $\sqrt{G} \theta^\beta$ to find

$$\begin{aligned}
\sum_{i=1}^3 \sqrt{G} \left(\frac{\partial \mathbf{F}^* \mathbf{S}^*}{\partial \theta^i} \right) \mathbf{G}^{*i} + \rho_0^* \sqrt{G} \mathbf{b} &= \rho_0^* \sqrt{G} \ddot{\mathbf{r}} + \sum_{\alpha=1}^2 \theta^\alpha \rho_0^* \sqrt{G} \ddot{\mathbf{d}}_\alpha, \\
\sum_{i=1}^3 \sqrt{G} \theta^\beta \left(\frac{\partial \mathbf{F}^* \mathbf{S}^*}{\partial \theta^i} \right) \mathbf{G}^{*i} + \rho_0^* \sqrt{G} \mathbf{b} &= \rho_0^* \sqrt{G} \theta^\beta \ddot{\mathbf{r}} + \sum_{\alpha=1}^2 \theta^\beta \theta^\alpha \rho_0^* \sqrt{G} \ddot{\mathbf{d}}_\alpha.
\end{aligned} \tag{7.111}$$

We shall use the traction vectors $\mathbf{T}^i = \sqrt{G} \mathbf{F}^* \mathbf{S}^* \mathbf{G}^{*i}$ in the sequel to define the forces \mathbf{n} , \mathbf{k}^β , and \mathbf{m}^α .

In hindsight, multiplying the local form of the balance of linear momentum by 1, θ^1 , and θ^2 and then integrating the resulting equations through the cross section of the rod-like body in order to arrive at a set of differential equations for the three vectors \mathbf{r} , \mathbf{d}_1 , and \mathbf{d}_2 may appear to be obvious. However, the development of this procedure took time and effort. We can only speculate at the alternative formulations attempted by Green, Naghdi, and their coworkers before they arrived at the final

form of their elegant procedure that appeared in [137]. The prescriptions for the assigned forces and assigned director forces that appear in this chapter are inspired by Rubin's treatment of this topic in [307, Appendix B]. We note that equivalent prescriptions using the traction vectors \mathbf{T}^i , which are not as transparent, can be found in [133, 137].

7.12.5 Balance of Linear Momentum for the Directed Curve

We now consider Eqn. (7.111)₁ and integrate this equation over the volume bounded by the lateral surface $F = 0$ and the ends $\xi = \xi_1$ and $\xi = \xi_2$:

$$\begin{aligned} & \int_{\xi_1}^{\xi_2} \int_{\mathcal{A}} \text{Div}(\mathbf{P}) \sqrt{G} d\theta^1 d\theta^2 d\xi + \int_{\xi_1}^{\xi_2} \int_{\mathcal{A}} \rho_0^* \sqrt{G} \mathbf{b} d\theta^1 d\theta^2 d\xi \\ &= \int_{\xi_1}^{\xi_2} \int_{\mathcal{A}} \ddot{\mathbf{r}} \rho_0^* \sqrt{G} d\theta^1 d\theta^2 d\xi + \sum_{\alpha=1}^2 \int_{\xi_1}^{\xi_2} \int_{\mathcal{A}} \ddot{\mathbf{d}}_\alpha \theta^\alpha \rho_0^* \sqrt{G} d\theta^1 d\theta^2 d\xi. \end{aligned} \quad (7.112)$$

Some of the terms in this equation can be rearranged using Eqn. (7.98):

$$\begin{aligned} \int_{\xi_1}^{\xi_2} \int_{\mathcal{A}} \ddot{\mathbf{r}} \rho_0^* \sqrt{G} d\theta^1 d\theta^2 d\xi &= \int_{\xi_1}^{\xi_2} \ddot{\mathbf{r}} \underbrace{\left(\int_{\mathcal{A}} \rho_0^* \sqrt{G} d\theta^1 d\theta^2 \right)}_{=\rho_0} d\xi, \\ \int_{\xi_1}^{\xi_2} \int_{\mathcal{A}} \ddot{\mathbf{d}}_\alpha \theta^\alpha \rho_0^* \sqrt{G} d\theta^1 d\theta^2 d\xi &= \int_{\xi_1}^{\xi_2} \ddot{\mathbf{d}}_\alpha \underbrace{\int_{\mathcal{A}} \theta^\alpha \rho_0^* \sqrt{G} d\theta^1 d\theta^2}_{=y^{0\alpha} \rho_0} d\xi. \end{aligned} \quad (7.113)$$

Others can be expanded using Eqn. (7.106) with $f = 1$:

$$\begin{aligned} \int_{\xi_1}^{\xi_2} \int_{\mathcal{A}} \text{Div}(\mathbf{P}) \sqrt{G} d\theta^1 d\theta^2 d\xi &= \int_{\xi_1}^{\xi_2} \underbrace{\oint_{\partial \mathcal{A}} \mathbf{t} du d\xi}_{\text{part of } \rho_0 \mathbf{f}} \\ &\quad + \underbrace{\int_{\mathcal{A}(\xi_2)} \mathbf{T}^3 d\theta^1 d\theta^2}_{=\mathbf{n}(\xi_2)} - \underbrace{\int_{\mathcal{A}(\xi_1)} \mathbf{T}^3 d\theta^1 d\theta^2}_{=\mathbf{n}(\xi_1)}. \end{aligned} \quad (7.114)$$

Substituting the results (7.113) and (7.114) into Eqn. (7.112) and then taking the $\frac{\partial}{\partial \xi}$ of the resulting equation we arrive at the balance of linear momentum for the directed curve:

$$\frac{\partial \mathbf{n}}{\partial \xi} + \rho_0 \mathbf{f} = \rho_0 \ddot{\mathbf{r}} + \sum_{\beta=1}^2 \rho_0 y^{0\beta} \ddot{\mathbf{d}}_\beta, \quad (7.115)$$

where (cf. Eqns. (7.38), (7.76), and (7.98))

$$\begin{aligned}\rho_0 &= \int_{\mathcal{A}} \rho_0^* da, \\ \rho_0 y^{0\alpha} &= \int_{\mathcal{A}} \theta^\alpha \rho_0^* da, \\ \rho_0 \mathbf{f} &= \int_{\mathcal{A}} \mathbf{b} \rho_0^* da + \oint_{\partial \mathcal{A}} \mathbf{t} du, \\ \mathbf{n} &= \int_{\mathcal{A}} \mathbf{T}^3 d\theta^1 d\theta^2.\end{aligned}\quad (7.116)$$

You should notice that we used all of these prescriptions earlier in this book.

7.12.6 Balances of Director Momenta for the Directed Curve

We now take Eqn. (7.111)₂ and integrate this equation over the volume bounded by the lateral surface $F = 0$ and the ends $\xi = \xi_1$ and $\xi = \xi_2$:

$$\begin{aligned}& \int_{\xi_1}^{\xi_2} \int_{\mathcal{A}} \theta^\beta \operatorname{Div}(\mathbf{P}) \sqrt{G} d\theta^1 d\theta^2 d\xi + \int_{\xi_1}^{\xi_2} \int_{\mathcal{A}} \rho_0^* \sqrt{G} \mathbf{b} \theta^\beta d\theta^1 d\theta^2 d\xi \\ &= \int_{\xi_1}^{\xi_2} \int_{\mathcal{A}} \ddot{\mathbf{r}} \theta^\beta \rho_0^* \sqrt{G} d\theta^1 d\theta^2 d\xi + \sum_{\alpha=1}^2 \int_{\xi_1}^{\xi_2} \int_{\mathcal{A}} \ddot{\mathbf{d}}_\alpha \theta^\alpha \theta^\beta \rho_0^* \sqrt{G} d\theta^1 d\theta^2 d\xi.\end{aligned}\quad (7.117)$$

With the help of Eqn. (7.98), we note that

$$\begin{aligned}& \int_{\xi_1}^{\xi_2} \int_{\mathcal{A}} \ddot{\mathbf{r}} \theta^\beta \rho_0^* \sqrt{G} d\theta^1 d\theta^2 d\xi = \int_{\xi_1}^{\xi_2} \rho_0 y^{0\alpha} \ddot{\mathbf{r}} d\xi, \\ & \sum_{\alpha=1}^2 \int_{\xi_1}^{\xi_2} \int_{\mathcal{A}} \ddot{\mathbf{d}}_\alpha \theta^\alpha \theta^\beta \rho_0^* \sqrt{G} d\theta^1 d\theta^2 d\xi = \sum_{\alpha=1}^2 \int_{\xi_1}^{\xi_2} \rho_0 y^{\beta\alpha} \ddot{\mathbf{d}}_\alpha d\xi,\end{aligned}\quad (7.118)$$

where

$$\rho_0 y^{\alpha\beta} = \int_{\mathcal{A}} \theta^\alpha \theta^\beta \rho_0^* da. \quad (7.119)$$

We now invoke the identity (7.106) with $f = \theta^\beta$ in a manner similar to that performed earlier with $f = 1$. Taking a partial derivative $\frac{\partial}{\partial \xi}$, using Eqns. (7.38) and (7.76), employing results of the form (7.113) and (7.114), and exploiting the fundamental theorem of calculus we arrive at the balances of director momenta:

$$\rho_0 y^{0\alpha} \ddot{\mathbf{r}} + \sum_{\beta=1}^2 \rho_0 y^{\alpha\beta} \ddot{\mathbf{d}}_\beta = \rho_0 \mathbf{l}^\alpha - \mathbf{k}^\alpha + \frac{\partial \mathbf{m}^\alpha}{\partial \xi}. \quad (7.120)$$

Here, in addition to the previous identifications, we have¹⁶

$$\begin{aligned}\mathbf{k}^\alpha &= \int_{\mathcal{A}} \mathbf{T}^\alpha d\theta^1 d\theta^2, \\ \mathbf{m}^\beta &= \int_{\mathcal{A}} \theta^\beta \mathbf{T}^3 d\theta^1 d\theta^2, \\ \rho_0 \mathbf{l}^\alpha &= \int_{\mathcal{A}} \mathbf{b} \theta^\alpha \rho_0^* da + \oint_{\partial \mathcal{A}} \mathbf{t} \theta^\alpha du.\end{aligned}\quad (7.121)$$

These results were referred to earlier (cf. Eqns. (7.38), (7.76), and (7.98)).

7.12.7 The Moment of Momentum and the Energy Balances for the Directed Curve

Following Green, Naghdi, and Wenner [137], the moment of momentum balance law and the energy balance are obtained by considering the corresponding balance laws for a three-dimensional body whose volume is bounded by the lateral surface $F = 0$ and the ends $\xi = \xi_1$ and $\xi = \xi_2$:

$$\begin{aligned}\frac{d}{dt} \int_{\xi_1}^{\xi_2} \int_{\mathcal{A}} \mathbf{r}^* \times \mathbf{v}^* \rho_0^* dV &= \int_{\xi_1}^{\xi_2} \int_{\mathcal{A}} \mathbf{r}^* \times \mathbf{b} \rho_0^* \sqrt{G} d\theta^1 d\theta^2 d\xi \\ &\quad + \int_{\mathcal{A}(\xi=\xi_2)} \mathbf{r}^* \times \mathbf{t} \sqrt{G} d\theta^1 d\theta^2 \\ &\quad - \int_{\mathcal{A}(\xi=\xi_1)} \mathbf{r}^* \times \mathbf{t} \sqrt{G} d\theta^1 d\theta^2 \\ &\quad + \int_{F=0} \mathbf{r}^* \times \mathbf{t} da,\end{aligned}\quad (7.122)$$

and

$$\begin{aligned}\frac{d}{dt} \int_{\xi_1}^{\xi_2} \int_{\mathcal{A}} \left(\psi^* + \frac{1}{2} \mathbf{v}^* \cdot \mathbf{v}^* \right) \rho_0^* dV &= \int_{\xi_1}^{\xi_2} \int_{\mathcal{A}} \mathbf{v}^* \cdot \mathbf{b} \rho_0^* \sqrt{G} d\theta^1 d\theta^2 d\xi \\ &\quad + \int_{\mathcal{A}(\xi=\xi_2)} \mathbf{v}^* \cdot \mathbf{t} \sqrt{G} d\theta^1 d\theta^2 \\ &\quad - \int_{\mathcal{A}(\xi=\xi_1)} \mathbf{v}^* \cdot \mathbf{t} \sqrt{G} d\theta^1 d\theta^2 \\ &\quad + \int_{F=0} \mathbf{v}^* \cdot \mathbf{t} da.\end{aligned}\quad (7.123)$$

Here, $dV = \sqrt{G} d\theta^1 d\theta^2 d\xi$. Substituting for \mathbf{r}^* and \mathbf{v}^* using the approximation (5.2), expanding the resulting equations, invoking the identities (7.38), (7.76), and (7.98), and finally taking the partial derivative with respect to ξ , the equations (7.122)

¹⁶ The intrinsic director forces \mathbf{k}^α can be attributed to the terms $\sum_{r=1}^3 \mathbf{T}^r \frac{\partial \theta^\alpha}{\partial \theta^r} = \mathbf{T}^\alpha$ in Eqn. (7.106).

and (7.123) will lead to the respective local forms of the balance of angular momentum and the balance of energy for the directed curve.

7.12.8 Balance of Material Momentum for the Directed Curve

It remains to consider the balance of material momentum. This law is not considered in the works of Green, Naghdi, and their coworkers, but we parallel their developments of the other balance laws in order to motivate the balance of material momentum (7.46) that was postulated earlier. To start, we recall the balance of material momentum for a three-dimensional continuum from Eqn. (8.97):

$$\left(\frac{\partial \sigma^*}{\partial \theta^i} \right) \mathbf{G}^{*i} + \rho_0^* \mathbf{b}_M^* = \dot{\mathbf{P}}^*, \quad (7.124)$$

where the energy momentum tensor σ^* , the pseudomomentum \mathbf{P}^* , and the assigned material force $\rho_0^* \mathbf{b}_M^*$ are respectively defined as

$$\begin{aligned} \sigma^* &= \left(\rho_0^* \psi^* - \frac{1}{2} \rho_0^* \mathbf{v}^* \cdot \mathbf{v}^* \right) \mathbf{I} - \mathbf{F}^{*T} \mathbf{P}, \\ \mathbf{P}^* &= -\rho_0^* \mathbf{F}^{*T} \mathbf{v}^*, \\ \rho_0^* \mathbf{b}_M^* &= -\nabla_{\text{exp}}^* \left(\rho_0^* \psi^* - \frac{1}{2} \rho_0^* \mathbf{v}^* \cdot \mathbf{v}^* \right) - \rho_0^* \mathbf{F}^{*T} \mathbf{b}. \end{aligned} \quad (7.125)$$

To motivate the corresponding balance law for the rod theory, we will consider the \mathbf{G}_3^* component of the balance law (7.124).

We note for future reference that

$$\begin{aligned} \mathbf{P}^* \cdot \mathbf{G}_3^* &= -(\rho_0^* \mathbf{F}^{*T} \mathbf{v}^*) \cdot \mathbf{G}_3^* = -\rho_0^* \mathbf{v}^* \cdot \mathbf{g}_3^*, \\ \rho_0^* \mathbf{b}_M^* \cdot \mathbf{G}_3^* &= -\left(\frac{\partial}{\partial \theta^3} \left(\rho_0^* \psi^* - \frac{1}{2} \rho_0^* \mathbf{v}^* \cdot \mathbf{v}^* \right) \right)_{\text{exp}} - \rho_0^* \mathbf{b} \cdot \mathbf{g}_3^*, \end{aligned} \quad (7.126)$$

where the explicit derivative $\left(\frac{\partial f}{\partial \xi} \right)_{\text{exp}}$ with $\theta^3 = \xi$ is defined by (1.113). The three-dimensional counterpart for this derivative is defined in Eqn. (8.101). In writing the above expressions, we have used the identity $\mathbf{F}^{*T} \mathbf{a} \cdot \mathbf{G}_3^* = \mathbf{a} \cdot \mathbf{F}^* \mathbf{G}_3^* = \mathbf{a} \cdot \mathbf{g}_3^*$ for any vector \mathbf{a} .

We now take the \mathbf{G}_3^* component of the balance law (7.124) and integrate this equation over the volume bounded by the lateral surface $F = 0$ and the ends $\xi = \xi_1$ and $\xi = \xi_2$. With the help of Eqn. (7.109), we find that

$$\begin{aligned}
-\frac{\partial}{\partial t} \int_{\xi_1}^{\xi_2} \int_{\mathcal{A}} \rho_0^* \mathbf{v}^* \cdot \mathbf{g}_3^* dV &= - \int_{\xi_1}^{\xi_2} \int_{\mathcal{A}} \rho_0^* \mathbf{b}_M^* \cdot \mathbf{g}_3^* dV - \int_{\xi_1}^{\xi_2} \oint_{\partial \mathcal{A}(\xi)} \mathbf{g}_3^* \cdot \mathbf{P} \mathbf{N} dA \\
&\quad - \int_{\mathcal{A}(\xi_2)} \mathbf{T}^3 \cdot \mathbf{g}_3^* d\theta^1 d\theta^2 - \int_{\mathcal{A}(\xi_2)} L^* \sqrt{G} d\theta^1 d\theta^2 \\
&\quad + \int_{\mathcal{A}(\xi_1)} \mathbf{T}^3 \cdot \mathbf{g}_3^* d\theta^1 d\theta^2 + \int_{\mathcal{A}(\xi_1)} L^* \sqrt{G} d\theta^1 d\theta^2 \\
&\quad + \int_{\xi_1}^{\xi_2} M_M d\xi,
\end{aligned} \tag{7.127}$$

where the Lagrangian density L^* was defined previously in Eqn. (7.108)₂ and

$$M_M = \int_{\mathcal{A}(\xi)} \sum_{r=1}^3 \mathbf{T}^r \cdot \left(\mathbf{F}^* \frac{\partial \mathbf{G}_3^*}{\partial \theta^r} \right) d\theta^1 d\theta^2. \tag{7.128}$$

The term M_M vanishes if $\mathbf{G}_3^* = \mathbf{R}' + \theta^1 \mathbf{D}_1' + \theta^2 \mathbf{D}_2'$ is constant.

After substituting the approximations $\mathbf{r}^* \approx \mathbf{r} + \theta^1 \mathbf{d}_1 + \theta^2 \mathbf{d}_2$ and the companion expressions for \mathbf{v}^* and \mathbf{g}_3^* into Eqn. (7.127), we find that

$$\begin{aligned}
-\frac{\partial}{\partial t} \int_{\xi_1}^{\xi_2} \int_{\mathcal{A}} \rho_0^* \mathbf{v}^* \cdot \mathbf{g}_3^* dV &= \int_{\xi_1}^{\xi_2} \dot{P} d\xi, \\
\int_{\mathcal{A}(\xi)} \mathbf{T}^3 \cdot \mathbf{g}_3^* d\theta^1 d\theta^2 - \int_{\mathcal{A}(\xi)} \left(\frac{1}{2} \rho_0^* \mathbf{v}^* \cdot \mathbf{v}^* - \rho_0^* \psi^* \right) \sqrt{G} d\theta^1 d\theta^2 &= C, \\
\int_{\xi_1}^{\xi_2} \int_{\mathcal{A}} \rho_0^* \mathbf{b}_M^* \cdot \mathbf{g}_3^* dV + \int_{\xi_1}^{\xi_2} \oint_{\partial \mathcal{A}(\xi)} \mathbf{g}_3^* \cdot \mathbf{P} \mathbf{N} dA &= \int_{\xi_1}^{\xi_2} b_p d\xi,
\end{aligned} \tag{7.129}$$

where the material momentum density P is defined by Eqn. (7.23), the kinetic energy density T is defined by Eqn. (7.26), the contact material force C is defined by Eqn. (7.37), and the assigned material force b_p is given by Eqn. (7.52). The identification (7.129)₃ can also be considered as a prescription for the assigned material force b_p from the fields associated with the three-dimensional body that the rod theory is being used to model.

Combining the previous results, we find the correspondences listed below:

$$\overbrace{\int_{\xi_1}^{\xi_2} \int_{\mathcal{A}} \text{Div}(\boldsymbol{\sigma}^*) \cdot \mathbf{G}_3^* dV + \rho^* \mathbf{b}_M^*}^{\int_{\xi_1}^{\xi_2} (\frac{\partial C}{\partial \xi} + b) d\xi + \int_{\xi_1}^{\xi_2} M_M d\xi} = \overbrace{- \frac{\partial}{\partial t} \int_{\xi_1}^{\xi_2} \int_{\mathcal{A}} \rho_0^* \mathbf{v}^* \cdot \mathbf{g}_3^* dV}^{\int_{\xi_1}^{\xi_2} \dot{P} d\xi}. \tag{7.130}$$

Thus, the three-dimensional balance of material momentum can be used to motivate the balance of material momentum for the directed curve. However, we need to assume that the term M_M vanishes in order for the correspondence to hold. Thus, we assume that the reference configuration of the rod is such that $\mathbf{R}'' = \mathbf{0}$ and $\mathbf{D}'_\alpha = \mathbf{0}$. We take this opportunity to note that while a material momentum balance law for Green and Naghdi's rod theory was postulated in [264] the correspondences

between this balance law and the balance of material momentum for a three-dimensional continuum were not explored in [264]. They are presented here for the first time.

7.12.9 Comments on the Integration Process

In summary, the balances of energy, angular momentum, material momentum, and linear momentum are obtained by substituting

$$\mathbf{R}^* = \mathbf{R} + \theta^1 \mathbf{D}_1 + \theta^2 \mathbf{D}_2, \quad \mathbf{r}^* \approx \mathbf{r} + \theta^1 \mathbf{d}_1 + \theta^2 \mathbf{d}_2, \quad (7.131)$$

into the corresponding balances for a three-dimensional continuum, integrating through the cross section, and then evaluating $\frac{\partial}{\partial \xi}$. After some identifications, the local form of the balance laws are obtained and these can then be used to motivate the conservation laws. The procedure we have just mentioned can be used with Kirchhoff's rod theory, the Cosserat rod theory that was presented in the previous chapter, the theory of a string, and Euler's elastica. For Green and Naghdi's rod theory, this procedure does not yield a sufficient number of equations to determine the motion of the directors. In fact, two new balance laws are needed. These balance laws are obtained by multiplying the local form of the balance of linear momentum for a three-dimensional continuum by θ^1 and θ^2 , respectively. One then integrates the resulting equations through the volume of the rod-like body and then evaluates $\frac{\partial}{\partial \xi}$ to arrive at a pair of balances of director momenta. The resulting local forms are then used to motivate the conservation laws with singular supplies.

It would be tempting to conclude that the strain energy function that is produced by the integration procedure,

$$\rho_0 \psi = \int_{\mathcal{A}} \psi^* \rho_0^* da, \quad (7.132)$$

will provide good results for the rod theory. Unfortunately, this is not the case and poor agreement between the bending and torsion solutions for a directed curve and those from three-dimensional linear elasticity are obtained [137, 138, 307]. The reasons for the discrepancy in the solutions lies in the fact that for bending and torsion $\mathbf{r}^* \approx \mathbf{r} + \theta^1 \mathbf{d}_1 + \theta^2 \mathbf{d}_2$ is not a good approximation. As discussed in [9, Section 11], [131, Page 297], [346, Sections 102 and 104], and [307, Section 7], among other sources, this approximation does not account for warping of the cross sections and does not capture the displacement field for the flexure of a three-dimensional body. Consequently, it should not be surprising that the integration procedure yields a bending stiffness of $EI_1 \left(\frac{1-v}{(1+v)(1-2v)} \right)$ as opposed to the correct value of EI_1 .¹⁷ This disparity is the reason for the extensive body of work in Green, Naghdi, et al. [131, 133, 137, 138] on comparisons between exact solutions from the three-

¹⁷ Details on this calculation can be found in [260, Section 4.1].

dimensional theory with exact solutions from the rod theory. You may recall that comparisons of this type were used to identify the parameters k_1, \dots, k_{17} for the linearized approximation to $\rho_0\psi$ (cf. Eqn. (7.35)). As discussed in [260], one perspective on these identifications is that the strain energy for the rod is given by

$$\rho_0\psi = \int_{\mathcal{A}} \psi^* \rho_0^* da + \text{extra piece}, \quad (7.133)$$

where the extra piece is determined by comparing solutions from three-dimensional linear elasticity to those for the infinitesimal theory of a directed curve. For the terms associated with the bending stiffness mentioned earlier, Eqn. (7.133) would read

$$\frac{k_{15}}{2} \kappa_{23}^2 = \underbrace{\frac{EI_1}{2} \left(\frac{1-\nu}{(1+\nu)(1-2\nu)} \right) \kappa_{23}^2}_{\text{from } \int_{\mathcal{A}} \psi^* \rho_0^* da} + \frac{EI_1}{2} \left(1 - \frac{1-\nu}{(1+\nu)(1-2\nu)} \right) \kappa_{23}^2, \quad (7.134)$$

where $k_{15} = EI_1$.

7.13 Applications

Green and Naghdi's theory has also been extended to an electromagnetic theory of rods, and a theory of fluid jets and elastic rods that have an arbitrary number of directors. It is arguably the most complete rod theory available. However, most numerical and analytical work on rods uses Euler's elastica, Kirchhoff's rod theory, and the Cosserat rod theory discussed in the previous chapter.

Of the research that has been performed using Green and Naghdi's theory, the most complete set of problems pertain to the linearized theory. As discussed in the exercises below, this linearized theory often decouples into sets of equations for flexure, torsion, and extension. These equations have been solved for a variety of wave propagation problems by Cohen and Whitman [64], vibrations of a parallelepiped by O'Reilly [261], drawn elastic rods (where the pulling devices couple extensional and flexural motions) in Nordenholz and O'Reilly [251], and a variety of flexure, torsion, and extension problems in Green et al. [137, 138]. The linearized theory, with some straightforward modifications, can also be used to examine the mechanics of a whirling rod (as in [184]).

7.14 Exercises

Exercise 7.1: Suppose one assumes that the strain energy function is a function of fifteen strains,

$$\psi = \psi(\gamma_{ik}, \kappa_{\alpha j}, \kappa_{3j}, \xi), \quad (7.135)$$

where, in addition to the twelve strains γ_{ik} and $\kappa_{\alpha j}$, the following additional three strains are also incorporated:

$$\kappa_{3k} = \frac{\partial \mathbf{d}_3}{\partial \xi} \cdot \mathbf{d}_k - \frac{\partial \mathbf{D}_3}{\partial \xi} \cdot \mathbf{D}_k. \quad (7.136)$$

Show that in order for the local form of the energy balance law (7.50) to be identically satisfied, ψ cannot depend on κ_{3k} .

Exercise 7.2: For a linearized theory corresponding to a straight elastic rod, show that the identifications (7.76) simplify considerably:

$$\begin{aligned} n_i &= \mathbf{n} \cdot \mathbf{E}_i = \int_{\mathcal{A}} \tau_{3i} dx_1 dx_2, \\ m_{\alpha i} &= \mathbf{m}^\alpha \cdot \mathbf{E}_i = \int_{\mathcal{A}} \tau_{3i} x_\alpha dx_1 dx_2, \\ \hat{k}_{\alpha i} &= \mathbf{k}^\alpha \cdot \mathbf{E}_i = \int_{\mathcal{A}} \tau_{\alpha i} dx_1 dx_2, \end{aligned} \quad (7.137)$$

where \mathcal{A} is the cross section of the rod, and $\mathbf{T} = \tau_{ik} \mathbf{E}_i \otimes \mathbf{E}_k$ is the Cauchy stress tensor. Note that $\mathbf{n} = \int_{\mathcal{A}} \mathbf{t} dx_1 dx_2$ and $\mathbf{m}^\alpha = \int_{\mathcal{A}} \mathbf{t} x_\alpha dx_1 dx_2$. Consequently, given the traction \mathbf{t} on the end surfaces, we can easily calculate \mathbf{n} and \mathbf{m}^α .

Exercise 7.3: In the presence of body forces and tractions on the lateral surface of the rod-like body, Green and Naghdi [133] have shown that the longitudinal and lateral displacements of the rod are governed by the following balance laws:

$$\begin{aligned} \frac{\partial n_3}{\partial \xi} + \rho_0 f_3 &= \rho_0 \frac{\partial^2 u_3}{\partial t^2}, \\ \frac{\partial m_{11}}{\partial \xi} - \hat{k}_{11} + \rho_0 l_{11} &= \rho_0 y^{11} \frac{\partial^2 \delta_{11}}{\partial t^2}, \\ \frac{\partial m_{22}}{\partial \xi} - \hat{k}_{22} + \rho_0 l_{22} &= \rho_0 y^{22} \frac{\partial^2 \delta_{22}}{\partial t^2}. \end{aligned} \quad (7.138)$$

In these equations, $\xi = x_3$ is the arc-length parameter of the rod in a fixed reference configuration, ρ_0 is the mass per unit length of ξ , and y^{11} and y^{22} are inertial coefficients. In the balance laws discussed above, certain components of the various forces are present: $n_3 = \mathbf{n} \cdot \mathbf{E}_3$, $f_3 = \mathbf{f} \cdot \mathbf{E}_3$, $m_{11} = \mathbf{m}^1 \cdot \mathbf{E}_1$, $m_{22} = \mathbf{m}^2 \cdot \mathbf{E}_2$, $\hat{k}_{11} = \mathbf{k}^1 \cdot \mathbf{E}_1$, $\hat{k}_{22} = \mathbf{k}^2 \cdot \mathbf{E}_2$, $l_{11} = \mathbf{l}^1 \cdot \mathbf{E}_1$, and $l_{22} = \mathbf{l}^2 \cdot \mathbf{E}_2$.

Assuming a linear isotropic elastic rod-like body with rectangular cross sections, the constitutive equations for the force components n_3 , m_{11} , m_{22} , \hat{k}_{11} , and \hat{k}_{22} are

$$\begin{aligned} m_{11} &= k_{10} \frac{\partial \delta_{11}}{\partial \xi} + k_{17} \frac{\partial \delta_{22}}{\partial \xi}, & m_{22} &= k_{17} \frac{\partial \delta_{11}}{\partial \xi} + k_{11} \frac{\partial \delta_{22}}{\partial \xi}, \\ \hat{k}_{11} &= 4k_1 \delta_{11} + 2k_7 \delta_{22} + 2k_8 \frac{\partial u_3}{\partial \xi}, & \hat{k}_{22} &= 2k_7 \delta_{11} + 4k_2 \delta_{22} + 2k_9 \frac{\partial u_3}{\partial \xi}, \\ n_3 &= 2k_8 \delta_{11} + 2k_9 \delta_{22} + 4k_3 \frac{\partial u_3}{\partial \xi}. \end{aligned} \quad (7.139)$$

For a rectangular rod of mass density ρ_0 , height h (in the \mathbf{E}_2 direction), width w (in the \mathbf{E}_1 direction), Young's modulus E , and Poisson's ratio ν , the coefficients k_1, \dots, k_{17} are summarized in Eqn. (7.35).

- Show that the equations (7.138) can be written as a set of three coupled partial differential equations for u_3 , δ_{11} , and δ_{22} .
- Show that a homogeneous deformation (i.e., one where u_3'' , δ_{11}' , and δ_{22}' vanish) can be supported in the rod given the appropriate traction fields on the ends of the rod.
- Referring to Figure 7.2, consider the following statics problem, which, in the context of circular rods, was first solved by Green, Naghdi, and Wenner [138, Section 9]. A rectangular rod of length ℓ is bonded at $x_3 = 0$ to a rigid surface. At the other end, $x_3 = \ell$, the rod is bonded to a rigid plate so it retains its dimensions and a traction $\sigma\mathbf{E}_3$ is applied. The lateral surface of the rod is free of tractions and there are no body forces. First, show that the boundary conditions are

$$\begin{aligned} u_3(0, t) &= 0, & \delta_{11}(0, t) &= \delta_{22}(0, t) = 0, \\ n_3(\ell, t) &= \sigma A, & \delta_{11}(\ell, t) &= \delta_{22}(\ell, t) = 0. \end{aligned} \quad (7.140)$$

Then, determine the static solution $(u_3, \delta_{11}, \delta_{22})$ to the boundary-value problem.¹⁸

- Assuming that the rod has a square or circular cross section and that $\delta_{11} = \delta_{22}$ for the boundary-value problem considered in (c), show that

$$\delta_{11}\left(\frac{\ell}{2}\right) = \frac{\alpha_1 n_3}{\alpha_2^2} \left(\operatorname{Sech}\left(\frac{\alpha_2 \ell}{2}\right) - 1 \right), \quad (7.141)$$

where

$$\alpha_1 = \frac{k_8}{2k_3k_{10}}, \quad \alpha_2^2 = \frac{4k_3}{k_{10}} \left(1 + \frac{k_7}{2k_3} - \frac{k_8^2}{2k_3^2} \right). \quad (7.142)$$

With the help of Eqn. (7.141) show that a finite $n_3 = \sigma A$ can result in a physically unrealistic deformation of the rod.¹⁹

- Show that by imposing the (linearized) constraints $\delta_{11} = 0$ and $\delta_{22} = 0$, the three partial differential equations you found in (a) simplify to a single differential equation for u_3 and two equations for the two functions λ_1 and λ_2 :

$$\hat{k}_{11} = \lambda_1, \quad \hat{k}_{22} = \lambda_2. \quad (7.143)$$

¹⁸ The general functional form of the solutions for the resulting ordinary differential equations can be found in [251, Eqns. (A4)–(A10)]. For a circular rod, the general solutions for $\delta_{11}(\xi) = \delta_{22}(\xi)$ and $\frac{\partial u_3}{\partial \xi}(\xi)$ are presented in [138, Eqns. (9.16)–(9.18)].

¹⁹ As emphasized in Antman [12], such deformations can be prevented by ensuring that the strain energy function has terms that prohibit unrealistic strains. For the linearized theory under consideration, the strain energy function is such that finite forces can produce physically meaningless results.

Comment on how the single differential equation differs from the wave equation:

$$\frac{E}{\rho} \frac{\partial^2 u}{\partial \xi^2} = \frac{\partial^2 u}{\partial t^2}. \quad (7.144)$$

Exercise 7.4: In the presence of body forces and tractions on the lateral surface of the rod-like body, Green and Naghdi [133] have shown that there are two sets of flexural equations. One of these pertains to flexure in the $\mathbf{E}_3 - \mathbf{E}_1$ plane and the other flexure in the $\mathbf{E}_3 - \mathbf{E}_2$ plane. Both sets of equations are similar, and we only address the former set here.

The balance laws are

$$\begin{aligned} \frac{\partial n_1}{\partial \xi} + \rho_0 f_1 &= \rho_0 \frac{\partial^2 u_1}{\partial t^2}, \\ \frac{\partial m_{13}}{\partial \xi} - \hat{k}_{13} + \rho_0 l_{13} &= \rho_0 y^{11} \frac{\partial^2 \delta_{13}}{\partial t^2}. \end{aligned} \quad (7.145)$$

In these equations, $\xi = x_3$ is the arc-length parameter of the rod in a fixed reference configuration, ρ_0 is the mass per unit length of ξ , and y^{11} is an inertial coefficient. In the balance laws discussed above, certain components of the various forces are present: $n_1 = \mathbf{n} \cdot \mathbf{E}_1$, $f_1 = \mathbf{f} \cdot \mathbf{E}_1$, $m_{13} = \mathbf{m}^1 \cdot \mathbf{E}_3$, $\hat{k}_{13} = \mathbf{k}^1 \cdot \mathbf{E}_3$, and $l_{13} = \mathbf{l}^1 \cdot \mathbf{E}_3$.

Assuming a linear isotropic elastic rod-like body with rectangular cross sections, the constitutive equations for the force components n_1 , m_{13} , and \hat{k}_{13} are

$$m_{13} = k_{16} \frac{\partial \delta_{13}}{\partial \xi}, \quad \hat{k}_{13} = n_1 = k_6 (\delta_{13} + \delta_{31}). \quad (7.146)$$

For a rectangular rod of mass density ρ_0 , height h , width w , Young's modulus E , and Poisson's ratio ν , the coefficients k_6 and k_{16} are presented in Eqn. (7.35).

- (a) Show that $-\delta_{13}$ is the transverse shear deformation of the rod. In addition, show that $-\delta_{13}$ corresponds to a counter-clockwise rotation of the cross section about \mathbf{E}_2 . What situation arises when $\delta_{13} + \delta_{31} = 0$? Similarly, show that $-m_{13}$ can be interpreted as a counter-clockwise moment about \mathbf{E}_2 .
- (b) With the assistance of the constitutive relations, show that the balance laws (7.145) can be written as a set of partial differential equations for u_1 and δ_{13} . Compare these equations to those for a beam theory proposed in [344] in 1921. The equations for Timoshenko's beam theory can be easily found in the literature, e.g., [74, 275, 310], and were presented earlier in Exercise 6.4 on Page 293. It is interesting to note that the linearized equations discussed below follow from balances of linear momentum, director momenta, angular momentum, and energy whereas in the earlier chapter, and in Timoshenko's original work, they follow from a balance of linear momentum, a balance of angular momentum, and a balance of energy.

- (c) Consider the flexural deformation of a rectangular beam of length ℓ which is subject to a gravitational force $-\rho_0 g \mathbf{E}_1$. Show that the static displacements of the beam, assuming that it is cantilevered, are

$$\begin{aligned} u_1(\xi) &= \left(-\frac{\sigma_1}{24} \frac{\xi^3}{\ell^3} + \frac{\sigma_1}{6} \frac{\xi^2}{\ell^2} + \frac{1}{4} (2\sigma_2 - \sigma_1) \frac{\xi}{\ell} - \sigma_2 \right) \xi, \\ \delta_{13}(\xi) &= \left(\frac{\sigma_1}{6} \frac{\xi^2}{\ell^2} - \frac{\sigma_1}{2} \frac{\xi}{\ell} + \frac{\sigma_1}{2} \right) \frac{\xi}{\ell}, \end{aligned} \quad (7.147)$$

where

$$\sigma_1 = \frac{\rho_0 g \ell^3}{EI_2}, \quad \sigma_2 = \frac{2(1+\nu)\rho_0 g \ell}{kEA}. \quad (7.148)$$

In your solution, you should justify the boundary conditions

$$u_1(0,t) = 0, \quad \delta_{13}(0,t) = 0, \quad n_1(\ell,t) = 0, \quad m_{13}(\ell,t) = 0. \quad (7.149)$$

Illustrate your solution with a sketch of the deformed beam (such as that shown in Figure 7.3(c)).

- (d) Consider the flexural deformation of a rectangular beam of length ℓ which is subject to a gravitational force $-\rho_0 g \mathbf{E}_1$. Show that the static displacements of the beam, assuming that it is clamped at both ends, are

$$\begin{aligned} u_1(\xi) &= \left(-\frac{\sigma_1}{24} \frac{\xi^3}{\ell^3} + \frac{\sigma_1}{12} \frac{\xi^2}{\ell^2} + \frac{1}{24} (12\sigma_2 - \sigma_1) \frac{\xi}{\ell} - \frac{\sigma_2}{2} \right) \xi, \\ \delta_{13}(\xi) &= \left(\frac{\sigma_1}{6} \frac{\xi^2}{\ell^2} - \frac{\sigma_1}{4} \frac{\xi}{\ell} + \frac{\sigma_1}{12} \right) \frac{\xi}{\ell}. \end{aligned} \quad (7.150)$$

In your solution, you should justify the boundary conditions:

$$u_1(0,t) = 0, \quad \delta_{13}(0,t) = 0, \quad u_1(\ell,t) = 0, \quad \delta_{13}(\ell,t) = 0. \quad (7.151)$$

Illustrate your solution with a sketch of the deformed beam (such as that shown in Figure 7.3(b)).

- (e) Show that imposing the linearized constraints $\delta_{13} = -\delta_{31}$ introduces a Lagrange multiplier,

$$n_1 = \hat{k}_{13} = \lambda, \quad (7.152)$$

which enforces the constraint. If, in addition, rotary inertia is ignored, then the linearized flexural equations from (d) reduce to those for the Bernoulli-Euler beam. Ignoring rotary inertia is equivalent to setting $\rho_0 y^{11} \frac{\partial \ddot{\delta}_{13}}{\partial \xi} = 0$.

Exercise 7.5: In the presence of body forces and tractions on the lateral surface of the rod-like body, and appropriate symmetry conditions on the material and geometry of the rod-like body that the rod is modeling, Green and Naghdi [133, Eqn. (9.23)] have shown that the equations governing the torsional mode of deformation of the rod decouple from the flexural and longitudinal modes. The strains

associated with this mode of deformation are

$$\gamma_{12} = \delta_{12} + \delta_{21}, \quad \kappa_{12} = \frac{\partial \delta_{12}}{\partial \xi}, \quad \kappa_{21} = \frac{\partial \delta_{21}}{\partial \xi}. \quad (7.153)$$

The balance laws for the torsional modes follow from the \mathbf{E}_2 and \mathbf{E}_1 components of the respective balances of director momenta:

$$\begin{aligned} \frac{\partial m_{12}}{\partial \xi} - \hat{k}_{12} + \rho_0 l_{12} &= \rho_0 y^{11} \frac{\partial^2 \delta_{12}}{\partial t^2}, \\ \frac{\partial m_{21}}{\partial \xi} - \hat{k}_{21} + \rho_0 l_{21} &= \rho_0 y^{22} \frac{\partial^2 \delta_{21}}{\partial t^2}. \end{aligned} \quad (7.154)$$

In these equations, $\xi = x_3$ is the arc-length parameter of the rod in a fixed reference configuration, ρ_0 is the mass per unit length of ξ , and y^{11} and y^{22} are inertial coefficients. In the balance laws discussed above, only certain components of the various forces are present: $m_{12} = \mathbf{m}^1 \cdot \mathbf{E}_2$, $m_{21} = \mathbf{m}^1 \cdot \mathbf{E}_2$, $\hat{k}_{12} = \mathbf{k}^1 \cdot \mathbf{E}_2$, $\hat{k}_{21} = \mathbf{k}^2 \cdot \mathbf{E}_1$, $l_{12} = \mathbf{l}^1 \cdot \mathbf{E}_2$, and $l_{21} = \mathbf{l}^2 \cdot \mathbf{E}_1$. The constitutive relations for the pair of contact director forces and intrinsic director forces are

$$\begin{aligned} m_{12} &= k_{12} \kappa_{12} + \frac{1}{2} k_{14} \kappa_{21}, & m_{21} &= k_{13} \kappa_{21} + \frac{1}{2} k_{14} \kappa_{12}, \\ \hat{k}_{12} &= \hat{k}_{21} = \frac{1}{2} k_4 (\gamma_{12} + \gamma_{21}) = k_4 (\delta_{12} + \delta_{21}). \end{aligned} \quad (7.155)$$

The coefficients in these expressions are recorded in Eqn. (7.35):

$$\begin{aligned} I_1 &= \frac{wh^3}{12}, & I_2 &= \frac{hw^3}{12}, \\ k_4 &= \frac{Ewh}{2(1+v)}, & k_{12} &= k_{13} = \frac{E(I_1 + I_2)}{8(1+v)} + \frac{\mathcal{D}}{4}, & k_{14} &= \frac{E(I_1 + I_2)}{4(1+v)} - \frac{\mathcal{D}}{2}, \end{aligned} \quad (7.156)$$

and

$$\mathcal{D} \approx k_4 \ell_1^2 \left(\frac{1}{3} - 0.21 \left(\frac{\ell_1}{\ell_2} \right) \left(1 - \frac{\ell_1^4}{12\ell_2^4} \right) \right), \quad (7.157)$$

where $\ell_1 = \min(h, w)$ and $\ell_2 = \max(h, w)$.

- (a) Explain why $\delta_{12} - \delta_{21}$ can be considered as a torsional deformation while the displacement $\delta_{12} + \delta_{21}$ can be considered as a shearing of the cross section of the rod.
- (b) Show that the equations governing the static behavior of δ_{12} and δ_{21} can be expressed in the form

$$\begin{aligned} \left(k_{12} - \frac{k_{14}}{2} \right) (\delta''_{12} - \delta''_{21}) + \rho_0 (l_{12} - l_{21}) &= 0, \\ \left(k_{12} + \frac{k_{14}}{2} \right) (\delta''_{12} + \delta''_{21}) + 2k_4 (\delta_{12} + \delta_{21}) + \rho_0 (l_{12} + l_{21}) &= 0, \end{aligned} \quad (7.158)$$

where the $'$ denotes $\frac{\partial}{\partial \xi}$. Determine the general solutions $\delta_{12}(\xi)$ and $\delta_{21}(\xi)$ to Eqn. (7.158) in the absence of tractions on the lateral surface and body forces.

- (c) Argue that $\delta = \delta_{12} - \delta_{21}$ is a measure of the torsional deformation of the rod and show that the equation governing the torsional vibrations of a rod with a square cross section can be expressed as

$$\mathcal{D}\ddot{\delta}'' + \rho_0 (l_{12} - l_{21}) = \frac{\rho_0 w^2}{12} \ddot{\delta}, \quad (7.159)$$

where the superposed dot denotes $\frac{\partial}{\partial t}$.

- (d) For the three examples shown in Figure 5.9 on Page 209, determine the corresponding contributions to $\rho_0 l_{12}$ and $\rho_0 l_{21}$. For a rod of length ℓ that is clamped at both ends, determine $\delta_{12}(\xi)$ and $\delta_{21}(\xi)$ for one of three examples.

Part III

Background Material

Chapter 8

A Rapid Review of Some Elements of Continuum Mechanics

“There are analogs of the energy-momentum tensor in branches of continuum mechanics other than the theory of elasticity. Some of them might repay investigation.”

J. D. Eshelby [103, Page 113]. His remarks foreshadow the use of the material force C in one-dimensional continua.

8.1 Introduction

Our interest lies in the application of one-dimensional theories of matter to various problems and the analysis of the resulting models. One central issue that arises at the onset is the development of a suitable model from a wide range of possible choices. Partially as a result of historical and pedagogical developments, it is often not transparent how various beam, rod, and cable theories can be considered in the context of continuum mechanics of three-dimensional continua. One of the goals of this textbook is to make these connections transparent. Fortunately, we have plenty of help and guidance from the literature to achieve this goal (see, e.g., [12, 137, 147, 243, 309]).

In this chapter, we review some needed background from continuum mechanics. Most of the kinematics we cover are standard and can be found in many introductory texts on continuum mechanics (such as Gurtin [147]). We supplement the kinematics with details on convected coordinates from a seminal textbook by Green and Zerna [140]. These coordinates play a key role in deriving rod and string theories from three-dimensional continuum mechanics and they also serve to illuminate the role played by various stress tensors. We then turn to a discussion of the balance laws and constitutive relations for the stress tensors. The chapter closes with a discussion of superposed rigid body motions, constraints, and a material (configurational) force balance. As discussed in Chapters 2, 4, and 5, the counterpart of the material force

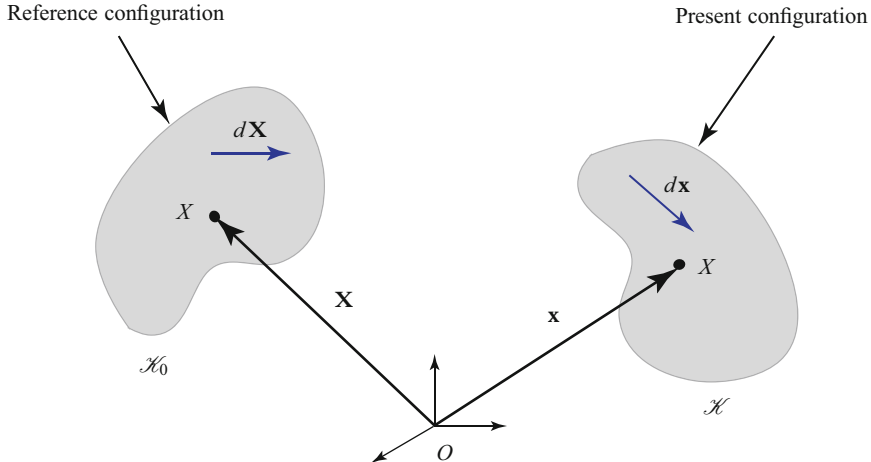


Fig. 8.1 The reference \mathcal{K}_0 and present \mathcal{K} configurations of a body \mathcal{B} .

balance for one-dimensional continua, such as strings and rods, plays a key role in solving problems where a discontinuity is present in the motion and often yields a useful conservation law in others.

8.2 Some Kinematical Results

Consider a body \mathcal{B} and let \mathcal{K}_0 and \mathcal{K} denote its reference and present configurations, respectively (see Figure 8.1). Here, we define a body \mathcal{B} to be a collection of material points X . For the present purposes, this collection of material points is fixed. The reference configuration occupies a fixed region of three-dimensional Euclidean space \mathbb{E}^3 and the position vector of a material point X in this configuration is denoted by $\mathbf{X} = \mathbf{R}^*$. The position vector of the same material point in the subset of \mathbb{E}^3 known as the present configuration \mathcal{K} is denoted by $\mathbf{x} = \mathbf{r}^*$.

The motion of \mathcal{B} is denoted by the vector-valued function

$$\mathbf{x} = \boldsymbol{\chi}(\mathbf{X}, t). \quad (8.1)$$

We also have the deformation gradient \mathbf{F} of this motion:

$$\mathbf{F} = \text{Grad}(\boldsymbol{\chi}). \quad (8.2)$$

This second-order tensor can also be viewed as a linear transformation of vectors $d\mathbf{X}$ which are tangent to material curves in \mathcal{K}_0 to their counterparts $d\mathbf{x}$ in the present configuration \mathcal{K} :

$$d\mathbf{x} = \mathbf{F} d\mathbf{X}. \quad (8.3)$$

We shall assume that \mathbf{F} preserves orientation and is invertible:

$$J = \det(\mathbf{F}) > 0. \quad (8.4)$$

The positiveness of J ensures that the motion is orientation preserving.

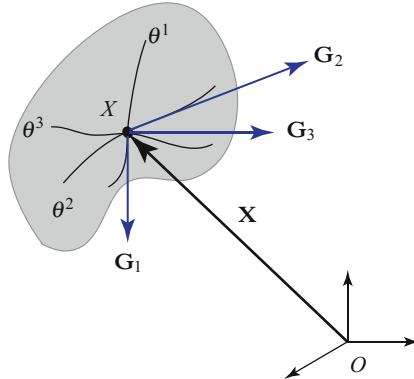


Fig. 8.2 The curvilinear coordinate system that is used to identify material points in the reference configuration.

8.2.1 Curvilinear Coordinates

Motivated by Green and Zerna [140], it is convenient to define a set of curvilinear coordinates $\{\theta^i\}$ which uniquely identify material points in \mathcal{K}_0 . That is, we assume that the curvilinear coordinates and their Cartesian counterparts are related by invertible functions:

$$\theta^k = \theta^k(X_1, X_2, X_3), \quad (8.5)$$

where $X_i = \mathbf{X} \cdot \mathbf{E}_i$. It follows from this assumption that any function $f = f(X_1, X_2, X_3)$ can be expressed as an equivalent function of the curvilinear coordinates: $f = \hat{f}(\theta^1, \theta^2, \theta^3)$. In particular,

$$\mathbf{X} = \mathbf{R}^*(\theta^1, \theta^2, \theta^3) = \mathbf{R}^*(\theta^i). \quad (8.6)$$

A schematic of such a coordinate system and its coordinate curves is shown in Figure 8.2. Where confusion may arise, we ornament quantities associated with three-dimensional fields with an asterisk so as to distinguish them from their one-dimensional counterparts: e.g., $\mathbf{R}(\xi)$ and $\mathbf{R}^*(\theta^1, \theta^2, \theta^3)$.

We define the covariant vectors associated with this coordinate system in \mathcal{K}_0 :

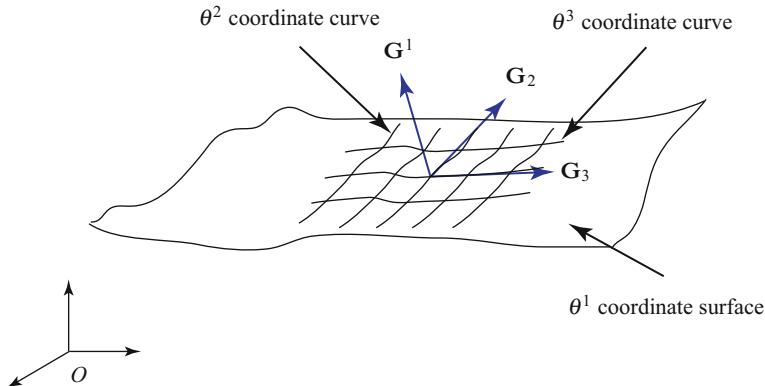


Fig. 8.3 Schematic of a θ^1 coordinate surface which is foliated by θ^2 and θ^3 coordinate curves. The vector \mathbf{G}^1 is normal to the θ^1 coordinate surface, while the vectors \mathbf{G}_2 and \mathbf{G}_3 are tangent to this surface.

$$\mathbf{G}_i = \frac{\partial \mathbf{R}^*}{\partial \theta^i} = \frac{\partial X_1}{\partial \theta^i} \mathbf{E}_1 + \frac{\partial X_2}{\partial \theta^i} \mathbf{E}_2 + \frac{\partial X_3}{\partial \theta^i} \mathbf{E}_3. \quad (8.7)$$

These vectors are tangent to their respective coordinate curves. For example, the vector \mathbf{G}_2 is tangent to a θ^2 coordinate curve. We also define the three dual or contravariant vectors \mathbf{G}^k :

$$\mathbf{G}^k = \text{Grad}(\theta^k) = \frac{\partial \theta^k}{\partial X_1} \mathbf{E}_1 + \frac{\partial \theta^k}{\partial X_2} \mathbf{E}_2 + \frac{\partial \theta^k}{\partial X_3} \mathbf{E}_3. \quad (8.8)$$

With the help of the chain rule, it is possible to show that

$$\mathbf{G}^k \cdot \mathbf{G}_i = \delta_i^k, \quad (8.9)$$

where δ_i^k is the Kronecker delta: $\delta_1^1 = \delta_2^2 = \delta_3^3 = 1$ and $\delta_2^1 = \delta_1^2 = \delta_2^3 = \dots = 0$. It follows that \mathbf{G}^k is normal to a θ^k coordinate surface (see Figure 8.3). In addition, solving the nine equations (8.9) for the nine components of the contravariant vectors, we find the well-known results

$$\mathbf{G}^1 = \frac{1}{\sqrt{G}} \mathbf{G}_2 \times \mathbf{G}_3, \quad \mathbf{G}^2 = \frac{1}{\sqrt{G}} \mathbf{G}_3 \times \mathbf{G}_1, \quad \mathbf{G}^3 = \frac{1}{\sqrt{G}} \mathbf{G}_1 \times \mathbf{G}_2, \quad (8.10)$$

where

$$\sqrt{G} = (\mathbf{G}_1 \times \mathbf{G}_2) \cdot \mathbf{G}_3. \quad (8.11)$$

It follows from the expressions (8.10) that

$$\frac{1}{\sqrt{G}} = (\mathbf{G}^1 \times \mathbf{G}^2) \cdot \mathbf{G}^3. \quad (8.12)$$

The set of vectors $\{\mathbf{G}_1, \mathbf{G}_2, \mathbf{G}_3\}$ form a basis for \mathbb{E}^3 which is known as a covariant basis. Similarly, the set $\{\mathbf{G}^1, \mathbf{G}^2, \mathbf{G}^3\}$ form a contravariant basis for \mathbb{E}^3 . All of the six vectors in these sets are not necessarily of unit magnitude and some of the vectors may depend on θ^1, θ^2 , and θ^3 .

As illustrative examples, consider the Cartesian coordinate system $\theta^k = x^k$:

$$\mathbf{G}_k = \mathbf{E}_k, \quad \mathbf{G}^j = \mathbf{E}_j, \quad (j, k = 1, 2, 3). \quad (8.13)$$

A more interesting example is the spherical polar coordinate system (R, φ, ϑ) :

$$R = \sqrt{x_1^2 + x_2^2 + x_3^2}, \quad \tan(\varphi) = \frac{\sqrt{x_2^2 + x_3^2}}{x_1}, \quad \tan(\vartheta) = \frac{x_2}{x_1}. \quad (8.14)$$

Whence,

$$\begin{aligned} \mathbf{G}_1 &= \mathbf{e}_R = \frac{1}{\sqrt{x_1^2 + x_2^2 + x_3^2}} (x_1 \mathbf{E}_1 + x_2 \mathbf{E}_2 + x_3 \mathbf{E}_3), \\ \mathbf{G}_2 &= R \mathbf{e}_\varphi = R \cos(\varphi) (\cos(\vartheta) \mathbf{E}_1 + \sin(\vartheta) \mathbf{E}_2) - R \sin(\varphi) \mathbf{E}_3, \\ \mathbf{G}_3 &= R \sin(\varphi) \mathbf{e}_\vartheta = R \sin(\varphi) (\cos(\vartheta) \mathbf{E}_2 - \sin(\vartheta) \mathbf{E}_1), \end{aligned} \quad (8.15)$$

and

$$\mathbf{G}^1 = \mathbf{G}_1, \quad \mathbf{G}^2 = \frac{1}{R^2} \mathbf{G}_2, \quad \mathbf{G}^3 = \frac{1}{R^2 \sin^2(\varphi)} \mathbf{G}_3. \quad (8.16)$$

For this coordinate system, $G = R^4 \sin^2(\varphi)$.

Any vector \mathbf{b} can be expressed as a linear combination of either the covariant or contravariant basis vectors:

$$\mathbf{b} = \sum_{i=1}^3 b^i \mathbf{G}_i = \sum_{k=1}^3 b_k \mathbf{G}^k. \quad (8.17)$$

To calculate the components, we note that

$$b^k = \mathbf{b} \cdot \mathbf{G}^k, \quad b_i = \mathbf{b} \cdot \mathbf{G}_i. \quad (8.18)$$

For the purposes of introducing the Christoffel symbols, it is useful to define

$$G_{ik} = \mathbf{G}_i \cdot \mathbf{G}_k, \quad G^{ik} = \mathbf{G}^i \cdot \mathbf{G}^k. \quad (8.19)$$

It is straightforward to show that $\sum_{r=1}^3 G_{ir} G^{rk} = \delta_i^k$.

Following [29, 59], we define the connection coefficients γ_{irk} and γ_{ir}^k :

$$\frac{\partial \mathbf{G}_i}{\partial \theta^r} = \sum_{k=1}^3 \gamma_{irk} \mathbf{G}^k = \sum_{k=1}^3 \gamma_{ir}^k \mathbf{G}_k. \quad (8.20)$$

As

$$\frac{\partial \mathbf{G}_i}{\partial \theta^r} = \frac{\partial^2 \mathbf{R}^*}{\partial \theta^r \partial \theta^i} = \frac{\partial \mathbf{G}_r}{\partial \theta^i}, \quad (8.21)$$

these coefficients are identical to the Christoffel symbols,

$$\begin{aligned} \Gamma_{irk} &= \frac{1}{2} \left(\frac{\partial G_{ik}}{\partial \theta^r} + \frac{\partial G_{rk}}{\partial \theta^i} - \frac{\partial G_{ir}}{\partial \theta^k} \right), \\ \Gamma_{ir}^k &= \sum_{s=1}^3 G^{ks} \Gamma_{irs}, \end{aligned} \quad (8.22)$$

respectively, that can be found in classic texts on differential geometry, such as [234, 325, 328], and texts on continuum mechanics, such as [140].¹

The gradient of a scalar-valued function $f = f(\theta^1, \theta^2, \theta^3)$ and the gradient of a vector-valued function $\mathbf{f} = \mathbf{f}(\theta^1, \theta^2, \theta^3)$ are defined as

$$\text{Grad}(f) = \sum_{i=1}^3 \frac{\partial f}{\partial \theta^i} \mathbf{G}^i, \quad \text{Grad}(\mathbf{f}) = \sum_{i=1}^3 \frac{\partial \mathbf{f}}{\partial \theta^i} \otimes \mathbf{G}^i. \quad (8.23)$$

Expressing \mathbf{f} in terms of its covariant or contravariant components and expanding the partial derivatives $\frac{\partial \mathbf{f}}{\partial \theta^i}$, an expression for $\text{Grad}(\mathbf{f})$ containing the connection coefficients (8.20) can be established.

8.2.2 A Material Curve

Consider a curve \mathcal{C} which is parameterized by $u \in [u_0, u_1]$ in \mathcal{X}_0 . That is, on this curve

$$\theta^i = \theta^i(u). \quad (8.24)$$

The length of \mathcal{C} is obtained by evaluating the following integral:

$$\begin{aligned} s(u_1) - s(u_0) &= \int_{u_0}^{u_1} \sqrt{\mathbf{G} \cdot \mathbf{G}} du \\ &= \int_{u_0}^{u_1} \sqrt{\sum_{i=1}^3 \sum_{k=1}^3 \frac{\partial \theta^i}{\partial u} \frac{\partial \theta^k}{\partial u} (\mathbf{G}_i \cdot \mathbf{G}_k)} du, \end{aligned} \quad (8.25)$$

where $\mathbf{G} = \sum_{i=1}^3 \frac{\partial \theta^i}{\partial u} \mathbf{G}_i$ is a tangent vector to \mathcal{C} . As we shall shortly observe, we can use the coordinates θ^i to readily parameterize this material curve in the present configuration \mathcal{X} .

¹ For the Euler basis vectors and dual Euler basis vectors that are discussed in Section 5.3.1 of Chapter 5, because $\frac{\partial \mathbf{e}_1}{\partial \alpha^3} \neq \frac{\partial \mathbf{e}_3}{\partial \alpha^1}$, some of the associated connection coefficients may differ from the corresponding Christoffel symbols. This is a property that the 3-2-3 set of Euler angles has in common with all of the other sets of Euler angles.

8.2.3 Metric Tensors and Identities

The determinant G of the metric tensor $[G_{ij}] = [\mathbf{G}_i \cdot \mathbf{G}_j]$ can be calculated using the identity²

$$\sqrt{G} = [\mathbf{G}_1, \mathbf{G}_2, \mathbf{G}_3]. \quad (8.26)$$

To see this result, you may wish to note that the identity tensor has the representations

$$\mathbf{I} = \sum_{i=1}^3 \mathbf{G}_i \otimes \mathbf{G}^i = \sum_{k=1}^3 \mathbf{G}^k \otimes \mathbf{G}_k = \sum_{i=1}^3 \sum_{j=1}^3 G^{ij} \mathbf{G}_i \otimes \mathbf{G}_j = \sum_{n=1}^3 \sum_{m=1}^3 G_{nm} \mathbf{G}^n \otimes \mathbf{G}^m, \quad (8.27)$$

and the determinant of any tensor \mathbf{A} satisfies the identity

$$[\mathbf{A}\mathbf{a}, \mathbf{A}\mathbf{b}, \mathbf{A}\mathbf{c}] = \det(\mathbf{A}) [\mathbf{a}, \mathbf{b}, \mathbf{c}], \quad (8.28)$$

where \mathbf{a} , \mathbf{b} , and \mathbf{c} are any three vectors. The tensor product \otimes that we use throughout this book is defined as follows:

$$(\mathbf{a} \otimes \mathbf{b}) \mathbf{c} = \mathbf{a} (\mathbf{b} \cdot \mathbf{c}), \quad (8.29)$$

for all vectors \mathbf{a} , \mathbf{b} , and \mathbf{c} .

8.2.4 Convected Coordinates

When the θ^i coordinate curves are identified with material curves in \mathcal{B} , then the θ^i coordinate system is said to be a convected (or material) coordinate system. We henceforth assume that this is the case. If a particle \bar{X} has coordinates $\bar{\theta}^i$ in \mathcal{K}_0 , then it can be identified with these same coordinates in \mathcal{K} :

$$\bar{\mathbf{x}} = \boldsymbol{\chi}(\bar{\mathbf{X}}, t) = \mathbf{r}^*(\bar{\theta}^1, \bar{\theta}^2, \bar{\theta}^3, t). \quad (8.30)$$

Needless to say the images of the θ^i coordinate curves in \mathcal{K} can be very intricate and a simple example is shown in Figure 8.4.

Associated with the convected coordinates, we define the following sets of covariant \mathbf{g}_i and contravariant \mathbf{g}^k bases vectors:

$$\mathbf{g}_i = \frac{\partial \mathbf{r}^*}{\partial \theta^i}, \quad (8.31)$$

and

$$\mathbf{g}^1 = \frac{1}{\sqrt{g}} \mathbf{g}_2 \times \mathbf{g}_3, \quad \mathbf{g}^2 = \frac{1}{\sqrt{g}} \mathbf{g}_3 \times \mathbf{g}_1, \quad \mathbf{g}^3 = \frac{1}{\sqrt{g}} \mathbf{g}_1 \times \mathbf{g}_2, \quad (8.32)$$

² Here, $[\mathbf{G}_1, \mathbf{G}_2, \mathbf{G}_3]$ denotes the scalar triple product $\mathbf{G}_1 \cdot (\mathbf{G}_2 \times \mathbf{G}_3)$.

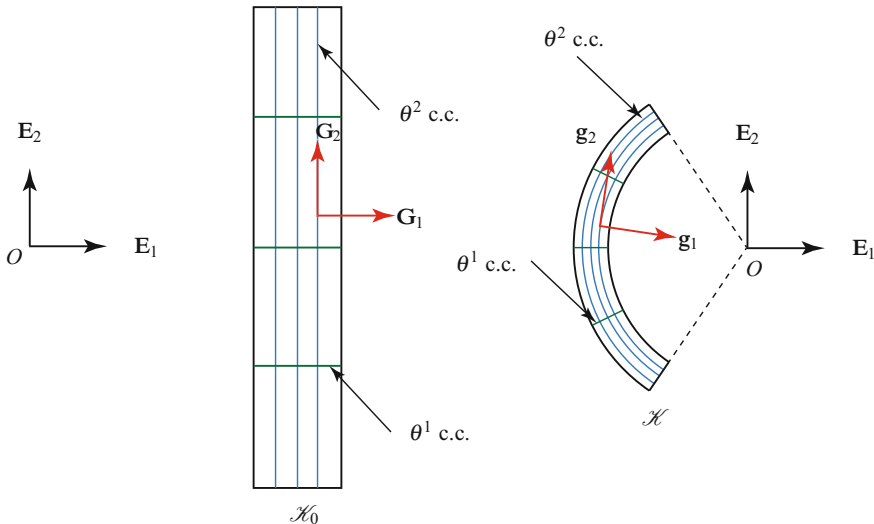


Fig. 8.4 Reference \mathcal{H}_0 and present \mathcal{H} configurations of a parallelepiped that is being deformed into a state of pure flexure. The abbreviation c.c. stands for coordinate curve. This problem is discussed in a seminal work by Rivlin [302, Sections 14–16] and the text by Green and Zerna [140, Section 3.11].

where, paralleling the definition of \sqrt{G} ,

$$\sqrt{g} = (\mathbf{g}_1 \times \mathbf{g}_2) \cdot \mathbf{g}_3. \quad (8.33)$$

It is a good exercise to consider the parallels in the representations involving \mathbf{g}^i and \mathbf{g}_k for the arc-length of a material curve in \mathcal{H} and the identity tensor \mathbf{I} (cf. Eqns. (8.25) and (8.27)). In addition, one can define Christoffel symbols and connection coefficients for these basis vectors.

We now turn to some very useful representations for tensors that are widely employed in continuum mechanics. First, consider the deformation gradient tensor \mathbf{F} . Recall that $\mathbf{x} = \mathbf{r}^*(\theta^1, \theta^2, \theta^3, t)$. Now, with the help of the definition (8.23),

$$\begin{aligned} \mathbf{F} &= \text{Grad}(\mathbf{r}^*) \\ &= \sum_{i=1}^3 \frac{\partial \mathbf{r}^*}{\partial \theta^i} \otimes \mathbf{G}^i \\ &= \sum_{i=1}^3 \mathbf{g}_i \otimes \mathbf{G}^i. \end{aligned} \quad (8.34)$$

From this representation, it follows that

$$\mathbf{g}_i = \mathbf{F} \mathbf{G}_i, \quad \mathbf{g}^i = \mathbf{F}^{-T} \mathbf{G}^i, \quad (8.35)$$

where $\mathbf{F}^{-1} = \mathbf{G}_1 \otimes \mathbf{g}^1 + \mathbf{G}_2 \otimes \mathbf{g}^2 + \mathbf{G}_3 \otimes \mathbf{g}^3$. A graphical summary of the transformations induced by \mathbf{F} and \mathbf{F}^{-T} is presented in Figure 8.5.

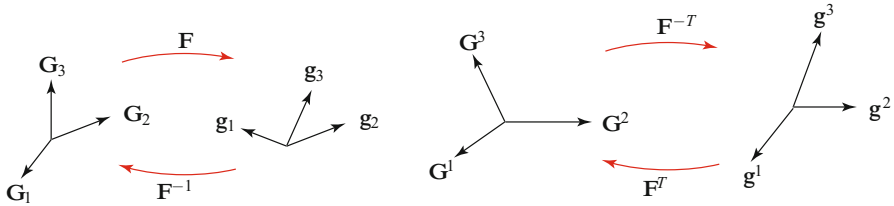


Fig. 8.5 Graphical representations of the transformations induced by \mathbf{F} and \mathbf{F}^{-T} and their inverses.

The representation for \mathbf{F} results in the following representations for the right Cauchy-Green strain tensor \mathbf{C} , the left Cauchy-Green strain tensor \mathbf{B} , the Lagrangian strain tensor \mathbf{E} , the determinant of \mathbf{F} , and the adjugate of \mathbf{F} :

$$\begin{aligned}\mathbf{C} &= \mathbf{F}^T \mathbf{F} = \sum_{i=1}^3 \sum_{k=1}^3 (\mathbf{g}_i \cdot \mathbf{g}_k) \mathbf{G}^i \otimes \mathbf{G}^k, \\ \mathbf{B} &= \mathbf{F} \mathbf{F}^T = \sum_{i=1}^3 \sum_{k=1}^3 (\mathbf{G}^i \cdot \mathbf{G}^k) \mathbf{g}_i \otimes \mathbf{g}_k, \\ \mathbf{E} &= \frac{1}{2} (\mathbf{C} - \mathbf{I}) = \sum_{i=1}^3 \sum_{k=1}^3 \frac{1}{2} (\mathbf{g}_i \cdot \mathbf{g}_k - \mathbf{G}_i \cdot \mathbf{G}_k) \mathbf{G}^i \otimes \mathbf{G}^k, \\ J &= \det(\mathbf{F}) = \frac{\sqrt{g}}{\sqrt{G}}, \\ \mathbf{F}^A &= J \mathbf{F}^{-T} = \sum_{i=1}^3 \frac{\sqrt{g}}{\sqrt{G}} \mathbf{g}^i \otimes \mathbf{G}_i.\end{aligned}\tag{8.36}$$

In the last of these results, \mathbf{F}^A denotes the adjugate of \mathbf{F} . It is easy to show from the representations listed above that $\det(\mathbf{C}) = \det(\mathbf{B}) = g/G$.

The adjugate of \mathbf{F} plays a key role in Nanson's formula:

$$\mathbf{n} d\mathbf{a} = \mathbf{F}^A \mathbf{N} dA.\tag{8.37}$$

Here, \mathbf{n} is the unit normal at a point on a material surface $F(\theta^1, \theta^2, \theta^3) = 0$ in \mathcal{K} , and \mathbf{N} is the unit normal at the same point of the corresponding surface in \mathcal{K}_0 . An example of such a material surface can be seen in Figure 8.6. For the material surface $\theta^3 = \xi_2$ in the reference configuration \mathcal{K}_0 , the area element $N dA$ has the representation

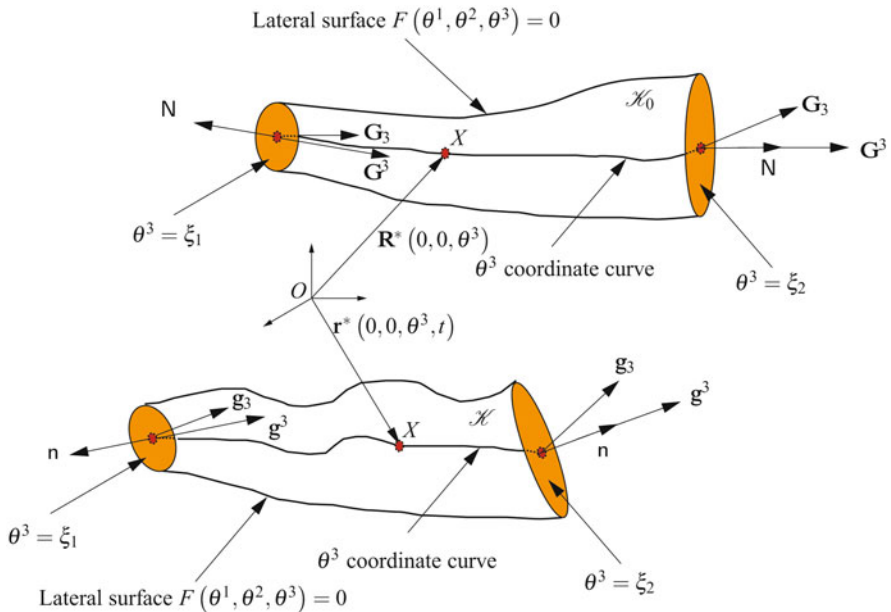


Fig. 8.6 Schematic of the reference \mathcal{K}_0 and present \mathcal{K} configurations of a rod-like body whose reference configuration is parameterized using a curvilinear coordinate system. The ends of the body are described using θ^3 coordinate surfaces, the centerline is described as a θ^3 coordinate curve where $\theta^1 = \theta^2 = 0$, and the lateral surface of the body is described using the function $F(\theta^1, \theta^2, \theta^3) = 0$.

$$\begin{aligned} NdA &= \frac{\partial \mathbf{R}^*}{\partial \theta^1}(\theta^1, \theta^2, \xi_2) d\theta^1 \times \frac{\partial \mathbf{R}^*}{\partial \theta^2}(\theta^1, \theta^2, \xi_2) d\theta^2 \\ &= \mathbf{G}_1(\theta^1, \theta^2, \xi_2) \times \mathbf{G}_2(\theta^1, \theta^2, \xi_2) d\theta^1 d\theta^2 \\ &= \mathbf{G}^3(\theta^1, \theta^2, \xi_2) \sqrt{G(\theta^1, \theta^2, \xi_2)} d\theta^1 d\theta^2. \end{aligned} \quad (8.38)$$

Paralleling (8.38), the area element nda in the present configuration for the material surface $\theta^3 = \xi_2$ has the representation

$$nda = \mathbf{g}^3(\theta^1, \theta^2, \xi_2) \sqrt{g(\theta^1, \theta^2, \xi_2)} d\theta^1 d\theta^2. \quad (8.39)$$

It is a useful exercise to verify how these representations for NdA and nda are in compliance with Nanson's formula.

8.3 Stress Tensors and Divergences

We next recall four stress tensors: the Cauchy stress tensor \mathbf{T} , the first Piola-Kirchhoff stress tensor \mathbf{P} , the nominal stress tensor Σ , and the second Piola-Kirchhoff stress tensor \mathbf{S} (see, e.g., [55, 147]). These four tensors are related:

$$\begin{aligned}\mathbf{P} &= \mathbf{T}\mathbf{F}^A, \\ \Sigma &= \mathbf{F}^{-1}\mathbf{P}\mathbf{F}^T = \mathbf{P}^T, \\ \mathbf{S} &= \mathbf{F}^{-1}\mathbf{P} = J\mathbf{F}^{-1}\mathbf{T}\mathbf{F}^{-T}.\end{aligned}\tag{8.40}$$

To see these definitions in a different light, let the Cauchy stress tensor have the representation

$$\mathbf{T} = \sum_{i=1}^3 \sum_{k=1}^3 \tau^{ik} \mathbf{g}_i \otimes \mathbf{g}_k.\tag{8.41}$$

Then,

$$\begin{aligned}J^{-1}\mathbf{P} &= \sum_{i=1}^3 \sum_{k=1}^3 \tau^{ik} \mathbf{g}_i \otimes \mathbf{G}_k, & J^{-1}\Sigma &= \sum_{i=1}^3 \sum_{k=1}^3 \tau^{ik} \mathbf{G}_k \otimes \mathbf{g}_i, \\ J^{-1}\mathbf{S} &= \sum_{i=1}^3 \sum_{k=1}^3 \tau^{ik} \mathbf{G}_i \otimes \mathbf{G}_k.\end{aligned}\tag{8.42}$$

Observe that the tensors have the same components and “legs” in different configurations: \mathbf{S} has both “legs” in \mathcal{H}_0 , \mathbf{T} has both “legs” in \mathcal{H} , and \mathbf{P} and Σ have one “leg” in \mathcal{H}_0 and the other in \mathcal{H} .

The representations of the stress tensors using the covariant basis vectors also illuminate the role played by a traction vector \mathbf{T}^i that was first introduced by Green and Zerna [140]³:

$$\begin{aligned}\mathbf{T}^i &= \sqrt{g} \mathbf{T} \mathbf{g}^i = \sum_{k=1}^3 \sqrt{g} \tau^{ki} \mathbf{g}_k \\ &= \sqrt{G} \mathbf{P} \mathbf{G}^i \\ &= \sqrt{G} \mathbf{F} \mathbf{S} \mathbf{G}^i.\end{aligned}\tag{8.43}$$

To further elaborate on \mathbf{T}^i and the role it plays in formulating the governing equations for rods and strings, consider the material surface \mathcal{A} defined by $\theta^3 = \xi_2$ that is shown in Figure 8.6. Suppose that a traction vector \mathbf{t} acts on this surface. From Cauchy’s lemma [55, 147], we know that $\mathbf{t} = \mathbf{T}\mathbf{n}$, where \mathbf{n} is the outward normal. Using Eqn. (8.39), the resultant force acting on this surface can be computed⁴:

³ Green and Zerna use the notation \mathbf{T}_i for these vectors. Our notation follows later papers by Green and Naghdi [133, 135, 137, 138]. As will shortly become apparent, the vector \mathbf{T}^i has similarities to the vector $\mathbf{t} = \mathbf{T}\mathbf{n}$ acting on a surface whose unit outward normal is \mathbf{n} .

⁴ Observe that $da \neq d\theta^1 d\theta^2$.

$$\begin{aligned}
\int_{\mathcal{A}} \mathbf{t} da &= \int_{\mathcal{A}} \mathbf{T} n da \\
&= \int_{\mathcal{A}} \mathbf{T} \mathbf{g}^3(\theta^1, \theta^2, \xi_2) \sqrt{g(\theta^1, \theta^2, \xi_2)} d\theta^1 d\theta^2 \\
&= \int_{\mathcal{A}} \mathbf{T}^3(\theta^1, \theta^2, \xi_2) d\theta^1 d\theta^2.
\end{aligned} \tag{8.44}$$

Concomitantly,

$$\mathbf{T}^1 = \mathbf{T}(\mathbf{g}_2 \times \mathbf{g}_3), \quad \mathbf{T}^2 = \mathbf{T}(\mathbf{g}_3 \times \mathbf{g}_1). \tag{8.45}$$

The elegance of the representation (8.44) is remarkable and it is often used to establish a representation for the contact force \mathbf{n} in rod and string theories. We leave it as an exercise to show that the corresponding representation for the referential traction vector $\mathbf{p} = \mathbf{P}\mathbf{n}$ is $\int_{\mathcal{A}} \mathbf{p} dA = \int_{\mathcal{A}} \mathbf{T}^3(\theta^1, \theta^2, \xi_2) d\theta^1 d\theta^2$.

8.3.1 Divergences

In the balance laws for a continuum, one finds a pair of distinct divergences of a tensor:

$$\text{Div}(\mathbf{P}) = \sum_{k=1}^3 \frac{\partial \mathbf{P}}{\partial \theta^k} \mathbf{G}^k, \quad \text{div}(\mathbf{T}) = \sum_{k=1}^3 \frac{\partial \mathbf{T}}{\partial \theta^k} \mathbf{g}^k. \tag{8.46}$$

To motivate these representations, we first consider a pair of gradient operators:

$$\text{grad}(a) = \nabla(a) = \sum_{r=1}^3 \mathbf{g}^r \frac{\partial a}{\partial \theta^r}, \quad \text{Grad}(a) = \nabla_0(a) = \sum_{r=1}^3 \mathbf{G}^r \frac{\partial a}{\partial \theta^r}, \tag{8.47}$$

where a is an arbitrary differentiable scalar-valued function. For any vector \mathbf{c} , we use the aforementioned gradient operators to define the divergences of a vector:

$$\text{Div}(\mathbf{c}) = \nabla_0 \cdot \mathbf{c} = \sum_{k=1}^3 \mathbf{G}^k \cdot \frac{\partial \mathbf{c}}{\partial \theta^k}, \quad \text{div}(\mathbf{c}) = \nabla \cdot \mathbf{c} = \sum_{k=1}^3 \mathbf{g}^k \cdot \frac{\partial \mathbf{c}}{\partial \theta^k}. \tag{8.48}$$

Following the treatment in Gurtin [147, Section 4], we next employ the definition (8.48) to define the divergences of a tensor \mathbf{H} :

$$\mathbf{a} \cdot \text{div}(\mathbf{H}) = \text{div}(\mathbf{H}^T \mathbf{a}), \quad \mathbf{a} \cdot \text{Div}(\mathbf{H}) = \text{Div}(\mathbf{H}^T \mathbf{a}), \tag{8.49}$$

where \mathbf{a} is any constant vector. This final step sets the stage to use Eqn. (8.49) to establish Eqn. (8.46). For example,

$$\begin{aligned}
\mathbf{a} \cdot \operatorname{div}(\mathbf{H}) &= \operatorname{div}(\mathbf{H}^T \mathbf{a}) \\
&= \sum_{r=1}^3 \mathbf{g}^r \cdot \frac{\partial}{\partial \theta^r} (\mathbf{H}^T \mathbf{a}) \\
&= \sum_{r=1}^3 \mathbf{g}^r \cdot \left(\frac{\partial \mathbf{H}^T}{\partial \theta^r} \mathbf{a} \right) \\
&= \sum_{r=1}^3 \left(\frac{\partial \mathbf{H}}{\partial \theta^r} \mathbf{g}^r \right) \cdot \mathbf{a}.
\end{aligned} \tag{8.50}$$

We used the property of the transpose of a second-order tensor $(\mathbf{A}\mathbf{b}) \cdot \mathbf{a} = \mathbf{b} \cdot (\mathbf{A}^T \mathbf{a})$ to manipulate the previous expression. As a consequence of the earlier manipulations, we can conclude that

$$\left(\operatorname{div}(\mathbf{H}) - \sum_{r=1}^3 \left(\frac{\partial \mathbf{H}}{\partial \theta^r} \mathbf{g}^r \right) \right) \cdot \mathbf{a} = 0. \tag{8.51}$$

As this result is true for all \mathbf{a} and the term inside the parentheses is independent of \mathbf{a} , we find that

$$\operatorname{div}(\mathbf{H}) = \sum_{r=1}^3 \frac{\partial \mathbf{H}}{\partial \theta^r} \mathbf{g}^r. \tag{8.52}$$

As expected, this result agrees with Eqn. (8.46)₂. A parallel derivation applies for Eqn. (8.46)₁.

8.3.2 The Traction Vector and a Divergence

Using \mathbf{T}^r , one finds very useful representations for the divergences of \mathbf{T} and \mathbf{P} . To see these results, we need to perform some lengthy but straightforward manipulations:

$$\begin{aligned}
\operatorname{div}(\mathbf{T}) &= \sum_{r=1}^3 \sum_{i=1}^3 \frac{\partial}{\partial \theta^r} \left(\frac{1}{\sqrt{g}} \mathbf{T}^i \otimes \mathbf{g}_i \right) \mathbf{g}^r \\
&= \sum_{r=1}^3 \sum_{i=1}^3 \frac{(\mathbf{g}_i \cdot \mathbf{g}^r)}{\sqrt{g}} \frac{\partial \mathbf{T}^i}{\partial \theta^r} + \sum_{i=1}^3 \mathbf{T}^i \underbrace{\left(\sum_{r=1}^3 \left(\frac{\partial}{\partial \theta^r} \left(\frac{\mathbf{g}_i}{\sqrt{g}} \right) \cdot \mathbf{g}^r \right) \right)}_{= 0 \text{ using Eqns. (8.56) and (8.59)}} \\
&= \sum_{r=1}^3 \sum_{i=1}^3 \frac{\delta_i^r}{\sqrt{g}} \frac{\partial \mathbf{T}^i}{\partial \theta^r} + \sum_{i=1}^3 \mathbf{T}^i(0) \\
&= \sum_{r=1}^3 \frac{1}{\sqrt{g}} \frac{\partial \mathbf{T}^r}{\partial \theta^r}.
\end{aligned} \tag{8.53}$$

Similarly,

$$\text{Div}(\mathbf{P}) = \sum_{r=1}^3 \frac{1}{\sqrt{G}} \frac{\partial \mathbf{T}^r}{\partial \theta^r}. \quad (8.54)$$

In summary,

$$\sum_{r=1}^3 \frac{\partial \mathbf{T}^r}{\partial \theta^r} = \sqrt{G} \text{Div}(\mathbf{P}) = \sqrt{g} \text{div}(\mathbf{T}). \quad (8.55)$$

To establish the representations (8.55), we used one of the following identities in Eqn. (8.53):

$$\sum_{r=1}^3 \sum_{i=1}^3 \left(\mathbf{T}^i \otimes \frac{\partial}{\partial \theta^r} \left(\frac{\mathbf{g}_i}{\sqrt{g}} \right) \right) \mathbf{g}^r = \mathbf{0}, \quad \sum_{r=1}^3 \sum_{i=1}^3 \left(\mathbf{T}^i \otimes \frac{\partial}{\partial \theta^r} \left(\frac{\mathbf{G}_i}{\sqrt{G}} \right) \right) \mathbf{G}^r = \mathbf{0}. \quad (8.56)$$

It suffices to consider Eqn. (8.56)₁ in order to show how its referential counterpart (8.56)₂ can be established. The proof starts by examining the derivative of \sqrt{g} and using the identities (8.32):

$$\begin{aligned} \frac{1}{\sqrt{g}} \frac{\partial \sqrt{g}}{\partial \theta^r} &= \frac{1}{\sqrt{g}} \frac{\partial \mathbf{g}_1}{\partial \theta^r} \cdot (\mathbf{g}_2 \times \mathbf{g}_3) + \frac{1}{\sqrt{g}} \frac{\partial \mathbf{g}_2}{\partial \theta^r} \cdot (\mathbf{g}_3 \times \mathbf{g}_1) + \frac{1}{\sqrt{g}} \frac{\partial \mathbf{g}_3}{\partial \theta^r} \cdot (\mathbf{g}_1 \times \mathbf{g}_2) \\ &= \sum_{k=1}^3 \frac{\partial \mathbf{g}_k}{\partial \theta^r} \cdot \mathbf{g}^k. \end{aligned} \quad (8.57)$$

Because $\mathbf{g}_k = \frac{\partial \mathbf{r}^*}{\partial \theta^k}$, the following identity for the mixed partial derivatives holds:

$$\frac{\partial \mathbf{g}_i}{\partial \theta^r} = \frac{\partial \mathbf{g}_r}{\partial \theta^i}. \quad (8.58)$$

Returning to the underbraced term in Eqn. (8.53), we can isolate the i th term and consider its expansion:

$$\begin{aligned} \sum_{r=1}^3 \frac{\partial}{\partial \theta^r} \left(\frac{\mathbf{g}_i}{\sqrt{g}} \right) \cdot \mathbf{g}^r &= \sum_{r=1}^3 \frac{\partial}{\partial \theta^r} \left(\frac{1}{\sqrt{g}} \right) \mathbf{g}_i \cdot \mathbf{g}^r + \frac{1}{\sqrt{g}} \sum_{r=1}^3 \frac{\partial \mathbf{g}_i}{\partial \theta^r} \cdot \mathbf{g}^r \\ &= \frac{\partial}{\partial \theta^i} \left(\frac{1}{\sqrt{g}} \right) + \frac{1}{\sqrt{g}} \sum_{r=1}^3 \underbrace{\frac{\partial \mathbf{g}_r}{\partial \theta^i}}_{\text{using Eqn. (8.58)}} \cdot \mathbf{g}^r \\ &= -\frac{1}{g} \frac{\partial \sqrt{g}}{\partial \theta^i} + \frac{1}{\sqrt{g}} \sum_{r=1}^3 \frac{\partial \mathbf{g}_r}{\partial \theta^i} \cdot \mathbf{g}^r \\ &= -\frac{1}{\sqrt{g}} \sum_{k=1}^3 \underbrace{\frac{\partial \mathbf{g}_k}{\partial \theta^i} \cdot \mathbf{g}^k}_{\text{using Eqn. (8.57)}} + \frac{1}{\sqrt{g}} \sum_{r=1}^3 \frac{\partial \mathbf{g}_r}{\partial \theta^i} \cdot \mathbf{g}^r \\ &= 0. \end{aligned} \quad (8.59)$$

The identity (8.56)₁ now follows in a straightforward manner.

8.4 Balance Laws

We recall the local forms of the balance laws for mass, linear momentum, and angular momentum for a three-dimensional continuum:

$$\begin{aligned}\dot{\rho}^* + \rho^* \operatorname{div}(\mathbf{v}^*) &= 0, \\ \operatorname{div}(\mathbf{T}) + \rho^* \mathbf{b} &= \rho^* \dot{\mathbf{v}}^*, \\ \mathbf{T} &= \mathbf{T}^T.\end{aligned}\tag{8.60}$$

In these equations, the superposed dot denotes the material time derivative, \mathbf{b} is the body force per unit mass, ρ^* is the mass density per unit volume of \mathcal{B} in \mathcal{K} , and $\mathbf{v}^* = \dot{\mathbf{r}}^*$.

Mass conservation (8.60)₁ integrates to

$$J\rho^* = \rho_0^*,\tag{8.61}$$

where ρ_0^* is the mass density per unit volume of \mathcal{B} in \mathcal{K}_0 . As $J = \frac{\sqrt{g}}{\sqrt{G}}$, we can write the linear momentum balance (8.60)₂ as

$$\frac{1}{\sqrt{G}} (\sqrt{g} \operatorname{div}(\mathbf{T})) + \rho_0^* \mathbf{b} = \rho_0^* \dot{\mathbf{v}}^*. \tag{8.62}$$

We next invoke Eqn. (8.55) to conclude that

$$\sum_{r=1}^3 \frac{1}{\sqrt{G}} \frac{\partial \mathbf{T}^r}{\partial \theta^r} + \rho_0^* \mathbf{b} = \rho_0^* \dot{\mathbf{v}}^*. \tag{8.63}$$

It is easy to write this result in terms of the divergence of \mathbf{P} . We also remark that, because the representation (8.63) is convenient to integrate over a three-dimensional continuum, Eqn. (8.63) is used in Green and Naghdi's papers [133, 137] to establish the linear momentum and director momentum balance laws.

8.5 Invariance Requirements under Superposed Rigid Body Motions

Consider two motions of \mathcal{B} . The two motions χ and χ^\perp differ by a rigid body motion if, and only if,

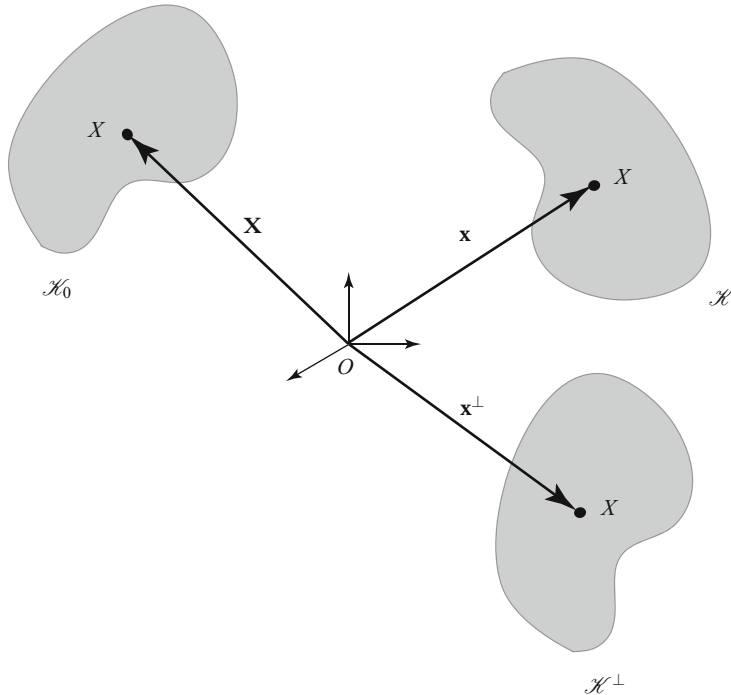


Fig. 8.7 Two configurations, \mathcal{K} and \mathcal{K}^\perp , of a body \mathcal{B} which differ by a superposed rigid body motion. The reference configuration \mathcal{K}_0 is also shown.

$$\begin{aligned}\mathbf{x}^\perp &= \boldsymbol{\chi}^\perp(\mathbf{X}, t^\perp = t + a) \\ &= \mathbf{Q}(t)\boldsymbol{\chi}(\mathbf{X}, t) + \mathbf{q}(t) \\ &= \mathbf{Q}(t)\mathbf{x}(t) + \mathbf{q}(t),\end{aligned}\quad (8.64)$$

where \mathbf{Q} , which is a rotation tensor, and \mathbf{q} are functions of t only and a is a constant. Notice that we are considering two distinct present configurations and a single reference configuration here (see Figure 8.7).⁵ For the two motions, it can be shown from Eqn. (8.64) that

$$\mathbf{F}^\perp = \mathbf{Q}\mathbf{F}, \quad \mathbf{C}^\perp = \mathbf{C}, \quad \mathbf{D}^\perp = \mathbf{Q}\mathbf{D}\mathbf{Q}^T. \quad (8.65)$$

Here, the stretching tensor \mathbf{D} is the symmetric part of the tensor $\mathbf{L} = \dot{\mathbf{F}}\mathbf{F}^{-1}$:

$$\mathbf{D} = \frac{1}{2} (\dot{\mathbf{F}}\mathbf{F}^{-1} + \mathbf{F}^{-T}\dot{\mathbf{F}}^T). \quad (8.66)$$

⁵ This is in contrast to the framework required to establish restrictions on constitutive relations using the principle of material frame indifference [242].

You might have noticed that

$$\begin{aligned}\mathbf{L} = \dot{\mathbf{F}}\mathbf{F}^{-1} &= \sum_{k=1}^3 \sum_{i=1}^3 \dot{\mathbf{g}}_i \otimes \mathbf{G}^i \left(\mathbf{G}_k \otimes \mathbf{g}^k \right) \\ &= \sum_{i=1}^3 \dot{\mathbf{g}}_i \otimes \mathbf{g}^i.\end{aligned}\quad (8.67)$$

Thus, the tensor $\mathbf{L} = \dot{\mathbf{F}}\mathbf{F}^{-1}$ transforms \mathbf{g}_k to $\dot{\mathbf{g}}_k$.

Supplementing the balance laws and response relations, it is necessary to impose invariance requirements under superposed rigid body motions. The invariance requirements we impose are standard:

$$(\psi^*)^\perp = \psi^*, \quad (\phi^*)^\perp = \phi^*, \quad (8.68)$$

where ψ^* is the strain energy function per unit volume in \mathcal{K}_0 and ϕ^* is an internal constraint on the motion of \mathcal{B} . Examples of such constraints include incompressibility ($\phi^* = \det(\mathbf{F}) - 1$).

8.6 Constitutive Relations for Hyperelastic Bodies

For a hyperelastic (or Green) elastic body, a strain energy function ψ^* exists which is a function of \mathbf{F} :

$$\psi^* = \hat{\psi}^*(\mathbf{F}, \mathbf{X}, t). \quad (8.69)$$

However, because we are imposing the invariance requirement (8.68)₁, ψ^* cannot depend on t and can only depend on \mathbf{F} through its invariant part. Consequently,

$$\psi^* = \psi^*(\mathbf{C}, \mathbf{X}). \quad (8.70)$$

We also assume that the body is subject to an internal constraint which is properly invariant:

$$\phi^* = \phi^*(\mathbf{C}, \mathbf{X}). \quad (8.71)$$

That is, $(\phi^*)^\perp = \phi^*$. We now seek constitutive relations for the stress tensor \mathbf{T} of the constrained hyperelastic continuum. Our treatment follows Ericksen and Rivlin [99] and benefits from the insights of later works by Antman and Marlow [14], Carlson et al. [46, 47], Casey et al. [49, 50], Green et al. [136], and Truesdell and Noll [351, Section 30].

In what follows, we make frequent use of the fact that, for any pair of tensors,

$$\mathbf{A} = \sum_{i=1}^3 \sum_{k=1}^3 A_{ik} \mathbf{E}_i \otimes \mathbf{E}_k, \quad \mathbf{B} = \sum_{i=1}^3 \sum_{k=1}^3 B_{ik} \mathbf{E}_i \otimes \mathbf{E}_k, \quad (8.72)$$

the trace operator,

$$\mathbf{A} \cdot \mathbf{B} = \text{tr}(\mathbf{AB}^T) = \sum_{i=1}^3 \sum_{k=1}^3 (A_{ik} B_{ik}), \quad (8.73)$$

provides an inner-product. We will also invoke the following result in the sequel: Assuming that \mathbf{A} and \mathbf{B} are independent of \mathbf{Z} , then the solution to the equation

$$\mathbf{A} \cdot \mathbf{Z} = 0 \text{ for all } \mathbf{Z} \text{ which satisfy } \mathbf{B} \cdot \mathbf{Z} = 0, \quad (8.74)$$

is $\mathbf{A} = \lambda \mathbf{B}$ where λ is a scalar. One proof of this result can be found in Green et al. [136, Page 902]. The result $\mathbf{A} = \lambda \mathbf{B}$, which also appears in Exercise 8.4, has a (well-known) geometric interpretation: \mathbf{A} is parallel to \mathbf{B} .

To prescribe constitutive relations for \mathbf{T} , we require that the stress power is equal to the rate of change of strain energy for all motions which satisfy the constraint⁶:

$$\text{tr}(\mathbf{TL}^T) = \rho^* \psi^* \text{ for all } \mathbf{C} \text{ which satisfy } \phi^*(\mathbf{C}, \mathbf{X}) = 0. \quad (8.75)$$

There are several representations for ψ^* :

$$\psi^* = \text{tr}\left(\frac{\partial \psi^*}{\partial \mathbf{C}} \dot{\mathbf{C}}\right) = \text{tr}\left(\left(\sum_{i=1}^3 \sum_{k=1}^3 \frac{\partial \psi^*}{\partial C_{ik}} \mathbf{E}_i \otimes \mathbf{E}_k\right) \dot{\mathbf{C}}\right) = \sum_{i=1}^3 \sum_{k=1}^3 \frac{\partial \psi^*}{\partial C_{ik}} \dot{C}_{ik}, \quad (8.76)$$

where

$$\mathbf{C} = \sum_{i=1}^3 \sum_{k=1}^3 C_{ik} \mathbf{E}_i \otimes \mathbf{E}_k, \quad \frac{\partial \psi^*}{\partial \mathbf{C}} = \sum_{i=1}^3 \sum_{k=1}^3 \frac{\partial \psi^*}{\partial C_{ik}} \mathbf{E}_i \otimes \mathbf{E}_k. \quad (8.77)$$

Further,

$$\dot{\mathbf{C}} = \dot{\mathbf{F}}^T \mathbf{F} + \mathbf{F}^T \dot{\mathbf{F}} = 2\mathbf{F}^T \mathbf{D}\mathbf{F}. \quad (8.78)$$

Invoking the moment of momentum balance law, we note that $\mathbf{T} = \mathbf{T}^T$. However, for all skew-symmetric tensors \mathbf{B} and symmetric tensors \mathbf{A} ,

$$\text{tr}(\mathbf{AB}) = 0. \quad (8.79)$$

Thus, the symmetry of \mathbf{T} implies that the expression $\text{tr}(\mathbf{TL}^T)$ can be simplified by removing the skew-symmetric part of \mathbf{L} :

$$\begin{aligned} \text{tr}(\mathbf{TL}^T) &= \text{tr}\left(\mathbf{T}\left(\mathbf{D} = \frac{1}{2}(\mathbf{L} + \mathbf{L}^T)\right)\right) + \frac{1}{2}\text{tr}(\mathbf{T}(\mathbf{L}^T - \mathbf{L})) \\ &= \text{tr}(\mathbf{TD}). \end{aligned} \quad (8.80)$$

We are now in a position to rephrase Eqn. (8.75) as

$$\text{tr}(\mathbf{TD}) = \text{tr}\left(2\rho^* \frac{\partial \psi^*}{\partial \mathbf{C}} \mathbf{F}^T \mathbf{DF}\right) \text{ for all } \mathbf{C} \text{ which satisfy } \phi^*(\mathbf{C}, \mathbf{X}) = 0. \quad (8.81)$$

⁶ Observe that $\frac{1}{\sqrt{G}} \mathbf{T}^i \cdot \dot{\mathbf{g}}_i = \text{tr}(\mathbf{P} \dot{\mathbf{F}}^T) = J \text{tr}(\mathbf{TF}^{-T} \dot{\mathbf{F}}^T) = J \text{tr}(\mathbf{TL}^T)$. The former representations for stress power are often more illuminating than $\text{tr}(\mathbf{TL}^T)$.

If \mathbf{C} satisfies the constraint $\phi^* = 0$, then its derivative satisfies

$$\text{tr} \left(\frac{\partial \phi^*}{\partial \mathbf{C}} \dot{\mathbf{C}} \right) = 0. \quad (8.82)$$

Or, equivalently, with the help of Eqn. (8.78),

$$\text{tr} \left(2 \frac{\partial \phi^*}{\partial \mathbf{C}} \mathbf{F}^T \mathbf{D} \mathbf{F} \right) = 0. \quad (8.83)$$

With this in mind, we rephrase Eqn. (8.81) as

$$\text{tr} \left(\left(\mathbf{T} - 2\rho^* \mathbf{F} \frac{\partial \psi^*}{\partial \mathbf{C}} \mathbf{F}^T \right) \mathbf{D} \right) = 0 \text{ for all } \mathbf{D} \text{ which satisfy } \text{tr} \left(2 \frac{\partial \phi^*}{\partial \mathbf{C}} \mathbf{F}^T \mathbf{D} \mathbf{F} \right) = 0. \quad (8.84)$$

If we assume that \mathbf{T} does not depend on \mathbf{D} and that Eqn. (8.84) is true for all \mathbf{D} , then, appealing to the solution to Eqn. (8.74), we find the classic response function for the Cauchy stress tensor:

$$\mathbf{T} = 2\rho^* \mathbf{F} \frac{\partial \psi^*}{\partial \mathbf{C}} \mathbf{F}^T + 2\lambda \mathbf{F} \frac{\partial \phi^*}{\partial \mathbf{C}} \mathbf{F}^T. \quad (8.85)$$

The scalar-valued function $\lambda = \lambda(\mathbf{X}, t)$ and is an unknown that must be determined as part of the solution to the boundary-value problem associated with the continuum. This function is sometimes identified as a Lagrange multiplier (cf. Ericksen and Rivlin [99, Section 4]). Following Casey and Carroll [49], we do not assume that the function λ that enforces the constraint $\phi^* = 0$ is invariant under superposed rigid body motions. That is, λ^\perp and λ are not necessarily identical. It is also important to note that the constitutive relations (8.85) guarantee that \mathbf{T} is symmetric and automatically satisfies the balance of angular momentum: $\mathbf{T} = \mathbf{T}^T$.

One useful interpretation of Eqn. (8.85) is that, for a constrained material, the stress response can be considered as an additive decomposition of a part associated with the deformation of the material and a part needed to ensure that the constraint is satisfied. The former part, $2\rho^* \mathbf{F} \frac{\partial \psi^*}{\partial \mathbf{C}} \mathbf{F}^T$, is known as the active stress and the latter part, $2\lambda \mathbf{F} \frac{\partial \phi^*}{\partial \mathbf{C}} \mathbf{F}^T$, is known as the reactive stress. Indeed, the alternative derivation of Eqn. (8.85) in Truesdell and Noll [351, Section 30] postulates the decomposition of the stress into active and reactive parts, assumes that the reactive stress is workless in any motion of the continuum that satisfies the constraints, and assumes that the active part identically satisfies the local form of the energy balance.

With the help of the identities

$$\frac{\partial \psi^*}{\partial \mathbf{F}} = 2\mathbf{F} \frac{\partial \psi^*}{\partial \mathbf{C}}, \quad \frac{\partial \phi^*}{\partial \mathbf{F}} = 2\mathbf{F} \frac{\partial \phi^*}{\partial \mathbf{C}}, \quad (8.86)$$

the constitutive relations for \mathbf{T} can also be expressed in a manner that is convenient for representations of the other stress tensors that appear in these pages:

$$\mathbf{T} = \rho^* \frac{\partial \psi^*}{\partial \mathbf{F}} \mathbf{F}^T + \lambda \frac{\partial \phi^*}{\partial \mathbf{F}} \mathbf{F}^T. \quad (8.87)$$

We leave it as an exercise to write out the corresponding response functions for \mathbf{T}^i , \mathbf{P} , $\boldsymbol{\Sigma}$, and \mathbf{S} . The representation for \mathbf{S} can be used to transparently demonstrate that the reactive stress is normal to the constraint manifold $\phi^*(\mathbf{C}) = 0$. This five-dimensional manifold corresponds to the set of all symmetric tensors \mathbf{C} which satisfy the constraint $\phi^*(\mathbf{C}) = 0$ and is a subset of the space of all symmetric second-order tensors. For additional details and perspectives on the constraint manifold, we refer the reader to [46, 50]. The geometric perspective in these papers also enables one to see that the prescription for the reactive stress in Eqn. (8.85) is equivalent to the Lagrange prescription for constraint forces and moments in particle and rigid body dynamics.⁷

8.6.1 A Mooney-Rivlin Material

One of the most prominent examples of constitutive relations for an incompressible, isotropic elastic body is due to Mooney and Rivlin:

$$\mathbf{T} = -p\mathbf{I} + \beta_1\mathbf{B} + \beta_{-1}\mathbf{B}^{-1}. \quad (8.88)$$

Here, p is the pressure associated with the incompressibility constraint,

$$\phi^*(\mathbf{C}) = \det(\mathbf{C}) - 1, \quad (8.89)$$

(i.e., $p = -\lambda$ in Eqn. (8.85)). Additionally, β_1 and β_{-1} are constants in the simplest Mooney-Rivlin material and, when $\beta_{-1} = 0$, the material is known, following Rivlin, as a neo-Hookean material. The strain energy function for the (simplest) Mooney-Rivlin material is

$$\rho_0^* \psi^* = \frac{1}{2} \beta_1 (I_C - 3) - \frac{1}{2} \beta_{-1} (II_C - 3), \quad (8.90)$$

where the two nontrivial invariants of \mathbf{C} are

$$I_C = \text{tr}(\mathbf{C}), \quad 2II_C = \text{tr}(\mathbf{C})^2 - \text{tr}(\mathbf{C}^2). \quad (8.91)$$

The third invariant $III_C = \det(\mathbf{C}) = 1$ for an incompressible continuum. The derivation of the relations (8.88) from the strain energy function given by Eqn. (8.90) is outlined in Exercise 8.4 at the end of this chapter.

⁷ In the case of a single particle, the Lagrange prescription implies that the constraint force is normal to surface or curve that the particle is constrained to move on. For this reason, this prescription is sometimes known as the normality prescription. We refer the reader to [271, 283, 284] for additional background on constraint forces and constraint moments in classical mechanics.

8.6.2 Additional Remarks

It is important to note that the constitutive relations (8.85), the balance laws, and the constraint may be used to provide a determinate system of equations to determine the motion \mathbf{r}^* of the body and λ :

$$\sum_{r=1}^3 \left(\frac{\partial}{\partial \theta^r} \left(2\mathbf{F} \left(\rho_0^* \sqrt{G} \frac{\partial \psi^*}{\partial \mathbf{C}} \mathbf{G}^r + \sqrt{g} \lambda \frac{\partial \phi^*}{\partial \mathbf{C}} \mathbf{G}^r \right) \right) \right) + \sqrt{G} \rho_0^* \mathbf{b} = \sqrt{G} \rho_0^* \dot{\mathbf{v}}^*,$$

$$\text{tr} \left(2 \frac{\partial \phi^*}{\partial \mathbf{C}} \mathbf{F}^T \mathbf{D} \mathbf{F} \right) = 0. \quad (8.92)$$

The corresponding set of equations for the unconstrained case were shown in Eqn. (8.63). Of course, both sets of equations need to be supplemented with boundary conditions and initial conditions.

8.7 Configurational, Material, or Eshelbian Forces

Following the seminal work of John D. Eshelby (1916–1981), it has become standard to consider the behavior of an energy-momentum tensor for hyperelastic bodies. For elastostatic problems, several alternative definitions of this tensor appear in the literature:

$$\boldsymbol{\sigma}_C = \rho_0^* \psi^* \mathbf{I} - \mathbf{S} \mathbf{C}, \text{ proposed by Chadwick [54]},$$

$$\boldsymbol{\sigma}_E = \rho_0^* \psi^* \mathbf{I} + (\mathbf{I} - \mathbf{F}^T) \boldsymbol{\Sigma}^T, \text{ proposed by Eshelby (cf. [103, Eqn. (13)]),}$$

$$\boldsymbol{\sigma}_G = \rho_0^* \psi^* \mathbf{I} - \mathbf{F}^T \boldsymbol{\Sigma}^T, \text{ proposed by Gurtin (cf. [149, Eqn. (5.14)]),}$$

$$\boldsymbol{\sigma}_M = \rho_0^* \psi^* \mathbf{I} - \mathbf{P} \mathbf{F}, \text{ proposed by Maugin and co-workers (cf. [231, Eqn. (3.7)]).}$$

The extension of these definitions to the dynamic case is obtained by subtracting the kinetic energy density from the strain energy function (cf., e.g., [103, Eqn. (53)]). For present purposes, we use a definition of the (dynamic) energy-momentum tensor that can be found in a variety of sources including [82, Eqn. (2.18)] and [149, Eqn. (7.8)]:

$$\boldsymbol{\sigma} = \left(\rho_0^* \psi^* - \frac{1}{2} \rho_0^* \mathbf{v}^* \cdot \mathbf{v}^* \right) \mathbf{I} - \mathbf{F}^T \mathbf{P}. \quad (8.93)$$

Concomitant with $\boldsymbol{\sigma}$, we follow Eshelby [103, Eqn. (55)] and define the material momentum \mathbf{P}^* :

$$\mathbf{P}^* = -\rho_0^* \mathbf{F}^T \mathbf{v}^*. \quad (8.94)$$

Among other uses, the momentum \mathbf{P}^* , which is alternatively referred to as the pseudomomentum or configurational momentum, and tensor $\boldsymbol{\sigma}$ can be used to establish a balance law for material momentum. This law provides a conservation law in certain instances and, as demonstrated by Eshelby [103], the energy release rate for a crack

in others. The force $\rho_0^* \mathbf{b}_M$ in this balance law is known as an assigned material (or configurational) force. As we shall see below, if the material is homogeneous and there are no body forces, $\mathbf{b} = \mathbf{0}$, then $\rho_0^* \mathbf{b}_M$ is identically zero. The vanishing of \mathbf{b}_M has been championed by Braun [36] as a test for the accuracy of numerical methods used in computational mechanics and we refer the reader to [240] for additional references and interesting examples.

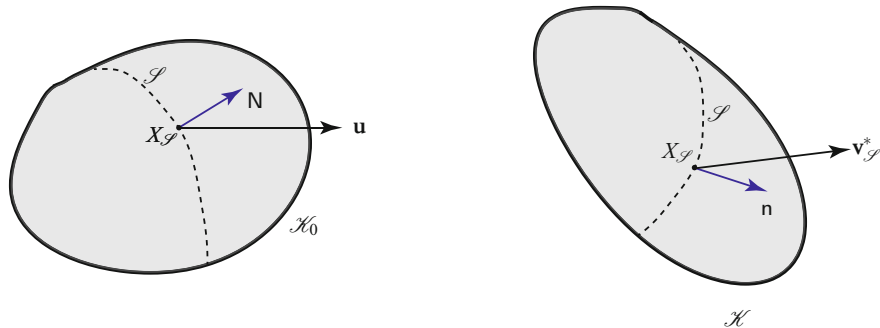


Fig. 8.8 The reference \mathcal{K}_0 and present \mathcal{K} configurations of a body \mathcal{B} showing a propagating surface of discontinuity \mathcal{S} and the associated velocity vectors \mathbf{u} and $\mathbf{v}_{\mathcal{S}}^*$ associated with a material point $X_{\mathcal{S}} \in \mathcal{S}$. The unit normal vectors to the shock surface in the reference and present configurations are \mathbf{N} and \mathbf{n} . The normal vectors are related by Nanson's formula (8.37) and the velocity vectors are related by Eqn. (8.95).

8.8 A Material Momentum Balance Law

The development of a balance law for material momentum follows from the aforementioned works by Gurin (cf. [149] and references therein) and Maugin (cf. [232] and references therein). Referring to Figure 8.8, we allow the existence of a surface of discontinuity \mathcal{S} in the body. A material point $X_{\mathcal{S}}$ on this surface has a position vector $\mathbf{X}_{\mathcal{S}}$ in a fixed reference configuration and a position vector $\mathbf{x}_{\mathcal{S}} = \chi(\mathbf{X}_{\mathcal{S}}, t)$ in the present configuration. This material point has the velocity vector $\mathbf{u} = \dot{\mathbf{X}}_{\mathcal{S}}$ in the reference configuration and a velocity vector $\mathbf{v}_{\mathcal{S}}^*$ in the present configuration. These velocity vectors are related by compatibility conditions:

$$\mathbf{v}_{\mathcal{S}}^* = (\mathbf{v}^* + \mathbf{F}\mathbf{u})^+ = (\mathbf{v}^* + \mathbf{F}\mathbf{u})^- . \quad (8.95)$$

The normal velocity of the shock or discontinuity as it propagates through material points in the fixed reference configuration is

$$U_n = \mathbf{u} \cdot \mathbf{N}, \quad (8.96)$$

where the unit normal vector \mathbf{N} is shown in Figure 8.8. We allow the existence of sources of material momentum $\mathbf{B}_\mathcal{S}^*$, linear momentum $\mathbf{F}_\mathcal{S}^*$, and power $\Phi_{E_\mathcal{S}}^*$ on \mathcal{S} . The source $\mathbf{B}_\mathcal{S}^*$ is vector-valued in contrast to the scalar-valued supply B_γ in one-dimensional theories.

The integral form of the balance law is equivalent to a local form,

$$\text{Div}(\boldsymbol{\sigma}) + \rho_0^* \mathbf{b}_M = \dot{P}^*, \quad (8.97)$$

and a companion jump condition,

$$[[\boldsymbol{\sigma}\mathbf{N} + U_n \mathbf{P}^*]]_\mathcal{S} = -\mathbf{B}_\mathcal{S}^*. \quad (8.98)$$

We also note that the associated jump conditions for mass, linear momentum, and energy are

$$\begin{aligned} [[\rho_0^* U_n]]_\mathcal{S} &= 0, \\ [[\mathbf{P}\mathbf{N} + U_n \rho_0^* \mathbf{v}^*]]_\mathcal{S} &= -\mathbf{F}_\mathcal{S}^*, \\ [[\mathbf{P}\mathbf{N} \cdot \mathbf{v}^*]]_\mathcal{S} + \left[\left[\rho_0^* \psi^* + \frac{\rho_0^*}{2} \mathbf{v}^* \cdot \mathbf{v}^* \right] \right]_\mathcal{S} U_n &= -\Phi_{E_\mathcal{S}}^*. \end{aligned} \quad (8.99)$$

In the sequel, we shall elaborate on the local form of the balance of material momentum and comment on the relationship between the jump condition (8.98) and related treatments in the literature. One of our intentions is to give context to the one-dimensional material momentum balance law that is used in this book. For certain problems in elastostatics, the balance law (8.97) can lead to a conservation law. Dating to the works of Günther [146] and Knowles and Sternberg [187], it is known that the resulting conservation law can also be established using Noether's theorem.⁸

8.8.1 The Local Form

The local form of the balance of material momentum is $\text{Div}(\boldsymbol{\sigma}) + \rho_0^* \mathbf{b}_M = \dot{P}^*$. By suitably specifying $\rho_0^* \mathbf{b}_M$, this law will be identically satisfied. The procedure has obvious parallels to the one used for one-dimensional theories, but the algebra is somewhat more involved.

To elaborate on the prescription for $\rho_0^* \mathbf{b}_M$, several preliminary results are needed.⁹ First, with the help of the constitutive relations $\mathbf{P} = \rho_0^* \frac{\partial \psi^*}{\partial \mathbf{F}}$, we find the following intermediate results:

⁸ Kinzler and Hermann [182, Chapter 1] and Olver [256] provide accessible treatments of infinitesimal transformations and their role in establishing conservation laws using Noether's theorem.

⁹ The corresponding developments for an incompressible hyperelastic material are easily inferred from Chadwick's lucid paper [54].

$$\begin{aligned} \operatorname{Div}\left(\left(\rho_0^*\psi^* - \frac{1}{2}\rho_0^*\mathbf{v}^*\cdot\mathbf{v}^*\right)\mathbf{I}\right) &= \sum_{r=1}^3 \frac{\partial}{\partial\theta^r} \left(\rho_0^*\psi^* - \frac{1}{2}\rho_0^*\mathbf{v}^*\cdot\mathbf{v}^*\right) \mathbf{G}^r \\ &= \sum_{r=1}^3 \left(\operatorname{tr}\left(\mathbf{P}\frac{\partial\mathbf{F}^T}{\partial\theta^r}\right)\right) \mathbf{G}^r + \rho_0^*\dot{\mathbf{F}}^T\mathbf{v}^* \\ &\quad + \nabla_{\exp}\left(\rho_0^*\psi^* - \frac{1}{2}\rho_0^*\mathbf{v}^*\cdot\mathbf{v}^*\right). \end{aligned} \quad (8.100)$$

The derivative ∇_{\exp} is defined for a function $f(\theta^1, \theta^2, \theta^3, \mathbf{C}, t)$ as

$$\nabla_{\exp}(f) = \sum_{r=1}^3 \frac{\partial f}{\partial\theta^r} \mathbf{G}^r \Bigg|_{\substack{\mathbf{C} = \text{const.} \\ t = \text{const.}}} . \quad (8.101)$$

For example, if a body is homogeneous, then ρ_0^* is independent of θ^k and $\nabla_{\exp}(\rho_0^*) = 0$. Invoking the balance of linear momentum, $\operatorname{Div}(\mathbf{P}) - \rho_0^*\dot{\mathbf{v}}^* = -\rho_0^*\mathbf{b}$, we find that

$$\begin{aligned} -\operatorname{Div}(\mathbf{F}^T\mathbf{P}) &= -\sum_{r=1}^3 \frac{\partial\mathbf{F}^T}{\partial\theta^r} \mathbf{P}\mathbf{G}^r - \mathbf{F}^T\operatorname{Div}(\mathbf{P}) \\ &= -\sum_{r=1}^3 \frac{\partial\mathbf{F}^T}{\partial\theta^r} \mathbf{P}\mathbf{G}^r + \rho_0^*\mathbf{F}^T\mathbf{b} - \rho_0^*\mathbf{F}^T\dot{\mathbf{v}}, \\ -\dot{\mathbf{P}}^* &= \rho_0^*\dot{\mathbf{F}}^T\mathbf{v}^* + \rho_0^*\mathbf{F}^T\dot{\mathbf{v}}^*. \end{aligned} \quad (8.102)$$

Choosing θ^r to be Cartesian coordinates in the reference configuration is the easiest method to see that

$$\sum_{r=1}^3 \left(\operatorname{tr}\left(\mathbf{P}\frac{\partial\mathbf{F}^T}{\partial\theta^r}\right)\mathbf{I} - \sum_{r=1}^3 \frac{\partial\mathbf{F}^T}{\partial\theta^r}\mathbf{P}\right) \mathbf{G}^r = \mathbf{0}. \quad (8.103)$$

That is,

$$\begin{aligned} \sum_{r=1}^3 \operatorname{tr}\left(\mathbf{P}\frac{\partial\mathbf{F}^T}{\partial\theta^r}\right) \mathbf{G}^r - \sum_{s=1}^3 \frac{\partial\mathbf{F}^T}{\partial\theta^s} \mathbf{P}\mathbf{G}^s &= \sum_{r=1}^3 \sum_{k=1}^3 \sum_{l=1}^3 P_{kl} \frac{\partial F_{kl}}{\partial X_r} \mathbf{E}_r - \sum_{s=1}^3 \sum_{k=1}^3 \sum_{l=1}^3 P_{ks} \frac{\partial F_{kl}}{\partial X_s} \mathbf{E}_l \\ &= \sum_{r=1}^3 \sum_{k=1}^3 \sum_{l=1}^3 P_{kl} \left(\frac{\partial x_k}{\partial X_r \partial X_l} - \frac{\partial x_k}{\partial X_l \partial X_r} \right) \mathbf{E}_r \\ &= \mathbf{0}, \end{aligned} \quad (8.104)$$

where

$$\mathbf{F} = \sum_{i=1}^3 \sum_{k=1}^3 \frac{\partial x_i}{\partial X_k} \mathbf{E}_i \otimes \mathbf{E}_k, \quad \mathbf{P} = \sum_{i=1}^3 \sum_{k=1}^3 P_{ik} \mathbf{E}_i \otimes \mathbf{E}_k. \quad (8.105)$$

It should be noted that the final step in the derivation above used the identity (8.58).

We now use the intermediate results (8.100), (8.102), and (8.103) to solve for a material force:

$$\rho_0^* \mathbf{b}_M = -\operatorname{Div}(\boldsymbol{\sigma}) + \dot{\mathbf{P}}^*. \quad (8.106)$$

The force $\rho_0^* \mathbf{b}_M$, which is known as the assigned material force, is given by

$$\rho_0^* \mathbf{b}_M = -\nabla_{\text{exp}} \left(\rho_0^* \psi^* - \frac{1}{2} \rho_0^* \mathbf{v}^* \cdot \mathbf{v}^* \right) - \rho_0^* \mathbf{F}^T \mathbf{b}. \quad (8.107)$$

This is the desired prescription for the assigned material force and it ensures that the balance law (8.97) is identically satisfied. For elastostatic problems where the body is homogeneous and the body force is zero, the balance law (8.97) immediately implies the conservation law $\operatorname{Div}(\boldsymbol{\sigma}) = \mathbf{0}$.

8.8.2 The Jump Condition

In the purely mechanical theory of interest, the primary singular supplies pertain to linear momentum and material momentum (cf. Figure 8.9). Further, the jump condition $[\![\boldsymbol{\sigma} \mathbf{n} + U_n \mathbf{P}^*]\!]_{\mathcal{S}} + \mathbf{B}_{\mathcal{S}}^* = \mathbf{0}$ that is associated with the balance of material momentum is related to a driving force (or driving force) on a discontinuity and Eshelby's notion of a force on a singularity. Before elaborating on these connections, we recall from [263] that the jump conditions for mass, material momentum, and linear momentum can be used in a straightforward manner to reduce the jump condition from the balance of energy to an identity for $\Phi_{E,\mathcal{S}}^*$:

$$\Phi_{E,\mathcal{S}}^* = \mathbf{F}_{\mathcal{S}}^* \cdot \mathbf{v}_{\mathcal{S}}^* + \mathbf{B}_{\mathcal{S}}^* \cdot \mathbf{u}. \quad (8.108)$$

Thus, the power supply $\Phi_{E,\mathcal{S}}^*$ can be related to the power of the sources of momenta. This parallels the situation for the supply $\Phi_{E,\gamma}$ for one-dimensional media that is presented throughout this book.

The normal component of the supply of material momentum $\mathbf{B}_{\mathcal{S}}^*$ can be related to a quantity known as the driving force f that appears in works by Abeyaratne and Knowles [1, 4, 5] and Truskinovsky [353, 354] and the force on a singularity that

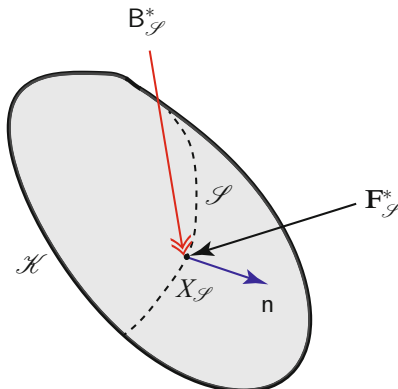


Fig. 8.9 Schematic of the singular supplies of linear momentum $\mathbf{F}_{\mathcal{S}}^*$ and material momentum acting at a point $X_{\mathcal{S}}$ on a surface of discontinuity.

appears in Eshelby [102]. Specifically, a driving force f is defined in [4, Eqn. (19)] (or [5, Eqn. (6.28)]),

$$f = [\![\rho_0^* \psi^*]\!]_{\mathcal{S}} - \{\mathbf{P}\}_{\mathcal{S}} \cdot [\![\mathbf{F}]\!]_{\mathcal{S}}. \quad (8.109)$$

Abeyaratne and Knowles interpret this force as “a normal traction applied to \mathcal{S} by the body” [1, Page 353] and prescriptions for f play a key role in developing discontinuous solutions to boundary-value problems. Prescribing f is equivalent to prescribing the sources of material and linear momenta. To see this, we note that we can expand $[\![\sigma N + U_n P^*]\!]_{\mathcal{S}} \cdot N$ by substituting for the energy-momentum tensor σ and P^* in terms of ρ_0^* , ψ^* , \mathbf{F} , and \mathbf{v}^* :

$$\begin{aligned} \sigma &= \left(\rho_0^* \psi^* - \frac{1}{2} \rho_0^* \mathbf{v}^* \cdot \mathbf{v}^* \right) \mathbf{I} - \mathbf{F}^T \mathbf{P}, \\ P^* &= -\rho_0^* \mathbf{F}^T \mathbf{v}^*. \end{aligned} \quad (8.110)$$

With some rearranging and elimination of terms using the jump conditions (8.99), we find that¹⁰

$$[\![\sigma N + U_n P^*]\!]_{\mathcal{S}} \cdot N = \underbrace{[\![\rho_0^* \psi^*]\!]_{\mathcal{S}} - \{\mathbf{P}\}_{\mathcal{S}} \cdot [\![\mathbf{F}]\!]_{\mathcal{S}}}_{+ \mathbf{F}_{\mathcal{S}}^* \cdot \{\mathbf{F}N\}_{\mathcal{S}}} + \mathbf{F}_{\mathcal{S}}^* \cdot \{\mathbf{F}N\}_{\mathcal{S}}. \quad (8.111)$$

After invoking the N component of the jump condition $[\![\sigma N + U_n P^*]\!]_{\mathcal{S}} = -\mathbf{B}_{\mathcal{S}}^*$ and identifying the driving force as the underbraced term in (8.111), we conclude that

$$f = -\mathbf{B}_{\mathcal{S}}^* \cdot N - \mathbf{F}_{\mathcal{S}}^* \cdot \{\mathbf{F}N\}_{\mathcal{S}}. \quad (8.112)$$

In [4], source terms such as $\mathbf{F}_{\mathcal{S}}^*$ are set to zero, so the “normal traction” quoted above is $\mathbf{B}_{\mathcal{S}}^* \cdot N$. However, the identity (8.112) implies that the driving force could also be supplied by $\mathbf{F}_{\mathcal{S}}^*$. The one-dimensional counterpart of the result (8.112) and its relation to Eshelby’s force on a singularity is discussed in Section 1.8.1 of Chapter 1 and Exercise 1.7.

Throughout this book, we advocate for, and exploit, the notion that the jump condition associated with the material momentum balance is helpful in solving problems associated with strings and rods. In the problems of interest in this book, the material momentum is supplied by adhesion and impacts. We hope however to have supplied sufficient detail for the reader to be able to appreciate how the balance is related to one-dimensional phase transformation problems that are discussed in [2, 3, 5, 296] and references therein.

8.9 Closing Comments

The partial differential equations (8.92) are formidable: only a small collection of exact static solutions (and an even smaller set of exact dynamic solutions) are known. Consequently, most analyses of the equations use numerical methods.

¹⁰ Further details of this calculation can be found in [263, Section 5].

The one-dimensional theories discussed in this book are designed to provide more tractable models compared to the three-dimensional theory. One important point to note as you explore these theories is that their structures are similar to that of the three-dimensional theory. Consequently, the one-dimensional theories do not necessarily have to be considered as a mishmash of assumptions that they often seem when one first encounters them in undergraduate courses.

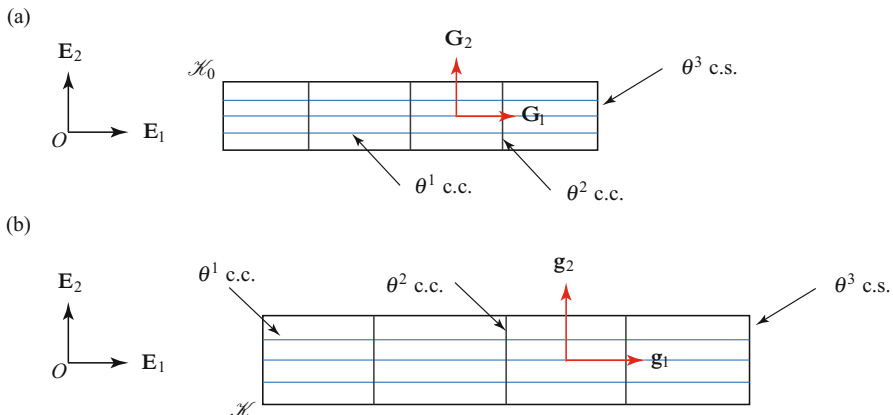


Fig. 8.10 An example of a θ^3 coordinate surface (c.s.) in (a) the reference configuration \mathcal{K}_0 and (b) the present \mathcal{K} configurations of a parallelepiped that is being dilated. The abbreviation c.c. stands for coordinate curve.

8.10 Exercises

Exercise 8.1: The covariant and contravariant basis vectors are related by the nine equations

$$\mathbf{g}_k \cdot \mathbf{g}^i = \delta_k^i, \quad (i, k = 1, 2, 3). \quad (8.113)$$

Assuming the contravariant basis vectors \mathbf{g}^i are known, show that

$$\mathbf{g}_1 = \sqrt{g} (\mathbf{g}^2 \times \mathbf{g}^3), \quad \mathbf{g}_2 = \sqrt{g} (\mathbf{g}^3 \times \mathbf{g}^1), \quad \mathbf{g}_3 = \sqrt{g} (\mathbf{g}^1 \times \mathbf{g}^2), \quad (8.114)$$

where

$$\frac{1}{\sqrt{g}} = (\mathbf{g}^1 \times \mathbf{g}^2) \cdot \mathbf{g}^3. \quad (8.115)$$

Exercise 8.2: Consider the dilation of a parallelepiped shown in Figure 8.10. In the reference configuration, the convected coordinate system coincides with a Cartesian

coordinate system:

$$\theta^k = x_k, \quad \mathbf{R}^*(\theta^1, \theta^2, \theta^3) = \theta^1 \mathbf{E}_1 + \theta^2 \mathbf{E}_2 + \theta^3 \mathbf{E}_3. \quad (8.116)$$

For the present configuration, the convected coordinate system can be described using Cartesian coordinates:

$$\theta^1 = f_1(x_1), \quad \theta^2 = f_2(x_2), \quad \theta^3 = f_3(x_3), \quad (8.117)$$

where f_k are smooth invertible functions.

(a) Show that

$$\mathbf{G}_1 = \mathbf{G}^1 = \mathbf{E}_1, \quad \mathbf{G}_2 = \mathbf{G}^2 = \mathbf{E}_2, \quad \mathbf{G}_3 = \mathbf{G}^3 = \mathbf{E}_3. \quad (8.118)$$

Compute \sqrt{G} .

(b) For the present configuration, show that

$$\mathbf{g}^1 = \frac{\partial f_1}{\partial x_1} \mathbf{E}_1, \quad \mathbf{g}^2 = \frac{\partial f_2}{\partial x_2} \mathbf{E}_2, \quad \mathbf{g}^3 = \frac{\partial f_3}{\partial x_3} \mathbf{E}_3. \quad (8.119)$$

(c) Verify that $\frac{1}{\sqrt{g}} = \frac{\partial f_1}{\partial x_1} \frac{\partial f_2}{\partial x_2} \frac{\partial f_3}{\partial x_3}$.

(d) Establish the following representations for the covariant basis vectors \mathbf{g}_k :

$$\mathbf{g}_1 = \left(\frac{\partial f_1}{\partial x_1} \right)^{-1} \mathbf{E}_1, \quad \mathbf{g}_2 = \left(\frac{\partial f_2}{\partial x_2} \right)^{-1} \mathbf{E}_2, \quad \mathbf{g}_3 = \left(\frac{\partial f_3}{\partial x_3} \right)^{-1} \mathbf{E}_3. \quad (8.120)$$

(e) Show that the deformation gradient \mathbf{F} associated with this problem has the representation

$$\mathbf{F} = \left(\frac{\partial f_1}{\partial x_1} \right)^{-1} \mathbf{E}_1 \otimes \mathbf{E}_1 + \left(\frac{\partial f_2}{\partial x_2} \right)^{-1} \mathbf{E}_2 \otimes \mathbf{E}_2 + \left(\frac{\partial f_3}{\partial x_3} \right)^{-1} \mathbf{E}_3 \otimes \mathbf{E}_3. \quad (8.121)$$

Show that the deformation is homogeneous if $f_k = a_k x_k + c_k$ where a_1, a_2, a_3, c_1, c_2 , and c_3 are constants. What are these functions if the body expands uniformly so that its volume in the present configuration is 8 times its volume in the reference configuration?

Exercise 8.3: Consider the flexure of a parallelepiped shown in Figure 8.4.¹¹ In the reference configuration, the convected coordinate system coincides with a Cartesian coordinate system:

$$\theta^k = x_k, \quad \mathbf{R}^*(\theta^1, \theta^2, \theta^3) = \theta^1 \mathbf{E}_1 + \theta^2 \mathbf{E}_2 + \theta^3 \mathbf{E}_3. \quad (8.122)$$

¹¹ Further details on the solution to this problem for specific constitutive equations can be found in [140]. The problem is of particular relevance because the rod theories we use give solutions to this flexure problem that are only approximations to the solution obtained using three-dimensional considerations.

For the present configuration, the convected coordinate system can be described using cylindrical polar coordinates (r, ϑ, z) :

$$\theta^1 = f_1(r), \quad \theta^2 = f_2(\vartheta), \quad \theta^3 = f_3(z), \quad (8.123)$$

where f_k are smooth invertible functions.

(a) Show that

$$\mathbf{G}_1 = \mathbf{G}^1 = \mathbf{E}_1, \quad \mathbf{G}_2 = \mathbf{G}^2 = \mathbf{E}_2, \quad \mathbf{G}_3 = \mathbf{G}^3 = \mathbf{E}_3. \quad (8.124)$$

Compute \sqrt{G} .

(b) For the present configuration, show that

$$\mathbf{g}^1 = \frac{\partial f_1}{\partial r} \mathbf{e}_r, \quad \mathbf{g}^2 = \frac{1}{r} \frac{\partial f_2}{\partial \vartheta} \mathbf{e}_\vartheta, \quad \mathbf{g}^3 = \frac{\partial f_3}{\partial z} \mathbf{E}_3, \quad (8.125)$$

where

$$\mathbf{e}_r = \cos(\vartheta) \mathbf{E}_1 + \sin(\vartheta) \mathbf{E}_2, \quad \mathbf{e}_\vartheta = \cos(\vartheta) \mathbf{E}_2 - \sin(\vartheta) \mathbf{E}_1. \quad (8.126)$$

(c) Verify that $\frac{1}{\sqrt{g}} = \frac{1}{r} \frac{\partial f_1}{\partial r} \frac{\partial f_2}{\partial \vartheta} \frac{\partial f_3}{\partial z}$.

(d) Establish the following representations for the covariant basis vectors \mathbf{g}_k :

$$\mathbf{g}_1 = \left(\frac{\partial f_1}{\partial r} \right)^{-1} \mathbf{e}_r, \quad \mathbf{g}_2 = r \left(\frac{\partial f_2}{\partial \vartheta} \right)^{-1} \mathbf{e}_\vartheta, \quad \mathbf{g}_3 = \left(\frac{\partial f_3}{\partial z} \right)^{-1} \mathbf{E}_3. \quad (8.127)$$

(e) Show that the deformation gradient \mathbf{F} associated with this problem has the representation

$$\mathbf{F} = \left(\frac{\partial f_1}{\partial r} \right)^{-1} \mathbf{e}_r \otimes \mathbf{E}_1 + r \left(\frac{\partial f_2}{\partial \vartheta} \right)^{-1} \mathbf{e}_\vartheta \otimes \mathbf{E}_2 + \left(\frac{\partial f_3}{\partial z} \right)^{-1} \mathbf{E}_3 \otimes \mathbf{E}_3. \quad (8.128)$$

(f) If the parallelepiped is composed of an incompressible material, then show that

$$\frac{\partial f_3}{\partial z} = r \left(\frac{\partial f_1}{\partial r} \frac{\partial f_2}{\partial \vartheta} \right)^{-1}. \quad (8.129)$$

Exercise 8.4: This exercise is devoted to an exploration of constitutive relations for a constrained hyperelastic continuum. We note that there are several treatments of this topic, among them [46, 50, 351], and these treatments have some overlaps to one that is used in the mechanics of rigid bodies and particles.

(a) Consider solving the following equation for $\mathbf{f}(x)$:

$$\mathbf{f} \cdot \dot{\mathbf{x}} = 0, \quad (8.130)$$

for all $\dot{\mathbf{x}}$ which satisfy the equation

$$\mathbf{g} \cdot \dot{\mathbf{x}} = 0. \quad (8.131)$$

Here, $\mathbf{g} = \mathbf{g}(\mathbf{x})$, the vector \mathbf{x} and vector-valued functions \mathbf{f} and \mathbf{g} are N -dimensional, and $\mathbf{a} \cdot \mathbf{b} = \sum_{K=1}^N a_K b_K$. Prove that the solution to Eqn. (8.130) is

$$\mathbf{f} = 0 + \lambda \mathbf{g}, \quad (8.132)$$

where λ is a scalar. That is, \mathbf{f} is parallel to \mathbf{g} .¹² Would this result hold if $\mathbf{f} = \mathbf{f}(\mathbf{x}, \dot{\mathbf{x}})$?

- (b) Using the results of (a), show that the constitutive equations for a constrained hyperelastic material whose strain energy function is $\psi^*(\mathbf{C})$ and which is subject to a constraint $\phi^*(\mathbf{C}) = 0$ is

$$\mathbf{S} = 2\rho_0^* \frac{\partial \psi^*}{\partial \mathbf{C}} + \lambda \frac{\partial \phi^*}{\partial \mathbf{C}}. \quad (8.133)$$

Your starting point should be the identity $\mathbf{S} \cdot \dot{\mathbf{C}} = 2\overline{\rho_0^* \psi^*}$, where the inner-product \cdot of two tensors is defined using the trace operator: $\mathbf{A} \cdot \mathbf{B} = \text{tr}(\mathbf{AB}^T)$.¹³

- (c) The prescription $\lambda \frac{\partial \phi^*}{\partial \mathbf{C}}$ for the constraint response is sometimes known as the normality prescription. Why is this the case? Give a brief discussion of the identical satisfaction of the moment of momentum balance law by the constitutive relations (8.133).
- (d) Show that the principal invariants of \mathbf{B} and \mathbf{C} are identical:

$$I_{\mathbf{B}} = I_{\mathbf{C}}, \quad II_{\mathbf{B}} = II_{\mathbf{C}}, \quad III_{\mathbf{B}} = III_{\mathbf{C}}, \quad (8.134)$$

where, for any second-order tensor \mathbf{A} ,

$$I_{\mathbf{A}} = \text{tr}(\mathbf{A}), \quad II_{\mathbf{A}} = \frac{1}{2} \left(\text{tr}(\mathbf{A})^2 - \text{tr}(\mathbf{A}^2) \right), \quad III_{\mathbf{A}} = \det(\mathbf{A}). \quad (8.135)$$

- (e) Using the results of (b) show that the constitutive relations for an incompressible hyperelastic body are

$$\mathbf{T} = 2\rho_0^* \mathbf{F} \frac{\partial \psi^*}{\partial \mathbf{C}} \mathbf{F}^T - p \mathbf{I}. \quad (8.136)$$

Here, the scalar function $p = p(\mathbf{X}, t)$ is known as the pressure. For this exercise, you may need to use the following identity:

$$\frac{\partial \det(\mathbf{C})}{\partial \mathbf{C}} = \det(\mathbf{C}) \mathbf{C}^{-1}. \quad (8.137)$$

- (f) Apply the results of (e) to the case of an incompressible Mooney-Rivlin material where $\rho_0^* \psi^*$ is given by Eqn. (8.90). Your final expression for \mathbf{T} should be

¹² For assistance with this exercise, it may be helpful to point out that a closely related proof can be found in Green et al. [136, Page 902].

¹³ You may wish to notice that $\mathbf{T} \cdot \mathbf{L}^T = \mathbf{J} \mathbf{P} \cdot \dot{\mathbf{F}} = \mathbf{J} \mathbf{S} \cdot \dot{\mathbf{E}}$, where, among others, the moment of momentum balance law $\mathbf{T} = \mathbf{T}^T$ is used to establish the equivalence. As mentioned on Page 361, the tensor \mathbf{L} has the representation $\mathbf{L} = \dot{\mathbf{F}} \mathbf{F}^{-1} = \sum_{k=1}^3 \dot{\mathbf{g}}_k \otimes \mathbf{g}^k$.

equivalent to Eqn. (8.88). In addition to the Cayley-Hamilton theorem for \mathbf{B} ,

$$\mathbf{B}^3 - I_{\mathbf{B}}\mathbf{B}^2 + II_{\mathbf{B}}\mathbf{B} - III_{\mathbf{B}}\mathbf{I} = \mathbf{0}, \quad (8.138)$$

the following identities will be helpful:

$$\frac{\partial \text{tr}(\mathbf{C})}{\partial \mathbf{C}} = \mathbf{I}, \quad \frac{1}{2} \frac{\partial}{\partial \mathbf{C}} \left(\text{tr}(\mathbf{C})^2 - \text{tr}(\mathbf{C}^2) \right) = \text{tr}(\mathbf{C})\mathbf{I} - \mathbf{C}. \quad (8.139)$$

- (g) Consider the theory of a nonlinear elastic string that is discussed in Chapter 1. Suppose that the string has a strain energy function $\rho_0\psi = \rho_0(\xi)\psi(\mu, \xi)$ where $\mu = \|\mathbf{r}'\|$ is the stretch of the string and ξ is a convected coordinate. Starting from the energy theorem (1.82)₂ and the local form of the balance of angular momentum (1.84) for the string,

$$\rho_0 \dot{\psi} = \mathbf{n} \cdot \mathbf{v}', \quad \mathbf{r}' \times \mathbf{n} = \mathbf{0}, \quad (8.140)$$

using the results of (a), and the identity $\mu \dot{\mu} = \mathbf{r}' \cdot \mathbf{v}'$, determine the constitutive relations for the contact force \mathbf{n} in the string. Specialize your results to the case of a strain energy function

$$\rho_0\psi = \frac{EA}{2} (\mu - 1)^2. \quad (8.141)$$

When would E and A depend on ξ ? What is $\rho_0\psi$ for a linearly elastic string?

- (h) Suppose that the string in (g) is inextensible. Using the results of (a), develop an expression for the constitutive relations for the string.

Chapter 9

Variational Methods

“Since the fabric of the universe is most perfect, and is the work of a most wise Creator, nothing whatsoever takes place in the universe in which some relation of maximum and minimum does not appear.”

L. Euler [106], as translated in [254, Page 76], introducing his seminal work on elastic curves.

9.1 Introduction

In this supplementary chapter, we give a brief review of methods from the calculus of variations. There are three seminal works on rods that employ these methods. First, Euler’s treatment [106] of the elastica in 1744, that we discussed in Chapter 4, where he examined curves of minimal and maximum curvature. The second work, which dates to 1859, is Kirchhoff’s development of the three-dimensional rod theory discussed in Chapter 5. The third work appeared in 1906 in the guise of the physicist Max Born’s dissertation [31]. In this work, Born (1882–1970) adopted newly developed variational methods to examine the stability of elastic curves. Comparing Kirchhoff’s treatment to Euler’s, we note the use of a principle, that is credited to William R. Hamilton (1805–1865), known as the Principle of Least Action (cf. [185, Eqn. (11)]). During the late 19th century and early 20th century, an explosion of work in the calculus of variations occurred. We are fortunate that the seminal textbook of Bolza [30] distilled and synthesized this work, some of which is discussed in Born’s dissertation, for a broader audience. Bolza’s book provides the framework for our discussion in this chapter of the necessary conditions for a function to extremize an integral. In so doing, we touch upon the connections between variational principles and the material momentum balance that appeared in the earlier chapters of this book.

Using variational principles to establish rod theories and to establish stability criteria has continued to the present day (see, e.g., [76, 217, 330]). Such treatments are not always easily read or comprehended and it is often difficult to imagine extending the formulations to include nonconservative forces and moments. We hope to overcome some of these challenges in this chapter by continually referring to other formulations of the string and rod theories that have been presented in the earlier chapters. In particular, we pay special attention to the application of variational principles to Green and Naghdi's rod theory, elastic strings, and the elastica.

9.2 Variations and Necessary Conditions

Consider a function $f = f\left(y, \frac{dy}{dx}, x\right)$ and the functional

$$I = I(y(x), x_1, x_0) = \int_{x_0}^{x_1} f\left(y, \frac{dy}{dx}, x\right) dx, \quad (9.1)$$

where x_0 and x_1 are fixed, and $y(x)$ satisfies the boundary conditions

$$y(x_0) = y_0, \quad y(x_1) = y_1. \quad (9.2)$$

The fundamental question we wish to answer is which function $y = y^*(x)$ extremizes¹ I ? Dating to Lagrange in the 1760s, the method of approach is to seek *necessary* conditions for a function $y = y^*(x)$ to extremize I .

The first necessary condition established is known as the Euler-Lagrange necessary condition: $y = y^*(x)$ must satisfy

$$\frac{d}{dx} \left(\frac{\partial f}{\partial \frac{dy}{dx}} \left(y^*, \frac{dy^*}{dx}, x \right) \right) - \frac{\partial f}{\partial y} \left(y^*, \frac{dy^*}{dx}, x \right) = 0. \quad (9.3)$$

With the implicit understanding that y and $\frac{dy}{dx}$ are both evaluated using y^* , we simply write this differential equation as

$$\frac{d}{dx} \left(\frac{\partial f}{\partial \frac{dy}{dx}} \right) - \frac{\partial f}{\partial y} = 0, \quad (9.4)$$

and refer to it as the Euler-Lagrange differential equation. In practice, we solve this differential equation to produce a series of candidate functions $y^*(x)$ which satisfy the boundary conditions (9.2), and which possibly extremize I . In other words, we view I as a function of $y(x)$ and seek candidate $y(x)$ s which extremize I .

¹ That is, minimizes or maximizes.

Other necessary conditions need to be satisfied by the candidate functions [30, 119]. These conditions are known as

- (i) the Legendre condition;
- (ii) the Weierstrass necessary condition; and
- (iii) the Jacobi condition.

For smooth functions $y(x)$, these conditions are complemented by the Weierstrass sufficiency condition. More general cases with non-smooth $y(x)$ are accommodated by incorporating the Weierstrass-Erdmann corner conditions (see Eqn. (9.26)). There has been considerable work in calculus of variations on problems with constraints and non-fixed end conditions, among other matters. In this chapter, we limit our scope to the Euler-Lagrange necessary condition and the corner conditions. The latter are often intimately related to the jump conditions for linear momentum, angular momentum, and material momentum that we discussed in earlier chapters of this book.² The Jacobi condition often provides a very useful stability criterion (cf. Section 4.8.2 of Chapter 4), while the Legendre condition,

$$\frac{\partial^2 f}{\partial \frac{dy}{dx} \partial \frac{dy}{dx}} \left(y^*, \frac{dy^*}{dx}, x \right) \geq 0, \quad (9.5)$$

is often identically satisfied for the applications of interest in this book.

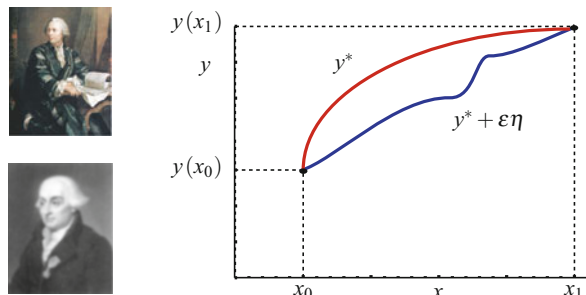


Fig. 9.1 The variations used to establish the Euler-Lagrange necessary condition. The inset images are of (top) Leonhard Euler (1707–1783) and (bottom) Joseph-Louis Lagrange (1736–1813).

9.3 The Euler-Lagrange Necessary Condition

We now examine from whence the Euler-Lagrange necessary condition arose. To start, we consider the following definite integral:

$$I(y(x), x_1, x_0) = \int_{x_0}^{x_1} f \left(y, \frac{dy}{dx}, x \right) dx, \quad (9.6)$$

² An example demonstrating this relationship can be seen in Section 9.3.3 on Page 384.

where x_0 and x_1 are fixed, and $y(x)$ satisfies the boundary conditions

$$y(x_0) = y_0, \quad y(x_1) = y_1. \quad (9.7)$$

Referring to Figure 9.1, suppose $y^*(x)$ is an extremizer, then we can consider a perturbation η to this function:

$$y(x) = y^*(x) + \varepsilon \eta(x), \quad \eta(x_0) = 0, \quad \eta(x_1) = 0. \quad (9.8)$$

After substituting for y in Eqn. (9.6) and then performing a Taylor series expansion about $\varepsilon = 0$, we find that

$$\begin{aligned} I(y^*(x) + \varepsilon \eta(x), x_1, x_0) &= \int_{x_0}^{x_1} f\left(y^*(x) + \varepsilon \eta(x), \frac{dy^*}{dx} + \varepsilon \frac{d\eta}{dx}, x\right) dx \\ &= I(y^*(x)) \\ &\quad + \varepsilon \int_{x_0}^{x_1} \underbrace{\left(-\frac{d}{dx} \left(\frac{\partial f}{\partial \frac{dy}{dx}} \left(y^*, \frac{dy^*}{dx}, x \right) \right) + \frac{\partial f}{\partial y} \left(y^*, \frac{dy^*}{dx}, x \right) \right) \eta}_{+ \mathcal{O}(\varepsilon^2)} dx \\ &\quad + \mathcal{O}(\varepsilon^2). \end{aligned} \quad (9.9)$$

Using an integration by parts on the underbraced term in the integrand, we find that

$$\begin{aligned} \Delta I &= I(y^*(x) + \varepsilon \eta(x), x_1, x_0) - I(y^*(x), x_1, x_0) \\ &= \varepsilon \int_{x_0}^{x_1} \left(-\frac{d}{dx} \left(\frac{\partial f}{\partial \frac{dy}{dx}} \left(y^*, \frac{dy^*}{dx}, x \right) \right) + \frac{\partial f}{\partial y} \left(y^*, \frac{dy^*}{dx}, x \right) \right) \eta dx \\ &\quad + \varepsilon \left[\frac{\partial f}{\partial \frac{dy}{dx}} \left(y^*, \frac{dy^*}{dx}, x \right) \eta \right]_{x_0}^{x_1} + \mathcal{O}(\varepsilon^2). \end{aligned} \quad (9.10)$$

Now, if $y^*(x)$ is a maximizer, say, then we require

$$\Delta I = I(y^*(x) + \varepsilon \eta(x), x_1, x_0) - I(y^*(x), x_1, x_0) \geq 0 \quad (9.11)$$

for all ε . However, ε can be positive or negative, so it is necessary for the $\mathcal{O}(\varepsilon)$ terms in Eqn. (9.10) to vanish. A related remark pertains to the minimizing case. Consequently, we see that it is necessary that

$$\begin{aligned} \int_{x_0}^{x_1} \left(-\frac{d}{dx} \left(\frac{\partial f}{\partial \frac{dy}{dx}} \left(y^*, \frac{dy^*}{dx}, x \right) \right) + \frac{\partial f}{\partial y} \left(y^*, \frac{dy^*}{dx}, x \right) \right) \eta dx \\ + \left[\frac{\partial f}{\partial \frac{dy}{dx}} \left(y^*, \frac{dy^*}{dx}, x \right) \eta \right]_{x_0}^{x_1} = 0. \end{aligned} \quad (9.12)$$

For the case at hand, $\eta(x_0) = 0$ and $\eta(x_1) = 0$ (see Eqn. (9.8)). Hence, the second term in this equation vanishes and we are left with

$$\int_{x_0}^{x_1} \left(-\frac{d}{dx} \left(\frac{\partial f}{\partial \frac{dy}{dx}} \left(y^*, \frac{dy^*}{dx}, x \right) \right) + \frac{\partial f}{\partial y} \left(y^*, \frac{dy^*}{dx}, x \right) \right) \eta dx = 0. \quad (9.13)$$

We now invoke the fundamental lemma of the calculus of variations³ to conclude that $y^*(x)$ must satisfy the differential equation

$$\frac{d}{dx} \left(\frac{\partial f}{\partial \frac{dy}{dx}} \left(y^*, \frac{dy^*}{dx}, x \right) \right) - \frac{\partial f}{\partial y} \left(y^*, \frac{dy^*}{dx}, x \right) = 0. \quad (9.14)$$

We refer to the differential equation (9.14) as the *Euler-Lagrange Necessary Condition*. The function η is known as a variation of y . Whence, the terminology calculus of variations.

9.3.1 Varying Boundary Conditions

In the event that say $y(x_1)$ is not prescribed, then we can return to Eqn. (9.12) to conclude that because $\eta(x_1)$ is now not necessarily zero, the following boundary condition must be satisfied:

$$\frac{\partial f}{\partial \frac{dy}{dx}} \left(y^*(x_1), \frac{dy^*}{dx}(x_1), x_1 \right) = 0. \quad (9.15)$$

In this manner, the calculus of variations often provides traction boundary conditions for problems involving equilibria of rods and strings.

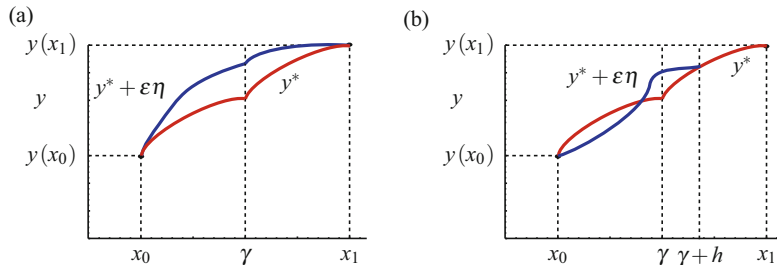


Fig. 9.2 The variations used to establish the Weierstrass-Erdmann corner conditions. (a) Variations to $y^*(x)$ which alter $y^*(\gamma)$ and (b) variations to $y^*(x)$ which alter both $y^*(\gamma)$ and change γ to $\gamma + h$.

³ According to Bolza [30], this lemma states that if g is a continuous function of $x \in (x_0, x_1)$ and if $\int_{x_0}^{x_1} \eta g(x) dx = 0$ for all functions $\eta(x)$ where $\eta(x_0) = 0$, $\eta(x_1) = 0$, and $\frac{\partial \eta}{\partial x}$ is continuous, then $g(x) = 0$ for all $x \in (x_0, x_1)$. This lemma is often referred to as the Du Bois-Reymond lemma.

9.3.2 Weierstrass-Erdmann Corner Conditions

If the function $y^*(x)$ is only piecewise-smooth, then the integration by parts we used to establish Eqn. (9.10) from Eqn. (9.9) can no longer be used. Suppose, as shown in Figure 9.2, that although $y^*(x)$ is continuous at $x = \gamma$, the derivative of $y^*(x)$ has a point of discontinuity at $x = \gamma$. This point of discontinuity is known as a corner. Our purpose here is to examine the additional conditions necessary for $y^*(x)$ to be an extremal.

When examining corners, it is useful to define the Weierstrass excess function

$$E(x, y, p_1, p_2) = f(y, p_2, x) - f(y, p_1, x) - (p_2 - p_1) \frac{\partial f}{\partial \frac{dy}{dx}}(y, p_1, x). \quad (9.16)$$

The variables $p_{1,2}$ in this function play the role of possible values of $\frac{dy}{dx}$.

To proceed, we split the integral I into two parts as we did earlier in establishing jump conditions:⁴

$$I(y(x), x_1, x_0) = I(y(x), \gamma, x_0) + I(y(x), x_1, \gamma). \quad (9.17)$$

Then it can be shown that Eqn. (9.9) now implies that the Euler-Lagrange equation (9.14) applies for all $x \in (x_0, \gamma^-)$ and for all $x \in (\gamma^+, x_1)$. To obtain the corner conditions, two classes of variations are considered. The first corner condition is obtained by considering variations $\varepsilon\eta(x)$ to y^* which only alter $y^*(\gamma)$ without altering the point $x = \gamma$. An example of such a variation is shown in Figure 9.2(a). Using the fact that y^* satisfies the Euler-Lagrange necessary condition for variations of this type we find that

$$\begin{aligned} \Delta I &= I(y^*(x) + \varepsilon\eta, x_1, x_0) - I(y^*(x), x_1, x_0) \\ &= -\varepsilon \left[\left[\frac{\partial f}{\partial \frac{dy}{dx}} \right] \right] \eta(\gamma) + \mathcal{O}(\varepsilon^2), \end{aligned} \quad (9.18)$$

where

$$\begin{aligned} \left[\left[\frac{\partial f}{\partial \frac{dy}{dx}} \right] \right] &= \frac{\partial f}{\partial \frac{dy}{dx}} \left(y^*(\gamma^+), \frac{dy^*}{dx}(\gamma^+), \gamma^+ \right) \\ &\quad - \frac{\partial f}{\partial \frac{dy}{dx}} \left(y^*(\gamma^-), \frac{dy^*}{dx}(\gamma^-), \gamma^- \right). \end{aligned} \quad (9.19)$$

Thus to order ε , we find that the following condition needs to hold at $x = \gamma$:

$$\left[\left[\frac{\partial f}{\partial \frac{dy}{dx}} \right] \right] = 0, \quad (9.20)$$

where $y = y^*(x)$.

⁴ See Section 1.5.3 in Chapter 1.

The second corner condition is obtained by considering a more general class of variations where the corner is moved: $\gamma \rightarrow \gamma + h$, where $h = \mathcal{O}(\varepsilon)$. Referring to Figure 9.2(b), we observe that

$$I(y^*(x) + \varepsilon\eta, x_1, x_0) = I(y^*(x) + \varepsilon\eta, \gamma + h, x_0) + I(y^*(x), x_1, \gamma + h). \quad (9.21)$$

The following compatibility condition for the variations h of x and η of y is readily established:

$$\varepsilon\eta(\gamma) \approx h \left(\frac{dy^*}{dx}(\gamma^+) - \frac{dy^*}{dx}(\gamma^-) \right). \quad (9.22)$$

Now, using the fact that y^* satisfies the Euler-Lagrange necessary condition and employing the mean-value theorem, one arrives at the following results:

$$\begin{aligned} \Delta I &= I(y^*(x) + \varepsilon\eta, x_1, x_0) - I(y^*(x), x_1, x_0) \\ &= I(y^*(x) + \varepsilon\eta, \gamma + h, x_0) - I(y^*(x), \gamma, x_0) - I(y^*(x), \gamma + h, \gamma) \\ &= h \left[\left[\frac{dy}{dx} \right] \right] \frac{\partial f}{\partial \frac{dy}{dx}} \left(y^*(\gamma^-), \frac{dy^*}{dx}(\gamma^-), \gamma^- \right) - h \llbracket f \rrbracket + \mathcal{O}(h), \end{aligned} \quad (9.23)$$

where $y = y^*(x)$.⁵ We can express this result compactly using the Weierstrass excess function:

$$\Delta I = -hE \left(\gamma, y^*(\gamma), \frac{dy^*}{dx}(\gamma^-), \frac{dy^*}{dx}(\gamma^+) \right) + \mathcal{O}(h). \quad (9.24)$$

As we can select h to be positive or negative, we conclude from our expansion of $I(y^*(x) + \varepsilon\eta, x_1, x_0) - I(y^*(x), x_1, x_0)$ that

$$E \left(\gamma, y^*(\gamma), \frac{dy^*}{dx}(\gamma^-), \frac{dy^*}{dx}(\gamma^+) \right) = 0. \quad (9.25)$$

This condition is known as the Weierstrass corner condition. It appears in Exercise 4.9 in Chapter 4.

Combining the conditions (9.20) and (9.25), we arrive at the celebrated Weierstrass-Erdmann corner conditions:

$$\begin{aligned} \left[\left[\frac{\partial f}{\partial \frac{dy}{dx}} \right] \right] &= 0, \\ \left[\left[f - \frac{dy}{dx} \frac{\partial f}{\partial \frac{dy}{dx}} \right] \right] &= 0, \end{aligned} \quad (9.26)$$

⁵ We have refrained from expressing the jumps in the final expression in their full form à la Eqn. (9.19) and we leave it to the reader to do so should they wish.

where $y = y^*(x)$. These conditions date to 1877, and we have followed Bolza [30] in our discussion and derivations. It is important to note that these conditions assume that $y^*(x)$ is continuous at $x = \gamma$.

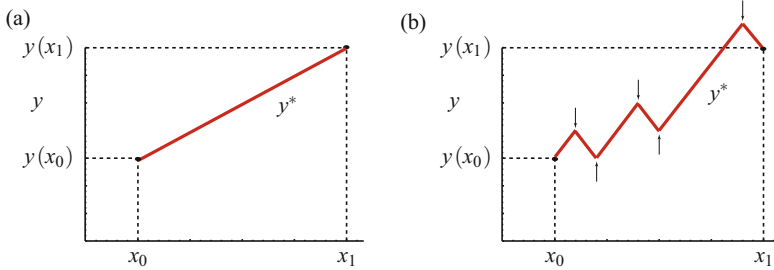


Fig. 9.3 Two examples of extremals. (a) The shortest distance between two points is a straight line. (b) An extremal of Eqn. (9.31) with five corner points (indicated by ↓ and ↑).

9.3.3 Examples

Consider the problem of finding the shortest path between two points y_0 and y_1 . This can be formulated as the problem of finding the function $y(x)$ which extremizes

$$I = \int_{x_0}^{x_1} \sqrt{1 + \left(\frac{dy}{dx}\right)^2} dx. \quad (9.27)$$

The Euler-Lagrange necessary condition for y^* is simply

$$\frac{d}{dx} \left(\frac{1}{\sqrt{1 + \left(\frac{dy^*}{dx}\right)^2}} \frac{dy^*}{dx} \right) = 0. \quad (9.28)$$

Further, the Weierstrass-Erdmann corner conditions are

$$\left[\left[\frac{1}{\sqrt{1 + \left(\frac{dy^*}{dx}\right)^2}} \frac{dy^*}{dx} \right] \right] = 0, \quad \left[\left[\frac{1}{\sqrt{1 + \left(\frac{dy^*}{dx}\right)^2}} \right] \right] = 0. \quad (9.29)$$

The Euler-Lagrange necessary condition is satisfied by all piecewise constant $y(x)$, and the corner conditions imply that the slope of $y(x)$ is continuous. Hence the extremizer is

$$y^*(x) = \left(\frac{y_1 - y_0}{x_1 - x_0} \right) (x - x_0) + y_0. \quad (9.30)$$

That is, as expected, the shortest distance between two points is a straight line (cf. Figure 9.3(a)).

A more intriguing example is the following which can be found in the textbooks [37, 107]. Consider finding the extremizer of

$$I = \int_{x_0}^{x_1} \left(\left(\frac{dy}{dx} \right)^2 - 1 \right)^2 dx. \quad (9.31)$$

There are two types of solutions to the Euler-Lagrange necessary condition and the corner conditions:

$$y^*(x) = \left(\frac{y_1 - y_0}{x_1 - x_0} \right) (x - x_0) + y_0, \quad y^*(x) = \pm x + c_i, \quad (9.32)$$

where c_i are constants which are used to keep $y^*(x)$ continuous at corners. The solutions of the first type are continuous straight lines between the endpoints. Solutions of the second type are far more interesting because it is often possible to construct an infinite number of such solutions joining any two endpoints, and each of these solutions will yield a global minimum $I = 0$. An example of such an extremal is shown in Figure 9.3(b).

Finally, a third example to find extremizers of the potential energy of an elastica of length ℓ subject to constant terminal loadings of $+R\mathbf{A}_1$ at $s = 0$ and $-R\mathbf{A}_1$ at $s = \ell$ (cf. Figure 9.4). Here, s is the arc-length parameter and the problem of interest is discussed in further detail in Chapter 4 (see Section 4.7 in particular). The potential energy of the applied forces can be calculated as follows⁶:

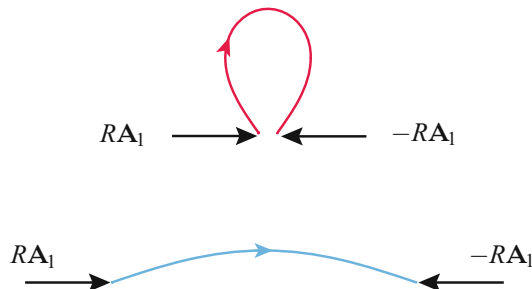


Fig. 9.4 Schematic of a pair of terminally loaded rods of length ℓ .

$$\begin{aligned} R\mathbf{A}_1 \cdot \mathbf{r}(s = \ell) - R\mathbf{A}_1 \cdot \mathbf{r}(s = 0) &= \int_0^\ell R\mathbf{A}_1 \cdot \frac{\partial \mathbf{r}}{\partial s} ds \\ &= \int_0^\ell R \cos(\theta) ds, \end{aligned} \quad (9.33)$$

⁶ You may wish to recall that the potential energy of a constant force \mathbf{P} acting on a particle whose position vector is \mathbf{x} is $-\mathbf{P} \cdot \mathbf{x}$.

where $\frac{\partial \mathbf{r}}{\partial s} = \cos(\theta) \mathbf{A}_1 + \sin(\theta) \mathbf{A}_2$. Combining this potential energy with the strain energy of the elastica we arrive at the functional

$$I = \int_0^\ell \frac{EI}{2} \left(\frac{\partial \theta}{\partial s} \right)^2 + R \cos(\theta) ds. \quad (9.34)$$

Evaluating the Euler-Lagrange necessary condition, we find the familiar equation for Euler's elastica:

$$EI \frac{\partial^2 \theta}{\partial s^2} + R \sin(\theta) = 0. \quad (9.35)$$

Turning to the Weierstrass-Erdmann corner conditions, we find that

$$\left[\left[EI \frac{\partial \theta}{\partial s} \right] \right] = 0, \quad \left[\left[R \cos(\theta) - \frac{EI}{2} \left(\frac{\partial \theta}{\partial s} \right)^2 \right] \right] = 0. \quad (9.36)$$

That is, the bending moment $EI \frac{\partial \theta}{\partial s}$ is continuous and the energy $\frac{EI}{2} \left(\frac{\partial \theta}{\partial s} \right)^2 - R \cos(\theta)$ is continuous. The energy here corresponds to the integral of motion (4.67) discussed in Section 4.5: it is none other than the material contact force C . An extension of this example to an adhesion problem is outlined in Exercise 4.9.

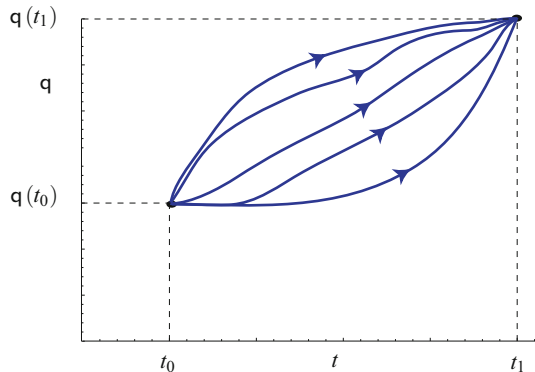


Fig. 9.5 Some of the possible paths $q(t)$ connecting two endpoints, $q(t_0)$ and $q(t_1)$, each of which corresponds to a configuration of a mechanical system. The actual path is the one that satisfies the Euler-Lagrange differential equation. For mechanical systems with a potential energy U and a kinetic energy T , Hamilton's principle states that this path extremizes $I = \int_{t_0}^{t_1} L dt$ where $L = T - U$ (see Eqn. (9.39)).

9.4 Hamilton's Principle of Least Action

The primary reason for the importance of the calculus of variations in mechanics can be traced to an observation by William R. Hamilton (1805–1865) in 1835 (see Figure 9.5). He noted that the solutions to Lagrange's equations of motion for an n degree-of-freedom mechanical system in the absence of constraints extremizes the so-called action integral:

$$A = \int_{t_0}^{t_1} L(\mathbf{q}, \dot{\mathbf{q}}, t) dt, \quad (9.37)$$

where L is the Lagrangian, $\mathbf{q} = (q^1, \dots, q^n)$ are the generalized coordinates, and $\dot{\mathbf{q}} = (\dot{q}^1, \dots, \dot{q}^n)$ are the generalized velocities. Extending the Euler-Lagrange equation (9.14) to this case, we see that the extremizer satisfies Lagrange's equations of motion:

$$\frac{d}{dt} \left(\frac{\partial L}{\partial \dot{q}^i} \right) - \frac{\partial L}{\partial q^i} = 0, \quad (i = 1, \dots, n). \quad (9.38)$$

For a mechanical system, Hamilton's Principle of Least Action then implies that we can calculate the equations of motion by simply computing L .⁷ Indeed, this is precisely the route taken by Kirchhoff [185] when he established the governing equations for his rod theory.

Hamilton's principle was extended in a variety of manners in the ensuing years. For instance, consider a system whose Lagrangian depends on $\frac{\partial q^i}{\partial t}$ and $\frac{\partial q^i}{\partial x}$. Then, the extremizer satisfies the partial differential equations⁸

$$\frac{d}{dt} \left(\frac{\partial L}{\partial \frac{\partial q^i}{\partial t}} \right) + \frac{d}{dx} \left(\frac{\partial L}{\partial \frac{\partial q^i}{\partial x}} \right) - \frac{\partial L}{\partial q^i} = 0. \quad (9.39)$$

The derivation of the associated Weierstrass-Erdmann corner conditions for this functional is beyond our present scope. We now turn to applying Eqn. (9.39) to a variety of strings and rods.

9.5 The Wave Equation

Consider an elastic string. Assume that it is stretched between two fixed points $\mathbf{r}(\xi_1) = \mathbf{0}$ and $\mathbf{r}(\xi_2) = \ell \mathbf{E}_1$. Suppose that the string has a strain energy function

$$\rho_0 \psi(\mu) = \frac{EA}{4} (\mu^2 - 1)^2, \quad (9.40)$$

⁷ As is well known, for the principle to apply for a mechanical system the only forces which do work need to be conservative, the constraints need to be holonomic, and the constraint forces need to be prescribed using Lagrange's prescription [265].

⁸ See the introductory text by Weinstock [358] for a discussion of how to derive this result.

where

$$\mu = \sqrt{\frac{\partial \mathbf{r}}{\partial \xi} \cdot \frac{\partial \mathbf{r}}{\partial \xi}}. \quad (9.41)$$

Once the string of initial length ℓ_0 is stretched between the end points, a constant stretch μ_0 is induced:

$$\mathbf{r}(\xi, t) = \mathbf{r}_0 = \left(\frac{\ell}{\ell_0} \right) \xi \mathbf{E}_1, \quad \mu_0 = \frac{\ell}{\ell_0}. \quad (9.42)$$

The contact force in the string is given by

$$\mathbf{n} = \rho_0 \frac{\partial \psi}{\partial \xi} = EA (\mu_0^2 - 1) \frac{\partial \mathbf{r}}{\partial \xi} = EA (\mu_0^2 - 1) \mu_0 \mathbf{E}_1. \quad (9.43)$$

For future purposes, we define T_0 :

$$T_0 = EA (\mu_0^2 - 1) \mu_0. \quad (9.44)$$

This is the tension in the string in its stretched state.

We now consider perturbations to this static solution:

$$\mathbf{r} = \mathbf{r}_0 + \varepsilon u \mathbf{E}_2. \quad (9.45)$$

Here, \mathbf{E}_2 is normal to the line connecting the points $\mathbf{r}(\xi_1)$ and $\mathbf{r}(\xi_2)$. We also define a new arc-length coordinate s :

$$s = \mu_0 \xi, \quad \frac{df}{ds} = \frac{\ell_0}{\ell} \frac{df}{d\xi} \quad (9.46)$$

It is also convenient to define a density ρ of the string in its stretched state: $\rho_0 = \mu_0 \rho$.

Substituting for T_0 and \mathbf{r} into the strain energy and the kinetic energy of the string, we can formulate the Lagrangian density:

$$\varepsilon \mathcal{L} = \varepsilon \left(\frac{\mu_0 \rho}{2} \dot{u}^2 - \frac{T_0}{2} \left(\frac{\partial u}{\partial \xi} \right)^2 \right). \quad (9.47)$$

Here, we have ignored terms of order ε^0 and ε^2 .

To formulate the equations of motion of the string, we invoke Hamilton's Principle of Least Action and seek extremizers $u(\xi, t)$ of the following integral⁹:

$$\int_{t_0}^{t_1} \int_{\xi_0}^{\xi_1} \frac{\mu_0 \rho}{2} \dot{u}^2 - \frac{T_0}{2} \left(\frac{\partial u}{\partial \xi} \right)^2 d\xi dt. \quad (9.48)$$

⁹ Note that we can change variables from ξ to s without any significant change to the analysis.

Using Eqn. (9.39), we find that

$$\frac{d}{dt} (\rho_0 \dot{u}) - \frac{d}{d\xi} \left(T_0 \frac{\partial u}{\partial \xi} \right) = 0. \quad (9.49)$$

As T_0 and ρ_0 are constant, this partial differential equation reduces to the familiar wave equation.

It is interesting to note that for static solutions, the Weierstrass-Erdman corner conditions (9.26) show that $\frac{du}{d\xi}$ is continuous.

9.6 Application to Green and Naghdi's Rod Theory

Consider Green and Naghdi's rod theory that is discussed at length in Chapter 7. Here, we consider an elastic rod in the absence of body forces and surface tractions, and seek to use Hamilton's Principle of Least Action to establish the equations of motion. While Green and Naghdi were probably well aware that the equations of motion for their rod theory satisfied a variational principle, we have not been able to find an explicit statement in their published works. We also note that the results below pertain to an elastic string if the directors are ignored. It may be advantageous on a first reading through the text to restrict attention to this case.

For a rod of length $\ell = \xi_1 - \xi_0$ in its reference configuration, the strain energy per unit length of the material coordinate ξ is $\rho_0 \psi$ and the kinetic energy is

$$T = \frac{\rho_0}{2} \left(\dot{\mathbf{r}} \cdot \dot{\mathbf{r}} + 2 \sum_{\alpha=1}^2 y^{0\alpha} \dot{\mathbf{r}} \cdot \dot{\mathbf{d}}_\alpha + \sum_{\alpha=1}^2 \sum_{\beta=1}^2 y^{\alpha\beta} \dot{\mathbf{d}}_\alpha \cdot \dot{\mathbf{d}}_\beta \right). \quad (9.50)$$

We construct a Lagrangian density

$$\mathcal{L} = T - \rho_0 \psi. \quad (9.51)$$

Note that

$$\psi = \psi(\gamma_{ik}, \kappa_{1j}, \kappa_{2j}, \xi) = \psi(\mathbf{r}', \mathbf{d}_\alpha, \mathbf{d}'_\beta, \xi), \quad (9.52)$$

where the prime denotes a partial derivative with respect to ξ . We next apply Hamilton's principle to the Lagrangian:

$$I = \int_{t_0}^{t_1} \int_{\xi_0}^{\xi_1} T - \rho_0 \psi d\xi. \quad (9.53)$$

The equations (9.39) can be expressed as

$$\begin{aligned}
& - \frac{d}{d\xi} \left(\underbrace{\rho_0 \frac{\partial \psi}{\partial \mathbf{r}'}}_{=\mathbf{n}} \right) + \frac{d}{dt} \left(\frac{\partial T}{\partial \dot{\mathbf{r}}} \right) + \underbrace{\rho_0 \frac{\partial \psi}{\partial \mathbf{r}}}_{=0} = \mathbf{0}, \\
& - \frac{d}{d\xi} \left(\underbrace{\rho_0 \frac{\partial \psi}{\partial \mathbf{d}'_\beta}}_{=\mathbf{m}^\beta} \right) + \frac{d}{dt} \left(\frac{\partial T}{\partial \dot{\mathbf{d}}_\beta} \right) + \underbrace{\rho_0 \frac{\partial \psi}{\partial \mathbf{d}_\beta}}_{=\mathbf{k}^\beta} = \mathbf{0}. \tag{9.54}
\end{aligned}$$

In these equations, we have identified the contact force \mathbf{n} , contact director forces \mathbf{m}^1 and \mathbf{m}^2 , and intrinsic director forces \mathbf{k}^1 and \mathbf{k}^2 using the constitutive relations.

Referring to Eqn. (7.50), it should be easy to see that the differential equations (9.54) are equivalent to the balances of linear and director momenta with $\mathbf{f} = \mathbf{0}$ and $\mathbf{l}^\alpha = \mathbf{0}$:

$$\begin{aligned}
\rho_0 \ddot{\mathbf{r}} + \sum_{\alpha=1}^2 \rho_0 y^{0\alpha} \ddot{\mathbf{d}}_\alpha &= \underbrace{\rho_0 \mathbf{f}}_{=0} + \frac{\partial \mathbf{n}}{\partial \xi}, \\
\rho_0 y^{0\alpha} \ddot{\mathbf{r}} + \sum_{\beta=1}^2 \rho_0 y^{\alpha\beta} \ddot{\mathbf{d}}_\beta &= \underbrace{\rho_0 l^\alpha}_{=0} - \mathbf{k}^\alpha + \frac{\partial \mathbf{m}^\alpha}{\partial \xi}. \tag{9.55}
\end{aligned}$$

Consequently, the balances of linear and director momenta can be expressed using a variational principle. Referring to Eqns. (7.53) and (9.26), the Weierstrass-Erdmann corner conditions for static solutions dictate that \mathbf{n} , \mathbf{m}^α , and \mathbf{C} are continuous - as expected.

We can extend the above results to the case where $\rho_0 \mathbf{f}$ and $\rho_0 \mathbf{l}^\beta$ are conservative:

$$\rho_0 \mathbf{f} = - \frac{\partial U}{\partial \mathbf{r}}, \quad \rho_0 \mathbf{l}^\beta = - \frac{\partial U}{\partial \mathbf{d}_\beta}, \tag{9.56}$$

where $U = U(\mathbf{r}, \mathbf{d}_\beta, \xi)$ is the potential energy. In this case, we would use a Lagrangian density

$$\mathcal{L} = T - \rho_0 \psi - U. \tag{9.57}$$

Note also that our results here can be readily applied to an elastic string by ignoring the directors and their associated fields.

9.7 Closing Remarks

The Euler-Lagrange necessary condition and the Weierstrass-Erdmann corner conditions for functionals in this chapter provide necessary conditions for a function to extremize a functional. As emphasized in the examples we have just presented, the

extremization is often equivalent to satisfaction of the balance laws and jump conditions for mechanical systems. One issue that then presents itself is the stability or instability of the resulting solution. In addressing this issue, methods from the calculus of variations are exceptional. In works ranging from Born's dissertation [31] and the more recent works by Maddocks and his collaborators [169, 215, 224–226], one finds that the calculus provides a framework for establishing nonlinear stability criteria and a clear pathway to relating these criteria to linear stability criteria obtained from linearization. In the chapter on Euler's elastica, Chapter 4, we discuss methods based on the second variation of a functional to determine stability criteria. The resulting criteria enable us to predict not only buckling but also adhesive instabilities.

References

1. Abeyaratne, R., Knowles, J.K.: On the driving traction acting on a surface of strain discontinuity in a continuum. *Journal of the Mechanics and Physics of Solids* **38**(3), 345–360 (1990). URL [http://dx.doi.org/10.1016/0022-5096\(90\)90003-M](http://dx.doi.org/10.1016/0022-5096(90)90003-M) [369, 370]
2. Abeyaratne, R., Knowles, J.K.: Kinetic relations and the propagation of phase boundaries in solids. *Archive for Rational Mechanics and Analysis* **114**(2), 119–154 (1991). URL <http://dx.doi.org/10.1007/BF00375400> [25, 44, 55, 309, 370]
3. Abeyaratne, R., Knowles, J.K.: Nucleation, kinetics and admissibility criteria for propagating phase boundaries. In: R. Fosdick, E. Dunn, H. Slemrod (eds.) Shock induced transitions and phase structures in general media, *IMA Volumes in Mathematics and its Applications*, vol. 52, pp. 1–33. Springer-Verlag, New York (1993). URL http://dx.doi.org/10.1007/978-1-4613-8348-2_1 [30, 309, 370]
4. Abeyaratne, R., Knowles, J.K.: A note on the driving traction acting on a propagating interface: Adiabatic and non-adiabatic processes of a continuum. *ASME Journal of Applied Mechanics* **67**(4), 829–831 (2000). URL [http://dx.doi.org/10.1016/S0167-2789\(05\)80008-9](http://dx.doi.org/10.1016/S0167-2789(05)80008-9) [369, 370]
5. Abeyaratne, R., Knowles, J.K.: Evolution of Phase Transitions: A Continuum Theory. Cambridge University Press, Cambridge (2006). URL <http://dx.doi.org/10.1017/CBO9780511547133> [25, 33, 37, 42, 43, 44, 55, 91, 369, 370]
6. Agoston, M.K.: Computer Graphics and Geometric Modelling: Mathematics. Springer-Verlag, London (2005). URL <http://dx.doi.org/10.1007/b138899> [98]
7. Aldinger, J., Klapper, I., Tabor, M.: Formulae for the calculation and estimation of writhe. *Journal of Knot Theory and its Ramifications* **4**(3), 343–372 (1995). URL <http://dx.doi.org/10.1142/S021821659500017X> [106, 109, 110]

8. Alexander, J.C., Antman, S.S.: The ambiguous twist of Love. *Quarterly of Applied Mathematics* **40**(1), 83–92 (1982/83) [161]
9. Antman, S.S.: The theory of rods. In: C. Truesdell (ed.) *Linear Theories of Elasticity and Thermoelasticity: Linear and Nonlinear Theories of Rods, Plates, and Shells*, pp. 641–703. Springer-Verlag, Berlin, Heidelberg (1973). URL http://dx.doi.org/10.1007/978-3-662-39776-3_6 [334]
10. Antman, S.S.: Kirchhoff's problem for nonlinearly elastic rods. *Quarterly of Applied Mathematics* **32**, 221–240 (1974) [188, 269, 270, 297]
11. Antman, S.S.: Multiple equilibrium states of nonlinearly elastic strings. *SIAM Journal of Applied Mathematics* **37**(3), 588–604 (1979). URL <http://dx.doi.org/10.1137/0137043> [80]
12. Antman, S.S.: Nonlinear Problems of Elasticity, *Applied Mathematical Sciences*, vol. 107, second edn. Springer-Verlag, New York (2005) [viii, 22, 32, 80, 187, 188, 189, 206, 270, 277, 290, 297, 304, 337, 345]
13. Antman, S.S., Liu, T.P.: Travelling waves in hyperelastic rods. *Quarterly of Applied Mathematics* **36**(4), 377–399 (1979). URL <http://www.jstor.org/stable/43636943> [291]
14. Antman, S.S., Marlow, R.S.: Material constraints, Lagrange multipliers, and compatibility. Applications to rod and shell theories. *Archive for Rational Mechanics and Analysis* **116**(3), 257–299 (1991). URL <http://dx.doi.org/10.1007/BF00375123> [361]
15. Arnol'd, V.I.: Mathematical Methods of Classical Mechanics, *Graduate Texts in Mathematics*, vol. 60, second edn. Springer-Verlag, New York (1989). Translated from the Russian by K. Vogtmann and A. Weinstein [225]
16. Autumn, K., Sitti, M., Liang, Y.A., Peattie, A.M., Hansen, W.R., Sponberg, S., Kenny, T.W., Fearing, R., Israelachvili, J.N., Full, R.J.: Evidence for van der Waals adhesion in gecko setae. *Proceedings of the National Academy of Sciences* **99**(19), 12,252–12,256 (2002). URL <http://dx.doi.org/10.1073/pnas.192252799> [137]
17. Batista, M.: Analytical treatment of equilibrium configurations of cantilever under terminal loads using Jacobi elliptical functions. *International Journal of Solids and Structures* **51**(13), 2308–2326 (2014). URL <http://dx.doi.org/10.1016/j.ijsolstr.2014.02.036> [135]
18. Bauer, W.R., Lund, R.A., White, J.H.: Twist and writhe of a DNA loop containing intrinsic bends. *Proceedings of the National Academy of Sciences* **90**(3), 833–837 (1993) [114]
19. Bechtel, S.E., Forest, M.G., Bogy, D.B.: A one-dimensional theory for viscoelastic fluid jets, with application to extrudate swell and draw-down under gravity. *Journal of Non-Newtonian Fluid Mechanics* **21**(3), 273–308 (1986). URL [http://dx.doi.org/10.1016/0377-0257\(86\)80041-6](http://dx.doi.org/10.1016/0377-0257(86)80041-6) [296, 324]
20. Berger, M.A.: Topological quantities: Calculating winding, writhing, linking, and higher order invariants. In: R.L. Ricca (ed.) *Lectures on Topological Fluid Mechanics, Lecture Notes in Mathematics*, pp. 75–97. Springer-Verlag, Berlin, Heidelberg (2009). URL http://dx.doi.org/10.1007/978-3-642-00837-5_2 [110]

21. Berger, M.A., Prior, C.: The writhe of open and closed curves. *Journal of Physics A: Mathematical and General* **39**(26), 8321 (2006). URL <http://dx.doi.org/10.1088/0305-4470/39/26/005> [110, 111]
22. Bergou, M., Wardetzky, M., Robinson, S., Audoly, B., Grinspan, E.: Discrete elastic rods. *ACM Transactions on Graphics (SIGGRAPH)* **27**(3), 63:1–63:12 (2008) [96, 97, 188, 239]
23. Biggins, J.S.: Growth and shape of a chain fountain. *Europhysics Letters* **106**(4), 44,001 (2014). URL <http://stacks.iop.org/0295-5075/106/i=4/a=44001> [50, 58, 69, 70, 78, 83, 85]
24. Biggins, J.S., Warner, M.: Understanding the chain fountain. *Proceedings of the Royal Society A: Mathematical, Physical and Engineering Science* **470**(2163) (2014). URL <http://dx.doi.org/10.1098/rspa.2013.0689> [78]
25. Bigoni, D., Bosi, F., Corso, F.D., Misseroni, D.: Instability of a penetrating blade. *Journal of the Mechanics and Physics of Solids* **64**, 411 – 425 (2014). URL <http://dx.doi.org/10.1016/j.jmps.2013.12.008> [147]
26. Bigoni, D., Bosi, F., Misseroni, D., Dal Corso, F., Noselli, G.: New phenomena in nonlinear elastic structures: from tensile buckling to configurational forces. In: D. Bigoni (ed.) *Extremely Deformable Structures*, pp. 55–135. Springer-Verlag, Vienna (2015). URL http://dx.doi.org/10.1007/978-3-7091-1877-1_2 [122, 135, 147]
27. Bigoni, D., Corso, F.D., Bosi, F., Misseroni, D.: Eshelby-like forces acting on elastic structures: Theoretical and experimental proof. *Mechanics of Materials* **80**, 368–374 (2015). URL <http://dx.doi.org/10.1016/j.mechmat.2013.10.009> [147, 165, 167]
28. Bishop, R.L.: There is more than one way to frame a curve. *The American Mathematical Monthly* **82**(3), 246–251 (1975). URL <http://dx.doi.org/10.2307/2319846> [96, 98, 117, 118]
29. Bishop, R.L., Goldberg, S.I.: *Tensor Analysis on Manifolds*. Dover Publications, New York (1980) [349]
30. Bolza, O.: *Lectures on the Calculus of Variations*, third edn. Chelsea, New York (1973) [122, 169, 185, 377, 379, 381, 384]
31. Born, M.: Untersuchungen über die Stabilität der elastischen Linie in Ebene und Raum, unter verschiedenen Grenzbedingungen. Dieterichsche Universitäts-Buchdruckerei, Göttingen (1906) [122, 377, 391]
32. Bosi, F., Misseroni, D., Dal Corso, F., Bigoni, D.: An elastica arm scale. *Proceedings of the Royal Society A: Mathematical, Physical and Engineering Science* **470**(2169), 20140,232 (2014). URL <http://dx.doi.org/10.1098/rspa.2014.0232> [121, 147, 148, 150, 154, 159, 160, 165, 167]
33. Bosi, F., Misseroni, D., Dal Corso, F., Bigoni, D.: Development of configurational forces during the injection of an elastic rod. *Extreme Mechanics Letters* **4**, 83–88 (2015). URL <http://dx.doi.org/10.1016/j.eml.2015.04.007> [147]

34. Bosi, F., Misseroni, D., Dal Corso, F., Bigoni, D.: Self-encapsulation, or the ‘dripping’ of an elastic rod. *Proceedings of the Royal Society of London A: Mathematical, Physical and Engineering Sciences* **471**(2179), 20150,195 (2015). URL <http://dx.doi.org/10.1098/rspa.2015.0195> [147]
35. Bouchiat, C., Mézard, M.: Elastic rod model of a supercoiled DNA molecule. *The European Physical Journal E* **2**(4), 377–402 (2000). URL <http://dx.doi.org/10.1007/s101890050020> [285]
36. Braun, M.: Configurational forces induced by finite element discretization. *Proceedings of the Estonian Academy of Sciences. Physics, Mathematics* **46**(1–2), 24–31 (1997) [366]
37. Breckken-Manderscheid, U.: *Introduction to the Calculus of Variations*. Chapman & Hall, London (1991). Translated from German by P. G. Engstrom [385]
38. Brun, P.T., Audoly, B., Goriely, A., Vella, D.: The surprising dynamics of a chain on a pulley: lift off and snapping. *Proceedings of the Royal Society of London A: Mathematical, Physical and Engineering Sciences* **472**(2190), 20160,187 (2016). URL <http://dx.doi.org/10.1098/rspa.2016.0187> [67]
39. Burridge, R., Keller, J.B.: Peeling, slipping and cracking - Some one-dimensional free-boundary problems in mechanics. *SIAM Review* **20**(1), 31–61 (1978). URL <http://dx.doi.org/10.1137/1020003> [30]
40. Bustamante, C., Bryant, Z., Smith, S.B.: Ten years of tension: Single-molecule DNA mechanics. *Nature* **421**, 423–427 (2003). URL <http://dx.doi.org/10.1038/nature01405> [115, 270, 284]
41. Byrd, P.F., Friedman, M.D.: *Handbook of Elliptic Integrals for Engineers and Scientists, Die Grundlehren der mathematischen Wissenschaften*, vol. 67. Springer-Verlag, New York (1971). Second edition, revised [142, 143, 146, 160]
42. Călugăreanu, G.: L’intégrale de Gauss et l’analyse des noeuds tridimensionnels. *Revue Roumaine Mathématique Pures et Appliqué* **4**, 5–20 (1959) [93, 98, 108, 114]
43. Călugăreanu, G.: Sur les classes d’isotopie des noeuds tridimensionnels et leurs invariants. *Czechoslovak Mathematical Journal* **11** (86), 588–625 (1961) [109, 110, 116]
44. Călugăreanu, G.: Sur les enlacements tridimensionnels des courbes fermées. *Comptes Rendus Academie R. P. Romîne* **11**, 829–832 (1961) [93, 108, 114]
45. Cambou, A.D., Gamari, B.D., Hamm, E., Hanna, J.A., Menon, N., Santangelo, C.D., Walsh, L.: Unwrapping chains (2012). URL <http://arxiv.org/abs/1209.0481> [67]
46. Carlson, D.E., Fried, E., Tortorelli, D.A.: Geometrically-based consequences of internal constraints. *Journal of Elasticity* **70**(1), 101–109 (2003). URL <http://dx.doi.org/10.1023/B:ELAS.0000005582.52534.2d> [317, 361, 364, 373]

47. Carlson, D.E., Tortorelli, D.A.: On hyperelasticity with internal constraints. *Journal of Elasticity* **42**(1), 91–98 (1996). URL <http://dx.doi.org/10.1007/BF00041225> [317, 321, 361]
48. Casey, J.: A treatment of rigid body dynamics. *ASME Journal of Applied Mechanics* **50**, 905–907 and 51 227 (1983). URL <http://dx.doi.org/10.1115/1.3167171> [205]
49. Casey, J., Carroll, M.M.: Discussion of “A treatment of internally constrained materials” by J. Casey. *ASME Journal of Applied Mechanics* **63**(1), 240 (1996). URL <http://dx.doi.org/10.1115/1.2787205> [34, 361, 363]
50. Casey, J., Krishnaswamy, S.: A characterization of internally constrained thermoelastic materials. *Mathematics and Mechanics of Solids* **3**(1), 71–89 (1998). URL <http://dx.doi.org/10.1177/108128659800300105> [317, 321, 361, 364, 373]
51. Casey, J., Lam, V.C.: On the relative angular velocity tensor. *ASME Journal of Mechanisms, Transmissions, and Automation in Design* **108**, 399–400 (1986). URL <http://dx.doi.org/10.1115/1.3258746> [196]
52. Casey, J., Naghdi, P.M.: On the Lagrangian description of vorticity. *Archive for Rational Mechanics and Analysis* **115**(1), 1–14 (1991). URL <http://dx.doi.org/10.1007/BF01881677> [56]
53. Cayley, A.: On a class of dynamical problems. *Proceedings of the Royal Society of London* **8**, 506–511 (1856). URL <http://dx.doi.org/10.1098/rspl.1856.0133> [60, 62, 64]
54. Chadwick, P.: Applications of an energy-momentum tensor in non-linear elastostatics. *Journal of Elasticity* **5**(3), 249–258 (1975). URL <http://dx.doi.org/10.1007/BF00126989> [365, 367]
55. Chadwick, P.: Continuum Mechanics, second corrected and enlarged edn. Dover Publications, New York (1999) [27, 355]
56. Chen, J.S.: Natural frequencies and stability of an axially-travelling string in contact with a stationary load system. *ASME Journal of Vibration and Acoustics* **119**(2), 152–157 (1997). URL <http://dx.doi.org/10.1115/1.2889696> [22]
57. Chen, L.Q.: Analysis and control of transverse vibrations of axially moving strings. *ASME Applied Mechanics Reviews* **58**(2), 91–116 (2005). URL <http://dx.doi.org/10.1115/1.1849169> [4]
58. Cheng, S.P., Perkins, N.C.: The vibration and stability of a friction-guided, translating string. *Journal of Sound and Vibration* **144**(2), 281–292 (1991). URL [http://dx.doi.org/10.1016/0022-460X\(91\)90749-A](http://dx.doi.org/10.1016/0022-460X(91)90749-A) [22]
59. Choquet-Bruhat, Y., DeWitt-Morette, C., Dillard Bleick, M.: Analysis, Manifolds, and Physics, revised edn. North-Holland Physics Publishing, Amsterdam (1982) [349]
60. Chouaieb, N., Goriely, A., Maddocks, J.H.: Helices. *Proceedings of the National Academy of Sciences* **103**(25), 9398–9403 (2006). URL <http://dx.doi.org/10.1073/pnas.0508370103> [225]

61. Clauvelin, N., Audoly, B., Neukirch, S.: Matched asymptotic expansions for twisted elastic knots: A self-contact problem with non-trivial contact topology. *Journal of the Mechanics and Physics of Solids* **57**(9), 1623–1656 (2009). URL <http://dx.doi.org/10.1016/j.jmps.2009.05.004> [239]
62. Cohen, H.: Homogeneous monotropic elastic rods: Normal uniform configurations and universal solutions. *Mecchanica* **31**(5), 527–546 (1996). URL <http://dx.doi.org/10.1007/BF00420824> [277]
63. Cohen, H., Epstein, M.: On a class of planar motions of flexible rods. *ASME Journal of Applied Mechanics* **61**(1), 206–208 (1994). URL <http://dx.doi.org/10.1115/1.2901402> [52]
64. Cohen, H., Whitman, A.B.: Waves in elastic rods. *Journal of Sound and Vibration* **51**(2), 283–302 (1977). URL [http://dx.doi.org/10.1016/S0022-460X\(77\)80037-0](http://dx.doi.org/10.1016/S0022-460X(77)80037-0) [312, 335]
65. Coleman, B.D., Dill, E.H.: Flexure waves in elastic rods. *Journal of the Acoustical Society of America* **91**(5), 2663–2673 (1992). URL <http://dx.doi.org/10.1121/1.402974> [52, 135]
66. Coleman, B.D., Dill, E.H., Swigon, D.: On the dynamics of flexure and stretch in the theory of elastic rods. *Archive for Rational Mechanics and Analysis* **129**(2), 147–174 (1995). URL <http://dx.doi.org/10.1007/BF00379919> [128, 291]
67. Coleman, B.D., Swigon, D.: Theory of supercoiled elastic rings with self-contact and its application to DNA plasmids. *Journal of Elasticity* **60**(3), 173–221 (2000). URL <http://dx.doi.org/10.1023/A:101091113919> [93, 239]
68. Coleman, B.D., Swigon, D.: Theory of self-contact in Kirchhoff rods with applications to supercoiling of knotted and unknotted DNA plasmids. *Philosophical Transactions of the Royal Society of London A: Mathematical, Physical and Engineering Sciences* **362**(1820), 1281–1299 (2004). URL <http://dx.doi.org/10.1098/rsta.2004.1393> [114, 239]
69. Coleman, B.D., Swigon, D., Tobias, I.: Elastic stability of DNA configurations. I. General theory. *Physical Review E* **61**, 747–758 (2000). URL <http://dx.doi.org/10.1103/PhysRevE.61.747>
70. Coleman, B.D., Swigon, D., Tobias, I.: Elastic stability of DNA configurations. II. Supercoiled plasmids with self-contact. *Physical Review E* **61**, 759–770 (2000). URL <http://dx.doi.org/10.1103/PhysRevE.61.759> [93]
71. Cosserat, E., Cosserat, F.: Sur la statique de la ligne déformable. *Compte Rendus de l'Académie des Sciences, Paris* **145**, 1409–1412 (1907) [188]
72. Cosserat, E., Cosserat, F.: *Théorie des Corps Déformables*. A. Hermann et Fils, Paris (1909) [188]
73. Costello, G.A.: *Theory of Wire Rope*. Springer-Verlag, New York (1990). URL <http://dx.doi.org/10.1007/978-1-4684-0350-3> [287]
74. Cowper, G.R.: The shear coefficient in Timoshenko's beam theory. *ASME Journal of Applied Mechanics* **33**(2), 335–340 (1966). URL <http://dx.doi.org/10.1115/1.3625046> [291, 338]

75. Coyne, J.: Analysis of the formation and elimination of loops in twisted cable. *IEEE Journal of Oceanic Engineering* **15**(2), 72–83 (1990). URL <http://dx.doi.org/10.1109/48.50692> [225, 233, 235, 239]
76. Crespo da Silva, M.R.M., Glynn, C.C.: Nonlinear flexural-flexural-torsional dynamics of inextensional beams. I. Equations of motion. *Journal of Structural Mechanics* **6**(4), 437–448 (1978). URL <http://dx.doi.org/10.1080/03601217808907348> [378]
77. Crick, F.H.: Linking numbers and nucleosomes. *Proceedings of the National Academy of Sciences* **73**(8), 2639–2643 (1976). URL <http://www.pnas.org/content/73/8/2639.abstract> [94, 110]
78. Cusumano, J.P., Moon, F.C.: Chaotic non-planar vibrations of the thin elastica: Part I: Experimental observation of planar instability. *Journal of Sound and Vibration* **179**(2), 185–208 (1995). URL <http://dx.doi.org/10.1006/jsvi.1995.0013> [188]
79. Cusumano, J.P., Moon, F.C.: Chaotic non-planar vibrations of the thin elastica: Part II: Derivation and analysis of a low-dimensional model. *Journal of Sound and Vibration* **179**(2), 209–226 (1995). URL <http://dx.doi.org/10.1006/jsvi.1995.0014> [188]
80. Dafermos, C.M.: Hyperbolic Conservation Laws in Continuum Physics, *Grundlehren der Mathematischen Wissenschaften [Fundamental Principles of Mathematical Sciences]*, vol. 325, fourth edn. Springer-Verlag, Berlin (2016). URL <http://dx.doi.org/10.1007/978-3-662-49451-6> [43, 91]
81. Darwin, C.R.: On the movements and habits of climbing plants. *Journal of the Linnean Society of London, Botany* **9**(33–34), 1–118 (1865). URL <10.1111/j.1095-8339.1865.tb00011.x>. Second edition printed in London in 1875 by J. Murray. [240]
82. Dascalu, C., Maugin, G.A.: The thermoelastic material-momentum equation. *Journal of Elasticity* **39**(3), 201–212 (1995). URL <http://dx.doi.org/10.1007/BF00041837> [365]
83. Daune, M.: Molecular Biophysics: Structures in Motion. Oxford University Press, New York (1999). Translated from the French by W. J. Duffin. [115]
84. Davies, M.A., Moon, F.C.: 3-D spatial chaos in the elastica and the spinning top: Kirchhoff analogy. *Chaos* **3**(1), 93–99 (1993). URL <http://dx.doi.org/10.1063/1.165969> [239]
85. Dennis, M.R., Hannay, J.H.: Geometry of Călugăreanu's theorem. *Proceedings of the Royal Society A: Mathematical, Physical and Engineering Science* **461**(2062), 3245–3254 (2005). URL <http://dx.doi.org/10.1098/rspa.2005.1527> [93, 110]
86. Dichmann, D.J., Li, Y., Maddocks, J.H.: Hamiltonian formulations and symmetries in rod mechanics. In: J.P. Mesirow, K. Schulten, D. Sumners (eds.) Mathematical approaches to biomolecular structure and dynamics (Minneapolis, MN, 1994), *The IMA Volumes in Mathematics and its Applications*, vol. 82, pp. 71–113. Springer-Verlag, New York (1996). URL http://dx.doi.org/10.1007/978-1-4612-4066-2_6 [193, 234, 270]

87. Dickey, R.W.: The nonlinear string under a vertical force. *SIAM Journal of Applied Mathematics* **17**, 172–178 (1969). URL <http://dx.doi.org/10.1137/0117016> [80]
88. Dickey, R.W.: *Bifurcation Problems in Nonlinear Elasticity*. Pitman Publishing, London, San Francisco, Melbourne (1976) [80]
89. Đuričković, B., Goriely, A., Maddocks, J.H.: Twist and stretch of helices explained via the Kirchhoff-Love rod model of elastic filaments. *Physical Review Letters* **111**, 108,103 (2013). URL <http://link.aps.org/doi/10.1103/PhysRevLett.111.108103> [253, 256, 257, 284]
90. Domokos, G., Healey, T.J.: Multiple helical perversions of finite, intrinsically curved rods. *International Journal of Bifurcation and Chaos* **15**(3), 871–890 (2005). URL <http://dx.doi.org/10.1142/S0218127405012430> [xiii, 240, 244, 247, 248, 252]
91. Domokos, G., Holmes, P., Royce, B.: Constrained Euler buckling. *Journal of Nonlinear Science* **7**(3), 281–314 (1997). URL <http://dx.doi.org/10.1007/BF02678090> [183]
92. Domokos, G., Ruina, A.: A circle construction based on elastostatics and hydrodynamics. *Mechanics Research Communications* **20**(3), 181–185 (1993). URL [http://dx.doi.org/10.1016/0093-6413\(93\)90054-R](http://dx.doi.org/10.1016/0093-6413(93)90054-R) [135]
93. Dong, S., Alpdogan, C., Taciroglu, E.: Much ado about shear correction factors in Timoshenko beam theory. *International Journal of Solids and Structures* **47**(13), 1651–1665 (2010). URL <http://dx.doi.org/10.1016/j.ijsolstr.2010.02.018> [291, 307]
94. Duhem, P.: Le potentiel thermodynamique et la pression hydrostatique. *Annales Scientifiques de l’École Normale Supérieure* **10**, 183–230 (1893). URL <http://eudml.org/doc/81051> [187, 188]
95. Epple, M.: Orbits of asteroids, a braid, and the first link invariant. *The Mathematical Intelligencer* **20**(1), 45–52 (1998). URL <http://dx.doi.org/10.1007/BF03024400> [101, 116]
96. Epple, M.: Topology, matter, and space, I: Topological notions in 19th-century natural philosophy. *Archive for History of Exact Sciences* **52**(4), 297–392 (1998). URL <http://www.jstor.org/stable/41134050> [101]
97. Erickson, J.L.: Simpler static problems in nonlinear theories of rods. *International Journal of Solids and Structures* **6**(3), 371–377 (1970). URL [http://dx.doi.org/10.1016/0020-7683\(70\)90045-4](http://dx.doi.org/10.1016/0020-7683(70)90045-4) [287]
98. Erickson, J.L.: Equilibrium of bars. *Journal of Elasticity* **5**(3), 191–201 (1975). URL <http://dx.doi.org/10.1007/BF00126984> [37, 55, 91]
99. Erickson, J.L., Rivlin, R.S.: Large elastic deformations of homogeneous anisotropic materials. *Journal of Rational Mechanics and Analysis* **3**(3), 281–301 (1954). URL http://dx.doi.org/10.1007/978-1-4612-2416-7_32 [361, 363]
100. Erickson, J.L., Truesdell, C.: Exact theory of stress and strain in rods and shells. *Archive for Rational Mechanics and Analysis* **1**(1), 295–323 (1958). URL <http://dx.doi.org/10.1007/BF00298012> [187, 269]

101. Eshelby, J.D.: The force on an elastic singularity. *Philosophical Transactions of the Royal Society of London. Series A. Mathematical and Physical Sciences* **244**, 84–112 (1951). URL <http://dx.doi.org/10.1098/rsta.1951.0016> [24, 41]
102. Eshelby, J.D.: The continuum theory of lattice defects. In: F. Seitz, D. Turnbull (eds.) *Solid State Physics*, vol. 3, pp. 79–144. Academic Press (1956). URL [http://dx.doi.org/10.1016/S0081-1947\(08\)60132-0](http://dx.doi.org/10.1016/S0081-1947(08)60132-0) [37, 40, 41, 184, 370]
103. Eshelby, J.D.: Energy relations and the energy-momentum tensor in continuum mechanics. In: J.M. Ball, D. Kinderlehrer, P. Podio-Guidugli (eds.) *Fundamental contributions to the continuum theory of evolving phase interfaces in solids*, pp. 82–119. Springer-Verlag, Berlin (1999). URL http://dx.doi.org/10.1007/978-3-642-59938-5_5 [16, 24, 41, 345, 365]
104. Eshelby, J.D.: *Collected Works of J. D. Eshelby. The Mechanics of Defects and Inhomogeneities*. Springer-Verlag, Berlin (2006). Edited by X. Marken scoff and A. Gupta. [24]
105. Estrada, R., Kanwal, R.P.: Nonclassical derivation of the transport theorems for wave fronts. *Journal of Mathematical Analysis and Applications* **159**(1), 290–297 (1991). URL [http://dx.doi.org/10.1016/0022-247X\(91\)90236-S](http://dx.doi.org/10.1016/0022-247X(91)90236-S) [27]
106. Euler, L.: *Methodus Inveniendi Lineas Curvas Maximi Minimive Proprietate Gaudentes, sive Solutio Problematis Isoperimetrii Lattissimo Sensu Accepti: Additamentum 1 De Curvis Elasticis*. Leonhardi Euleri Opera Omnia, Series prima (Opera mathematica), Vol. XXIV, Auctoritate et impensis Societatis Scientiarum Naturalium Helveticae. Orell Füssli, Zürich (1952). An English translation of this work can be found in [254]. [121, 132, 135, 250, 377]
107. Ewing, G.M.: *Calculus of Variations with Applications*. Norton & Co., New York (1969) [385]
108. Farjoun, Y., Neu, J.: The tallest column: A dynamical system approach using a symmetry solution. *Studies in Applied Mathematics* **115**(3), 319–337 (2005). URL <http://dx.doi.org/10.1111/j.1467-9590.2005.00316.x> [162]
109. Faruk Senan, N.A., O'Reilly, O.M., Tresierras, T.N.: Modeling the growth and branching of plants: A simple rod-based model. *J. Mech. Phys. Solids* **56**(10), 3021–3036 (2008). URL <http://dx.doi.org/10.1016/j.jmps.2008.06.005> [25, 183]
110. Fuller, F.B.: The writhing number of a space curve. *Proceedings of the National Academy of Sciences* **68**, 815–819 (1971). URL <http://www.pnas.org/content/68/4/815.abstract> [107, 110]
111. Fuller, F.B.: Decomposition of the linking number of a closed ribbon: A problem from molecular biology. *Proceedings of the National Academy of Sciences* **75**(8), 3557–3561 (1978). URL <http://dx.doi.org/10.1073/pnas.75.8.3557> [106, 111]

112. Gavrilov, S.: Nonlinear investigation of the possibility to exceed the critical speed by a load on a string. *Acta Mechanica* **154**(1), 47–60 (2002). URL <http://dx.doi.org/10.1007/BF01170698> [25]
113. Gelfand, I.M., Fomin, S.V.: Calculus of Variations. Prentice-Hall, Englewood Cliffs, N. J. (1964) [169, 173, 174]
114. Gibney, E.: Physicists explain “gravity-defying” chain trick: Leaping beads get a push from the pot. *Nature News* (2014). URL <http://dx.doi.org/10.1038/nature.2014.14523> [70]
115. Ginsberg, J.H.: Advanced Engineering Dynamics, second edn. Cambridge University Press, Cambridge (1995) [193]
116. Glassmaker, N., Jagota, A., Hui, C., Noderer, W., Chaudhury, M.: Biologically inspired crack trapping for enhanced adhesion. *Proceedings of the National Academy of Sciences* **104**(26), 10,786–10,791 (2007). URL <http://dx.doi.org/10.1073/pnas.0703762104> [137]
117. Glassmaker, N.J., Hui, C.Y.: Elastica solution for a nanotube formed by self-adhesion of a folded thin film. *Journal of Applied Physics* **96**(6), 3429–3434 (2004). URL <http://dx.doi.org/10.1063/1.1779974> [137, 139]
118. Goldstein, R.E., Goriely, A.: Dynamic buckling of morphoelastic filaments. *Physical Review E* **74**, 010,901 (2006). URL <http://dx.doi.org/10.1103/PhysRevE.74.010901> [183]
119. Goldstine, H.H.: A History of the Calculus of Variations From the 17th Through the 19th Century, *Studies in the History of Mathematics and Physical Sciences*, vol. 5. Springer-Verlag, New York (1980) [379]
120. Gore, J., Bryant, Z., Nöllmann, M., Le, M.U., Cozzarelli, N.R., Bustamante, C.: DNA overwinds when stretched. *Nature* **442**, 836–839 (2006). URL <http://dx.doi.org/10.1038/nature04974> [257, 284, 285, 287]
121. Goriely, A.: The Mechanics and Mathematics of Biological Growth. Springer-Verlag, New York (2017) [183, 240]
122. Goriely, A., Neukirch, S.: The mechanics of attachment in twining plants. *Physical Review Letters* **97**, 184,302 (2006). URL <http://dx.doi.org/10.1103/PhysRevLett.97.184302> [183, 188]
123. Goriely, A., Tabor, M.: Spontaneous helix hand reversal and tendril perversion in climbing plants. *Physical Review Letters* **80**, 1564–1567 (1998). URL <http://dx.doi.org/10.1103/PhysRevLett.80.1564> [240, 242, 244]
124. Goyal, S., Perkins, N.C.: Looping mechanics of rods and DNA with non-homogeneous and discontinuous stiffness. *International Journal of Non-Linear Mechanics* **43**(10), 1121–1129 (2008). URL <http://dx.doi.org/10.1016/j.ijnonlinmec.2008.06.013> [93, 239]
125. Goyal, S., Perkins, N.C., Lee, C.L.: Nonlinear dynamics and loop formation in Kirchhoff rods with implications to the mechanics of DNA and cables. *Journal of Computational Physics* **209**(1), 371–389 (2005). URL <http://dx.doi.org/10.1016/j.jcp.2005.03.027>
126. Goyal, S., Perkins, N.C., Lee, C.L.: Non-linear dynamic intertwining of rods with self-contact. *International Journal of Non-Linear Mechanics* **43**(1), 65–73 (2008). URL <http://dx.doi.org/10.1016/j.ijnonlinmec.2007.10.004> [239]

127. Green, A., Knops, R., Laws, N.: Large deformations, superposed small deformations and stability of elastic rods. *International Journal of Solids and Structures* **4**(5), 555 – 577 (1968). URL [http://dx.doi.org/10.1016/0020-7683\(68\)90065-6](http://dx.doi.org/10.1016/0020-7683(68)90065-6) [295, 302]
128. Green, A.E., Laws, N.: A general theory of rods. *Proceedings of the Royal Society. London. Series A. Mathematical, Physical and Engineering Sciences* **293**(1433), 145–155 (1966). URL <http://dx.doi.org/10.1098/rspa.1966.0163> [295, 312]
129. Green, A.E., Laws, N.: Ideal fluid jets. *International Journal of Engineering Science* **6**(6), 317–328 (1968). URL [http://dx.doi.org/10.1016/0020-7225\(68\)90053-0](http://dx.doi.org/10.1016/0020-7225(68)90053-0) [51, 296]
130. Green, A.E., Laws, N.: Remarks on the theory of rods. *Journal of Elasticity* **3**(3), 179–184 (1973). URL <http://dx.doi.org/10.1007/BF00052892> [188, 269, 270, 297, 309, 320]
131. Green, A.E., Laws, N., Naghdi, P.M.: A linear theory of straight elastic rods. *Archive for Rational Mechanics and Analysis* **25**(4), 285–298 (1967). URL <http://dx.doi.org/10.1007/BF00250931> [190, 248, 295, 305, 334]
132. Green, A.E., Naghdi, P.M.: A derivation of jump condition for entropy in thermomechanics. *Journal of Elasticity* **8**(2), 119–182 (1978). URL <http://dx.doi.org/10.1007/BF00052481> [22, 25, 127, 210]
133. Green, A.E., Naghdi, P.M.: On thermal effects in the theory of rods. *International Journal of Solids and Structures* **15**(11), 829–853 (1979). URL [http://dx.doi.org/10.1016/0020-7683\(79\)90053-2](http://dx.doi.org/10.1016/0020-7683(79)90053-2) [13, 28, 277, 305, 307, 329, 334, 336, 338, 339, 355, 359]
134. Green, A.E., Naghdi, P.M.: A direct theory of viscous fluid flow in pipes. I: Basic general developments. *Philosophical Transactions of the Royal Society. London. Series A. Mathematical, Physical and Engineering Sciences* **342**(1666), 525–542 (1993). URL <http://dx.doi.org/10.1098/rsta.1993.0031> [13, 295, 296]
135. Green, A.E., Naghdi, P.M.: A unified procedure for construction of theories of deformable media. II. Generalized continua. *Proceedings of the Royal Society. London. Series A. Mathematical, Physical and Engineering Sciences* **448**(1934), 357–377 (1995). URL <http://dx.doi.org/10.1098/rspa.1995.0021> [295, 355]
136. Green, A.E., Naghdi, P.M., Trapp, J.A.: Thermodynamics of a continuum with internal constraints. *International Journal of Engineering Science* **8**(11), 891–908 (1970). URL [http://dx.doi.org/10.1016/0020-7225\(70\)90069-8](http://dx.doi.org/10.1016/0020-7225(70)90069-8) [361, 362, 374]
137. Green, A.E., Naghdi, P.M., Wenner, M.L.: On the theory of rods. I Derivations from three-dimensional equations. *Proceedings of the Royal Society. London. Series A. Mathematical, Physical and Engineering Sciences* **337**(1611), 451–483 (1974). URL <http://dx.doi.org/10.1098/rspa.1974.0061> [33, 190, 200, 208, 295, 299, 305, 307, 320, 323, 329, 331, 334, 335, 345, 355, 359]

138. Green, A.E., Naghdi, P.M., Wenner, M.L.: On the theory of rods. II Developments by direct approach. *Proceedings of the Royal Society. London. Series A. Mathematical, Physical and Engineering Sciences* **337**(1611), 485–507 (1974). URL <http://dx.doi.org/10.1098/rspa.1974.0062> [33, 248, 277, 299, 301, 304, 305, 307, 312, 334, 335, 337, 355]
139. Green, A.E., Rivlin, R.S.: On Cauchy’s equations of motion. *Zeitschrift für Angewandte Mathematik und Physik. ZAMP. Journal of Applied Mathematics and Physics. Journal de Mathématiques et de Physique Appliquées* **15**(3), 290–292 (1964). URL <http://dx.doi.org/10.1007/BF01607019> [21]
140. Green, A.E., Zerna, W.T.: *Theoretical Elasticity*, second edn. Clarendon Press, Oxford (1968) [196, 345, 347, 350, 352, 355, 372]
141. Greenhill, A.G.: On the strength of shafting when exposed both to torsion and to end thrust. *Proceedings of the Institution of Mechanical Engineers* **34**(1), 182–225 (1883). URL http://dx.doi.org/10.1243/PIME_PROC_1883_034_013_02 [225, 230, 262, 264]
142. Grewal, A., Johnson, P., Ruina, A.: A chain that speeds up, rather than slows, due to collisions: How compression can cause tension. *American Journal of Physics* **79**(7), 723–729 (2011). URL <http://dx.doi.org/10.1119/1.3583481> [50, 60, 64, 68, 69, 71, 87, 89]
143. Gruttmann, F., Wagner, W.: Shear correction factors in Timoshenko’s beam theory for arbitrary shaped cross-sections. *Computational Mechanics* **27**(3), 199–207 (2001). URL <http://dx.doi.org/10.1007/s004660100239> [291]
144. Guggenheimer, H.: Computing frames along a trajectory. *Computer Aided Geometric Design* **6**(1), 77–78 (1989). URL [http://dx.doi.org/10.1016/0167-8396\(89\)90008-3](http://dx.doi.org/10.1016/0167-8396(89)90008-3) [97]
145. Guillou, T., Dumont, Y., Fourcaud, T.: A new mathematical framework for modelling the biomechanics of growing trees with rod theory. *Mathematical and Computer Modelling* **55**(9–10), 2061–2077 (2012). URL <http://dx.doi.org/10.1016/j.mcm.2011.12.024> [183]
146. Günther, W.: Über einige randintegrale der elastomechanik. *Abhandlungen der Braunschweigischen Wissenschaftlichen Gesellschaft* **14**, 53–72 (1962). URL <http://www.digibib.tu-bs.de/?docid=00047859> [367]
147. Gurtin, M.E.: *An Introduction to Continuum Mechanics*. Academic Press, New York (1981) [345, 355, 356]
148. Gurtin, M.E.: The nature of configurational forces. *Archive for Rational Mechanics and Analysis* **131**(1), 67–100 (1995). URL <http://dx.doi.org/10.1007/BF00386071> [26]
149. Gurtin, M.E.: *Configurational Forces as Basic Concepts of Continuum Physics, Applied Mathematical Sciences*, vol. 137. Springer-Verlag, New York (2000) [24, 26, 28, 365, 366]
150. Hamel, G.: *Theoretische Mechanik: Eine Einheitliche Einführung in die Gesamte Mechanik*. Springer-Verlag, Berlin, Göttingen and Heidelberg (1949) [75, 77]

151. Hamm, E., Géminard, J.C.: The weight of a falling chain, revisited. *American Journal of Physics* **78**(8), 828–833 (2010). URL <http://dx.doi.org/10.1119/1.3429983> [50, 58, 68, 71, 72]
152. Han, S.M., Benaroya, H., Wei, T.: Dynamics of transversely vibrating beams using four engineering theories. *Journal of Sound and Vibration* **225**(5), 935–988 (1999). URL <http://dx.doi.org/10.1006/jsvi.1999.2257> [293]
153. Hanna, J.A., King, H.: An instability in a straightening chain (2011). URL <http://arxiv.org/abs/1110.2360v1>. ArXiv:1110.2360v1 [78]
154. Hanna, J.A., Santangelo, C.D.: Slack dynamics on an unfurling string. *Physical Review Letters* **109**, 134,301 (2012). URL <http://dx.doi.org/10.1103/PhysRevLett.109.134301> [78]
155. Hanson, A.J.: Visualizing Quaternions. Morgan Kaufmann, San Francisco, CA; Amsterdam; Boston (2006) [96, 97, 98]
156. Haslwanter, T.: Mathematics of three-dimensional eye rotations. *Vision Research* **35**(12), 1727–1739 (1995). URL [http://dx.doi.org/10.1016/0042-6989\(94\)00257-M](http://dx.doi.org/10.1016/0042-6989(94)00257-M) [193]
157. Healey, T.J.: Stability of axial motions of nonlinearly elastic loops. *Zeitschrift für Angewandte Mathematik und Physik. ZAMP. Journal of Applied Mathematics and Physics. Journal de Mathématiques et de Physique Appliquées* **47**(5), 809–816 (1996). URL <http://dx.doi.org/10.1007/BF00915277> [52, 56]
158. Healey, T.J.: Material symmetry and chirality in nonlinearly elastic rods. *Mathematics and Mechanics of Solids* **7**(4), 405–420 (2002). URL <http://dx.doi.org/10.1177/108128028482> [197, 206, 270, 278, 283]
159. Healey, T.J., Mehta, P.G.: Straightforward computation of spatial equilibria of geometrically exact Cosserat rods. *International Journal of Bifurcation and Chaos* **15**(3), 949–965 (2005). URL <http://dx.doi.org/10.1142/S0218127405012387> [248]
160. Healey, T.J., Papadopoulos, J.N.: Steady axial motions of strings. *ASME Journal of Applied Mechanics* **57**(3), 785–787 (1990). URL <http://dx.doi.org/10.1115/1.2897094> [52, 54]
161. Heidug, W., Lehner, F.K.: Thermodynamics of coherent phase transformations in nonhydrostatically stressed solids. *Pure and Applied Geophysics* **123**(1), 91–98 (1985). URL <http://dx.doi.org/10.1007/BF00877051> [37]
162. van der Heijden, G.H.M., Neukirch, S., Goss, V.G.A., Thompson, J.M.T.: Instability and self-contact phenomena in the writhing of clamped rods. *International Journal of Mechanical Sciences* **45**(1), 161–196 (2003). URL [http://dx.doi.org/10.1016/S0020-7403\(02\)00183-2](http://dx.doi.org/10.1016/S0020-7403(02)00183-2) [239]
163. van der Heijden, G.H.M., Peletier, M.A., Planqué, R.: On end rotation for open rods undergoing large deformations. *Quarterly of Applied Mathematics* **65**(2), 385–402 (2007). URL <http://dx.doi.org/10.1090/S0033-569X-07-01049-X> [161]

164. van der Heijden, G.H.M., Thompson, J.M.T.: Helical and localised buckling in twisted rods: A unified analysis of the symmetric case. *Nonlinear Dynamics* **21**(1), 71–99 (2000). URL <http://dx.doi.org/10.1023/A:1008310425967> [188, 207, 220, 233, 234, 239, 262]
165. van der Heijden, G.H.M., Yagasaki, K.: Horseshoes for the nearly symmetric heavy top. *Zeitschrift für Angewandte Mathematik und Physik. ZAMP. Journal of Applied Mathematics and Physics. Journal de Mathématiques et de Physique Appliquées* **65**(2), 221–240 (2014). URL <http://dx.doi.org/10.1007/s00033-013-0319-z> [239]
166. Helmholtz, H.: Ueber die normalen Bewegungen des menschlichen Auges. *Archiv für Ophthalmologie* **9**(2), 153–214 (1863). URL <http://dx.doi.org/10.1007/BF02720895> [193]
167. von Helmholtz, H.: A Treatise on Physiological Optics, vol. III. Dover Publications, New York (1962). Translated from the (1910) third German edition and edited by J.P.C. Southall [193]
168. Hess, W.: Ueber die Beigung und Drillung eines unendlich dünnen elastischen Stabes mit zwei gleichen Widersänden, auf dessen freies Ende eine Kraft und ein um die Hauptaxe ungleichen Widerstandes drehendes Kräftepaar einwirkt. *Mathematische Annalen* **25**(1), 1–38 (1885). URL <http://dx.doi.org/10.1007/BF01446419> [135]
169. Hoffman, K.A., Manning, R.S., Maddocks, J.H.: Link, twist, energy, and the stability of DNA minicircles. *Biopolymers* **70**(2), 145–157 (2003). URL <http://dx.doi.org/10.1002/bip.10430> [93, 110, 113, 122, 234, 391]
170. Ilyukhin, A.A.: Three-Dimensional Problems of the Nonlinear Theory of Elastic Rods. Naukova Dumka, Kiev, Ukraine (1979) [220]
171. Irschik, H., Humer, A.: A rational treatment of the relations of balance for mechanical systems with a time-variable mass and other non-classical supplies. In: H. Irschik, A.K. Belyaev (eds.) *Dynamics of Mechanical Systems with Variable Mass, CISM International Centre for Mechanical Sciences*, vol. 557, pp. 1–50. Springer, Vienna (2014). URL http://dx.doi.org/10.1007/978-3-7091-1809-2_1 [60]
172. Israelachvili, J.R.: *Intermolecular and Surface Forces: With Applications to Colloidal and Biological Systems (Colloid Science)*, second edn. Academic Press, San Diego (1992) [137]
173. Jawed, M.K., Dieleman, P., Audoly, B., Reis, P.M.: Untangling the mechanics and topology in the frictional response of long overhand elastic knots. *Physical Review Letters* **115**(11), 118,302 (2015). URL <http://dx.doi.org/10.1103/PhysRevLett.115.118302> [239]
174. Jeans, J.H.: *An Elementary Treatise on Theoretical Mechanics*, second edn. Ginn & Co., Boston, New York (1907) [68, 89, 90]
175. Johnson, K.L., Kendall, K., Roberts, A.D.: Surface energy and the contact of elastic solids. *Proceedings of the Royal Society. London. Series A. Mathematical, Physical and Engineering Sciences* **324**(1558), 301–313 (1971). URL <http://dx.doi.org/10.1098/rspa.1971.0141> [137, 185]

176. Kamien, R.D.: Local writhing dynamics. *The European Physical Journal B* **1**(1), 1–4 (1998). URL <http://dx.doi.org/10.1007/s100510050145> [106, 110]
177. Kamien, R.D., Lubensky, T.C., Nelson, P., O’Hern, C.S.: Twist-stretch elasticity of DNA. In: *Symposia EE - Statistical Mechanics in Physics and Biology, MRS Online Proceedings Library Archive*, vol. 463, pp. 43–48 (1996). URL <http://dx.doi.org/10.1557/PROC-463-43> [257, 270]
178. Kehrbaum, S., Maddocks, J.H.: Elastic rods, rigid bodies, quaternions and the last quadrature. *Philosophical Transactions of the Royal Society of London. Series A. Mathematical, Physical Sciences and Engineering* **355**(1732), 2117–2136 (1997). URL <http://dx.doi.org/10.1098/rsta.1997.0113> [193, 220, 234, 270]
179. Keller, J.B.: Tendril shape and lichen growth. In: G.F. Oster (ed.) *Some Mathematical Questions in Biology; Symposium On Mathematical Biology At The Annual Meeting of The American Association for the Advancement Of Science, San Francisco, California, USA, Jan. 6, 1980, Lectures On Mathematics in the Life Sciences*, pp. 257–274. American Mathematical Society, Providence, Rhode Island (1980) [240]
180. Kelvin, L., Tait, P.G.: *A Treatise on Natural Philosophy*, Reprinted edn. Cambridge University Press, Cambridge (1912) [193, 256]
181. Kendall, K.: The adhesion and surface energy of elastic solids. *Journal of Physics D: Applied Physics* **4**(8), 1186–1195 (1971). URL <http://dx.doi.org/10.1088/0022-3727/4/8/320> [166]
182. Kienzler, R., Herrmann, G.: *Mechanics in Material Space: With Applications to Defect and Fracture Mechanics*. Springer-Verlag, Berlin (2000) [24, 26, 128, 184, 367]
183. Kienzler, R.R., Herrmann, G.G.: On material forces in elementary beam theory. *ASME Journal of Applied Mechanics* **53**(3), 561–564 (1986). URL <http://dx.doi.org/10.1115/1.3171811> [26, 37, 40, 128, 184]
184. Kinkaid, N.M., O'Reilly, O.M., Turcotte, J.S.: On the steady motions of a rotating elastic rod. *ASME Journal of Applied Mechanics* **68**(5), 766–771 (2001). URL <http://dx.doi.org/10.1115/1.1381003> [335]
185. Kirchhoff, G.: Über des gleichgewicht und die Bewegung eines unendlich dünnen elastischen Stabes. *Crelles Journal für die reine und angewandte Mathematik* **56**, 285–313 (1859). URL <http://dx.doi.org/10.1515/crll.1859.56.285> [122, 188, 206, 214, 220, 377, 387]
186. Knops, R., Wilkes, N.: The elastic instability of a director rod. *International Journal of Solids and Structures* **14**(6), 527–533 (1978). URL [http://dx.doi.org/10.1016/0020-7683\(78\)90015-X](http://dx.doi.org/10.1016/0020-7683(78)90015-X) [295, 302]
187. Knowles, J.K., Sternberg, E.: On a class of conservation laws in linearized and finite elastostatics. *Archive for Rational Mechanics and Analysis* **44**(3), 187–211 (1972). URL <http://dx.doi.org/10.1007/BF00250778> [367]
188. Kreyszig, E.: *Differential Geometry*, Revised and reprinted edn. Toronto University Press, Toronto (1964) [7, 101, 216]

189. Kucharski, W.: Zur Kinetik dehnungsloser Seile mit Knickstellen. *Archive of Applied Mechanics (Ingenieur Archiv)* **12**(2), 109–123 (1941) [75]
190. Kumar, A., Healey, T.J.: A generalized computational approach to stability of static equilibria of nonlinearly elastic rods in the presence of constraints. *Computer Methods in Applied Mechanics and Engineering* **199**(25), 1805–1815 (2010). URL <http://dx.doi.org/10.1016/j.cma.2010.02.007> [248]
191. Lagrange, J.L.: Mécanique Analytique. In: J.A. Serret, G. Darboux (eds.) *Joseph Louis de Lagrange Oeuvres*, vol. 11/12, fourth edn. Georg Olms Verlag, Heidelberg (1973) [225]
192. Lagrange, J.L.: Analytical Mechanics, *Boston Studies in the Philosophy of Science*, vol. 191. Kluwer Academic Publishers Group, Dordrecht (1997). Translated from the 1811 French original, with an introduction and edited by A. Boissonnade and V. N. Vagliente, and with a preface by C. G. Fraser [225]
193. Lamb, H.: Dynamics, second reprinted edn. Cambridge University Press, Cambridge (1929) [49, 51, 64, 67, 68, 90]
194. Lamb, H.: Hydrodynamics, sixth edn. Dover Publications, New York (1999) [56]
195. Lanczos, C.: The Variational Principles of Mechanics, fourth edn. University of Toronto Press, Toronto (1970) [33]
196. Langer, J., Singer, D.A.: Lagrangian aspects of the Kirchhoff elastic rod. *SIAM Review* **38**(4), 605–618 (1996). URL <http://dx.doi.org/10.1137/S0036144593253290> [96, 220]
197. Larmor, J.: On the direct application of the principle of least action to the dynamics of solid and fluid systems, and analogous elastic problems. *Proceedings of the London Mathematical Society* **s1-15**(1), 170–185 (1883). URL <http://dx.doi.org/10.1112/plms/s1-15.1.170> [265]
198. Lauderdale, T.A., O'Reilly, O.M.: On transverse and rotational symmetries in elastic rods. *Journal of Elasticity* **82**(1), 31–47 (2006). URL <http://dx.doi.org/10.1007/s10659-005-9022-4> [206, 277]
199. Lauderdale, T.A., O'Reilly, O.M.: On the restrictions imposed by non-affine material symmetry groups for elastic rods: Application to helical substructures. *European Journal of Mechanics. A. Solids* **26**(4), 701–711 (2007). URL <http://dx.doi.org/10.1016/j.euromechsol.2006.10.003> [197, 199, 278]
200. Lawden, D.F.: Elliptic Functions and Applications, *Applied Mathematical Sciences*, vol. 80. Springer-Verlag, New York (1989) [142, 160]
201. Lee, S.Y., Mote, Jr., C.D.: Travelling wave dynamics in a translating string coupled to stationary constraints: Energy transfer and mode localization. *Journal of Sound and Vibration* **212**(1), 1–22 (1998). URL <http://dx.doi.org/10.1006/jsvi.1997.1285> [22]
202. LeFloch, P.G.: Hyperbolic Systems of Conservation Laws. *Lectures in Mathematics ETH Zürich*. Birkhäuser Verlag, Basel (2002). URL <http://dx.doi.org/10.1007/978-3-0348-8150-0> [43, 91]

203. LeFloch, P.G., Mohammadian, M.: Why many theories of shock waves are necessary: Kinetic functions, equivalent equations, and fourth-order models. *Journal of Computational Physics* **227**(8), 4162–4189 (2008). URL <http://dx.doi.org/10.1016/j.jcp.2007.12.026> [43, 91]
204. Levinson, M., Cooke, D.: On the two frequency spectra of Timoshenko beams. *Journal of Sound and Vibration* **84**(3), 319–326 (1982). URL [http://dx.doi.org/10.1016/0022-460X\(82\)90480-1](http://dx.doi.org/10.1016/0022-460X(82)90480-1) [293]
205. Lewis, D., Ratiu, T., Simo, J.C., Marsden, J.E.: The heavy top: A geometric treatment. *Nonlinearity* **5**(1), 1–48 (1992). URL <http://dx.doi.org/10.1088/0951-7715/5/1/001> [225]
206. Liepmann, H.W., Roshko, A.: Elements of Gas Dynamics. John Wiley & Sons, Inc., New York (1957) [20]
207. Lionnet, T., Joubaud, S., Lavery, R., Bensimon, D., Croquette, V.: Wringing out DNA. *Physical Review Letters* **96**, 178,102 (2006). URL <http://link.aps.org/doi/10.1103/PhysRevLett.96.178102> [257]
208. Listing, J.B.: Vorstudien zur Topologie. Göttinger Studien. Vandenhoeck & Ruprecht, Göttingen (1848). URL <https://archive.org/details/vorstudienzur000listgoog> [240]
209. Liu, J., Huang, J., Su, T., Bertoldi, K., Clarke, D.R.: Structural transition from helices to hemihelices. *PLoS ONE* **9**(4), e93,183 (2014). URL <http://dx.doi.org/10.1371/journal.pone.0093183> [241, 248]
210. Livingston, C.: Knot Theory. Mathematical Association of America, Washington, DC (1993) [94]
211. Lotz, J.C., O'Reilly, O.M., Peters, D.M.: Some comments on the absence of buckling of the ligamentous human spine in the sagittal plane. *Mechanics Research Communications* **40**(1), 11–15 (2012). URL <http://dx.doi.org/10.1016/j.mechrescom.2011.11.010> [176]
212. Love, A.E.H.: Theoretical Mechanics. Cambridge University Press, Cambridge (1897) [51, 73, 74, 75, 77]
213. Love, A.E.H.: A Treatise on the Mathematical Theory of Elasticity, fourth edn. Cambridge University Press, Cambridge (1927) [viii, 3, 107, 128, 135, 136, 137, 150, 176, 184, 188, 191, 193, 198, 207, 214, 216, 217, 225, 231, 233, 252, 253, 256, 262, 265]
214. Luo, C., O'Reilly, O.M.: On the material symmetry of elastic rods. *Journal of Elasticity* **60**(1), 35–56 (2000). URL <http://dx.doi.org/10.1023/A:1007624328427> [278]
215. Maddocks, J.H.: Stability of nonlinearly elastic rods. *Archive for Rational Mechanics and Analysis* **85**(4), 311–354 (1984). URL <http://dx.doi.org/10.1007/BF00275737> [122, 176, 391]
216. Mahadevan, L., Keller, J.B.: Periodic folding of thin sheets. *SIAM Journal on Applied Mathematics* **55**(6), 1609–1624 (1995). URL <http://dx.doi.org/10.1137/S0036139994263410> [183]
217. Majidi, C.: Remarks on formulating an adhesion problem using Euler's elastica. *Mechanics Research Communications* **34**(1), 85–90 (2007). URL <http://dx.doi.org/10.1016/j.mechrescom.2006.06.007> [137, 139, 166, 378]

218. Majidi, C., Adams, G.G.: Adhesion and delamination boundary conditions for elastic plates with arbitrary contact shape. *Mechanics Research Communications* **37**(2), 214–218 (2010). URL <http://dx.doi.org/10.1016/j.mechrescom.2010.01.002> [166]
219. Majidi, C., O'Reilly, O.M., Williams, J.A.: On the stability of a rod adhering to a rigid surface: Shear-induced stable adhesion and the instability of peeling. *Journal of the Mechanics and Physics of Solids* **60**(5), 827–843 (2012). URL <http://dx.doi.org/10.1016/j.jmps.2012.01.015> [xii, 122, 123, 137, 165, 168, 174, 178, 181]
220. Majidi, C., O'Reilly, O.M., Williams, J.A.: Bifurcations and instability in the adhesion of intrinsically curved rods. *Mechanics Research Communications* **49**, 13–16 (2013). URL <http://dx.doi.org/10.1016/j.mechrescom.2013.01.004> [xii, 122, 123, 137, 168, 181]
221. Majumdar, A., Prior, C., Goriely, A.: Stability estimates for a twisted rod under terminal loads: A three-dimensional study. *Journal of Elasticity* **109**(1), 75–93 (2012). URL <http://dx.doi.org/10.1007/s10659-012-9371-8> [xiii, 188]
222. Majumdar, A., Raisch, A.: Stability of twisted rods, helices and buckling solutions in three dimensions. *Nonlinearity* **27**(12), 2841–2867 (2014). URL <http://dx.doi.org/10.1088/0951-7715/27/12/2841> [xiii, 188, 234]
223. Männer, J.: On the form problem of embryonic heart loops, its geometrical solutions, and a new biophysical concept of cardiac looping. *Annals of Anatomy - Anatomischer Anzeiger* **195**(4), 312–323 (2013). URL <http://dx.doi.org/10.1016/j.aanat.2013.02.008> [240]
224. Manning, R.S.: Conjugate points revisited and Neumann-Neumann problems. *SIAM Review* **51**(1), 193–212 (2009). URL <http://dx.doi.org/10.1137/060668547> [122, 188, 391]
225. Manning, R.S., Bulman, G.B.: Stability of an elastic rod buckling into a soft wall. *Proceedings of the Royal Society of London. Series A: Mathematical, Physical and Engineering Sciences* **461**(2060), 2423–2450 (2005). URL <http://dx.doi.org/10.1098/rspa.2005.1458>
226. Manning, R.S., Rogers, K.A., Maddocks, J.H.: Isoperimetric conjugate points with application to the stability of DNA minicircles. *Proceedings of the Royal Society of London. Series A: Mathematical, Physical and Engineering Sciences* **454**(1980), 3047–3074 (1998). URL <http://dx.doi.org/10.1098/rspa.1998.0291> [122, 188, 391]
227. Marko, J.F.: Stretching must twist DNA. *Europhysics Letters* **38**(3), 183–188 (1997). URL <http://stacks.iop.org/0295-5075/38/i=3/a=183> [257, 270]
228. Marko, J.F., Siggia, E.D.: Bending and twisting elasticity of DNA. *Macromolecules* **27**(4), 981–988 (1994). URL <http://dx.doi.org/10.1021/ma00082a015>. Errata for this paper were published on page 4820 of Volume 29 [197, 206, 270, 285]

229. Marsden, J.E., Ratiu, T.S.: Introduction to Mechanics and Symmetry: A Basic Exposition of Classical Mechanical Systems, *Texts in Applied Mathematics*, vol. 17, second edn. Springer-Verlag, New York (1999). URL <http://dx.doi.org/10.1007/978-0-387-21792-5> [225]
230. Marshall, J.S., Naghdi, P.M.: A thermodynamical theory of turbulence. I. Basic developments. Philosophical Transactions of the Royal Society of London. Series A. Mathematical and Physical Sciences **327**(1595), 415–448 (1989). URL <http://dx.doi.org/10.1098/rsta.1989.0001> [22, 25, 127, 210]
231. Maugin, G.A.: Material forces: concepts and applications. ASME Applied Mechanics Reviews **48**(5), 213–245 (1995). URL <http://dx.doi.org/10.1115/1.3005101> [26, 28, 365]
232. Maugin, G.A.: Configurational forces: Thermomechanics, physics, mathematics, and numerics. CRC Series: Modern Mechanics and Mathematics. CRC Press, Boca Raton, FL (2011) [24, 366]
233. Maxwell, J.C.: A Treatise on Electricity and Magnetism, vol. 2, third edn. Clarendon Press, Oxford (1892) [103]
234. McConnell, A.J.: Applications of the Absolute Differential Calculus. Blackie and Son, London (1947). Corrected reprinted edition [101, 350]
235. McMillen, T., Goriely, A.: Tendril perversion in intrinsically curved rods. Journal of Nonlinear Science **12**(3), 241–281 (2002). URL <http://dx.doi.org/10.1007/s00332-002-0493-1> [114, 188, 240, 242, 244, 247]
236. Meriam, J.L.: Dynamics, first edn. John Wiley & Sons, New York (1966) [68, 89, 90]
237. Meriam, J.L., Kraige, L.G.: Engineering Mechanics: Dynamics, seventh edn. John Wiley & Sons, New York (2012) [89, 90]
238. Mielke, A., Holmes, P.: Spatially complex equilibria of buckled rods. Archive for Rational Mechanics and Analysis **101**(4), 319–348 (1988). URL <http://dx.doi.org/10.1007/BF00251491> [xiii, 239, 270]
239. Moffatt, H.K., Ricca, R.L.: Helicity and the Călugăreanu invariant. Proceedings of the Royal Society A: Mathematical, Physical and Engineering Science **439**(1906), 411–429 (1992). URL <http://www.jstor.org/stable/52228> [93, 98, 109, 114]
240. Mueller, R., Maugin, G.A.: On material forces and finite element discretizations. Computational Mechanics **29**(1), 52–60 (2002). URL <http://dx.doi.org/10.1007/s00466-002-0322-2> [366]
241. Murasugi, K.: Knot theory and its applications. Birkhäuser Boston Inc., Boston, MA (1996). Translated from the 1993 Japanese original by Bohdan Kurpita [115]
242. Murdoch, A.I.: Objectivity in classical continuum physics: a rationale for discarding the ‘principle of invariance under superposed rigid body motions’ in favour of purely objective considerations. Continuum Mechanics and Thermodynamics **15**(3), 309–320 (2003). URL <http://dx.doi.org/10.1007/s00161-003-0121-9> [360]

243. Naghdi, P.M.: The theory of shells and plates. In: C. Truesdell (ed.) *Linear Theories of Elasticity and Thermoelasticity: Linear and Nonlinear Theories of Rods, Plates, and Shells*, pp. 425–640. Springer-Verlag, Berlin, Heidelberg (1973). URL http://dx.doi.org/10.1007/978-3-662-39776-3_5 [187, 345]
244. Naghdi, P.M.: On the formulation of contact problems of shells and plates. *Journal of Elasticity* **5**(3–4), 379–398 (1975). URL <http://dx.doi.org/10.1007/BF00126998> [202]
245. Naghdi, P.M.: Finite deformation of elastic rods and shells. In: D.E. Carlson, R.T. Shield (eds.) *Proceedings of the IUTAM Symposium on Finite Elasticity*, Bethlehem PA 1980, pp. 47–104. Martinus Nijhoff, The Hague (1982) [187, 189, 296, 298, 299, 324]
246. Naghdi, P.M., Rubin, M.B.: Constrained theories of rods. *Journal of Elasticity* **14**, 343–361 (1984). URL <http://dx.doi.org/10.1007/BF00125605> [188, 312, 316]
247. Naghdi, P.M., Rubin, M.B.: On the significance of normal cross-sectional extension in beam theory with application to contact problems. *International Journal of Solids and Structures* **25**(3), 249–265 (1989). URL [http://dx.doi.org/10.1016/0020-7683\(89\)90047-4](http://dx.doi.org/10.1016/0020-7683(89)90047-4) [209, 295, 296, 299]
248. Neukirch, S., Starostin, E.L.: Writhe formulas and antipodal points in plectonemic DNA configurations. *Physical Review E* **78**(4), 041,912, 9 (2008). URL <http://dx.doi.org/10.1103/PhysRevE.78.041912> [93]
249. Nizette, M., Goriely, A.: Towards a classification of Euler-Kirchhoff filaments. *Journal of Mathematical Physics* **40**(6), 2830–2866 (1999). URL <http://dx.doi.org/10.1063/1.532731> [234]
250. Nordenholz, T.R., O'Reilly, O.M.: On kinematical conditions for steady motions of strings and rods. *ASME Journal of Applied Mechanics* **62**(3), 820–822 (1995). URL <http://dx.doi.org/10.1115/1.2897023> [51]
251. Nordenholz, T.R., O'Reilly, O.M.: On steady motions of an elastic rod with application to contact problems. *International Journal of Solids and Structures* **34**(9), 1123–1143 & 3211–3212 (1997). URL [http://dx.doi.org/10.1016/S0020-7683\(96\)00054-6](http://dx.doi.org/10.1016/S0020-7683(96)00054-6) [22, 209, 311, 335, 337]
252. Novelia, A., O'Reilly, O.M.: On geodesics of the rotation group SO(3). *Regular and Chaotic Dynamics* **20**(6), 729–738 (2015). URL <http://dx.doi.org/10.1134/S1560354715060088> [13]
253. Novelia, A., O'Reilly, O.M.: On the dynamics of the eye: geodesics on a configuration manifold, motions of the gaze direction and Helmholtz's theorem. *Nonlinear Dynamics* **80**(3), 1303–1327 (2015). URL <http://dx.doi.org/10.1007/s11071-015-1945-0> [13, 193]
254. Oldfather, W.A., Ellis, C.A., Brown, D.M.: Leonhard Euler's elastic curves. *Isis* **20**(1), 72–160 (1933). URL <http://www.jstor.org/stable/224885> [135, 250, 377, 401]
255. Olsson, M.: On the fundamental moving load problem. *Journal of Sound and Vibration* **145**(2), 299–307 (1991). URL [http://dx.doi.org/10.1016/0022-460X\(91\)90593-9](http://dx.doi.org/10.1016/0022-460X(91)90593-9) [25]

256. Olver, P.J.: Conservation laws in elasticity. II. Linear homogeneous elastostatics. *Archive for Rational Mechanics and Analysis* **85**(2), 131–160 (1984). URL <http://dx.doi.org/10.1007/BF00281448> [367]
257. Oprea, J.: Differential Geometry and its Applications, second edn. Pearson Prentice Hall, Upper Saddle River, NJ (2003) [101, 104]
258. O'Reilly, O.M.: A properly invariant theory of small deformations superposed on large deformations of an elastic rod. *Journal of Elasticity* **39**(2), 97–131 (1995). URL <http://dx.doi.org/10.1007/BF00043412> [302, 324]
259. O'Reilly, O.M.: On steady motions of a drawn cable. *ASME Journal of Applied Mechanics* **63**(1), 180–189 (1996). URL <http://dx.doi.org/10.1115/1.2787196> [4, 80]
260. O'Reilly, O.M.: On constitutive relations for elastic rods. *International Journal of Solids and Structures* **35**(11), 1009–1024 (1998). URL [http://dx.doi.org/10.1016/S0020-7683\(97\)00100-5](http://dx.doi.org/10.1016/S0020-7683(97)00100-5) [208, 305, 320, 323, 334, 335]
261. O'Reilly, O.M.: On coupled longitudinal and lateral vibrations of elastic rods. *Journal of Sound and Vibration* **247**(5), 835–856 (2001). URL <http://dx.doi.org/10.1006/jsvi.2001.3753> [335]
262. O'Reilly, O.M.: The dual Euler basis: Constraints, potentials, and Lagrange's equations in rigid body dynamics. *ASME Journal of Applied Mechanics* **74**(2), 256–258 (2007). URL <http://dx.doi.org/10.1115/1.2190231> [195]
263. O'Reilly, O.M.: The energy jump condition for thermomechanical media in the presence of configurational forces. *Continuum Mechanics and Thermodynamics* **18**(6), 361–365 (2007). URL <http://dx.doi.org/10.1007/s00161-006-0036-3> [25, 131, 369, 370]
264. O'Reilly, O.M.: A material momentum balance law for rods. *Journal of Elasticity* **86**(2), 155–172 (2007). URL <http://dx.doi.org/10.1007/s10659-006-9089-6> [3, 29, 30, 73, 131, 137, 204, 207, 303, 307, 333, 334]
265. O'Reilly, O.M.: Intermediate Engineering Dynamics: A Unified Treatment of Newton-Euler and Lagrangian Mechanics. Cambridge University Press, Cambridge (2008) [161, 193, 196, 387]
266. O'Reilly, O.M.: Some perspectives on Eshelby-like forces in the elastica arm scale. *Proceedings of the Royal Society of London. Series A: Mathematical, Physical and Engineering Sciences* **471**(2174), 20140785 (2015). URL <http://dx.doi.org/10.1098/rspa.2014.0785> [147]
267. O'Reilly, O.M., Payen, S.: The attitudes of constant angular velocity motions. *International Journal of Non-Linear Mechanics* **41**(6–7), 1–10 (2006). URL <http://dx.doi.org/10.1016/j.ijnonlinmec.2006.05.001> [13, 288]
268. O'Reilly, O.M., Peters, D.M.: On the stability analyses of three classical buckling problems for the elastic strut. *Journal of Elasticity* **105**(1–2), 117–136 (2011). URL <http://dx.doi.org/10.1007/s10659-010-9299-9> [xii, 122, 123]

269. O'Reilly, O.M., Peters, D.M.: Nonlinear stability criteria for tree-like structures composed of branched elastic rods. *Proceedings of the Royal Society of London. Series A: Mathematical, Physical and Engineering Sciences* **468**(2137), 206–226 (2012). URL <http://dx.doi.org/10.1098/rspa.2011.0291> [xii, 25, 122, 123, 183]
270. O'Reilly, O.M., Sena, M., Feeley, B.T., Lotz, J.C.: On representations for joint moments using a joint coordinate system. *ASME Journal of Biomechanical Engineering* **135**(11), 114,504–114,504 (2013). URL <http://dx.doi.org/10.1115/1.4025327> [195]
271. O'Reilly, O.M., Srinivasa, A.R.: A simple treatment of constraint forces and constraint moments in the dynamics of rigid bodies. *ASME Applied Mechanics Reviews* **67**(1), 014,801–014,801–8 (2014). URL <http://dx.doi.org/10.1115/1.4028099> [195, 364]
272. O'Reilly, O.M., Tan, M.H.: Steady motions of an axisymmetric satellite: An atlas of their bifurcations. *International Journal of Non-Linear Mechanics* **39**(6), 921–940 (2004). URL [http://dx.doi.org/10.1016/S0020-7462\(03\)00075-1](http://dx.doi.org/10.1016/S0020-7462(03)00075-1) [266]
273. O'Reilly, O.M., Tresierras, T.N.: On the evolution of intrinsic curvature in rod-based models of growth in long slender plant stems. *International Journal of Solids and Structures* **48**(9), 1239–1247 (2011). URL <http://dx.doi.org/10.1016/j.ijsolstr.2010.12.006> [183, 240]
274. O'Reilly, O.M., Tresierras, T.N.: On the static equilibria of branched elastic rods. *International Journal of Engineering Science* **49**(2), 212–227 (2011). URL <http://dx.doi.org/10.1016/j.ijengsci.2010.11.008> [25, 183]
275. O'Reilly, O.M., Turcotte, J.S.: Another mode of vibration in a Timoshenko beam. *Journal of Sound and Vibration* **198**(4), 517–521 (1996). URL <http://dx.doi.org/10.1006/jsvi.1996.0585> [293, 338]
276. O'Reilly, O.M., Turcotte, J.S.: Some remarks on invariance requirements for constrained rods. *Mathematics and Mechanics of Solids* **1**(3), 343–348 (1996). URL <http://dx.doi.org/10.1177/108128659600100306> [309, 312, 316, 320]
277. O'Reilly, O.M., Varadi, P.C.: A treatment of shocks in one-dimensional thermomechanical media. *Continuum Mechanics and Thermodynamics* **11**(6), 339–352 (1999). URL <http://dx.doi.org/10.1007/s001610050116> [23, 30, 34, 73, 77]
278. O'Reilly, O.M., Varadi, P.C.: On energetics and conservations for strings in the presence of singular sources of momentum and energy. *Acta Mechanica* **165**(1–2), 27–45 (2003). URL <http://dx.doi.org/10.1007/s00707-003-0032-7> [3]
279. O'Reilly, O.M., Varadi, P.C.: On some peculiar aspects of axial motions of closed loops of string in the presence of a singular supply of momentum. *ASME Journal of Applied Mechanics* **71**(4), 541–545 (2004). URL <http://dx.doi.org/10.1115/1.1756139> [22, 52]

280. Ouyang, H.: Moving-load dynamic problems: A tutorial (with a brief overview). *Mechanical Systems and Signal Processing* **25**(6), 2039–2060 (2011). URL <http://dx.doi.org/10.1016/j.ymssp.2010.12.010> [25]
281. Pai, D.K.: Strands: Interactive simulation of thin solids using Cosserat models. *Computer Graphics Forum* **21**(3), 347–352 (2002). URL <http://dx.doi.org/10.1111/1467-8659.00594> [188]
282. Pamp, A., Adams, G.G.: Deformation of bowed silicon chips due to adhesion and applied pressure. *Journal of Adhesion Science and Technology* **21**(11), 1021–1043 (2007). URL <http://dx.doi.org/10.1163/156856107782105963> [167]
283. Papastavridis, J.G.: *Tensor Calculus and Analytical Dynamics: A Classical Introduction to Holonomic and Nonholonomic Tensor Calculus; And Its Principal Applications to the Lagrangean Dynamics of Constrained Mechanical Systems, for Engineers, Physicists, and Mathematicians*. Library of Engineering Mathematics. CRC Press, Boca Raton, FL (1999) [364]
284. Papastavridis, J.G.: *Analytical Mechanics: A Comprehensive Treatise on the Dynamics of Constrained Systems; for Engineers, Physicists, and Mathematicians*. Oxford University Press, Oxford (2002) [364]
285. Parker, D.F.: The role of Saint Venant's solutions in rod and beam theories. *ASME Journal of Applied Mechanics* **46**(4), 861–866 (1979). URL <http://dx.doi.org/10.1115/1.3424668> [323]
286. de Payrebrune, K.M., O'Reilly, O.M.: On constitutive relations for a rod-based model of a pneu-net bending actuator. *Extreme Mechanics Letters* **8**(C), 38–46 (2016). URL <http://dx.doi.org/10.1016/j.eml.2016.02.007> [126, 202]
287. Perkins, N.C., Mote, Jr., C.D.: Three dimensional vibration of travelling elastic cables. *Journal of Sound and Vibration* **114**(2), 325–340 (1987). URL [http://dx.doi.org/10.1016/S0022-460X\(87\)80157-8](http://dx.doi.org/10.1016/S0022-460X(87)80157-8) [4, 52]
288. Perkins, N.C., Mote, Jr., C.D.: Theoretical and experimental stability of two translating cable equilibria. *Journal of Sound and Vibration* **128**(3), 397–410 (1989). URL [http://dx.doi.org/10.1016/0022-460X\(89\)90782-7](http://dx.doi.org/10.1016/0022-460X(89)90782-7) [4, 52, 80]
289. Peters, D.M.: Nonlinear stability criteria for elastic rod structures. Ph.D. thesis, University of California at Berkeley (2011). URL <https://escholarship.org/uc/item/6km3q6b7> [174]
290. Plaut, R.H., Dalrymple, A.J., Dillard, D.A.: Effect of work on contact of an elastica with a flat surface. *Journal of Adhesion Science and Technology* **15**(5), 565–581 (2001). URL <http://dx.doi.org/10.1163/156856101300189934> [137]
291. Plaut, R.H., Williams, N.H., Dillard, D.A.: Elastica analysis of the loop tack adhesion test for pressure sensitive adhesives. *Journal of Adhesion* **76**(1), 37–53 (2001). URL <http://dx.doi.org/10.1080/00218460108029616> [137]

292. Podio-Guidugli, P.: Peeling tapes. In: P. Steinmann, G.A. Maugin (eds.) Mechanics of Material Forces, *Advances in Mechanics and Mathematics*, vol. 11, pp. 253–260. Springer-Verlag, New York (2005). URL http://dx.doi.org/10.1007/0-387-26261-X_25 [137]
293. Pohl, W.F.: The self-linking number of a closed space curve. *Journal of Mathematics and Mechanics* **17**, 975–985 (1967/1968) [110, 113]
294. Pohl, W.F.: DNA and differential geometry. *The Mathematical Intelligencer* **3**(1), 20–27 (1980/81). URL <http://dx.doi.org/10.1007/BF03023391> [94, 104, 114, 115]
295. Prusinkiewicz, P.: Modeling plant growth and development. *Current Opinion in Plant Biology* **7**(1), 79–83 (2004). URL <http://dx.doi.org/10.1016/j.pbi.2003.11.007> [240]
296. Purohit, P.K., Bhattacharya, K.: Dynamics of strings made of phase-transforming materials. *Journal of the Mechanics and Physics of Solids* **51**(3), 393–424 (2003). URL [http://dx.doi.org/10.1016/S0022-5096\(02\)00097-2](http://dx.doi.org/10.1016/S0022-5096(02)00097-2) [55, 370]
297. Reeken, M.: The equation of motion of a chain. *Mathematische Zeitschrift* **155**(3), 219–237 (1977). URL <http://dx.doi.org/10.1007/BF02028442> [30, 73]
298. Reid, W.T.: Riccati Differential Equations. Academic Press, New York (1972) [172]
299. Reissner, E.: On one-dimensional large-displacement finite-strain beam theory. *Studies in Applied Mathematics* **52**(2), 87–95 (1973). URL <http://dx.doi.org/10.1002/sapm197352287> [269]
300. Reissner, E.: On finite deformations of space-curved beams. *Zeitschrift für Angewandte Mathematik und Physik. ZAMP. Journal of Applied Mathematics and Physics. Journal de Mathématiques et de Physique Appliquées* **32**(6), 734–744 (1981). URL <http://dx.doi.org/10.1007/BF00946983> [269]
301. Ricca, R.L., Nipoti, B.: Gauss' linking number revisited. *Journal of Knot Theory and its Ramifications* **20**(10), 1325–1343 (2011). URL <http://dx.doi.org/10.1142/S0218216511009261> [101, 116]
302. Rivlin, R.S.: Large elastic deformations of isotropic materials. VI. Further results in the theory of torsion, shear and flexure. *Philosophical Transactions of the Royal Society of London A: Mathematical, Physical and Engineering Sciences* **242**(845), 173–195 (1949). URL <http://dx.doi.org/10.1098/rsta.1949.0009> [352]
303. Rolfsen, D.: Knots and Links, *Mathematics Lecture Series*, vol. 7. Publish or Perish, Inc., Houston, Texas (1990). Corrected reprint of the 1976 original [104]
304. Rosenberg, R.M.: Analytical Dynamics of Discrete Systems. Plenum Press, New York (1977) [75, 77]
305. Routh, E.J.: The Advanced Part of a Treatise on the Dynamics of a System of Rigid Bodies, sixth, revised and enlarged edn. MacMillan & Co., London (1905) [52, 53, 193, 228]

306. Routh, E.J.: The Elementary Part of a Treatise on the Dynamics of a System of Rigid Bodies, seventh edn. Macmillan, London (1905) [193]
307. Rubin, M.B.: Restrictions on nonlinear constitutive equations for elastic rods. *Journal of Elasticity* **44**(1), 9–36 (1996). URL <http://dx.doi.org/10.1007/BF00042190> [324, 326, 329, 334]
308. Rubin, M.B.: An intrinsic formulation for nonlinear elastic rods. *International Journal of Solids and Structures* **34**(31–32), 4191–4212 (1997). URL [http://dx.doi.org/10.1016/S0020-7683\(96\)00158-8](http://dx.doi.org/10.1016/S0020-7683(96)00158-8) [312, 323]
309. Rubin, M.B.: Cosserat Theories: Shells, Rods, and Points. Kluwer Academic Press, Dordrecht (2000). URL <http://dx.doi.org/10.1007/978-94-015-9379-3> [189, 200, 208, 295, 296, 307, 323, 345]
310. Rubin, M.B.: On the quest for the best Timoshenko shear coefficient. *ASME Journal of Applied Mechanics* **70**(1), 154–157 (2002). URL <http://dx.doi.org/10.1115/1.1526122> [291, 293, 338]
311. Rumiyansev, V.V.: Stability of steady-state satellite motion. *Cosmic Research* **6**, 135–138 (1968) [266]
312. Santillan, S.T., Virgin, L.N.: Numerical and experimental analysis of the static behavior of highly deformed risers. *Ocean Engineering* **38**(13), 1397–1402 (2011). URL <http://dx.doi.org/10.1016/j.oceaneng.2011.06.009> [183]
313. Santillan, S.T., Virgin, L.N., Plaut, R.H.: Static and dynamic behavior of highly deformed risers and pipelines. *ASME Journal of Offshore Mechanics and Arctic Engineering* **132**(2), 021,401 (2010). URL <http://dx.doi.org/10.1115/1.4000555> [183]
314. Sarkar, A., Léger, J.F., Chatenay, D., Marko, J.F.: Structural transitions in DNA driven by external force and torque. *Physical Review E* **63**(5), 051,903 (2001). URL <http://link.aps.org/doi/10.1103/PhysRevE.63.051903> [114, 115]
315. Schagerl, M., Steindl, A., Steiner, W., Troger, H.: On the paradox of the free falling folded chain. *Acta Mechanica* **125**(1–4), 155–168 (1997). URL <http://dx.doi.org/10.1007/BF01177305> [51, 73, 77]
316. Schajer, G.S.: The vibration of a rotating circular string subject to a fixed elastic restraint. *Journal of Sound and Vibration* **92**(1), 11–19 (1984). URL [http://dx.doi.org/10.1016/0022-460X\(84\)90369-9](http://dx.doi.org/10.1016/0022-460X(84)90369-9) [22]
317. Schlick, T.: Modeling superhelical DNA: recent analytical and dynamic approaches. *Current Opinion in Structural Biology* **5**(2), 245–262 (1995). URL [http://dx.doi.org/10.1016/0959-440X\(95\)80083-2](http://dx.doi.org/10.1016/0959-440X(95)80083-2) [188]
318. Seifert, U.: Adhesion of vesicles in two dimensions. *Physical Review A* **43**(12), 6803–6814 (1991). URL <http://dx.doi.org/10.1103/PhysRevA.43.6803> [165, 166]
319. Shi, Y., Hearst, J.E.: The Kirchhoff elastic rod, the nonlinear Schrödinger equation, and DNA supercoiling. *The Journal of Chemical Physics* **101**(6), 5186–5200 (1994). URL <http://dx.doi.org/10.1063/1.468506> [188, 220, 222, 225, 239]

320. Shi, Y., Hearst, J.E., Bishop, T.C., Halvorson, H.R.: Erratum: “The Kirchhoff elastic rod, the nonlinear Schrödinger equation, and DNA supercoiling” [J. Chem. Phys. 101, 5186 (1994)]. *The Journal of Chemical Physics* **109**(7), 2959–2961 (1998). URL <http://dx.doi.org/10.1063/1.476848> [188, 225]
321. Shuster, M.D.: A survey of attitude representations. *American Astronautical Society. Journal of the Astronautical Sciences* **41**(4), 439–517 (1993) [8, 193]
322. Silk, W., Erickson, R.O.: Kinematics of hypocotyl curvature. *American Journal of Botany* **65**(3), 310–319 (1978). URL <http://www.jstor.org/stable/2442271> [183]
323. Silk, W., Erickson, R.O.: Kinematics of plant growth. *Journal of Theoretical Botany* **76**(4), 481–501 (1979). URL [http://dx.doi.org/10.1016/0022-5193\(79\)90014-6](http://dx.doi.org/10.1016/0022-5193(79)90014-6) [240]
324. Silk, W., Wang, L.L., Cleland, R.E.: Mechanical properties of the rice panicle. *Plant Physiology* **70**(2), 460–464 (1982) [183]
325. Simmonds, J.G.: A Brief on Tensor Analysis, second edn. Springer-Verlag, New York (1994). URL <http://dx.doi.org/10.1007/978-1-4419-8522-4> [196, 350]
326. Simo, J.C., Marsden, J.E., Krishnaprasad, P.S.: The Hamiltonian structure of nonlinear elasticity: The material and convective representations of solids, rods, and plates. *Archive for Rational Mechanics and Analysis* **104**(2), 125–183 (1988). URL <http://dx.doi.org/10.1007/BF00251673> [270]
327. Simo, J.C., Vu-Quoc, L.: On the dynamics in space of rods undergoing large motions - a geometrically exact approach. *Computer Methods in Applied Mechanics and Engineering* **66**(2), 125–161 (1988). URL [http://dx.doi.org/10.1016/0045-7825\(88\)90073-4](http://dx.doi.org/10.1016/0045-7825(88)90073-4) [193, 270]
328. Sokolnikoff, I.S.: *Tensor Analysis: Theory and Applications*. John Wiley & Sons, Inc., London (1951) [207, 350]
329. Spivak, M.: *A Comprehensive Introduction to Differential Geometry*, vol. I, second edn. Publish or Perish, Inc., Wilmington, Delaware (1979) [102]
330. Steigmann, D.J., Faulkner, M.G.: Variational theory for spatial rods. *Journal of Elasticity* **33**(1), 1–26 (1993). URL <http://dx.doi.org/10.1007/BF00042633> [378]
331. Steiner, W., Troger, H.: On the equations of motion of the folded inextensible string. *Zeitschrift für Angewandte Mathematik und Physik. ZAMP. Journal of Applied Mathematics and Physics. Journal de Mathématiques et de Physique Appliquées* **46**(6), 960–970 (1995). URL <http://dx.doi.org/10.1007/BF00917880> [51, 73, 75, 77]
332. Steinmann, P., Maugin, G.A. (eds.): *Mechanics of Material Forces, Advances in Mechanics and Mathematics*, vol. 11. Springer-Verlag, New York (2005). URL <http://dx.doi.org/10.1007/b137232> [24]
333. Stepanov, S.I.: On the steady motions of a gyrostat satellite. *Journal of Applied Mathematics and Mechanics* **33**(1), 121–126 (1969). URL [http://dx.doi.org/10.1016/0021-8928\(69\)90120-8](http://dx.doi.org/10.1016/0021-8928(69)90120-8) [266]

334. Stump, D.M.: The hockling of cables: A problem in shearable and extensible rods. *International Journal of Solids and Structures* **37**(3), 515–533 (2010). URL [http://dx.doi.org/10.1016/S0020-7683\(99\)00019-0](http://dx.doi.org/10.1016/S0020-7683(99)00019-0) [291]
335. Swigon, D., Coleman, B.D., Tobias, I.: The elastic rod model for DNA and its application to the tertiary structure of DNA minicircles in mononucleosomes. *Biophysical Journal* **74**(5), 2515–2530 (1998). URL [http://dx.doi.org/10.1016/S0006-3495\(98\)77960-3](http://dx.doi.org/10.1016/S0006-3495(98)77960-3) [114, 115]
336. Tait, P.G.: On the rotation of a rigid body about a fixed point. *Proceedings of the Royal Society of Edinburgh* **25** (1868). Reprinted in pages 86–127 of [338] [193]
337. Tait, P.G.: Note on the measure of beknottedness. *Proceedings of the Royal Society of Edinburgh* **9**, 289–298 (1877–1878). URL <http://www.maths.ed.ac.uk/~aar/papers/beknot.pdf> [93]
338. Tait, P.G.: *Scientific Papers*, vol. 1. Cambridge University Press, Cambridge (1898) [419]
339. Tait, P.G., Steele, W.J.: *A Treatise on the Dynamics of a Particle with Numerous Examples*, second edn. MacMillan & Co., Cambridge and London (1865) [90]
340. Thompson, J.M.T., Champneys, A.R.: From helix to localized writhing in the torsional post-buckling of elastic rods. *Proceedings of the Royal Society of London A: Mathematical, Physical and Engineering Sciences* **452**(1944), 117–138 (1996). URL <http://dx.doi.org/10.1098/rspa.1996.0007> [233, 234, 239]
341. Thomson, W., Tait, P.G.: *Treatise on Natural Philosophy*. Oxford University Press, Oxford (1867) [99]
342. Tian, J., Hutton, S.G.: Lateral vibrational instability mechanisms in a constrained rotating string. *ASME Journal of Applied Mechanics* **65**(3), 774–776 (1998). URL <http://dx.doi.org/10.1006/jsvi.1999.2237> [22]
343. Tian, J., Hutton, S.G.: On the mechanisms of vibrational instability in a constrained rotating string. *Journal of Sound and Vibration* **225**(1), 111–126 (1999). URL <http://dx.doi.org/10.1006/jsvi.1999.2237> [22]
344. Timoshenko, S.P.: On the correction for shear of the differential equation for transverse vibrations of prismatic bars. *Philosophical Magazine Series 6* **41**(245), 744–746 (1921). URL <http://dx.doi.org/10.1080/14786442108636264> [270, 292, 293, 338]
345. Timoshenko, S.P., Gere, J.M.: *Theory of Elastic Stability*, second edn. McGraw-Hill, New York (1961) [176, 184, 250, 252, 262]
346. Timoshenko, S.P., Goodier, J.N.: *Theory of Elasticity*, third edn. McGraw-Hill, New York (1970) [54, 334]
347. Tomassetti, G.: On configurational balance in slender bodies. *Archive of Applied Mechanics* **81**(8), 1041–1050 (2010). URL <http://dx.doi.org/10.1007/s00419-010-0470-3> [26]

348. Toupin, R.A.: Theories of elasticity with couple-stress. *Archive for Rational Mechanics and Analysis* **17**(2), 85–112 (1964). URL <http://dx.doi.org/10.1007/BF00253050> [269]
349. Truesdell, C.: *The Kinematics of Vorticity*. Indiana University Press, Bloomington, Indiana (1954) [56]
350. Truesdell, C.: *The Rational Mechanics of Flexible or Elastic Bodies*, 1638–1788. Leonhardi Euleri Opera Omnia, Series secunda (Opera mechanica et astronoca), Vol. XI, sectio secunda. Auctoritate et impensis Societatis Scientiarum Naturalium Helveticae. Orell Füssli, Zürich (1960) [121, 135, 176, 295]
351. Truesdell, C., Noll, W.: *The Non-Linear Field Theories of Mechanics*, third edn. Springer-Verlag, Berlin (2004). Edited, and with a preface, by Stuart S. Antman [32, 304, 361, 363, 373]
352. Truskinovskii, L.M.: Equilibrium phase interfaces. *Soviet Physics Doklady* **27**(7), 551–552 (1982) [37]
353. Truskinovskii, L.M.: Dynamics of non-equilibrium phase boundaries in a heat conducting non-linearly elastic medium. *Journal of Applied Mathematics and Mechanics* **51**(6), 777–784 (1987). URL [http://dx.doi.org/10.1016/0021-8928\(87\)90140-7](http://dx.doi.org/10.1016/0021-8928(87)90140-7) [369]
354. Truskinovsky, L.: Kinks versus shocks. In: R. Fosdick, E. Dunn, H. Slemrod (eds.) *Shock induced transitions and phase structures in general media, IMA Volumes in Mathematics and its Applications*, vol. 52, pp. 185–229. Springer-Verlag, New York (1993). URL http://dx.doi.org/10.1007/978-1-4613-8348-2_11 [37, 43, 91, 369]
355. Umetani, N., Schmidt, R., Stam, J.: Position-based elastic rods. In: K. Erleben, J. Pettré (eds.) *Proceedings of the ACM SIGGRAPH/Eurographics Symposium on Computer Animation*, pp. 21–30. Eurographics Association (2014) [188]
356. Virga, E.G.: Chain paradoxes. *Proceedings of the Royal Society A: Mathematical, Physical and Engineering Science* **471**(2173), 1–24 (2014). URL <http://dx.doi.org/10.1098/rspa.2014.0657> [71, 77, 78]
357. Virga, E.G.: Dissipative shocks in a chain fountain. *Physical Review E* **89**(5), 053,201 (2014). URL <http://dx.doi.org/10.1103/PhysRevE.89.053201> [78]
358. Weinstock, R.: *Calculus of Variations with Applications to Physics and Engineering*. Dover Publications, New York (1974) [387]
359. White, J.H.: Self-linking and the Gauss integral in higher dimensions. *American Journal of Mathematics* **91**, 693–728 (1969). URL <http://www.jstor.org/stable/2373348> [114]
360. White, J.H., Bauer, W.R.: Calculation of the twist and the writhe for representative models of DNA. *Journal of Molecular Biology* **189**(2), 329–341 (1986). URL [http://dx.doi.org/10.1016/0022-2836\(86\)90513-9](http://dx.doi.org/10.1016/0022-2836(86)90513-9) [111, 113, 114, 117]

361. White, J.H., Bauer, W.R.: Applications of the twist difference to DNA structural analysis. *Proceedings of the National Academy of Sciences* **85**(3), 772–776 (1988). URL <http://www.pnas.org/content/85/3/772.full.pdf> [114]
362. Whittaker, E.T.: *A Treatise on the Analytical Dynamics of Particles and Rigid Bodies*, fourth edn. Cambridge University Press, Cambridge (1937) [193, 225, 229]
363. Wickert, J.A., Mote, Jr., C.D.: On the energetics of axially moving continua. *Journal of the Acoustical Society of America* **85**(3), 1365–1368 (1989). URL <http://dx.doi.org/10.1121/1.397418> [4]
364. Williams, J.A.: Adhesional instabilities and gecko locomotion. *Journal of Physics D: Applied Physics* **48**(1), 015,401 (2015). URL <http://dx.doi.org/10.1088/0022-3727/48/1/015401> [137]
365. Wilson, B.F.: Apical control of branch growth and angle in woody plants. *American Journal of Botany* **87**(5), 601–607 (2000). URL <http://www.amjbot.org/content/87/5/601.abstract> [240]
366. Wong, C.W., Yasui, K.: Falling chains. *American Journal of Physics* **74**(6), 490–496 (2006). URL <http://dx.doi.org/10.1119/1.2186686> [60, 64, 87]
367. Wong, C.W., Youn, S.H., Yasui, K.: The falling chain of Hopkins, Tait, Steele and Cayley. *European Journal of Physics* **28**(3), 385 (2007). URL <http://dx.doi.org/10.1088/0143-0807/28/3/001> [60, 64, 87]
368. Yamamoto, H., Yoshida, M., Okuyama, T.: Growth stress controls negative gravitropism in woody plant stems. *Planta* **216**(2), 280–292 (2002). URL <http://dx.doi.org/10.1007/s00425-002-0846-x> [183]
369. Zheng, Q.S.: On transversely isotropic, orthotropic and relative isotropic functions of symmetric tensors, skew-symmetric tensors and vectors. II. The representations for three-dimensional transversely isotropic functions. *International Journal of Engineering Science* **31**(10), 1411–1423 (1993). URL [http://dx.doi.org/10.1016/0020-7225\(93\)90006-G](http://dx.doi.org/10.1016/0020-7225(93)90006-G) [282]
370. Zheng, Q.S.: On transversely isotropic, orthotropic and relative isotropic functions of symmetric tensors, skew-symmetric tensors and vectors. III. The irreducibility of the representations for three-dimensional transversely isotropic functions. *International Journal of Engineering Science* **31**(10), 1425–1433 (1993). URL [http://dx.doi.org/10.1016/0020-7225\(93\)90007-H](http://dx.doi.org/10.1016/0020-7225(93)90007-H)
371. Zheng, Q.S.: Theory of representations for tensor functions - A unified invariant approach to constitutive equations. *ASME Applied Mechanics Reviews* **47**(11), 545–587 (1994). URL <http://dx.doi.org/10.1115/1.3111066> [281, 282]
372. Zhou, X., Majidi, C., O'Reilly, O.M.: Flexing in motion: A locomotion mechanism for soft robots. *International Journal of Non-Linear Mechanics* **74**, 7–17 (2015). URL <http://dx.doi.org/10.1016/j.ijnonlinmec.2015.03.001> [126, 183]

373. Zhou, X., Majidi, C., O'Reilly, O.M.: Soft hands: An analysis of some gripping mechanisms in soft robot design. *International Journal of Solids and Structures* **64–65**, 155–165 (2015). URL <http://dx.doi.org/10.1016/j.ijsolstr.2015.03.021> [126, 183]
374. Zhou, X., O'Reilly, O.M.: On adhesive and buckling instabilities in the mechanics of carbon nanotubes bundles. *ASME Journal of Applied Mechanics* **82**(10), 101,007 (2015). URL <http://dx.doi.org/10.1115/1.4030976> [137, 183]
375. Ziegler, H.: Principles of Structural Stability, second edn. Birkhäuser, Basel (1977). URL <http://dx.doi.org/10.1007/978-3-0348-5912-7> [161, 250, 262]

Index

A

adhesion, 137
adhesion boundary condition, 140, 166
angular momentum \mathbf{H}_O , 204, 273, 302
angular momentum \mathbf{h}_O , 125, 302
assigned director force \mathbf{l}^β , 207, 208, 273, 307
example, 208, 310
prescription, 208, 307, 331
assigned force \mathbf{f} , 23, 127, 207, 273, 307
example, 208, 310
prescription, 208, 307, 330
assigned material force \mathbf{b} , 35, 130, 207, 273, 307
prescription, 314, 333
assigned material force $\rho_a^* \mathbf{b}_M$, 369
assigned moment \mathbf{m}_a , 127, 207, 273
prescription, 208, 307
axial motions, 14, 51

B

bead chain, 58, 78
Bernoulli-Euler beam, 184, 302, 339
Bernoulli-Euler constitutive relations, 129
Bishop frame, 95, 107, 117, 215, 218
Bonnet-Meusnier relations, 216
buckling, 240, 262

C

Călugăreanu's Theorem, 108
Cauchy's representation theorem, 304
Cayley-Hamilton theorem, 375
chain fountain, 78
Christoffel symbol
 γ_{ir}^k , 349
 γ_{irk} , 349

circulation, 16
closed loops of string, 51
configuration
natural, 276
present, 346
reference, 346
conservative force, 162
conservative moment, 162
constitutive relations
constrained elastic rod, 316
Cosserat rod, 274
elastic rod, 315
elastic string, 30
elastica, 125
hyperelastic body, 361
inextensible string, 30
Kirchhoff elastic rod, 213
Mooney-Rivlin, 364, 375
neo-Hookean, 364
constrained rod theories, 316, 320
constraint manifold, 364
constraints, 34, 316, 320, 361, 373
contact director force \mathbf{m}^β , 307
contact force \mathbf{n} , 23, 127, 207, 273, 307
contact material force \mathbf{C} , 23, 127, 207, 273, 307
contact moment \mathbf{m} , 127, 207, 273
coordinates
arc-length parameter, 13
convected, 13, 323, 351, 371, 373
curvilinear, 323, 347, 373
material, 13, 351
Cosserat curve, 270
curvature κ , 5, 95, 123

D

- Darboux vector ω_{SF} , 5, 95, 117, 215
 directed curve, 189, 270
 director momentum L^β , 204, 273, 302
 directors, 189, 270
 divergence
 tensor-valued function, 356, 359
 vector-valued function, 356, 359
 DNA
 supercoiling, 114, 239
 twist-stretch coupling, 284
 driving force, 24, 42, 44, 91, 369
 dual Euler basis, 193, 227

E

- elastic bar, 37
 elastica, 121, 385
 adhesion, 137, 164
 adhesion instability, 173, 174
 buckling, 173, 174, 176
 constitutive relations, 129
 stability criteria, 167
 terminally loaded, 133, 161
 variational formulation, 161
 elastica arm scale, 147
 energy release rate, 24, 42, 366
 Erickson's uniform states, 287
 Eshelby's force on a singularity, 42, 369
 Euler angles, 193, 215, 235, 258, 266
 Euler basis, 193
 Euler-Lagrange necessary condition, 378, 381
 Eulerian formulation, 19

F

- flexural strains $v_{1,2}$, 272
 flexure of a rod, 121, 291, 338
 Frenet frame, 6, 94
 Frenet triad, 5, 94, 215

G

- Gauss map, 101
 Gauss-Bonnet theorem, 99, 107
 geodesic, 100
 geodesic curvature κ_g , 100
 geometric torsion τ , 5, 95, 215
 Gibbs free energy ϕ_G , 33, 47
 gradient
 scalar-valued function, 350, 356
 vector-valued function, 356

H

- Hamilton's Principle of Least Action, 387
 helical spring, 252

- helix, 10, 97, 101, 107, 112
 hocking of marine cables, 236

I

- inverted catenary, 78
 irreducible function bases, 281

J

- Jacobi condition, 172, 379
 Jacobi equation, 172

K

- kinetic analogue, 132, 154, 265
 kinetic energy T , 125, 204, 273, 302
 Kirchhoff's constraints, 191
 Kirchhoff's rod theory, 187, 284, 320

L

- Lagrange multipliers, 363
 Lagrange's equations of motion, 227, 261, 387
 Lagrangian formulation, 19
 Legendre condition, 379
 Legendre transformation, 33
 Leibnitz rule, 17, 166
 linear momentum \mathbf{G} , 125, 204, 273, 302
 link chain, 58
 linking number $L_k(\mathcal{S}_1, \mathcal{S}_2)$, 101
 example, 116, 117
 looping, 236

M

- material curve, 13, 346, 351
 material momentum P , 16, 125, 204, 273, 302
 material momentum P^* , 365
 material symmetry, 277
 transverse hemitropy, 281
 transverse isotropy, 207, 281
 material time derivative, 13

N

- Nanson's formula, 353
 Noether's theorem, 26, 367

P

- parallel propagation, 95
 phase transformation, 41, 91
 planar pendulum, 132
 plane curve, 9, 95, 117

R

- relatively parallel, 96
 ribbon, 98, 112
 Riccati equation, 172
 rotations, 8, 21, 193

S

- self-contact, 236, 239
- self-linking number SL , 113
- Serret-Frenet relations, 5, 215
- shear correction factor, 291, 306
- signed crossings, 102
- singular supply
 - angular momentum \mathbf{M}_γ , 131
 - example, 139, 145, 152, 154
 - angular momentum \mathbf{M}_{O_γ} , 24, 127, 309
 - director momentum \mathbf{F}_γ^β , 309
 - prescription, 310
 - linear momentum \mathbf{F}^*_γ , 367
 - linear momentum \mathbf{F}_γ , 24, 127, 309
 - example, 60, 66, 70, 74, 81, 139, 152, 154, 164
 - prescription, 310
 - material momentum \mathbf{B}^*_γ , 367
 - material momentum \mathbf{B}_γ , 24, 127, 309
 - example, 50, 58, 60, 61, 70, 74, 81, 139, 152, 164
 - prescription, 310
 - power $\Phi_{E_\gamma}^*$, 367
 - power Φ_{E_γ} , 24, 127, 309
 - example, 60, 70, 74, 139
- small on large, 302
- soft robots, 125, 182
- space curve, 5, 15, 215
- spiral spring, 252
- strain energy function
 - constrained elastic rod, 316
 - Cosserat rod, 274
 - elastic rod, 303, 334
 - elastica, 125
 - Kirchhoff rod, 205, 214
 - linearly elastic rod, 305
 - string, 30
- strain measure
 - $\mathbf{v} - \mathbf{v}_0$, 123
 - \mathbf{v} , 205, 273
 - \mathbf{q} , 273
 - γ_{ij} , 301
 - $\kappa - \kappa_0$, 123
 - $\kappa_{\beta k}$, 301
 - μ , 123
- stretch, 14
- superposed rigid body motions, 21, 34, 126, 192, 271, 298, 303, 315, 316, 320, 359

T

- tangent indicatrix c_t , 100
- tendril perversion, 240
- tensor
 - adjugate, 279, 353
 - Cauchy stress \mathbf{T} , 355
 - deformation gradient \mathbf{F} , 346, 352
 - deformation gradient \mathbf{F}^* , 323
 - energy-momentum $\boldsymbol{\sigma}$, 365
 - first Piola-Kirchhoff stress \mathbf{P} , 355
 - Lagrangian strain \mathbf{E} , 353
 - left Cauchy-Green strain \mathbf{B} , 353
 - metric tensor, 350
 - nominal stress Σ , 355
 - orthogonal, 278
 - proper-orthogonal, 191
 - right Cauchy-Green strain \mathbf{C} , 353
 - rotation, 8, 21, 191, 193, 270
 - second Piola-Kirchhoff stress \mathbf{S} , 355
 - stretching \mathbf{D} , 361
- Timoshenko beam theory, 293, 338
- torsion of a rod, 339
- torsional rigidity \mathcal{D} , 306
- torsional strain v_3 , 272
- torsional strains $\gamma_{12}, \kappa_{12}, \kappa_{21}$, 339
- tortuosity $\Sigma = 1/\tau$, 216
- total geometric torsion $T_w(\mathcal{S}, \mathbf{e}_n)$, 106
- total twist $T_w(\mathcal{S}, \mathbf{u})$, 107
- traction vector \mathbf{T}^i , 355
- trefoil knot, 113
- twist, 215
- twist-stretch coupling, 287
- twisting number T_w , 114

V

- volumetric deformation of a rod, 336

W

- wave equation, 338, 387
- Weierstrass conditions, 379
- Weierstrass excess function, 383
- Weierstrass-Erdmann corner conditions, 30, 185, 382, 384, 389, 390
- wire rope, 287
- wrench, 252, 287
- writhing number $W_r(\mathcal{S})$, 109
 - example, 111